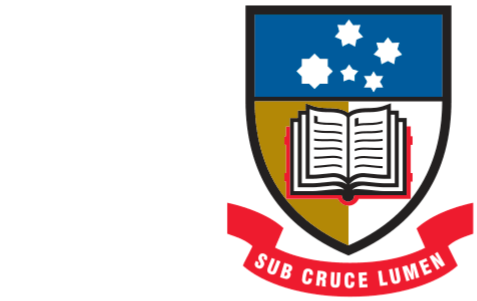

THE UNIVERSITY of ADELAIDE

Reconstructing Australia's late Quaternary climate from the geochemistry of lake sediments and snail shells

GEORGINA MAJA FALSTER

Department of Earth Sciences
School of Physical Sciences
The University of Adelaide

This thesis is submitted in fulfilment of the requirements for the degree of Doctor of Philosophy

March 2019

Table of contents

Chapter Four: Environmental controls on the carbon and oxygen stable isotope ratios of modern land snail shells in Australia

Chapter Five: Clarifying the climate-isotope relationship in Australian land snail shells using clumped isotopes and flux balance models

Chapter Six: Clumped isotopes in freshwater snail shells: a new quantitative temperature proxy for Australia and its application to fossil *Glyptophysa* shells from Blanche Cave

Abstract

Australia's climate is influenced by ocean-atmosphere interactions in the adjacent Indian, Pacific, and Southern oceans, as well as major atmospheric circulation patterns. Australian climates exhibit high inter-annual variability, arising in part from complex interactions between these drivers. Understanding the nature and drivers of Australian climate variability is not only important for land use and management, but also has global relevance, due to Australia's contribution to the global terrestrial carbon budget. Measurements of Australian temperature and rainfall only extend back to the early 20th century, and hence do not capture the full range of natural climate variability. Proxy-based climate reconstructions are therefore required to understand Australian climate variability on long (centennial to millennial) time scales. The late Quaternary—defined in this thesis as 30 to 10 thousand years before the year 1950 (ka BP)—is a particularly informative interval. It encompasses large changes in global climate dynamics, including both the global Last Glacial Maximum (LGM; 23 to 19 ka BP) and subsequent deglaciation, allowing assessment of the Australian climate response to global change. However, the arid to semi-arid nature of most the continent is not conducive to sedimentary record accumulation, limiting spatial and temporal resolution of existing late Quaternary climate reconstructions.

This thesis therefore presents both new late Quaternary palaeoclimate data and new methods for inferring past climate across the Australian continent, through the following research components:

1) A record of late Quaternary moisture balance, inferred from highly resolved x-ray fluorescence and organic carbon isotope measurements of a sedimentary sequence from Lake Surprise in south-eastern Australia (Chapter 3). The regional significance of this record is assessed using a Monte Carlo Empirical Orthogonal Function approach.
2) The high-resolution record is supported by three discrete quantitative temperature estimates, based on the clumped isotope composition (Δ_{47}) of freshwater snail shells from Blanche Cave, also in south-eastern Australia (Chapter 6). Δ_{47} analysis allows calculation of the growth temperature of carbonate minerals (e.g. snail shells), independent of organism, carbonate phase, or formation water geochemistry. Carbonate Δ_{47} analysis therefore offers a uniquely direct estimate of past temperatures, that has not previously been applied in Australian palaeoclimate studies.
3) Clumped isotope analysis is highly susceptible to contamination, so this thesis provides a new pretreatment method for obtaining precise and accurate data from carbonates preserved within an organic-rich matrix (Chapter 2).
4) The influence of remote drivers of Australian climate often manifests in distinct spatial patterns of temperature or rainfall. However, the low spatial resolution of existing palaeoclimate records across the continent inhibits detection of spatio-temporal climate trends that would facilitate inference of these drivers. This thesis therefore evaluates the

climate proxy potential of land snail shells in Australia, by combining flux balance models with clumped and stable isotope measurements of modern shells collected from a wide spatial and climatic gradient across the continent (Chapters 4 and 5).

The palaeoclimate reconstructions provide a coherent record of climate variability prior to and throughout the late Quaternary, and suggest that drivers of south-eastern Australian climate have varied on multi-millennial time scales in response to major shifts in global circulation. Δ_{47} analysis of freshwater snail shells suggests that between ~41 and 32 ka BP, mean annual air temperatures at Blanche Cave decreased from approximately 12 ± 3.2 °C to 5 ± 4.4 °C i.e. almost ten degrees cooler than modern. These relatively low temperatures preceded a period of regional aridity between 28 and 18.5 ka BP as recorded at Lake Surprise. Together, the data suggest that the south-east Australian climate was probably responding to very different drivers to those that affect the modern climate, possibly dominated by cold Southern Ocean processes. Centennial- to millennial-scale hydroclimate variability was maintained throughout the 28–18.5 ka BP interval. Peak aridity between 21 and 18.5 ka BP probably represents the local expression of the global LGM. A rapid deglacial climate shift occurred between ~18.5 and 16 ka BP, culminating in warmer (15.5 ± 3.6 °C) and wetter conditions probably more like those of the present.

The stable isotope geochemistry of modern land snail shells records precipitation amount via two mechanisms: (1) its influence on the $\delta^{18}O$ of precipitation (a wet season signal), and (2) its effect on vegetation $\delta^{13}C$ (an annual to multi-annual signal). Unlike freshwater snails, land snail Δ_{47} growth temperatures do not have a straightforward relationship with average air temperatures, but rather are useful for extracting the temperature influence from snail shell $\delta^{18}O$. This is the first study to report $\delta^{13}C$, $\delta^{18}O$, and Δ_{47} measurements from land snail shells spanning such a large climatic gradient, and also the first to investigate snail isotope-climate relationships across the variable and largely arid Australian environments. The isotope-climate relationships are robust irrespective of species or regional climatology. With land snails widely distributed in Australia, including in arid climates that lack other suitable proxies, these consistent relationships demonstrate that land snail shell isotopes will be a valuable tool for assessing spatio-temporal precipitation variability at a continental scale.

Thesis declaration

I certify that this work contains no material which has been accepted for the award of any other degree or diploma in my name in any university or other tertiary institution and, to the best of my knowledge and belief, contains no material previously published or written by another person, except where due reference has been made in the text. In addition, I certify that no part of this work will, in the future, be used in a submission in my name for any other degree or diploma in any university or other tertiary institution without the prior approval of the University of Adelaide.

I acknowledge that copyright of published works contained within this thesis resides with the copyright holders of those works.

I give permission for the digital version of my thesis to be made available on the web, via the University's digital research repository, the Library Search, and also through web search engines, unless permission has been granted by the University to restrict access for a period of time.

I acknowledge the support I have received for my research through the provision of an Australian Government Research Training Program Scholarship.

GEORGINA FALSTER . DATE 12th March 2019

Publications arising from this thesis

Journal articles

Falster, G., Delean, S., Tyler, J. (2018). Hydrogen Peroxide Treatment of Natural Lake Sediment Prior to Carbon and Oxygen Stable Isotope Analysis of Calcium Carbonate. *Geochemistry, Geophysics, Geosystems*, 19, 3583-3595. https://doi.org/10.1029/2018GC007575

Falster, G., Tyler, J., Grant, K., Tibby, J., Turney, C., Löhr, S., Jacobsen, G., Kershaw, A. P. (2018). Millennial-scale variability in south-east Australian hydroclimate between 30,000 and 10,000 years ago. *Quaternary Science Reviews*, 192, 106-122. https://doi.org/10.1016/j.quascirev.2018.05.031

Conference abstracts

Falster G., Tyler, J., Kluge, T., Dux, F., Drysdale, R., Chivas, A., Tibby, J., Reed, L., 2018. Leaving a trail: reconstructing past climates from stable and clumped isotope analysis of snail shells. Australasian Quaternary Association biennial meeting, Canberra.

Falster, G., Tyler, J., Grant, K., Tibby, J., Turney, C., Jacobsen, G., Kershaw, A. P., 2018. Millennial-scale variability in south-east Australasian hydroclimate between 30,000 and 10,000 years ago. Southern Hemisphere Assessment of PalaeoEnvironments (SHAPE) workshop, Wollongong.

Falster, G., Tyler, J., Tibby, J., Kershaw, A. P., Barr, C., Grant, K., Turney, C., 2017. Coherent millennial-scale variability in southern Australasia during the Last Glacial Period. 5th PAGES Open Science Meeting, Zaragoza.

Falster, G., Tyler, J., Tibby, J., Barr, C., Grant, K., Kershaw, A. P., 2016. Hydroclimate variability in southern Australia during the Last Glacial Period: a multi-proxy record from Lake Surprise. Australasian Quaternary Association biennial meeting, Auckland.

Falster, G., Tyler, J., Tibby, J., Barr, C., Grant, K., Kershaw, A. P., 2016. Climate variability in southern Australia during the Last Glacial Period: a multi-proxy record from Lake Surprise. Australian Earth Sciences Convention, Adelaide.

Falster, G., Tyler, J., Tibby, J., Barr, C., Grant, K., Kershaw, A. P., 2015. Climate variability in southern Australia during the last glacial-interglacial transition: toward new insights from lake sediments using conventional and clumped isotope geochemistry. XIX INQUA Congress, Nagoya.

Acknowledgments

I thank AINSE Limited for providing financial assistance in the form of a Postgraduate Research Award and an International Travel Scholarship, the latter allowing me to spend time in the clumped isotope laboratory at the Institute of Environmental Physics at Heidelberg University. I am also very grateful to the Walter and Dorothy Duncan Trust, the Adelaide University Graduates Union, CRC LEME, and Soroptimist International of Adelaide for awarding generous grants enabling my participation in workshops, international training courses, and conferences. Part of this research was funded by an ARC Discovery Project (DP140014093).

I gratefully acknowledge the time that Katharine Grant, Tobias Kluge, Ivan Prokhorov, Fiona Bertuch, Peter Self, and the staff at Adelaide Microscopy spent training me in the laboratory. Each of these people went out of their way to help me become proficient in various analytical techniques, when they could undoubtedly have done the work much faster themselves! Special thanks to Florian Dux, for spending several weeks training me in clumped isotope analysis near the start of my PhD, and providing me with ongoing support in the subsequent years. Thanks also to Mark Rollog, Russell Drysdale, and David Wheeler for providing assistance with data acquisition.

Thanks to Allan Chivas, for not only providing snail shells carefully collected over many years of fieldwork, but also providing a wonderful example of the foresight, dedication, enthusiasm, and imagination that it takes to make a great scientist. Thanks also to Liz Reed for providing fossil shells from Blanche Cave, and to Tony Robinson, Winston Ponder, Michael Shea, and John Stanisic for performing taxonomic identifications.

Many thanks to the co-authors on the peer-reviewed publications included in this thesis; your insight and encouragement throughout the publication process helped me to become a better writer. Special thanks to Martin Kennedy and Katharine Grant for providing honest criticism and encouraging clarity of thought and expression. Thanks also two my two thesis examiners, who provided generous and thoughtful comments that both improved the quality of this thesis, and will be of great assistance in publishing the remainder of my work in peer-reviewed journals.

I sincerely thank my primary supervisor Jon Tyler for his guidance, inspiration, and academic support, despite a continuing—and I am sure rather irritating—lack of self-confidence on my part. Thanks also to my secondary supervisor John Tibby for his support and encouragement, and particularly for his valuable editorial and stylistic suggestions that improved the quality of both my written and oral presentations.

Finally, thanks to my wonderful family and friends for support throughout my PhD studies, and for your ongoing interest in my work.

Chapter 1

1 Introduction

1.1 Global climate change

Anthropogenic greenhouse gas emissions have contributed to present-day atmospheric greenhouse gas concentrations exceeding the range of the past 800,000 years (Masson-Delmotte et al., 2013). This unprecedented rise in greenhouse gas concentrations has resulted in rapid changes in global temperature and the global water cycle, with major implications for both natural and human systems (IPCC, 2014; Trenberth, 2011). The principal tools for predicting the magnitude and impact of future climate change are climate models–mathematical representations of climate systems that are based on the laws of physics and parameterised by theoretical and empirical observations of interactions between the atmosphere, the oceans, and the continents. By the year 2100, climate model simulations predict a global mean surface temperature increase of between 0.3 and 4.8 °C relative to the beginning of the 21st century, along with major changes in the distribution of global precipitation (IPCC, 2014). The large range in projected warming is due in part to uncertainty in future anthropogenic emission rates, but also results from an incomplete understanding of global and regional climate dynamics, including natural climate variability (Whetton, 2015). Instrumental climate records used to test the veracity of climate model simulations do not capture the full range of natural climate variability, limiting the ability of climate models to accurately model dynamic climate systems, particularly on time scales beyond the decadal.

1.2 Australian climate variability

Uncertainty in future climate change is of particular concern for Australia, a country with climates that are subject to a diverse range of remote drivers, arising from various atmospheric circulation patterns and the adjacent ocean basins (Power et al., 1999), as well as the Atlantic Ocean, via trans-basin ocean and atmosphere teleconnections (Johnson et al., 2018). Drivers directly influencing Australian climate include the Southern Annular Mode (SAM; Marshall, 2003), the El Niño-Southern Oscillation (ENSO; Forootan et al., 2016; Nicholls et al., 1997), the Indian Ocean Dipole (IOD; Pepler et al., 2014; Saji and Yamagata, 2003), the Interdecadal Pacific Oscillation (IPO; Palmer et al., 2015; Power et al., 1999), atmospheric blocking (Pook and Gibson, 1999; Tozer and Kiem, 2017), and the position and intensity of the subtropical ridge (Murphy and Timbal, 2008; Timbal and Drosdowsky, 2013). These ocean-atmosphere circulation patterns operate on spatial scales from synoptic to hemispheric, and on temporal scales ranging from daily to multi-decadal (Gallant et

al., 2013). The relative influence of these remote drivers on Australian climates varies along with complex interactions between the drivers themselves (Gergis and Henley, 2017; Johnson et al., 2018). Interrelationships are further clouded as the influence of each driver on the key climatic variables—temperature and rainfall—varies across seasons, regions, and time periods (Crimp et al., 2018).

The complexity of Australia's climate systems is reflected in a high degree of uncertainty in model projections of Australian climate change, both in terms of changes in the strength and latitudinal position of Australia's remote climate drivers, and their influence on regional temperature and rainfall (Colman et al., 2015; Watterson et al., 2015; Watterson, 2001; Whetton et al., 2015). This uncertainty has major implications for land use and resource planning in Australia, where improved knowledge of long-term spatio-temporal variability in temperature and rainfall will be critically important in responsible management of natural resources (Hennessy et al., 2015; Jaffres et al., 2018; Tozer and Kiem, 2017).

1.3 Global relevance of Australian climate variability

Understanding Australian climate variability is relevant at global as well as local and regional scales. Australian landscapes play an important role in global carbon budgets (Long et al., 2019), and vegetation cover in Australia's semi-arid interior in particular can have a significant effect on global CO_2 drawdown (Ahlstrom et al., 2015; Poulter et al., 2014). Under current global climate boundary conditions, absolute *uptake* of CO_2 by terrestrial ecosystems is mainly by tropical forests, but both *trends* and inter-annual *variability* in CO_2 uptake are dominated by semi-arid lands, due to their high dependence on temperature and rainfall (Ahlstrom et al., 2015). These contributions are heavily dependent on modern climatologies, and may be different under alternate global climate baselines such as may occur in the future (Brown et al., 1993; Sitch et al., 2008). Consequently, extended pluvial conditions in Australia may be expected to cause a slight reduction in atmospheric CO_2 (Poulter et al., 2014). Understanding the interplay between temperature, rainfall, and vegetation cover has further implications for land management; for example, grazing significantly affects the capacity of semi-arid Australian ecosystems to assimilate CO_2 (Long et al., 2019).

Understating the controls on Australian rainfall and temperature, and the magnitude of their variability on centennial to millennial time scales is therefore of great importance. However, times-series data for Australian weather is relatively short, and

cannot resolve low-frequency climate variations that may clarify relationships with remote drivers. Combined with the non-stationary nature of interactions between these drivers, this causes major uncertainty in Australian climate variability on all time scales beyond the decadal (Gallant et al., 2013; Gergis and Henley, 2017; Jaffres et al., 2018; Tozer and Kiem, 2017). It is here that palaeoclimatology—the study of past climates—plays an important role in understanding the nature of climate variability on long (centennial to millennial time) scales.

1.4 Australian late Quaternary palaeoclimate records

Climate proxies—natural materials preserved in sedimentary archives that can be interpreted in terms of climate—are therefore necessary to understand long-term Australian climate variability. Reconstruction of Australian climates under different global boundary conditions may be particularly informative. The late Quaternary (defined here as 30–10 thousand calendar years before the year 1950; ka BP) is one such time, as it was characterised by abrupt shifts in climate dynamics (Thomas 2016). The late Quaternary also encompasses the Last Glacial Maximum (LGM; 23–19 ka BP), which was the most recent period of maximum global ice sheet volume (Clark et al., 2009), and the subsequent deglaciation, which involved a re-arrangement of major ocean-atmosphere circulation patterns (e.g. Anderson et al., 2009; Du et al., 2018; Partin et al., 2007; Xu et al., 2010). The late Quaternary therefore offers an excellent natural laboratory to assess the response of Australian climates to large shifts in remote drivers under different conditions to those encompassed by historic records, and on long time scales.

A detailed understanding of the long-term response of Australian climates to various drivers is contingent on robust reconstructions of spatial and temporal trends in these climates. This requires sedimentary records spanning the late Quaternary, of sufficiently high resolution to capture centennial- to millennial-scale variability. The potential resolution of a record is dependent both on the methods used to analyse the sediment, and the sedimentary archives themselves. Lakes are particularly useful archives, as they adapt to environmental change via physical, chemical, and biological shifts, evidence for which may be preserved in the lake sediment (Battarbee, 2000). Where suitable environmental conditions have persisted for the duration of the record, lakes may therefore provide high-resolution and continuous records of terrestrial climate change.

Unfortunately, Australian climates are dominantly arid to semi-arid (Peel et al., 2007), and these environments are not conducive to rapid or continuous sediment accumulation. This was especially the case during the LGM, which was probably colder, drier, and winder than the present (Bowler, 1976; Reeves et al., 2013a). Additionally, there is a strong spatial bias toward the south-east of the continent i.e. a region with a relatively high density of both sedimentary accumulations and Quaternary researchers. These issues were comprehensively reviewed by Reeves et al. (2013a). Since that review, eight new records of palaeoclimate change have been published that span at least the global LGM, including work forming part of this thesis. Most of these records—and indeed the majority of palaeoclimate records for the Australian late Quaternary—reflect 'hydroclimate' i.e. the combined influence of rainfall and temperature (Falster et al., 2018; Reeves et al., 2013a). Most proxy-environment relationships retain sufficient unexplained variance to make quantitative estimates of past rainfall or temperature rather tenuous (Juggins, 2013). The hydrological cycle, on the other hand, has a strong influence on a range of sedimentological, palaeoecological, and geochemical proxies that may be interpreted relatively easily in terms of 'wetter' or 'drier' conditions.

The relative ease of producing hydroclimate records has resulted in over 70 published records of Australian late Quaternary hydroclimate (Falster et al., 2018; Reeves et al., 2013a; Reeves et al., 2013b). However, many of these records are fragmentary, low resolution, and/or have sparse chronological control, thus limiting opportunities for inter-site comparisons or the reliable identification of millennial-scale variability (Hesse et al., 2018). Although recently published high-resolution records allow an increasingly nuanced understanding of climatic trends throughout the late Quaternary (e.g. Barr et al., 2017; DeDeckker et al., 2012; Petherick et al., 2017), high-resolution records remain rare for Australia. Additionally, a factor that remains largely overlooked in Australian hydroclimate records is imprint of the seasonal cycle on proxy records (Crimp et al., 2018). For example, modern climatologies demonstrate that a proxy reflecting spring maximum temperatures may record different trends to one recording minimum summer temperatures, or only record activity in very wet years (Alexander et al., 2007; Jakob and Walland, 2016; Nicholls et al., 1997). This may be a contributing factor to the lack of consensus.

For informative climate reconstructions that can be assessed in the context of historical data and climate model simulations, hydroclimate records should be supported by quantitative estimates of temperature or rainfall. This would also allow

determination of how records compare with those from farther afield. Absolute temperature or rainfall amount reconstructions rely on a response of a proxy to these variables which can be quantified through various calibration techniques. Proxy calibration approaches fall into three broad groups (von Gunten et al., 2012):

1. Calibration-in-time, where proxy measurements are regressed against coincident historical climate data, and the relationship is extrapolated beyond the monitoring period. This approach is only applicable to sedimentary records that continue to the present, and have excellent chronological control.
2. Calibration-in-space, where modern samples from a wide (spatial) climatic gradient are used to develop a proxy-environment calibration.
3. Empirical calibrations, where the response (biological or geochemical) of a proxy to environmental parameters can be measured directly, either in a laboratory, or *in situ*.

Successful application of these calibrations is dependent on the stability of the relationships through time, as well as the quality of the modern data. In Australia, calibration of rainfall proxies is particularly difficult, as historical rainfall measurements have poor accuracy (Jones et al., 2009; Viney and Bates, 2004). Therefore any modern proxy-climate relationship must be supported by strong mechanistic relationships, which can be expected with reasonable confidence to have also held under different climate boundary conditions.

Even high-resolution, well dated, and/or quantitative records of Australian late Quaternary climates still may dominantly reflect local climates, rather than being representative of regional conditions. Meaningful regional climate information is therefore dependent on either a network of directly comparable reconstructions across the continent, or use of numerical methods to extract regional trends from disparate records. Some advances have been made in the latter field recently, particularly in application of techniques such as Monte Carlo Empirical Orthogonal Function analysis to identify trends common to multiple sites (Anchukaitis and Tierney, 2012; Field et al., 2018; Shakun and Carlson, 2010; Tyler et al., 2015). This is a promising approach that will become more applicable as more suitably high-resolution records are published. Only with consistent spatial and temporal coverage will regional assessments of Australian climates be possible, after which point we may attempt to understand their response to remote drivers on long time scales. Comparison of robust proxy reconstructions with climate model outputs will allow assessment of the ability of climate models to reproduce past climate change, an essential step in evaluating their ability to accurate predict future change.

2 Notation used in this thesis

Throughout the thesis, carbon and oxygen stable isotope ratios ($^{13}C/^{12}C$ and $^{18}O/^{16}O$) are presented in the conventional delta (δ) notation i.e.

$$\delta^{13}\mathrm{C} = \frac{(^{13}\mathrm{C}/^{12}\mathrm{C})_{sample} - (^{13}\mathrm{C}/^{12}\mathrm{C})_{standard}}{(^{13}\mathrm{C}/^{12}\mathrm{C})_{standard}} \times 1000$$

$$\delta^{18}\mathrm{O} = \frac{(^{18}\mathrm{O}/^{16}\mathrm{O})_{sample} - (^{18}\mathrm{O}/^{16}\mathrm{O})_{standard}}{(^{18}\mathrm{O}/^{16}\mathrm{O})_{standard}} \times 1000$$

where a 'standard' is a reference material of known stable isotopic composition. Delta values of solid material (e.g. carbonate and organic matter) are reported relative to the Vienna Pee Dee Belemnite calcite standard, and delta values for water are reported relative to the Vienna Standard Mean Ocean Water standard. $\delta^{13}C$ and $\delta^{18}O$ are presented as per mil (‰) deviations from the relevant standard.

Clumped isotope values are presented in the conventional Δ_{47} notation i.e.

$$\Delta_{47} = \left[\left(\frac{R^{47}}{R^{47*}} - 1\right) - \left(\frac{R^{46}}{R^{46*}} - 1\right) - \left(\frac{R^{45}}{R^{45*}} - 1\right)\right] \times 1000$$

where

$$R^i = \frac{mass\ i}{mass\ 44}$$

i.e. the R^i values are abundance ratios of the mass 45, 46, and 47 CO_2 isotopologues, relative to mass 44 CO_2. The parameter R^{i*} is analogous to R^i, but corresponds to the expected ratios given a stochastic distribution of all possible isotopologues. These R^i values are derived in turn from the measured δ values for each isotopologue in the sample gas, relative to the laboratory-specific working gas:

$$\delta^i = \left[\frac{R_{i(sample\ gas)}}{R_{i\ (working\ gas)}} - 1\right] \times 1000$$

These 'raw' Δ_{47} values are then converted into a common reference frame, following methods described in the text.

3 Thesis aims

With this thesis, I have two overarching goals:

- Contribute to understanding the evolution of the Australian climate through the late Quaternary, with a view to gaining insight into the long-term nature and drivers of variability in Australian climates.
- Provide new, robust methods that may be applied to future palaeoclimate studies.

Specifically, I seek to address the following aims:

1. Provide a new high-resolution, well-dated 'baseline' palaeoclimate record for the late Quaternary, which is of sufficient resolution and quality to compare with regional and distal records (understand temporal change).
2. Develop and test new proxy and numerical methods to improve spatial coverage of palaeoclimate inferences across Australia (understand spatial change).
3. Develop a quantitative palaeoclimate reconstruction technique, and apply it to late Quaternary sediment.

4 Thesis outline

A diagram summarising the components of this thesis is provided in Figure 1.1.

4.1 Chapter Two

I describe a new method for the treatment of organic matter-rich sediment prior to carbon ($\delta^{13}C$) and oxygen ($\delta^{18}O$) stable isotope analysis of carbonate. The $\delta^{13}C$ and $\delta^{18}O$ of lacustrine carbonates are commonly used as proxies for terrestrial palaeoclimates, and these carbonates may be preserved in an organic-matter rich matrix. Organic matter has been shown to release CO_2 during phosphoric acid digestion of carbonate prior to analysis, biasing the data. My aim was therefore to develop a pretreatment method that would result in consistently accurate data.

I report the results of a controlled experiment, where I measured the $\delta^{13}C$ and $\delta^{18}O$ of fine-grained carbonate of known isotopic composition, present in low concentrations within organic-rich lake sediment. Prior to analysis, I subjected these mixtures to oxidation with acidic or alkaline hydrogen peroxide (H_2O_2), at various temperatures. Many of the combinations of experimental parameters resulted in a 'treatment bias',

but oxidation of sediment using alkaline H_2O_2 maintained at 50 °C yielded accurate and precise results. I applied this method to all carbonate isotope data presented in the remainder of the thesis.

This chapter is published as: Falster, G., Delean, S., Tyler, J. (2018). 'Hydrogen Peroxide Treatment of Natural Lake Sediment Prior to Carbon and Oxygen Stable Isotope Analysis of Calcium Carbonate' *Geochemistry, Geophysics, Geosystems*, 19, 3583-3595.

4.2 Chapter Three

I present a new well-dated, continuous, high-resolution record of hydroclimate spanning 30–10 ka BP, based on x-ray fluorescence and organic carbon isotope measurements of a sedimentary sequence from Lake Surprise in south-eastern Australia. The data provide a locally coherent record of the hydrological cycle, and preserve evidence for millennial-scale climate variability throughout the global LGM.

In this chapter, I assess my results in the context of two other high-resolution palaeoclimate records—one each from south-eastern Australia and New Zeland—using a Monte Carlo Empirical Orthogonal Function (MCEOF) approach. The MCEOF analysis identifies a regionally coherent trend in the three datasets. This trend suggests that south-east Australasian climates during the LGM responded to very different drivers to modern conditions, where a strong Southern Ocean influence likely resulted in a weakened hydrological cycle. This work also highlights an urgent need for more high-resolution, well dated records from adjacent ocean basins i.e. the likely remote drivers.

This chapter is published as: Falster, G., Tyler, J., Grant, K., Tibby, J., Turney, C., Löhr, S., Jacobsen, G., Kershaw, A. P. (2018). 'Millennial-scale variability in south-east Australian hydroclimate between 30,000 and 10,000 years ago'. *Quaternary Science Reviews*, 192, 106-122.

4.3 Chapter Four

Land snails are ubiquitous across Australia. The $\delta^{13}C$ and $\delta^{18}O$ of land snail shells should preserve information about past climates, but to date have not been used in Australian palaeoclimate studies. In this chapter, I therefore explore the potential of the $\delta^{13}C$ and $\delta^{18}O$ of land snail shells as a proxy for past Australian climates that should be applicable across a wide spatial gradient.

I report new measurements of the $\delta^{13}C$ and $\delta^{18}O$ of land snail shells collected from Australian sites covering a broad climatic range. As an initial exploratory exercise, I compare these measurements with a range of annually-averaged local climate variables, derived from gridded observational data. I find that both $\delta^{13}C$ and $\delta^{18}O$ are most strongly correlated with precipitation amount.

I suggest that the negative correlation of shell $\delta^{13}C$ and precipitation ultimately reflects a physiological adaptation of C_3 vegetation eaten by the snails i.e. changes in stomatal conductance in response to moisture availability. Snail shell $\delta^{18}O$ mirrors the spatial trend in the distribution of oxygen isotopes in Australian precipitation, suggesting that shell $\delta^{18}O$ reflects precipitation $\delta^{18}O$, which in turn is largely driven by precipitation amount.

4.4 Chapter Five

In this chapter I use flux balance models and clumped isotope analysis to interrogate the coarse environment-isotope relationships identified in Chapter Four, thereby gaining a more thorough mechanistic understanding of the precipitation influence on the shell isotopes.

In the context of modelling stable isotope systematics in animals, flux balance models are simple forward models that incorporate information about the physiology and environment of an animal to predict the isotopic composition of a specific part of its anatomy (Bryant and Froelich, 1995; Kohn, 1996). In the case of land snail shells, flux balance models explicitly incorporate snail-specific factors such as kinetic isotope effects resulting from respiratory gas exchange, evaporation, and slime excretion. These metabolic factors are combined with environmental information– such as temperature, diet, and water intake—to predict the $\delta^{13}C$ and $\delta^{18}O$ of shell aragonite secreted by the snails (Balakrishnan and Yapp, 2004).

I evaluate the supposition that the snails ate mostly C_3 plants by inverting the carbon flux balance model to predict the *absolute* $\delta^{13}C$ values of food ingested by the snails. I find that snail dietary $\delta^{13}C$ is indeed consistent with a C_3 plant- dominated diet. I also suggest that land snail shell $\delta^{13}C$ preserves an annual to multi-annual climate signal, depending on the residence time of vegetation in the landscape.

Most land snails are distinctly seasonal in their activity, being active during moist conditions and avoiding hot and dry weather. $\delta^{18}O$ in particular is likely to be affected

by this seasonality, given the transient nature of surface water compared with vegetation. I therefore use the oxygen flux balance model to evaluate the most likely growth season for the snails, and find that this is probably the wettest months at each location.

A major confounding influence in the snail shell $\delta^{18}O$-precipitation relationship is that carbonate $\delta^{18}O$ is a function of the formation water $\delta^{18}O$ *and* the temperature at the time of mineral growth. To decouple snail body fluid $\delta^{18}O$ and snail growth temperature, I measure the clumped isotope composition (Δ_{47}) of a subset of shells. I use the shell Δ_{47} to calculate snail growth temperatures, and find that they do not have a straightforward relationship with seasonal average temperatures. I use this temperature information to extricate snail body fluid $\delta^{18}O$ from shell $\delta^{18}O$, and observe a strong relationship between snail body fluid $\delta^{18}O$ and total precipitation during the wettest months.

Chapters Four and Five therefore demonstrate that snail shell isotopes track precipitation amount via two mechanisms i.e. its influence on $\delta^{18}O$ of precipitation (a seasonal signal), and its effect on vegetation $\delta^{13}C$ (an annual to multi-annual signal). These findings indicate that the $\delta^{13}C$ and $\delta^{18}O$ of ancient land snail shells will provide valuable insight into Australian palaeoclimate over a broad spatial and temporal range.

4.5 Chapter Six

In this chapter I supplement the high-resolution palaeoclimate record presented in Chapter Three with discrete clumped isotope measurements on freshwater gastropods from Blanche Cave, also in south-eastern Australia. I had originally intended on applying the findings from Chapters Four and Five to fossil land snails from this cave, however taxonomic identification of shells found in the cave sediment revealed them to be freshwater rather than terrestrial. Unlike land snails, freshwater snails tend to grow their shells year-round, and the clumped isotope composition of their shells has been previously shown to have a reasonably straightforward relationship with mean annual air temperature.

I measure the clumped isotope composition of three individual freshwater snail shells—two from prior to the LGM (approx. 41 and 32 ka BP), and one from the early deglacial (approx. 16 ka BP)—and use the snail growth temperatures to infer mean annual air temperatures. In conjunction with existing palaeoenvironmental data for

the area, temperatures up to ~5 °C (41 ka BP) and up to ~10 °C (32 ka BP) cooler than modern suggest cool and wet conditions prior to the LGM. An early deglacial temperature in the range of 13-18 °C supports previous suggestions that this period saw the onset of conditions more like the present. Although of very low resolution, these new temperature data are also consistent with the four pre-existing temperature reconstructions for the late Quaternary in Australia, suggesting that (1) there may be a consistent trend in late Quaternary temperature variability along the eastern Australian margin, and (2) the clumped isotope composition of freshwater snail shells reflects growth temperatures that are not wildly implausible, potentially providing a valuable new quantitative palaeotemperature proxy.

4.6 Chapter Seven

I summarise the findings of this thesis, offer some concluding statements, and provide recommendations for the direction of future research.

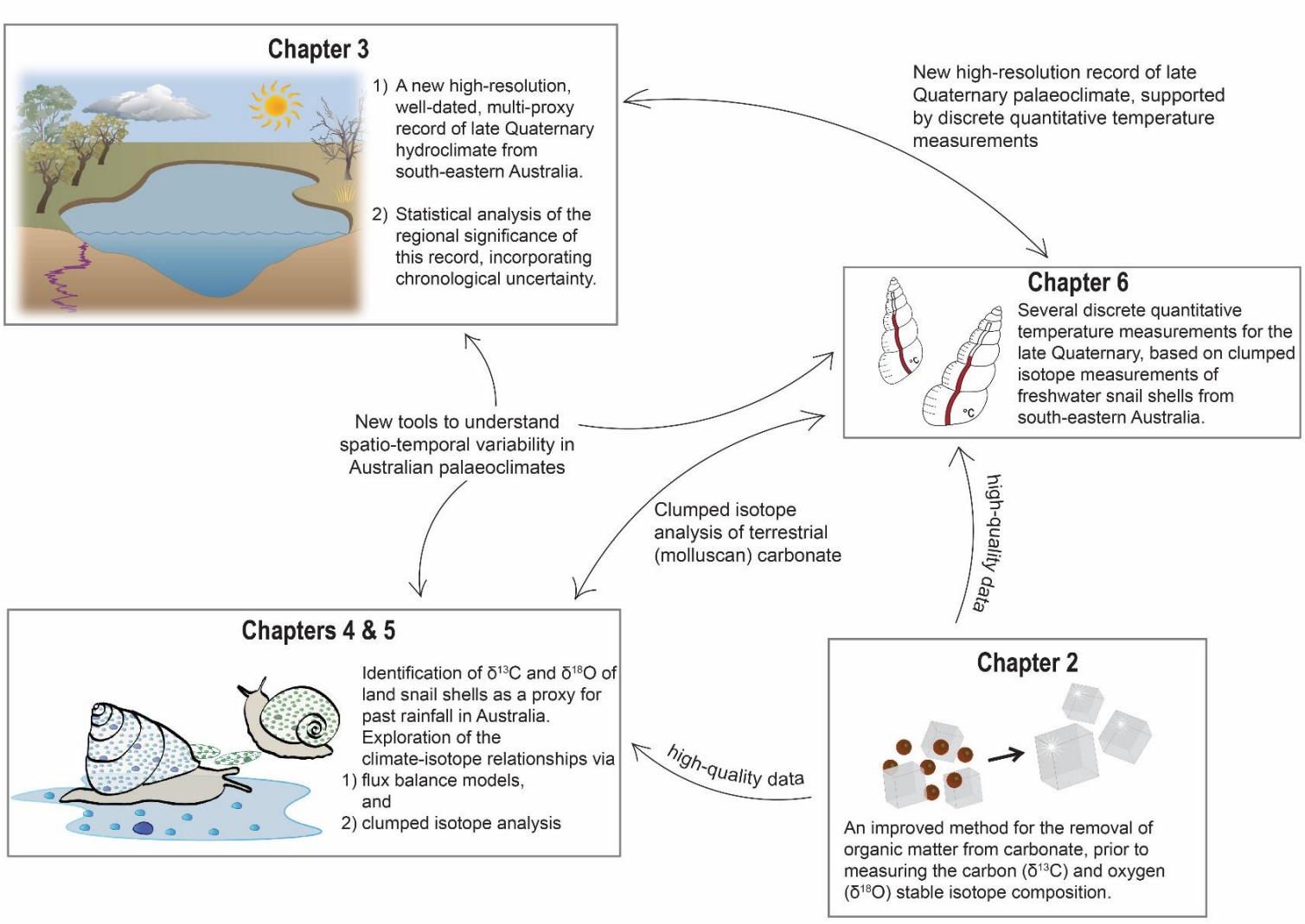

Figure 1.1. Conceptual flow diagram summarising the research components of this thesis.

5 References cited

Ahlstrom, A., Raupach, M.R., Schurgers, G., Smith, B., Arneth, A., Jung, M., Reichstein, M., Canadell, J.G., Friedlingstein, P., Jain, A.K., Kato, E., Poulter, B., Sitch, S., Stocker, B.D., Viovy, N., Wang, Y.P., Wiltshire, A., Zaehle, S., Zeng, N., 2015. The dominant role of semi-arid ecosystems in the trend and variability of the land CO_2 sink. Science 348, 895-899.

Alexander, L.V., Hope, P., Collins, D., Trewin, B., Lynch, A., Nicholls, N., 2007. Trends in Australia's climate means and extremes: a global context. Australian Meteorological Magazine 56, 1-18.

Anchukaitis, K.J., Tierney, J.E., 2012. Identifying coherent spatiotemporal modes in time-uncertain proxy paleoclimate records. Climate Dynamics 41, 1291-1306.

Anderson, R.F., Ali, S., Bradtmiller, L.I., Nielsen, S.H.H., Fleisher, M.Q., Anderson, B.E., Burckle, L.H., 2009. Wind-Driven Upwelling in the Southern Ocean and the Deglacial Rise in Atmospheric CO_2. Science 323, 1443-1448.

Balakrishnan, M., Yapp, C.J., 2004. Flux balance models for the oxygen and carbon isotope compositions of land snail shells. Geochimica et Cosmochimica Acta 68, 2007-2024.

Barr, C., Tibby, J., Moss, P.T., Halverson, G.P., Marshall, J.C., McGregor, G.B., Stirling, E., 2017. A 25,000-year record of environmental change from Welsby Lagoon, North Stradbroke Island, in the Australian subtropics. Quaternary International 449, 106-118.

Battarbee, R.W., 2000. Palaeolimnological approaches to climate change, with special regard to the biological record. Quaternary Science Reviews 19, 107-124.

Bowler, J.M., 1976. Aridity in Australia: Age, Origins and Experssion in Aeolian Landforms and Sediments. Earth-Science Reviews 12, 279-310.

Brown, S., Hall, C.A.S., Knabe, W., Raich, J., Trexler, M.C., Woomer, P., 1993. Tropical forests: Their past, present, and potential future role in the terrestrial carbon budget. Water, Air, and Soil Pollution 70, 71-94.

Bryant, J.D., Froelich, P.N., 1995. A model of oxygen isotope fractionation in body water of large mammals. Geochimica et Cosmochimica Acta 59, 4523-4537.

Clark, P.U., Dyke, A.S., Shakun, J.D., Carlson, A.E., Clark, J., Wohlfarth, B., Mitrovica, J.X., Hostetler, S.W., McCabe, A.M., 2009. The Last Glacial Maximum. Science 325, 710-714.

Colman, R., Moise, A., Power, S., Braganza, K., Watterson, I., 2015. Global climate change science, in: Whetton, P. (Ed.), Climate Change in Australia. Information for Australia's Natural Resource Management Regions: Technical Report. CSIRO and Bureau of Meteorology, Australia, pp. 23-39.

Crimp, S., Nicholls, N., Kokic, P., Risbey, J.S., Gobbett, D., Howden, M., 2018. Synoptic to large-scale drivers of minimum temperature variability in Australia - long-term changes. International Journal of Climatology 38, E237-E254.

DeDeckker, P., Moros, M., Perner, K., Jansen, E., 2012. Influence of the tropics and southern westerlies on glacial interhemispheric asymmetry. Nature Geoscience 5, 266-269.

Du, J., Haley, B.A., Mix, A.C., Walczak, M.H., Praetorius, S.K., 2018. Flushing of the deep Pacific Ocean and the deglacial rise of atmospheric CO2 concentrations. Nature Geoscience 11, 749-755.

Falster, G., Tyler, J., Grant, K., Tibby, J., Turney, C., Löhr, S., Jacobsen, G., Kershaw, A.P., 2018. Millennial-scale variability in south-east Australian hydroclimate between 30,000 and 10,000 years ago. Quaternary Science Reviews 192, 106-122.

Field, E., Tyler, J., Gadd, P.S., Moss, P., McGowan, H., Marx, S., 2018. Coherent patterns of environmental change at multiple organic spring sites in northwest Australia: Evidence of Indonesian-Australian summer monsoon variability over the last 14,500 years. Quaternary Science Reviews 196, 193-216.

Forootan, E., Khandu, Awange, J.L., Schumacher, M., Anyah, R.O., van Dijk, A.I.J.M., Kusche, J., 2016. Quantifying the impacts of ENSO and IOD on rain gauge and remotely sensed precipitation products over Australia. Remote Sensing of Environment 172, 50-66.

Gallant, A.J.E., Phipps, S.J., Karoly, D.J., Mullan, A.B., Lorrey, A.M., 2013. Nonstationary Australasian Teleconnections and Implications for Paleoclimate Reconstructions. Journal of Climate 26, 8827-8849.

Gergis, J., Henley, B.J., 2017. Southern Hemisphere rainfall variability over the past 200 years. Climate Dynamics 48, 2087-2105.

Hennessy, K., Webb, L., Clarke, J., 2015. Using climate change data in impact assessment and adaptation planning, in: Whetton, P. (Ed.), Climate Change in Australia. Information for Australia's Natural Resource Management Regions: Technical Report. CSIRO and Bureau of Meteorology, Australia.

Hesse, P.P., Williams, R., Ralph, T.J., Fryirs, K.A., Larkin, Z.T., Westaway, K.E., Farebrother, W., 2018. Palaeohydrology of lowland rivers in the Murray-Darling Basin, Australia. Quaternary Science Reviews 200, 85-105.

IPCC, 2014. Climate Change 2014: Synthesis Report. Contributions of Working Groups I, II and III to the Fifth Assessment Report of the Intergovernmental Panel on Climate Change, in: Core Writing Team, IPCC, Geneva, Switzerland, p. 151 pp.

Jaffres, J.B.D., Cuff, C., Rasmussen, C., Hesson, A.S., 2018. Teleconnection of atmospheric and oceanic climate anomalies with Australian weather patterns: a review of data availability. Earth-Science Reviews 176, 117-146.

Jakob, D., Walland, D., 2016. Variability and long-term change in Australian temperature and precipitation extremes. Weather and Climate Extremes 14, 36-55.

Johnson, Z.F., Chikamoto, Y., Luo, J.J., Mochizuki, T., 2018. Ocean Impacts on Australian Interannual to Decadal Precipitation Variability. Climate 6.

Jones, D.A., Wang, W., Fawcett, R., 2009. High-quality spatial climate data-sets for Australia. Australian Meteorological and Oceanographic Journal 58, 233-248.

Juggins, S., 2013. Quantitative reconstructions in palaeolimnology: new paradigm or sick science? Quaternary Science Reviews 64, 20-32.

Kohn, M.J., 1996. Predicting animal $\delta^{18}O$: Accounting for diet and physiological adaptation. Geochimica et Cosmochimica Acta 60, 4811-4829.

Long, X.J., Guan, H.D., Sinclair, R., Batelaan, O., Facelli, J.M., Andrew, R.L., Bestland, E., 2019. Response of vegetation cover to climate variability in protected and grazed arid rangelands of South Australia. Journal of Arid Environments 161, 64-71.

Marshall, G.J., 2003. Trends in the southern annular mode from observations and reanalyses. Journal of Climate 16, 4134-4143.

Masson-Delmotte, V., Schulz, M., Abe-Ouchi, A., Beer, J., Ganopolski, A., Ruoco, J.F.G., Jansen, E., Lamback, K., Luterbacher, J., Naish, T., Osborn, T., Otto-Bliesner, B., Quinn, T., Ramesh, R., Rojas, M., Shao, X., Timmermann, A., 2013. Information from Paleoclimate Archives, in: Stocker, T.F., Win, D., Plattner, G.-K., Tignor, M., Allen, S.K., Boschung, J., Nauels, A., Xia, Y., Bex, V., Midgley, P.M. (Eds.), Climate Change 2013: The Physical Science Basis. Contributions of Working Group I to the Fifth Assessment Report of the Intergovernmenal Panel on Climate Change. Cambridge University Press, Cambridge, United Kingdom and New York, NY, USA, pp. 383-464.

Murphy, B.F., Timbal, B., 2008. A review of recent climate variability and climate change in southeastern Australia. International Journal of Climatology 28, 859-879.

Nicholls, N., Drosdowsky, W., Lavery, B., 1997. Australian rainfall variability and change. Weather 52, 66-72.

Palmer, J.G., Cook, E.R., Turney, C.S.M., Allen, K., Fenwick, P., Cook, B.I., O'Donnell, A., Lough, J., Grierson, P., Baker, P., 2015. Drought variability in the eastern Australia and New Zealand summer drought atlas (ANZDA, CE 1500–2012) modulated by the Interdecadal Pacific Oscillation. Environmental Research Letters 10, 124002.

Partin, J.W., Cobb, K.M., Adkins, J.F., Clark, B., Fernandez, D.P., 2007. Millennial-scale trends in west Pacific warm pool hydrology since the Last Glacial Maximum. Nature 449, 452-455.

Peel, M.C., Finlayson, B.L., McMahon, T.A., 2007. Updated world map of the Köppen-Geiger climate classification. Hydrol. Earth Syst. Sci. 11, 1633-1644.

Pepler, A., Timbal, B., Rakich, C., Coutts-Smith, A., 2014. Indian Ocean Dipole Overrides ENSO's Influence on Cool Season Rainfall across the Eastern Seaboard of Australia. Journal of Climate 27, 3816-3826.

Petherick, L.M., Moss, P.T., McGowan, H.A., 2017. An extended Last Glacial Maximum in subtropical Australia. Quaternary International 432, 1-12.

Pook, M., Gibson, T., 1999. Atmospheric blocking and storm tracks during SOP-1 of the FROST Project. Australian Meteorological Magazine, 51-60.

Poulter, B., Frank, D., Ciais, P., Myneni, R.B., Andela, N., Bi, J., Broquet, G., Canadell, J.G., Chevallier, F., Liu, Y.Y., Running, S.W., Sitch, S., van der Werf, G.R., 2014. Contribution of semi-arid ecosystems to interannual variability of the global carbon cycle. Nature 509, 600-603.

Power, S., Tseitkin, F., Mehta, V., Lavery, B., Torok, S., Holbrook, N., 1999. Decadal climate variability in Australia during the twentieth century. International Journal of Climatology 19, 169-184.

Reeves, J.M., Barrows, T.T., Cohen, T.J., Kiem, A.S., Bostock, H.C., Fitzsimmons, K.E., Jansen, J.D., Kemp, J., Krause, C., Petherick, L., Phipps, S.J., OZ-INTIMATE Members, 2013a. Climate variability over the last 35,000 years recorded in marine and terrestrial archives in the Australian region: an OZ-INTIMATE compilation. Quaternary Science Reviews 74, 21-34.

Reeves, J.M., Bostock, H.C., Ayliffe, L.K., Barrows, T.T., De Deckker, P., Devriendt, L.S., Dunbar, G.B., Drysdale, R.N., Fitzsimmons, K.E., Gagan, M.K., Griffiths, M.L., Haberle, S.G., Jansen, J.D., Krause, C., Lewis, S., McGregor, H.V., Mooney, S.D., Moss, P., Nanson, G.C., Purcell, A., van der Kaars, S., 2013b. Palaeoenvironmental change in tropical Australasia over the last 30,000 years – a synthesis by the OZ-INTIMATE group. Quaternary Science Reviews 74, 97-114.

Saji, N.H., Yamagata, T., 2003. Possible impacts of Indian Ocean Dipole mode events on global climate. Climate Research 25, 151-169.

Shakun, J.D., Carlson, A.E., 2010. A global perspective on Last Glacial Maximum to Holocene climate change. Quaternary Science Reviews 29, 1801-1816.

Sitch, S., Huntingford, C., Gedney, N., Levy, P.E., Lomas, M., Piao, S.L., Betts, R., Ciais, P., Cox, P., Friedlingstein, P., Jones, C.D., Prentice, I.C., Woodward, F.I., 2008. Evaluation of the terrestrial carbon cycle, future plant geography and climate-carbon cycle feedbacks using five Dynamic Global Vegetation Models (DGVMs). Global Change Biology 14, 2015-2039.

Timbal, B., Drosdowsky, W., 2013. The relationship between the decline of Southeastern Australian rainfall and the strengthening of the subtropical ridge. International Journal of Climatology 33, 1021-1034.

Tozer, C.R., Kiem, A.S., 2017. Large-scale ocean-atmospheric processes and seasonal rainfall variability in South Australia: accounting for non-linearity and establishing the hierarchy of influence. International Journal of Climatology 37, 1180-1198.

Trenberth, K.E., 2011. Changes in precipitation with climate change. Climate Research 47, 123-138.

Tyler, J.J., Mills, K., Barr, C., Sniderman, J.M.K., Gell, P.A., Karoly, D.J., 2015. Identifying coherent patterns of environmental change between multiple, multivariate records: an application to four 1000-year diatom records from Victoria, Australia. Quaternary Science Reviews 119, 94-105.

Viney, N.R., Bates, B.C., 2004. It never rains on Sunday: The prevalence and implications of untagged multi-day rainfall accumulations in the Australian high quality data set. International Journal of Climatology 24, 1171-1192.

von Gunten, L., D'Andrea, W.J., Bradley, R.S., Huang, Y., 2012. Proxy-to-proxy calibration: Increasing the temporal resolution of quantitative climate reconstructions. Scientific Reports 2, 609.

Watterson, I., Rafter, T., Wilson, L., Bhend, J., Heady, C., 2015. Projections: Atmosphere and the land (surface temperature), in: Whetton, P. (Ed.), Climate

Change in Australia: Information fo Australia's Natural Resource Management Regions: Technical Report. CSIRO and Bureau of Meteorology, Australia, pp. 91-98.

Watterson, I.G., 2001. Wind-Induced Rainfall and Surface Temperature Anomalies in the Australian Region. Journal of Climate 14, 1901.

Whetton, P., 2015. Executive Summary, in: Whetton, P. (Ed.), Climate Change in Australia Information for Australia's Natural Resource Management Regions: Technical Report. CSIRO and Bureau of Meteorology, Australia.

Whetton, P., Moise, A., Kirono, D., Rafter, T., Wilson, L., Hennessy, K., Bhend, J., Hope, P., Timbal, B., Dowdy, A., Watterson, I., Grose, M., Narsey, S., Bathols, J., 2015. Projections: Atmosphere and the land (rainfall), in: Whetton, P. (Ed.), Climate Change in Australia. Information for Australia's Natural Resource Management Regions: Technical Report. CSIRO and Bureau of Meteorology, Australia, pp. 99-124.

Xu, J., Kuhnt, W., Holbourn, A., Regenberg, M., Andersen, N., 2010. Indo-Pacific Warm Pool variability during the Holocene and Last Glacial Maximum. Paleoceanography 25, 183-195.

Chapter 2

This chapter is published as:

Falster, G., Delean, S., Tyler, J. (2018). Hydrogen Peroxide Treatment of Natural Lake Sediment Prior to Carbon and Oxygen Stable Isotope Analysis of Calcium Carbonate. *Geochemistry, Geophysics, Geosystems*, 19, 3583-3595. https://doi.org/10.1029/2018GC007575

Note: Stable isotope data associated with this chapter are provided in Appendix 2 Table A1.

I have re-formatted the published article to match the rest of the thesis. The text remains exactly the same, except for the figure and table numbers, which are now prefaced with the chapter number e.g. Table 1 is now Table 2.1. The published version of the chapter is provided in Appendix 3.

Statement of Authorship

Title of Paper	Hydrogen Peroxide Treatment of Natural Lake Sediment Prior to Carbon and Oxygen Stable Isotope Analysis of Calcium Carbonate
Publication Status	☑ Published ☐ Accepted for Publication ☐ Submitted for Publication ☐ Unpublished and Unsubmitted work written in manuscript style
Publication Details	Falster, G., Delean, S., & Tyler, J. (2018). Hydrogen Peroxide Treatment of Natural Lake Sediment Prior to Carbon and Oxygen Stable Isotope Analysis of Calcium Carbonate. *Geochemistry, Geophysics, Geosystems, 19*, 3583-3595. https://doi.org/10.1029/2018GC007575

Principal Author

Name of Principal Author (Candidate)	Georgina Falster		
Contribution to the Paper	Devised experiment, prepared, imaged, and analysed all samples, interpreted data, wrote manuscript, acted as corresponding author.		
Overall percentage (%)	90 %		
Certification:	This paper reports on original research I conducted during the period of my Higher Degree by Research candidature and is not subject to any obligations or contractual agreements with a third party that would constrain its inclusion in this thesis. I am the primary author of this paper.		
Signature		Date	11/3/2019

Co-Author Contributions

By signing the Statement of Authorship, each author certifies that:

i. the candidate's stated contribution to the publication is accurate (as detailed above);

ii. permission is granted for the candidate in include the publication in the thesis; and

iii. the sum of all co-author contributions is equal to 100% less the candidate's stated contribution.

Name of Co-Author	Steven Delean		
Contribution to the Paper	Provided guidance and assistance with statistical analysis and presentation of the data.		
Signature		Date	31/01/2019

Name of Co-Author	Jonathan Tyler		
Contribution to the Paper	Provided lake sediment, evaluated and edited manuscript.		
Signature		Date	31/01/2019

Hydrogen peroxide treatment of natural lake sediment prior to carbon and oxygen stable isotope analysis of calcium carbonate

Abstract

The carbon and oxygen stable isotope ratios ($\delta^{13}C$ and $\delta^{18}O$) of authigenic and biogenic lacustrine carbonates are commonly used as past climate proxies, and these carbonates are often preserved within organic-rich bulk sediment. We measured the $\delta^{13}C$ and δ18O of carbon dioxide evolved from fine-grained crystalline calcite and biogenic aragonite, mixed with natural organic-rich lake sediment. We found that if the ratio of total inorganic carbon (TIC) to total organic carbon (TOC) in lacustrine bulk sediment is low, then organic compounds evolve detectable CO_2 during phosphoric acid digestion, leading to an "organic bias" in the measured $\delta^{13}C$ and $\delta^{18}O$. We tested the effect of oxidative pretreatment of the bulk sediment with acidic or alkaline hydrogen peroxide (H_2O_2), at a range of temperatures. Pretreatment with acidic H_2O_2 not only had a negligible effect on the TIC/TOC but also resulted in dissolution and reprecipitation of carbonate, and a consequent "treatment bias" that was particularly strong for $\delta^{18}O$. Oxidation with alkaline H_2O_2 removed a greater proportion of organic material, with no evidence for carbonate dissolution at temperatures of ≤50 °C. The $\delta^{13}C$ and $\delta^{18}O$ values obtained from sediment treated with alkaline H_2O_2 at 50 °C were both accurate and precise, even for sediment with very low initial TIC/TOC. Our results show that it is possible to obtain accurate $\delta^{13}C$ and $\delta^{18}O$ values from carbonates preserved within organic-rich lacustrine sediment, suitable for use in paleoclimate reconstructions.

1 Introduction

The stable isotope composition of lacustrine carbonate minerals is dependent on the chemistry, hydrology, and biological productivity of the host lake, which in turn are dependent on ambient environmental conditions. Carbonates therefore record climatic conditions at the time of precipitation, and serve as paleoclimate indicators when preserved in lacustrine sediment. In particular, the $\delta^{13}C$ and $\delta^{18}O$ of authigenic and biogenic lake carbonates have long been used to derive records of a range of climate-related variables, including temperature, hydrology, and lake productivity (e.g., Holmes, 1996; Leng & Marshall, 2004; Stuiver, 1970). In the case of $\delta^{18}O$, fluctuations as small as a few per mille are interpreted to represent major changes in temperature and hydroclimate (e.g., Holmes et al., 2016; Hyvåinen et al., 1990; McCrea, 1950; Schwander et al., 2000; von Grafenstein et al., 1992). It is therefore critical that reported stable isotope values are accurate and precise.

The accumulative natures of lakes is such that lacustrine sediment is often a rich source of materials that may be used as paleoclimate proxies, including allochthonous and autochthonous organic material as well as various carbonate phases. While this compositional variety is excellent for the creation of multiproxy paleoclimate reconstructions, lacustrine carbonates consequently are often preserved in a matrix that has a low ratio of total inorganic carbon (TIC) to total organic carbon (TOC). Oehlerich et al. (2013) and Lebeau et al. (2014) demonstrated that when using the phosphoric acid (H_3PO_4) digestion method to measure carbonate stable isotope ratios of bulk sediment with low TIC/TOC (<0.3), organic compounds release CO_2, leading to bias in the measured $\delta^{13}C$ and $\delta^{18}O$ that is dependent on the specific sample matrix. For coarse-grained carbonates, such as large snail, bivalve, or foraminiferal shells, manual cleaning is typically sufficient to remove much of the organic material (Keatings et al., 2006). For fine-grained carbonates, such as very small ostracod shells and authigenic carbonate, this may not be possible, in which case the TIC/TOC may be increased by oxidizing as much of the organic material as possible prior to analysis of the sediment.

Methods commonly used to oxidize organic matter prior to stable isotope analysis are bleaching with sodium hypochlorite (NaOCl) or hydrogen peroxide (H_2O_2), or thermal treatments (vacuum roasting, plasma ashing). However, both chemical and thermal pretreatment methods are demonstrated sources of error in isotope determinations, with different methods resulting in different biases (Grottoli et al., 2005; Lebeau et al., 2014; Nagtegaal et al., 2012; Serrano et al., 2008; Wierzbowski, 2007). After several decades of debate, there is yet no consensus in either the literature or stable isotope geochemistry community as to which method results in the most accurate carbonate $\delta^{13}C$ and $\delta^{18}O$, or indeed whether pretreatment is necessary. This is in part due to the wide compositional variety in lacustrine sediment, including carbonate phase, TIC/TOC, and specific organic compounds, all of which may respond differently to the same treatment. In paleoclimate studies where lake sediment has been subjected to oxidative treatment prior to analysis, many different methods are used, and with low methodological consistency, for example, temperature and duration of reaction, concentration, and purity of reagent. Comparison of isotope proxy data from different laboratories may therefore potentially be misleading, in the absence of quantitative assessment of potential treatment effects on carbonate $\delta^{13}C$ and $\delta^{18}O$.

Table 2.1. Summary of published results of three most commonly used treatments for the removal of organic matter from carbonates—bleaching with sodium hypochlorite (NaOCl) or hydrogen peroxide (H_2O_2), and thermal treatments (vacuum roasting or plasma ashing).

Treatment	Methodological detail	Carbonate phase	Change in stable isotope composition relative to untreated samples	Authors' possible explanations for observations	Reference
NaOCl	5%, 18 hr, room temperature	Biogenic aragonite	Negative shift in $\delta^{13}C$, no change in $\delta^{18}O$	Isotope exchange with reagent, precipitation of $Ca(OH)_2$	Wierzbowski (2007)
	5%, 18 hr, room temperature	Biogenic calcite	Negative shift in $\delta^{13}C$ and $\delta^{18}O$	Isotope exchange with reagent, precipitation of $Ca(OH)_2$	Wierzbowski (2007)
	Household bleach, 5.25%, 24 hr	Coral aragonite	Negative shift in $\delta^{13}C$ and $\delta^{18}O$	Partial dissolution of carbonate, isotope exchange with reagent	Grottoli et al. (2005)
	Reagent grade, 5%, 24 hr, room temperature	Coral aragonite	No change		Nagtegaal et al. (2012)
	10%, 10 mins, 20°C	Foraminiferal calcite	No change		Serrano et al. (2008)
	5%, 18 hr, room temperature	Inorganic aragonite	No change		Wierzbowski (2007)
	5%, 18 hr, room temperature	Inorganic calcite	No change		Wierzbowski (2007)
	5%, 18 hr, room temperature	Inorganic calcite (ground)	Negative shift in $\delta^{13}C$ and $\delta^{18}O$	Isotope exchange with reagent, precipitation of $Ca(OH)_2$	Wierzbowski (2007)
	5%, 4 hr, room temperature	Ostracod calcite	Negative shift in $\delta^{13}C$ and $\delta^{18}O$, increase in variability	Isotope exchange with reagent	Keatings et al. (2006)
	3.5%, three days, room temperature	Siderite	Negative shift in $\delta^{13}C$ (not significant), no change in $\delta^{18}O$	Partial dissolution of carbonate	Lebeau et al. (2014)
H_2O_2	30%, 12 hr, room temperature	Biogenic aragonite	No change		Wierzbowski (2007)
	30%, 12 hr, room temperature	Biogenic calcite	No change		Wierzbowski (2007)
	30%, 24 hr	Coral aragonite	Negative shift in $\delta^{13}C$, no change in $\delta^{18}O$, increase in variability	Partial dissolution of carbonate, precipitation of $Ca(OH)_2$, possible isotope exchange with reagent	Grottoli et al. (2005)
	30%, 12 hr, room temperature	Coral aragonite	Variable, but mainly negative shifts in $\delta^{13}C$ and $\delta^{18}O$	Elimination of organic matter, partial dissolution of carbonate	Boiseau & Juillet-Leclerc (1997)
	30%, 10 mins, 20°C	Foraminiferal calcite	No change in $\delta^{13}C$, Negative shift in $\delta^{18}O$	Partial dissolution of carbonate	Serrano et al. (2008)
	10%, one hour, room temperature	Foraminiferal calcite	No change		Feldmeijer et al. (2013)
	10%, 20 min, buffered to pH = 7.5 with ammonia	Foraminiferal calcite	No change		Ganssen (1981)
	30%, 12 hr, room temperature	Inorganic calcite	No change in $\delta^{13}C$, negative shift or no change in $\delta^{18}O$	Partial dissolution of carbonate	Wierzbowski (2007)
	5%, 80°C, 15 min	Ostracod calcite	Negative shift in $\delta^{13}C$, no change in $\delta^{18}O$, increase in variability	Potential isotope exchange with reagent	Keatings et al. (2006)
	30%, three days, room temperature	Siderite	Negative shift in $\delta^{13}C$ and $\delta^{18}O$ (not significant)	Partial dissolution of carbonate	Lebeau et al. (2014)
Thermal	Plasma ashing, 125°C, 16 hr	Ostracod calcite	No change		Keatings et al. (2006)
	Plasma ashing, 5 - 33 hr	Siderite	Negative shift in $\delta^{13}C$ (not significant), no change in $\delta^{18}O$		Lebeau et al. (2014)
	Vacuum roasting, 200°C, 30 min	Foraminiferal calcite	No change		Ganssen (1981)
	Vacuum roasting, 200°C, 45 min	Biogenic aragonite	No change in $\delta^{13}C$, Negative shift in $\delta^{18}O$	Isotope exchange with internal water	Wierzbowski (2007)
	Vacuum roasting, 200°C, 45 min	Biogenic calcite	No change		Wierzbowski (2007)
	Vacuum roasting, 340-350°C, 45 min	Biogenic aragonite	No change in $\delta^{13}C$, Negative shift in $\delta^{18}O$	Isotope exchange with internal water	Wierzbowski (2007)
	Vacuum roasting, 340-350°C, 45 min	Biogenic calcite	No change		Wierzbowski (2007)

Table 2.1 contd.

Treatment	Methodological detail	Carbonate phase	Change in stable isotope composition relative to untreated samples	Authors' possible explanations for observations	Reference
Thermal	Vacuum roasting, 340-350°C, 45 min	Inorganic aragonite	No change		Wierzbowski (2007)
	Vacuum roasting, 340-350°C, 45 min	Inorganic calcite	No change		Wierzbowski (2007)
	Vacuum roasting, 350°C, 2 hr	Coral aragonite	Negative shift in $\delta^{13}C$ and $\delta^{18}O$	Conversion of aragonite to calcite, presence of organic carbon	Boiseau & Juillet-Leclerc (1997)
	Vacuum roasting, 380°C, 1 hour	Ostracod calcite	Negative shift in $\delta^{13}C$ and $\delta^{18}O$, increase in variability	Disruption of calcite lattice facilitating isotope exchange with atmospheric CO_2	Keatings et al. (2006)
	Vacuum roasting, 400°C, 60 min	Foraminiferal calcite	No change		Ganssen (1981)
	Vacuum roasting, 450°C, 45 min	Biogenic aragonite	Negative shift in $\delta^{13}C$ and $\delta^{18}O$	Isotope exchange with internal water	Wierzbowski (2007)
	Vacuum roasting, 450°C, 45 min	Biogenic calcite	No change		Wierzbowski (2007)
	Vacuum roasting, 450°C, 45 min	Inorganic aragonite	No change		Wierzbowski (2007)
	Vacuum roasting, 450°C, 45 min	Inorganic calcite	Negative shift or no change in $\delta^{13}C$, no change in $\delta^{18}O$		Wierzbowski (2007)

Note. For the sake of clarity, we only report findings from studies that specifically tested for the effects of these treatments.

Several studies have tested the effect of chemical pretreatment on the stable isotope composition of specific carbonate phases, including foraminiferal calcite (Fallet et al., 2009; Feldmeijer et al., 2013; Ganssen, 1981; Serrano et al., 2008), coral aragonite (Boiseau & Juillet-Leclerc, 1997; Grottoli et al., 2005; Nagtegaal et al., 2012), ostracod calcite (Keatings et al., 2006), and siderite (Lebeau et al., 2014). The findings from these studies are not consistent (see Table 2.1). Wierzbowski (2007) performed perhaps the most universally applicable study, investigating the effect of NaOCl, H_2O_2, and vacuum roasting treatments on skeletal and inorganic calcites and aragonites, mixed with a variety of pure organic compounds. Results from this study indicated that pretreatment may introduce severe isotopic biases, and is generally unnecessary. However, this study was conducted on mixtures with TIC/TOC ≥ 0.85.

Pretreatment with NaOCl typically leads to negative bias in both $\delta^{13}C$ and $\delta^{18}O$ (Table 2.1), which is likely due to both isotope exchange between the carbonate and the NaOCl, and precipitation of calcium hydroxide; authors therefore generally suggest avoiding oxidation with NaOCl (Keatings et al., 2006; Wierzbowski, 2007). Thermal treatments are similarly prone to inducing bias, through disruption of the carbonate structure, and isotope exchange with internal water (Boiseau & Juillet-Leclerc, 1997; Keatings et al., 2006; Wierzbowski, 2007). Commercially available laboratory-grade H_2O_2 is acidic, leading to partial dissolution of carbonate, and has been reported to be less effective in the removal of organic material than NaOCl (Gaffey & Bronnimann, 1993). However, no isotope exchange occurs between H_2O_2 and carbonate (Boiseau & Juillet-Leclerc, 1997). Pretreatment with H_2O_2 therefore has the potential to result in accurate stable isotope values, if carbonate dissolution can be prevented by raising the pH of the solution (cf. Fallet et al., 2009). Alkaline H_2O_2 is not routinely used as an oxidative reagent, as a high pH promotes rapid decomposition of H_2O_2,

particularly at the higher temperatures that may be used to speed up oxidation (Hosking, 1932; Mikutta et al., 2005). Fine-grained lacustrine carbonates are likely to be particularly susceptible to partial dissolution by acidic H_2O_2; however, the efficacy of alkaline H_2O_2 in oxidative pretreatment of natural lake sediment has not been directly tested.

The aim of this study is therefore to test the effect of treatment with both acidic and alkaline H_2O_2 on the measured $\delta^{13}C$ and $\delta^{18}O$ of fine-grained calcium carbonate within a natural lake sediment matrix. We also test the effect of carrying out the reaction at different temperatures. We measured the $\delta^{13}C$ and $\delta^{18}O$ of treated and untreated simulated very low TIC/TOC lake sediment, created by mixing fine-grained carbonate standards—one crystalline calcite and one relatively poorly structured aragonite—with carbonate-free lake sediment from Lake Purrumbete, a maar lake in the Newer Volcanics Province of south-eastern Australia. This province hosts several crater lakes that preserve long sediment records, potentially representing valuable paleoclimate archives (e.g., Chivas et al., 1986; Cook, 2009; Falster et al., 2018; Timms, 1976; Wilkins et al., 2013). We evaluated the influence of both the organic matter and the oxidative treatments, by comparison with the stable isotope composition of the pure, untreated carbonate. We designed the experiment to test the following hypotheses:

1. Organic matter will be more efficiently oxidized by acidic than alkaline H_2O_2, but the former will lead to partial dissolution of carbonate.
2. Higher TIC/TOC will result in less contribution of organic material to the measured CO_2, with negligible influence above TIC/TOC = 0.3 (cf. Oehlerich et al., 2013).
3. Increasing reaction temperature will result in more efficient oxidation of organic material.

2 Materials and Methods

2.1 Preparation of Experimental Material

We simulated realistic, very low TIC/TOC lake sediment by mixing natural lake sediment with two different calcium carbonate standards of known $\delta^{13}C$ and $\delta^{18}O$. The sediment was obtained from core PB86–5 A, a core raised from near the southern margin of Lake Purrumbete in 1986. Lake Purrumbete is a large, deep (>40 m), cheimomictic freshwater maar located in south-eastern Australia (38°16’48″S, 143°13’48″E; Timms, 1976). The lake is contained by a ring of basaltic phreatomagmatic deposits, and the water is alkaline and eutrophic (Ollier, 1967; Tibby et al., 2011). The lake sediment has a high organic matter content (24%), including substantial plant matter, and a low C/N ratio of ~12.5 (Timms,

Table 2.1. Summary of treatments applied to mixtures of fine-grained carbonate in varying concentrations, within natural lake sediment obtained from Lake Purrumbete.

Parameter	Variables
$CaCO_3$ material	M2 (calcite marble), P3 (biogenic aragonite)
$CaCO_3$ concentration	1, 3, 5 % (0, 100 %)
Oxidising agent	acidic 18% H_2O_2, alkaline 18% H_2O_2 (no treatment)
Reaction temperature	4 °C, 25 °C, 50 °C, 75 °C (no treatment)

Note. All reactions were carried out for 24 hr, with each possible combination of variables tested in quadruplicate. To assess the effect of the different oxidative pretreatments, we also measured the $\delta^{13}C$ and $\delta^{18}O$ of pure lake sediment and pure carbonate (0 and 100% carbonate), as well as mixtures that were not subject to any pretreatment.

1976). Two fine-grained calcium carbonate standards were used: M2 ($\delta^{13}C$: 2.8‰ Vienna Pee Dee belemnite (VPDB), $\delta^{18}O$: -7.26‰ VPDB), and P3 ($\delta^{13}C$: 2.23‰ VPDB, $\delta^{18}O$: -0.31‰ VPDB). M2 is a calcite marble, formed during Devonian-aged contact metamorphism of a Silurian limestone, and collected from Marulan, New South Wales. P3 is aragonitic shell carbonate from a giant clam (*Tridacna gigas*), collected live in the 1980s from Palm Island, Queensland.

To ensure that no carbonate was present aside from the two standards, the Lake Purrumbete sediment was acidified prior to creating the mixtures. Approximately 250 cm3 wet sediment was taken from the top 30 cm of the core, and placed in a large beaker with 200 mL of 1% hydrochloric acid. The sediment was agitated every 30 min for 2 hr, and then the solution was made up to 1 L with ultrapure water, and left to react overnight. After a total of 24 hr of reaction time, the supernatant was decanted off, and the beaker was refilled with ultrapure water, stirred, and left to settle. The rinsing process was repeated 3 times, before the sediment was placed in a freeze drier. The dry sediment was homogenized by gentle grinding with an agate mortar and pestle.

The acid-treated Lake Purrumbete sediment was analyzed with an elemental analyzer to determine the $\delta^{13}C$ of the organic matter, and check for carbonate content. Four subsamples of approximately 2 mg were weighed into silver capsules, and four into tin capsules. Testing for residual carbonate was via the acid-fumigation method—approximately 50 µL deionized water was added to each silver capsule, and then subsamples were acidified for 4 hr in concentrated hydrochloric acid vapor and then left to dry overnight in a 40 °C oven (e.g., Harris et al., 2001). Once dry, the silver capsules were placed inside tin capsules and crimped. The acidified sediment was analyzed alongside the four non-acidified samples. The $\delta^{13}C$ values were indistinguishable (-23.09 ± 0.1‰ VPDB) and uncorrelated with carbon content, and sediment was therefore regarded as carbonate-free.

Pretreatment parameters tested were the pH of the oxidizing agent (H_2O_2), and the temperature at which oxidation occurred. For each combination of reagent and temperature, sufficient Lake Purrumbete sediment was added to 1 mg of each of the pure reference

carbonates to make mixtures of approximately 1, 3, and 5% carbonate. Samples containing 0 and 100% carbonate were also subject to each pretreatment. Prior to oxidation at each temperature, two solutions of fresh 18% H_2O_2 were prepared from reagent-grade 30% H_2O_2: one pure (pH ≈ 4), and one buffered to a pH of 8 using sodium hydroxide (NaOH), following the NIOZ protocol outlined in Fallet et al. (2009; hereafter referred to as acidic H_2O_2 and alkaline H_2O_2). In brief, the acidic 18% H_2O_2 solution was prepared by mixing 300 mL 30% H_2O_2 with 200 mL ultrapure water, and the alkaline 18% H_2O_2 solution was prepared by mixing 20 mL 0.5 M NaOH, 240 mL 30% H_2O_2, and 200 mL ultrapure water. All samples were tested in quadruplicate, resulting in a total of 324 samples; a summary of all tested variables is provided in Table 2.2.

2.2 Organic Matter Oxidation

To test oxidation at 4 °C, the NaOH, 30% H_2O_2, and ultrapure water were refrigerated overnight prior to preparation of the oxidizing solutions as above. A 2-mL aliquot of reagent was added to each vial, and gently shaken to thoroughly mix the reagent with the sediment. The samples were placed in a refrigerator at 4 °C, and gently agitated every 15 min. After 1 hr of reaction time, a further 2 mL of reagent was added. This procedure was repeated until a total of 10 mL of reagent had been added to each vial. Each time the samples were agitated, the pH of several vials was measured using pH indicator paper, to check that the pH did not fluctuate by more than one unit. The samples were subsequently agitated each hour for 5 hr, and then left to react in the refrigerator overnight. After a total reaction time of 24 hr, each vial was filled with ultrapure water and centrifuged, and then the supernatant liquid was decanted. The samples were rinsed 4 times with ultrapure water and then freeze-dried.

To test oxidation at 25 °C, the above procedure was repeated, but the reaction was performed out in a room with the temperature controlled at 25 °C, using solutions that were previously equilibrated to room temperature. For oxidation at 50 °C and 75 °C, the reaction was carried out in an oven.

2.3 Sample Analysis

2.3.1 Stable Isotope Analysis

All pretreated samples were transferred to borosilicate exetainers for stable isotope analysis at the University of Adelaide. We also analyzed samples at each concentration that had not undergone any pretreatment. Samples were digested in 105% H_3PO_4 at 70 °C for a minimum of 1 hr, and measurements were made on the evolved CO_2 gas following the

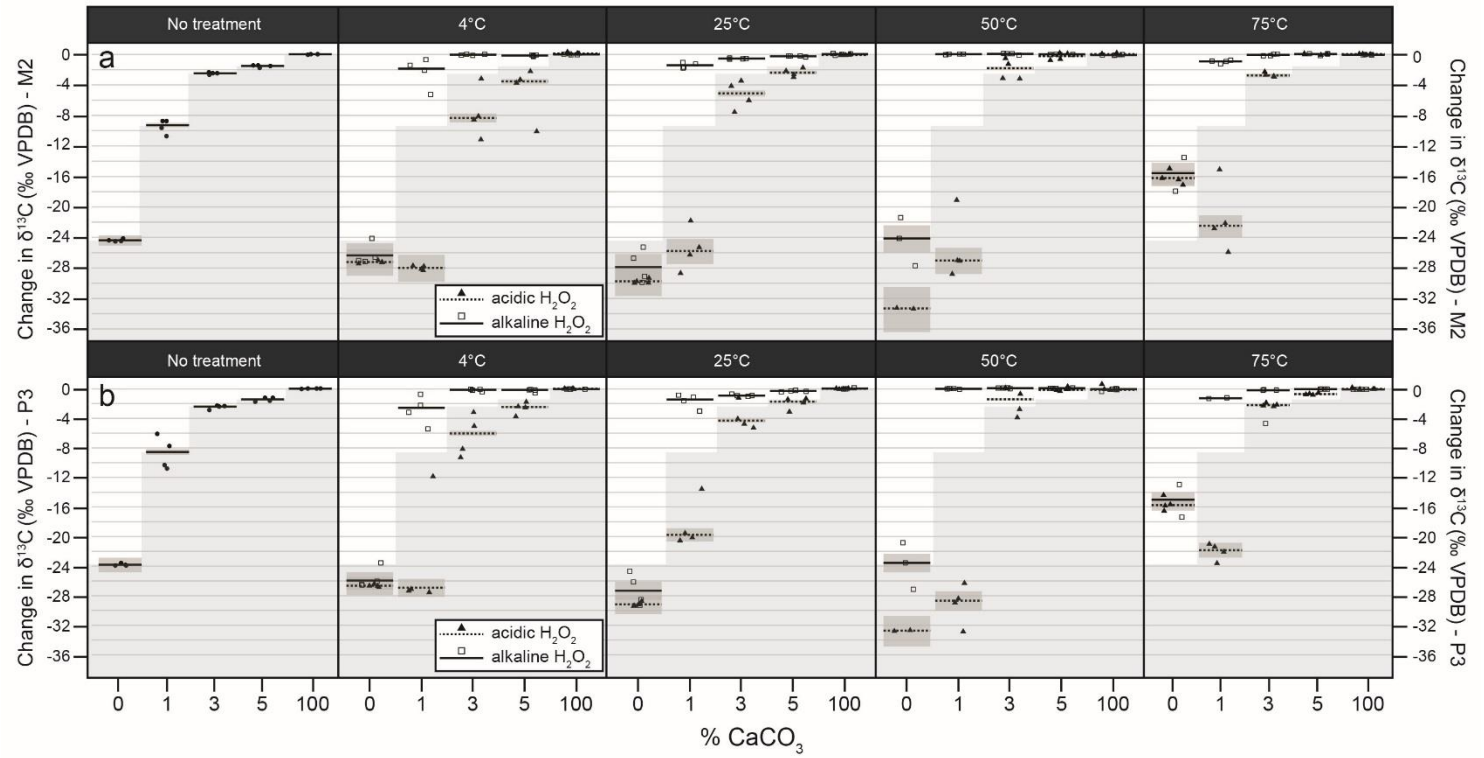

Figure 2.1. **a)** Comparison of the effect of oxidative pre-treatments on the measured $\delta^{13}C$ of mixtures of M2 carbonate standard (calcite; $\delta^{13}C$: 2.8 ‰VPDB) in varying concentrations, within natural lake sediment. Sediment mixtures were treated with 18% H_2O_2 (dotted line/filled triangles) or 18% H_2O_2 that was buffered to a pH of 8 with NaOH (solid line/outlined squares), at four different temperatures. Values are presented as deviations from the $\delta^{13}C$ of pure, untreated M2 carbonate. Horizontal bars denote the fitted model value for each combination of experimental parameters, and grey windows show the 95% confidence interval. Points denote the partial residuals from individual analyses. The left-most panel shows results from mixtures of M2 carbonate and lake sediment, that were not subject to any pre-treatment; these are shown as grey steps on each plot window for comparison; **b)** All as per **a)**, but for the P3 carbonate standard (aragonite; $\delta^{13}C$: 2.23 ‰VPDB).

method of Spötl and Vennemann (2003). Measurements were made on a Nu Instruments GasPrep in-line with a Nu-Horizon continuous flow isotope ratio mass spectrometer. Standardization was based on in-house ANU-P3 ($\delta^{13}C$: 2.24‰, $\delta^{18}O$: -0.32‰), UAC-1 ($\delta^{13}C$: -15‰, $\delta^{18}O$: -18.4‰), and IAEA CO-8 ($\delta^{13}C$: -5.76‰, $\delta^{18}O$: -22.7‰) standards, which have been calibrated against international standards. Analytical precision (1σ) for replicate measurements of the standards was ±0.1‰. The CO_2 peak heights returned by the continuous flow isotope ratio mass spectrometer were used to calculate the volume of carbonate measured in each sample, which in turn was used to approximate the post-treatment carbonate concentration. Seven of the 324 samples returned CO_2 peak sizes that were too small for reliable calculation of isotopic composition. The $\delta^{13}C$ and $\delta^{18}O$ values are reported in per mille units relative to the Vienna Pee Dee belemnite (VPDB) standard.

2.3.2 Scanning Electron Microscope Imaging

To investigate any structural or mineralogical alteration to the carbonate during pretreatment, the simulated lake sediment was imaged using a Phillips XL30 field emission scanning

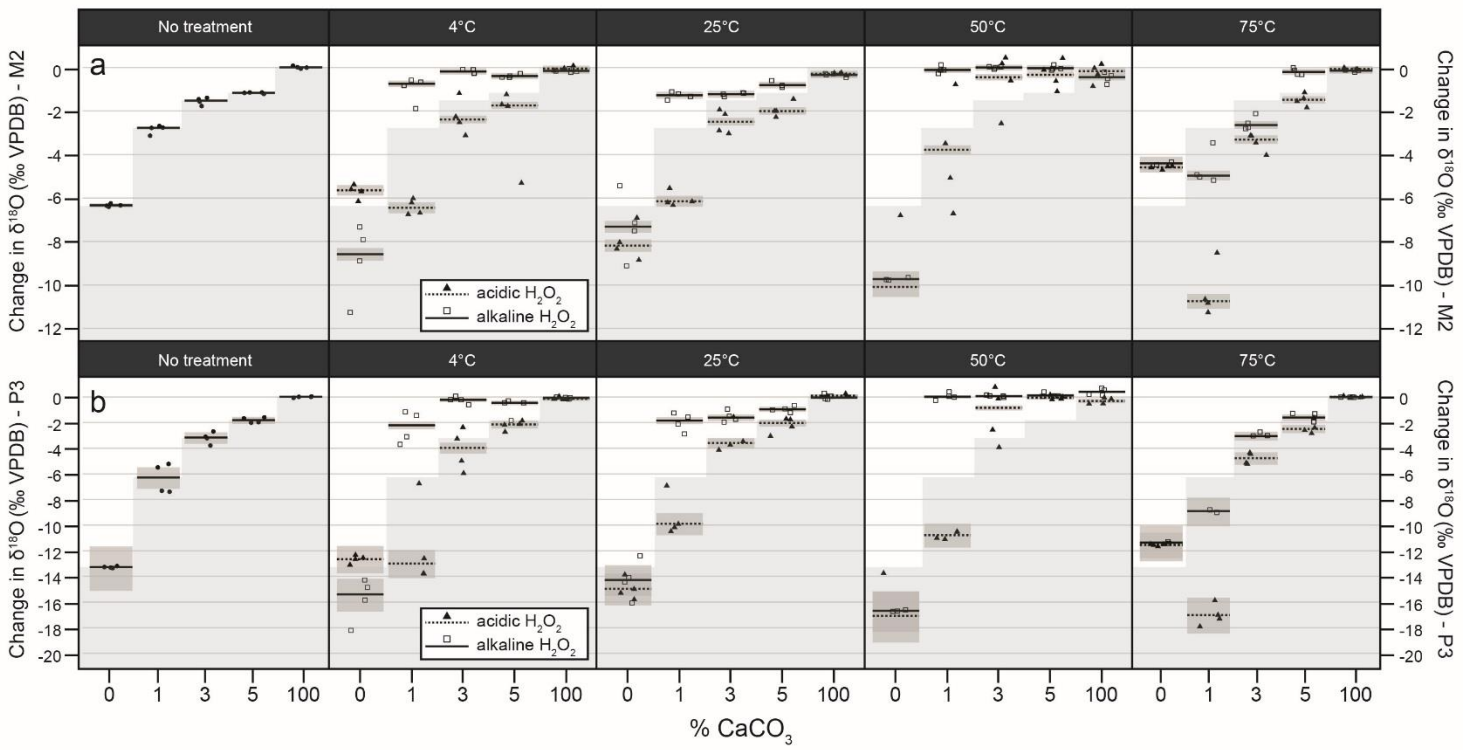

Figure 2.2. As per Figure 2.1, but for $\delta^{18}O$ (M2 $\delta^{18}O$: -7.26‰VPDB; P3 $\delta^{18}O$: -0.31‰VPDB).

electron microscope equipped with a thin film energy-dispersive x-ray spectroscopy detector, at 30-mm working distance and 10-kV accelerating voltage. We imaged untreated carbonate grains, as well as mixtures of sediment and carbonate that were treated with either acidic or alkaline H_2O_2, in both cases at 25 °C.

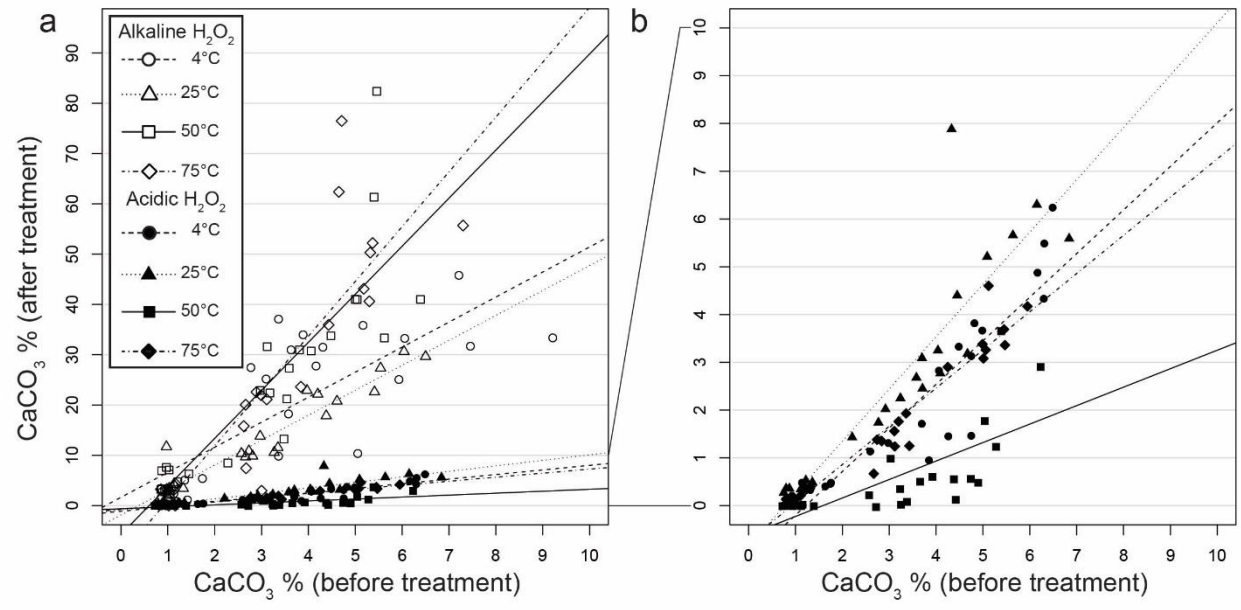

Figure 2.3. Cross-plots showing the percentage of calcium carbonate after treatment with either acidic (pH ≈ 4) or alkaline (pH ≈ 8) H_2O_2 at four different temperatures, compared with the initial percentage within natural lake sediment: **a)** All samples plotted on the same axes, showing two distinct populations: samples that were treated with acidic H_2O_2 (lower slopes) and samples that were treated with alkaline H_2O_2 (higher slopes); **b)** Only samples that were treated with acidic H_2O_2, with the same scale on the x and y axes.

2.4 Statistical Analysis

We used a balanced three-way analysis of variance to determine whether the treatment parameters (acidic or alkaline H_2O_2, reaction temperature) and initial carbonate concentration resulted in significantly different $\delta^{13}C$ and $\delta^{18}O$ values. The response variables ($\delta^{13}C$ and $\delta^{18}O$) were rescaled so that all values were positive prior to analysis. We used robust linear models for model fitting because the variance more closely approximated a *t*-distribution than a Gaussian distribution. We used type II sums of squares and set α to 0.05 a priori. All analysis of variance computations were performed using the "MASS" package (Venables & Ripley, 2002) in R (R Core Team, 2017) and estimated marginal mean effects were calculated using the "visreg" package (Breheny & Burchett, 2017). Estimates were back-transformed to their original scale for plotting.

3 Results

For each carbonate standard, the highest-order interaction among all three factors (temperature, reagent, and carbonate concentration) was significant for both $\delta^{13}C$ and $\delta^{18}O$ (Supp. Table 2.1). The $\delta^{13}C$ and $\delta^{18}O$ data are presented in Figures 2.1 and 2.2 as deviation from the stable isotope composition of the pure, untreated carbonate.

For samples that were not subject to any pretreatment, the measured $\delta^{13}C$ and $\delta^{18}O$ of all mixtures differed significantly from the true values for both the M2 and P3 standards (Figures 2.1 and 2.2 and Supp. Table 2.1). Detectable CO_2 was evolved from the pure lake sediment, which returned the most negative $\delta^{13}C$ and $\delta^{18}O$ values. The values of all mixtures were negatively biased, and the bias increased with decreasing carbonate concentration.

The posttreatment carbonate concentrations for the eight different treatments fell into two distinct populations—samples subject to oxidation by acidic H_2O_2 at the four temperatures and samples subject to oxidation by alkaline H_2O_2 at the four temperatures (Figure 2.3). In all cases, the posttreatment carbonate concentration was significantly higher in the samples treated with alkaline H_2O_2. A linear relationship with slopes ranging from 5 to 10.9 indicates a high degree of organic matter removal (Figure 2.3a). Conversely, samples oxidized with acidic H_2O_2 lie along slopes between 0.4 and 1.1, indicating either very little removal of organic matter, or in fact some loss of carbonate (Figure 2.3b). For alkaline H_2O_2 and acidic H_2O_2, the most organic matter removal occurred at 75 °C and 25 °C, respectively. Both the pH of the H_2O_2 and the temperature of reaction had a significant effect on the measured $\delta^{13}C$ and $\delta^{18}O$ of the simulated lake sediment (Supp. Table 2.1), with a larger effect at lower starting carbonate concentrations (Figures 2.1 and 2.2). Pretreatment of the simulated lake sediment with alkaline H_2O_2 resulted in model $\delta^{13}C$ values that were invariably more

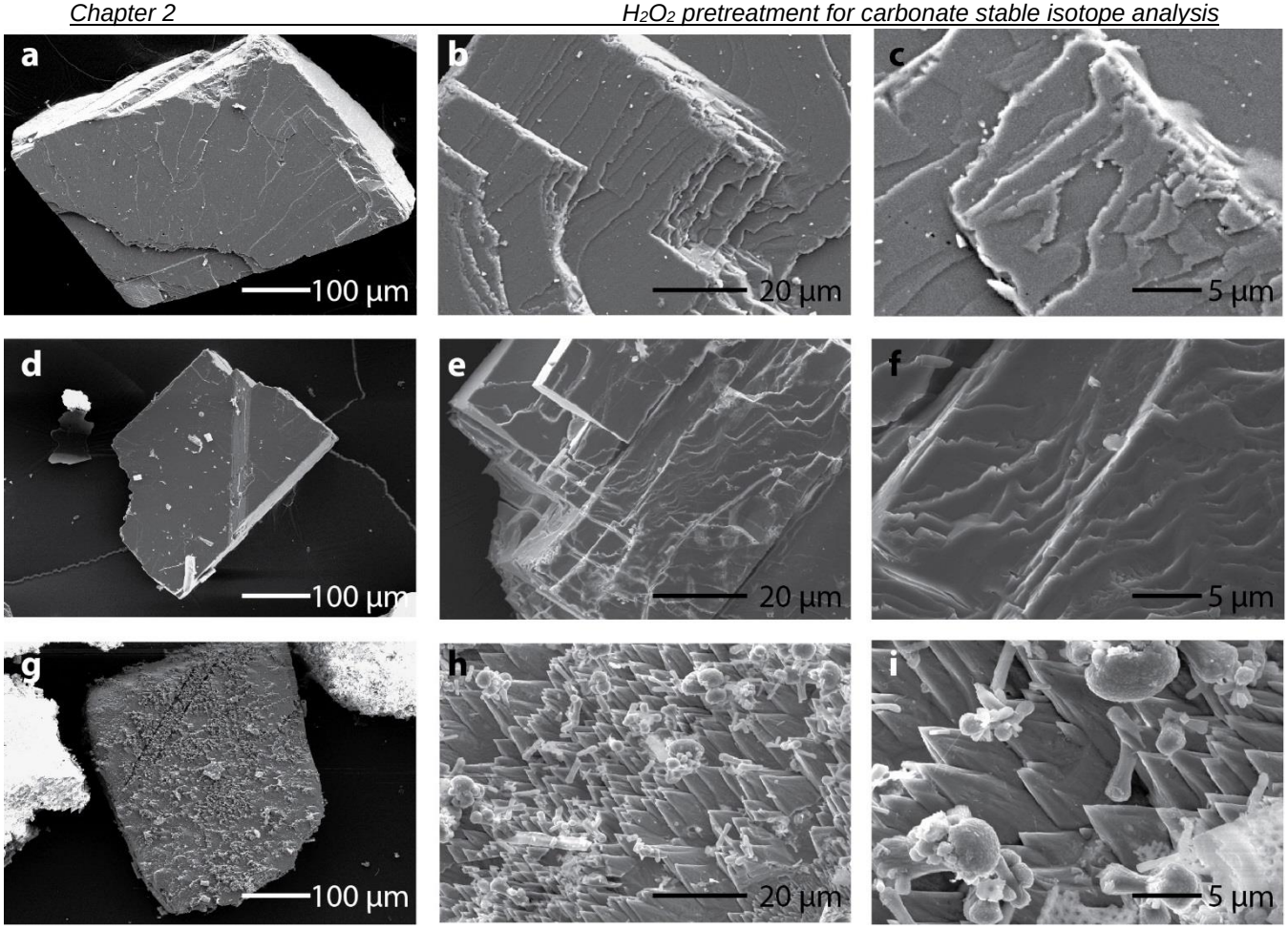

Figure 2.4. Scanning electron micrographs of M2 calcite grains, showing the effect of acidic or alkaline oxidative pre-treatment on crystal morphology. Both reactions were carried out for 24 hr, at 25 °C: **a-c)** M2 standard prior to any pre-treatment: regular, plate-like calcite crystalline morphology; **d-f)** M2 carbonate after reaction with alkaline 18% H_2O_2. Note that the crystal structure remains unchanged at all scales; **g-i)** M2 carbonate after reaction with acidic 18% H_2O_2, in the presence of natural lake sediment. Note the appearance of new carbonate morphologies, including elongated laminated micro particles on the grain surface, with rhombohedral calcite crystals, alongside with dumbbell-like crystals, and cauliflower-like polycrystalline aggregates typical of vaterite **(h & i)**.

accurate than both the sediment that was not pretreated, and the sediment that was treated with acidic H_2O_2 (Figure 2.1). The $\delta^{18}O$ values of sediment treated with alkaline H_2O_2 were generally more accurate than those resulting from pretreatment with acidic H_2O_2, or from sediment that was not pretreated (Figure 2.2). The major exception to this was treatment at 75 °C, where the accuracy of the H_2O_2 values was not improved by any pretreatment. For both standards, the most accurate values were returned by mixtures subject to oxidation with alkaline H_2O_2 at 50 °C.

The negative bias in $\delta^{18}O$ was much greater for the P3 (biogenic aragonite; $\delta^{18}O$: -0.31‰VPDB) standard than the M2 (crystalline calcite; $\delta^{18}O$: -7.26‰VPDB) standard (note the difference in the scale of the *y* axis in Figures 2.2a and 2.2b). Where samples of 100%

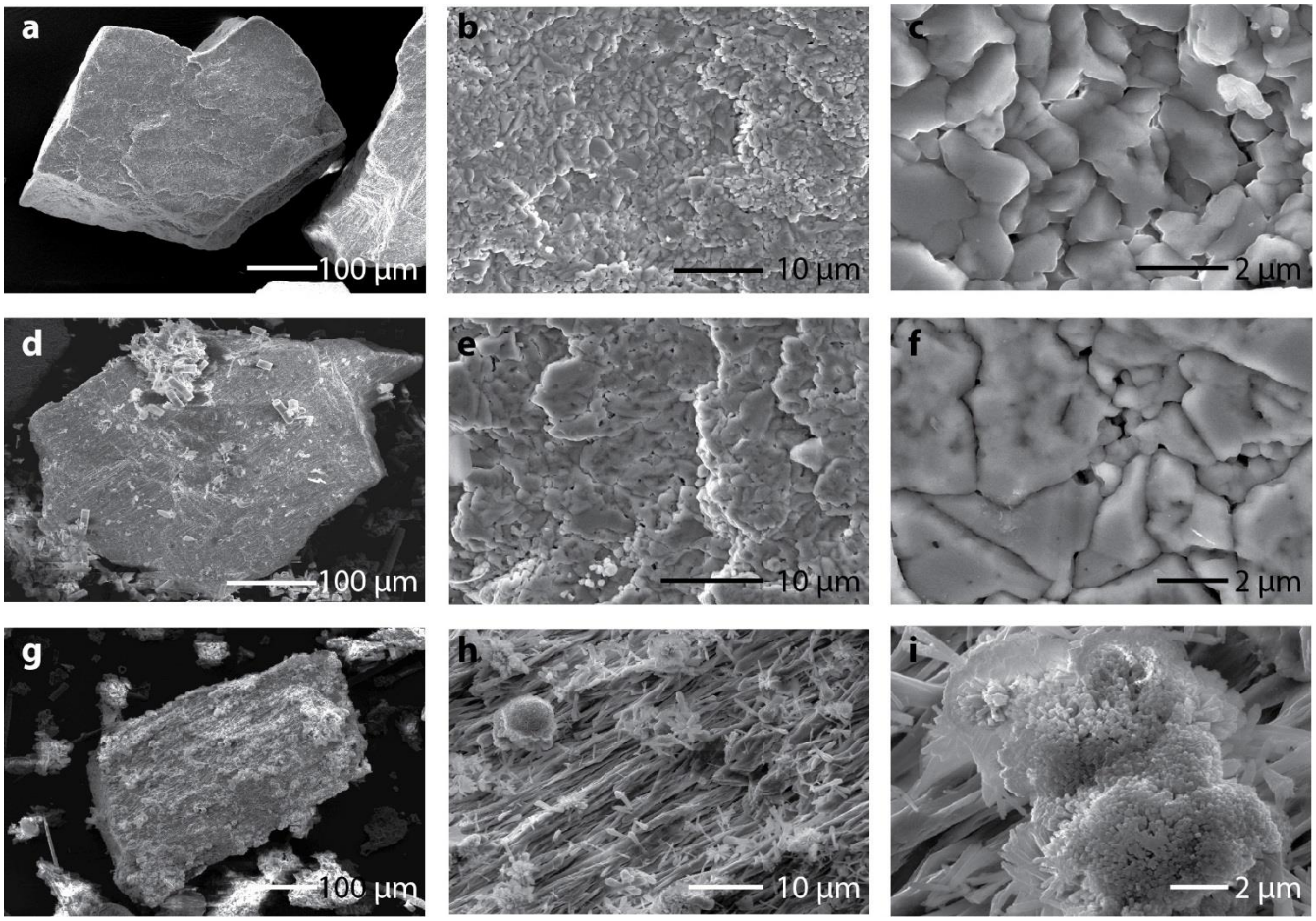

Figure 2.5. Scanning electron micrographs of P3 aragonite grains, as per Figure 2.4: **a-c)** P3 standard prior to any pre-treatment: an aragonite crystal with irregular thalloid surface morphology; **d-f)** P3 carbonate after reaction with alkaline 18% H_2O_2. Note that the crystal structure remains unchanged at all scales; **g-i)** P3 carbonate after reaction with acidic 18% H_2O_2, in the presence of natural lake sediment. Note the appearance of new carbonate morphologies, including discrete needle-like and cauliflower-shaped crystals **(h)** alongside aggregates of rod-like crystals **(i)**.

carbonate were subject to pretreatment, in all cases, the $\delta^{13}C$ values were both accurate and precise. The $\delta^{18}O$ values are slightly less accurate, and display some scatter, especially for samples treated with acidic H_2O_2.

4 Discussion

Our results clearly demonstrate that $\delta^{13}C$ and $\delta^{18}O$ values of fine-grained carbonate in very low concentrations within natural lake sediment, measured with no pretreatment, differ significantly from those of the pure carbonate. This confirms the findings of similar studies (e.g., Lebeau et al., 2014), indicating that sediment with low TIC/TOC is affected by an "organic bias," and requires pretreatment in order to obtain accurate C and O stable isotope determinations. For lake sediment that was treated with H_2O_2 to oxidize organic matter prior to analysis, different reaction parameters resulted in significant differences in both the efficacy of organic matter removal, and the measured $\delta^{13}C$ and $\delta^{18}O$ values.

Bias in the measured stable isotope composition of pretreated sediment/carbonate mixtures was almost uniformly negative, that is, toward the values returned from analysis of carbonate-free lake sediment. This effect was particularly strong in samples with extremely low TIC/TOC, and in sediment that was subject to oxidation with acidic H_2O_2. The effect was also larger for $\delta^{18}O$ at high temperatures, indicating that chemical treatment of carbonate at high temperature could be particularly detrimental to accurate oxygen stable isotope analyses.

For paleoclimate studies where oxidation of organic matter is required, H_2O_2 is generally used in its pure form despite being acidic, as it has been considered a less effective oxidizing agent if buffered to an alkaline pH (Gaffey & Bronnimann, 1993; Hosking, 1932). H_2O_2 is thermodynamically unstable, and decomposes into water and oxygen; this decomposition is accelerated by both high pH, and the higher temperatures that are often applied to reduce reaction time (Nicoll & Smith, 1955; Schultz et al., 1999). However, our results indicate that oxidation with alkaline H_2O_2 removes around 5 times as much organic matter as oxidation with acidic H_2O_2 (Figure 2.3). This apparent contradiction may be due in part to the composition of the Lake Purrumbete sediment. The molecular composition of the organic matter in Lake Purrumbete has not been determined; however, the sediment contains abundant plant material (Timms, 1976). Vascular plants produce lignin, a complex organic polymer that is resistant to diagenesis, so that it is preferentially preserved in lake sediment (Meyers & Ishiwatari, 1993). Solubilization of lignin by H_2O_2 has been shown to be more effective at high pH, owing to increased presence of molecular oxygen and other radical species produced by the rapid decomposition of H_2O_2 (Xiang & Lee, 2000). The ability for these species to degrade lignin is increased at higher temperatures; this fits well with our results, where the greatest removal of organic matter by alkaline H_2O_2 occurred at 75 °C (Figure 2.3). This also suggests that lignins contribute to residual organic carbon in mixtures treated with acidic H_2O_2, and confirms that specific lake sediment composition is an important factor in choice of reagent; for example, for lake sediment that is rich in terrestrial plant matter, the organic bias may be more effectively reduced by oxidation with alkaline H_2O_2.

Not only did oxidation with alkaline H_2O_2 remove a much larger proportion of organic matter from the simulated lake sediment samples than oxidation with acidic H_2O_2, but it also resulted in uniformly more accurate $\delta^{13}C$ and $\delta^{18}O$. This must be due in part to the greater increase in TIC/TOC (cf. Oehlerich et al., 2013), resulting in relatively less organic bias. The deviation of values following exposure to acidic H_2O_2 is also a strong argument for partial dissolution of fine-grained carbonate, that is, a “treatment bias.” This is supported by the

scanning electron microscope imaging. Images of the standards prior to treatment reveal distinct carbonate morphologies: M2 grains are characterized by well-defined platy calcite layers (Figures 2.4a–2.4c), and P3 grains are composed of relatively poorly structured aragonite (Figures 2.5a–2.5c). Grains that were subject to the alkaline H2O2 pretreatment are structurally indistinguishable from untreated grains, both at the scale of an entire grain and on a submicron scale (Figures 2.4a–2.24f and 2.5a–2.5f). However, grains within sediment treated with the acidic H_2O_2 show major structural changes on their surface, as well as the appearance of new carbonate morphologies (Figures 2.4g–2.4i and 2.5g–2.5i). M2 calcite grains developed a surficial morphology characterized by elongate rhombohedral crystals, and adhered to the grain surfaces were discrete rhombohedral calcite crystals, dumbbell-shaped crystals, and cauliflower-like polycrystalline aggregates (Figures 2.4h and 2.4i). The latter are characteristic of vaterite (Boyjoo et al., 2014), a metastable polymorph of calcium carbonate ($CaCO_3$) that may form subject to certain conditions including pH, water chemistry, presence of organic compounds, and the substrate (Pochitalkina et al., 2016; Ren et al., 2011; Zhao et al., 2011). The surficial structure of the P3 aragonite grains was altered from an irregular thalloid texture (Figure 2.5b) to elongate platy crystals (Figure 2.5h). Individual needle-shaped crystals and clusters of rod-like crystals—both typical aragonite morphologies—also appeared, alongside rare cauliflower-shaped aggregates similar to those seen on the M2 carbonate (Figures 2.5h and 2.5i). The composition—including presence of organic compounds—of a solution from which $CaCO_3$ precipitates is an important factor in determining the morphology of $CaCO_3$ crystals (Konopacka-Łyskawa et al., 2017). The variety of morphologies present in samples treated with acidic H_2O_2 indicates unequivocally that new carbonate was precipitated during the reaction. By contrast, the absence of new carbonate morphologies in the samples treated with alkaline H_2O_2 suggests that dissolution and reprecipitation was prevented by buffering the H_2O_2 to pH 8.

While the alkaline H_2O_2 treatment resulted in more accurate $\delta^{13}C$ and $\delta^{18}O$ values than the acidic H_2O_2 at all tested temperatures, the temperature of reaction also had a significant influence on the measured values. During treatment with alkaline H_2O_2 at 4 °C and 25 °C, the $\delta^{13}C$ and $\delta^{18}O$ of both carbonates at 1% concentration maintained a negative bias of several per mille, and this bias was also present at 3 and 5% in the $\delta^{18}O$ of samples treated at 25 °C. These are the two temperatures at which the least organic matter was removed (Figure 2.3), resulting in lower TIC/TOC at the time of measurement. Given there was no evidence for the precipitation of new carbonate during treatment with alkaline H_2O_2, it is likely that the residual organic matter evolved detectable CO_2, resulting in an organic bias.

The $\delta^{13}C$ of the mixtures treated at 75 °C was accurate for starting concentrations of 3 and 5%, and only slightly offset at 1%. However, the $\delta^{18}O$ values are heavily biased, with negative offsets of up to -5 and -9‰ in mixtures of 1% M2 and P3 carbonates, respectively (Figure 2.2). There was also generally no improvement on samples that were subject to no pretreatment. The organic bias in these samples was most likely minimal, given that this was the treatment at which the most organic matter was removed (Figure 2.3), and so this must represent a treatment bias. The similarity in $\delta^{18}O$ between the samples treated with acidic versus alkaline H_2O_2 at 75 °C suggests that at high temperatures, some new carbonate precipitation did occur. At temperatures over >70 °C, H_2O_2 decomposes rapidly, particularly at an alkaline pH (Schultz et al., 1999). We did not image samples treated at high temperature; however, at a temperature >70 °C, the supply of alkaline reagent may have been exhausted (Mikutta et al., 2005), allowing acidic oxidation products to lower the solution pH sufficiently to dissolve carbonate. Hence, 50 °C was the only temperature at which treatment with alkaline H_2O_2 did not result in any discernible organic or treatment bias.

Regarding the use of $\delta^{13}C$ and $\delta^{18}O$ from fine-grained lacustrine carbonate for paleoclimate reconstructions, our results demonstrate that with appropriate pretreatment, lake sediment with very low TIC/TOC may indeed yield accurate values that may be used to interpret past environmental change. However, given the large between-treatment range—especially for $\delta^{18}O$, which is commonly used in quantitative climate reconstructions—a degree of circumspection is essential when comparing published results where different H_2O_2 treatment parameters were used. This will be particularly important where pretreatment was carried out at a high temperature, with an acidic reagent, or on sediment that has very low starting TIC/TOC. We also note that these results are specific to the Lake Purrumbete sediment and that sediments containing different organic compounds will almost certainly result in different degrees of bias (Mikutta et al., 2005; Oehlerich et al., 2013). Nevertheless, alkaline H_2O_2 is clearly efficient in removal of organic compounds commonly found in lakes, and provides a starting point for determination of optimal treatment parameters for a wider variety of lake sediments. For individual lakes, a straightforward test may be to acidify a sediment subsample, subject this subsample to oxidation by alkaline H_2O_2 at varying temperatures and durations, and in this way determine optimal parameters for removal of organic compounds specific to the sediment. Our results may also be applicable to diatom $\delta^{18}O$ studies, where it is essential that all organic material in the surrounding sediment is removed prior to analysis (Leng & Barker, 2006; Tyler et al., 2007).

One parameter not tested here is the temperature at which H_3PO_4 digestion occurs prior to analysis. In our case, this was performed at 70 °C. However, digestion at lower

temperatures for a longer time period may result in a lower organic bias. This should be tested in future work.

5 Conclusions

The $\delta^{13}C$ and $\delta^{18}O$ of fine-grained carbonate preserved within organic-rich lacustrine sediments may provide valuable information about how the climate has varied in the past. If the TIC/TOC of the measured bulk sediment is low (<0.3; Oehlerich et al., 2013), then an organic bias arises due to contribution of CO_2 evolved from organic compounds. The TIC/TOC may be raised by oxidation of organic matter with H_2O_2; however, this may induce a treatment bias resulting from dissolution and reprecipitation of carbonate under acidic conditions. We tested the effects of pretreatment with acidic or alkaline H_2O_2 at different temperatures, on the measured $\delta^{13}C$ and $\delta^{18}O$ of very small amounts (≤5%) of fine-grained carbonate standards within a natural lake sediment matrix, and present the following key findings and recommendations:

1. Pretreatment of lacustrine sediment with alkaline H_2O_2 at 50 °C results in accurate carbonate $\delta^{13}C$ and $\delta^{18}O$ values, even for initial carbonate concentrations as low as 1%. This combination of treatment parameters not only avoids the bias associated with partial dissolution of carbonate but also is more efficient in the oxidation of some organic compounds. This may be particularly relevant to lacustrine sediment that contains a high proportion of material derived from vascular land plants.
2. Oxidation of organic material with acidic H_2O_2 results in partial dissolution and reprecipitation of carbonate, leading to a treatment bias. Oxidation with hot (75 °C) alkaline H_2O_2 also results in a treatment bias, possibly due to the production of organic acids in conjunction with rapid decomposition of the alkaline reagent. We recommend avoiding treatment with hot or acidic H_2O_2 in all cases.
3. Scanning electron microscope imaging of sediment before and after treatment is a useful tool to determine if new carbonate has precipitated during treatment; the appearance of new crystal morphologies is a reliable positive indicator of carbonate dissolution and reprecipitation.
4. The lack of methodological consistency in oxidative pretreatments that is evident in the paleoclimatological literature, even between H_2O_2-based treatments, may preclude rigorous comparison of climate interpretations derived from the absolute $\delta^{13}C$ and $\delta^{18}O$ values of lacustrine carbonates.

6 References cited

Boiseau, M., & Juillet-Leclerc, A. (1997). H_2O_2 treatment of recent coral aragonite: Oxygen and carbon isotopic implications. Chemical Geology, 143(3-4), 171–180. https://doi.org/10.1016/S0009-2541(97)00112-5

Boyjoo, Y., Pareek, V. K., & Liu, J. (2014). Synthesis of micro and nano-sized calcium carbonate particles and their applications. Journal of Materials Chemistry A, 2(35), 14,270–14,288. https://doi.org/10.1039/C4TA02070G

Breheny, P., & Burchett, W., 2017. visreg: Visualization of regression models, R package version 2.4–1 ed.

Chivas, A. R., Deckker, P. D., & Shelley, J. M. G. (1986). Magnesium and strontium in non-marine ostracod shells as indicators of palaeosalinity and palaeotemperature. Hydrobiologia, 143(1), 135–142. https://doi.org/10.1007/BF00026656

Cook, E. J. (2009). A record of late Quaternary environments at lunette-lakes Bolac and Turangmoroke, western Victoria, Australia, based on pollen and a range of non-pollen palynomorphs. Review of Palaeobotany and Palynology, 153(3-4), 185–224. https://doi.org/10.1016/j. revpalbo.2008.07.001

R Core Team (2017). R: A Language and Environment for Statistical Computing. Vienna, Austria: R Foundation for Statistical Computing.

Fallet, U., Boer, W., van Assen, C., Greaves, M., & Brummer, G.-J. A. (2009). A novel application of wet oxidation to retrieve carbonates from large organic-rich samples for ocean-climate research. Geochemistry, Geophysics, Geosystems, 10, Q08004. https://doi.org/10.1029/ 2009GC002573

Falster, G., Tyler, J., Grant, K., Tibby, J., Turney, C., Löhr, S., et al. (2018). Millennial-scale variability in south-east Australian hydroclimate between 30,000 and 10,000 years ago. Quaternary Science Reviews, 192, 106–122. https://doi.org/10.1016/j.quascirev.2018.05.031

Feldmeijer, W., Metcalfe, B., Scussolini, P., & Arthur, K. (2013). The effect of chemical pretreatment of sediment upon foraminiferal-based proxies. Geochemistry, Geophysics, Geosystems, 14, 3996–4014. https://doi.org/10.1002/ggge.20233

Gaffey, S. J., & Bronnimann, C. E. (1993). Effects of bleaching on organic and mineral phases in biogenic carbonates. Journal of Sedimentary Petrology, 63(4), 752–754. https://doi.org/10.1306/D4267BE0-2B26-11D7-8648000102C1865D

Ganssen, G. (1981). Isotopic analysis of foraminifera shells: Interference from chemical treatment. Palaeogeography, Palaeoclimatology, Palaeoecology, 33(1-3), 271–276. https://doi.org/10.1016/0031-0182(81)90043-2

Grottoli, A. G., Rodrigues, L. J., Matthews, K. A., Palardy, J. E., & Gibb, O. T. (2005). Pre-treatment effects on coral skeletal δ13C and $\delta^{18}O$. Chemical Geology, 221(3-4), 225–242. https://doi.org/10.1016/j.chemgeo.2005.05.004

Harris, D., Horwath, W. R., & van Kessel, C. (2001). Acid fumigation of soils to remove carbonates prior to total organic carbon or carbon-13 analysis. Soil Science Society of America Journal, 65(6), 1853–1856. https://doi.org/10.2136/sssaj2001.1853

Holmes, J. A. (1996). Trace-element and stable-isotope geochemistry of non-marine ostracod shells in quaternary palaeoenvironmental reconstruction. Journal of Paleolimnology, 15(3), 223–235. https://doi.org/10.1007/BF00213042

Holmes, J. A., Tindall, J., Roberts, N., Marshall, W., Marshall, J. D., Bingham, A., et al. (2016). Lake isotope records of the 8200-year cooling event in western Ireland: Comparison with model simulations. Quaternary Science Reviews, 131, 341–349. https://doi.org/10.1016/j. quascirev.2015.06.027

Hosking, J. S. (1932). The influence of hydrogen-ion concentration on the decomposition of soil organic matter by hydrogen peroxide. The Journal of Agricultural Science, 22(01), 92–100. https://doi.org/10.1017/S0021859600053119

Hyvåinen, H., Martma, T., & Punning, J.-M. (1990). Stable isotope and pollen stratigraphy of a Holocene lake marl section from NE Finland. Boreas, 19, 17–24.

Keatings, K. W., Holmes, J. A., & Heaton, T. H. E. (2006). Effects of pre-treatment on ostracod valve chemistry. Chemical Geology, 235(3-4), 250–261. https://doi.org/10.1016/j.chemgeo.2006.07.003

Konopacka-Łyskawa, D., Kościelska, B., & Karczewski, J. (2017). Controlling the size and morphology of precipitated calcite particles by the selection of solvent composition. Journal of Crystal Growth, 478, 102–110. https://doi.org/10.1016/j.jcrysgro.2017.08.033

Lebeau, O., Busigny, V., Chaduteau, C., & Ader, M. (2014). Organic matter removal for the analysis of carbon and oxygen isotope compositions of siderite. Chemical Geology, 372, 54–61. https://doi.org/10.1016/j.chemgeo.2014.02.020

Leng, M. J., & Barker, P. A. (2006). A review of the oxygen isotope composition of lacustrine diatom silica for palaeoclimate reconstruction. Earth-Science Reviews, 75(1-4), 5–27. https://doi.org/10.1016/j.earscirev.2005.10.001

Leng, M. J., & Marshall, J. D. (2004). Palaeoclimate interpretation of stable isotope data from lake sediment archives. Quaternary Science Reviews, 23(7-8), 811–831. https://doi.org/10.1016/j.quascirev.2003.06.012

McCrea, J. M. (1950). On the isotopic chemistry of carbonates and a paleotemperature scale. The Journal of Chemical Physics, 18(6), 849–857. https://doi.org/10.1063/1.1747785 Meyers, P. A., &

Ishiwatari, R. (1993). Lacustrine organic geochemistry—An overview of indicators of organic matter sources and diagenesis in lake sediments. Organic Geochemistry, 20(7), 867–900. https://doi.org/10.1016/0146-6380(93)90100-

Mikutta, R., Kleber, M., Kaiser, K., & Jahn, R. (2005). Organic matter removal from soils using hydrogen peroxide, sodium hypochlorite, and disodium peroxodisulfate. Soil Science Society of America Journal, 69(1), 120–135. https://doi.org/10.2136/sssaj2005.0120

Nagtegaal, R., Grove, C. A., Kasper, S., Zinke, J., Boer, W., & Brummer, G.-J. A. (2012). Spectral luminescence and geochemistry of coral aragonite: Effects of whole-core treatment. Chemical Geology, 318–319, 6–15.

Nicoll, W. D., & Smith, A. F. (1955). Stability of dilute alkaline solutions of hydrogen peroxide. Industrial and Engineering Chemistry, 47(12), 2548–2554. https://doi.org/10.1021/ie50552a051

Oehlerich, M., Baumer, M., Lücke, A., & Mayr, C. (2013). Effects of organic matter on carbonate stable isotope ratios (δ13C, δ^{18}O values)— Implications for analyses of bulk sediments. Rapid Communications in Mass Spectrometry, 27(6), 707–712. https://doi.org/10.1002/rcm.6492

Ollier, C. D. (1967). Maars their characteristics, varieties and definition. Bulletin Volcanologique, 31(1), 45–73. https://doi.org/10.1007/ BF02597005

Pochitalkina, I. A., Kekin, P. A., Morozov, A. N., Kondakov, D. F., & Petropavlovskii, I. A. (2016). Morphology of calcium carbonate prepared via homogeneous synthesis. Russian Journal of Inorganic Chemistry, 61(11), 1392–1396. https://doi.org/10.1134/S0036023616110152

Ren, D., Feng, Q., & Bourrat, X. (2011). Effects of additives and templates on calcium carbonate mineralization in vitro. Micron, 42(3), 228–245. https://doi.org/10.1016/j.micron.2010.09.005

Schultz, M. K., Biegalski, S. R., Inn, K. G. W., Yu, L., Burnett, W. C., Thomas, J. L. W., & Smith, G. E. (1999). Optimizing the removal of carbon phases in soils and sediments for sequential chemical extractions by coulometry. Journal of Environmental Monitoring, 1(2), 183–190. https://doi.org/10.1039/a900534j

Schwander, J., Eicher, U., & Ammann, B. (2000). Oxygen isotopes of lake marl at Gerzensee and Leysin (Switzerland), covering the younger Dryas and two minor oscillations, and their correlation to the GRIP ice core. Palaeogeography, Palaeoclimatology, Palaeoecology, 159(3-4), 203–214. https://doi.org/10.1016/S0031-0182(00)00085-7

Serrano, O., Serrano, L., & Mateo, M. A. (2008). Effects of sample pre-treatment on the δ13C and $\delta^{18}O$ values of living benthic foraminifera. Chemical Geology, 257(3-4), 218–220. https://doi.org/10.1016/j.chemgeo.2008.09.013

Spötl, C., & Vennemann, T. W. (2003). Continuous-flow isotope ratio mass spectrometric analysis of carbonate minerals. Rapid Communications in Mass Spectrometry, 17(9), 1004–1006. https://doi.org/10.1002/rcm.1010

Stuiver, M. (1970). Oxygen and carbon isotope ratios of fresh-water carbonates as climatic indicators. Journal of Geophysical Research, 75(27), 5247–5257. https://doi.org/10.1029/JC075i027p05247

Tibby, J., Penny, D., Leahy, P., & Kershaw, A. P. (2011). Vegetation and water quality responses to Holocene climate variability in Lake Purrumbete, western Victoria. Terra Australis, 43, 359–373.

Timms, B. V. (1976). A comparative study of the limnology of three Maar Lakes in western Victoria. I. Physiography and Physicochemical Features. Australian Journal of Marine and Freshwater Research, 27(1), 35–60. https://doi.org/10.1071/MF9760035

Tyler, J. J., Leng, M. J., & Sloane, H. J. (2007). The effects of organic removal treatment on the integrity of $\delta^{18}O$ measurements from biogenic silica. Journal of Paleolimnology, 37(4), 491–497. https://doi.org/10.1007/s10933-006-9030-9

Venables, W. N., & Ripley, B. D. (2002). Modern Applied Statistics with S (4th ed.). New York: Springer.

von Grafenstein, U., Erlenkeuser, H., Müller, J., & Kleinmann-Eisenmann, A. (1992). Oxygen isotope records of benthic ostracods in Bavarian lake sediments. Naturwissenschaften, 79(4), 145–152. https://doi.org/10.1007/BF01134431

Wierzbowski, H. (2007). Effects of pre-treatments and organic matter on oxygen and carbon isotope analyses of skeletal and inorganic calcium carbonate. International Journal of Mass Spectrometry, 268(1), 16–29. https://doi.org/10.1016/j.ijms.2007.08.002

Wilkins, D., Gouramanis, C., Deckker, P. D., Fifield, L. K., & Olley, J. (2013). Holocene lake-level fluctuations in lakes Keilambete and Gnotuk, southwestern Victoria, Australia. The Holocene, 23(6), 784–795. https://doi.org/10.1177/0959683612471983

Xiang, Q., & Lee, Y. Y. (2000). Oxidative cracking of precipitated hardwood lignin by hydrogen peroxide. Applied Biochemistry and Biotechnology, 84, 153–162.

Zhao, Y., Li, S., Yu, L., Liu, Y., Wang, X., & Jiao, J. (2011). The preparation of calcium carbonate crystals regulated by mixed cationic/cationic surfactants. Journal of Crystal Growth, 324(1), 278–283. https://doi.org/10.1016/j.jcrysgro.2011.03.052

Supporting information for Chapter Two

Hydrogen peroxide treatment of natural lake sediment prior to carbon and oxygen stable isotope analysis of calcium carbonate

Supplementary Table 2.1. Balanced three-way ANOVA (type II) of $\delta^{13}C_{M2}$, $\delta^{13}C_{P3}$, $\delta^{18}O_{M2}$, and $\delta^{18}O_{P3}$ values following oxidative pretreatment.

Response	Predictor	*df*	*F*	*p*-value
$\delta^{18}O$ (M2)	Temperature	3	154.24	<0.0001
	Reagent	1	682.687	<0.0001
	Carbonate concentration	4	2536.875	<0.0001
	Temperature*Reagent	3	29.136	<0.0001
	Temperature*Carbonate concentration	12	158.526	<0.0001
	Reagent*Carbonate concentration	4	380.616	<0.0001
	Temperature*Reagent*Carbonate concentration	12	22.902	<0.0001
$\delta^{18}O$ (P3)	Temperature	3	137.121	<0.0001
	Reagent	1	598.882	<0.0001
	Carbonate concentration	4	1635.355	<0.0001
	Temperature*Reagent	3	18.808	<0.0001
	Temperature*Carbonate concentration	12	33.592	<0.0001
	Reagent*Carbonate concentration	4	154.664	<0.0001
	Temperature*Reagent*Carbonate concentration	12	13.887	<0.0001
$\delta^{13}C$ (M2)	Temperature	3	67.963	<0.0001
	Reagent	1	1457.66	<0.0001
	Carbonate concentration	4	1916.351	<0.0001
	Temperature*Reagent	3	12.286	<0.0001
	Temperature*Carbonate concentration	12	11.545	<0.0001
	Reagent*Carbonate concentration	4	389.273	<0.0001
	Temperature*Reagent*Carbonate concentration	12	12.432	<0.0001
$\delta^{13}C$ (P3)	Temperature	3	45.5552	<0.0001
	Reagent	1	978.3151	<0.0001
	Carbonate concentration	4	1773.1875	<0.0001
	Temperature*Reagent	3	4.4383	0.005477
	Temperature*Carbonate concentration	12	11.0485	<0.0001
	Reagent*Carbonate concentration	4	289.4319	<0.0001
	Temperature*Reagent*Carbonate concentration	12	11.7729	<0.0001

Denominator degrees of freedom = 115

df = degrees of freedom

Chapter 3

This chapter is published as:

Falster, G., Tyler, J., Grant, K., Tibby, J., Turney, C., Löhr, S., Jacobsen, G., Kershaw, A. P. (2018). Millennial-scale variability in south-east Australian hydroclimate between 30,000 and 10,000 years ago. *Quaternary Science Reviews*, 192, 106-122. https://doi.org/10.1016/j.quascirev.2018.05.031

Note: Organic matter elemental and stable isotope data associated with this chapter are provided in Appendix 2 Table A2. The scanning XRF dataset is very large, and is not presented here. The data are permanently hosted on the University of Adelaide's Figshare site along with all primary data arising from this chapter:

https://adelaide.figshare.com/articles/Falster_et_al_2018_Lake_Surprise_xlsx/7246031

I have re-formatted the published article to match the rest of the thesis. The text remains exactly the same, except for the figure and table numbers, which are now prefaced with the chapter number e.g. Table 1 is now Table 3.1. The published version of the chapter is provided in Appendix 3.

Statement of Authorship

Title of Paper	Millennial-scale variability in south-east Australian hydroclimate between 30,000 and 10,000 years ago
Publication Status	☑ Published ☐ Accepted for Publication ☐ Submitted for Publication ☐ Unpublished and Unsubmitted work written in manuscript style
Publication Details	Falster, G., Tyler, J., Grant, K., Tibby, J., Turney, C., Löhr, S., Jacobsen, G., Kershaw, A. P. (2018). Millennial-scale variability in south-east Australian hydroclimate between 30,000 and 10,000 years ago. *Quaternary Science Reviews, 192*, 106-122. https://doi.org/10.1016/j.quascirev.2018.05.031

Principal Author

Name of Principal Author (Candidate)	Georgina Falster		
Contribution to the Paper	Prepared and analysed samples, interpreted data, wrote manuscript, acted as corresponding author.		
Overall percentage (%)	75%		
Certification:	This paper reports on original research I conducted during the period of my Higher Degree by Research candidature and is not subject to any obligations or contractual agreements with a third party that would constrain its inclusion in this thesis. I am the primary author of this paper.		
Signature		Date	11/3/2019

Co-Author Contributions

By signing the Statement of Authorship, each author certifies that:

i. the candidate's stated contribution to the publication is accurate (as detailed above);

ii. permission is granted for the candidate in include the publication in the thesis; and

iii. the sum of all co-author contributions is equal to 100% less the candidate's stated contribution.

Name of Co-Author	Jonathan Tyler		
Contribution to the Paper	Provided conceptual guidance, assisted with statistical analyses, evaluated and edited manuscript.		
Signature		Date	31/1/2019

Name of Co-Author	Katharine Grant		
Contribution to the Paper	Assisted with acquisition and processing of x-ray fluorescence data, evaluated and edited manuscript.		
Signature		Date	1/2/2019

Name of Co-Author	John Tibby		
Contribution to the Paper	Provided conceptual guidance, evaluated and edited manuscript.		
Signature		Date	31/01/2019

Name of Co-Author	Chris Turney		
Contribution to the Paper	Evaluated and edited manuscript, assisted with initial interpretation of radiocarbon dates.		
Signature		Date	31 January 2019

Name of Co-Author	Stefan Löhr		
Contribution to the Paper	Assisted with interpretation of x-ray diffraction data, evaluated and edited manuscript.		
Signature		Date	01/02/2019

Name of Co-Author	Geraldine Jacobsen		
Contribution to the Paper	Assisted with acquisition of radiocarbon data, evaluated and edited manuscript.		
Signature		Date	01/02/2019

Name of Co-Author	A. Peter Kershaw		
Contribution to the Paper	Provided sediment for analysis, evaluated and edited manuscript.		
Signature		Date	31/1/2019

Millennial-scale variability in south-east Australian hydroclimate between 30,000 and 10,000 years ago

Abstract

Global climate variability during the late Quaternary is commonly framed in terms of the 'bipolar seesaw' pattern of asynchronous temperature variations in the northern and southern polar latitudes. However, the terrestrial hydrological response to this pattern in south-eastern Australia is not fully understood, as continuous, high-resolution, well-dated proxy records for the hydrological cycle in the region are sparse. Here we present a well-dated, highly-resolved record of moisture balance spanning 30000–10000 calendar years before present (30–10 ka BP), based on x-ray fluorescence (XRF) and organic carbon isotope ($\delta^{13}C_{OM}$) measurements of a sedimentary sequence from Lake Surprise in south-eastern Australia. The data provide a locally coherent record of the hydrological cycle. Elevated Si (reflecting windblown quartz and clays), and relatively high $\delta^{13}C_{OM,}$ indicate an extended period of relative aridity between 28–18.5 ka BP, interrupted by millennial-scale episodes of decreased Si and $\delta^{13}C_{OM}$, suggesting increased moisture balance. This was followed by a rapid deglacial shift to low Si and $\delta^{13}C_{OM}$ at 18.5 ka BP, indicative of wetter conditions. We find that these changes are coeval with other records from south-eastern Australia and New Zealand, and use a Monte Carlo Empirical Orthogonal Function approach to extract a common trend from three high-resolution records. Our analyses suggest that drivers of the regional hydrological cycle have varied on multi-millennial time scales, in response to major shifts in global atmosphere-ocean dynamics during the last glacial-interglacial transition. Southern Ocean processes were the dominant control on hydroclimate during glacial times, via a strong influence of cold sea surface temperatures on moisture uptake and delivery onshore. Following the last deglaciation (around 18 ka BP), the southward migration of cold Southern Ocean fronts likely resulted in the establishment of conditions more similar to those of the present day. Millennial-scale variability in records from the region is dominated by a persistent ca. 2300-year periodicity, consistent with other records across the Southern Hemisphere mid-latitudes; however, a mechanism for this pervasive periodicity remains equivocal.

1 Introduction

The late Quaternary (defined here as 30000–10000 calendar years before present; 30–10 ka BP) is the most recent period in the geological record that is characterised by abrupt shifts in global atmosphere and ocean circulation (Thomas, 2016). Unravelling patterns of climate variability during this period is key to understanding long-term atmosphere-ocean dynamics, and their environmental impact on centennial to millennial time scales. High-

resolution methane-synchronised ice core records from the northern and southern polar regions are characterised by marked, asynchronous climate changes during the late Quaternary (c.f. the 'bipolar seesaw'), and much research has been devoted to understanding the mechanisms driving these high-latitude climate phase relationships (Blunier et al., 1998; Broecker, 1998; Blunier and Brook, 2001; EPICA Community Members, 2006). However, the manifestation of these events in the terrestrial hydrological cycle beyond the high latitudes is less well constrained. This is particularly the case in the Southern Hemisphere (SH) mid-latitudes (defined here as spanning 25–45°S) where a relative dearth of continuous, high-resolution records has limited our ability to investigate the timing and drivers of change (Vandergoes et al., 2005; Bayon et al., 2017).

Within the ocean-dominated SH mid-latitudes, coastal sites in southern Australia and New Zealand (NZ) are highly sensitive to atmosphere-ocean interactions (Gentilli, 1971; Barrows et al., 2007; Gouramanis et al., 2013), and hence are ideally located to investigate long-term drivers of terrestrial hydroclimate. Large-scale climate systems that directly influence modern southern Australian and NZ climates include the mid-latitude Southern Westerly Winds (SWW) (Hall and Visbeck, 2002; Cai et al., 2005; Meneghini et al., 2007; Pepler et al., 2016), Southern Ocean and Antarctic ice sheet dynamics (Pezza et al., 2008; Williams and Stone, 2009), and zonal sea surface temperature (SST) gradients including the El Niño Southern Oscillation (ENSO) and the Indian Ocean Dipole (IOD) (Ashok et al., 2007; Risbey et al., 2009; Pepler et al., 2014; Forootan et al., 2016). However, the extent to which these systems influence southern Australian and NZ hydroclimate on multi-millennial time scales is not clear, especially considering the confounding effect of the sea level changes associated with glacial cycles (Clark and Mix, 2002).

A range of sedimentological, palaeoecological and geochemical tracers respond strongly to changes in the terrestrial hydrological cycle, and accordingly, there are over 60 hydroclimate-related proxy records from southern Australia and New Zealand, that span the late Quaternary (Table 3.1, Fig. 3.3.1). Early work, relying largely on fragmentary aeolian deposits, suggested that the last glacial period was cold, windy, and mostly dry relative to deglacial and interglacial periods (Bowler, 1976). This hypothesis has been generally supported by subsequent hydroclimate records (e.g. Gingele et al., 2001; Petherick et al., 2009; Barrell et al., 2013; Petherick et al., 2013), though some exceptions have been reported (Shulmeister et al., 2016; Treble et al., 2016; Barr et al., 2017).

Unfortunately, most records shown in Table 3.1 are fragmentary, or at too coarse a resolution to reliably identify millennial-scale variability. This is primarily because the largely

Table 3.1. Records of late Quaternary hydroclimate variability (spanning the majority of the period 30–10 ka BP), from southern Australia and New Zealand. Listed by country, in order of decreasing latitude. Map reference numbers correspond to Figure 3.1.

Country	Site name	Hydroclimate proxy(s)	Reference(s)	Latitude	Longitude	Map reference
Australia	Welsby Lagoon	Pollen, charcoal, total organic carbon content	Moss et al. (2013); Barr et al. (2017)	27°27'00"S	153°28'00"E	1
	Tortoise Lagoon	Pollen, charcoal, clastic sediment flux, particle size analysis	Moss et al. (2013); Petherick et al. (2017)	27°30'59"S	153°28'26"E	2
	Native Companion Lagoon	ICP-MS trace element analysis, pollen, charcoal, particle size analysis	Petherick et al. (2008); Petherick et al. (2009), Moss et al. (2013)	27°40'36"S	153°24'39"E	3
	Lake Eyre	Dates (OSL, TL, AMS ^{14}C, TIMS U-Th, amino acid racemisation determinations on bird eggshells and molluscs) on lake and lake-margin sediments	Magee et al. (2004)	28°31'2"S	137°13'51"E	4
	Lake Mega-Frome	OSL, TL and ^{14}C dates from lake palaeoshorelines	Cohen et al. (2011)	29°49'34"S	140°10'6"E	5
	Little Llangothlin Lagoon	OSL dating of geomorphology (lake margin shoreline features) via GPR, and sediments in a couple of cores	Shulmeister et al. (2016)	30° 5'9"S	151°46'53"E	6
	Lake Eyre, Lake Frome	OSL dating of palaeoshorelines	Cohen et al. (2015)	30°43'19"S	139°49'43"E	4, 7
	Lake Frome	Pollen	Singh and Luly (1991)	30°43'19"S	139°49'43"E	7
	Ulungra Springs	Pollen	Dodson and Wright (1989)	31°44'25"S	149° 5'38"E	8
	Burraga Swamp	Pollen	Sweller and Martin (2001)	32° 5'50"S	151°35'29"E	9
	Mairs Cave	MC-ICP-MS growth-phase, δ^{18}O, δ^{13}C, and trace element analyses on speleothems	Cohen et al. (2011); Treble et al. (2016)	32°13'25"S	138°53'5"E	10
	Redhead Lagoon	Pollen, charcoal	Williams (2005); Williams et al. (2006)	32°59'43"S	151°43'22"E	11
	Lachlan River	OSL dates from river terraces	Kemp and Rhodes (2010)	33°21'34"S	147°40'41"E	12
	Mountain Lagoon	Pollen	Robbie and Martin (2007)	33°26'40"S	150°38'15"E	13
	Willandra Lakes	^{14}C and TL dates within stratigraphic sections	Bowler (1998); Bowler et al. (2003); Bowler et al. (2012)	33°42'31"S	143° 4'18"E	14
	Darling Lakes	δ^{18}O (emu eggshells)	Miller and Fogel (2016)	33°42'31"S	143° 4'18"E	15
	Lake Baraba	Pollen, charcoal, LOI	Black et al. (2006)	34°13'S	150°13'E	16
	Murrumbidgee Valley	TL dates from riverine source-bordering dunes	Page et al. (2001)	35° 4'13"S	147°12'38"E	17
	Lake George	Radiocarbon dates on abandoned lake shorelines, pollen, ostracod ecology, charcoal	Coventry (1976); Singh et al. (1981); De Deckker (1982); Singh and Geissler (1985)	35° 6'37"S	149°26'5"E	18
	Lake Tyrrell	OSL dating of dune sediments	Stone (2006)	35°14'17"S	142°50'28"E	19
	Kelly Hill Caves	U/Th dates from speleothems	Cohen et al. (2011)	35°58'31"S	136°54'15"E	20
	Snowy Mountains	^{10}Be dates from glacial moraines	Barrows et al. (2001)	36°25'25"S	148°16'37"E	21
	Marine Core MD03-2611	Scanning XRF (Fe and Ti), XRD	DeDeckker et al. (2012)	36°43'48"S	136°32'54"E	22
	Naracoorte Caves (including Blanche Cave, Robertson Cave, and Wet Cave)	230Th/234U ages from speleothems and flowstones, XRF-derived major element geochemistry, LA-ICP-MS-derived REE and trace element composition, Nd isotopes, pollen, morphologicla analysis of quartz grains, grain size analysis, petrography, NMR, δ^{13}C and δ^{15}N (bulk sediment), δ^{13}C (charcoal), XRD	Ayliffe et al. (1998); Moriarty et al. (2000); Forbes et al. (2007); Darrénougué et al. (2009); Macken et al. (2013); Macken and Reed (2014)	37° 4'50"S	140°48'38"E	23
	Caledonia Fen	Pollen, charcoal, magnetic susceptibility, δ^{13}C (pollen grains)	Kershaw et al. (2007); Nelson et al. (2016)	37°20'0"S	146°43'60"E	24
	Lake Leake	Pollen	Dodson (1975)	37°37'27"S	140°36'14"E	25
	Wyrie Swamp	Pollen	Dodson (1977)	37°38'0"S	140°16'56"E	26
	Lake Turangmoroke	Pollen, palynomorphs, charcoal	Cook (2009)	37°43'33"S	142°53'34"E	27
	Lake Bolac	Pollen, palynomorphs, charcoal	Cook (2009)	37°43'49"S	142°51'39"E	28
	Lake Keilambete	^{14}C dates within stratigraphic sections	Bowler and Hamada (1971)	38°12'28"S	142°52'35"E	29
	Tower Hill	Pollen, microfauna, diatoms, charcoal, δ^{13}C (pollen grains)	D'Costa et al. (1989); Nelson et al. (2016)	38°19'1"S	142°21'46"E	30
	Marine core E55-6	Pollen, charcoal	Harle (1997)	38°51'12"S	141° 3'48"E	31
	Egg Lagoon	Mollusc assemblages, pollen, charcoal	D'Costa et al. (1993)	39°38'39"S	143°59'30"E	32
	Pulbeena Swamp	Pollen	Colhoun et al. (1982)	40°52'35"S	145° 8'36"E	33
	Tullabardine Dam	Pollen, charcoal	Colhoun and Geer (1986)	41°40'30"S	145°39'8"E	34
	Lake Selina	Pollen, charcoal, NMR intensity	Colhoun et al. (1999)	41°52'43"S	145°36'32"E	35
	Central Ice Plateau	^{36}Cl and ^{10}Be dates on glacial moraines	Barrows et al. (2002)	41°58'44"S	145°36'36"E	36
	Hazards Lagoon	Pollen, charcoal	Mackenzie and Moss (2017)	42°10'20"S	148°17'21"E	37
	Tasman Sea (deep sea cores)	Sedimentology (aeolian content, dry bulk density), particle size analysis of mineral fraction	Hesse (1994); Hesse and McTainsh (1999)	Multiple locations within the Tasman Sea		n/a
	Australian Highlands (Snowy Mountains, Tasmania)	Presence of periglacial landforms and LGM-aged lake shorelines	Galloway (1965)	Multiple locations		n/a
New Zealand	Marine Core S803	Pollen	Wright et al. (1995)	36°41'49"S	176°36'22"E	38
	Onepoto Maar	Sediment grain size, XRF (Al, Ti, Ni, Cr, Fe/Mn), TOC, TN, TS, δ^{13}C and δ^{15}N (bulk sediment), biogenic silica, diatoms, cladocerans, pollen, charcoal	Kattel and Augustinus (2010); Augustinus et al. (2011); Augustinus et al. (2012)	36°48'31"S	175°45'05"E	39
	Mt Richmond	Pollen	Sandiford et al. (2002)	36°55'58"S	174°50'26"E	40
	Kohuora Crater	Pollen, charcoal	Newnham et al. (2007)	36°58'42"S	174°50'34"E	41
	Pukaki Crater	Pollen, charcoal	Sandiford et al. (2003)	36°58'57"S	174°48'38"E	42
	central Taranaki	XRD determination of aerosolic quartz	Alloway et al. (1992)	39° 6'11"S	174°15'17"E	43
	North Island	^{3}He surface dates on glacial moraines, tephrochronology, tephrostratigraphy	Eaves et al. (2016)	39° 7'48"S	175°39'0"E	44
	Marine Core P69	Pollen	McGlone (2001)	40°23'48"S	177°59'48"E	45

Table 3.1 contd.

Country	Site name	Hydroclimate proxy(s)	Reference(s)	Latitude	Longitude	Map reference
	North-West Nelson	Pollen, charcoal	Shulmeister et al. (2003)	41° 5'57"S	172°38'5"E	46
	Mt Arthur	$\delta^{18}O$ and $\delta^{13}C$ (speleothem)	Hellstrom et al. (1998)	41°12'35"S	172°43'46"E	47
	Hollywood Cave	$\delta^{18}O$ and $\delta^{13}C$ (speleothem)	Whittaker et al. (2011)	41°57'0"S	171°28'0"E	48
	Okarito Bog	Pollen	Vandergoes et al. (2013)	43°14'30"S	170°13'6"E	49
	Galway Tarn	Pollen	Vandergoes et al. (2013)	43°24'30"S	169°52'24"E	50
	Skiffington Swamp	Pollen	Vandergoes et al. (2013)	43°25'15"S	169°59'30"E	51
	Rakaia Valley	IRSL dates within sedimentary sections	Shulmeister et al. (2010)	43°27'49"S	171°36'9"E	52
	Southern Alps Icefield	Topographically-constrained ice sheet modelling	Golledge et al. (2012)	43°42'1"S	170°4'6"E	53
	Lake Ohau	^{10}Be surface exposure dates on terminal moraines	Putnam et al. (2013)	44°13'20"S	169°51'17"E	54
	South Island	^{36}Cl and ^{10}Be dates and tephrochronology of glacial landforms	Barrows et al. (2013)	Multiple locations on the South Island of New Zealand		n/a
	Offshore NZ (marine cores)	Mass accumulation rates of terrigenous and biogenic sediments	Carter et al. (2000)	Multiple locations around New Zealand		n/a

arid- to semi-arid climates of south-eastern Australia in particular are generally not conducive to continuous accumulation of sediments. The region therefore suffers from there only being a limited network of high-resolution, temporally well-constrained, late Quaternary hydroclimate proxy records, in turn hindering precise inter-site comparison of climatic events on both regional and global scales. This is problematic, as single-site reconstructions may be confounded by local or proxy-specific effects, rather than providing a robust representation of regional palaeoclimate that may be directly compared with high-resolution and precisely dated palaeoclimate records from more distal locations (Turney et al., 2006; Moss et al., 2013; Petherick et al., 2013; Harrison et al., 2016; Prentice et al., 2017)

This uncertainty has resulted in ambiguity in the expression of the Last Glacial Maximum (LGM) in southern Australia and NZ. The global LGM is generally considered to have occurred between 23–19 ka BP, when sea level was at a minimum and the global climate was relatively stable (Mix et al., 2001; Clark et al., 2009). However, the LGM has no formal stratigraphic definition *per se* (Hughes and Gibbard, 2014), and several southern Australian and NZ palaeoclimate records preserve evidence for an 'extended LGM' that manifests as a period of extreme aridity, and most likely commenced between 32 and 28 ka BP (e.g. Heusser et al., 1999; Williams et al., 2006; Kershaw et al., 2007; Newnham et al., 2007; Fogwill et al., 2015; Petherick et al., 2017), but possibly as early as ~38 ka BP (e.g. Barrows et al., 2001; Petherick et al., 2008). Furthermore, some high-resolution records from southern Australia and NZ preserve evidence for (a) two relatively arid phases centred around ~31 and 22 ka BP, separated by an interval of increased moisture balance around ~24 ka BP (Alloway et al., 2007; Petherick et al., 2008; Augustinus et al., 2011; Petherick et al., 2017), or (b) variable hydroclimate superimposed on generally dry conditions (Moss et al., 2013). Interpretation of the timing, nature, and spatial distribution of LGM conditions in southern Australia and NZ is therefore equivocal, highlighting the need for more highly resolved palaeoclimate records.

Here we present a new high-resolution, multi-proxy hydroclimate record spanning 30–10 ka BP from Lake Surprise, a small, steep-walled crater lake located in south-eastern Australia (38°03'42"S, 141°55'22"E; Fig. 3.1). Lake Surprise is a sensitive archive of climate variability, lying at the modern northern margin of influence of the SWW (Hendon et al., 2007; Barr et al., 2014), with climate variability also modulated by the IOD and ENSO (Ashok et al., 2007; Risbey et al., 2009; Ummenhofer et al., 2009). Using comprehensive radiocarbon (^{14}C) dating in combination with high-resolution quantitative elemental composition data, and the carbon isotope composition of bulk organic matter, we infer past changes in aeolian input and variation in plant water stress within a robust geochronological framework. We subsequently apply a Monte Carlo Empirical Orthogonal Function (MCEOF) approach to key published records to objectively define a regionally coherent record of hydroclimate change. These records are all from south-eastern Australia and NZ, so we then use our findings to explore the timing and potential drivers of change in this region.

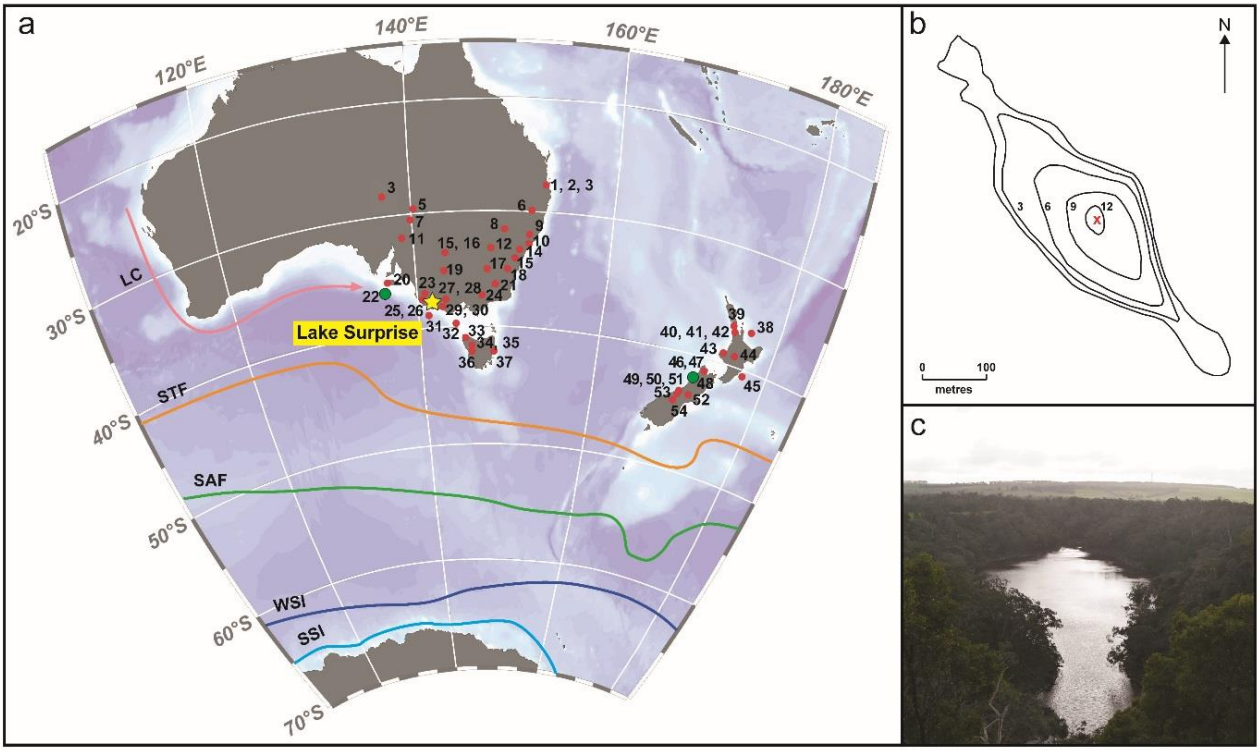

Figure 3.1. Location of sites mentioned in the text: **a**) Records of hydroclimate variability for southern Australia and New Zealand during the period 30-10 ka BP (Table 3.1), with the approximate modern position of the Southern Ocean subtropical front (STF), subantarctic front (SAF), maximum winter sea ice extent (WSI), and maximum summer sea ice extent (SSI), as well as the Leeuwin Current (LC). Location of published records included in the MCEOF analysis shown in green. Southern Ocean fronts and sea ice distribution adapted from Gersonde et al. (2005); Leeuwin Current path adapted from De Deckker et al. (2012). Map generated using the Ocean Data View software; **b**) Bathymetry of Lake Surprise, with depth contours in metres, and core location shown by the red cross; **c)** Lake Surprise, looking north-west from the rim of the Mt Eccles crater.

2 Methods

2.1 Study site and core acquisition

Lake Surprise occupies the crater complex of Mt Eccles, a dormant scoria cone volcano composed of nepheline hawaiite, located in the Newer Volcanics Province of south-eastern Australia (Fig. 3.1; Timms, 1975; Irving and Green, 1976; Boyce, 2013). Cosmogenic exposure dating of the surrounding Tyrendarra lava flow, which originated in Mt Eccles, indicates that the eruption of the volcano probably occurred 36 ± 3 ka BP (Gillen et al., 2010). Radiocarbon dates from lakes and swamps that formed following drainage diversion due to the extrusion of the Tyrendarra basalt provide minimum eruption ages of between 32 and 29 ka BP (Head et al., 1991; Builth et al., 2008); this chronological discrepancy is most likely due to the time taken for the porous basalt substrate to mature sufficiently to allow the accumulation of water and sediment. Following the eruption of Mt Eccles—and several other volcanos that erupted around the same time—there appears to have been no further volcanic activity in the Newer Volcanics Province until approximately the mid-Holocene (Sherwood et al., 2004). Based on analysis of archaeological evidence of human patterns of occupation of Australia, it is likely that Indigenous people lived in the general area from before the eruption of Mt Eccles (O'Connor and Allen, 2015), however there is no strong evidence for their exploitation of the landscape prior to the mid-Holocene (Builth et al., 2008).

The Mt Eccles crater complex is an amalgam of three contiguous craters (Boutakoff, 1963), resulting in an elongate lake with large littoral areas at each end (Fig. 3.1b; Timms, 1975). The crater walls are high and steep, protecting Lake Surprise from wind disturbance (Fig. 3.1c). This limits deep mixing, resulting in a sharp boundary between the oxygenated epilimnion and the anoxic hypolimnion (Timms, 1975). The lake has no fluvial input or output, such that the hydrological balance is mainly a function of precipitation and evaporation (Barr et al., 2014), and detrital input is restricted to run-off from the crater walls and wind-blown particles. The lake water level is also maintained by some groundwater input. The lake water is hard, and slightly alkaline (Timms, 1975). The modern climate at Lake Surprise is temperate, with a mean daily temperature of 13.6 °C and mean annual precipitation of 798 mm recorded at Heywood Forestry, approximately 45 km to the west (Peel et al., 2007; BOM, 2013). Precipitation is winter-dominated, with the majority delivered by prevailing westerly and south-westerly winds that bring moist air onshore from the Southern Ocean. The area is also affected by north-easterly and north-westerly winds, especially in the warmer months (Gentilli, 1971).

The modern crater slopes are dominated by a *Eucalyptus viminalis* woodland with abundant *Acacia melanoxylon*, and ground cover is predominantly composed of bracken, with some grasses on the drier slopes (Tibby et al., 2006). The shallow water margins of the lake support a variable, but generally narrow, band of aquatic vegetation composed mainly of emergent macrophytes, but incorporating floating plants in sheltered open water (Tibby et al., 2006).

Here we present data from core LS04, which was retrieved from the deepest point of Lake Surprise in March 2004 in a contemporary water depth of approximately 10.4 m (Barr et al., 2014). The core was recovered from 1–13 m using a hand-operated Livingstone sampler, and core recovery was extended to the base of the sequence at 18.4 m using a piston sampler operated with a winch and pulley system (Builth et al., 2008). All core segments were split longitudinally, and have been stored at 4 °C since acquisition.

The sediment in the analysed section of core LS04 (9.25–18.4m) is uniformly very dark brown and very fine-grained, with few visible grains or sedimentary features. The absence of any desiccation or erosion features indicates perennial water in the lake since the onset of sedimentation. Due to the limited nature of the catchment, core LS04 therefore provides a continuous record of the surrounding vegetation, as well as pluvial, colluvial, and aeolian input to Lake Surprise.

2.2 Chronological control

A chronology for core LS04 has been defined by a total of 32 accelerator mass spectrometry (AMS) ^{14}C dates, all obtained from concentrated pollen samples. Sixteen AMS ^{14}C dates existed for Lake Surprise prior to this study (Supp. Table 3.1).

Here we report sixteen new AMS ^{14}C dates, all within the 30–10 ka BP period. The location of each sample was selected in order to optimise AMS ^{14}C dates to identify change points in sediment accumulation rate. Wet sediment samples of approximately 5–10 g were sieved to retain the 5–150 µm fraction that contained the pollen. The samples were reacted with 10 % HCl at 60 °C for 20 minutes to remove carbonates, and then with 40 % HF at room temperature overnight to remove silicate minerals. The organic matter was separated from mineral residue using LST heavy liquid with a specific gravity of 1.8. To remove humic acids, the <1.8 g/mL sample fraction was reacted with 10 % NaOH at 60°C for 30 minutes repeatedly until the supernatant was completely clear. The samples were reacted with 5 % NaOCl for five minutes at room temperature to reduce the level of organic contamination (e.g. chitin, cellulose), and then once more with 10 % HCl for 10 minutes at room

temperature. Each sample was rinsed three times with 18 MΩ Milli-Q water between each step.

The concentrated pollen samples were screened for contamination under an optical microscope, then transferred to a clean vial and dried in a 60°C oven overnight. The pollen samples were then combusted and graphitised for AMS ^{14}C analysis on the STAR accelerator mass spectrometer at the Australian Nuclear Science and Technology Organisation (Hua et al., 2001; Fink et al., 2003).

All radiocarbon ages were calibrated to calendar ages using the SH radiocarbon calibration curve (SHCal13; Hogg et al., 2013). We developed a composite age-depth model in R using the 'Bacon' software for Bayesian age modelling (Blaauw and Christen, 2011). Ages are reported as 'ka BP' – thousands of calendar years before the year 1950 (Supp. Fig. 3.1).

2.3 XRF core scanning

High-resolution elemental analyses of core LS04 were obtained using an Avaatech XRF core scanner at the Australian National University. Half-core segments were covered with 4 µm SPEX SamplePrep Ultralene film to prevent desiccation of the sediment and avoid contamination of the instrument. Measurements were acquired every 2 mm at 10 kv, with a 500 µA current and count time of 20 seconds, and with a 2 mm down-core slit size and a 12 mm across-core slit size. Only elements that were reliably detected above background levels were included in subsequent analysis (i.e. Si, S, Ca, Ti, Mn, and Fe) (Supp. Fig. 3.2).

The semi-quantitative scanning XRF count data were converted to quantitative element concentrations (Fig. 3.2) using wavelength-dispersive (WD) XRF analyses of 10 discrete sub-samples from core LS04, following the multivariate log ratio calibration method outlined by Weltje et al. (2015) and applied by Grant et al. (2017). The location for each sample was selected using Ward's method in conjunction with a Euclidean distance matrix to divide the count data into ten clusters. The data point closest to the cluster centroid was selected for sampling. The predictive power of the calibration was assessed by plotting the measured values against the values predicted by the calibration model (Supp. Fig. 3.3). High r^2 values and p-values << 0.05 for all elements indicates a robust calibration.
WD-XRF analyses were performed at the Commonwealth Scientific and Industrial Research Organisation's (CSIRO) Waite Campus. Approximately one gram of oven-dried (105°C) sample was weighed into a Pt/Au crucible with four grams of 12-22 lithium borate flux. To remove organic matter, the mixtures were slowly heated to 700°C in a furnace, held at 700°C for seven hours, and then slowly cooled overnight. Each oxidised mixture was heated

to 1050°C until completely liquefied, and then poured into a Pt/Au mould and rapidly cooled. The resulting glass discs were analysed on a PANalytical Axios Advanced WD-XRF system using the CSIRO in-house silicates calibration programme (Supp. Table 3.2).

Principal Components Analysis (PCA) was used to identify major patterns of change in the calibrated data (Fig. 3.2). The data were scaled according to variance to give each element equal importance, and the mean was subtracted from each analysis. The PCA was performed on the centred and scaled data, using the 'vegan' package (Okansen et al., 2008) in R (R Core Team, 2017). The number of principal components (PCs) that are likely to contain meaningful information was determined using a 'broken-stick' model (Bennett, 1996), which compares the variance explained by each PC with that expected from a random distribution (Fig. 3.2b). Results from the PCA are provided in Supp. Table 3.3. A principal curve was also fitted to the PCA axis scores, to isolate a single vector that describes the majority of variance in the XRF data. The principal curve was fitted using the 'analogue' package in R (Simpson, 2007; Simpson and Oksanen, 2016).

2.4 Mineral identification

Bulk mineralogy of ten samples was determined using x-ray diffractometry (XRD) performed on randomly oriented powders. The samples were dried in a freeze-drier, and lightly ground using an agate mortar and pestle. Powder diffraction patterns were collected using a Bruker D8 Advance x-ray diffractometer with a Cu-radiation source. Minerals were identified using Bruker Diffrac.Eva software and Crystallography Open Database reference patterns. Phase identification was complicated by the abundant presence of biogenic opal in all samples, particularly for low abundance phases. Interpretation of the x-ray diffractograms was therefore assisted by SEM imaging and mineral mapping of several samples. Samples for imaging were embedded in resin, manually polished, ion polished (Hitachi IM4000 Argon Ion Mill) and carbon coated. SEM analyses were performed on an FEI Teneo LoVac field emission SEM equipped with dual EDS (energy dispersive x-ray spectroscopy) detectors (Bruker XFlash Series 6), at a 13 mm working distance and 15 kV accelerating voltage. Back-scatter electron images and EDS spectra (2 µm step size, 16 ms acquisition time) for mineral mapping were collected sequentially using the FEI Maps Mineralogy software, followed by classification of the individual EDS spectra using the FEI Nanomin software. Mineral classification was achieved by comparing EDS spectra collected in the mapped area against reference spectra collected on known mineral standards. A summary of minerals identified in each sample is provided in Supp. Table 3.4, with qualitative estimates of relative mineral abundance.

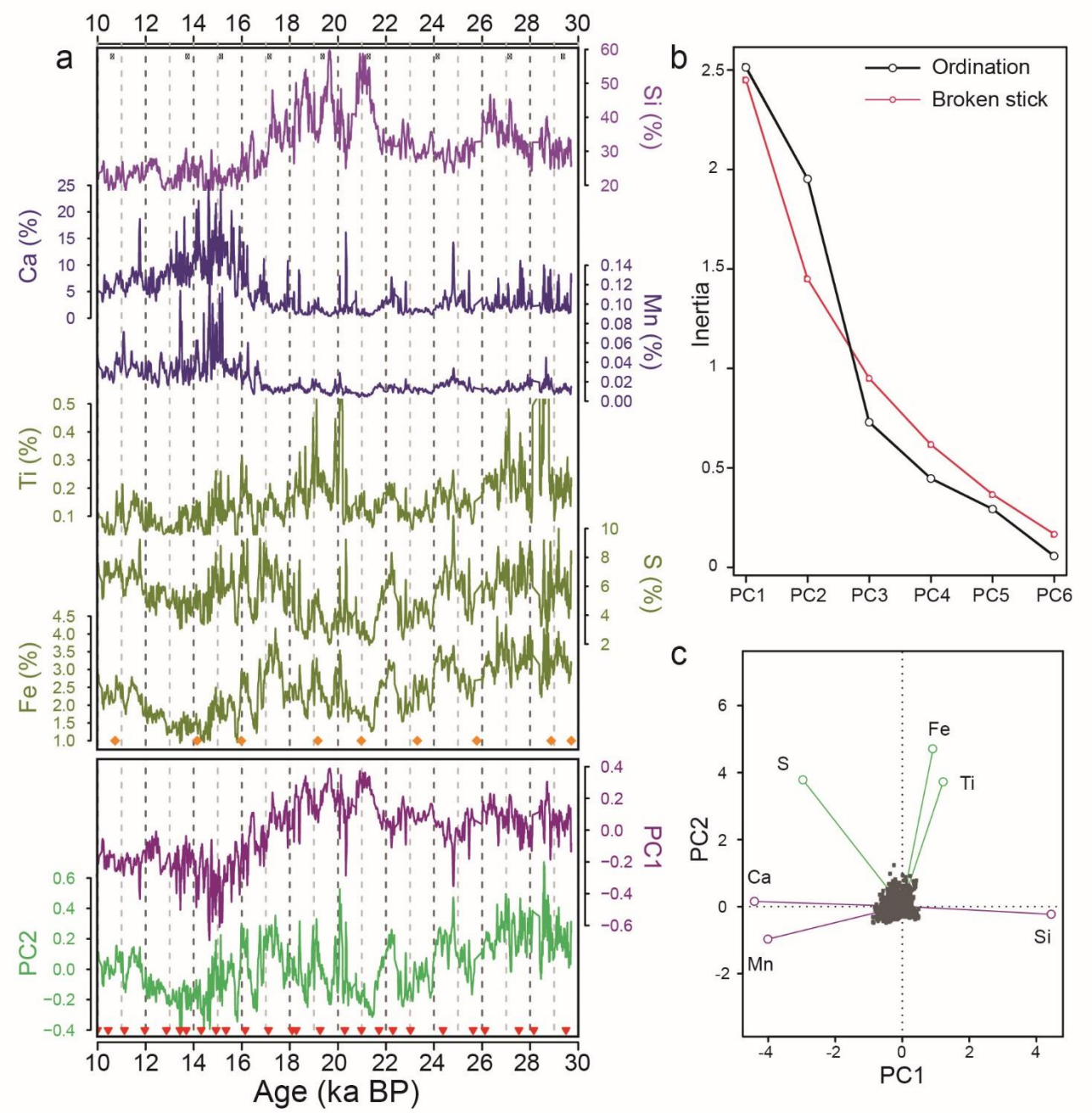

Figure 3.2. Calibrated Lake Surprise scanning XRF data, and results of the Principal Components Analysis (PCA): **a)** Upper panel: Five-point running mean of calibrated concentrations for all elements detected above background levels. Black points denote the location of WD-XRF calibration samples (Supp. Table 3.2). Orange diamonds denote the location of XRD samples (Supp. Table 3.4). Lower panel: First and second principal components of the scanning XRF data. Note strong similarity between PC1 and Si, and PC2 and Ti/Fe/S. Red triangles denote the location of age control points; **b)** Broken stick test performed on the PCA of the scanning XRF data, indicating that the first two principal components preserve interpretable information; **c)** Biplot representation of the PCA, showing the loadings of each sample (grey circles) and element (vectors) on the first two principal components.

2.5 Organic matter elemental and stable isotope ratios

Concentrations of organic carbon (total organic carbon; TOC) and nitrogen (total nitrogen; TN), and the $^{13}C/^{12}C$ isotope ratio of the bulk organic matter ($\delta^{13}C_{OM}$) were determined on samples that were freeze-dried and lightly ground in a ball mill. $\delta^{13}C_{OM}$ and TOC were

determined at 5 cm resolution from 9.25–18.4 m, and TN at 10 cm resolution. Sub-samples of approximately 2 mg were weighed into silver capsules. Carbonate was removed from the sub-samples via acid fumigation, whereby approximately 50 µL deionised water was added to each capsule, then sub-samples were acidified for four hours in concentrated hydrochloric acid vapour and dried overnight in a 40°C oven (e.g. Harris et al., 2001). Once dry, the silver capsules were placed inside larger tin capsules and crimped. The acid fumigation step was omitted for TN analyses.

All capsules were combusted in a Eurovector elemental analyser, and the evolved gas was transferred to a Nu Horizon isotope-ratio mass spectrometer. Standardisation was based on in-house glycine ($\delta^{13}C$: -31.2 ‰), glutamic acid ($\delta^{13}C$: -16.72 ‰) and triphenylamine ($\delta^{13}C$: -29.3 ‰) standards which have been calibrated against international standards. Analytical precision (1σ) for replicate measurements of the standards was ± 0.06 ‰. Each run of samples also included at least 10 % replicate analyses. $\delta^{13}C_{OM}$ is reported in per mille units relative to the Vienna Pee Dee belemnite standard (VPDB) (Supp. Fig. 3.4).

2.6 Multi-proxy synthesis

Published hydroclimate reconstructions for southern Australia and New Zealand were systematically reviewed, and are summarised in Table 3.1. We used the following four criteria to screen these records for inclusion in a regional data synthesis alongside the record from Lake Surprise: (1) the record is continuous through the majority of the period 30–10 ka BP, (2) the data have been interpreted to primarily reflect the terrestrial hydrological cycle, (3) the record is independently dated with a minimum of one date per 2000 years, and (4) the data have an average time resolution per sample of 200 years or less. In addition to our new record from Lake Surprise, two records met all criteria—a speleothem $\delta^{13}C$ record from Hollywood Cave, on the south island of New Zealand (Whittaker et al., 2011), and an XRF-derived record of Ti variation from ocean core MD03-2611, located south of South Australia (DeDeckker et al., 2012) (green circles in Fig. 3.1a). No suitable records exist for western Australia.

We used the Monte Carlo Empirical Orthogonal Function (MCEOF) approach to identify significant trends common to all records. Our method follows Anchukaitis and Tierney (2012) using code modified from Tyler et al. (2015). To maintain consistency in the chronological control, we updated each age-depth model using the 'Bacon' software in R (Blaauw and Christen, 2011). We extracted an ensemble of 1000 individual iterations from the Bayesian age-depth model for each site, and, for each iteration, each dataset was modelled using a Generalised Additive Model (GAM). This replaces the interpolation step of previous studies,

which potentially alters the variance structure of the data (Tyler et al., 2015), although we acknowledge that this is still an imperfect solution in terms of maintaining the variance structure, and will require further attention. GAMs were fitted using the Mixed GAM Computational Vehicle ('mgcv') package (Wood, 2006) in R, with model parameters estimated using the 'restricted maximum likelihood' method (Fig. 3.3a).

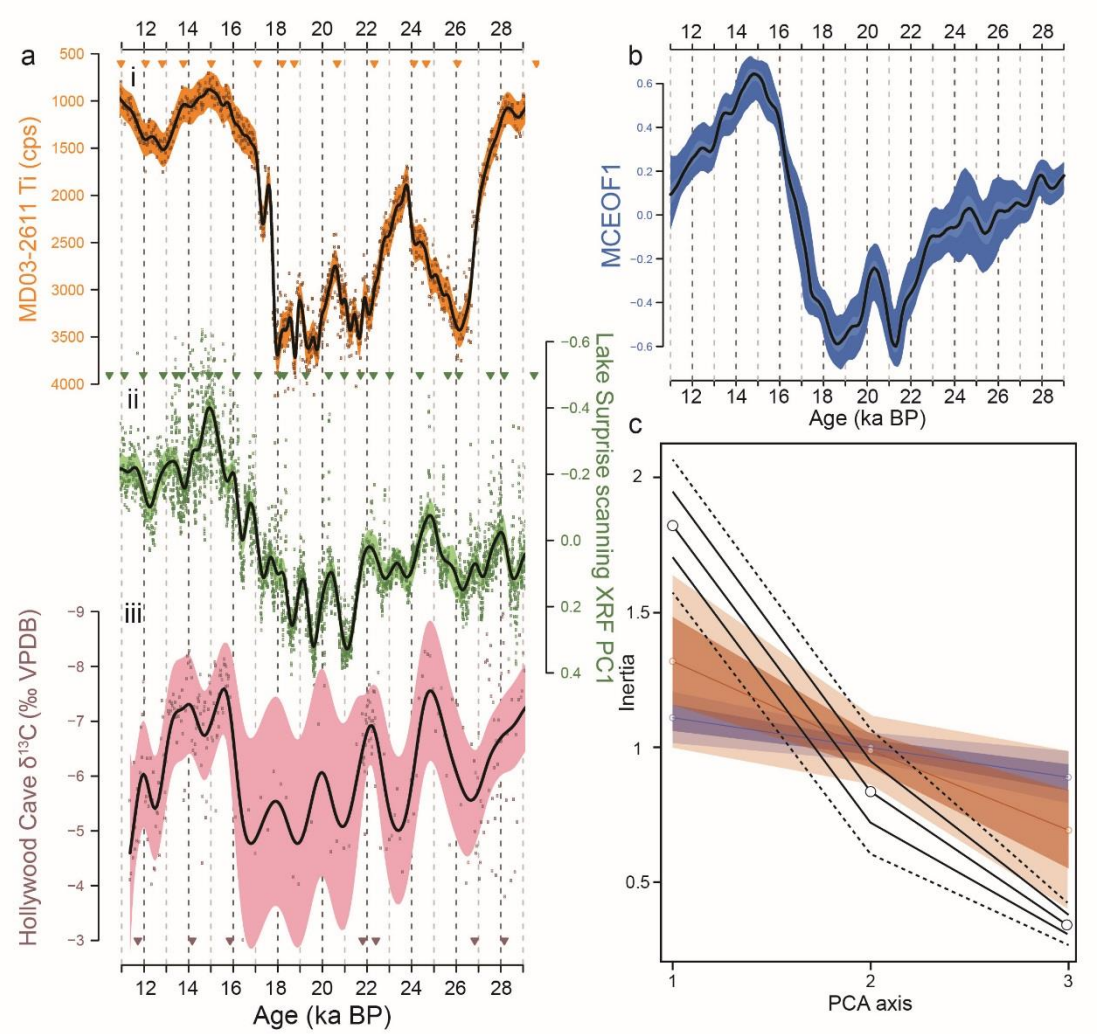

Figure 3.3. Results of the MCEOF analysis on three key hydroclimate records from the south-east Australia and NZ region: **a)** Example Generalised Additive Models (GAMs) derived for each site, using published age models. **i)** Total counts per second (cps) of Ti from core MD03-2611, located south of South Australia (Fig. 3.1). Interpreted to reflect regional aridity in southern Australia (DeDeckker et al., 2012); **ii)** Lake Surprise scanning XRF PC1 (this study); **iii)** Speleothem $\delta^{13}C$ from Hollywood Cave in New Zealand, interpreted to reflect changes in precipitation (Whittaker et al., 2011). Black line = GAM, shading = 95% confidence interval, points = individual data points, triangles = age control points on published chronologies. For input to the MCEOF analysis, a GAM was derived for each of 1000 age ensemble members extracted from a Bayesian age-depth model created using the 'Bacon' software in R (Blaauw and Christen, 2011); **b)** Results of the MCEOF analysis. Black line = median timeseries, dark and light shading = 90% and 68% confidence intervals; **c)** Variance explained by each MCEOF, compared with simulated random and red noise. White circles with a black outline represent the ensemble mean, with one and two standard deviations shown by solid and dashed black lines, respectively. The blue line shows the mean of the white noise test, with one and two standard deviations shown by the dark and light blue envelopes. The same applies for the orange envelope, but showing results of the red noise test, following Anchukaitis and Tierney (2012).

In each case, the data were resampled from the GAM at consistent intervals and truncated to the period 29 – 11 ka BP. The time period was defined by the limit of overlapping coverage of the three datasets. The data were standardised to unit variance, and PCA was performed for each age realisation. For each EOF, 68 % and 90 % confidence intervals were calculated, to provide estimates of the error in the EOFs associated with age model determination (Fig. 3.3).

Significance testing was performed using two 'Rule N' tests following Anchukaitis and Tierney (2012). For the null hypotheses, we generated 1000 sets of synthetic timeseries, using (1) Gaussian white noise, and (2) 'red noise', with parameters derived from the autoregressive structure of the component timeseries. The synthetic timeseries were then input to the PCA as described above, and the eigenvalues compared with those from the actual data (Fig. 3.3c).

2.7 Spectral analysis

To investigate characteristic timescales of variability in the data, we performed spectral analysis on the Lake Surprise XRF PC1, PC2, and $\delta^{13}C_{OM}$ timeseries, as well as each component record of the MCEOF analysis, and several other timeseries for comparison. We used Lomb-Scargle periodograms to identify frequencies present in each timeseries, as the Lomb-Scargle method may be applied to unevenly spaced timeseries, avoiding the need for an interpolation step that may introduce artificial periodicities to the data. Lomb-Scargle periodograms were computed using the 'lomb' package in R (Ruf, 1999), along with estimates of the significance ($\alpha = 0.05$) of spectral peaks (Supp. Fig. 3.5).

3 Results

3.1 Chronology

The core chronology indicates continuous sediment accumulation in Lake Surprise from ~30 ka BP until the time of coring in 2004 (Supp. Table 3.1, Supp. Fig. 3.1). All ages are shown as median radiocarbon ages with 2σ errors. The modelled sediment accumulation for the bottom section of core LS04 shows a reasonably consistent accumulation rate between 30 and 13 ka, with a decrease in accumulation rate between 25 and 23 ka BP, and peaks in the accumulation rate at 22–21 ka BP, 20–19.5 ka BP, and 17.5 ka BP. A sharp drop in accumulation rate between 13 and 10 ka BP is followed by a rapid return to higher accumulation rates.

3.2 Geochemical analyses

3.2.1 Inorganic geochemistry and mineralogy

The Avaatech XRF scans yielded interpretable data for six elements, and each has been calibrated to quantitative WD-XRF measurements (Si, S, Ca, Ti, Mn, Fe – Supp. Fig. 3.3). The elemental trends fall visually into three distinct groups, within which elements display similar stratigraphic variation: (1) Si; (2) Ca and Mn; (3) Fe, Ti and S (Fig. 3.2). Ca and Mn are mostly present only in trace concentrations, except for a broad peak between 17 and 12 ka BP which corresponds to the only core section where the calcite tests of ostracods are preserved. This is reflected in the XRD data, where calcite is abundant between 14 and 15.9 ka BP, but absent from the remainder of the samples (Supp. Table 3.4).

Si is by far the most abundant inorganic element, and is present as both quartz and biogenic opal (diatoms and sponge spicules were both identified by visual inspection of the sediment), as well as a range of silicate minerals. The x-ray diffractograms indicate that amorphous (biogenic) silica is a major component of the sediment throughout the core. However, the abundance of quartz, feldspars, and clays is relatively variable, and these minerals are likely the main contributors to downcore variability in Si, although this is difficult to quantify given that amorphous silica does not manifest as a distinct pattern in the diffractograms, but rather a diffuse ‘hump’. Moderate to abundant quartz is present in all samples from 28.8–15.9 ka BP, but subsequently decreases and is present only in trace to minor amounts between 14–8.5 ka BP. Similarly, feldspars and silt-sized illite/kaolinite aggregates are present in minor to moderate amounts from 29.7–19.1 ka BP, but were either not identified, or present only in trace amounts in younger samples.

PCA performed on the calibrated XRF data captures the two dominant trends in the first two principal components (PC1 and PC2). Both axes are significant according to the broken stick test, and summarise the majority of the variance in the dataset (Fig. 3.2, Supp. Table 3.3). PC1 explains 42% of the total variability, and is strongly dominated by Si. PC1 is relatively stable between 30 and 21 ka BP, with minor negative peaks at 24.8 and 22 ka BP (Fig. 3.2). The pattern of change during the global LGM features an increase in both variability and absolute values, with distinct negative peaks at 20 and 19 ka BP. PC1 then exhibits a gradual decline until ca. 15 ka BP, followed by a slight increase to the start of the Holocene, and then relatively stable values during the early Holocene (Fig. 3.2).

PC2 explains a further 33% of the total variance, and is strongly correlated to Ti, Fe, and S; the former two are elements that are present both in the Lake Surprise catchment, and in

Australian dust sources (DeDeckker et al., 2012; Petherick et al., 2009). The overall variability of PC2 is dominated by a cyclicity with a period of ca. 2300 years (significant at 95% confidence level; Supp. Fig. 3.5), superimposed on a slight decreasing trend from 30 to 21 ka BP, and an overall increase from 15 ka BP into the Holocene, along with a reduction in variability (Fig. 3.2).

A plot of the first and second principal components yields a 'horseshoe' shape (Fig. 3.2c). This is characteristic of a long environmental gradient in the data that is not sufficiently captured by an unconstrained ordination, but may be more accurately modelled by fitting a principal curve. The principal curve for the Lake Surprise XRF data describes 80 % of the total variance, however, the trend is near identical to PC1.

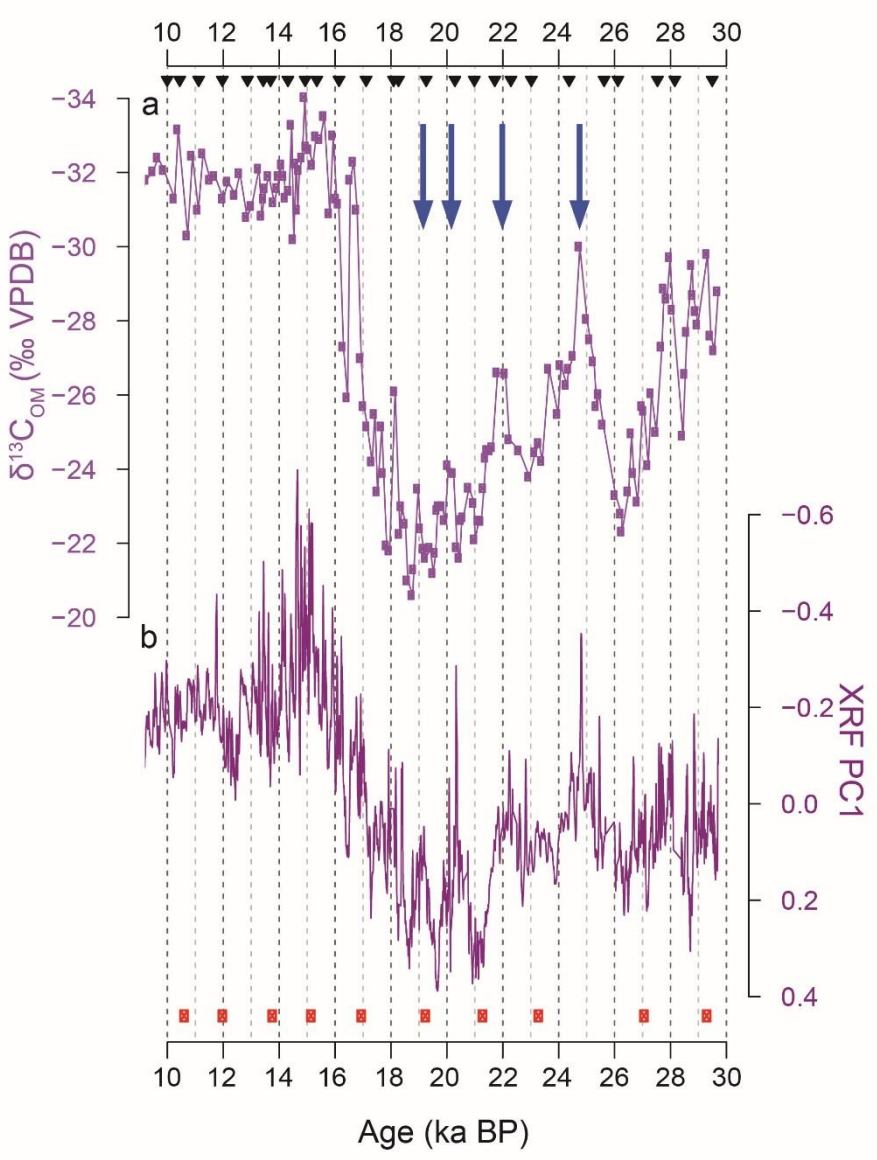

Figure 3.4. Selected data from the 30-10 ka BP geochemical record from Lake Surprise: **a**) Bulk sediment carbon isotope ratios ($\delta^{13}C_{OM}$), interpreted to reflect plant moisture stress; **b**) First principal component (PC1) of the calibrated scanning XRF dataset, interpreted to reflect aeolian deposition of Si in the lake. Blue arrows indicate periods of increased effective moisture within the relatively arid LGM. Filled triangles denote ^{14}C age control points. Red circles denote the location of XRD samples (Supp. Table 3.4).

3.2.2 Organic geochemistry

TOC concentrations in core LS04 are highly variable, with a range of 33% around a mean of 27% and median of 28%. The broad trend is characterised by fluctuations around a mean that is relatively stable between 30 and 20 ka BP, then follows a slight upward trend from 20 – 10 ka BP. Organic C:N ratios are relatively invariant, with a range of 8 around a mean and median of 18. There is no long-term trend in the mean C:N throughout the analysed section of the core (Supp. Fig. 3.4).

The $\delta^{13}C_{OM}$ is also highly variable, with a range of 13 ‰ around a mean and median of -28 ‰. $\delta^{13}C_{OM}$ increases by ~4 ‰ between 28 and 26 ka BP, then rapidly decreases to ~-30 ‰ by 25 ka BP. This is followed by an overall increase to the highest values of ~-21 ‰ at 21 – 18.5 ka BP, punctuated by distinct millennial-scale periods of lower $\delta^{13}C_{OM}$. A sharp negative shift of over 10 ‰ between 18 and 16 ka BP is interrupted by a brief return to more positive values at 16.5 ka BP. The remainder of the record from 16 – 10 ka BP features relatively stable values around -32‰, the most negative in the record (Fig. 3.4). $\delta^{13}C_{OM}$ is linearly correlated with XRF PC1 ($r^2 = 0.56$, $p << 0.05$) (Supp. Fig. 3.6).

4 Discussion

Our new high-resolution data from the sediments of Lake Surprise complement existing palaeoecological data (Builth et al., 2008), and record distinct climate variability in south-eastern Australia throughout the period from 30–10 ka BP. The highly resolved age-depth model for Lake Surprise makes it one of the most well constrained late Quaternary palaeoclimate records for southern Australia. The excellent control on the timing of climate fluctuations at Lake Surprise allows for robust inter-site comparison; both (1) regionally, to determine the geographic significance of these events, and (2) globally, to establish likely mechanisms underpinning the variability.

4.1 Interpretation of Lake Surprise geochemical data

4.1.1 XRF and mineralogical data

High-resolution core scanning is increasingly used to characterise the elemental composition of lake sediments (e.g. Hahn et al., 2014; Turner et al., 2015; Weltje et al., 2015; Burrows et al., 2016), which varies as a function of the accumulation of autochthonous and allochthonous minerals. This in turn is driven by the flux of alluvial and aeolian sediment, as well as changes in lake water chemistry. The elemental composition therefore archives various environmental and climate processes, including lake hydrological balance, exposure and inundation of littoral areas, biogeochemical cycling, catchment erosion and dust

deposition (Davies et al., 2015). These factors are difficult to deconvolve, however here we propose likely scenarios, given the specific environmental setting.

At Lake Surprise, scanning XRF PC1 is dominated by Si (Fig. 3.2c), and may therefore represent the deposition of aeolian sediment (quartz, feldspars, and clays), colluvial feldspars and clays, or biogenic opal from diatoms and sponge spicules. Diatom concentration data are currently not available for these sediments, however variation in opal peak heights on the x-ray diffractograms is not consistent with trends in XRF Si (Supp. Table 3.4, Fig. 3.2). This suggests a primary lithogenic driver of Si variability. Abundant quartz silt is associated with high Si between ~28 and 17 ka BP, and this must represent aeolian deposition, given the catchment bedrock is basaltic (Irving and Green, 1976). An aeolian source is supported by the low concentration of plagioclase and apparent absence of lithic grains, which together indicate a predominance of distally- versus locally-sourced detritus. Secondary clay minerals (kaolinite, smectite, and illite) were present in sufficient abundances to be detected via bulk powder XRD only prior to 19 ka BP, also corresponding to high Si, and the occurrence of kaolinite as discrete, silt-size aggregates indicates that it was windblown.

Comparison with regional palaeoclimate records provides support for this interpretation. Despite sampling and age uncertainties, the majority of palaeoclimate records for south-eastern Australia indicate that 30–18.5 ka BP (high Si at Lake Surprise) was generally dry relative to the deglacial (lower Si at Lake Surprise). The consequent reduction in vegetation cover probably increased sediment deflation in sediment source areas to the north-east and north-west, and this would have been supplemented by the lower sea level providing a greater potential source area on the exposed continental shelf along the path of the prevailing westerly winds (Hesse and McTainsh, 1999; Hesse and McTainsh, 2003; Petherick et al., 2013). Furthermore, PC1 follows a similar trend to two direct records of aeolian dust accumulation from eastern Australia (Supp. Fig. 3.7) (De Deckker et al., 2012; Petherick et al., 2009). We are therefore confident in the inference that at Lake Surprise, an increase in PC1 reflects increased aeolian sediment supply, potentially due to (1) reduced regional vegetation cover in source areas to the west, north-east, and north-west (depending on seasonal wind direction), and (2) lower sea level resulting in an overall greater potential sediment source area.

PC2 is dominated by the concentrations of Ti, Fe, and S (Fig. 3.2c). Ti is redox-insensitive, and accumulates in lacustrine sediments following detrital input via catchment erosion or aeolian deposition. Fe preservation in lacustrine sediments is affected both by detrital input

(bound to clay minerals, and deposited in the lake without reaction), and, to a lesser extent, by redox conditions in the lake (Davison, 1993; Davies et al., 2015). The strong correspondence of the Fe and Ti profiles (Fig. 3.2a) suggests that first-order variability in Fe at Lake Surprise relates to the former i.e. changes in lithogenic detrital input. Fe and Ti in Lake Surprise may have originated from both local and distal sources. The basalt that forms the crater walls contains Fe- and Ti-bearing minerals, including olivine, labradorite, and augite, however, windblown dust in Australia tends to be rich in goethite (Petherick et al., 2009), and may supply clay-bound Fe. According to the XRD and SEM EDS-based mineral mapping analysis, potentially Ti- and Fe-bearing minerals in the Lake Surprise sediments include clays (Fe only), and rutile and ilmenite, present as 2 – 3 µm grains. Each of these minerals may be colluvially transported from the basaltic crater walls, or wind-blown, and may therefore reflect either changes in catchment weathering and erosion, or a different mode of aeolian deposition to that preserved in PC1.

Sulphur is largely delivered to lake water via deposition of marine aerosols, and leaching from catchment soils (Davies et al., 2015), with subsequent accumulation in the lake sediments dependent on lake water chemistry. Sulphur in the Lake Surprise sediment therefore reflects (1) the amount of S being delivered to the lake, and (2) the occurrence of conditions conductive to the preservation of sulphate minerals. Regarding (1), Chivas et al. (1991) found that the majority of sulphate in modern southern and central Australian lakes is of marine origin, with comparatively little from weathering of local bedrock. This may therefore provide support to an aeolian control on PC2.

Potential mechanisms for preservation of S in the Lake Surprise sediments are rather more complex than those for its delivery. Sulphur is present in Lake Surprise as iron sulphide minerals, including pyrite (during the early last deglacial), and jarosite (abundant in one sample only, around 28.8 ka BP). Pyrite is present only in trace to minor quantities during the early last interglacial-glacial transition (LGIT), and may reflect increased supply of S to the lake due to a strengthening of the onshore south-westerly winds, which are prevalent over the modern Lake Surprise particularly during winter (Gentilli, 1971).

Jarosite is a mineral that precipitates in acidic, saline lake waters, and has been identified as an early diagenetic phase in several such settings in southern Australia (e.g. Alpers et al., 1992; Benison and Bowen, 2013). Factors that may cause the acidic conditions necessary for jarosite precipitation in lakes include the oxidation of sulphides, seepage of acidic groundwater, or large inputs of acid rain (Long et al., 1992). In each of these cases, jarosite precipitation is also dependent on evaporative concentration of constituent ions, generally

resulting in crusts or cements, but there is no evidence for these in the Lake Surprise sediments. However, jarosite (Bani et al., 2009) and schwertmannite (a metastable mineral that tends to alter to jarosite) (Ohsawa et al., 2014) have also been identified in modern volcanic lakes, where precipitation is a result of degassing of sulphur-rich gas into the lake water following eruptive activity. We therefore speculate that the unique appearance of jarosite in the Lake Surprise sediments, early in the lake's history, was the result of some similar residual degassing activity following the eruption of Mt Eccles several thousand years prior.

Sulphur is also present in Lake Surprise as gypsum, which precipitates in lake environments under evaporative conditions. There is no evidence for periods of a dry lake bed in core LS04, which was taken from the deepest part of Lake Surprise. However, minor gypsum is present in the early Holocene section of the core, when we might expect higher lake levels (Supp. Table 3.4) (Petherick et al., 2013). This is counter-intuitive, as evaporative minerals would be expected to accumulate during the driest periods in a lake's history. We suggest that this may be a result of the unusual morphology of Lake Surprise. It is possible that gypsum precipitated in the large littoral areas at either end of the lake during periods of relatively low lake level (Fig. 3.1b). When lake level rose during periods of increased moisture balance, sediment was washed down to the core site in the profundal zone. Gypsum in core LS04 may therefore signify an increase in water depth following a period of relative aridity.

Given the complex controls on the elements that load most strongly on PC2, it is difficult to confidently ascribe PC2 to a specific environmental variable. One driver that is common to all three elements, however, is westerly and south-westerly wind strength, which influences the delivery of both marine sulphate and Fe- and Ti-bearing sediment to the lake, and colluvial weathering of the crater walls. This may indicate that whilst PC1 is representative of regional sediment availability, PC2 records the local influence of changes in wind strength. Although negatively correlated with PC1, Ca and Mn are present only in trace amounts other than a broad peak between 17 and 12 ka BP (Fig. 3.2), corresponding with the only analysed section of LS04 with an accumulation of calcite ostracod tests. Ostracods are cosmopolitan organisms that occur across a wide spectrum of environmental conditions in south-eastern Australia (e.g. De Deckker, 1982; Chivas et al., 1986). The ostracod proliferation in these sediments may reflect changes in water oxygen profile, habitat availability, water chemistry, or taphonomic conditions, and will be the subject of future investigation.

4.1.2 Organic geochemical data

The $\delta^{13}C$ of bulk organic matter (OM) in a lake may have several controls, dependent in part on the OM source. The C:N ratio of OM is commonly used to separate autochthonous and allochthonous sources of OM in lakes; C:N values of OM from terrestrial and aquatic plants are typically >20 and <10, respectively (Meyers and Ishiwatari, 1993). C:N in the LS04 OM is stratigraphically stable around a mean of 18, and the aquatic/terrestrial pollen ratio is consistently low (Builth et al., 2008). These lines of evidence suggest a dominant contribution of terrestrial plants to the OM (Supp. Fig. 3.8).

Three main factors affect the $\delta^{13}C_{OM}$ of terrestrial plants: (1) the photosynthetic pathway used by the source plants, where more arid conditions favour a dominance of C_4 (less negative $\delta^{13}C$) over C_3 (more negative $\delta^{13}C$) plant types, (2) changes in stomatal conductivity in C_3 plants, where increased moisture stress results in closure of stomatal pores and reduced discrimination against ^{13}C (i.e. less negative $\delta^{13}C$), and (3) partial pressure of atmospheric CO_2 (ρCO_2), where lower ρCO_2 results in reduced discrimination against ^{13}C during photosynthesis in C_3 plants (O'Leary, 1981; Farquhar et al., 1989; Prentice et al., 2011; Schubert and Jahren, 2012; Rao et al., 2017). With respect to (3), a shift of approximately -2 ‰ in $\delta^{13}C_{OM}$ may be ascribed to the ~100 ppm rise in ρCO_2 between the LGM and the Holocene (Schubert and Jahren, 2012, 2015). This is much smaller than the deglacial shift of approximately -10 ‰ recorded at Lake Surprise (Fig. 3.4), indicating a relatively minor influence of ρCO_2 on $\delta^{13}C_{OM}$ variability. Regarding factors (1) and (2), a reduction in effective moisture results in less negative $\delta^{13}C_{OM}$ values in both cases (Stewart et al., 1995; Kohn, 2010; Prentice et al., 2011; Rao et al., 2017;).

We also acknowledge potential minor environmental impacts from (1) the local Indigenous people, and (2) fire. However, regarding (1), there is no definitive evidence for Indigenous people modifying the surrounding environmental until the mid-Holocene (Builth et al., 2008). Regarding (2), the pollen to charcoal ratio does not vary much through the record, indicating at most a minor influence of fire on the environmental variability (Builth et al., 2008). Hence, given the limited effect of glacial-interglacial atmospheric ρCO_2 and the relatively low and invariant contribution of autochthonous OM to Lake Surprise, we interpret changes in $\delta^{13}C_{OM}$ as an indirect tracer of terrestrial plant moisture stress, which is a direct response to local hydroclimate variability.

4.2 Hydroclimate change at Lake Surprise

Lake Surprise scanning XRF PC1 (interpreted to reflect increased aeolian sediment supply to Lake Surprise during periods of aridity) and $\delta^{13}C_{OM}$ (interpreted to reflect terrestrial

vegetation moisture stress) are positively correlated (Supp. Fig. 3.6), and provide a locally coherent record of changes in the hydrological cycle. This interpretation is supported by pollen data from Lake Surprise (Builth et al., 2008). Evidence for a slight increase in aeolian input to the lake from 28 – 18 ka BP coincides with relatively high $\delta^{13}C_{OM}$, and a dominance of open herbaceous grassland and semi-arid shrublands over forest or woodland. Together, these data suggest that 28 – 18 ka BP was a period of greatest aridity both at Lake Surprise and in the surrounding region. During this time, local vegetation was subject to greater moisture stress; regional pollen records clearly indicate reduced tree and shrub cover during the glacial period (e.g. Builth et al., 2008; Cook, 2009), most likely resulting in increased supply of aeolian sediment to the lake. The timing is in agreement with palaeoclimate records from northern and eastern Australia (De Deckker, 2001; Petherick et al., 2008) and New Zealand (Hellstrom et al., 1998; Suggate and Almond, 2005; Alloway et al., 2007; Newnham et al., 2007), which all record arid conditions and increased dust transport coincident with local glacial maxima in New Zealand from around 28 ka BP, significantly earlier than the global LGM (Mix et al., 2001).

Within this interval, peak aridity occurs between 21 and 18.5 ka BP, possibly representing the expression of the global LGM at Lake Surprise. However, the Lake Surprise data also record distinct millennial-scale episodes of increased effective moisture, centred on 24.8, 22, 20, and 19 ka BP (indicated by arrows on Fig. 3.4). These are reflected in reduced detrital input in conjunction with lower $\delta^{13}C_{OM}$, and are also coeval with peaks in *Eucalyptus* pollen at the expense of Asteraceae (Builth et al., 2008). In south-eastern Australia, expansion of eucalypts most likely reflects a regional increase in effective precipitation (Builth et al., 2008), and this adds weight to our interpretation of a succession of humid intervals within an arid period. The alternation of wetter and drier conditions at Lake Surprise provides further evidence that the global LGM in south-eastern Australia was not a prolonged, stable period of cold and dry conditions, but rather that the climate remained variable (Moss et al., 2013; Petherick et al., 2013; Reeves et al., 2013).

The period of increased moisture balance at 24.8 ka BP is particularly distinct, and coincides with the climate amelioration proposed for both Australia and New Zealand (Alloway et al., 2007; Newnham et al., 2007; Petherick et al., 2008; Augustinus et al., 2011), concurrent with oscillating lake levels in the Willandra region (Bowler et al., 2012) and warming in the Southern Ocean to the south of Australia (Calvo et al., 2007). The interpretation of a wetter period at 24.8 ka BP in our well-dated record provides strong support for the regional nature

of this event, indicating that it may have been a period of major environmental change at least in southern Australia.

A major deglacial shift in hydroclimate commences at 18.5 ka BP at Lake Surprise, approximately concomitant with the rapid rise in global sea level (Clark and Mix, 2002). The transition is marked in the geochemical data by reduced detrital input and a sharp reduction in plant moisture stress. This implies a rapid transition from the period of peak aridity, to relatively moist conditions at the start of the LGIT, possibly with a decreased source area for aeolian sediment. The geochemical shift precedes a more gradual transition in the palaeoecological data, from open herbaceous vegetation to Casuarinaceae woodland (Builth et al., 2008). This lag implies a delayed response of the vegetation to deglacial climate change, perhaps due to the time taken for long-lived trees to become established following a major climatic shift (Builth et al., 2008).

The transition to deglacial conditions is interrupted by a temporary return to drier conditions at 16.5 ka BP, after which the $\delta^{13}C_{OM}$ remains remarkably stable. The inorganic geochemical data continues to exhibit variability, suggesting some disparity between local conditions within the crater rim, and regional climate. Detrital input to the lake decreases to a minimum around 14.5 ka BP, signifying a period of peak moisture balance for the period 30-10 ka BP. The subsequent increase in detrital input between 14.5 – 12 ka BP implies a minor drying into a relatively stable couple of millennia at the beginning of the Holocene (Fig. 3.4).

4.3 Multi-site analysis

There is a growing demand for objective numerical approaches to inferring regional scale climate variability, through integration of multiple palaeoclimate records that have secure chronological control and high temporal resolution (Shakun and Carlson, 2010; Shanahan et al., 2015). The MCEOF method is one such approach, and incorporates the chronological uncertainty inherent in individual records. The MCEOF method has been applied to late Holocene records from Africa and southern Australia (Anchukaitis and Tierney, 2012; Tierney et al., 2013; Tyler et al., 2015), but until now has not been used for longer time periods.

The Lake Surprise record exhibits clear visual similarity with numerous high and low resolution records of climate variability from the region, but most notably with the two records that met the criteria for inclusion in the MCEOF analysis: a speleothem $\delta^{13}C$ record from the south island of New Zealand (Whittaker et al., 2011), and an XRF-derived record of Ti variation from offshore South Australia (DeDeckker et al., 2012) (Fig. 3.1 & Supp. Fig. 3.9).

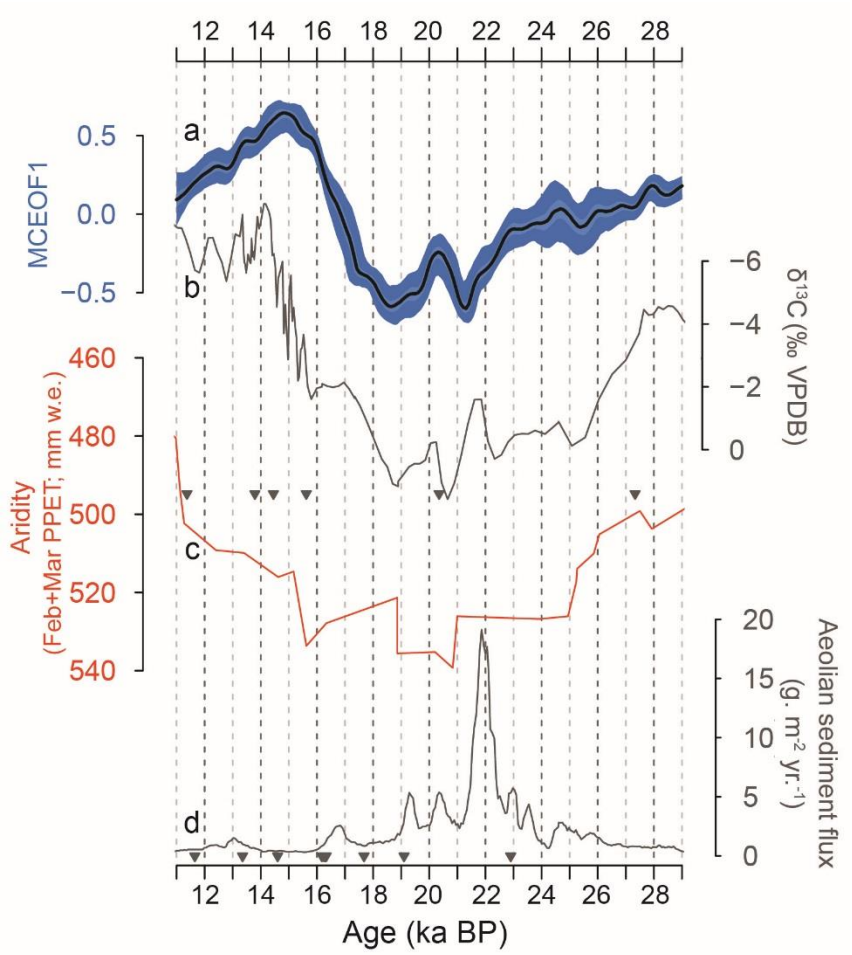

Figure 3.5. Comparison of the first Empirical Orthogonal Function (MCEOF1) of three high-resolution hydroclimate records, with Australian and New Zealand hydroclimate records not included in the MCEOF analysis: **a**) MCEOF1, representing regional hydroclimate change in the south-east Australian and NZ region, during the period from 29-11 ka BP. Black line = median timeseries, dark and light shading = 90% and 68% confidence intervals, respectively; **b**) Speleothem $\delta^{13}C$ from Mt. Arthur in New Zealand, interpreted to reflect changes in regional forest productivity (Hellstrom et al., 1998); **c**) aridity index (February and March point-potential evapotranspiration, in mm of water equivalent) for arid southern Australia, derived from the $\delta^{18}O$ of emu eggshells (Miller and Fogel, 2016); **d**) total aeolian sediment flux to Native Companion Lagoon (Petherick et al., 2009). Timeseries **a**)-**c**) oriented so that 'up' indicates a wetter climate. Location of age control points for **b**) and **d**) denoted by grey triangles.

The coherence between the records is remarkable given that the records are derived from disparate proxies spanning a longitudinal distance of over 2000 km, and points to a regional hydroclimate signal that transcends the influence of local or proxy-specific factors. The visual similarity is confirmed by the MCEOF analysis, which isolated one mode of hydroclimate variability (EOF1) that contains interpretable information, and explains 61% of the common variance (Fig. 3.3b-c). The trend described by EOF1 is broadly consistent with Australian aeolian sedimentation records (Petherick et al., 2008; Darrénougué et al., 2009; Petherick et al., 2009; Fitzsimmons et al., 2013), as well as many additional records of terrestrial Australasian hydroclimate that did not meet the criteria for inclusion in the MCEOF analysis; examples are provided in Figure 3.5. To test the robustness of the MCEOF analysis, we tried including several records that failed to meet criteria 3) or 4) i.e. chronological or sampling resolution. In each case, the first mode of variability was almost indistinguishable from EOF1, apart from some loss of finer-scale variability.

This consistency indicates that the trends and millennial-scale variability observed in the three records reflect the regional hydrological cycle in south-eastern Australasia between 30–10 ka BP, and that the trend is accurately captured by the MCEOF analysis. The pattern of change in EOF1 indicates a gradual decrease in regional moisture balance from 30 ka BP to 23.5 ka BP, with a small reversal at ca. 24.5 ka BP. The lowest values of EOF1 occur between 21.5 and 18.5 ka BP, indicating peak aridity at this time, but punctuated by a moisture peak at 21–20 ka BP. The minor 24.5 ka BP event coincides with the period of increased moisture balance identified in the Lake Surprise multi-proxy record (Fig. 3.4), but is considerably less distinct. This may reflect smoothing due to incorporation of the chronological uncertainty, especially considering that this is a period of relatively sparse age control for Hollywood Cave (Fig. 3.3aiii). Nevertheless, this provides some evidence that this wetter period within a generally arid interval may have been a regional event that lasted for up to 1500 years. This is relatively brief considering the low sediment accumulation rates characteristic of many Australian wetlands in particular, where data can only be collected at millennial-scale resolution, and is a possible reason for the event remaining largely undetected in hydroclimate records for south-eastern Australia and NZ.

The rapid deglacial switch from relatively dry to relatively wet conditions observed at Lake Surprise is maintained in EOF1, where the transition occurs between 18.5 and 16 ka BP, and is then followed by an overall decrease in moisture balance into the Holocene.

4.4 Potential drivers of regional hydroclimate

Between 29 ka BP and 16 ka BP, the EOF1 pattern of change is comparable to records of SH ocean and atmospheric circulation, within dating uncertainty (Anderson et al., 2009; De Deckker et al., 2012; Lopes dos Santos et al., 2013; Weber et al., 2014; WAIS Divide Project Members, 2015) (Fig. 3.6b–i). Relatively arid conditions in south-eastern Australia and New Zealand were associated with increased sea ice extent around Antarctica, along with reduced wind strength and cooler SSTs in the Southern Ocean south of Australia i.e. the dominant moisture source for the region. This relationship is unsurprising for coastal margin climates that are strongly subject to variations in both SST and atmospheric circulation (Mullan, 1998; Watterson, 2001). The decrease in latent heat flux from the ocean implies a weakened continental hydrological cycle (e.g. Hesse and McTainsh, 1999; Hesse and McTainsh, 2003), and consequent widespread reduction in precipitation. This is likely to have been compounded by the lower eustatic sea level (Clark and Mix, 2002), as each site lay further from the moisture source offshore.

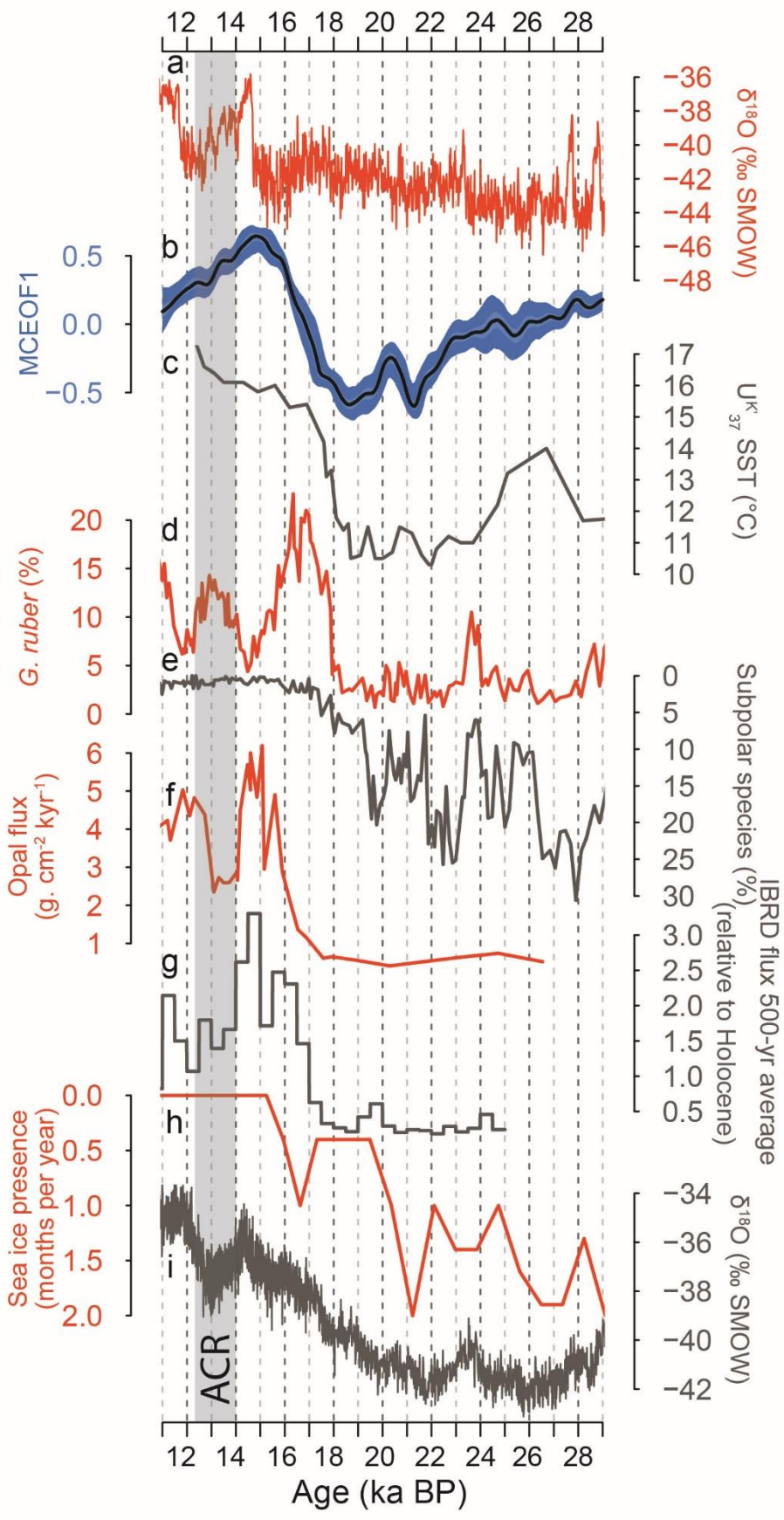

Figure 3.6. Trends in south-east Australian and NZ hydroclimate, compared with a range of global palaeoclimate records: **a**) $\delta^{18}O$ record from NGRIP ice core, indicative of mean annual surface air temperature in the NH high latitudes (WAIS Divide Project Members, 2013); **b**) Regional south-east Australian and NZ hydroclimate (this study). Black line = median timeseries, dark and light shading = 90% and 68% confidence intervals, respectively; **c**) Mean annual SST for offshore south-eastern Australia, derived using the $U^{K'}_{37}$ alkenone index (Lopes dos Santos et al., 2013); **d**-**e** Percentages of planktic foraminifera from core MD03-2611, located south of Australia near the modern location of the subtropical front: **d**) *Globigerinoides ruber*, a subtropical near-surface dweller that tracks the position of the Leeuwin Current, and **e**) subpolar species, indicative of subantarctic/Antarctic water masses, and hence the proximity of the subantarctic front (SAF) (De Deckker et al., 2012); **f**) Biogenic silica flux south of the Antarctic Polar Front, indicative of the rate of upwelling in the Southern Ocean (Anderson et al., 2009); **g**) 500-yr average of iceberg-rafted debris flux to the Scotia Sea, relative to the Holocene average. Reflects iceberg flux from the Antarctic ice sheet (Weber et al., 2014); **h**) Duration of sea-ice presence (months per year) over a core location near the LGM maximum winter sea ice extent, in the Indian sector of the Southern Ocean (Crosta et al., 2004); **i**) $\delta^{18}O$ record from WDC ice core, indicative of mean annual surface air temperature in the SH high latitudes (WAIS Divide Project Members, 2013). Records are plotted from north to south, and are oriented so that 'up' indicates a warmer/wetter climate. Approximate duration of the Antarctic Cold Reversal (ACR) highlighted by grey window.

Hesse and McTainsh (1999) and Shulmeister et al. (2016) suggested that the strength and position of the SWW (i.e. the key mechanism for the delivery of the moisture onshore) did not vary greatly over the past 25 ka BP. If this were the case, then SH SST must have had a greater influence than wind strength on regional hydroclimate during the last glacial period. This is supported by slight increases in Southern Ocean SST, coincident with southward migration of the cold subantarctic front (Fig. 3.1a) (Lopes dos Santos et al., 2013), which match the timing of the peaks in regional moisture balance inferred from EOF1, particularly at 21–20 ka BP (Fig. 3.6).

The onset of more rapid Antarctic warming post 18 ka BP was associated with i) melting of the ice sheet (Weber et al., 2014), ii) reduced sea ice extent (Crosta et al., 2004; Ferry et al., 2015), iii) poleward displacement of the cold subantarctic front (De Deckker et al., 2012), iv) increased upwelling strength in the Southern Ocean (Anderson et al., 2009), and v) a rapid increase in SST off the southern coast of Australia between 18 and 16 ka BP (Lopes dos Santos et al., 2013) (Fig. 3.6). This was matched by a switch from arid to more humid conditions in south-eastern Australia and New Zealand, implying a re-invigoration of the hydrological cycle. The Australian sites may also have been affected by the opening of the Indonesian Throughflow, and renewed delivery of warm Indian Ocean water to southern Australia by the Leeuwin Current (Fig. 3.1a, Fig. 3.6d) (Gingele et al., 2001; De Deckker et al., 2012).

The Last Glacial-Interglacial Transition (LGIT) in each of the SH high latitude records (Fig. 3.6c-i) is characterised by a reasonably uniform warming/wetting trend between 18-12 ka BP, interrupted by a two-millennia-duration event. This event coincides with the Antarctic Cold Reversal (ACR), a millennial-scale high latitude cooling event which occurred between ca. 14 and 12.2 ka BP (grey window in Fig. 3.6) (Pedro et al., 2016). The stabilisation of the Antarctic ice sheet and northward migration of cold SO fronts (Fig. 3.1) during the ACR is reflected in EOF1 as a slight increase in the rate of decline of the moisture balance, also consistent with a weakening of the SWW at this time (Anderson et al., 2009).

Following these major shifts in SH ocean-atmosphere circulation between 18 and 15 ka BP, the strength of the relationship between EOF1 and SH high latitude drivers weakens. Likewise, the rapid climate shift that characterises the start of the Holocene in many palaeoclimate records from both the SH and NH high latitudes is not present in EOF1, which instead reflects a continued gradual drying trend until at least 11 ka BP (Fig. 3.6). A parsimonious explanation may simply be that with the removal of a strong SO influence on south-east Australian and NZ climates, a more complex array of climate drivers—including

the modern drivers that originate in the equatorial regions, such as ENSO and the IOD (e.g. Ashok et al., 2007)—began to exert a stronger influence on the SH mid-latitudes.

Our data and analyses therefore suggest that the mechanisms controlling the regional hydrological cycle in south-eastern Australasia varied over multi-millennial time scales, with a strong dominant Southern Ocean influence during the last glacial giving way to more complex drivers during the deglacial and early Holocene. These conclusions are corroborated by Bayon et al. (2017), who use sediment provenance proxy data from a marine core from southern Australia to advocate a combined northern and southern high latitude control on SH subtropical climates during the last glacial period (90–20 ka BP). It is important to note, however, that any potential mechanism remains equivocal without additional high-resolution reconstructions of SST and terrestrial hydroclimate across the region.

4.5 Spectral analysis

Spectral analysis performed on the Lake Surprise data returned no persistent frequencies in the $\delta^{13}C_{OM}$ or XRF PC1 records, but yielded two significant peaks in XRF PC2, centred around 1600 and 2300 years (Supp. Fig. 3.5). A significant peak at 2300 ± 200 years is also present in the hydroclimate records from Hollywood Cave and core MD03-2611 (Supp. Fig. 3.5), both of which are well-dated, and sampled at appropriate resolution to discern cyclicity on millennial time scales. This hints at a climate oscillation that is consistent on at least a regional scale. Intriguingly, a similar periodicity is present in several late Pleistocene climate reconstructions from a diverse geographical range, including northern Australian hydroclimate (De Deckker, 2001; Denniston et al., 2013), East African hydroclimate (van Bree et al., 2014), Antarctic air temperature (WAIS Divide Project Members, 2015), and iceberg rafted debris in the Southern Ocean (Weber et al., 2014) (Supp. Fig. 3.5), as well as two low-resolution records of sea-ice presence around Antarctica, where the cycle is present but not significant (Crosta et al., 2004; Ferry et al., 2015). We acknowledge that this is only a tiny fraction of all late Pleistocene records, however due to aliasing, a signal can only be identified in records that are both well dated, and of sufficiently high resolution. However, the occurrence of this periodicity in a broad range of high-resolution records suggests that a ca. 2300 year cycle may be a real climatic feature of late Quaternary climate, but also poses the significant challenge of identifying the driver of a potentially globally coherent climate response.

One such link has previously been proposed for the persistence of a ca. 2300 year cycle throughout climate records of the Holocene. The presence this periodicity in both solar

activity and palaeoclimate proxy records has led to the suggestion that cyclical changes in solar insolation may be a contributing influence on millennial-scale climate variation in south-east Australia (McGowan et al., 2010) as well as a broad range of climatic regimes globally (e.g. Damon and Jirikowic, 1992; Engels and van Geel, 2012; Scafetta et al., 2016; Soon et al., 2014; Steinhilber et al., 2009; van Bree et al., 2014). A potential causal relationship between small changes in solar irradiance and global climate remains elusive for the Holocene (Haigh, 2007; Versteegh, 2005), and this uncertainty is amplified considering the only record of cosmogenic ^{14}C production that extends beyond the Holocene does not preserve any significant periodicity (Hughen et al., 2006). Additionally, the direct influence of solar irradiance on climate variability is likely to be small in comparison to that of ocean and atmospheric circulation on glacial-interglacial timescales, and requires amplification by internal climate processes (de Garidel-Thoron et al., 2001; Khider et al., 2014; Ogurtsov et al., 2010). Nonetheless, a persistent spectral signature across a broad range of climatic zones for at least 30,000 years does suggest a consistent external forcing, and a solar origin of the 2300-year periodicity should probably not be discounted, although we also acknowledge the possibility that the periodicity is a heterodyne of higher-frequency cycles (Clemens, 2005). This potential modulation of global millennial-scale climate variability warrants further investigation, and will require further well dated, high-resolution records of both climate, and solar activity.

5 Conclusions

1. A multi-proxy record of late Quaternary (30–10 ka BP) hydroclimate change from Lake Surprise, south-eastern Australia, is accompanied by a well-constrained age-depth model, allowing detailed comparison with existing records.
2. Quantitative high-resolution XRF data provide a record of aeolian sediment supply to the lake, whilst the carbon isotope composition of bulk organic matter reflects local terrestrial vegetation moisture stress. Together these data provide a coherent record of hydroclimate change in south-eastern Australia.
3. The onset of arid ‘LGM-like’ conditions at Lake Surprise occurred around 28 ka BP, providing further evidence that the LGM in the SH mid-latitudes may have commenced considerably earlier than the global LGM around 23 ka BP. Similarly, a period of increased moisture balance around 24.8 ka BP is coincident with similar events in Australian and New Zealand records, suggesting that this climate amelioration may have been a regional event. The combined proxy data indicate that peak aridity was reached at Lake Surprise between ~21 and 18.5 ka BP.
4. An MCEOF approach was used to extract a pattern of change (EOF1) that is common to three high-resolution, well-dated hydroclimate records from south-eastern

Australia and NZ. EOF1 incorporates the chronological uncertainty inherent in each record, and is free from site-specific idiosyncrasies. We argue that EOF1 is representative of changes in the regional hydrological cycle, and consequently explore the relationship of this pattern with potential drivers, with a higher degree of confidence than may be obtained from a traditional single-site approach.

5. Evidence for a regionally coherent early LGM is ambiguous in EOF1, as is the interval of increased moisture balance at 25–24 ka BP. However, this may be a result of smoothing due to the geochronological uncertainty in the component records. EOF1 indicates that peak aridity in south-eastern Australia and NZ occurred between ~21.5 and 18.5 ka BP.
6. Our analysis indicates that drivers of the regional hydrological cycle varied over multi-millennial time scales. At the end of the last glacial period (30–18.5 ka BP), a strong Southern Ocean influence led to cold SSTs south of Australia and NZ, resulting in a weakened terrestrial hydrological cycle, and widespread aridity. During the last glacial-interglacial transition, retreating Antarctic sea ice and a southward migration of the subantarctic front resulted in a marked decrease in Southern Ocean influence on south-eastern Australian and NZ hydroclimate, making way for more complex controls on regional hydroclimate, potentially similar to those of the modern day.
7. A ca. 2300 year periodicity that is present in climate records from a broad range of climate regimes globally is also present in the component records of the MCEOF, and may represent a solar modulation of millennial-scale climate variability. However, a mechanism for this influence remains equivocal.

6 References cited

Alloway, B.V., Lowe, D.J., Barrell, D.J.A., Newnham, R.M., Almond, P.C., Augustinus, P.C., Bertler, N.A.N., Carter, L., Litchfield, N.J., McGlone, M.S., Shulmeister, J., Vandergoes, M.J., Williams, P.W., 2007. Towards a climate event stratigraphy for New Zealand over the past 30 000 years (NZ-INTIMATE project). Journal of Quaternary Science 22, 9-35.

Alpers, C.N., Rye, R.O., Nordstrom, D.K., White, L.D., King, B.-S., 1992. Chemical, crystallographic and stable isotopic properties of alunite and jarosite from acid—Hypersaline Australian lakes. Chemical Geology 96, 203-226.

Anchukaitis, K.J., Tierney, J.E., 2012. Identifying coherent spatiotemporal modes in time-uncertain proxy paleoclimate records. Climate Dynamics 41, 1291-1306.

Anderson, R.F., Ali, S., Bradtmiller, L.I., Nielsen, S.H.H., Fleisher, M.Q., Anderson, B.E., Burckle, L.H., 2009. Wind-Driven Upwelling in the Southern Ocean and the Deglacial Rise in Atmospheric CO_2. Science 323, 1443-1448.

Ashok, K., Nakamura, H., Yamagata, T., 2007. Impacts of ENSO and Indian Ocean Dipole Events on the Southern Hemisphere Storm-Track Activity during Austral Winter. Journal of Climate 20, 3147-3163.

Augustinus, P., Cochran, U., Kattel, G., D'Costa, D., Shane, P., 2012. Late Quaternary paleolimnology of Onepoto maar, Auckland, New Zealand: Implications for the drivers of regional paleoclimate. Quaternary International 253, 18-31.

Augustinus, P., D'Costa, D., Deng, Y., Hagg, J., Shane, P., 2011. A multi-proxy record of changing environments from ca. 30 000 to 9000 cal. a BP: Onepoto maar palaeolake, Auckland, New Zealand. Journal of Quaternary Science 26, 389-401.

Ayliffe, L.K., Marianelli, P.C., Moriarty, K.C., Wells, R.T., McCulloch, M.T., Mortimer, G.E., Hellstrom, J.C., 1998. 500 ka precipitation record from southeastern Australia: Evidence for interglacial relative aridity. Geology 26, 147-150.

Bani, P., Oppenheimer, C., Varekamp, J.C., Quinou, T., Lardy, M., Carn, S., 2009. Remarkable geochemical changes and degassing at Voui crater lake, Ambae volcano, Vanuatu. Journal of Volcanology and Geothermal Research 188, 347-357.

Barr, C., Tibby, J., Gell, P., Tyler, J., Zawadzki, A., Jacobsen, G.E., 2014. Climate variability in south-eastern Australia over the last 1500 years inferred from the high-resolution diatom records of two crater lakes. Quaternary Science Reviews 95, 115-131.

Barr, C., Tibby, J., Moss, P.T., Halverson, G.P., Marshall, J.C., McGregor, G.B., Stirling, E., 2017. A 25,000-year record of environmental change from Welsby Lagoon, North Stradbroke Island, in the Australian subtropics. Quaternary International 449, 106-118.

Barrell, D.J.A., Almond, P.C., Vandergoes, M.J., Lowe, D.J., Newnham, R.M., 2013. A composite pollen-based stratotype for inter-regional evaluation of climatic events in New Zealand over the past 30,000 years (NZ-INTIMATE project). Quaternary Science Reviews 74, 4-20.

Barrows, T.T., Juggins, S., De Deckker, P., Calvo, E., Pelejero, C., 2007. Long-term sea surface temperature and climate change in the Australian–New Zealand region. Paleoceanography 22.

Barrows, T.T., Stone, J.O., Fifield, L.K., Cresswell, R.G., 2001. Late Pleistocene Glaciation of the Kosciuszko Massif, Snowy Mountains, Australia. Quaternary Research 55, 179-189.

Bayon, G., De Deckker, P., Magee, J.W., Germain, Y., Bermell, S., Tachikawa, K., Norman, M.D., 2017. Extensive wet episodes in Late Glacial Australia resulting from high-latitude forcings. Scientific Reports 7, 44-54.

Benison, K.C., Bowen, B.B., 2013. Extreme sulfur-cycling in acid brine lake environments of Western Australia. Chemical Geology 351, 154-167.

Bennett, K.D., 1996. Determination of the number of zones in a biostratigraphical sequence. New Phytologist 132, 155-170.

Blaauw, M., Christen, J.A., 2011. Flexible Paleoclimate Age-Depth Models Using an Autoregressive Gamma Process. Bayesian Analysis 6, 457-474.

Black, M.P., Mooney, S.D., Martin, H.A., 2006. A >43,000-year vegetation and fire history from Lake Baraba, New South Wales, Australia. Quaternary Science Reviews 25, 3003-3016.

Blunier, T., Brook, E.J., 2001. Timing of Millennial-Scale Climate Change in Antarctica and Greenland During the Last Glacial Period. Science 291, 109-112.

Blunier, T., Chappellaz, J., Schwander, J., Dallenbach, A., Stauffer, B., Stocker, T.F., Raynaud, D., Jouzel, J., Clausen, H.B., Hammer, C.U., Johnsen, S.J., 1998. Asynchrony of Antarctic and Greenland climate change during the last glacial period. Nature 394, 739-743.

Boutakoff, N., 1963. The Geology and Geomorphology of the Portland Area. Department of Mines Melbourne, Victoria.

Bowler, J.M., 1976. Aridity in Australia: Age, Origins and Experssion in Aeolian Landforms and Sediments. Earth-Science Reviews 12, 279-310.

Bowler, J.M., Gillespie, R., Johnston, H., Boljkovac, K., 2012. Wind v water: Glacial maximum records from the Willandra Lakes, In: Haberle, S.G., David, B. (Eds.), Peopled Landscapes: Archaeological and Biogeographic Approaches to Landscapes. ANU E-Press, Canberra, pp. 271-296.

Bowler, J.M., 1998. Willandra Lakes revisited: environmental framework for human occupation. Archaeology in Oceania 33, 120-155.

Bowler, J.M., Gillespie, R., Johnston, H., Boljkovac, K., 2012. Wind v water: Glacial maximum records from the Willandra Lakes, In: Haberle, S.G., David, B. (Eds.), Peopled Landscapes: Archaeological and Biogeographic Approaches to Landscapes. ANU E-Press, Canberra, pp. 271-296.

Bowler, J.M., Hamada, T., 1971. Late Quaternary Stratigraphy and Radiocarbon Chronology of Water Level Fluctuations in Lake Keilambete, Victoria. Nature 232, 330-332.

Bowler, J.M., Johnston, H., Olley, J.M., Prescott, J.R., Roberts, R.G., Shawcross, W., Spooner, N.A., 2003. New ages for human occupation and climatic change at Lake Mungo, Australia. Nature 421, 837.

Boyce, J., 2013. The Newer Volcanics Province of southeastern Australia: a new classification scheme and distribution map for eruption centres. Australian Journal of Earth Sciences 60, 449-462.

Broecker, W.S., 1998. Paleocean circulation during the Last Deglaciation: A bipolar seesaw? Paleoceanography 13, 119-121.

Builth, H., Kershaw, A.P., White, C., Roach, A., Hartney, L., McKenzie, M., Lewis, T., Jacobsen, G., 2008. Environmental and cultural change on the Mt Eccles lava-flow landscapes of southwest Victoria, Australia. The Holocene 18, 413-424.

Burrows, M.A., Heijnis, H., Gadd, P., Haberle, S.G., 2016. A new late Quaternary palaeohydrological record from the humid tropics of northeastern Australia. Palaeogeography, Palaeoclimatology, Palaeoecology 451, 164-182.

Cai, W., Shi, G., Cowan, T., Bi, D., Ribbe, J., 2005. The response of the Southern Annular Mode, the East Australian Current, and the southern mid-latitude ocean circulation to global warming. Geophysical Research Letters 32.

Calvo, E., Pelejero, C., De Deckker, P., Logan, G.A., 2007. Antarctic deglacial pattern in a 30 kyr record of sea surface temperature offshore South Australia. Geophysical Research Letters 34, 1-6.

Carter, L., Neil, H.L., McCave, I.N., 2000. Glacial to interglacial changes in non-carbonate and carbonate accumulation in the SW Pacific Ocean, New Zealand. Palaeogeography, Palaeoclimatology, Palaeoecology 162, 333-356.

Castañeda, I.S., Schouten, S., Pätzold, J., Lucassen, F., Kasemann, S., Kuhlmann, H., Schefuß, E., 2016. Hydroclimate variability in the Nile River Basin during the past 28,000 years. Earth and Planetary Science Letters 438, 47-56.

Chivas, A.R., Andrews, A.S., Lyons, W.B., Bird, M.I., Donnelly, T.H., 1991. Isotopic constraints on the origin of salts in Australian playas. 1. Sulphur. Palaeogeography, Palaeoclimatology, Palaeoecology 84, 309-332.

Chivas, A.R., Deckker, P.D., Shelley, J.M.G., 1986. Magnesium and strontium in non-marine ostracod shells as indicators of palaeosalinity and palaeotemperature. Hydrobiologia 143, 135-142.

Clark, P.U., Dyke, A.S., Shakun, J.D., Carlson, A.E., Clark, J., Wohlfarth, B., Mitrovica, J.X., Hostetler, S.W., McCabe, A.M., 2009. The Last Glacial Maximum. Science 325, 710-714.

Clark, P.U., Mix, A.C., 2002. Ice sheets and sea level of the Last Glacial Maximum. Quaternary Science Reviews 21, 1-7.

Clemens, S.C., 2005. Millennial-band cliate spectrum resolved and linked to centennial-scale solar cycles. Quaternary Science Reviews 24, 521-531.

Cohen, T.J., Jansen, J.D., Gliganic, L.A., Larsen, J.R., Nanson, G.C., May, J.-H., Jones, B.G., Price, D.M., 2015. Hydrological transformation coincided with megafaunal extinction in central Australia. Geology 43, 195-198.

Cohen, T.J., Nanson, G.C., Jansen, J.D., Jones, B.G., Jacobs, Z., Treble, P., Price, D.M., May, J.-H., Smith, A.M., Ayliffe, L.K., Hellstrom, J.C., 2011. Continental aridification and the vanishing of Australia's megalakes. Geology 39, 167-170.

Colhoun, E.A., Geer, G.V.D., 1986. Holocene to Middle Last Glaciation Vegetation History at Tullabardine Dam, Western Tasmania. Proceedings of the Royal Society of London. Series B, Biological Sciences 229, 177-207.

Colhoun, E.A., Pola, J.S., Barton, C.E., Heijnis, H., 1999. Late Pleistocene vegetation and climate history of Lake Selina, western Tasmania. Quaternary International 57–58, 5-23.

Colhoun, E.A., van de Geer, G., Mook, W.G., 1982. Stratigraphy, pollen analysis, and paleoclimatic interpretation of Pulbeena Swamp, northwestern Tasmania. Quaternary Research 18, 108-126.

Cook, E.J., 2009. A record of late Quaternary environments at lunette-lakes Bolac and Turangmoroke, Western Victoria, Australia, based on pollen and a range of non-pollen palynomorphs. Review of Palaeobotany and Palynology 153, 185-224.

Coventry, R.J., 1976. Abandoned shorelines and the late quaternary history of lake George, New South Wales. Journal of the Geological Society of Australia 23, 249-273.

Crosta, X., Sturm, A., Armand, L., Pichon, J.-J., 2004. Late Quaternary sea ice history in the Indian sector of the Southern Ocean as recorded by diatom assemblages. Marine Micropaleontology 50, 209-223.

D'Costa, D.M., Edney, P., Kershaw, A.P., Deckker, P.D., 1989. Late Quaternary Palaeoecology of Tower Hill, Victoria, Australia. Journal of Biogeography 16, 461-482.

D'Costa, D.M., Grindrod, J., Ogden, R., 1993. Preliminary environmental reconstructions from late Quaternary pollen and mollusc assemblages at Egg Lagoon, King Island, Bass Strait. Australian Journal of Ecology 18, 351-366.

Damon, P.E., Jirikowic, J.L., 1992. The Sun as a Low-Frequency Harmonic Oscillator. Radiocarbon 34, 199-205.

Darrénougué, N., De Deckker, P., Fitzsimmons, K.E., Norman, M.D., Reed, L., van der Kaars, S., Fallon, S., 2009. A late Pleistocene record of aeolian sedimentation in Blanche Cave, Naracoorte, South Australia. Quaternary Science Reviews 28, 2600-2615.

Davies, S.J., Lamb, H.F., Roberts, S.J., 2015. Micro-XRF Core Scanning in Palaeolimnology: Recent Developments, in: Croudace, I.W., Rothwell, R.G. (Eds.), Micro-XRF Studies of Sediment Cores: Applications of a non-destructive tool for the environmental sciences. Springer Netherlands, Dordrecht, pp. 189-226.

Davison, W., 1993. Iron and manganese in lakes. Earth-Science Reviews 34, 119-163.

De Deckker, P., 1982. Late Quaternary ostracods from Lake George, New South Wales. Alcheringa: An Australasian Journal of Palaeontology 6, 305-318.

De Deckker, P., 2001. Late Quaternary cyclic aridity in tropical Australia. Palaeogeography, Palaeoclimatology, Palaeoecology 170, 1-9.

De Deckker, P., Moros, M., Perner, K., Jansen, E., 2012. Influence of the tropics and southern westerlies on glacial interhemispheric asymmetry. Nature Geoscience 5, 266-269.

de Garidel-Thoron, T., Beaufort, L., Linsley, B.K., Dannenmann, S., 2001. Millennial-scale dynamics of the east Asian winter monsoon during the last 200,000 years. Paleoceanography 16, 491-502.

Denniston, R.F., Wyrwoll, K.-H., Asmerom, Y., Polyak, V.J., Humphreys, W.F., Cugley, J., Woods, D., LaPointe, Z., Peota, J., Greaves, E., 2013. North Atlantic forcing of millennial-scale Indo-Australian monsoon dynamics during the Last Glacial period. Quaternary Science Reviews 72, 159-168.

Deplazes, G., Luckge, A., Peterson, L.C., Timmermann, A., Hamann, Y., Hughen, K.A., Rohl, U., Laj, C., Cane, M.A., Sigman, D.M., Haug, G.H., 2013. Links between tropical rainfall and North Atlantic climate during the last glacial period. Nature Geoscience 6, 213-217.

Dodson, J., 1977. Late Quaternary palaeoecology of Wyrie Swamp, southeastern South Australia. Quaternary Research 8, 97-114.

Dodson, J., Wright, R., 1989. Humid to Arid to Subhumid Vegetation Shift on Pilliga Sandstone, Ulungra Springs, New South Wales. Quaternary Research 32, 182-192.

Dodson, J.R., 1975. Vegetation History and Water Fluctuations at Lake Leake, South-eastern South Australia. II*. 50,000 B.P. to 10,000 B.P. Australian Journal of Botany 23, 815-831.

Eaves, S.R., N. Mackintosh, A., Winckler, G., Schaefer, J.M., Alloway, B.V., Townsend, D.B., 2016. A cosmogenic 3He chronology of late Quaternary glacier fluctuations in North Island, New Zealand (39°S). Quaternary Science Reviews 132, 40-56.

Engels, S., van Geel, B., 2012. The effects of changing solar activity on climate: contributions from palaeoclimatological studies. Journal of Space Weather and Space Climate 2, A09.

Farquhar, G.D., Ehleringer, J.R., Hubick, K.T., 1989. Carbon Isotope Discrimination and Photosynthesis. Annual Review of Plant Physiology and Plant Molecular Biology 40, 503-537.

Ferry, A.J., Crosta, X., Quilty, P.G., Fink, D., Howard, W., Armand, L.K., 2015. First records of winter sea ice concentration in the southwest Pacific sector of the Southern Ocean. Paleoceanography 30, 1525-1539.

Fink, D., Hotchkis, M., Hua, Q., Jacobsen, G., Smith, A.M., Zoppi, U., Child, D., Mifsud, C., van der Gaast, H., Williams, A., Williams, M., 2004. The ANTARES AMS facility at ANSTO. Nuclear Instruments & Methods in Physics Research Section B-Beam Interactions with Materials and Atoms 223, 109-115.

Fitzsimmons, K.E., Cohen, T.J., Hesse, P.P., Jansen, J., Nanson, G.C., May, J.-H., Barrows, T.T., Haberlah, D., Hilgers, A., Kelly, T., Larsen, J., Lomax, J., Treble, P., 2013. Late Quaternary palaeoenvironmental change in the Australian drylands. Quaternary Science Reviews 74, 78-96.

Fogwill, C.J., Turney, C.S.M., Hutchinson, D.K., Taschetto, A.S., England, M.H., 2015. Obliquity Control On Southern Hemisphere Climate During The Last Glacial. Scientific Reports 5.

Forootan, E., Khandu, Awange, J.L., Schumacher, M., Anyah, R.O., van Dijk, A.I.J.M., Kusche, J., 2016. Quantifying the impacts of ENSO and IOD on rain gauge and remotely sensed precipitation products over Australia. Remote Sensing of Environment 172, 50-66.

Forbes, M.S., Bestland, E.A., Wells, R.T., Krull, E.S., 2007. Palaeoenvironmental reconstruction of the Late Pleistocene to Early Holocene Robertson Cave sedimentary deposit, Naracoorte, South Australia. Australian Journal of Earth Sciences 54, 541-559.

Galloway, R.W., 1965. Late Quaternary Climates in Australia. The Journal of Geology 73, 603-618.

Gentilli, J., 1971. Climates of Australia and New Zealand, in: Landsberg, H.E. (Ed.), World Survey of Climatology. Elsevier Publishing Company, The Netherlands.

Gillen, D., Honda, M., Chivas, A.R., Yatsevich, I., Patterson, D.B., Carr, P.F., 2010. Cosmogenic 21Ne exposure dating of young basaltic lava flows from the Newer Volcanic Province, western Victoria, Australia. Quaternary Geochronology 5, 1-9.

Gingele, F.X., De Deckker, P., Hillenbrand, C.D., 2001. Late Quaternary fluctuations of the Leeuwin Current and palaeoclimates on the adjacent land masses: clay mineral evidence. Australian Journal of Earth Sciences 48, 867-874.

Golledge, N.R., Mackintosh, A.N., Anderson, B.M., Buckley, K.M., Doughty, A.M., Barrell, D.J.A., Denton, G.H., Vandergoes, M.J., Andersen, B.G., Schaefer, J.M., 2012. Last Glacial Maximum climate in New Zealand inferred from a modelled Southern Alps icefield. Quaternary Science Reviews 46, 30-45.

Gouramanis, C., De Deckker, P., Switzer, A.D., Wilkins, D., 2013. Cross-continent comparison of high-resolution Holocene climate records from southern Australia — Deciphering the impacts of far-field teleconnections. Earth-Science Reviews 121, 55-72.

Grant, K.M., Rohling, E.J., Westerhold, T., Zabel, M., Heslop, D., Konijnendijk, T., Lourens, L., 2017. A 3 million year index for North African humidity/aridity and the implication of potential pan-African Humid periods. Quaternary Science Reviews 171, 100-118.

Hahn, A., Kliem, P., Oehlerich, M., Ohlendorf, C., Zolitschka, B., 2014. Elemental composition of the Laguna Potrok Aike sediment sequence reveals paleoclimatic changes over the past 51 ka in southern Patagonia, Argentina. Journal of Paleolimnology 52, 349-366.

Haigh, J.D., 2007. The Sun and the Earth's Climate. Living Reviews in Solar Physics 4, 2.

Håkansson, S., 1985. A review of various factors influencing the stable carbon isotope ratio of organic lake sediments by the change from glacial to post-glacial environmental conditions. Quaternary Science Reviews 4, 135-146.

Hall, A., Visbeck, M., 2002. Synchronous Variability in the Southern Hemisphere Atmosphere, Sea Ice, and Ocean Resulting from the Annular Mode. Journal of Climate 15, 3043.

Harle, K.J., 1997. Late Quaternary vegetation and climate change in southeastern Australia: palynological evidence from marine core E55-6. Palaeogeography, Palaeoclimatology, Palaeoecology 131, 465-483.

Harris, D., Horwath, W.R., van Kessel, C., 2001. Acid fumigation of soils to remove carbonates prior to total organic carbon or carbon-13 analysis. Soil Science Society of America Journal 65, 1853-1856.

Harrison, S.P., Bartlein, P.J., Prentice, I.C., 2016. What have we learnt from palaeoclimate simulations? Journal of Quaternary Science 31, 363-385.

Head, L., D'Costa, D., Edney, P., 1991. Pleistocene dates for volcanic activity in western Victoria and implications for Aboriginal occupation., In: Williams, M.A.J., De Deckker, P., Kershaw, A.P. (Eds.), The Cainozoic in Australia: a re-appraisal of the evidence. Geological Society of Australia, pp. 302-308.

Hellstrom, J., McCulloch, M., Stone, J., 1998. A Detailed 31,000-Year Record of Climate and Vegetation Change, from the Isotope Geochemistry of Two New Zealand Speleothems. Quaternary Research 50, 167-178.

Hendon, H.H., Thompson, D.W.J., Wheeler, M.C., 2007. Australian Rainfall and Surface Temperature Variations Associated with the Southern Hemisphere Annular Mode. Journal of Climate 20, 2452-2467.

Hesse, P.P., McTainsh, G.H., 1999. Last Glacial Maximum to Early Holocene Wind Strength in the Mid-latitudes of the Southern Hemisphere from Aeolian Dust in the Tasman Sea. Quaternary Research 52, 343-349.

Hesse, P.P., McTainsh, G.H., 2003. Australian dust deposits: modern processes and the Quaternary record. Quaternary Science Reviews 22, 2007-2035.

Heusser, L., Heusser, C., Kleczkowski, A., Crowhurst, S., 1999. A 50,000-yr Pollen Record from Chile of South American Millennial-Scale Climate Instability during the Last Glaciation. Quaternary Research 52, 154-158.

Hogg, A.G., Quan, H., Blackwell, P.G., Mu, N., Buck, C.E., Guilderson, T.P., Heaton, T.J., Palmer, J.G., Reimer, P.J., Reimer, R.W., Turney, C.S.M., Zimmerman, S.R.H., 2013. SHCAL13 Southern Hemisphere Calibration, 0-50,000 years cal BP. Radiocarbon 55, 1889-1903.

Hua, Q., Jacobsen, G.E., Zoppi, U., Lawson, E.M., Williams, A.A., Smith, A.M., McGann, M.J., 2001. Progress in radiocarbon target preparation at the ANTARES AMS Centre. Radiocarbon 43, 275-282.

Hughen, K., Southon, J., Lehman, S., Bertrand, C., Turnbull, J., 2006. Marine-derived 14C calibration and activity record for the past 50,000 years updated from the Cariaco Basin. Quaternary Science Reviews 25, 3216-3227.

Hughes, P.D., Gibbard, P.L., 2014. Evaluating the Concept of a Global “Last Glacial Maximum” (LGM): A Terrestrial Perspective, in: Rocha, R., Pais, J., Kullberg, J.C., Finney, S. (Eds.), STRATI 2013: First International Congress on Stratigraphy At the Cutting Edge of Stratigraphy. Springer International Publishing, Cham, pp. 943-945.

Irving, A.J., Green, D.H., 1976. Geochemistry and petrogenesis of the newer basalts of Victoria and South Australia. Journal of the Geological Society of Australia 23, 45-66.

Kattel, G.R., Augustinus, P.C., 2010. Cladoceran-inferred environmental change during the LGM to Holocene transition from Onepoto maar paleolake, Auckland, New Zealand. New Zealand Journal of Geology & Geophysics 53, 31-42.

Kelts, K., Hsü, K.J., 1978. Freshwater carbonate sedimentation, in: Lerman, A. (Ed.), Lakes: Chemistry, Geology and Physics. Springer-Verlag, Berlin Heidelberg, pp. 295-323.

Kemp, J., Rhodes, E.J., 2010. Episodic fluvial activity of inland rivers in southeastern Australia: Palaeochannel systems and terraces of the Lachlan River. Quaternary Science Reviews 29, 732-752.

Kershaw, A.P., McKenzie, G.M., Porch, N., Roberts, R.G., Brown, J., Heijnis, H., Orr, M.L., Jacobsen, G., Newall, P.R., 2007. A high-resolution record of vegetation and climate through the last glacial cycle from Caledonia Fen, southeastern highlands of Australia. Journal of Quaternary Science 22, 481-500.

Khider, D., Jackson, C.S., Stott, L.D., 2014. Assessing millennial-scale variability during the Holocene: A perspective from the western tropical Pacific. Paleoceanography 29, 143-159.

Kohn, M.J., 2010. Carbon isotope compositions of terrestrial C3 plants as indicators of (paleo)ecology and (paleo)climate. Proceedings of the National Academy of Sciences 107, 19691-19695.

Long, D.T., Fegan, N.E., McKee, J.D., Lyons, W.B., Hines, M.E., Macumber, P.G., 1992. Formation of alunite, jarosite and hydrous iron oxides in a hypersaline system: Lake Tyrrell, Victoria, Australia. Chemical Geology 96, 183-202.

Lopes dos Santos, R.A., Spooner, M.I., Barrows, T.T., De Deckker, P., Sinninghe Damsté, J.S., Schouten, S., 2013. Comparison of organic ($U^{K'}_{37}$, TEX^{H}_{86}, LDI) and faunal proxies (foraminiferal assemblages) for reconstruction of late Quaternary sea surface temperature variability from offshore southeastern Australia. Paleoceanography 28, 377-387.

Macken, A.C., McDowell, M.C., Bartholomeusz, D.N., Reed, E.H., 2013. Chronology and stratigraphy of the Wet Cave vertebrate fossil deposit, Naracoorte, and relationship to paleoclimatic conditions of the Last Glacial Cycle in south-eastern Australia. Australian Journal of Earth Sciences 60, 271-281.

Macken, A.C., Reed, E.H., 2014. Postglacial reorganization of a small-mammal paleocommunity in southern Australia reveals thresholds of change. Ecological Monographs 84, 563-577.

Mackenzie, L., Moss, P., 2017. A late Quaternary record of vegetation and climate change from Hazards Lagoon, eastern Tasmania. Quaternary International 432, 58-65.

Magee, J.W., Miller, G.H., Spooner, N.A., Questiaux, D., 2004. Continuous 150 k.y. monsoon record from Lake Eyre, Australia: Insolation-forcing implications and unexpected Holocene failure. Geology 32, 885-888.

McGlone, M.S., 2001. A late Quaternary pollen record from marine core P69, southeastern North Island, New Zealand. New Zealand Journal of Geology and Geophysics 44, 69-77.

McGowan, H.A., Marx, S.K., Soderholm, J., Denholm, J., 2010. Evidence of solar and tropical-ocean forcing of hydroclimate cycles in southeastern Australia for the past 6500 years. Geophysical Research Letters 37, L10705.

EPICA Community Members, 2006. One-to-one coupling of glacial climate variability in Greenland and Antarctica. Nature 444, 195-198.

WAIS Divide Project Members, 2015. Precise interpolar phasing of abrupt climate change during the last ice age. Nature 520, 661-665.

Meneghini, B., Simmonds, I., Smith, I.N., 2007. Association between Australian rainfall and the Southern Annular Mode. International Journal of Climatology 27, 109-121.

Bureau of Meteorology, 2013. Climate statistics for Australian locations - Heywood Forestry. Bureau of Meteorology, Commonwealth of Australia.

Meyers, P.A., Ishiwatari, R., 1993. Lacustrine organic geochemistry—an overview of indicators of organic matter sources and diagenesis in lake sediments. Organic Geochemistry 20, 867-900.

Miller, G.H., Fogel, M.L., 2016. Calibrating $\delta^{18}O$ in *Dromaius novaehollandiae* (emu) eggshell calcite as a paleo-aridity proxy for the Quaternary of Australia. Geochimica et Cosmochimica Acta 193, 1-13.

Mix, A.C., Bard, E., Schneider, R., 2001. Environmental processes of the ice age: land, oceans, glaciers (EPILOG). Quaternary Science Reviews 20, 627-657.

Moriarty, K.C., McCulloch, M.T., Wells, R.T., McDowell, M.C., 2000. Mid-Pleistocene cave fills, megafaunal remains and climate change at Naracoorte, South Australia: towards a predictive model using U-Th dating of speleothems. Palaeogeography, Palaeoclimatology, Palaeoecology 159, 113-143.

Moss, P.T., Tibby, J., Petherick, L., McGowan, H., Barr, C., 2013. Late Quaternary vegetation history of North Stradbroke Island, Queensland, eastern Australia. Quaternary Science Reviews 74, 257-272.

Mullan, A.B., 1998. Southern hemisphere sea-surface temperatures and their contemporary and lag association with New Zealand temperature and precipitation. International Journal of Climatology 18, 817-840.

Nelson, D.M., Urban, M.A., Kershaw, A.P., Hu, F.S., 2016. Late-Quaternary variation in C3 and C4 grass abundance in southeastern Australia as inferred from δ13C analysis: Assessing the roles of climate, pCO2, and fire. Quaternary Science Reviews 139, 67-76.

Newnham, R.M., Lowe, D.J., Giles, T., Alloway, B.V., 2007. Vegetation and climate of Auckland, New Zealand, since ca. 32 000 cal. yr ago: support for an extended LGM. Journal of Quaternary Science 22, 517-534.

O'Connor, J.F. and Allen, J., 2015. The process, biotic impact, and global implications of the human colonization of Sahul about 47,000 years ago. Journal of Archaeological Science 56, 73-84.

O'Leary, M.H., 1981. Carbon isotope fractionation in plants. Phytochemistry 20, 553-567.

Ogurtsov, M.G., Raspopov, O.M., Oinonen, M., Jungner, H., Lindholm, M., 2010. Possible manifestation of nonlinear effects when solar activity affects climate changes. Geomagnetism and Aeronomy 50, 15-20.

Ohsawa, S., Sugimori, K., Yamauchi, H., Koeda, T., Inaba, H., Kataoka, Y., Kagiyama, T., 2014. Brownish discoloration of the summit crater lake of Mt. Shinmoe-dake, Kirishima Volcano, Japan: volcanic–microbial coupled origin. Bulletin of Volcanology 76, 809.

Okansen, J., Kindt, R., Legendre, P., O'Hara, B., Simpson, G.L., Solymos, P., Stevens, M.H.H., Wagner, H., 2008. Vegan: Community Ecology Package.

Page, K.J., Dare-Edwards, A.J., Owens, J.W., Frazier, P.S., Kellett, J., Price, D.M., 2001. TL chronology and stratigraphy of riverine source bordering sand dunes near Wagga Wagga, New South Wales, Australia. Quaternary International 83, 187-193.

Pedro, J. B., Bostock, H. Hc., Bitz, C. M., He, F., Vandergoes, M. J., Steig, E. J., Chase, B. M., Krause, C. E., Rasmussen, S. O., Markle, B. R., Cortese, G., 2016. The spatial extent and dynamics of the Antarctic Cold Reversal. Nature Geoscience 9, 51-55.

Peel, M.C., Finlayson, B.L., McMahon, T.A., 2007. Updated world map of the Köppen-Geiger climate classification. Hydrology and Earth Sysem. Sciences 11, 1633-1644.

Pepler, A., Timbal, B., Rakich, C., Coutts-Smith, A., 2014. Indian Ocean Dipole Overrides ENSO's Influence on Cool Season Rainfall across the Eastern Seaboard of Australia. Journal of Climate 27, 3816-3826.

Pepler, A.S., Alexander, L.V., Evans, J.P., Sherwood, S.C., 2016. Zonal winds and southeast Australian rainfall in global and regional climate models. Climate Dynamics 46, 123-133.

Petherick, L.M., Moss, P.T., McGowan, H.A., 2017. An extended Last Glacial Maximum in subtropical Australia. Quaternary International 432, 1-12.

Petherick, L., Bostock, H., Cohen, T.J., Fitzsimmons, K., Tibby, J., Fletcher, M.-S., Moss, P., Reeves, J., Mooney, S., Barrows, T., Kemp, J., Jansen, J., Nanson, G., Dosseto, A., 2013. Climatic records over the past 30 ka from temperate Australia - a synthesis from the Oz-INTIMATE workgroup. Quaternary Science Reviews 74, 58-77.

Petherick, L., McGowan, H., Moss, P., 2008. Climate variability during the Last Glacial Maximum in eastern Australia: evidence of two stadials? Journal of Quaternary Science 23, 787-802.

Petherick, L.M., McGowan, H.A., Kamber, B.S., 2009. Reconstructing transport pathways for late Quaternary dust from eastern Australia using the composition of trace elements of long traveled dusts. Geomorphology 105, 67-79.

Pezza, A.B., Durrant, T., Simmonds, I., Smith, I., 2008. Southern Hemisphere Synoptic Behavior in Extreme Phases of SAM, ENSO, Sea Ice Extent, and Southern Australia Rainfall. Journal of Climate 21, 5566-5584.

Prentice, I.C., Cleator, S.F., Huang, Y.H., Harrison, S.P., Roulstone, I., 2017. Reconstructing ice-age palaeoclimates: Quantifying low-CO_2 effects on plants. Global and Planetary Change 149, 166-176.

Prentice, I.C., Meng, T., Wang, H., Harrison, S.P., Ni, J., Wang, G., 2011. Evidence of a universal scaling relationship for leaf CO_2 drawdown along an aridity gradient. New Phytologist 190, 169-180.

Putnam, A.E., Schaefer, J.M., Denton, G.H., Barrell, D.J.A., Birkel, S.D., Andersen, B.G., Kaplan, M.R., Finkel, R.C., Schwartz, R., Doughty, A.M., 2013. The Last Glacial Maximum at 44°S documented by a ^{10}Be moraine chronology at Lake Ohau, Southern Alps of New Zealand. Quaternary Science Reviews 62, 114-141.

R Core Team, 2017. R: A language and environment for statistical computing. R Foundation for Statistical Computing, Vienna, Austria.

Rao, Z., Guo, W., Cao, J., Shi, F., Jiang, H., Li, C., 2017. Relationship between the stable carbon isotopic composition of modern plants and surface soils and climate: A global review. Earth-Science Reviews 165, 110-119.

Reeves, J.M., Barrows, T.T., Cohen, T.J., Kiem, A.S., Bostock, H.C., Fitzsimmons, K.E., Jansen, J.D., Kemp, J., Krause, C., Petherick, L., Phipps, S.J., Members, O.-I., 2013. Climate variability over the last 35,000 years recorded in marine and terrestrial archives in the Australian region: an OZ-INTIMATE compilation. Quaternary Science Reviews 74, 21-34.

Risbey, J.S., Pook, M.J., McIntosh, P.C., Wheeler, M.C., Hendon, H.H., 2009. On the Remote Drivers of Rainfall Variability in Australia. Monthly Weather Review 137, 3233-3253.

Robbie, A., Martin, H.A., 2007. The History of the Vegetation from the Last Glacial Maximum at Mountain Lagoon, Blue Mountains, New South Wales. Proceedings of the Linnean Society of New South Wales 128, 57-80.

Ruf, T., 1999. The Lomb-Scargle Periodogram in Biological Rhythm Research: Analysis of Incomplete and Unequally Spaced Time-Series. Biological Rhythm Research 30, 178 - 201.

Sandiford, A., Horrocks, M., Newnham, R., Ogden, J., Alloway, B., 2002. Environmental change during the last glacial maximum (c. 25 000-c. 16 500 years BP) at Mt Richmond, Auckland Isthmus, New Zealand. Journal of the Royal Society of New Zealand 32, 155-167.

Sandiford, A., Newnham, R., Alloway, B., Ogden, J., 2003. A 28 000–7600 cal yr BP pollen record of vegetation and climate change from Pukaki Crater, northern New Zealand. Palaeogeography, Palaeoclimatology, Palaeoecology 201, 235-247.

Scafetta, N., Milani, F., Bianchini, A., Ortolani, S., 2016. On the astronomical origin of the Hallstatt oscillation found in radiocarbon and climate records throughout the Holocene. Earth-Science Reviews 162, 24-43.

Schubert, B.A., Jahren, A.H., 2012. The effect of atmospheric CO_2 concentration on carbon isotope fractionation in C_3 land plants. Geochimica et Cosmochimica Acta 96, 29-43.

Schubert, B.A., Jahren, A.H., 2015. Global increase in plant carbon isotope fractionation following the Last Glacial Maximum caused by increase in atmospheric pCO_2. Geology 43, 435-438.

Shakun, J.D., Burns, S.J., Fleitmann, D., Kramers, J., Matter, A., Al-Subary, A., 2007. A high-resolution, absolute-dated deglacial speleothem record of Indian Ocean climate from Socotra Island, Yemen. Earth and Planetary Science Letters 259, 442-456.

Shakun, J.D., Carlson, A.E., 2010. A global perspective on Last Glacial Maximum to Holocene climate change. Quaternary Science Reviews 29, 1801-1816.

Shanahan, T.M., McKay, N.P., Hughen, K.A., Overpeck, J.T., Otto-Bliesner, B., Heil, C.W., King, J., Scholz, C.A., Peck, J., 2015. The time-transgressive termination of the African Humid Period. Nature Geoscience 8, 140-144.

Sherwood, J, Oyston, B. and Kershaw, A.P., 2004. The age and contemporary environments of Tower Hill volcano, southwest Victoria, Australia. Proceedings of the Royal Society of Victoria 116, 71-78.

Shulmeister, J., Kemp, J., Fitzsimmons, K.E., Gontz, A., 2016. Constant wind regimes during the Last Glacial Maximum and early Holocene: evidence from Little Llangothlin Lagoon, New England Tablelands, eastern Australia. Climate of the Past 12, 1435-1444.

Shulmeister, J., McLea, W.L., Singer, C., McKay, R.M., Hosie, C., 2003. Late Quaternary pollen records from the Lower Cobb Valley and adjacent areas, North-West Nelson, New Zealand. New Zealand Journal of Botany 41, 503-533.

Simpson, G.L., 2007. Analogue Methods in Palaeoecology: Using the analogue Package. 2007 22, 29.

Simpson, G.L., Oksanen, J., 2016. analogue: Analogue matching and Modern Analogue Technique transfer function models, R package version 0.17-0 ed.

Singh, G., Geissler, E.A., 1985. Late Cainozoic History of Vegetation, Fire, Lake Levels and Climate, at Lake George, New South Wales, Australia. Philosophical Transactions of the Royal Society of London. B, Biological Sciences 311, 379-447.

Singh, G., Luly, J., 1991. Changes in vegetation and seasonal climate since the last full glacial at Lake Frome, South Australia. Palaeogeography, Palaeoclimatology, Palaeoecology 84, 75-86.

Singh, G., Opdyke, N.D., Bowler, J.M., 1981. Late Cainozoic stratigraphy, palaeomagnetic chronology and vegetational history from Lake George, N.S.W. Journal of the Geological Society of Australia 28, 435-452.

Soon, W., Velasco Herrera, V.M., Selvaraj, K., Traversi, R., Usoskin, I., Chen, C.-T.A., Lou, J.-Y., Kao, S.-J., Carter, R.M., Pipin, V., Severi, M., Becagli, S., 2014. A review of Holocene solar-linked climatic variation on centennial to millennial timescales: Physical processes, interpretative frameworks and a new multiple cross-wavelet transform algorithm. Earth-Science Reviews 134, 1-15.

Steinhilber, F., Beer, J., Fröhlich, C., 2009. Total solar irradiance during the Holocene. Geophysical Research Letters 36, L19704.

Stewart, G.R., Turnbull, M.H., Schmidt, S., Erskine, P.D., 1995. ^{13}C Natural Abundance in Plant Communities Along a Rainfall Gradient: a Biological Integrator of Water Availability. Functional Plant Biology 22, 51-55.

Stone, T., 2006. Last glacial cycle hydrological change at Lake Tyrrell, southeast Australia. Quaternary Research 66, 176-181.

Suggate, R.P., Almond, P.C., 2005. The Last Glacial Maximum (LGM) in western South Island, New Zealand: implications for the global LGM and MIS 2. Quaternary Science Reviews 24, 1923-1940.

Sweller, S., Martin, H.A., 2001. A 40,000 year vegetation history and climatic interpretations of Burraga Swamp, Barrington Tops, New South Wales. Quaternary International 83, 233-244.

Thomas, Z.A., 2016. Using natural archives to detect climate and environmental tipping points in the Earth System. Quatern Sci Rev 152, 60-71.

Tibby, J., Kershaw, A.P., Builth, H., Philibert, A., White, C., 2006. Environmental Change and Variability in South-western Victoria: Changing Constraints and Opportunities for Occupation and Land Use, in: David, B., Barker, B., McNiven, I.J. (Eds.), The Social Archaeology of Australian Indigenous Societies. Aboriginal Studies Press, Canberra, pp. 254-269.

Tierney, J.E., Russell, J.M., Huang, Y., Damsté, J.S.S., Hopmans, E.C., Cohen, A.S., 2008. Northern Hemisphere Controls on Tropical Southeast African Climate during the Past 60,000 Years. Science 322, 252-255.

Tierney, J.E., Smerdon, J.E., Anchukaitis, K.J., Seager, R., 2013. Multidecadal variability in East African hydroclimate controlled by the Indian Ocean. Nature 493, 389-392.

Timms, B.V., 1975. Basic Limnology of Two Crater Lakes in Western Victoria. Proceedings of the Royal Society of Victoria 87, 159-166.

Treble, P.C., Baker, A., Ayliffe, L.K., Cohen, T.C., Hellstrom, J.C., Gagan, M.K., Frisia, S., Drysdale, R.N., Griffiths, A.D., Borsato, A., 2016. Hydroclimate of the Last Glacial Maximum and deglaciation in southern Australia's arid margin interpreted from speleothem records (23-15 ka). Climate of the Past Discussions 2016, 1-43.

Turner, J.N., Holmes, N., Davis, S.R., Leng, M.J., Langdon, C., Scaife, R.G., 2015. A multiproxy (micro-XRF, pollen, chironomid and stable isotope) lake sediment record for the Lateglacial to Holocene transition from Thomastown Bog, Ireland. Journal of Quaternary Science 30, 514-528.

Turney, C.S.M., 1999. Lacustrine Bulk Organic $\delta^{13}C$ in the British Isles during the Last Glacial-Holocene Transition (14-9 ka ^{14}C BP). Arctic, Antarctic, and Alpine Research 31, 71-81.

Turney, C.S.M., Haberle, S., Fink, D., Kershaw, A.P., Barbetti, M., Barrows, T.T., Black, M., Cohen, T.J., Corrège, T., Hesse, P.P., Hua, Q., Johnston, R., Morgan, V., Moss, P., Nanson, G., van Ommen, T., Rule, S., Williams, N.J., Zhao, J.X., D'Costa, D., Feng, Y.X., Gagan, M., Mooney, S., Xia, Q., 2006. Integration of ice-core, marine and terrestrial records for the Australian Last Glacial Maximum and Termination: a contribution from the OZ INTIMATE group. Journal of Quaternary Science 21, 751-761.

Tyler, J.J., Mills, K., Barr, C., Sniderman, J.M.K., Gell, P.A., Karoly, D.J., 2015. Identifying coherent patterns of environmental change between multiple, multivariate records: an application to four 1000-year diatom records from Victoria, Australia. Quaternary Science Reviews 119, 94-105.

Ummenhofer, C.C., England, M.H., McIntosh, P.C., Meyers, G.A., Pook, M.J., Risbey, J.S., Gupta, A.S., Taschetto, A.S., 2009. What causes southeast Australia's worst droughts? Geophysical Research Letters 36.

van Bree, L.G.J., Rijpstra, W.I.C., Cocquyt, C., Al-Dhabi, N.A., Verschuren, D., Sinninghe Damsté, J.S., de Leeuw, J.W., 2014. Origin and palaeoenvironmental significance of C25 and C27 n-alk-1-enes in a 25,000-year lake-sedimentary record from equatorial East Africa. Geochimica et Cosmochimica Acta 145, 89-102.

Vandergoes, M.J., Newnham, R.M., Denton, G.H., Blaauw, M., Barrell, D.J.A., 2013. The anatomy of Last Glacial Maximum climate variations in south Westland, New Zealand, derived from pollen records. Quaternary Science Reviews 74, 215-229.

Vandergoes, M.J., Newnham, R.M., Preusser, F., Hendy, C.H., Lowell, T.V., Fitzsimons, S.J., Hogg, A.G., Kasper, H.U., Schluchter, C., 2005. Regional insolation forcing of late Quaternary climate change in the Southern Hemisphere. Nature 436, 242-245.

Versteegh, G.J.M., 2005. Solar Forcing of Climate. 2: Evidence from the Past. Space Science Reviews 120, 243-286.

Watterson, I.G., 2001. Wind-Induced Rainfall and Surface Temperature Anomalies in the Australian Region. Journal of Climate 14, 1901.

Weber, M.E., Clark, P.U., Kuhn, G., Timmermann, A., Sprenk, D., Gladstone, R., Zhang, X., Lohmann, G., Menviel, L., Chikamoto, M.O., Friedrich, T., Ohlwein, C., 2014. Millennial-scale variability in Antarctic ice-sheet discharge during the last deglaciation. Nature 510, 134-138.

Weltje, G.J., Bloemsma, M.R., Tjallingii, R., Heslop, D., Röhl, U., Croudace, I.W., 2015. Prediction of Geochemical Composition from XRF Core Scanner Data: A New Multivariate Approach Including Automatic Selection of Calibration Samples and Quantification of Uncertainties, in: Croudace, I.W., Rothwell, R.G. (Eds.), Micro-XRF Studies of Sediment Cores. Springer Netherlands, pp. 507-534.

Whittaker, T.E., Hendy, C.H., Hellstrom, J.C., 2011. Abrupt millennial-scale changes in intensity of Southern Hemisphere westerly winds during marine isotope stages 2–4. Geology 39, 455-458.

Williams, A.A.J., Stone, R.C., 2009. An assessment of relationships between the Australian subtropical ridge, rainfall variability, and high-latitude circulation patterns. International Journal of Climatology 29, 691-709.

Williams, N.J., Harle, K.J., Gale, S.J., Heijnis, H., 2006. The vegetation history of the last glacial–interglacial cycle in eastern New South Wales, Australia. Journal of Quaternary Science 21, 735-750.

Wood, S.N., 2006. Generalized Additive Models: An Introduction with R. Chapman and Hall/CRC Boca Raton, Florida.

Wright, I.C., McGlone, M.S., Nelson, C.S., Pillans, B.J., 1995. An integrated Late Quaternary (Stage 3 to Present-day) paleoclimate and paleoceanographic record from offshore northern New Zealand. Quaternary Research 44, 283-293.

Supporting information for Chapter Three

Millennial-scale variability in south-east Australian hydroclimate between 30,000 and 10,000 years ago

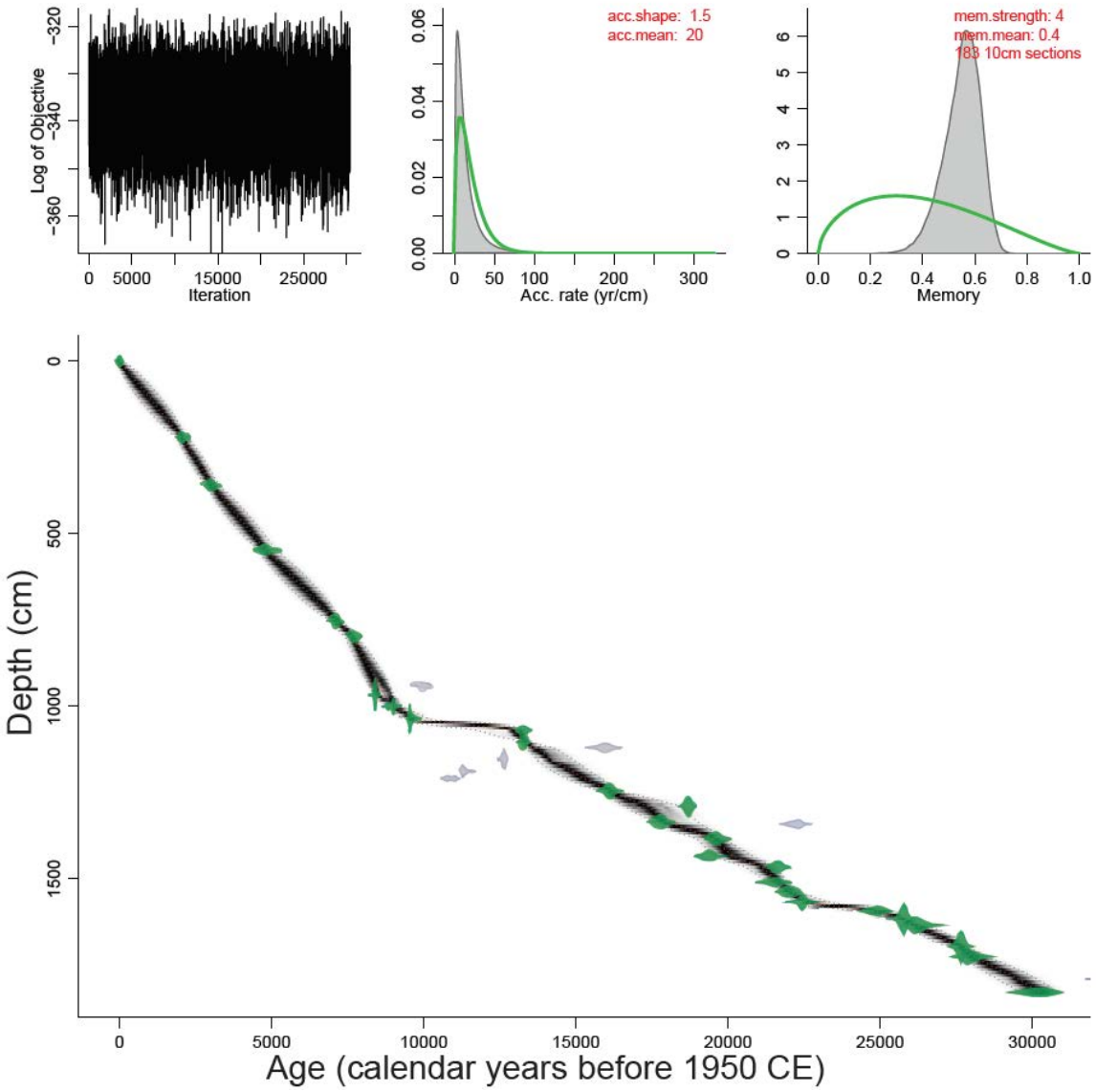

Supplementary Figure 3.1. Age-depth model for Lake Surprise, created in the 'Bacon' software in R (Blaauw and Christen, 2011), using 32 radiocarbon (^{14}C) analyses of concentrated pollen samples (Supp. Table 3.1). The model was derived from ^{14}C analyses coloured in green; the remained were identified as outliers, and excluded from the model. All ^{14}C dates were calibrated to SHCal13 (Hogg et al., 2013).

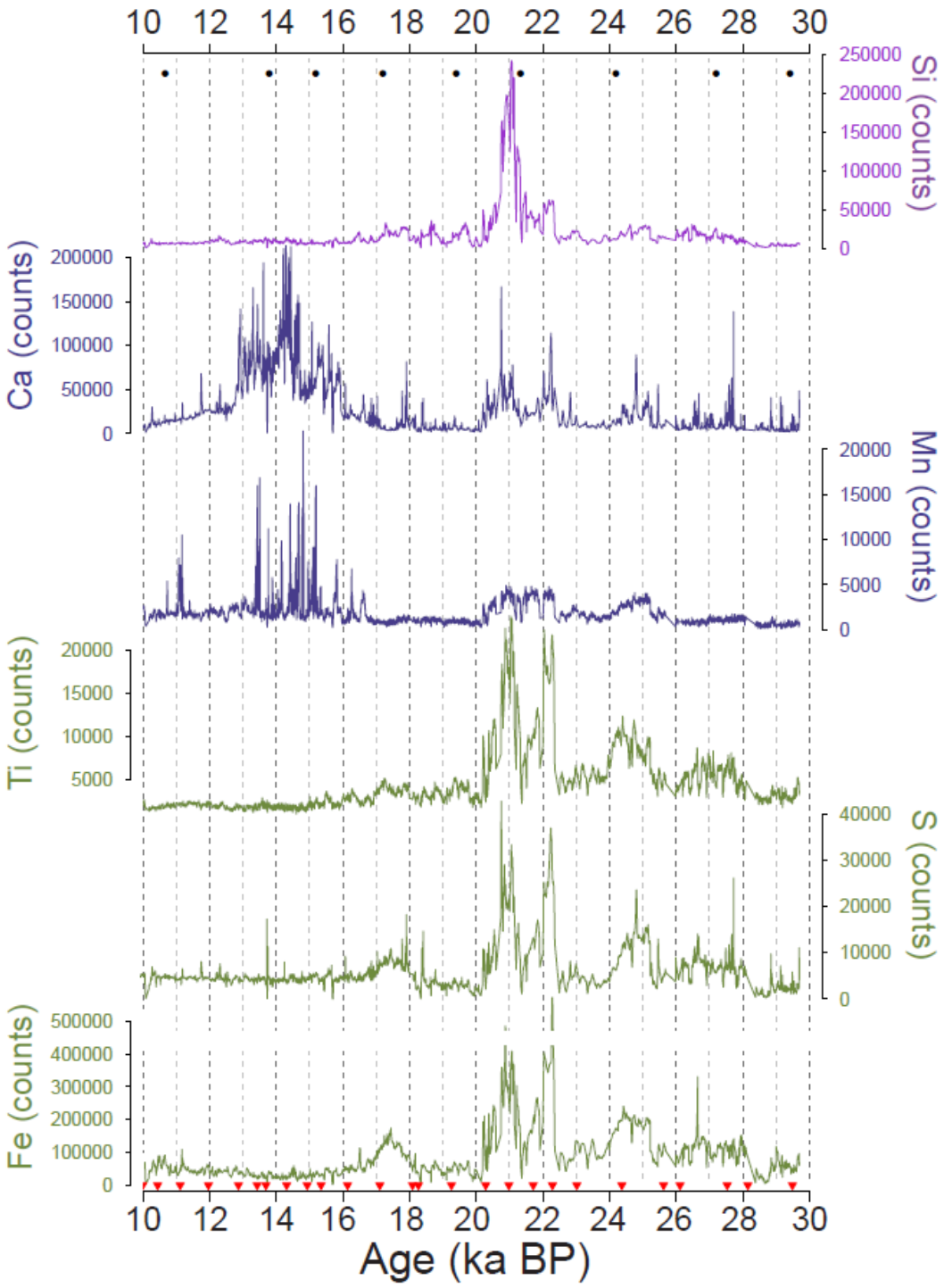

Supplementary Figure 3.2. Lake Surprise scanning XRF data, presented as raw counts. Black points denote the location of WD-XRF calibration samples (Supp. Table 3.2). Red triangles denote the location of age control points.

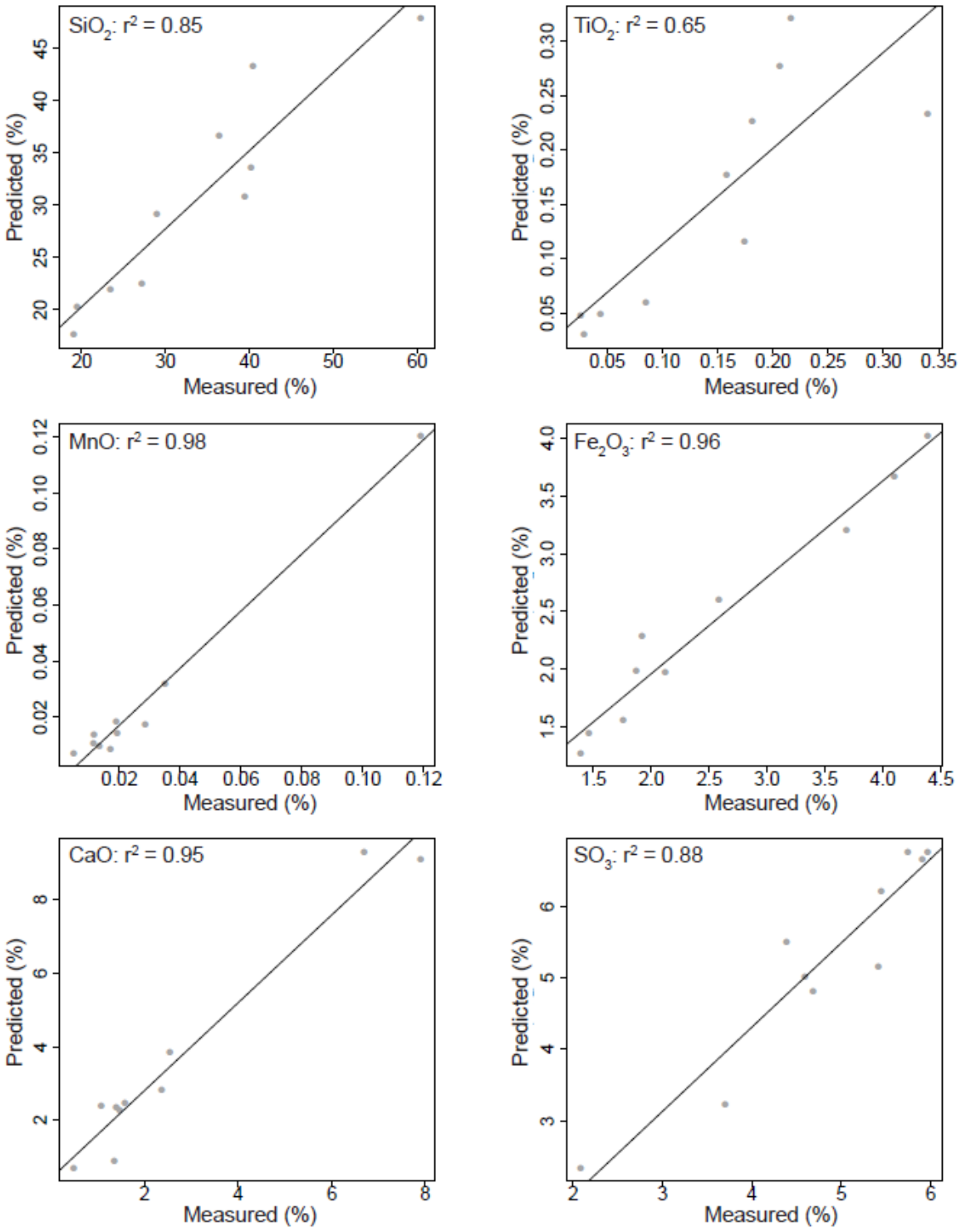

Supplementary Figure 3.3. Measured versus predicted element concentrations for the Lake Surprise scanning and WD-XRF data, based on the multivariate log ratio calibration model of Weltje et al. (2015).

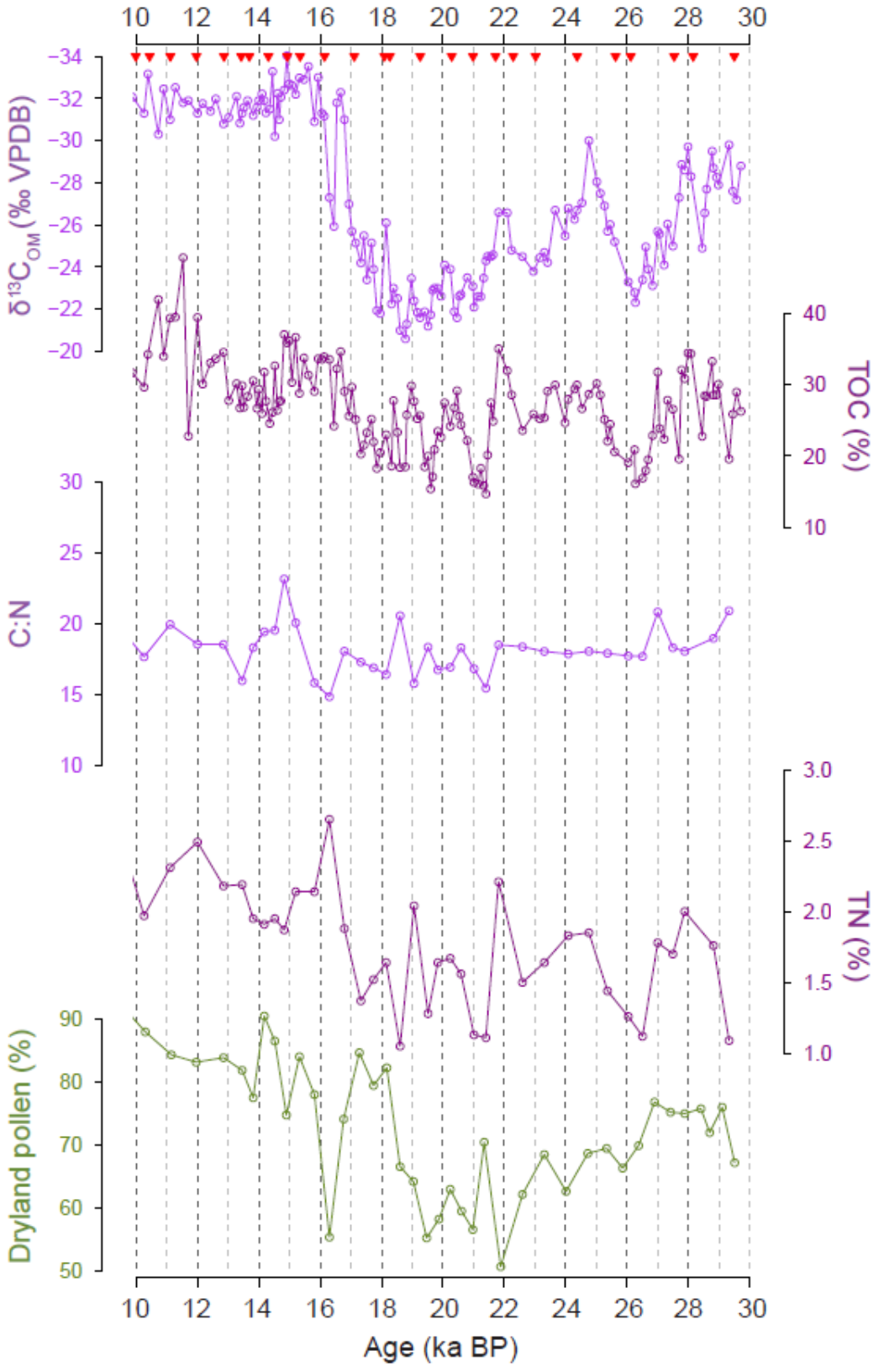

Supplementary Figure 3.4. All new organic geochemical data for Lake Surprise (purple), along with the percentage of dryland pollen (green) (Builth et al., 2008). Filled triangles denote ^{14}C age control points. TOC = total organic carbon, TN = total nitrogen.

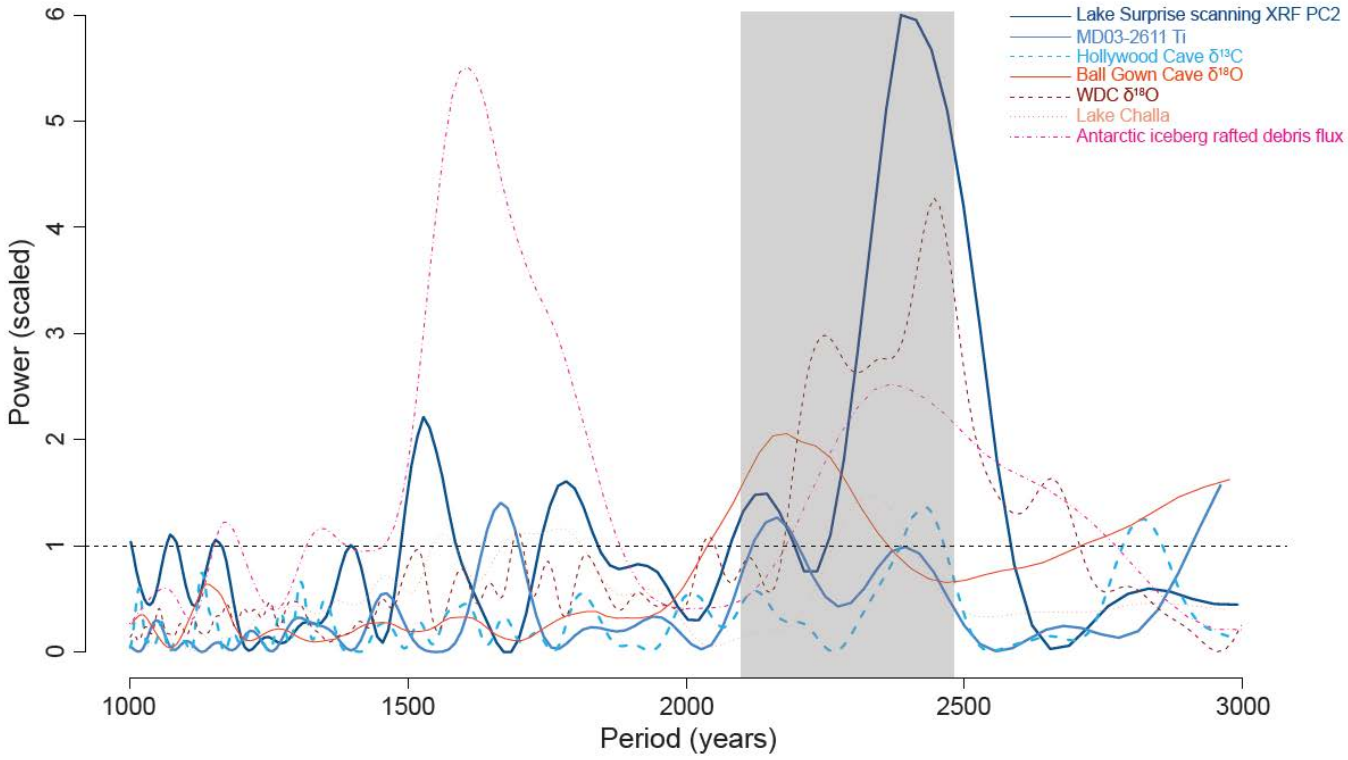

Supplementary Figure 3.5. Lomb-Scargle periodograms for various timeseries, computed using the 'lomb' package in R (Ruf, 1999). Timeseries included in the MCEOF analysis are shown in cool colours; the remainder in warm colours. Each periodograms has been scaled by 95% confidence level to facilitate comparison i.e. all peaks above the horizontal dashed line are considered significant. Grey window highlights a window within which each timeseries preserves a significant period i.e. between 2150 and 2470 years.

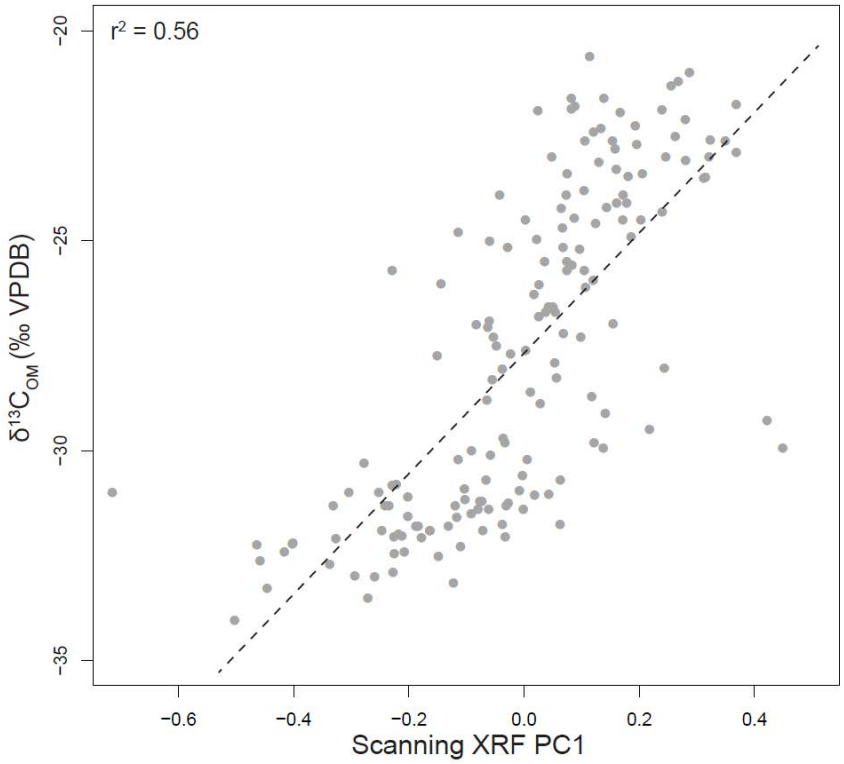

Supplementary Figure 3.6. Comparison of two Lake Surprise datasets: the first principal component (PC1) of the calibrated scanning XRF dataset, and the bulk sediment carbon isotope ratios ($\delta^{13}C_{OM}$). PC1 was interpolated to the depth scale of the $\delta^{13}C_{OM}$ data.

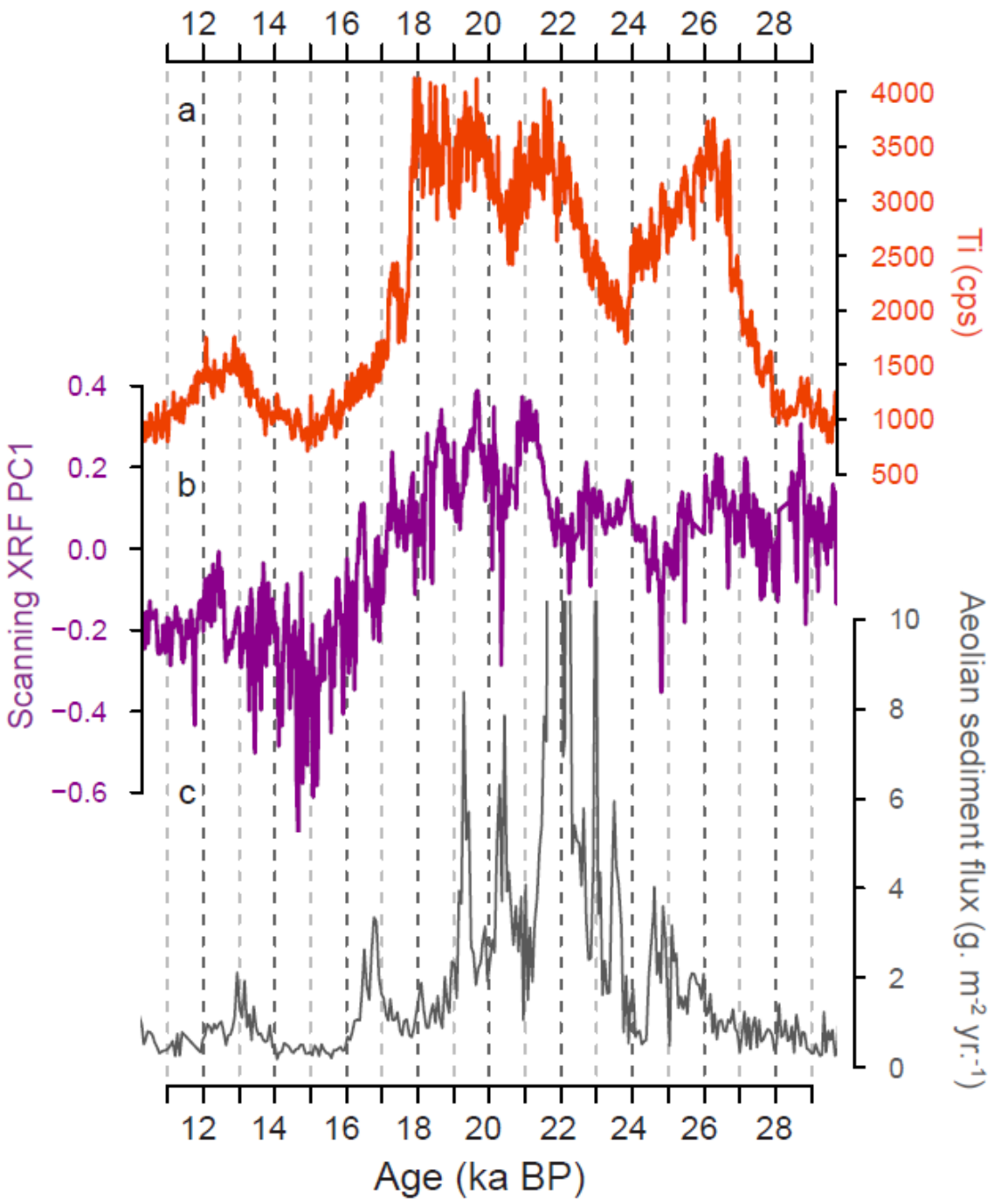

Supplementary Figure 3.7. Comparison of Lake Surprise scanning XRF PC1 (**b**) with two records of aeolian sedimentation in Australia: **a)** Total counts per second (cps) of Ti from core MD03-2611, located south of South Australia (Fig. 3.1). Interpreted to reflect regional aridity in southern Australia (De Deckker et al., 2012); **c)** total aeolian sediment flux to Native Companion Lagoon (Petherick et al., 2009). All records oriented so that 'up' indicates higher aeolian sedimentation.

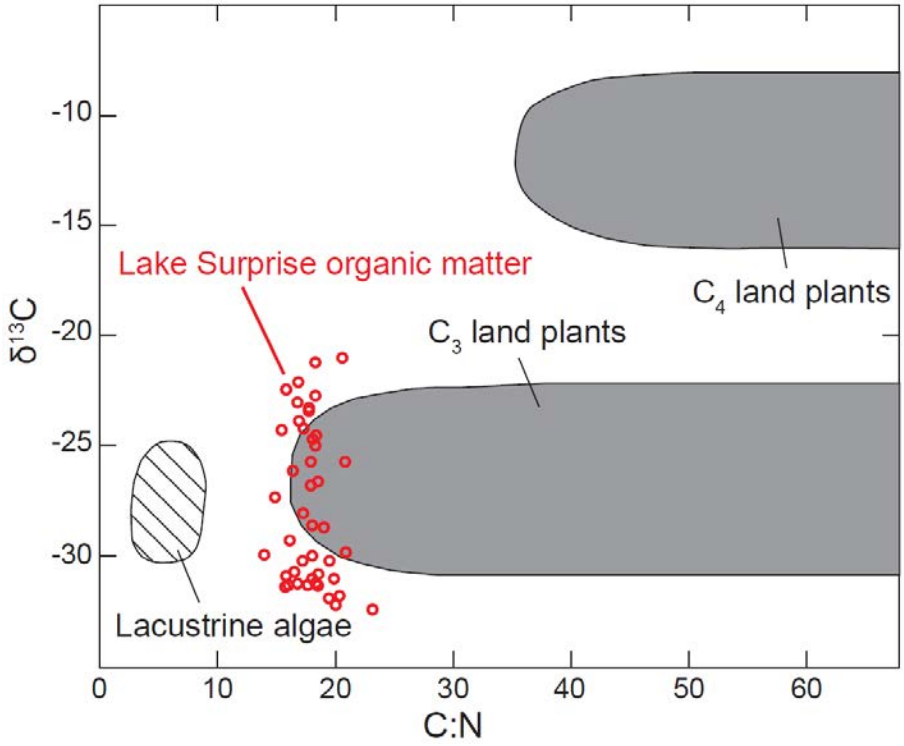

Supplementary Figure 3.8. Cross plot of Lake Surprise C:N and $\delta^{13}C_{OM}$ values (red circles) overlain on shaded zones representing the typical range of C:N and $\delta^{13}C$ values of organic matter derived from lacustrine algae, C_3 land plants, and C_4 land plots (adapted from Meyers and Lallier-Vergés, 1999). Note that the data fall within the range typical of C_3 plants, with minimal variation in C:N.

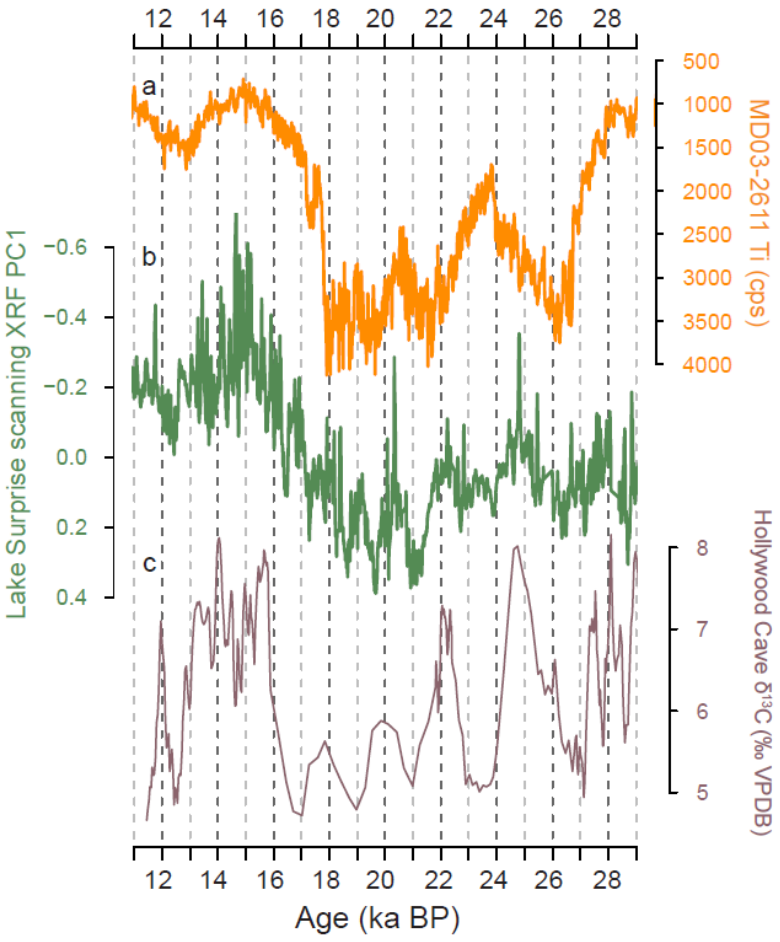

Supplementary Figure 3.9. Comparison of three timeseries included in the MCEOF analysis, presented in each case on the published chronology: **a)** Total counts per second (cps) of Ti from core MD03-2611, located south of South Australia. Interpreted to reflect regional aridity in southern Australia (DeDeckker et al., 2012); **b)** Lake Surprise scanning XRF PC1 (this study); **c)** Speleothem $\delta^{13}C$ from Hollywood Cave in New Zealand, interpreted to reflect changes in precipitation (Whittaker et al., 2011). For location of each site, see Figure 3.1. Each record has been oriented so that 'up' indicates a wetter climate.

Supplementary Table 3.1. List of radiocarbon dates obtained from Lake Surprise core LS04.

Laboratory	Laboratory ID	Material dated	Depth	Conventional ^{14}C age		Source
			cm	years BP	1σ error	
ANSTO	OZH380	pollen fraction	220	2130	50	Builth et al. (2008)
ANSTO	OZG 890	pollen fraction	360	2900	50	Builth et al. (2008)
ANSTO	OZJ031	pollen fraction	547	4270	70	unpublished
ANSTO	OZG891	pollen fraction	754	6260	50	unpublished
ANSTO	OZJ 032	pollen fraction	798	6910	70	Builth et al. (2008)
ANSTO	OZH 381	pollen fraction	940	8940	70	Builth et al. (2008)
ANSTO	OZT498	pollen fraction	968	7635	30	this study
ANSTO	OZT499	pollen fraction	1000.5	8100	35	this study
ANSTO	OZT500	pollen fraction	1036	8635	40	this study
ANSTO	OZG 892	pollen fraction	1069	11480	80	Builth et al. (2008)
ANSTO	OZT501	pollen fraction	1103.5	11500	40	this study
ANSTO	OZH 382	pollen fraction	1120	13310	110	unpublished
ANSTO	OZT502	pollen fraction	1156	10700	40	this study
ANSTO	OZT503	pollen fraction	1189	9945	40	this study
ANSTO	OZH 383	pollen fraction	1210	9570	60	Builth et al. (2008)
ANSTO	OZT504	pollen fraction	1246.5	13420	50	this study
ANSTO	OZT505	pollen fraction	1291	15460	60	this study
ANSTO	OZH 384	pollen fraction	1335	14670	80	Builth et al. (2008)
Waikato	LS 1342	pollen fraction	1342	18430	132	unpublished
ANSTO	OZT506	pollen fraction	1384.5	16320	70	this study
ANSTO	OZH 385	pollen fraction	1435	16100	100	Builth et al. (2008)
ANSTO	OZT507	pollen fraction	1466.5	17890	70	this study
ANSTO	OZJ 034	pollen fraction	1512	17840	120	unpublished
ANSTO	OZT508	pollen fraction	1538	18200	80	this study
ANSTO	OZT509	pollen fraction	1567	18570	80	this study
ANSTO	OZT510	pollen fraction	1594	20680	80	this study
ANSTO	OZT511	pollen fraction	1617.5	21490	80	this study
ANSTO	OZH 386	pollen fraction	1635	21990	140	Builth et al. (2008)
ANSTO	OZT512	pollen fraction	1697.5	23570	90	this study
ANSTO	OZH 387	pollen fraction	1727	23890	180	Builth et al. (2008)
ANSTO	OZT513	pollen fraction	1791	28780	140	this study
ANSTO	OZJ 034	pollen fraction	1829	25990	220	unpublished

Supplementary Table 3.2. Wavelength-dispersive x-ray fluorescence analyses obtained from Lake Surprise core LS04.

Sample name	Midpoint depth	LOI	SiO_2	TiO_2	Al_2O_3	Fe_2O_3	MnO	MgO	CaO	Na_2O	K_2O	P_2O_5	SO_3
	(cm)	(%)	concentration (%)										
LS04-1	980.25	65.74	23.42	0.03	0.32	2.12	0.04	0.25	2.36	0.14	0.02	0.18	5.42
LS04-2	1038.50	69.58	19.46	0.03	0.37	1.87	0.03	0.28	2.54	0.16	0.03	0.23	5.45
LS04-3	1128.25	58.79	27.13	0.04	0.58	1.39	0.02	0.36	6.69	0.14	0.05	0.23	4.59
LS04-4	1204.25	64.44	19.04	0.09	1.36	1.46	0.12	0.37	7.90	0.15	0.14	0.28	4.69
LS04-5	1287.00	46.06	40.18	0.16	1.66	3.69	0.01	0.24	1.58	0.19	0.13	0.22	5.91
LS04-6	1387.00	49.22	40.44	0.18	2.37	1.92	0.01	0.31	1.35	0.19	0.19	0.13	3.70
LS04-7	1489.50	32.53	60.43	0.17	1.90	1.76	0.01	0.23	0.48	0.22	0.14	0.10	2.09
LS04-8	1575.25	53.76	28.92	0.34	4.48	4.10	0.01	0.44	1.39	0.40	0.32	0.18	5.75
LS04-9	1679.25	51.64	36.37	0.22	2.62	2.58	0.02	0.46	1.07	0.29	0.21	0.17	4.39
LS04-10	1785.50	45.17	39.43	0.21	2.29	4.39	0.02	0.44	1.46	0.28	0.16	0.21	5.97

Supplementary Table 3.3. Results of principal components analysis (PCA) of the Lake Surprise calibrated scanning XRF dataset: a) Fraction of total variance explained by each PC; b) Element loadings for the first two (significant) PCs.

a)	Eigenvalue	% explained
PC1	2.52	42
PC2	1.95	33
PC3	0.73	12
PC4	0.45	7
PC5	0.29	5
PC6	0.06	1

b)	PC1	PC2
Si	4.44	-0.22
Ti	1.23	3.72
Fe	0.93	4.72
Mn	-4.01	-0.97
Ca	-4.4	0.15
S	-2.95	3.78

Supplementary Table 3.4. Minerals inferred from x-ray diffractograms, with interpretation assisted by scanning electron microscope imaging and energy dispersive x-ray spectroscopy mineral mapping. Where possible, hrelative mineral abundance has been inferred from peak heights.

Sample name	Depth (cm)	Approximate age (ka BP)	Mineral	Inferred abundance
LS1	928	8494	Opal	dominant
			Gypsum	
			Calcite	
			Weddelite	
			Halite	trace
			Labradorite	trace
			Quartz	trace
LS2	1037	10601	Opal	dominant
			Gypsum	
			Weddelite	
			Smectite	
			Labradorite	trace
			Quartz	trace
LS3	1144	14070	Calcite	dominant
			Opal	abundant
			Quartz	minor
			Smectite	
			Weddelite	
			Labradorite	trace
			Pyrite	trace
LS4	1234	15910	Calcite	abundant
			Opal	abundant
			Quartz	abundant
			Pyrite	minor
			Smectite	
			Weddelite	
			Labradorite	trace
LS5	1376	19167	Opal	abundant
			Quartz	abundant
			Labradorite	moderate
			Illite/muscovite	
			Weddelite	
			Smectite	uncertain

Supplementary Table 3.4 contd.

Sample name	Depth (cm)	Approximate age (ka BP)	Mineral	Inferred abundance
LS6	1467	20921	Opal	dominant
			Quartz	moderate
			Feldspar	minor
			Illite/muscovite	
			Weddelite	
			Smectite	
LS7	1547	23196	Opal	abundant
			Quartz	abundant
			Labradorite	minor
			Weddelite	
			Illite/muscovite	
			Smectite	uncertain
LS8	1627	25778	Opal	abundant
			Quartz	abundant
			Labradorite	minor
			Weddelite	
			Illite/muscovite	
			Smectite	uncertain
LS9	1756	28814	Jarosite	abundant
			Quartz	abundant
			Anorthoclase/labradorite	moderate
			Opal	moderate
			Illite/muscovite	
			Kaolinite	
			Smectite	
LS10	1832	29700	Opal	dominant
			Albite	minor
			Calcite	minor
			Quartz	minor

References cited

Blaauw, M., Christen, J.A., 2011. Flexible Paleoclimate Age-Depth Models Using an Autoregressive Gamma Process. Bayesian Analysis 6, 457-474.

De Deckker, P., Moros, M., Perner, K., Jansen, E., 2012. Influence of the tropics and southern westerlies on glacial interhemispheric asymmetry. Nature Geoscience 5, 266-269.

Meyers, P.A., Lallier-Vergés, E., 1999. Lacustrine Sedimentary Organic Matter Records of Late Quaternary Paleoclimates. Journal of Paleolimnology 21, 345-372.

Ruf, T., 1999. The Lomb-Scargle Periodogram in Biological Rhythm Research: Analysis of Incomplete and Unequally Spaced Time-Series. Biological Rhythm Research 30, 178 - 201.

Weltje, G.J., Bloemsma, M.R., Tjallingii, R., Heslop, D., Röhl, U., Croudace, I.W., 2015. Prediction of Geochemical Composition from XRF Core Scanner Data: A New Multivariate Approach Including

Automatic Selection of Calibration Samples and Quantification of Uncertainties, In: Croudace, I.W., Rothwell, R.G. (Eds.), Micro-XRF Studies of Sediment Cores. Springer Netherlands, pp. 507-534.

Whittaker, T.E., Hendy, C.H., Hellstrom, J.C., 2011. Abrupt millennial-scale changes in intensity of Southern Hemisphere westerly winds during marine isotope stages 2–4. Geology 39, 455-458.

Chapter 4

Statement of Authorship

Title of Paper	Environmental controls on the carbon and oxygen stable isotope ratios of modern land snail shells in Australia.
Publication Status	☐ Published ☐ Accepted for Publication ☐ Submitted for Publication ☑ Unpublished and Unsubmitted w ork w ritten in manuscript style
Publication Details	Falster, G., Tyler, J., Drysdale, R.,Tibby, J., Chivas, A. (2019). Environmental controls on the carbon and oxygen stable isotope ratios of modern land snail shells in Australia.

Principal Author

Name of Principal Author (Candidate)	Georgina Falster		
Contribution to the Paper	Devised study, prepared and analysed samples, interpreted data, wrote manuscript, acted as corresponding author.		
Overall percentage (%)	90 %		
Certification:	This paper reports on original research I conducted during the period of my Higher Degree by Research candidature and is not subject to any obligations or contractual agreements with a third party that would constrain its inclusion in this thesis. I am the primary author of this paper.		
Signature		Date	11/3/2019

Co-Author Contributions

By signing the Statement of Authorship, each author certifies that:

i. the candidate's stated contribution to the publication is accurate (as detailed above);

ii. permission is granted for the candidate in include the publication in the thesis; and

iii. the sum of all co-author contributions is equal to 100% less the candidate's stated contribution.

Name of Co-Author	Jonathan Tyler		
Contribution to the Paper	Provided conceptual guidance, evaluated and edited manuscript.		
Signature		Date	31/1/2019

Name of Co-Author	Russell Drysdale		
Contribution to the Paper	Assisted with acquisition of stable isotope data.		
Signature		Date	31 January 2019

Name of Co-Author	John Tibby		
Contribution to the Paper	Evaluated and edited manuscript.		
Signature		Date	31/1/2019

Name of Co-Author	Allan Chivas		
Contribution to the Paper	Collected and provided samples for analysis, assisted with acquisition of stable isotope data.		
Signature		Date	01 February 2019

Environmental controls on the carbon and oxygen stable isotope ratios of modern land snail shells in Australia

Abstract

Land snails are present across Australia, and their shells are found in sedimentary accumulations, including important archaeological and palaeontological sites. Research from elsewhere in the world has shown that the carbon and oxygen stable isotope ratios ($\delta^{13}C$ and $\delta^{18}O$) of land snail shells reflect various aspects of the snails' ambient environment. However, relationships between the $\delta^{13}C$ and $\delta^{18}O$ values of modern land snail shells in Australia and contemporary climate variables have not yet been tested.

This study reports measurements of the $\delta^{13}C$ and $\delta^{18}O$ values of land snail shells collected from Australian sites covering a broad climatic range. These measurements are compared with annually-averaged local climate variables, derived from gridded observational data. The strongest relationship observed was a negative correlation between snail shell $\delta^{13}C$ and precipitation amount. Where a collection site yielded more than one species, the different species generally preserve distinct shell $\delta^{13}C$ values. The spatial distribution of shell $\delta^{13}C$ values relative to vegetation types expected from seasonal rainfall totals indicates that the diet of all snails was dominated by C_3 vegetation. Snail shell $\delta^{18}O$ is also negatively correlated with precipitation amount, but the species offset is less pronounced.

The results suggest that the shell $\delta^{13}C$-precipitation relationship mirrors the influence of moisture availability on the $\delta^{13}C$ of C_3 plant tissues. This is probably a 'smoothed' signal, as vegetation may remain in the landscape for several years. Inter-specific variability in snail shell $\delta^{13}C$ suggests that species favour different plant species or parts of plants, or that different species metabolise carbon with distinct plant-carbonate fractionation factors. Shell $\delta^{18}O$ values likely reflect the $\delta^{18}O$ of local precipitation, thereby recording the continent-scale trend of decreasing precipitation $\delta^{18}O$ values with increasing annual precipitation. Residual variability in both relationships is probably due to uncertainties in snail age, growth year, ecology, and physiology.

The $\delta^{13}C$ and $\delta^{18}O$ values of Australian land snail shells therefore track mean annual precipitation via two mechanisms. These results indicate that the $\delta^{13}C$ and $\delta^{18}O$ values of ancient land snail shells may provide qualitative insight into past precipitation in Australia.

1 Introduction

The late Quaternary (defined in this thesis as 30,000–10,000 years before present) is the most recent interval in geological history featuring abrupt changes in global climates (Blunier and Brook, 2001). Understanding the evolution of Australian landscapes and climates throughout the late Quaternary potentially offers great reward. Australia's location at the intersection of the Indian, Pacific, and Southern oceans means that continental climates are influenced by complex ocean-atmosphere interactions (McIntosh et al., 2008; Risbey et al., 2009). Unravelling the relative influence of these over centennial to millennial time scales may provide insight into the drivers of long-term variability in Australian climates. Records of hydroclimate are particularly valuable, as they provide an intuitive reflection of environmental conditions. However, understanding continental hydroclimate regimes requires a spatial network of palaeoclimate reconstructions across the continent. Much of the Australian continent is dominated by arid- to semi-arid climates, which are not conducive to the accumulation or preservation of sediment that may be interpreted in terms of past hydroclimate (Chapter 3, this thesis; Reeves et al., 2013) (Table 3.1). An exception is the stable carbon and oxygen isotope ratios ($\delta^{13}C$ and $\delta^{18}O$ values) of biogenic carbonates including vertebrate fossils (Forbes et al., 2010) and emu eggshells (Miller and Fogel, 2016), which have proved to be valuable proxies for past hydroclimate. However, neither of these fossil types is ubiquitous across the continent. In contrast, Australia has an exceptionally rich land snail fauna, with extensive distribution across a wide range of habitats (Stanisic et al., 2017). The $\delta^{13}C$ and $\delta^{18}O$ values of these snails' shells represents a potentially valuable new proxy—with a broad spatial and climatic range—if the isotope-environment relationships between snail and climate can be understood.

1.1 Stable isotopes in modern land snails

Terrestrial pulmonate gastropods—air-breathing land snails—absorb water through a permeable foot. This water is rapidly lost via evaporation, as well as secretion of a mucus trail required for locomotion, while the snail is active (Prior, 1985). This results in a very high body fluid turnover rate in active snails, such that the $\delta^{13}C$ and $\delta^{18}O$ values of bicarbonate dissolved in the body fluid are a close approximation of the $\delta^{13}C$ and $\delta^{18}O$ values of food and water recently ingested by the snail (Goodfriend et al., 1989; Leng and Lewis, 2016; Liu et al., 2007). Land snails use this bicarbonate to secrete a protective aragonite shell. The $\delta^{13}C$ and $\delta^{18}O$ values of land snail shells therefore reflect the local environment during the active period of the snail, plus some offset due to isotope fractionation during metabolic processing of C and O (Balakrishnan et al., 2005b; Goodfriend and Ellis, 2002; McConnaughey et al., 1997; Yapp, 1979).

1.2 $\delta^{13}C$ in modern land snails

Controlled feeding experiments have demonstrated that land snail shell $\delta^{13}C$ is linearly correlated with the $\delta^{13}C$ of the snail's diet, this in turn being mostly determined by the local vegetation (eg. Balakrishnan and Yapp, 2004; Liu et al., 2007; McConnaughey et al., 1997; Stott, 2002). The $\delta^{13}C$ of plant matter consumed by snails may vary widely, due to three primary factors: (1) dietary preference, (2) the photosynthetic pathway used by any ingested plants, where more arid conditions or climates with summer-dominated precipitation favour a dominance of C_4 (higher $\delta^{13}C$) over C_3 (lower $\delta^{13}C$) plant types, and (3) the stomatal conductance response of C_3 plants to moisture availability, where increased moisture stress results in stomatal narrowing to avoid moisture loss, and hence reduced discrimination against ^{13}C (i.e. higher $\delta^{13}C$) (Farquhar et al., 1982; O'Leary, 1981; Prentice et al., 2011; Rao et al., 2017). Regarding (1), snails do not eat indiscriminately, but rather have species-specific dietary preferences that may vary seasonally. Snails may also prefer senescent over green vegetation (Hatziioannou et al., 1994; Iglesias and Castillejo, 1999). Factors (2) and (3) are contingent on (1), however a reduction in effective moisture results in higher $\delta^{13}C$ in both cases (Kohn, 2010; Prentice et al., 2011; Rao et al., 2017; Stewart et al., 1995; Tibby et al., 2016).

1.3 $\delta^{18}O$ in modern land snails

To a first-order approximation, snail shell $\delta^{18}O$ is a function of (1) the $\delta^{18}O$ of the formation water i.e. the snail's body fluid, and (2) temperature at the time of mineral growth i.e. snail body temperature (Epstein et al., 1951). The snail body fluid $\delta^{18}O$ in turn is influenced by environmental variables including the $\delta^{18}O$ of meteoric water, relative humidity, and ambient air temperature, and the relative influence of these appears to be location-specific (Leng and Lewis, 2016; Yanes et al., 2018; Yanes et al., 2009; Yapp, 1979). These relationships are further complicated by the various controls on the $\delta^{18}O$ of meteoric water, including temperature, evaporation, and the origin and trajectory of moisture-bearing air masses (Dansgaard, 1964; Hollins et al., 2018). Plant water represents a very small fraction of total moisture ingested by the snail relative to water absorbed through the foot, and therefore has a negligible influence on the body water $\delta^{18}O$ value (Balakrishnan and Yapp, 2004).

1.4 Challenges of interpreting land snail stable isotopes

In common with isotope-based palaeoenvironment reconstructions from most biogenic carbonates, inferring past environmental change from the $\delta^{13}C$ and (particularly) $\delta^{18}O$ values of fossil land snail shells is not straightforward (eg. Goodfriend, 1992; Goodfriend and Magaritz, 1987; Leng and Lewis, 2016; Leng and Marshall, 2004; Watkins et al.,

2014). Two environmental variables commonly inferred from snail shell $\delta^{13}C$ are the relative abundance of C_3 versus C_4 plants (eg. Goodfriend, 1990), and hydroclimate, via the influence of moisture availability on the $\delta^{13}C$ of C_3 plant tissues eaten by snails (eg. Colonese et al., 2013; Goodfriend and Ellis, 2000). However, vegetation-snail relationships are confounded by species-specific dietary preferences (eg. Bao et al., 2018), and ingestion of carbonate-rich detritus, which biases the shell $\delta^{13}C$ to higher values (eg. Goodfriend, 1987; Stott, 2002).

For $\delta^{18}O$ values, there are many potential confounding factors in shell $\delta^{18}O$-climate relationships, and many are due to the ecology and phenology of the snails (e.g. Yanes et al., 2017, and references therein). Although land snails are found in a wide range of climates, this is partially because snails are active only in optimal conditions (Prior, 1985). Snails desiccate rapidly in dry weather, and are therefore most active immediately after rain events, especially in the early evening when falling temperatures lead to increased relative humidity (Ward and Slotow, 1992). When ambient conditions are hot and dry, snails aestivate i.e. they retreat into their shells, and seal the shell aperture with a layer of dried mucus. During aestivation, snail metabolism is drastically slowed, and new shell aragonite is not secreted (Barnhart, 1986). The environmental tolerance—and therefore periods of activity—of a snail is also dependent on physiological factors including size (Yanes and Fernández-Lopez-de-Pablo, 2017; Yanes et al., 2017), shell colour (Heath, 1975; Knigge et al., 2017), and shell morphology (Goodfriend, 1986; Stankowski, 2011). Snail-based climate reconstructions can therefore be improved by gaining some understanding of modern snail ecology and phenology (eg. Colonese et al., 2013), although many studies have used snail carbonate isotopes as palaeoclimate proxies without direct modern calibration (Balakrishnan et al., 2005a; Goodfriend, 1990; Murelaga et al., 2012; Yanes et al., 2018).

1.5 Land snail isotopes as palaeoenvironmental indicators

Despite these challenges, land snail shell $\delta^{13}C$ and $\delta^{18}O$ values have been used to reconstruct Quaternary palaeoenvironments in Europe (e.g. Bonadonna and Leone, 1995; Colonese et al., 2007; Colonese et al., 2013; Kehrwald et al., 2010; Murelaga et al., 2012), North America (e.g. Balakrishnan et al., 2005a; Stevens et al., 2012), Asia (e.g. Milano et al., 2018; Wu et al., 2018), South America (e.g. Bonadonna et al., 1999; Yanes et al., 2014), Africa (Prendergast et al., 2016), and several low-latitude islands (Chiba and Davison, 2009; Yanes and Romanek, 2013; Yanes et al., 2011). Land snail shells have also been identified in late Quaternary sediment accumulations across Australia, including significant palaeontological and archaeological sites (Mick Morrison, Liz Reed, and Fenja Theden-Ringl pers. comm.), and in arid areas that are often lacking in other proxies.

However, the presence of land snails is rarely reported, and $\delta^{13}C$ or $\delta^{18}O$ data from late Quaternary-aged snail shells in Australia is restricted to a handful of measurements in one PhD thesis (McDowell, 2013).

Relationships between $\delta^{13}C$ or $\delta^{18}O$ values of modern snail shells with climate in Australia have never been explored, which is surprising given > 70 articles have been published on the subject, covering every other continent except Antarctica (Yanes et al., 2018). This may have led to some reluctance in using fossil snails as palaeoclimate indicators in the unique—and largely arid to semi-arid—Australian environment. This work reports measurements of the $\delta^{13}C$ and $\delta^{18}O$ of modern land snail shells, collected from a wide spatial and climatic gradient across Australia (Fig. 4.1). The spatial scale is unprecedented for studies reporting both $\delta^{13}C$ and $\delta^{18}O$ values from snail shells, potentially providing valuable new insight into the main controls on shell isotopes at a coarse spatial scale. These values are compared with measured environmental variables for the estimated snail growth years, to test the hypothesis that snail shell $\delta^{13}C$ and $\delta^{18}O$ values reflect prevailing local environmental conditions.

2 Methods

2.1 Study area

Australia spans a broad range of climate zones, most of which exhibit rainfall variability higher than otherwise similar climates elsewhere in the world (Nicholls et al., 1997). This is largely because Australian climates are influenced by multiple large-scale ocean-atmosphere circulation patterns, including the El Niño Southern Oscillation, the Indian Ocean Dipole, the Interdecadal Pacific Oscillation, the Southern Annular Mode, atmospheric blocking, and variations in the strength and position of the subtropical jet (McIntosh et al., 2008; Risbey et al., 2009). These drivers of Australian climate, as well as local influences, result in large spatial differences in both temperature and precipitation, as well as marked seasonality. Australia's geographically diverse climate conditions also result in considerable spatial variability in the relative abundance of C_3 and C_4 plants. Areas that receive most precipitation in the warm months tend to have a higher relative abundance of C_4; the opposite is true in areas where cool-season precipitation dominates (Hattersley, 1983; Nelson et al., 2016).This range of climate zones, each responding to distinct drivers, provides an excellent natural laboratory to examine the influence of local environmental variables on the stable isotope composition of land snail shells.

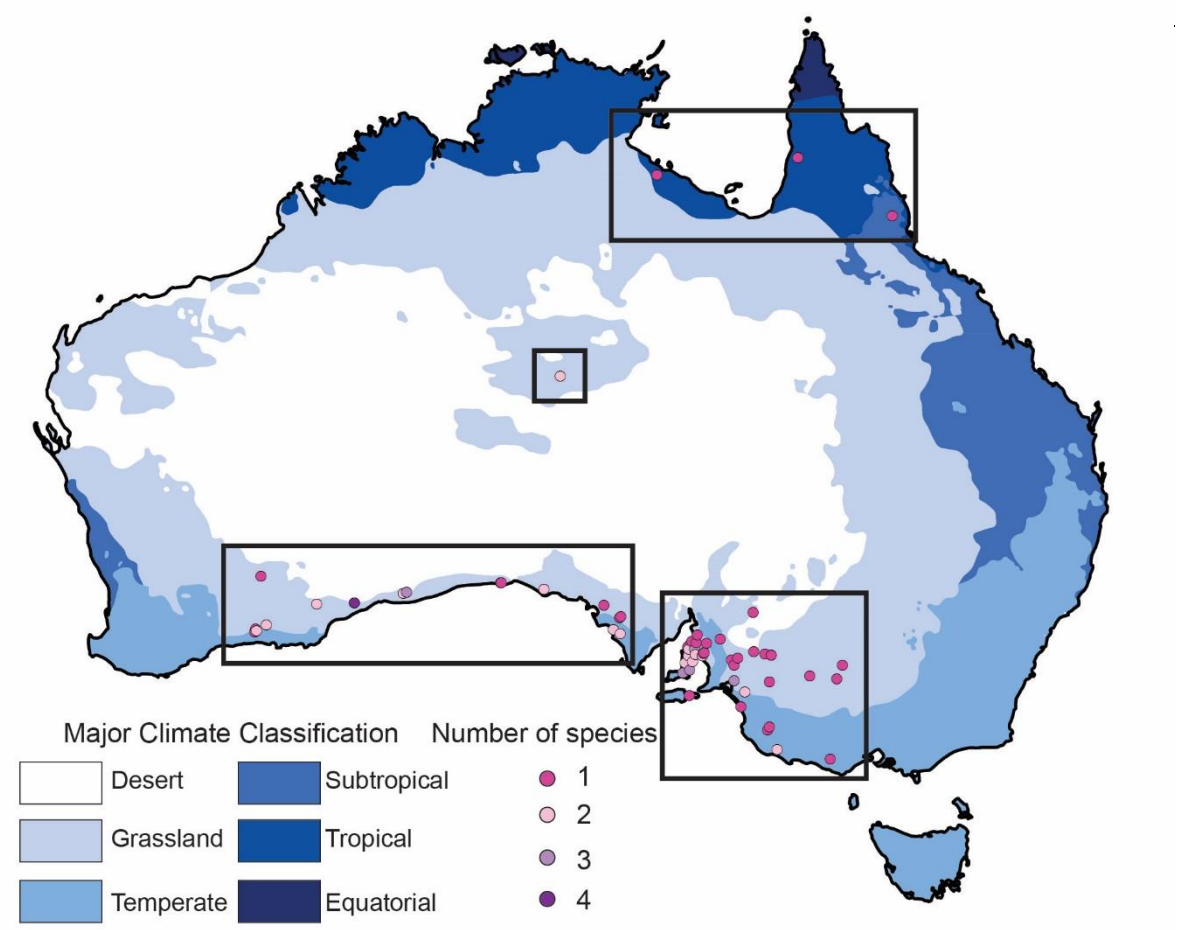

Figure 4.1. Location of snail shell collection sites. Pink circles are shaded according to the number of species identified at each site. The map of Australia is coloured according to major Köppen-Geiger climate classes, based on long-term monthly precipitation and temperature data (Peel et al., 2007). Black boxes denote geographical regions discussed in the text i.e. south-central, south-east, central Australia, and north-east.

2.2 Sample collection

The shells for this study were procured from an existing collection of modern Australian snail shells, comprising samples collected by Allan Chivas during fieldwork over the past 15 years. Samples represent 62 different sites, and are biased toward a) the southern coast of Australia, where the majority of the fieldwork was conducted, and b) areas with extensive outcropping limestone e.g. the Nullarbor Plain (Fig. 4.1, Supp. Table 4.1). Living snails were generally not present, so well-preserved empty shells with some remnant organic matter—indicating a recently deceased snail—were collected instead. All species identified at each site were sampled, but all shells for each site were commingled in one sample bag. To facilitate comparison between regions with potentially disparate climate drivers, isotope data are coloured by geographical region in all relevant figures. The regions (denoted on Fig. 4.1) are: south-central (south of the South Australian border and west of Spencer Gulf), south-east (south of the South Australian border and east of Spencer Gulf), central Australia (one sample only, from Alice Springs), and north-east (north of Townsville and east of the Queensland border).

2.3 Climate data

Climate data was extracted from the Scientific Information for Land Owners (SILO) database, spanning the estimated growth period of the snails. The SILO database is hosted by the Queensland Government (https://silo.longpaddock.qld.gov.au/), and contains products constructed from data collected by the Australian Bureau of Meteorology (BOM) since 1889 (Jeffrey et al., 2001). SILO provides primary and derived climatic variables in the form of gridded datasets that are interpolated from the raw BOM data, to provide spatially and temporally continuous information. Comparison of raw BOM data with interpolated SILO data from selected locations indicates that the SILO data are reliable (Fig. 4.2). As the snails were collected dead, there is uncertainty in the snail shell growth years. Therefore, for each snail sampling site, data was downloaded for the five years preceding sample collection, assuming that the snails probably grew within this interval. Variables include annual averages for temperature (minimum, maximum, and mean), precipitation, evaporation, and maximum relative humidity.

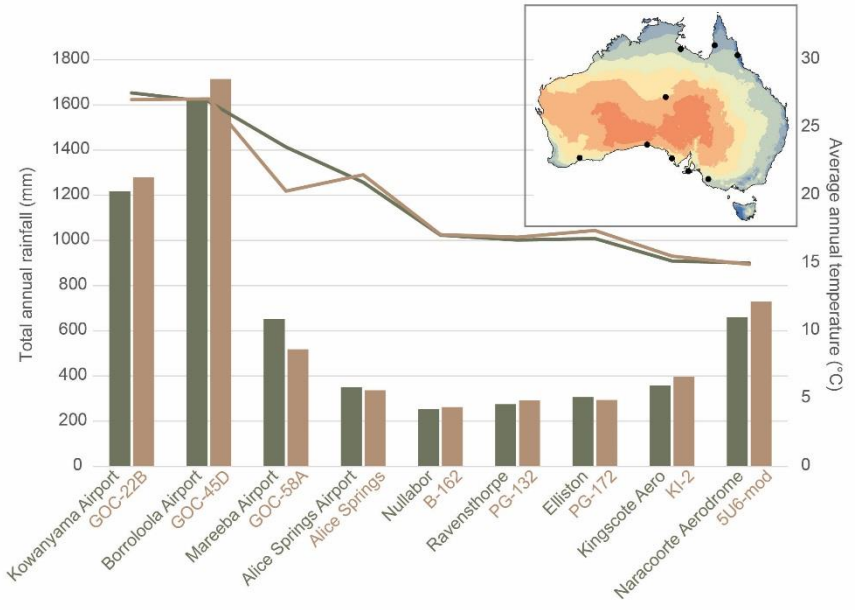

Figure 4.2. Comparison of annual rainfall and temperature data collected by BOM (green), with data downloaded from the SILO database (brown), from nine sample sites with disparate climates. In each case, the climate data correspond to the year of sample collection. Vertical bars show total annual rainfall, and the lines show average annual temperature. Inset map shows site locations, overlain on a grid of mean annual precipitation (BOM, 2010).

2.4 Sample identification, preparation, and analysis

Taxonomic identification of individual snails was based solely on shell morphology and locality. Eighteen species were identified, including 14 native and 4 invasive (Table 4.1). Where more than one species was present at a site, these species were analysed separately.

Each sample consisted of five individual shells. To avoid analysing the shells of juvenile snails, the largest five shells were selected from each sample bag. Intra-sample variability was assessed by analysing the five individual shells separately in a subset of samples (Appendix 2 Table A3). Prior to isotope analysis, all shells were manually cleaned with a

toothbrush, then treated with buffered H_2O_2 to dissolve any remaining organic matter that may bias the results (Chapter 2, this thesis). The cleaned shells were finely ground using an agate mortar and pestle, creating a homogeneous powder representing average environmental conditions over the snail's active lifespan. This whole-shell sampling approach mirrors that of many similar studies investigating the stable isotope composition of land snails (eg. Balakrishnan et al., 2005b; Bao et al., 2018; Colonese et al., 2014; Yanes et al., 2008), making this work directly comparable with these publications.

Table 4.1. Summary of the shell morphology, distribution, and preferred habitat of all land snail species contributing to this dataset. All information summarised from Stanisic et al. (2010, 2017).

Species	Common name	Shell size	Shell thickness	Shell colour	Current distribution	Habitat	Native?
Austrosuccinea australis	Southern Ambersnail	Height to 15 mm	thin	Pale yellow to orange to brown	Southern Australia from inland NSW, Victoria, Tasmania, and SA, to the central west coast of WA	Semi-arid woodland and limestone outcrops; living under logs amonst grass and under bark on trees	Yes
Bothriembryon barretti	Barrett's Tapered Snail	Height 30-40 mm	thin	White to pink	Nullarbor Plain, from Penong (central SA) to Cocklebiddy (eastern WA)	Woodland and scrub on limestone; lives in soil under rocks and litter	Yes
Bothriembryon dux	Balladonia Tapered Snail	Height 60 mm	solid	Ivory white to pink	Nullarbor Plain, east of Norseman (WA)	Malle and scrub on limestone; living under rocks and litter beneath shrubs	Yes
Bothriembryon esperantia	Esperance Tapered Snail	Height to 30 mm	solid	Cream with sparse brown bands and speckles	Cape Le Grande, east of Esperance to Pallinup River, south coast of WA	Coastal scrub on dunes and limestone; living under litter at the base of shrubs	Yes
Bothriembryon indictus	Eucla Tapered Snail	Height to 42 mm	thin to solid	White to pink	Nullarbor Plain from Minnipa (Eyra Peninsula, SA) to Eucla (WA)	Mallee and low scrub on limestone; living under rocks and litter beneath trees and bushes	Yes
Bothriembryon melo	Torndirrup Tapered Snail	Height to 22 m	thin	Variable; pale greenish yellow with reddish markings, to reddish brown with yellow markings, to dark brown with pale markings	Tor Bay (west of Albany, WA) to Bremer Bay (southern WA coast)	Coastal scrub, tall heath and mallee on dunes, limestone, granite; usually seen crawling on trees and shrubs after rain	Yes
Crikey steveirwini	Steve Irwin's Treesnail	Height to 15 mm		Yellowish cream to creamy brown with black and coppery brown spiral bands	Central wet tropics (northeast Qld)	Rainforest; arboreal, living on leaves of trees	Yes
Pleuroxia adcockiana	Adcock's Sculptured Snail	Diameter 12-18 mm		Pale yellow with reddish brown spiral bands	MacDonnell, Krichauff, and James ranges (NT)	Semi-arid woodland and palm forest; living under rocks and forest debris	Yes
Pleuroxia elfina	Elfin Sculptured Snail	Diameter 11-18 mm		Light brown	Nullarbor Plain, from Nullarbor (SA) to east of the Fraser Range (WA)	Semi-arid scrub; living under slabs of rock	Yes
Pleuroxia polypleura	Densely Sculptured Snail	Diameter 10-18 mm		Pale grey-brown with white ribs	Nullarbor Plain, from Koonalda (SA) to Caiguna (WA)	Semi-arid scrub; living under slabs of rock	Yes
Sinumelon expositum	Finke River Dwarfmelon	Diameter 14-25 mm	solid	Greenish yellow with some brown	Finke River and western MacDonnell Ranges, Krichauff and James ranges (NT)	Open scrub and woodland; buried in soil under logs, rocks, and litter	Yes
Sinumelon nullarboricum	Nullarbor Dwarfmelon	Diameter 12-22 mm	solid	Yellowish grey	Colona (SA) to Balladonia and Cape Arid (southern WA)	Open scrub; buried in soil under logs, rocks, and grass	Yes
Spurlingia gemma	Rounded Chillagoe Thicket Snail	Diameter 22.5 mm		Pale grey with a white lip	Chillagoe limestones (northeast Qld)	Vine thicket on limestone outcrops; living under rocks	Yes
Xanthomelon durvillii	Durvill's Melon Snail	Diameter 33-47 mm	solid	Greenish brown	Cobourg Peninsula (NT)	Vine thicket to dry woodland and littoral vegetation; living under rocks and litter	Yes
Cornu asperum	European Garden Snail	Diameter to 40 mm		Brown with darker spiral bands and yellow speckles	Most of southern and eastern Australia, as far north as the Atherton Tablelands (QLD)	Gardens, parks, nurseries, and agricultural land; living under pots, rocks, and debris	No
Theba pisana	White Italian Snail	Diameter to 20 mm		White , sometimes with thin brown spiral bands	Throughout drier coastal southern Australia	Dry, open grassy areas and dunes, grain crops, vineyards, and roadside vegetation; living sealed to any upright surface	No
Cernuella virgata	Vinyard Snail	Diameter 12-18 mm		White to yellowish, sometimes with dark brown spiral bands	Widespread through drier areas of southern Australia	Coastal vegetation, cereal crops and pasture; living sealed to posts, grass, and vegetation	No
Cochicella acuta	Pointed Snail	Height to 18 mm	thin	Creamy white with a single brown band and/or dense speckles and flame-shaped patterns	Widespread through coastal areas of WA, SA, and Victoria, and the Murray-Darling Basin of inland NSW	Dunes, gardens, roadside vegetation, pasture and grain crops; living on vegetation and fence posts	No

All pre-treated powders were transferred to borosilicate exetainers for stable isotope analysis by a continuous flow isotope ratio mass spectrometer at either the University of Melbourne or the University of Wollongong. Detailed sample preparation and analytical methods for each laboratory are provided in Appendix 1. Forty-seven powders (representing 17 different samples) were measured at both laboratories, and there was no systematic offset between the two (Fig. 4.3). $\delta^{13}C$ and $\delta^{18}O$ values are reported in per mille units relative to the Vienna Pee Dee belemnite standard (VPDB).

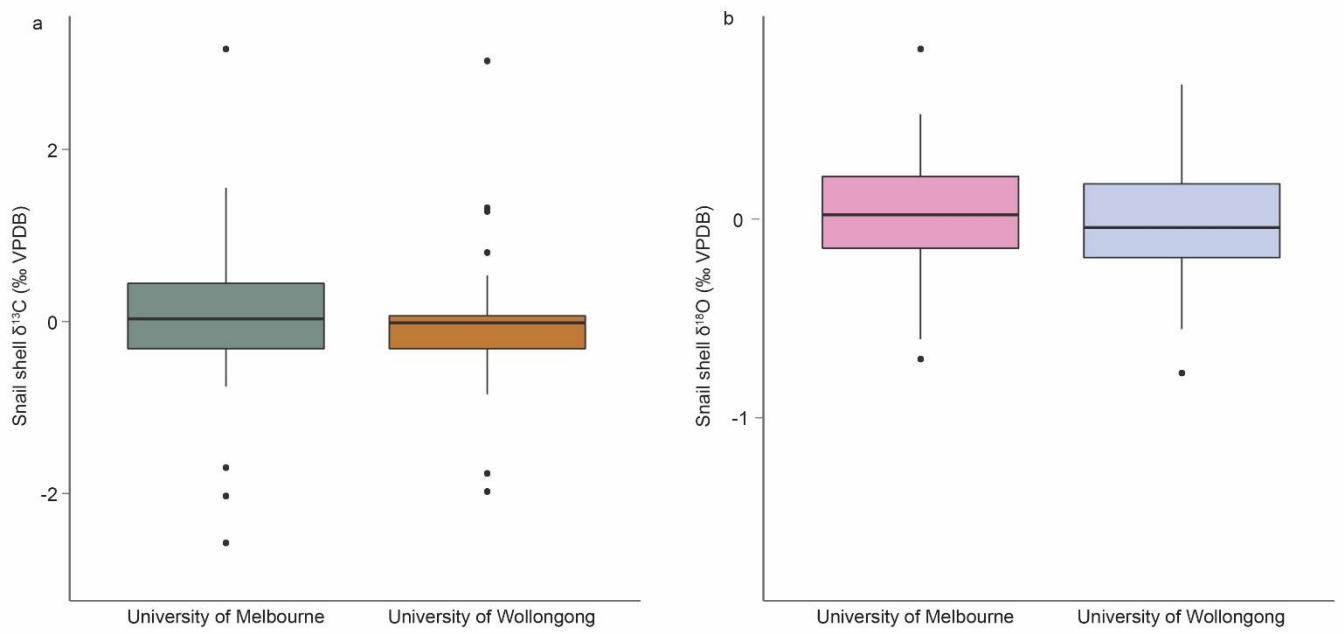

Figure 4.3. Comparison of snail shell **a)** $\delta^{13}C$ and **b)** $\delta^{18}O$ data acquired from the University of Melbourne, and the University of Wollongong. Only samples that were measured in both laboratories are plotted here. Values are presented as the deviation from the average value from both laboratories.

2.5 Numerical analyses

Pearson correlations were used to compare snail shell $\delta^{13}C$ and $\delta^{18}O$ values with potential major environmental influences i.e. temperature, precipitation amount, evapotranspiration, and relative humidity. These environmental variables were chosen using basic knowledge of land snail ecology and phenology (Michael Shea, pers. comm.). For this initial exploratory analysis, annual average values were used to determine broad-scale influences. For the annual climate values, the average of the five years preceding the date of collection of the shell was used, to account for uncertainty in the actual snail growth years. For samples where individual snails were analysed, the mean value of the five analyses was used for direct comparison with grouped samples. Linear regression equations were calculated to determine the slopes and coefficients of determination, and used these broad indicators to assess the influence of any environmental variable significantly correlated with $\delta^{13}C$ or $\delta^{18}O$. The Kruskal-Wallis test was applied to evaluate

whether median values of groups of samples were significantly different, combined with Dunn's post-hoc pair-wise tests.

3 Results

The $\delta^{13}C$ and $\delta^{18}O$ values of all analysed shell samples (n = 243) range from -14.09 to -1.79 ‰, and -5.61 to +4.2 ‰, respectively (Appendix 2 Table A3). These results are comparable with the published ranges of snails in their natural habitats, which fall between approximately -17.75 and +1.7 ‰ for $\delta^{13}C$, and -11.9 and +4.5 ‰ for $\delta^{18}O$ (eg. Balakrishnan et al., 2005b and references therein; Bao et al., 2018; Yanes, 2015; Yanes et al., 2008). The isotopic range covered by our samples is rather wide for a single study, reflecting the broad climatic gradient covered by the sites. Shell $\delta^{13}C$ and $\delta^{18}O$ values are not linearly correlated, although this may be due in part to the dense spacing of samples in the south-east (Fig. 4.1), where measured climate variables are fairly similar, but snails probably inhabit a range of different microhabitats (Table 4.1).

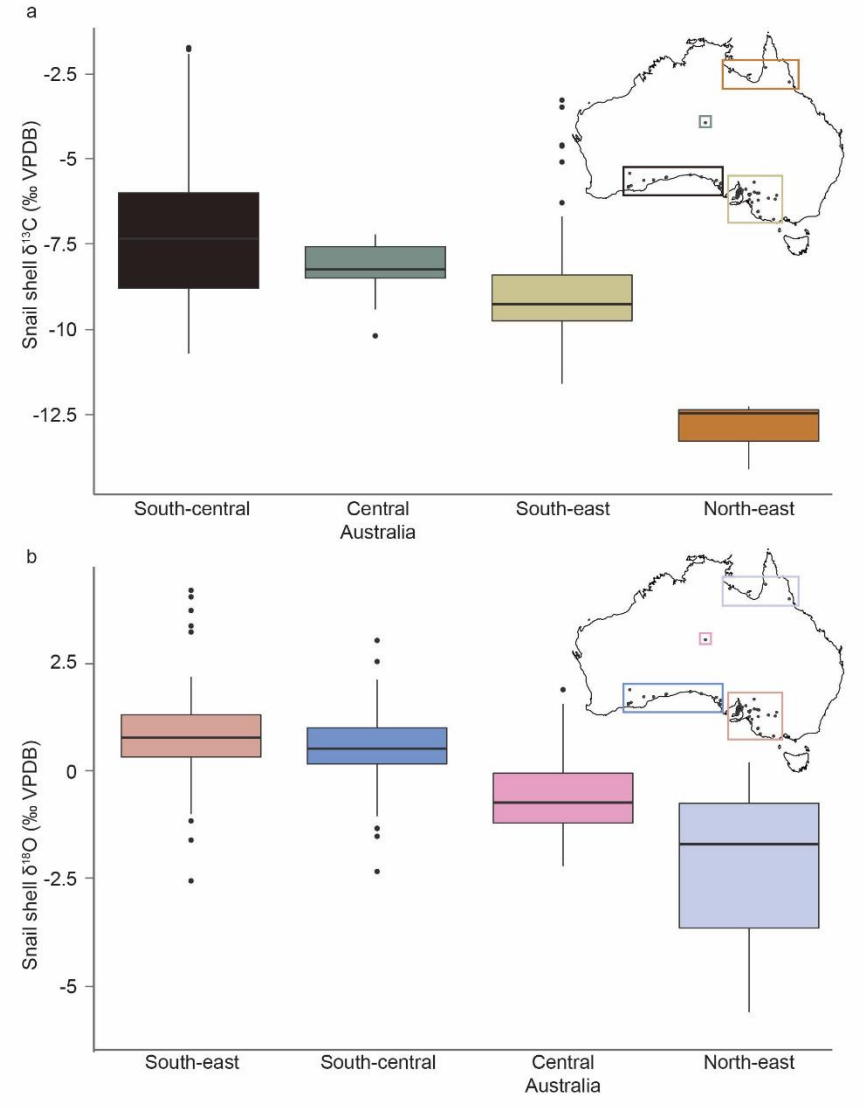

Figure 4.4. a) Comparison of snail shell $\delta^{13}C$ data from the four geographical regions discussed in the text. Where individual shells and/or multiple species were measured, only the site average is shown. Post-hoc Dunn's tests indicate that median regional values for the south-central, central Australia, and the south-east are indistinguishable. The median value of samples from the north-east is distinct from the other regions. Inset map shows the boundaries of the four regions; **b)** as per **a)**, but for $\delta^{18}O$. The median regional values for the south-central and south-east are indistinguishable, but all are regions are distinct.

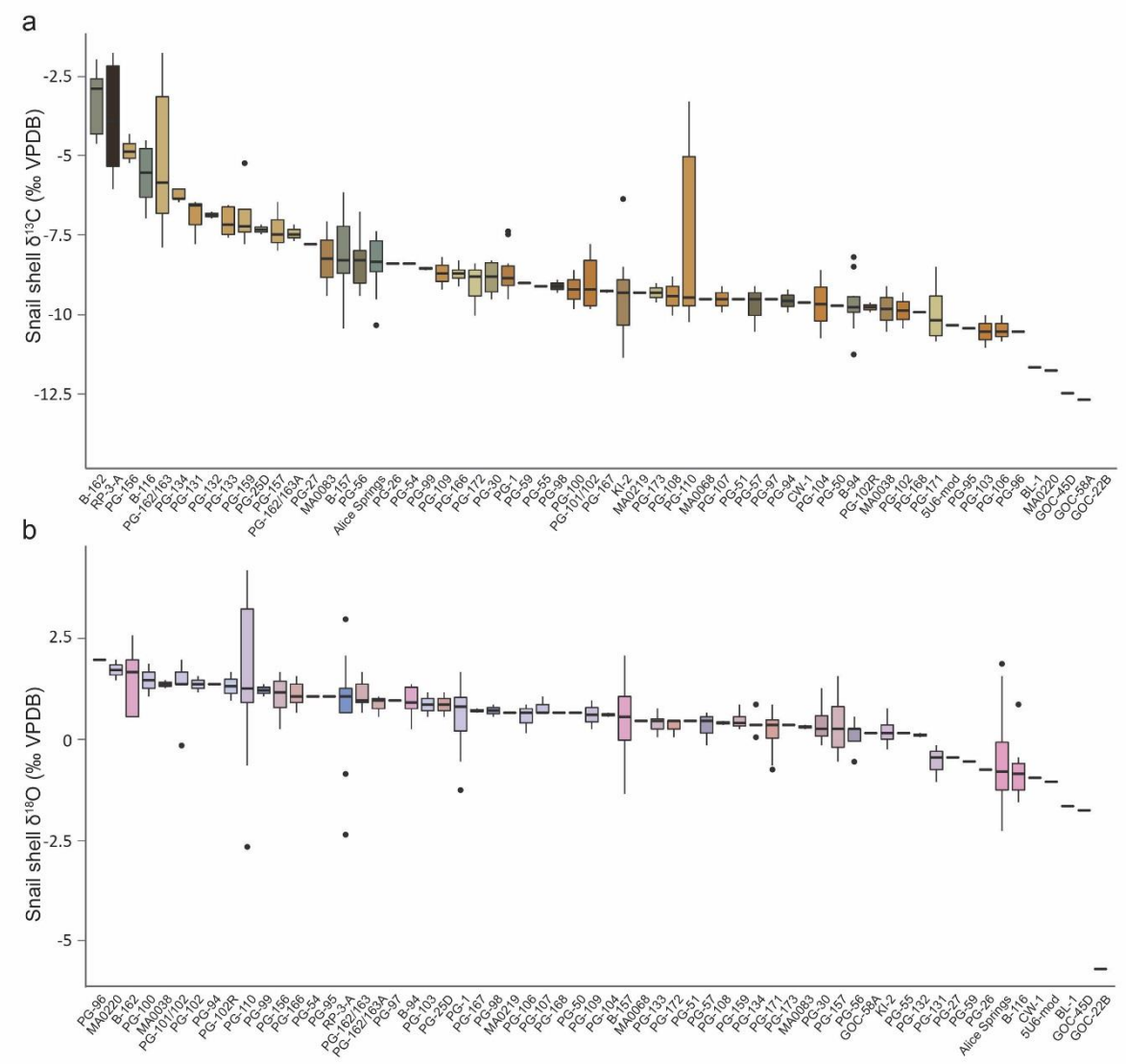

Figure 4.5. a) Comparison of snail shell $\delta^{13}C$ from all sites. The boxplot includes all analyses i.e. measurements made on individual shells are included as discrete points rather than site averages; **b)** as per **a)** but for $\delta^{18}O$.

At a regional scale, there is spatial variability in both $\delta^{13}C$ and $\delta^{18}O$ values, although post-hoc pair-wise tests indicate that the spatial control is stronger for $\delta^{18}O$ than $\delta^{13}C$ (Fig. 4.4). The median $\delta^{18}O$ is indistinguishable between the sites in the south-central and south-east of Australia, but distinct for all other pair-wise comparisons. For $\delta^{13}C$, only the samples from north-eastern Australia are distinct from the other regions. At the individual site level, there are significant differences (Kruskal-Wallis $p < 0.05$) between median site values for both $\delta^{13}C$ and $\delta^{18}O$ (Fig. 4.5), although post-hoc tests show that not all sites are distinct from all other sites. There is also variability in shell isotope compositions within samples (Fig. 4.6), and between species (Fig. 4.7). This variability probably reflects local variations in the snails' micro-habitat, physiology, age, and dietary preferences, as well as some uncertainty in the specific year of snail growth.

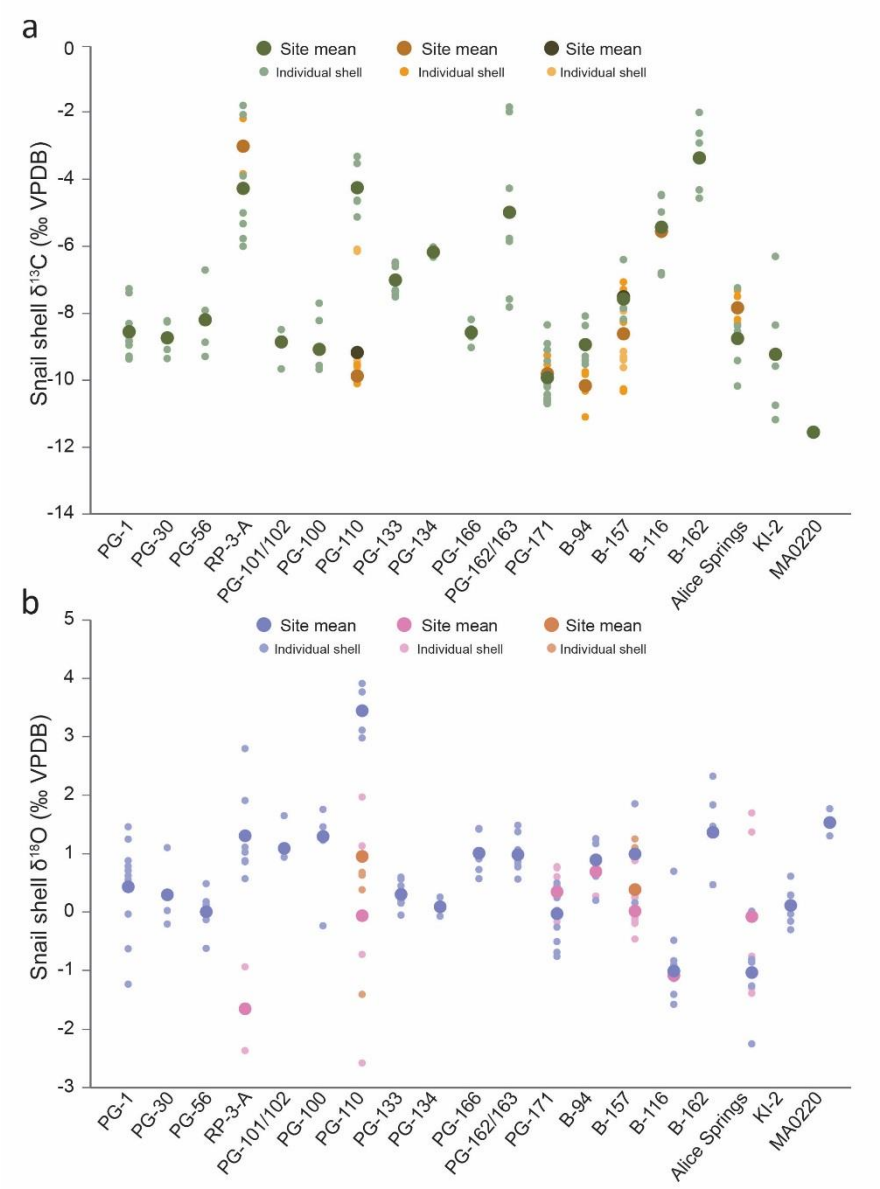

Figure 4.6 (left). a) Plot showing intra-sample variability in snail shell $\delta^{13}C$. Only samples where individual shells were measured are shown. Where individuals from more than one species were measured from one site, species are differentiated by colour. Large points denote the site mean for each species, and smaller points denote measurements from individual shells. Site names are listed on the horizontal axis, and are arranged by date of collection; **b)** as per **a)** but for $\delta^{18}O$.

Figure 4.7 (below). Comparison of snail shell **a)** $\delta^{13}C$ and **b)** $\delta^{18}O$ data from sites where more than one species was present. Where individual shells were measured, the site average is shown for each species. Values are presented as the deviation of the species average from the site average (grey dashed line), and are ordered by total offset (from most positive to most negative).

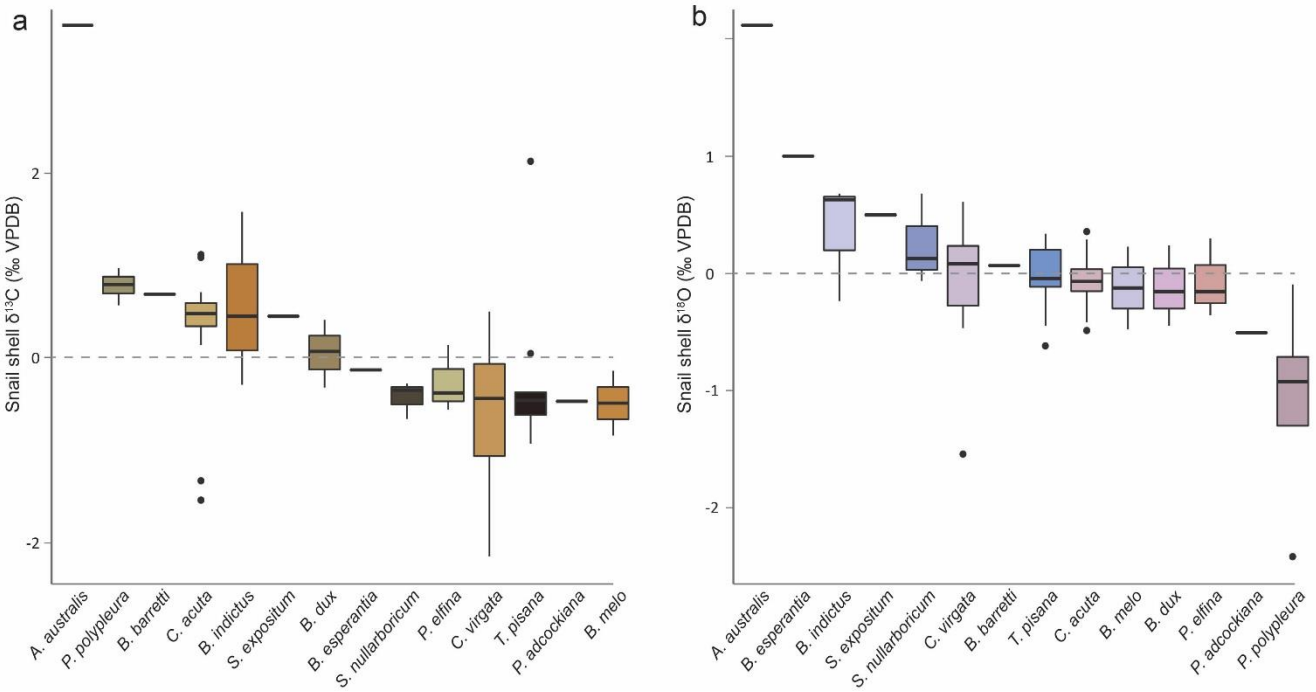

3.1 Relationship between shell isotopes and environmental variables

Of the variables tested here, $\delta^{13}C$ is most strongly correlated with mean annual precipitation for the five years preceding collection of the sample ($p << 0.05$, $R^2 = 0.34$). Shell $\delta^{13}C$ has a weaker or non-significant relationship with the other variables tested. Shell $\delta^{18}O$ is also most strongly correlated with mean annual precipitation ($p << 0.05$, $R^2 = 0.26$) (Fig. 4.8). It is highly likely that some of the scatter in these relationships is due to uncertainty in the time that the snails were alive. Precipitation at most sites is highly variable (Fig. 4.9), and this was accounted for by regressing against five-year averages. However, most small (<5 cm) snails generally live for one or two years (e.g. Baker, 2008; Kempster and Charwat, 2003; Smallridge and Kirby, 1988), and therefore will not reflect rainfall for the entire five-year comparison interval.

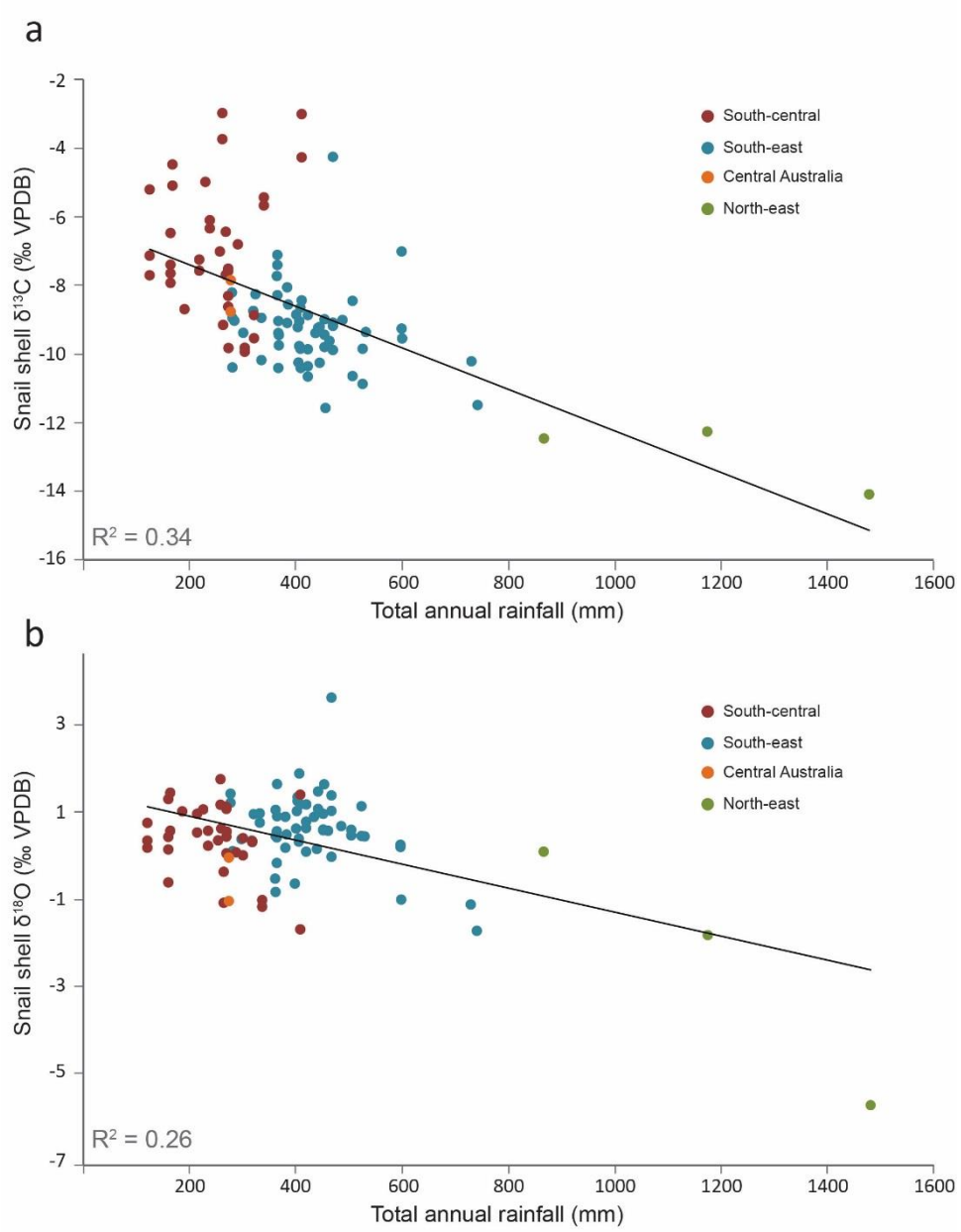

Figure 4.8. a) Relationship of snail shell $\delta^{13}C$ with mean total annual rainfall for the five years preceding collection of the sample. All shell $\delta^{13}C$ values shown are the site average, but if more than one species was present at a site then the species averages for that site are plotted separately. Points are coloured according to geographical region; **b)** as per **a)** but for $\delta^{18}O$.

4 Discussion

4.1 Main influences on snail shell $\delta^{13}C$ and $\delta^{18}O$

Correlation of both the $\delta^{13}C$ and $\delta^{18}O$ values of the land snail shells analysed in this study with mean annual precipitation indicates a strong hydrological influence on Australian snail shell isotope composition. This reflects similar relationships identified in other locations, and suggests that fossil shells may provide a valuable proxy for past hydroclimate in Australia. However, the low coefficients of determination (Fig. 4.8) indicate (unsurprisingly) that snail shell $\delta^{13}C$ and $\delta^{18}O$ values are influenced by variables not accounted for by the simple isotope-rainfall relationships. Figure 4.6 demonstrates large within-sample variability in both $\delta^{13}C$ and $\delta^{18}O$ values, probably reflecting differences in diet, age, life span, physiology, and the particular environmental conditions experienced by that individual snail (i.e. weather). The most informative values from a site may therefore obtained by averaging values from as many shells of a particular species as possible (Apolinarska et al., 2015), unless the range of environmental variability is of particular interest.

One potentially major source of variability is that our sample set comprised of empty-collected shells i.e. snails with uncertain growth years. Much of Australia has significant interannual variability in precipitation (Fig. 4.9), and the climatic variables obtained from the SILO database are not precisely coincident with the snail growth times. Additionally, the annually integrated variables are probably closely correlated with equivalent seasonal variables, and hence may not reflect the true snail active season per se, but rather an approximation of the 'true' relationship. Nevertheless, these comparisons provide an informative foundation for understanding broad shell-isotope relationships at a coarse spatial resolution.

4.2 Snail shell isotopes and the ambient environment

4.2.1 Carbon isotopes

The simplest explanation for the negative relationship of snail shell $\delta^{13}C$ and precipitation is that proposed by equivalent studies conducted elsewhere i.e. a reflection of the influence of hydroclimate on the local vegetation. Although the $\delta^{13}C$ of terrestrial vegetation is controlled on the first order by the photosynthetic pathway used by the plant, I suggest that in the case of this dataset, the main control on snail shell $\delta^{13}C$ is the C_3 plant stomatal aperture response to moisture availability. C_4 vegetation is favoured by summer-dominated rainfall regimes, leading to increased abundance of C_4 vegetation in Australia's monsoonal tropics (Hattersley, 1983). If the relative abundance of C_3 versus C_4

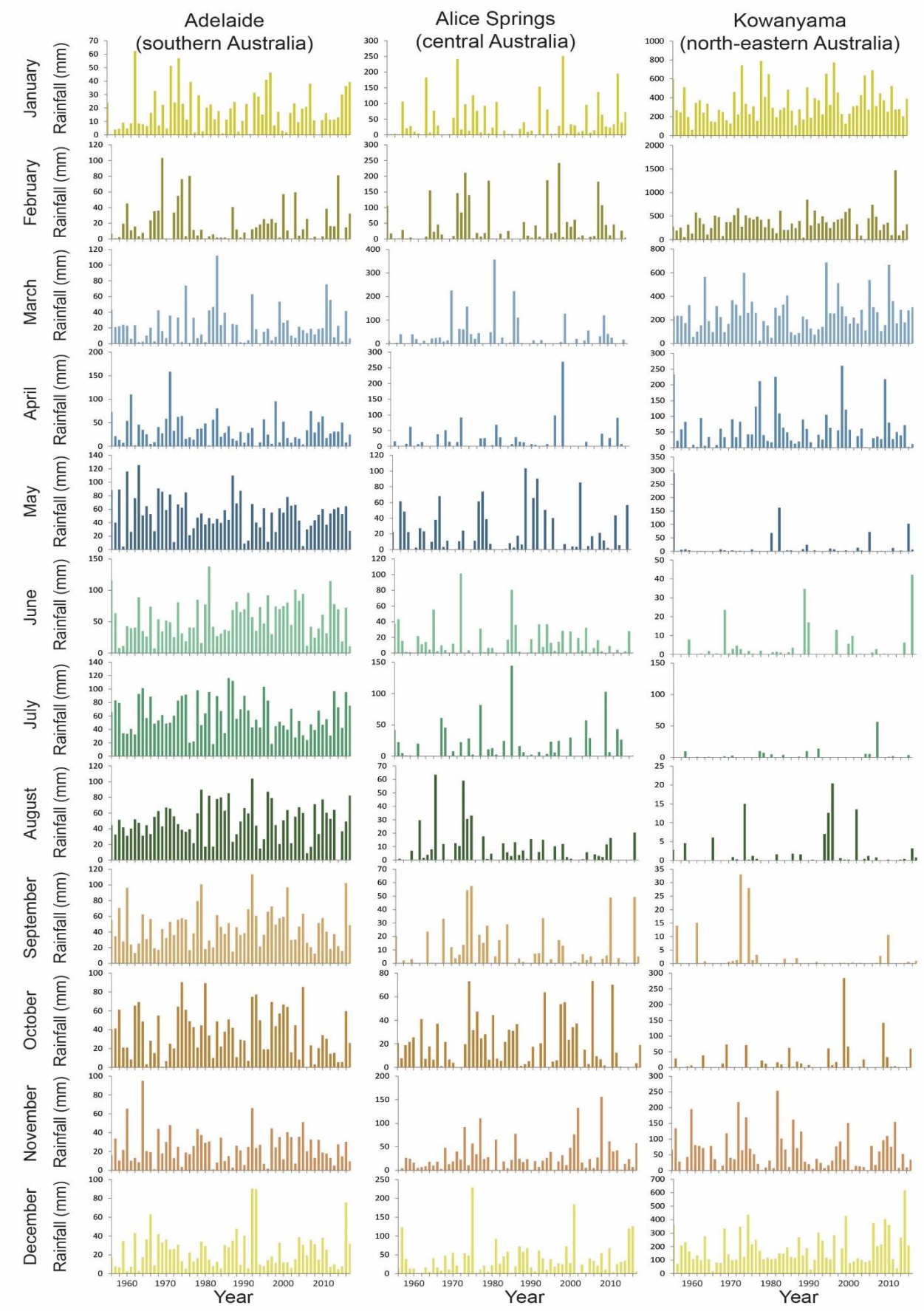

Figure 4.9. Monthly rainfall totals from 1956 to 2017, representative of three distinct geographical regions and climate types: temperate south coast (Adelaide), arid to semi-arid continental interior (Alice Springs), and tropical north-east (Kowanyama). Note variation on the vertical axes, indicating a high degree of both intra- and inter-annual variability in total rainfall.

vegetation eaten by a snail was the primary control on shell $\delta^{13}C$, then we would expect that the three samples from northern Queensland might have the highest $\delta^{13}C$ (Fig. 4.1). Instead, these samples have the lowest $\delta^{13}C$ values, as expected from snails eating C_3 plants in high-humidity conditions. This apparent contradiction may be due to dietary preferences of these snail species. Snails do not eat plants in direct proportion with their abundance, but rather prefer plants with higher attractiveness, palatability, or provision of shelter (Hatziioannou et al., 1994; Iglesias and Castillejo, 1999), and generally tend to prefer C_3 plants over C_4 (Metref et al., 2003). In the case of these data, *Crikey steveirwini* is a tree-dwelling snail (Table 4.1), and therefore probably does not encounter C_4 grasses. Although the preferred vegetation types of the remaining two species—*Spurlingia gemma*, and *Xanthomelon durvillii*—are unknown, it seems from the relatively low $\delta^{13}C$ of their shells that all three species prefer plants using the C_3 metabolic pathway, in accordance with the observations of Metref et al. (2003). So, whilst acknowledging the unquantified proportion of C_4 plants in the snails' diets, I suggest that C_4 plant consumption by snails is probably neither major nor systematic.

A corollary of the interpretation of the $\delta^{13}C$-precipitation relationship as a reflection of plant moisture availability is that the snail shell $\delta^{13}C$ represents a precipitation signal integrated over the time taken for plant tissues to respond to changes in moisture availability. If the preference of snails for senescent over green vegetation applies to Australian snails, this may also result in snail shell $\delta^{13}C$ lagging large shifts in precipitation by several years (Hatziioannou et al., 1994), although this lag would be negligible on centennial–millennial time scales. Figure 4.7 also demonstrates that where more than one species was present at a site, some species either had distinct species-specific fractionation factors, or fed on different plants. I therefore suggest that if snail shell $\delta^{13}C$ is used as a proxy for past precipitation, then it would be best to first observe modern snails of the same species in their natural habitat, to understand their dietary preferences. If this is not possible, then I suggest analysing all species present at a site and using the site mean, which may approximate 'average' local vegetation.

4.2.2 Oxygen isotopes

Hollins et al. (2018) recently demonstrated that the $\delta^{18}O$ of rainwater in Australia correlates negatively with total annual precipitation, albeit weakly. I therefore suggest that the negative correlation between snail shell $\delta^{18}O$ and mean annual precipitation is a result of this relationship i.e. snail shell $\delta^{18}O$ reflects surface water $\delta^{18}O$, which in turn is dependent on precipitation $\delta^{18}O$. This is supported by a close spatial correspondence of mean annual precipitation $\delta^{18}O$ trends with snail shell $\delta^{18}O$ (Fig. 4.10), which mirrors similar results recently published for North America. Yanes et al. (2018) identified a strong

linear relationship between snail shell $\delta^{18}O$ and the average $\delta^{18}O$ of mean annual precipitation that applies regardless of snail taxon, ecology, size, or behaviour, at least on a broad spatial scale. Unfortunately, the database used by Yanes et al. (2018) to derive precipitation $\delta^{18}O$ relies on data with a strong Northern Hemisphere bias, and does not always provide accurate values for Australian precipitation (Bowen, 2017; Hollins et al., 2018). I therefore did not attempt to perform a direct snail $\delta^{18}O$/precipitation $\delta^{18}O$ comparison, but note that the similarity of continent-scale results from Australia and North America is an encouraging sign that a snail $\delta^{18}O$ proxy for hydroclimate may be globally applicable.

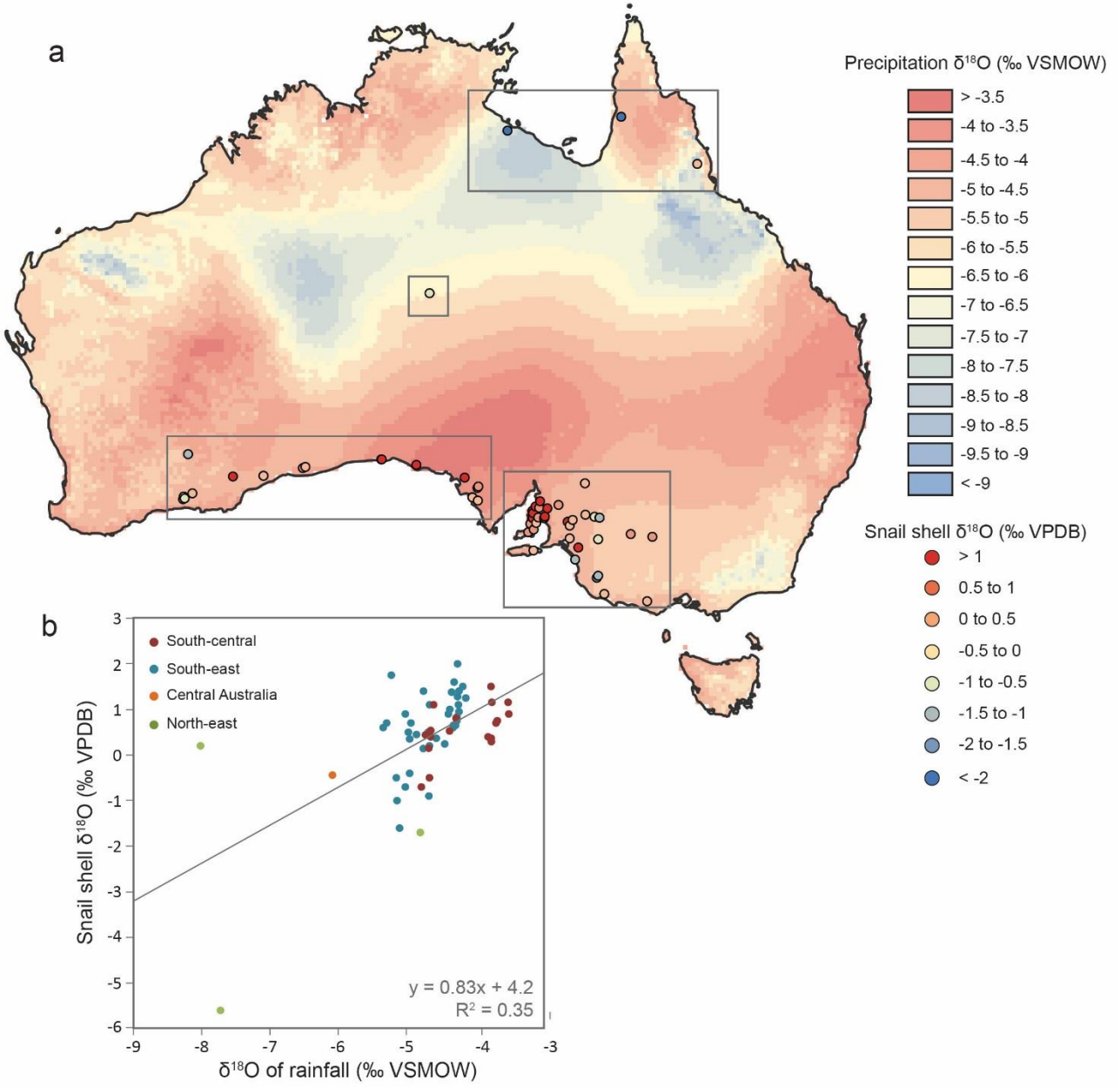

Fig. 4.10. a) Annual precipitation $\delta^{18}O$ isoscape (Hollins et al., 2018), with site average snail shell $\delta^{18}O$; **b)** comparison between site average snail shell $\delta^{18}O$ and the corresponding precipitation $\delta^{18}O$ value interpolated from the annual isoscape. Points are coloured according to geographical regions, denoted by grey boxes in **a)**.

However, the precipitation amount-precipitation $\delta^{18}O$ relationship is based on complex climatic and spatial interactions (Hollins et al., 2018), which are further complicated by incorporation of this signal into snail shell carbonate. Compared with $\delta^{13}C$, the slightly poorer relationship of snail shell $\delta^{18}O$ values with mean annual precipitation is probably due to the diverse climatic and environmental influences on the $\delta^{18}O$ of water absorbed by a snail. A key source of variability not accounted for by this simple relationship is the narrow environmental tolerance of snails, relative to environmental conditions across much of the Australian continent. Specific snail active periods and behaviour are unknown for most Australian species, and we must therefore make broad assumptions about the time intervals most likely sampled in the shell isotopes. Accordingly, assuming snails only secrete shell aragonite during the moist conditions suitable for snail activity, the shell $\delta^{18}O$ values should represent environmental conditions integrated over these snail-preferred periods. If these conditions are concentrated in one particular season (e.g. winter), then palaeoenvironmental records based on snail shell $\delta^{18}O$ values may be biased toward synoptic weather patterns peculiar to that particular season, possibly with very different moisture source $\delta^{18}O$ and trajectories to other seasons (e.g. summer) (Dansgaard, 1964; Hollins et al., 2018; Risbey et al., 2009). If the seasonality at a particular site is pronounced, then the precipitation amount in the wettest season will have a causal relationship with mean annual precipitation, resulting in a relatively weak, but still significant correlation of $\delta^{18}O$ with mean annual conditions. The imprint of this seasonality should be a focus of future work.

An additional source of variability in this spatially broad data is the different moisture pathways and oceanic moisture sources that deliver precipitation across Australia (Hollins et al., 2018; Nicholls et al., 1997; Risbey et al., 2009; Williams and Stone, 2009) (Fig. 4.4b). The distinct isotopic populations formed by the shells from southern, central, and north-eastern Australia are probably in part a reflection of moisture derived from the three major ocean basins that surround Australia (Hollins et al., 2018; Liu et al., 2010). However, moisture source and pathway are closely linked with precipitation amount (Hollins et al., 2018), and in a palaeo context, the source influence may be difficult to extricate without equivalent records of $\delta^{18}O$ from moisture source regions. For a qualitative precipitation record derived from snails at one location, this would not be a major issue, unless moisture sources changed dramatically during the period of reconstruction. This influence would, however, become important if attempting a regional or continent-scale analysis of past rainfall trends from snail shell $\delta^{18}O$ values.

Temperature is another variable that influences snail shell $\delta^{18}O$ values, and is neither explicitly accounted for here, nor linearly related to mean annual precipitation. As the shell

$\delta^{18}O$ is composed of two unknowns (snail body fluid, reflecting environmental water, and snail body temperature) this influence is impossible to quantify from this data alone, restricting climatic interpretation of shell $\delta^{18}O$ values to qualitative observations.

4.2.3 Factors influencing carbon and oxygen isotopes

The low coefficient of determination for both isotope-mean annual precipitation relationships ($\delta^{13}C$: 0.34, $\delta^{18}O$: 0.26) demonstrates that there are environmental influences not accounted for. I have discussed potential major sources of variability specific to each tracer, but there are also variables that influence both, mostly pertaining to snail ecology and ecophysiology. As neither of these is well understood for most Australian snails, I discuss these factors briefly only to highlight them as a target for future investigations.

In addition to the broad-scale influences described above, the food and water ingested by a snail, which contributes to the stable isotope composition of its body fluid and ultimately its shell, is determined by the growth season, age, and micro-habitat of the individual; the latter in turn comprises variations in micro-topography and micro-climate (Bao et al., 2018). For example, an obvious outlier on Figure 4.10 is the shell from Cape York, which preserves a greater negative offset from precipitation $\delta^{18}O$ than most other shells. The snail in question, *C. steveirwini*, is the only confirmed tree-dweller in our dataset, and it is very likely that *C. steveirwini* absorbs moisture from different pools to ground-dwelling snails. This highlights the importance of performing modern species-specific studies where possible.

The relationship of snail body fluid $\delta^{13}C$ and $\delta^{18}O$ values to that of the shell carbonate is presumably also affected by species-specific isotope fractionation factors (Goodfriend et al., 1989). The latter seems to be less of a problem for $\delta^{18}O$, given the smaller systematic species offsets observed in this multi-taxa dataset (Fig. 4.7), as well as similar conclusions reached in previous studies (Balakrishnan et al., 2005b; Yanes and Romanek, 2013; Yanes et al., 2009). However, it may also be that whilst all snails obtain moisture from surface waters—thereby absorbing similar $\delta^{18}O$—different species prefer to eat different vegetation types, hence ingesting food with distinct $\delta^{13}C$. If snails eat environmental carbonate, then this may influence the shell $\delta^{13}C$ and $\delta^{18}O$ values (eg. Yanes et al., 2008; Yanes et al., 2012; Zhang et al., 2014), although this finding is not universal (eg. Chiba and Davison, 2009; Stott, 2002), and probably depends on the specific combination of species, habitat, and climate (Zhang et al., 2014).

4.3 Land snail shell isotopes as a palaeohydrology archive

Confounding variables notwithstanding, the fact that both $\delta^{13}C$ and $\delta^{18}O$ values dominantly reflect mean annual precipitation is an encouraging result for land snail shells as a palaeohydrology archive for Australia, and provides a foundation for more detailed investigation of these relationships. The data presented here confirm work from a variety of climatological regimes elsewhere in the world, showing that the $\delta^{13}C$ and $\delta^{18}O$ values of land snail shells provide clues to environmental conditions during the snails' lifetime. However, due to large inter-annual variability in Australian precipitation, and possible species-specific effects, three key recommendations are suggested:

1. If possible, perform a 'calibration' study on modern snails prior to using fossil snails as palaeohydrological indicators. This should clarify much of the unexplained variability discussed in our broader-scale study. However, such studies may not always be feasible, especially if fossil species are rare or extinct.
2. Representative environmental reconstructions will be gained only from samples comprising as many individual shells as possible within a sediment layer. This should 'smooth' annual variability and snail dietary preferences, ideally providing a representative signal of both the climatology, and local vegetation.
3. For broad spatio-temporal studies, it will likely be necessary to employ the shells of snails from a variety of species. Given the apparent inter-specific variability for both $\delta^{13}C$ and $\delta^{18}O$, such reconstructions will probably only be informative where environmental variability is large enough to swamp 'noise' arising from ecological and physiological influences.

5 Conclusions

In a multi-taxon dataset from a wide climatic gradient across Australia, both the $\delta^{13}C$ and $\delta^{18}O$ values of land snail shells are negatively correlated with mean annual precipitation, albeit via different mechanisms. This is the first study of its kind to be conducted in Australia, and the first study in the world to examine both $\delta^{13}C$ and $\delta^{18}O$ values across such a diverse range of climates.

Snail shell $\delta^{13}C$ values are considered to reflect the $\delta^{13}C$ of C_3 vegetation, which in turn is controlled by moisture availability. With respect to inferring past hydroclimate from snail shells, large climate shifts resulting in a transition to strongly C_4 dominated vegetation should be clearly identifiable by a shift to more positive shell $\delta^{13}C$ values. By contrast, snail shell $\delta^{18}O$ values reflect the $\delta^{18}O$ of meteoric water, which—on the Australian continent—ultimately reflects precipitation amount. This may be a seasonal signal, with individual snails preferentially sampling precipitation during conditions most conducive to activity, although this requires further investigation.

Reconstructions of past precipitation from snail shell $\delta^{13}C$ and/or $\delta^{18}O$ values will now benefit from a deeper understanding of snail ecology and phenology. Specifically, knowledge of the dietary preferences of species would aid interpretation of shell $\delta^{13}C$. More information is also needed to deconvolve the multiple influences on snail shell $\delta^{18}O$, including—but not limited to—snail growth season, and the influence of temperature and relative humidity on the shell $\delta^{18}O$ values. In the absence of such information, I suggest that the $\delta^{13}C$ and $\delta^{18}O$ values of land snails may be useful as a qualitative indicator of major changes past hydroclimate.

6 References cited

Apolinarska, K., Pełechaty, M., Kossler, A., 2015. Within-sample variability of $\delta^{13}C$ and $\delta^{18}O$ values of freshwater gastropod shells and the optimum number of shells to measure per sediment layer in the Paddenluch palaeolacustrine sequence, Germany. Journal of Paleolimnology 54, 305-323.

Baker, G.H., 2008. The population dynamics of the mediterranean snails *Cernuella virgata, Cochlicella acuta* (Hygromiidae) and *Theba pisana* (Helicidae) in pasture/cereal rotations in South Australia: a 20-year study. Australian Journal of Experimental Agriculture 48, 1514-1522.

Balakrishnan, M., Yapp, C.J., 2004. Flux balance models for the oxygen and carbon isotope compositions of land snail shells. Geochimica et Cosmochimica Acta 68, 2007-2024.

Balakrishnan, M., Yapp, C.J., Meltzer, D.J., Theler, J.L., 2005a. Paleoenvironment of the Folsom archaeological site, New Mexico, USA, approximately 10,500 14C yr B.P. as inferred from the stable isotope composition of fossil land snail shells. Quaternary Research 63, 31-44.

Balakrishnan, M., Yapp, C.J., Theler, J.L., Carter, B.J., Wyckoff, D.G., 2005b. Environmental significance of $^{13}C/^{12}C$ and $^{18}O/^{16}O$ ratios of modern land-snail shells from the southern great plains of North America. Quaternary Research 63, 15-30.

Bao, R., Sheng, X., Teng, H.H., Ji, J., 2018. Reliability of shell carbon isotope composition of different land snail species as a climate proxy: A case study in the monsoon region of China. Geochimica et Cosmochimica Acta 228, 42-61.

Barnhart, M.C., 1986. Respiratory Gas Tensions and Gas Exchange in Active and Dormant Land Snails, Otala lactea. Physiological Zoology 59, 733-745.

Blunier, T., Brook, E.J., 2001. Timing of Millennial-Scale Climate Change in Antarctica and Greenland During the Last Glacial Period. Science 291, 109-112.

Bonadonna, F., Leone, G., 1995. Palaeoclimatological reconstruction using stable isotope data on continental molluscs from Valle di Castiglione, Roma, Italy. Holocene 5, 461-469.

Bonadonna, F.P., Leone, G., Zanchetta, G., 1999. Stable isotope analyses on the last 30 ka molluscan fauna from Pampa grassland, Bonaerense region, Argentina. Palaeogeography Palaeoclimatology Palaeoecology 153, 289-308.

Bowen, G.J., 2017. The Online Isotopes in Precipitation Calculator, version 3.1.

Bureau of Meteorology, 2010. Average annual rainfall over the period 1961 to 1990. Commonwealth of Australia.

Chiba, S., Davison, A., 2009. Associations Between Stable Carbon Isotope Ratio and Vegetation in Modern and Fossil Land Snails *Mandarina chichijimana* on Chichijima of the Ogasawara Islands. Paleontological Research 13, 151-157.

Colonese, A.C., Zanchetta, G., Fallick, A.E., Manganelli, G., Lo Cascio, P., Hausmann, N., Baneschi, I., Regattieri, E., 2014. Oxygen and carbon isotopic composition of modern terrestrial gastropod shells from Lipari Island, Aeolian Archipelago (Sicily). Palaeogeography, Palaeoclimatology, Palaeoecology 394, 119-127.

Colonese, A.C., Zanchetta, G., Fallick, A.E., Martini, F., Manganelli, G., Lo Vetro, D., 2007. Stable isotope composition of Late Glacial land snail shells from Grotta del Romito (Southern Italy): Palaeoclimatic implications. Palaeogeography, Palaeoclimatology, Palaeoecology 254, 550-560.

Colonese, A.C., Zanchetta, G., Perlès, C., Drysdale, R.N., Manganelli, G., Baneschi, I., Dotsika, E., Valladas, H., 2013. Deciphering late Quaternary land snail shell $\delta^{18}O$ and $\delta^{13}C$ from Franchthi Cave (Argolid, Greece). Quaternary Research 80, 66-75.

Dansgaard, W., 1964. Stable isotopes in precipitation. Tellus 16, 436-468.

Epstein, S., Buchsbaum, R., Lowenstam, H., Urey, H.C., 1951. Carbonate-water isotopic temperature scale. Geological Society of America Bulletin 62, 417-426.

Falster, G., Delean, S., Tyler, J., 2018a. Hydrogen Peroxide Treatment of Natural Lake Sediment Prior to Carbon and Oxygen Stable Isotope Analysis of Calcium Carbonate. Geochemistry, Geophysics, Geosystems 19, 3583-3595.

Falster, G., Tyler, J., Grant, K., Tibby, J., Turney, C., Löhr, S., Jacobsen, G., Kershaw, A.P., 2018b. Millennial-scale variability in south-east Australian hydroclimate between 30,000 and 10,000 years ago. Quaternary Science Reviews 192, 106-122.

Farquhar, G.D., O'Leary, M.H., Berry, J.A., 1982. On the relationship between carbon isotope discrimination and the intercellular carbon dioxide concentration in leaves. Australian Journal of Plant Physiology 9, 121-137.

Forbes, M.S., Kohn, M.J., Bestland, E.A., Wells, R.T., 2010. Late Pleistocene environmental change interpreted from $\delta^{13}C$ and $\delta^{18}O$ of tooth enamel from the Black Creek Swamp Megafauna site, Kangaroo Island, South Australia. Palaeogeography, Palaeoclimatology, Palaeoecology 291, 319-327.

Goodfriend, G.A., 1986. Variation in Land-Snail Shell Form and Size and its Causes: A Review. Systematic Zoology 35, 204-223.

Goodfriend, G.A., 1987. Radiocarbon Age Anomalies in Shell Carbonate of Land Snails from Semi-Arid Areas. Radiocarbon 29, 159-167.

Goodfriend, G.A., 1990. Rainfall in the Negev Desert during the middle Holocene, based on ^{13}C of organic matter in land snail shells. Quaternary Research 34, 186-197.

Goodfriend, G.A., 1992. The use of land snail shells in paleoenvironmental reconstruction. Quaternary Science Reviews 11, 665-685.

Goodfriend, G.A., Ellis, G.L., 2000. Stable carbon isotope record of middle to late Holocene climate changes from land snail shells at Hinds Cave, Texas. Quaternary International 67, 47-60.

Goodfriend, G.A., Ellis, G.L., 2002. Stable carbon and oxygen isotopic variations in modern Rabdotus land snail shells in the southern Great Plains, USA, and their relation to environment. Geochimica et Cosmochimica Acta 66, 1987-2002.

Goodfriend, G.A., Magaritz, M., 1987. Carbon and oxygen isotope composition of shell carbonate of desert land snails. Earth and Planetary Science Letters 86, 377-388.

Goodfriend, G.A., Magaritz, M., Gat, J.R., 1989. Stable isotope composition of land snail body-water and its relation to environmental waters and shell carbonate. Geochimica et Cosmochimica Acta 53, 3215-3221.

Hattersley, P.W., 1983. The distribution of C3 and C4 grasses in Australia in relation to climate. Oecologia 57, 113-128.

Hatziioannou, M., Eleutheriadis, N., Lazaridoudimitriadou, M., 1994. Food preferences and dietary overlap by terrestrial snails in Logos area (Edessa, Macedonia, northern Greece). Journal of Molluscan Studies 60, 331-341.

Heath, D.J., 1975. Colour, sunlight and internal temperatures in the land-snail Cepaea nemoralis (L.). Oecologia 19, 29-38.

Hollins, S.E., Hughes, C.E., Crawford, J., Cendon, D.I., Meredith, K.T., 2018. Rainfall isotope variations over the Australian continent - Implications for hydrology and isoscape applications. Science of the Total Environment 645, 630-645.

Iglesias, J., Castillejo, J., 1999. Field observations on feeding of the land snail *Helix aspersa* Muller. Journal of Molluscan Studies 65, 411-423.

Jeffrey, S.J., Carter, J.O., Moodie, K.B., Beswick, A.R., 2001. Using spatial interpolation to construct a comprehensive archive of Australian climate data. Environmental Modelling & Software 16, 309-330.

Kehrwald, N.M., McCoy, W.D., Thibeault, J., Burns, S.J., Oches, E.A., 2010. Paleoclimatic implications of the spatial patterns of modern and LGM European land-snail shell $\delta^{18}O$. Quaternary Research 74, 166-176.

Kempster, V., Charwat, S., 2003. Soil surface temperature and mortality in land snails: implications for successful management. Australian Journal of Experimental Agriculture 43, 1351-1356.

Knigge, T., Di Lellis, M.A., Monsinjon, T., Köhler, H.-R., 2017. Relevance of body size and shell colouration for thermal absorption and heat loss in white garden snails, *Theba pisana* (Helicidae), from Northern France. Journal of Thermal Biology 69, 54-63.

Kohn, M.J., 2010. Carbon isotope compositions of terrestrial C3 plants as indicators of (paleo)ecology and (paleo)climate. Proceedings of the National Academy of Sciences 107, 19691-19695.

Leng, M.J., Lewis, J.P., 2016. Oxygen isotopes in Molluscan shell: Applications in environmental archaeology. Environmental Archaeology 21, 295-306.

Leng, M.J., Marshall, J.D., 2004. Palaeoclimate interpretation of stable isotope data from lake sediment archives. Quaternary Science Reviews 23, 811-831.

Liu, J., Fu, G., Song, X., Charles, S.P., Zhang, Y., Han, D., Wang, S., 2010. Stable isotopic compositions in Australian precipitation. Journal of Geophysical Research: Atmospheres 115, 1 - 16.

Liu, Z., Gu, Z., Wu, N., Xu, B., 2007. Diet control on carbon isotopic composition of land snail shell carbonate. Chin. Sci. Bull. 52, 388-394.

McConnaughey, T.A., Burdett, J., Whelan, J.F., Paull, C.K., 1997. Carbon isotopes in biological carbonates: Respiration and photosynthesis. Geochimica Et Cosmochimica Acta 61, 611-622.

McDowell, M.C., 2013. Late Quaternary faunal responses to environmental change and isolation on a large Australian land-bridge island (PhD thesis), School of Biological Sciences. The Flinders University of South Australia.

McIntosh, P., Pook, M.J., Risbey, J.S., Hope, P.K., Wang, G., Alves, O., 2008. Australia's Regional Climate Drivers, Canberra, Australia.

Metref, S., Rousseau, D.D., Bentaleb, I., Labonne, M., Vianey-Liaud, M., 2003. Study of the diet effect on $\delta^{13}C$ of shell carbonate of the land snail *Helix aspersa* in experimental conditions. Earth and Planetary Science Letters 211, 381-393.

Miller, G.H., Fogel, M.L., 2016. Calibrating $\delta^{18}O$ in *Dromaius novaehollandiae* (emu) eggshell calcite as a paleo-aridity proxy for the Quaternary of Australia. Geochimica et Cosmochimica Acta 193, 1-13.

Murelaga, X., Ortega, L., Sancho, C., Muñoz, A., Osácar, C., Larraz, M., 2012. Succession and stable isotope composition of gastropods in Holocene semi-arid alluvial sequences (Bardenas Reales, Ebro Basin, NE Spain): Palaeoenvironmental implications. The Holocene 22, 1047-1060.

Nelson, D.M., Urban, M.A., Kershaw, A.P., Hu, F.S., 2016. Late-Quaternary variation in C3 and C4 grass abundance in southeastern Australia as inferred from $\delta^{13}C$ analysis: Assessing the roles of climate, pCO_2, and fire. Quaternary Science Reviews 139, 67-76.
Nicholls, N., Drosdowsky, W., Lavery, B., 1997. Australian rainfall variability and change. Weather 52, 66-72.

O'Leary, M.H., 1981. Carbon isotope fractionation in plants. Phytochemistry 20, 553-567.

Peel, M. C., Finlayson, B. L., McMahon, T. A., 2007. Updated world map of the Köppen-Geiger climate classification. Hydrology and Earth System Sciences 11, 1633-1644/

Prendergast, A.L., Stevens, R.E., O'Connell, T.C., Hill, E.A., Hunt, C.O., Barker, G.W., 2016.
A late Pleistocene refugium in Mediterranean North Africa? Palaeoenvironmental reconstruction from stable isotope analyses of land snail shells (Haua Fteah, Libya). Quaternary Science Reviews 139, 94-109.

Prentice, I.C., Meng, T., Wang, H., Harrison, S.P., Ni, J., Wang, G., 2011. Evidence of a universal scaling relationship for leaf CO_2 drawdown along an aridity gradient. New Phytologist 190, 169-180.

Prior, D.J., 1985. Water-regulatory behaviour in terrestrial gastropods. Biological Reviews 60, 403-424.

Rao, Z., Guo, W., Cao, J., Shi, F., Jiang, H., Li, C., 2017. Relationship between the stable carbon isotopic composition of modern plants and surface soils and climate: A global review. Earth-Science Reviews 165, 110-119.

Reeves, J.M., Barrows, T.T., Cohen, T.J., Kiem, A.S., Bostock, H.C., Fitzsimmons, K.E., Jansen, J.D., Kemp, J., Krause, C., Petherick, L., Phipps, S.J., Members, O.-I., 2013. Climate variability over the last 35,000 years recorded in marine and terrestrial archives in the Australian region: an OZ-INTIMATE compilation. Quaternary Science Reviews 74, 21-34.

Risbey, J.S., Pook, M.J., McIntosh, P.C., Wheeler, M.C., Hendon, H.H., 2009. On the Remote Drivers of Rainfall Variability in Australia. Monthly Weather Review 137, 3233-3253.

Smallridge, M.A., Kirby, G.C., 1988. Competitive interactions between the land snails *Theba pisana* (Müller) and *Cernuella Virgata* (Da Costa) from South Australia. Journal of Molluscan Studies 54, 251-258.

Stanisic, J., Shea, M., Potter, D., Griffiths, O., 2017. Australian land snails. Volume 2. A field guide to southern, central and western species. Bioculture Press, Mauritius.

Stankowski, S., 2011. Extreme, continuous variation in an island snail: local diversification and association of shell form with the current environment. Biological Journal of the Linnean Society 104, 756-769.

Stevens, R.E., Metcalfe, S.E., Leng, M.J., Lamb, A.L., Sloane, H.J., Naranjo, E., González, S., 2012. Reconstruction of late Pleistocene climate in the Valsequillo Basin (Central Mexico) through isotopic analysis of terrestrial and freshwater snails. Palaeogeography, Palaeoclimatology, Palaeoecology 319-320, 16-27.

Stewart, G.R., Turnbull, M.H., Schmidt, S., Erskine, P.D., 1995. ^{13}C Natural Abundance in Plant Communities Along a Rainfall Gradient: a Biological Integrator of Water Availability. Functional Plant Biology 22, 51-55.

Stott, L.D., 2002. The influence of diet on the $\delta^{13}C$ of shell carbon in the pulmonate snail *Helix aspersa*. Earth and Planetary Science Letters 195, 249-259.

Tibby, J., Barr, C., McInerney, F.A., Henderson, A.C.G., Leng, M.J., Greenway, M., Marshall, J.C., McGregor, G.B., Tyler, J.J., McNeil, V., 2016. Carbon isotope discrimination in leaves of the broad-leaved paperbark tree, Melaleuca quinquenervia, as a tool for quantifying past tropical and subtropical rainfall. Global Change Biology 22, 3474-3486.

Ward, D., Slotow, R., 1992. The effects of water availability on the life-history of the desert snail, *Trochoidea seetzenii* - an experimental field manipulation. Oecologia 90, 572-580.

Watkins, J.M., Hunt, J.D., Ryerson, F.J., DePaolo, D.J., 2014. The influence of temperature, pH, and growth rate on the $\delta^{18}O$ composition of inorganically precipitated calcite. Earth and Planetary Science Letters 404, 332-343.

Williams, A.A.J., Stone, R.C., 2009. An assessment of relationships between the Australian subtropical ridge, rainfall variability, and high-latitude circulation patterns. International Journal of Climatology 29, 691-709.

Yanes, Y., 2015. Stable isotope ecology of land snails from a high-latitude site near Fairbanks, interior Alaska, USA. Quaternary Research 83, 588-595.

Yanes, Y., Al-Qattan, N.M., Rech, J.A., Pigati, J.S., Dodd, J.P., Nekola, J.C., 2018. Overview of the oxygen isotope systematics of land snails from North America. Quaternary Research, 1-16.

Yanes, Y., Delgado, A., Castillo, C., Alonso, M.R., Ibáñez, M., De la Nuez, J., Kowalewski, M., 2008. Stable isotope ($\delta^{18}O$, $\delta^{13}C$, and δD) signatures of recent terrestrial communities from a low-latitude, oceanic setting: Endemic land snails, plants, rain, and carbonate sediments from the eastern Canary Islands. Chemical Geology 249, 377-392.

Yanes, Y., Fernández-Lopez-de-Pablo, J., 2017. Calibration of the stable isotope composition and body size of the arid-dwelling land snail *Sphincterochila candidissima*, a climatic archive abundant in Mediterranean archaeological deposits. The Holocene 27, 890-899.

Yanes, Y., Gutiérrez-Zugasti, I., Delgado, A., 2012. Late-glacial to Holocene transition in northern Spain deduced from land-snail shelly accumulations. Quaternary Research 78, 373-385.

Yanes, Y., Izeta, A.D., Cattáneo, R., Costa, T., Gordillo, S., 2014. Holocene (~4.5–1.7 cal. kyr BP) paleoenvironmental conditions in central Argentina inferred from entire-shell and intra-shell stable isotope composition of terrestrial gastropods. Holocene 24, 1193-1205.

Yanes, Y., Nekola, J.C., Rech, J.A., Pigati, J.S., 2017. Oxygen stable isotopic disparities among sympatric small land snail species from northwest Minnesota, USA. Palaeogeography, Palaeoclimatology, Palaeoecology 485, 715-722.

Yanes, Y., Romanek, C.S., 2013. Quaternary interglacial environmental stability in San Salvador Island (Bahamas): A land snail isotopic approach. Palaeogeography, Palaeoclimatology, Palaeoecology 369, 28-40.

Yanes, Y., Romanek, C.S., Delgado, A., Brant, H.A., Noakes, J.E., Alonso, M.R., Ibanez, M., 2009. Oxygen and carbon stable isotopes of modern land snail shells as environmental indicators from a low-latitude oceanic island. Geochimica Et Cosmochimica Acta 73, 4077-4099.

Yanes, Y., Yapp, C.J., Ibáñez, M., Alonso, M.R., De-la-Nuez, J., Quesada, M.L., Castillo, C., Delgado, A., 2011. Pleistocene–Holocene environmental change in the Canary Archipelago as inferred from the stable isotope composition of land snail shells. Quaternary Research 75, 658-669.

Yapp, C.J., 1979. Oxygen and carbon isotope measurements of land snail shell carbonate. Geochimica Et Cosmochimica Acta 43, 629-635.

Zhang, N., Yamada, K., Suzuki, N., Yoshida, N., 2014. Factors controlling shell carbon isotopic composition of land snail *Acusta despecta sieboldiana* estimated from laboratory culturing experiment. Biogeosciences 11, 5335-5348.

Supporting information for Chapter Four

Environmental controls on the carbon and oxygen stable isotope ratios of modern land snail shells in Australia

Supplementary Table 4.1. Sample collection details for all land snail shell stable isotope data presented in the text. Samples at each location consisted of empty shells, although an effort was made to choose samples that appeared to have died recently e.g. completely intact, and ideally with organic matter still attached. Species identified from shell morphology, with assistance from Tony Robinson at the South Australian Museum.

Site name	Date of collection	Latitude	Longitude	Altitude m	Species
PG-132	27/03/2003	-33.43	121.27	174	*Bothriembryon dux*
PG-133	27/03/2003	-33.30	121.30	206	*Bothriembryon dux*
PG-131	27/03/2003	-33.38	121.34	178	*Bothriembryon dux*
					Bothriembryon melo
B-116	28/06/2004	-31.30	121.51	384	*Bothriembryon indictus*
					Sinumelon nullarboricum
PG-134	27/03/2003	-33.15	121.71	238	*Bothriembryon dux*
					Bothriembryon melo
PG-156	30/03/2003	-32.35	123.62	180	*Bothriembryon dux*
					Cernuella virgata
B-157	27/06/2004	-32.32	125.05	131	*Bothriembryon indictus*
					Pleuroxia elfina
					Pleuroxia polypleura
					Sinumelon nullarboricum
PG-157	30/03/2003	-32.32	125.05	143	*Bothriembryon esperantia*
					Pleuroxia elfina
					Pleuroxia polypleura
					Sinumelon nullarboricum
RP-3-A	12/02/2002	-31.96	126.91	29	*Bothriembryon indictus*
					Cernuella virgata
					Pleuroxia polypleura
PG-159	31/03/2003	-31.90	127.02	63	*Bothriembryon indictus*
					Cernuella virgata
					Sinumelon nullarboricum
B-162	1/07/2004	-31.55	130.59	61	*Bothriembryon indictus*
PG-162/163	31/03/2003	-31.55	130.62	62	*Bothriembryon barretti*
PG-162/163A	31/03/2003	-31.81	132.24	37	*Cernuella virgata*
					Cochlicella acuta
Alice Springs	14/05/2016	-23.73	132.87	746	*Pleuroxia adcockiana*
					Sinumelon expositum
PG-166	1/04/2003	-32.41	134.52	80	*Cernuella virgata*
					Cernuella virgata
PG-171	1/04/2003	-33.33	134.88	70	*Cernuella virgata*
					Theba pisana
PG-172	1/04/2003	-33.34	134.88	77	*Cochlicella acuta*
					Theba pisana
PG-168	1/04/2003	-32.89	135.12	112	*Cernuella virgata*
PG-173	1/04/2003	-33.49	135.14	50	*Cernuella virgata*
					Cochlicella acuta
PG-167	1/04/2003	-32.82	135.16	186	*Cernuella virgata*
GOC-22B	2/05/2004	-16.08	136.53	47	*Xanthomelon durvillii*
PG-107	8/07/2002	-34.98	137.51	16	*Cernuella virgata*
					Cochlicella acuta
					Theba pisana
PG-104	7/07/2002	-34.58	137.60	75	*Cernuella virgata*
					Cochlicella acuta
PG-101/102	7/07/2002	-33.97	137.70	53	*Cernuella virgata*
PG-103	7/07/2002	-34.31	137.72	188	*Cernuella virgata*
					Theba pisana

Supplementary Table 4.1 contd.

Site name	Date of collection	Latitude	Longitude	Altitude m	Species
PG-102	7/07/2002	-34.08	137.73	91	*Cernuella virgata*
					Cochlicella acuta
PG-102R	10/04/2004	-34.08	137.73	60	*Cernuella virgata*
					Cochlicella acuta
KI-2	15/07/2016	-35.84	137.75	22	*Cernuella virgata*
PG-106	7/07/2002	-34.85	137.76	52	*Cernuella virgata*
					Cochlicella acuta
					Theba pisana
PG-100	7/07/2002	-33.77	137.85	58	*Cernuella virgata*
PG-108	8/07/2002	-34.54	137.88	38	*Cochlicella acuta*
					Theba pisana
PG-110	8/07/2002	-34.07	137.96	108	*Austrosuccinea australis*
					Cernuella virgata
					Cochlicella acuta
PG-109	8/07/2002	-34.28	137.98	33	*Cernuella virgata*
					Cochlicella acuta
PG-98	7/07/2002	-33.83	138.02	124	*Cernuella virgata*
PG-99	7/07/2002	-33.52	138.06	33	*Cernuella virgata*
PG-94	6/07/2002	-34.31	138.26	23	*Cochlicella acuta*
					Theba pisana
B-94	11/04/2004	-34.31	138.26	13	*Cochlicella acuta*
					Theba pisana
PG-95	6/07/2002	-34.24	138.29	39	*Cernuella virgata*
PG-96	7/07/2002	-34.21	138.32	40	*Cernuella virgata*
PG-97	6/07/2002	-33.85	138.41	123	*Cernuella virgata*
PG-50	27/08/2001	-33.69	138.93	474	*Cernuella virgata*
PG-54	28/08/2001	-34.49	139.36	213	*Cernuella virgata*
PG-55	28/08/2001	-34.67	139.46	124	*Cernuella virgata*
PG-57	29/08/2001	-35.27	139.46	4	*Cernuella virgata*
					Cochlicella acuta
PG-57					*Theba pisana*
PG-51	28/08/2001	-34.40	139.60	44	*Cernuella virgata*
CW-1	27/10/2017*	-36.26	139.71	4	*Cernuella virgata*
MA0038	4/04/2016	-35.70	139.86	31	*Cernuella virgata*
					Cochlicella acuta
PG-56	29/08/2001	-32.67	140.17	85	*Cernuella virgata*
PG-30	24/08/2001	-34.15	140.19	54	*Cernuella virgata*
PG-27	24/08/2001	-34.25	140.62	56	*Cernuella virgata*
BL-1	27/10/2017*	-37.12	140.73	52	*Cernuella virgata*
PG-59	29/08/2001	-35.31	140.79	108	*Cernuella virgata*
5U6-mod (Blanche Cave)	26/10/2017	-37.03	140.80	67	*Cernuella virgata*
PG-25D	24/08/2001	-34.29	140.86	23	*Cernuella virgata*
					Pleuroxia elfina
PG-26	24/08/2001	-34.29	140.86	24	*Cernuella virgata*
MA0083	6/04/2016	-37.88	141.08	70	*Cernuella virgata*
					Cochlicella acuta
MA0082	6/04/2016	-37.89	141.10	60	*Cochlicella acuta*
GOC-45D	9/05/2004	-15.42	141.88	11	*Crikey steveirwini*
MA0219	26/02/2017	-35.07	142.33	39	*Cernuella virgata*
MA0068	5/04/2016	-38.23	143.10	111	*Cornu aspersum*
PG-1	22/08/2001	-35.19	143.35	63	*Cernuella virgata*
MA0220	26/02/2017	-34.67	143.56	65	*Cernuella virgata*
GOC-58A	19/05/2004	-17.64	145.46	796	*Spurlingia gemma*

*denotes live at the time of collection

Chapter 5

Statement of Authorship

Title of Paper	Clarifying the climate-isotope relationship in Australian land snails using clumped isotopes and flux balance models
Publication Status	☐ Published ☐ Accepted for Publication ☐ Submitted for Publication ☑ Unpublished and Unsubmitted w ork w ritten in manuscript style
Publication Details	Falster, G., Tyler, J., Dux, F., Drysdale, R., Tibby, J., Chivas, A. (2019). Clarifying the climate-isotope relationship in Australian land snails using clumped isotopes and flux balance models

Principal Author

Name of Principal Author (Candidate)	Georgina Falster		
Contribution to the Paper	Devised study, prepared and analysed samples, interpreted data, wrote manuscript, acted as corresponding author.		
Overall percentage (%)	90 %		
Certification:	This paper reports on original research I conducted during the period of my Higher Degree by Research candidature and is not subject to any obligations or contractual agreements with a third party that would constrain its inclusion in this thesis. I am the primary author of this paper.		
Signature		Date	11/3/2019

Co-Author Contributions

By signing the Statement of Authorship, each author certifies that:

i. the candidate's stated contribution to the publication is accurate (as detailed above);

ii. permission is granted for the candidate in include the publication in the thesis; and

iii. the sum of all co-author contributions is equal to 100% less the candidate's stated contribution.

Name of Co-Author	Jonathan Tyler		
Contribution to the Paper	Provided conceptual guidance, evaluated and edited manuscript.		
Signature		Date	31/1/2019

Name of Co-Author	Florian Dux		
Contribution to the Paper	Assisted with acquisition and processing of clumped isotope data.		
Signature		Date	5.2.2019

Name of Co-Author	Russell Drysdale		
Contribution to the Paper	Provided access to facilities for clumped and stable isotope analysis.		
Signature		Date	31 January 2019

Name of Co-Author	John Tibby		
Contribution to the Paper	Evaluated and edited manuscript.		
Signature		Date	31/1/2019

Name of Co-Author	Allan Chivas		
Contribution to the Paper	Collected and provided samples for analysis, assisted with acquisition of clumped and stable isotope data.		
Signature		Date	01 February 2019

Clarifying the climate-isotope relationship in Australian land snail shells using clumped isotopes and flux balance models

Abstract

Quantitative palaeoclimate data are required to interpret palaeoclimate reconstructions in the context of historical records and climate model results. However, quantification of past precipitation in Australia has rarely been attempted beyond the Holocene due to a lack of reliable proxies. Modern and fossil land snails are abundant across Australia, and the carbon and oxygen stable isotope compositions ($\delta^{13}C$ and $\delta^{18}O$) of their shells preserve information about past precipitation. However, these relationships are confounded by various environmental factors. Snail shell $\delta^{18}O$ values record a convolution of snail body temperature and formation water (snail body fluid) information. The latter is dependent on factors including snail active season and variability in the $\delta^{18}O$ of precipitation. Spatial variability in snail shell $\delta^{13}C$ values suggest that Australian snails favour C_3 plants such that shell $\delta^{13}C$ values reflect the influence of moisture stress on plant tissue $\delta^{13}C$, although this mechanism has yet to be tested.

A steady state flux balance model is used to determine the likely seasons of shell growth for land snails from a wide climatic gradient across Australia, based on their shell $\delta^{18}O$. The shells preserve a $\delta^{18}O$ signal biased to the rainiest months at each location. The clumped isotope composition (ratio of $^{13}C^{18}O^{16}O$ to $^{12}C^{16}O^{16}O$; Δ_{47}) of 16 Australian land snail shells from 15 different sites is also measured. Snail growth temperatures calculated from the shell Δ_{47} do not have a straightforward relationship with seasonal average temperatures, probably reflecting the narrow environmental tolerance of land snails. This temperature information is used to decouple snail body fluid $\delta^{18}O$ from shell $\delta^{18}O$, revealing a strong relationship between snail body fluid $\delta^{18}O$ and total precipitation during the wettest months ($p < 0.05$, $R^2 = 0.67$). It is suggested that with detailed modern calibration studies, a combined Δ_{47} and $\delta^{18}O$ approach may provide a quantitative palaeoprecipitation proxy that is applicable across much of the Australian continent.

Shell $\delta^{13}C$ values are also combined with general snail physiological parameters, to estimate absolute $\delta^{13}C$ values of food eaten by the snails. Dietary $\delta^{13}C$ values fall mostly within the range of C_3 plants, providing support for a C_3-dominated diet of Australian land snails, although some higher dietary $\delta^{13}C$ values may reflect limestone consumption by some snails.

Like many palaeoenvironmental indicators, snail shell isotopes are complicated by the myriad controls on isotope composition. However, the results of this study indicate that even where it is not possible to obtain an empirical understanding of the ecophysiology of fossil snails, interrogation of snail shell geochemistry beyond bulk shell $\delta^{13}C$ and $\delta^{18}O$ values may allow detailed reconstruction of past environmental change.

1 Introduction

Australia is subject to influence from major ocean-atmosphere circulation patterns, resulting in greater rainfall variability than otherwise similar climates elsewhere in the world (McIntosh et al., 2008; Risbey et al., 2009). Understanding this variability is crucial for land-use management, as well as planning and preparation for extreme rainfall events (Barr et al., 2019; Cook et al., 2016; Ho et al., 2015). However, reliable rainfall measurements only extend back to the early 20th century (Viney and Bates, 2004). This interval does not sample the natural range of possible rainfall variability in Australia, including changes of a magnitude similar to those that may occur in the future (e.g. Clark et al., 2016; Sanchez Goñi and Harrison, 2010). Reconstructing past climate change may clarify the response of Australian rainfall to changes in the strength and relative influence of remote drivers under different boundary conditions to modern. The Late Pleistocene is particularly informative, as it is the most recent time interval featuring abrupt and extreme centennial- to millennial-scale climate fluctuations, beyond what is preserved in instrumental records (e.g. Blockley et al., 2012; Turney et al., 2017). Interactions between the remote drivers of Australian rainfall often manifest in distinct spatial rainfall patterns across the continent (Risbey et al., 2009), and a detailed understanding of the influence of drivers throughout the climatic fluctuations of the Late Pleistocene therefore requires a spatial network of reliable proxy data.

Whilst Australian climate archives have yielded a wealth of qualitative hydroclimate-related palaeoclimate data (Chapter 3, this thesis), most of these records do not extend to the present day, and therefore cannot be directly calibrated or interpreted in the context of historical rainfall. Inter-comparison of these ‘floating’ records to gauge spatial variability in rainfall patterns is similarly challenging, in the absence of a common baseline. Quantitative palaeoprecipitation data are required to anchor qualitative records, enabling direct comparison with contemporaneous and modern rainfall.

Quantitative rainfall reconstructions require a thorough characterisation of the relationship between rainfall amount and the proxy response variable. The considerable challenge of mathematically defining these relationships is enhanced by the wide range of factors influencing rainfall in Australia, resulting in non-linear and potentially non-stationary

interactions (Gallant et al., 2013; Risbey et al., 2009). At present, quantitative information for past Australian precipitation during the Late Pleistocene is restricted to two records based on fossil pollen assemblages (Kershaw et al., 2004; van der Kaars et al., 2006). Models that have been published but not yet applied to fossil sediment include predictions of rainfall amount from various different pollen assemblages (Cook and van der Kaars, 2006; Herbert and Harrison, 2016), beetle assemblages (Porch, 2010), and the $\delta^{13}C$ of surface charcoal (Turney, 2012). A rainfall calibration based on the $\delta^{13}C$ of *Melaleuca quinquenervia* (broad-leafed paperbark) leaves (Tibby et al., 2016) was recently applied to sub-fossil leaves from Swallow Lagoon in eastern Australia (Barr et al., 2019). However, this record extends only to the mid-Holocene, and the broad-leafed paperbark is restricted to the east Australian coastal margin. Regarding the pollen and beetle-based methods, the wide array of influences on biological assemblages and the lack of modern analogue assemblages for a range of climate states may result in reconstructions that do not strictly reflect Quaternary reality (Jackson and Williams, 2004; Porch, 2010).

A new quantitative proxy for precipitation amount, that is applicable across Australia, will therefore contribute to understanding the long-term evolution of continental rainfall patterns. The stable isotope composition of land snail shells is one such potential proxy. Land snails occur in a broad range of habitats across Australia, and both the oxygen and carbon stable isotope ratios ($\delta^{18}O$ and $\delta^{13}C$ values) of their aragonite shells can be linked to annual precipitation amount, albeit via different mechanisms (Chapter 4, this thesis). Snail shell $\delta^{18}O$ values reflect the $\delta^{18}O$ of surface water absorbed by the snail, which in turn reflects meteoric water. In Australia, the $\delta^{18}O$ of meteoric water is correlated with weakly precipitation amount, although this relationship is also influenced by temperature, moisture source, and continentality (Hollins et al., 2018). Snail shell $\delta^{13}C$ values reflect the $\delta^{13}C$ of vegetation ingested by the snail (Liu et al., 2007), which varies mostly according to plant moisture stress and seasonality of precipitation, although this is also dependent on the specific plant component (Farquhar et al., 1989; O'Leary, 1981; Prentice et al., 2011; Rao et al., 2017). The relationships of both $\delta^{18}O$ and $\delta^{13}C$ values with annual precipitation retain considerable scatter, indicating contributions from variables not accounted for by these simple correlations.

If one or both of these isotope-precipitation relationships is to be developed into a quantitative palaeoclimate proxy, then these confounding variables must be accounted for. This is challenging without detailed knowledge of the ecology and phenology of specific snail species (Yanes et al., 2017). The $\delta^{18}O$ of land snail shells in particular is dependent on a wide array of environmental variables, and extracting any single environmental influence from the many is not straightforward (Fig. 5.1). Even the relatively clear relationship between

shell $\delta^{13}C$ and the $\delta^{13}C$ of the snail's diet is muddied by unknown dietary preferences of particular snail species (Goodfriend and Magaritz, 1987), although $\delta^{13}C$ values from Australian snail shells suggest that Australian snails favour C_3 vegetation, even in environments with a high relative abundance of C_4 vegetation (Chapter 4, this thesis). However, this behaviour has not been directly observed.

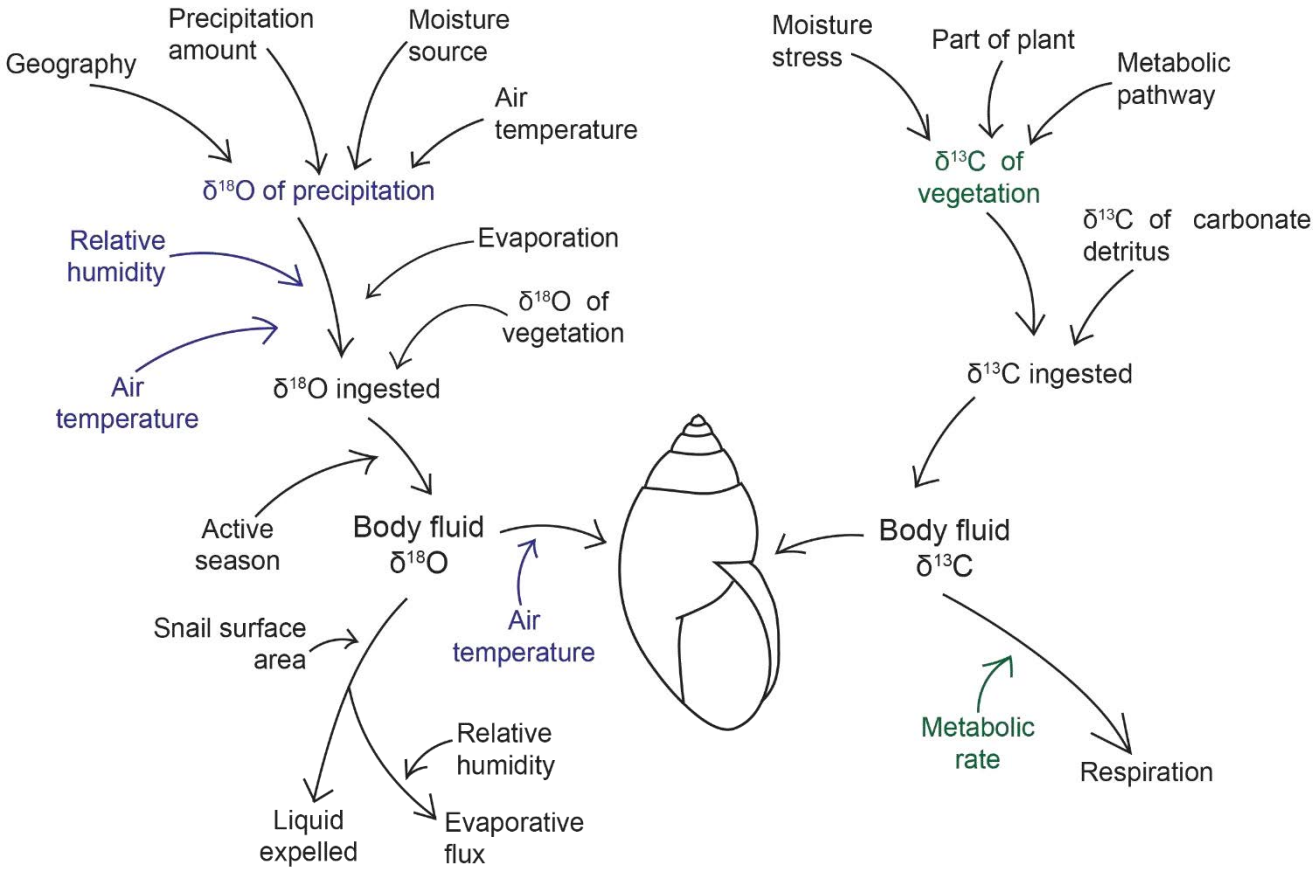

Figure 5.1. Environmental, ecological, and physiological controls on the $\delta^{18}O$ and $\delta^{13}C$ of land snail shell carbonate. Parameters that are explicit inputs to the $\delta^{18}O$ snail flux balance model are coloured blue, and inputs to the $\delta^{13}C$ model are coloured green.

A first-order complication in interpreting snail shell $\delta^{18}O$ values is that they are a function of *two* factors: $\delta^{18}O$ of the carbonate formation water (the snail body fluid) and the snail's body temperature at the time that the snail secretes the shell carbonate. As land snails are poikilothermic (i.e. internal temperature fluctuates as a consequence of the ambient environmental temperature), variability in body temperature is not trivial. Extracting the temperature component of shell $\delta^{18}O$ should result in a closer reflection of meteoric water $\delta^{18}O$ (Prendergast et al., 2015), and hence precipitation amount (Hollins et al., 2018). This may be accomplished via carbonate 'clumped isotope' analysis. Clumped isotope analysis is a relatively new technique that enables calculation of the growth temperature of carbonate

minerals, independent on the $\delta^{18}O$ of the formation water (Eiler, 2007). Temperature estimation from clumped isotope analysis (the 'clumped isotope thermometer') is based on measurement of the excess of ^{13}C-^{18}O bonds in the carbonate lattice, above a theoretical random distribution (Ghosh et al., 2006; Schauble et al., 2006). This excess—denoted Δ_{47}—occurs with greater frequency at lower temperatures, and this temperature dependence results in a Δ_{47} decrease of approximately 0.0033 ‰ per degree Celsius (Kele et al., 2015). Δ_{47} can generally be measured with precision of around ± 0.01 ‰, corresponding to a temperature sensitivity of around ± 2 °C (Dennis et al., 2011). $\delta^{18}O$ is measured simultaneously with Δ_{47}, allowing calculation of the formation water $\delta^{18}O$. The clumped isotope-temperature calibration is mostly unaffected by carbonate phase (Eiler, 2011; Thiagarajan et al., 2011; Tripati et al., 2010), with only a handful of documented exceptions (Affek et al., 2008; Affek et al., 2014; Daëron et al., 2011; Meckler et al., 2009). Fortunately, Zhang et al. (2018) demonstrated that the shells of land snails cultivated under controlled conditions faithfully record growth temperatures; however, wild snails have a relatively narrow environmental tolerance, and actively seek out clement conditions which may not be representative of the ambient climate (Prior, 1985; Zaarur et al., 2011). Given the potentially unpredictable relationship between snail growth temperature and average environmental temperatures, the clumped isotope thermometer should therefore be particularly useful in deconvolving temperature and body fluid $\delta^{18}O$.

Here the carbonate clumped isotope thermometer is used to calculate snail shell growth temperatures and body fluid $\delta^{18}O$, with the intention of reducing the number of confounding factors in the $\delta^{18}O$ shell-precipitation amount relationship. This relationship is explored further by combining the temperature information with a published snail flux balance model, to assess the potential of snail shell $\delta^{18}O$ and Δ_{47} as a quantitative precipitation proxy. The snail physiological information inherent in the flux balance model is also used to better understand snail shell $\delta^{13}C$ values.

2 Methods

2.1 Study area

Australia spans a broad range of climate zones, often featuring intra- and inter-annual precipitation more variable than places elsewhere on earth with similar mean annual precipitation (Nicholls et al., 1997). This is largely because Australian climates are influenced by multiple drivers from adjacent ocean basins, resulting in spatial variability in both temperature and precipitation (McIntosh et al., 2008; Risbey et al., 2009). This range of climate zones provides an excellent natural laboratory to examine the stable isotope composition of snail shells grown in a range of environmental conditions. Following the

approach taken in Chapter Four, Australian climates are considered here in terms of four broad geographical regions: south-central and south-east (arid to temperate climates), central Australia (arid climate), and north-east (tropical to equatorial climates).

The land snail sample set described in Chapter Four was also used in this study (data provided in Appendix 2 Table A3). In brief, the samples are from 62 sites, spanning a broad spatial and climatic gradient, but biased toward the southern coast of Australia (Fig. 5.2). Living snails were generally not present, so well-preserved empty shells were targeted instead. For a detailed description of the sample set, see Chapter Four Section 2, Table 4.1 and Supplementary Table 4.1.

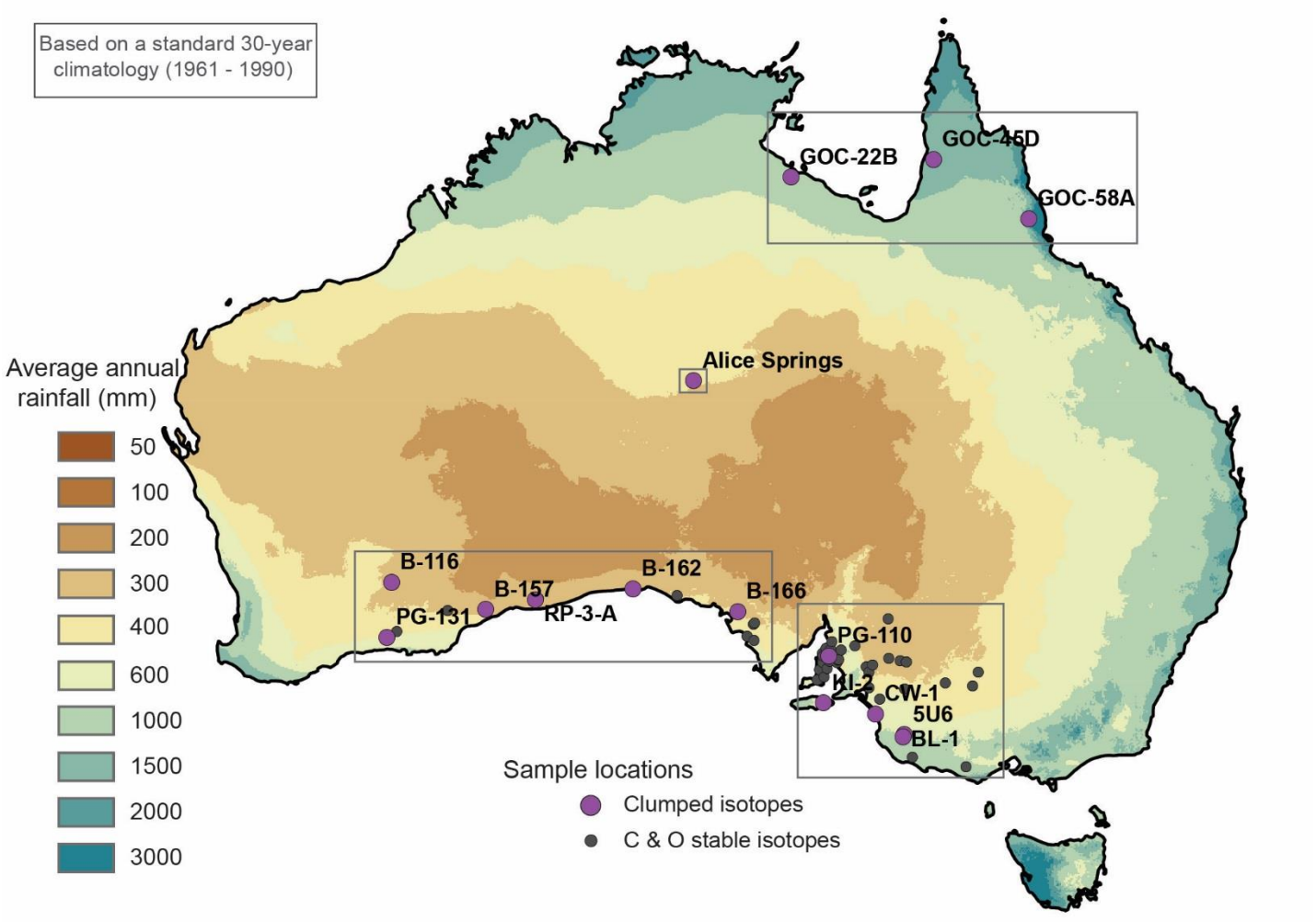

Figure 5.2. Location of snail shell collection sites. Smaller grey circles denote conventional stable isotope samples (Chapter 4), and larger purple circles denote the location of sites with clumped isotope analyses. The map of Australia is coloured according to average annual rainfall (BOM, 2010). Grey boxes denote geographical regions discussed in the text.

2.2 Climate data

A key finding from Chapter Four was the need to compare snail shell $\delta^{18}O$ with seasonal—rather than annual average—climate data. Here, monthly average climate data previously obtained from the Scientific Information for Land Owners (SILO) database were used to calculate seasonal averages i.e. the austral summer (DJF), autumn (MAM), winter (JJA), and spring (SON); see Chapter Four Section 2.3 for a description of SILO data products. In addition, the average monthly $\delta^{18}O$ of precipitation was calculated for each site, using the Online Isotopes in Precipitation Calculator (OIPC; Bowen, 2017). The OIPC provides an estimate of monthly precipitation $\delta^{18}O$ at a specified location, based on data derived mostly from the International Atomic Energy Association/World Meteorological Organization Global Network for Isotopes in Precipitation (GNIP; IAEA/WMO, 2015). These data have been interpolated to provide global maps of monthly precipitation $\delta^{18}O$, following the method outlined by Bowen et al. (2005). In common with most published isoscapes, the interpolation algorithms include latitude, altitude, and meteorological variables, theoretically resulting in realistic predictions. However, the GNIP dataset has a strong Northern Hemisphere bias and does not always provide accurate values for Australian precipitation, particularly for areas influenced by tropical cyclones (Hollins et al., 2018). Nevertheless, these are the only monthly estimates currently available for Australia, so they are used here as indicators of broad spatial variability in precipitation $\delta^{18}O$, whilst recognising that absolute values are unlikely to be strictly accurate.

2.3 Sample preparation and analysis

The snail shell $\delta^{18}O$ and $\delta^{13}C$ data discussed in Chapter Four are used here (Appendix 2 Table A3). In summary: the $\delta^{18}O$ and $\delta^{13}C$ values of samples consisting five individual shells was measured for each of the 62 sites. Where more than one species was present at a site, these species were analysed separately. For a subset of samples, five individual shells were analysed separately—these data are presented here as site averages. For details of the sample preparation and analysis, see Chapter Four Section 2.4 and Appendix 1.

2.4 Clumped isotope analysis

To clarify the influence of temperature on the snail shell $\delta^{18}O$, the clumped isotope composition of a subset of the powdered shell samples was analysed (Table 5.1). Fifteen of the most geographically, climatologically, and isotopically disparate sites were selected, to ensure analysis of a representative suite of samples. Site PG-110 featured one species that was particularly isotopically distinct (Fig. 4.6), so two species from this site were analysed, for a total of 16 analyses. The samples were selected by using Ward's method in conjunction

with a Euclidean distance matrix to divide the sites into fifteen clusters based on the average isotopic and climatological (mean average temperature and precipitation) data for each locality. The site closest to the cluster centroid was selected for clumped isotope analysis. Clumped isotope analysis was performed on residual powders from the stable isotope analyses i.e. the shell carbonate had been manually cleaned, subject to oxidation with buffered hydrogen peroxide (Chapter 2, this thesis), air dried, and then gently ground to a homogeneous fine-grained powder (see Chapter 4 Section 2.4 and Appendix 1 for details).

Clumped isotope analysis was undertaken at The University of Wollongong (UOW) and The University of Melbourne (UOM). Detailed analytical methods for each laboratory are provided in Appendix 1, but the broad approach (extraction, purification, and measurement of CO_2 gas) is common to both laboratories. In summary, ortho-phosphoric acid was used to transform aliquots of powdered snail shell to gaseous CO_2. The gas was purified using temperature-controlled gas chromatography (UOW) or transport of the CO_2 through a trap packed with Porapak™ Q (UOM). A Thermo Finnigan MAT 253 (UOW) or Nu Instruments Perspective-IS (UOM) dual inlet mass spectrometer was used to measure the $\delta^{18}O$, $\delta^{13}C$, and Δ_{47} of the purified gas relative to an ultra-high purity working gas of known isotopic composition. The raw sample Δ_{47} was calculated as

$$\Delta_{47} = \left[\left(\frac{R^{47}}{R^{47*}} - 1\right) - \left(\frac{R^{46}}{R^{46*}} - 1\right) - \left(\frac{R^{45}}{R^{45*}} - 1\right)\right] \times 1000$$

where

$$R^i = \frac{mass\ i}{mass\ 44}$$

i.e. the R^i values are abundance ratios of the mass 45, 46, and 47 CO_2 isotopologues, relative to mass 44 CO_2. The parameter R^{i*} is analogous to R^i, but corresponds to the expected ratios given a stochastic distribution of all possible isotopologues. These R^i values are derived in turn from the measured δ values for each isotopologue in the sample gas, relative to the working gas:

$$\delta^i = \left[\frac{R_{i(sample\ gas)}}{R_{i\ (working\ gas)}} - 1\right] \times 1000$$

The two laboratories use different methods to account for methodological and analytical artifacts, allowing conversion of raw Δ_{47} values into a common reference frame. At UOW, the isotopic composition of a) heated, and b) equilibrated CO_2 gases are used to calibrate the raw sample data into the absolute reference frame (Dennis et al., 2011).

Table 5.1. Clumped and stable isotope data for modern Australian land snail shells. Temperatures calculated using the Δ_{47}-T calibration equation of Bernasconi et al. (2018). $\delta^{18}O_{snail\ body\ fluid}$ calculated using the Δ_{47} temperatures and shell $\delta^{18}O$ (Kim et al., 2007). 'n' denotes the number of replicate measurements for each sample.

Lab	Sample name	Latitude	Longitude	Species	Specimens in sample	n	$\delta^{13}C$	$\delta^{18}O$	Δ_{47} (corrected)	SE	Temperature	SE	$\delta^{18}O_{snail\ body\ fluid}$	SE
							‰ VPDB	‰ VPDB	‰		°C		‰ VSMOW	
Melbourne	B-116	-31.30	121.51	*Bothriembryon indictus*	5	7	-4.0	0.4	0.680	0.006	23	1.6	0.1	0.3
Melbourne	B-157	-32.32	125.05	*Bothriembryon indictus*	5	6	-6.1	1.0	0.680	0.004	22	1.2	1.4	0.2
Melbourne	RP-3-A	-31.96	126.91	*Bothriembryon indictus*	5	8	-3.8	2.2	0.690	0.008	20	2.4	1.6	0.5
Melbourne	B-166	-32.41	134.52	*Cernuella virgata*	5	8	-9.0	-0.4	0.680	0.007	24	2.2	0.2	0.4
Melbourne	KI-2	-35.84	137.75	*Cochlicella acuta*	5	3	-9.2	0.1	0.670	0.004	25	1.2	0.1	0.2
Melbourne	CW-1	-36.26	139.71	*Cernuella virgata*	5	2	-9.2	0.6	0.690	0.004	20	1.0	-0.7	0.2
Melbourne	BL-1	-37.12	140.73	*Cernuella virgata*	5	3	-11.1	-0.1	0.680	0.004	23	1.1	-0.6	0.2
Melbourne	5U6	-37.03	140.80	*Cernuella virgata*	5	3	-9.8	0.5	0.670	0.003	24	0.9	1.1	0.2
Wollongong	PG-131	-33.38	121.34	*Bothriembryon melo*	5	2	-6.9	-0.6	0.720	0.003	12	0.8	1.4	0.2
Wollongong	B-162	-31.55	130.59	*Bothriembryon indictus*	5	2	-4.1	1.5	0.730	0.001	10	0.1	2.8	0.0
Wollongong	Alice Springs	-23.73	132.87	*Sinumelon expositum*	5	1	-8.6	2.2	0.735	NA	8	NA	2.7	NA
Wollongong	GOC-22B	-16.08	136.53	*Xanthomelon durvillii*	2	2	-14.1	-5.6	0.730	0.005	8	1.2	-4.2	0.3
Wollongong	GOC-45D	-15.42	141.88	*Crikey steveirwini*	1	1	-12.3	-1.7	0.719	NA	12	NA	0.3	NA

The former are heated to 1000°C to reach a stochastic distribution of isotopologues i.e. Δ_{47} = 0, and the latter are equilibrated with water at 10, 25, and 50 °C. At UOM, a carbon dioxide equilibration scale is used to normalise sample measurements to internationally distributed clumped isotope carbonate standards. These standardisation steps are necessary to account for mass spectrometric artifacts, thereby allowing inter-laboratory comparison of results (Bernasconi et al., 2018; Dennis et al., 2011). Although the data from both laboratories are presented on the same absolute scale and are theoretically comparable, gas extraction and instrument-specific effects are both non-negligible and poorly understood (Bernasconi et al., 2018) and may result in differences in the calculated temperature of the same sample of up to 10 °C (Dennis et al., 2011). The data from each laboratory are therefore differentiated on all figures, and we do not place much emphasis on environmental implications of the absolute temperatures, but rather the temperature-corrected $\delta^{18}O$ values described below. Shell $\delta^{18}O$ and $\delta^{13}C$ values are reported in per mille units relative to the Vienna Pee Dee belemnite standard (VPDB).

Several measurements from the UOW were deemed to be unsuccessful due to a suspected leak in the stainless steel U-trap used to collect the purified CO_2 gas following the gas chromatography step (Appendix 1). This leak was inferred due to a) low yield of purified sample CO_2 gas compared with the volume initially evolved from the sample, and b) anomalously high Δ_{47} values. These measurements were rejected and are not reported here. Several other measurements from UOW had CO_2 yields that were somewhat higher, but still with associated Δ_{47} values higher than might be expected given snail ecology.

Results of the analyses and calibrations are listed in Table 5.1 (average values) and Supplementary Table 5.1 (all measurements). All data are presented in the absolute

reference frame (Dennis et al., 2011). Unless otherwise noted, uncertainty is reported as standard error

$$\sigma_{\overline{x}} = \frac{\sigma}{\sqrt{n}}$$

where σ denotes the standard deviation of the Δ_{47} replicates, and n is the number of replicates.

2.4.1 Calibration equations

The Δ_{47}-T calibration equation published by Bernasconi et al. (2018) was used to calculate temperatures of shell growth. The calibration equation is

$$\Delta_{47} = 0.0449\ (\pm 0.001) * \frac{10^6}{T^2} + 0.167\ (\pm 0.01)$$

where T is the temperature in Kelvin. This calibration was chosen as it is derived from samples covering a wide temperature range that encompasses all likely snail growth temperatures. The calibration samples also cover a wide compositional, environmental, and bulk stable isotopic ($\delta^{13}C$ and $\delta^{18}O$) range with no apparent bias, suggesting convergence of these samples on a universal Δ_{47}-T relationship. Prior to calculating the average values presented in Table 5.1, the measurements were screened for unrealistic temperatures, which probably reflect measurement error or contamination. A broad filter of 5–40°C was used; this slightly exceeds the known range of snail environmental tolerance, excepting hibernation or aestivation (Ansart and Vernon, 2003; Cowie, 1985; Riddle, 1990). Measurements rejected on this basis are highlighted in red in Supplementary Table 5.1 and are not included in the average values of Table 5.1.

The water-aragonite oxygen isotope fractionation equation of Kim et al. (2007) was used to calculate the snail body water $\delta^{18}O$:

$$1000 \ln \alpha_{aragonite-water} = 17.88\ (\pm 0.13) * \left(\frac{10^3}{T}\right) - 31.14\ (\pm 0.46)$$

In this case, T is the snail growth temperature calculated using the Δ_{47}-T calibration equation, and $\alpha_{aragonite-water}$ is the fractionation factor between aragonite and water:

$$\alpha_{aragonite-water} = \frac{R_{aragonite}}{R_{water}}$$

where R is the ratio of ^{18}O to ^{16}O. $R_{aragonite}$ is measured directly during the clumped isotope measurements, allowing calculation of the R—and hence $\delta^{18}O$—of the formation water. Uncertainties in the $\delta^{18}O$ of the formation water (the snail body fluid) are based on the Δ_{47}-derived temperature uncertainties, as the analytical uncertainties are relatively negligible. Snail body water $\delta^{18}O$ values are reported in per mille units relative to Vienna Standard Mean Ocean Water (VSMOW).

2.5 Steady state flux balance models

2.5.1 Oxygen steady state flux balance model

Land snail shell $\delta^{18}O$ is not a direct reflection of local precipitation $\delta^{18}O$, but rather a convolution of many environmental variables (Fig. 5.1). A land snail-specific steady-state flux balance model was therefore employed to better understand the contribution of these variables (Balakrishnan and Yapp, 2004). The model requires information about the snail's ambient environment and combines this with physiological parameters to predict the $\delta^{18}O$ of aragonite shells extruded by the snails (Table 5.2). Requisite environmental variables are the temperature, relative humidity, and $\delta^{18}O$ of precipitation in the snail's local environment (highlighted in blue on Fig. 5.1), integrated over the total active period of the snail. Given the highly variable nature of Australian climates, and preference for snails to be active in warm and moist conditions, the latter is not trivial and probably highly seasonal (Chapter 4, this thesis). Unfortunately, information about the specific active seasons of Australian snails is scarce. In general, snails cease aestivation during the first large storm following the dry season and then continue to be active after rain events throughout the wetter months, especially in the evenings when relative humidity is higher (Baker, 2008; Kempster and Charwat, 2003; Prior, 1985; Smallridge and Kirby, 1988), although activity may cease at very cold temperatures (Segal, 1961). It was therefore assumed that shells sample the rainiest months at each site, possibly with a bias to warmer conditions. If these assumptions are accurate, then modelled shell $\delta^{18}O$ values constrained by environmental data averaged over the relevant seasons should closely match measured shell $\delta^{18}O$ (i.e. a linear relationship with a slope of one and intercept of zero).

Four likely snail growing seasons were therefore defined, based on seasonal precipitation trends in southern, central, and north-eastern Australia (Fig. 4.9). For the snails from the north-east and central Australia, it was assumed in all cases that snails are active from November to April (NDJFMA). The four possible growth seasons that tested for the snails from southern Australia were: autumn (MAM), spring (SON), autumn and spring (MAM-SON), and autumn, winter, and spring (MAMJJASON). For comparison, the model was also constrained using annual average values. All seasonal averages were calculated from the

Table 5.2. Summary of key inputs to the land snail oxygen isotope steady state flux balance model (Balakrishnan and Yapp, 2004), including the values of parameters used where applicable. 'Variables' are inputs requiring specific information for each sample. Inputs marked with an asterisk in the last column have a substantial effect on the modelled $\delta^{18}O$.

Term	Description	Value	Variable?
$^{18}\alpha_k$	kinetic fractionation factor	1.0284	N
$^{18}\alpha_{w\text{-}v}$	equilibrium oxygen isotope fractionation between H_2O_{liquid} and H_2O_{vapour}	$1000\ln{}^{18}\alpha_{w\text{-}v} = 1.137[10^6/T^2] - 0.4156[10^3/T] - 2.0667$	Y (temperature)
h	relative humidity	Site-specific	Y*
$^{18}R_{IN}$	$^{18}O/^{16}O$ of water imbibed by the snail	$\delta^{18}O$ of local rainfall (from OIPC)	Y*
$^{18}R_A$	$^{18}O/^{16}O$ of water in the atmosphere	Calculated from $^{18}R_{IN}$ and $^{18}\alpha_{w\text{-}v}$	N
θ	F_{OUT}/F_{IN} i.e. liquid H_2O output from the snail body fluid as a fraction of input	Dependent on species; assume 0.4	N
F_{EV}	evaporative flux of H_2O from snail body flud	2.7×10^{-6} mol of H_2O/g wet body weight/s	N
n_L	moles of H_2O in well-mixed snail body fluid	2×10^{-2} mol of H_2O/g wet body weight	N

SILO and OIPC data. Following Balakrishnan and Yapp (2004), average daily temperatures and average daily maximum relative humidity were used. and θ was maintained at 0.4 (Table 5.2). For each of the five cases, modelled shell $\delta^{18}O$ values were compared with the measured values.

2.5.2 Carbon steady state flux balance model

The most important input to the snail shell $\delta^{13}C$ steady-state flux balance model (Balakrishnan and Yapp, 2004) is the $\delta^{13}C$ of vegetation eaten by the snail (Table 5.3, coloured green on Fig. 5.1). This information is not currently available for the majority of our sites. Instead, I inverted the flux balance model i.e. the snail physiological parameters included in the model were used to predict the $\delta^{13}C$ of vegetation consumed by the snails from the measured shell $\delta^{13}C$, thereby gaining insight into whether dietary $\delta^{13}C$ reflects a particularly obvious C_3 or C_4 source. The other key parameter is φ, which is the proportion of carbon expelled by the snail as bicarbonate dissolved in the body fluid (a function of metabolic rate, probably scaling with body size) (Table 5.3). This parameter is not available for individual species, so equal φ was used for all species.

In Chapter Four, it was speculated that the $\delta^{13}C$ of snail shells in our dataset reflects the $\delta^{13}C$ of C_3 vegetation. To evaluate this, the calculated 'snail-derived vegetation $\delta^{13}C$' was compared with a continent-wide grid predicting the $\delta^{13}C$ of C_3 vegetation. This grid was created using Equation 1 of Kohn (2010):

$$\delta^{13}C\ (‰\ VPDB) = -10.29 + 1.9 * 10^{-4} * altitude\ (m) - 5.61 * \log_{10}(MAP + 300) - 0.0124 * abs(latitude)$$

where $\delta^{13}C$ is the $\delta^{13}C$ of C_3 vegetation, MAP is mean annual precipitation in mm/year and latitude is in decimal degrees. This model is most sensitive to changes in MAP. The grid was calculated in ArcMap 10.2, using MAP based on a standard 30-year climatology (BOM, 2010) and a digital elevation model of Australia incorporating data from 236 individual LiDAR surveys (Geoscience Australia, 2015).

Table 5.3. Summary of key inputs to the land snail carbon isotope steady state flux balance model (Balakrishnan and Yapp, 2004), including the values of parameters used where applicable. 'Variables' are inputs requiring specific information for each sample. Inputs marked with an asterisk in the last column have a substantial effect on the modelled $\delta^{13}C$. Information for $\delta^{13}C_{IN}$ (the $\delta^{13}C$ of local vegetation) was not available for all sites, so instead we used the measured snail shell $\delta^{13}C$ to estimate absolute values for $\delta^{13}C_{IN}$.

Term	Description	Value	Variable?
$^{13}\alpha_k$	kinetic fractionation factor	1.0044	N
$^{13}\alpha_{a\text{-}b}$	equilibrium carbon isotope fractionation between aragonite and HCO_3^-	1.0027 at 10 - 25°C	N
$^{13}\alpha_{b\text{-}g}$	equilibrium carbon isotope fractionation between HCO_3^- and $CO_{2(gas)}$	$1000\ln\alpha_{b\text{-}g} = 9.552[10^3/T] - 24.1$; assume T = 25°C	N
η	P_A/P_O	0.0228	N
$\delta^{13}C_{IN}$	$\delta^{13}C$ of HCO_3^- input to snail body fluid	Assume equal to local vegetation ^{13}R	Y*
$\delta^{13}C_A$	$\delta^{13}C$ of CO_2 in the atmosphere	-8 ‰	N
φ	F_{OUT}/F_{IN} i.e. HCO_3^- output from the snail body fluid as a fraction of input	Dependent on species; assume 0	Y*
F_{rs}	respired flux of CO_2 from the body fluid	9.7×10^{-10} mol of respired CO_2/g wet body weight/s	N
n_b	moles of HCO_3^- in well-mixed body fluid	1.6×10^{-7} mol of HCO_3^- /g wet body weight	N
P_O	partial pressure of CO_2 in the lungs of the snail	16 mb ≈ 15800 ppm	N
P_A	partial pressure of CO_2 in the open atmosphere	0.365 mb ≈ 361 ppm	N

3 Results

3.1 Clumped isotope composition of land snail shells

A summary of the isotope composition (Δ_{47}, $\delta^{18}O$, $\delta^{13}C$) of the land snail shells is provided in Table 5.1, with calculated growth temperatures and formation water (snail body fluid) $\delta^{18}O$. Δ_{47} values range from 0.730 ± 0.005 ‰ to 0.67 ± 0.004 ‰, corresponding to growth temperatures between 8 ± 1.2 °C and 25 ± 1.2 °C. This temperature range is comparable with, but slightly narrower than the full range of environmental temperatures experienced across the sites (approximately 5 °C to 36 °C) (BOM, 2018). The growth temperatures are generally cooler than the published range of Δ_{47} temperatures from wild Northern Hemisphere snails, which span 19 ± 3.5 °C to 37 ± 2 °C (Eagle et al., 2013; Wang et al., 2016; Zaarur et al., 2011). It was not possible to directly test inter-species variation in the dataset; shells from two different species were measured from site PG-110, but all measurements from this site were discarded (Supp. Table 5.1). The $\delta^{18}O$ and $\delta^{13}C$ values of the shells are well within the range of the analyses from Chapter Four. However, where no correlation between $\delta^{18}O$ and $\delta^{13}C$ was present in the full stable isotope dataset, here the stable isotope values are positively correlated (R^2 = 0.53; Fig. 5.3). This correlation may have been masked in the full stable isotope dataset, which includes samples from sites in close geographical proximity. Many of these sites have very similar climates, but probably a relatively large range of micro-habitats. Calculated snail body fluid $\delta^{18}O$ values range from -4.2 ± 0.3 ‰ to 2.8 ‰ VSMOW.

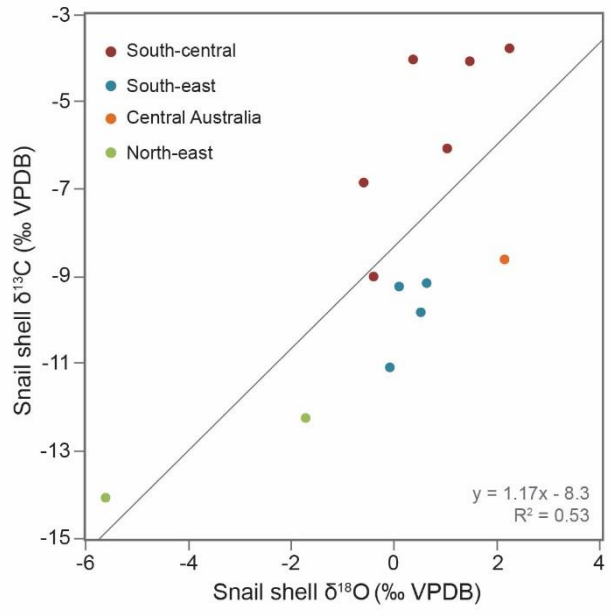

Figure 5.3. Relationship between snail shell $\delta^{18}O$ and $\delta^{13}C$ values. Points are coloured according to geographical region.

3.1.1 Inter-laboratory differences

Calculated growth temperatures from the two laboratories form distinct populations, with a significant difference in mean values (Welch's t-test, $p << 0.01$). Samples analysed at the UOW and UOM have mean calculated growth temperatures of 10 °C and 22.6 °C, respectively. Due to time and sample size constraints we were not able to replicate any measurements across the two laboratories, and therefore cannot confirm that the difference

in mean values is due to inter-laboratory differences. However, given a) the samples analysed at UOW are generally from warmer climates than those analysed at UOM (Fig. 5.6), and b) the possibility of a slightly leaky U-trap at UOW (Section 2.4), it is suspected that the difference may be due in larger part to inter-laboratory measurement artifacts than a 'real' environmental difference. The data are therefore discussed separately in Section 4.2.

3.2 Estimation of snail growth season

According to simple linear regressions, the modelled snail shell $\delta^{18}O$ values that most closely match the measured values were constrained by environmental data averaged over NDJFMA (snails from northern and central Australia) or MAMJJASON (snails from southern Australia) (slope = 0.83, R^2 = 0.38; Fig. 5.4a, Table 5.4). This was a slight improvement on the model constrained by MAM averages for the southern snails (slope = 0.82, R^2 = 0.24), and a distinct improvement on values calculated from annual climate averages (slope = 0.41, R^2 = 0.08).

Table 5.4. Results of linear regressions of measured and modelled snail shell $\delta^{18}O$ values. Data periods are the months for which the model input variables were averaged. A slope of 1 and intercept of 0 would indicate that the model has produced results that are a good reflection of reality i.e. the environmental data period is a reasonable approximation of the snail active season.

Environmental data period	Slope	Intercept	R^2
Annual	0.41	0.20	0.08
NDJFMA or MAMJJASON	0.83	0.62	0.38
NDJFMA or MAM-SON	0.69	-0.33	0.19
NDJFMA or MAM	0.82	-0.68	0.24
NDJFMA or SON	0.57	0.01	0.13

3.3 Estimation of $\delta^{13}C$ of snail diet

Assuming φ = 0, vegetation $\delta^{13}C$ inferred from snail shell $\delta^{13}C$ ranges from -29.7 ‰ to -18.8 ‰ i.e. mostly within the range of C_3 plants (O'Leary, 1981). If φ = 0.4 (i.e. snails expel a greater fraction of bicarbonate), then all $\delta^{13}C$ values increase by approximately 5 ‰ (Supp. Table 5.3). The snail-inferred vegetation $\delta^{13}C$ values are a direct reflection of shell $\delta^{13}C$ values, and hence are geographically distinct as discussed in Chapter Four: shells from north-eastern Australia have the lowest $\delta^{13}C$ values, whereas almost all snail-inferred vegetation values higher than -22 ‰ are from shells collected in south-central Australia (the Nullarbor Plain) (Fig. 5.5).

Snail-inferred vegetation $\delta^{13}C$ is positively correlated with the distribution of C_3 plant $\delta^{13}C$ predicted (mainly) from mean annual precipitation (Kohn, 2010) (Fig. 5.5). Snail shell $\delta^{13}C$ values predict a much wider range of vegetation $\delta^{13}C$ than the global model of Kohn (2010), possibly reflecting the influence of snail micro-habitats. The shells from south-central Australia appear to form a distinct population (red points in Fig. 5.5 inset) and are not well correlated with the precipitation-based predictions. This may indicate ingestion of limestone by these snails (Goodfriend, 1987; Goodfriend and Stipp, 1983), particularly given the limestone-dominated surficial geology of the region (O'Connell et al., 2012).

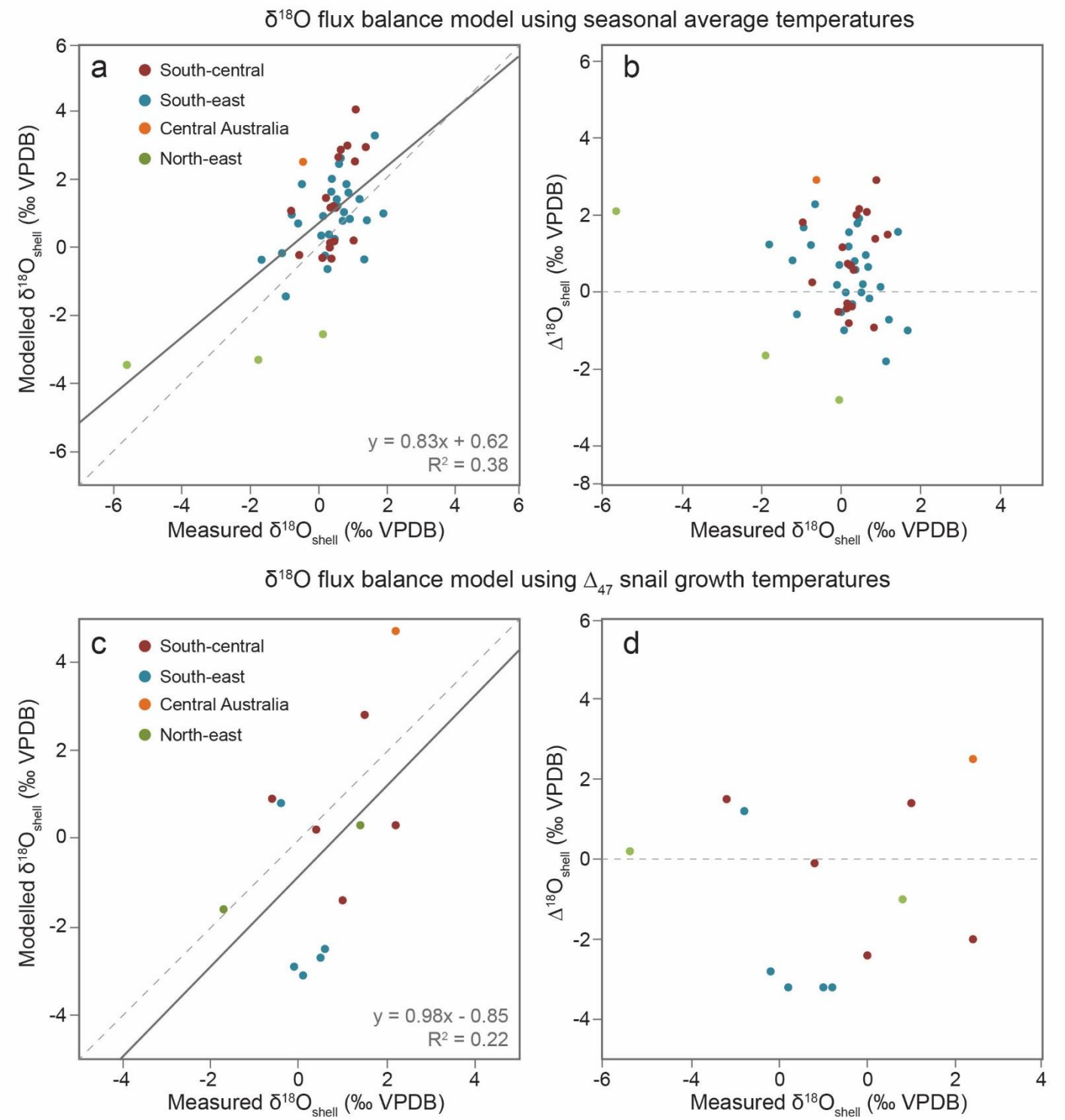

Figure 5.4. a) Relationship between measured snail shell $\delta^{18}O$ values, and model predictions of shell $\delta^{18}O$, assuming isotopic equilibrium between shell carbonate and snail body fluid, which in turn is calculated from temperature and relative humidity data from SILO, and precipitation $\delta^{18}O$ data from the OIPC. Points are coloured according to geographical region. For north-eastern and central Australia, assumed active season is NDJFMA. For the south-central and south-east, assumed active season is MAMJJASON; **b)** comparison between measured snail shell $\delta^{18}O$ values, and the offset of model predictions in **a)** from the measured values i.e. $\Delta^{18}O = \delta^{18}O_{modelled} - \delta^{18}O_{measured}$. Dashed grey line denotes an exact match between $\delta^{18}O_{modelled}$ and $\delta^{18}O_{measured}$; **c)–d)** as per **a)–b)**, but using Δ_{47} snail growth temperatures in place of average seasonal temperatures.

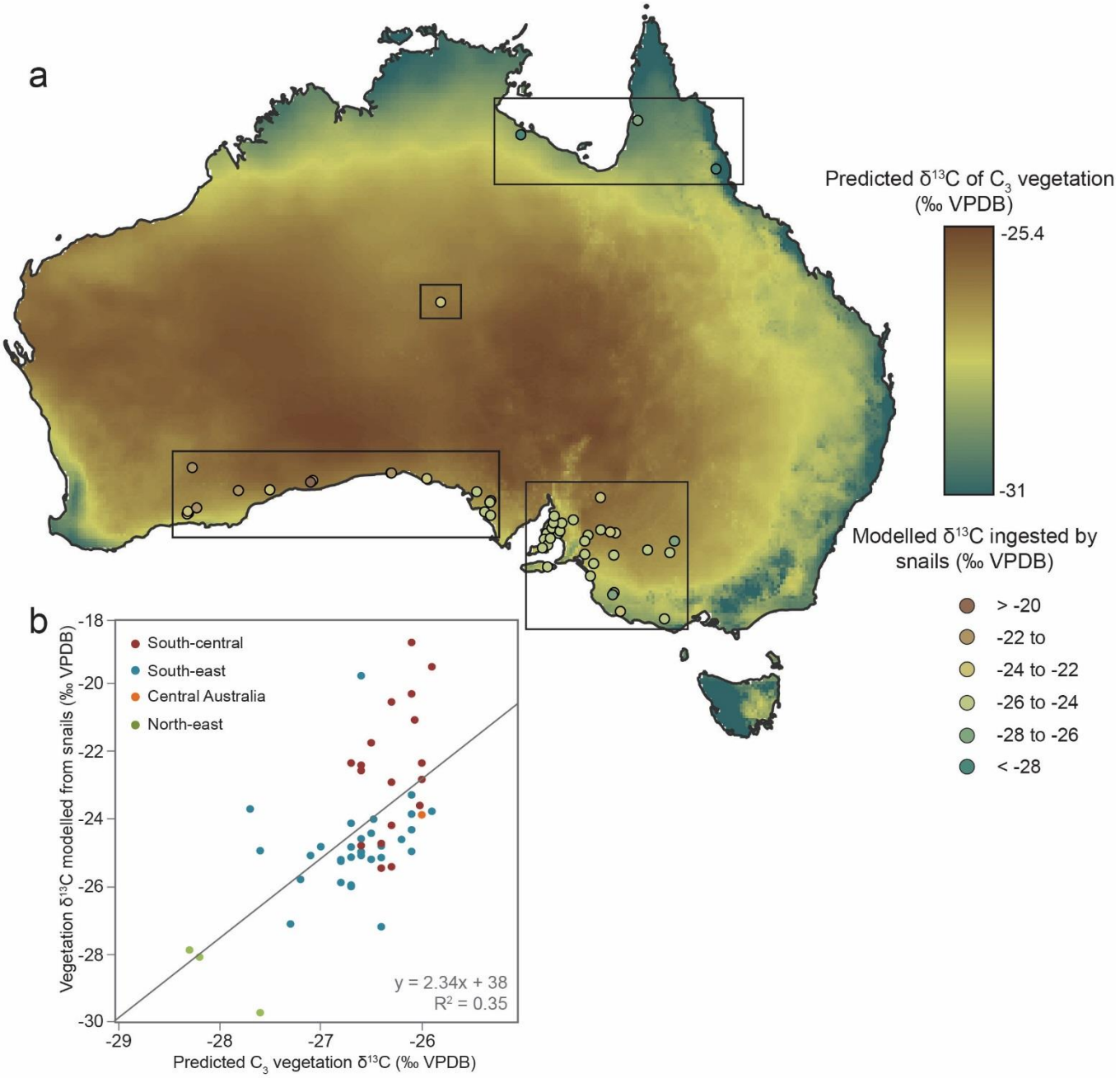

Figure 5.5. a) Grid of the predicted $\delta^{13}C$ of C_3 vegetation, based on mean annual precipitation, latitude, and elevation (Kohn, 2010) with the $\delta^{13}C$ of food eaten by snails predicted from their shell $\delta^{13}C$ (site average); **b)** comparison between site average snail dietary $\delta^{13}C$ and the corresponding predicted C_3 $\delta^{13}C$ value interpolated from the grid. Points are coloured according to geographical regions, denoted by grey boxes in **a)**.

4 Discussion

Chapter Four concluded that snail shell $\delta^{18}O$ and $\delta^{13}C$ both reflect precipitation amount, but highlighted an incomplete understanding of these relationships. Clumped isotope analyses and interrogation of the isotope-precipitation relationships with steady state flux balance models have refined these relationships, resulting in increased confidence in the inferred mechanisms.

4.1 Land snail growth season

To test assumptions of the seasons sampled in the shell $\delta^{18}O$, five scenarios were evaluated. In four of the five cases, snails from central and north-eastern Australia were active from November to April. In these four cases, snails from southern Australia were active during 1) autumn, winter, and spring (MAMJJASON), 2) autumn and spring (MAM-SON), 3) autumn (MAM), or 4) spring (SON). In the fifth scenario, the snails were active and growing their shells year-round. The steady state flux balance model accurately predicted snail shell $\delta^{18}O$ when constrained by climate data for the wet seasons, but performed very poorly when constrained by annual climate averages (Table 5.4). This supports the hypothesis arising from Chapter Four i.e. snails record seasonal, rather than annual averages. The results also support empirical observations of increased snail activity during the moist conditions following rainfall events, and snails aestivating during dry weather (Baker, 2008; Butcher and Grove, 2005; Kempster and Charwat, 2003; Smallridge and Kirby, 1988; Michael Shea, pers. comm.). A whole-shell signal should therefore integrate the rainy months that occur during a snail's lifetime, which can evidently be approximated by MAMJJASON for temperate climates and NDJFMA for the monsoonal tropics (Table 5.4). It is likely that snails aestivate during the particularly hot and dry conditions of the Australian summer and then are active—even if sporadically—until the onset of the following summer (Fig. 4.9). It follows that a palaeoclimate reconstruction based on the $\delta^{18}O$ values of land snail shells will be biased to the wettest parts of the year. Curiously, this slightly contrasts recent work from North America. In a study much like our own, Yanes et al. (2018) demonstrated that snail shell $\delta^{18}O$ from a variety of taxa covering a broad latitudinal and climatic gradient track precipitation amount, but in the case of North America, the annual and seasonal signals are equally strong. This may be a result of the large inter-annual variability in Australian rainfall, or perhaps a reflection of a longer period of aestivation by Australian snails in the drier climates.

Fortunately, despite substantial unexplained variance in the relationship between modelled and measured shell $\delta^{18}O$ (Fig. 5.4), the offset is not systematic, suggesting that there are no major environmental influences that are not accounted for. A possible source of uncertainty is the species and age of the snails. The flux balance model assumes the same physiological parameters for all snails, including θ (evaporative flux of ^{18}O from the snail). However, this almost certainly differs between species (Balakrishnan and Yapp, 2004). Within species, juvenile snails have higher surface area to volume ratio and thinner shells and are therefore more prone to evaporative effects (Prendergast et al., 2015).

A second likely source of uncertainty is the precipitation $\delta^{18}O$ data used to constrain the model. As outlined in Section 2.2, precipitation isotope data for Australia is spatially inconsistent, and the values here are probably more representative of broad regional trends than the specific local habitats of snails. The OIPC estimates of $\delta^{18}O$ are also known to be particularly inaccurate for the tropics (Hollins et al., 2018), possibly accounting for the relatively large offset of the snail shells from north-eastern Australia (Fig. 5.4). The short lifespan of a snail (one to two years) probably means that they are largely dependent on a few large rain events, which may have distinct trajectories and very different rainwater $\delta^{18}O$, especially given the large number of influences on Australian rainfall (Hollins et al., 2018; Risbey et al., 2009; Treble et al., 2005).

Nevertheless, the strength of the correlation compared with the annual averages demonstrates that by considering the $\delta^{18}O$ as 'wet season' rather than annual signal, we are approaching a relationship with the potential to infer wet season rainfall.

4.2 Snail growth temperatures

Comparison of the Δ_{47} snail growth temperatures with the average temperature of inferred snail active seasons reveals that not only do land snails actively manage their environmental temperatures, but in fact they maintain an inverse relationship with ambient temperature i.e. as average ambient temperatures increase, the temperature tolerated by the snail decreases (Fig. 5.6). This suggests that at more extreme temperatures, snails seek to be active only in clement conditions, but at more moderate temperatures, snails are less discriminating. A plot of the offset of snail growth temperatures from average growth season temperatures suggests that an ideal temperature for snail activity is around 18°C (Fig. 5.6). The distinct populations formed by measurements from the two laboratories may reflect inter-laboratory bias, especially if the leak in the extraction line at UOW caused a systematic overestimation of Δ_{47} values. However, the negative relationship between ambient and snail growth temperatures is maintained even when the data from each laboratory are evaluated separately. We are therefore reasonably confident in the observed trend of an increased offset of snail growth temperatures away from an optimal air temperature. The offset is higher (positive) when the average seasonal air temperature is lower, and lower (negative) when the average temperature is higher.

This inference that land snails seek optimal conditions, rather than passively sampling seasonal average temperatures, mirrors the relationship observed in the sole previous study of land snail shell Δ_{47} (Zaarur et al., 2011). This study similarly sampled a range of snail species from climatologically disparate regions, but includes environments with growing

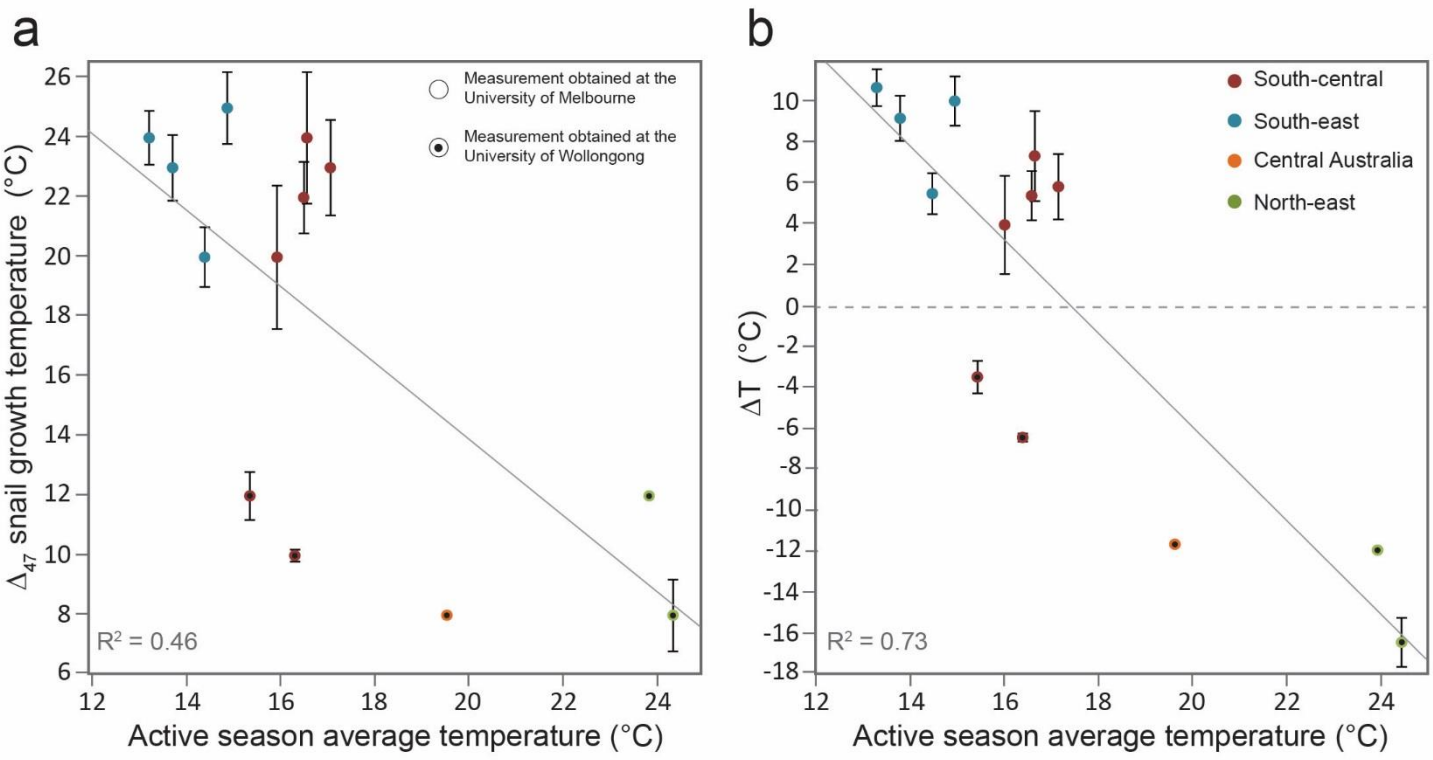

Figure 5.6. a) Comparison of the measured Δ_{47} snail growth temperatures with the local average air temperature during the snails' activity period. Points are coloured according to geographical regions discussed in the text, and analyses made at the University of Wollongong are denoted by a filled circle. Δ_{47} temperatures without error bars are calculated from only one replicate, and therefore have high (unquantifiable) uncertainty; **b)** the offset of Δ_{47} snail growth temperatures from average active season temperatures, plotted according to the average active season temperatures. Grey dashed line denotes an exact correspondence of snail growth temperatures and average active season temperatures.

season temperatures of 5–10 °C i.e. much colder than any of our sites. Accordingly, where the Australian snails record temperatures variably warmer or cooler than ambient, the shells measured by Zaarur et al. (2011) returned growth temperatures uniformly above seasonal averages. This is unsurprising, given our sites include areas that experience hot and dry conditions, where snails might seek shelter outside of cooler, moister periods.

The disparity between snail growth temperatures and ambient environmental temperatures has implications for use of snail shell $\delta^{18}O$ as a palaeoprecipitation proxy for a broad range of climates. Given the influence of growth temperature on snail shell $\delta^{18}O$ (Kim et al., 2007), clumped isotopes are especially important to reconstruct snail body fluid $\delta^{18}O$, which should closely reflect precipitation $\delta^{18}O$ (Goodfriend et al., 1989; Prendergast et al., 2015).

4.2.1 Influence of temperature on shell $\delta^{18}O$

Given the apparent temperature preferences of Australian land snails, average seasonal temperatures should be poorly correlated with the temperature recorded in the shell $\delta^{18}O$. The seasonal average temperature data in the MAMJJASON flux balance model was therefore replaced with Δ_{47} snail growth temperatures, maintaining all other inputs (Supp.

Table 5.4). This resulted in further improvement in the relationship (Fig. 5.4c–d), confirming that whilst snails sample precipitation $\delta^{18}O$ integrated across the rainiest months at a site, they do so within a specific temperature window.

Combining the flux balance model and clumped isotope analyses, it is clear that snail shell $\delta^{18}O$ reflects the $\delta^{18}O$ of *seasonal* precipitation, as well as the influences of local temperature, humidity, and snail physiology. This supports the conclusion from Chapter Four i.e. the relationship between snail shell $\delta^{18}O$ is a direct reflection of rainwater $\delta^{18}O$ and retains the same negative correlation with precipitation amount (Hollins et al., 2018). These new insights result in a distinct improvement in the numerical relationship between shell $\delta^{18}O$ values and annual precipitation (Chapter 4). Using the Δ_{47} measurements to extract the temperature influence from shell $\delta^{18}O$ and comparing the resultant snail body fluid $\delta^{18}O$ values with seasonal (NDJFMA or MAMJJASON) precipitation totals results in a $\delta^{18}O$-precipitation relationship ($p < 0.05$, $R^2 = 0.67$) clearer than the shell $\delta^{18}O$-mean annual precipitation relationship previously identified ($R^2 = 0.26$) (Fig 5.7), although we acknowledge the likely influence of moisture source and continentality on this relationship (c.f. Hollins et al., 2018).

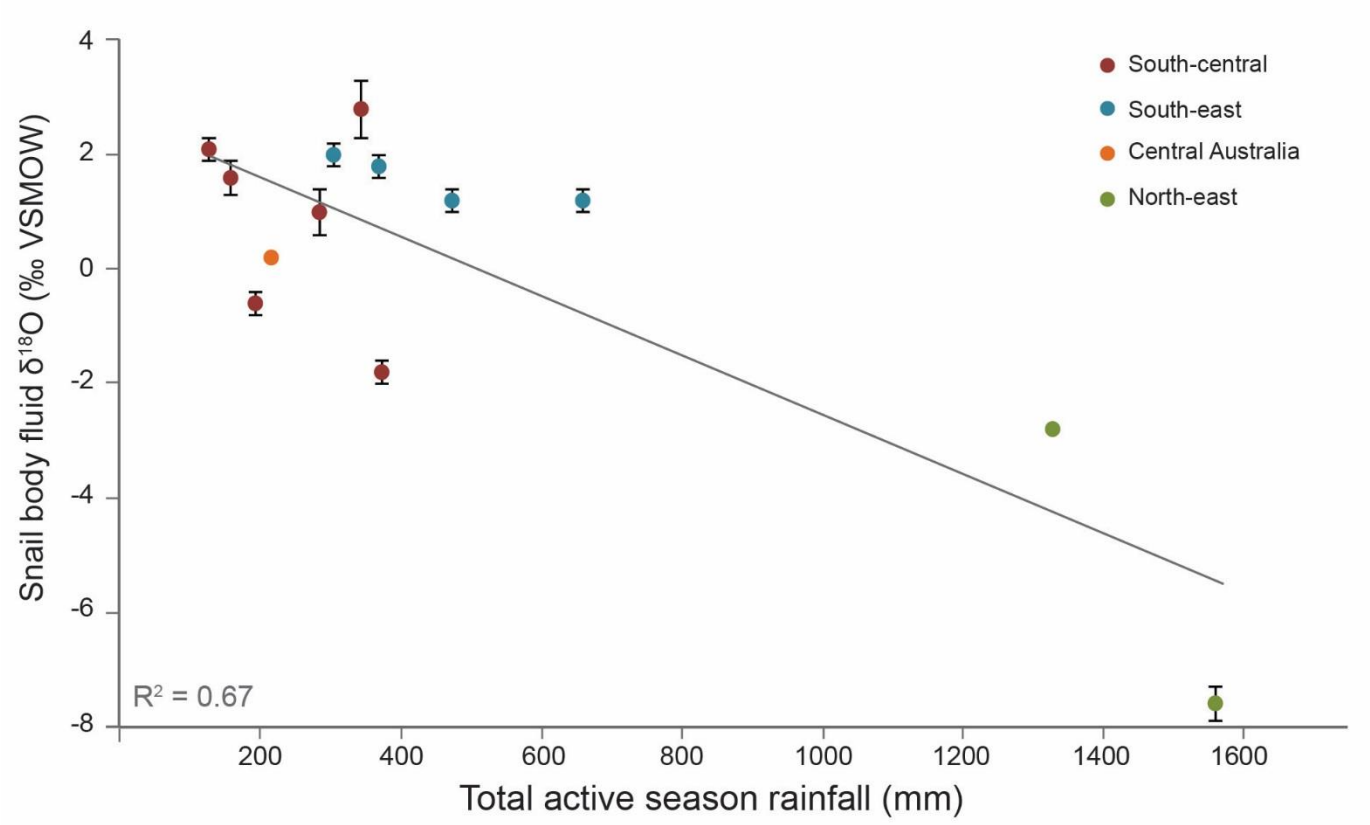

Figure 5.7. a) Relationship of snail body fluid $\delta^{18}O$ (calculated from shell $\delta^{18}O$ and Δ_{47} snail growth temperatures) with mean total active season rainfall for the five years preceding collection of the sample. Points are coloured according to geographical region. Vertical bars denote standard error derived from Δ_{47} measurements.

4.3 $\delta^{13}C$ of material ingested by snails

Assuming the snails in our dataset consumed only plant matter, modelled dietary $\delta^{13}C$ values mostly between -30 and -23 ‰ suggest a C_3-dominated diet for all snails from north-eastern, central, and south-eastern Australia (Fig. 5.5 inset). Most shells with $\delta^{13}C$ values suggesting a diet *not* solely of C_3 plants are from south-central Australia. This is the area with the lowest C_4 plant abundance (Hattersley, 1983; Nelson et al., 2016). The region with the highest proportion of C_4 plants (i.e. plant matter with more positive $\delta^{13}C$) is north-eastern Australia, where the shells returned the most negative ('C_3-like') values of the dataset. This apparent paradox may be due to snail nutritional requirements. Many of the snails from south-central Australia are of the genus *Bothriembryon*, which secrete large, thick shells, and generally inhabit limestone-dominated areas (Table 4.1). I suggest that like other large snails inhabiting areas with a calcareous substrate (Goodfriend and Ellis, 2000; Goodfriend and Hood, 1983; Romaniello et al., 2008), snails from south-central Australia supplement their diet with detrital limestone, thereby obtaining the calcium necessary to build their shells and also resulting in higher shell $\delta^{13}C$. Therefore it appears that Australian snails, like those from elsewhere in the world, prefer to eat C_3 over C_4 vegetation.

Comparison of the modelled absolute $\delta^{13}C$ values of the snails' food—indicative of a mainly C_3 diet—with the $\delta^{13}C$ of C_3 vegetation predicted by trends in MAP reveals a close correspondence in spatial variability (Fig. 5.5). This supports my hypothesis that the shell $\delta^{13}C$-precipitation relationship reflects a plant physiological response to moisture stress in C_3 plants (Farquhar et al., 1989). This spatial covariation also confirms that on a broad scale, the climate signal overrides the influence of snail dietary preferences on the shell $\delta^{13}C$. A possible exception to this is in south-central Australia, where relatively positive dietary $\delta^{13}C$ values probably reflect minor consumption of limestone (or perhaps C_4 plants) (Fig. 5.5).

Hence I reaffirm the important corollary of this mechanism: snail shell $\delta^{13}C$ reflects the longer-term climatic signal that is integrated in plant material at each site i.e. a smoothed response to changing environmental conditions. This contrasts the snail shell $\delta^{18}O$ signal, which is both highly seasonal and susceptible to inter-annual variability in precipitation.

4.4 Snail shell isotopes as palaeoenvironmental indicators

The combined analysis and modelling of Australian land snail shell $\delta^{18}O$, $\delta^{13}C$, and Δ_{47} values reveals snail shells to be an archive of multiple environmental parameters. The shells record precipitation amount not only via two different mechanisms, but for two distinct seasons. Due to the high turnover of water in a snail's body, the $\delta^{13}C$ and $\delta^{18}O$ values of a snail's body fluid—and hence shell carbonate—reflect the snail's immediate environment.

The environmental feature with the strongest influence on snail $\delta^{13}C$ is local plant matter, which itself preserves a smoothed climate signal resulting from the influence of moisture stress on stomatal aperture size and hence degree of discrimination against ^{13}C. The factor with the strongest influence on snail $\delta^{18}O$ is surface water $\delta^{18}O$ (as also observed by Goodfriend et al., 1989; Prendergast et al., 2015) i.e. a transient climate signal. Although the relationship of snail shell $\delta^{18}O$ with body fluid $\delta^{18}O$ is confounded by temperature, clumped isotope analysis can quantify this influence, allowing a close mechanistic connection of shell $\delta^{18}O$ with precipitation amount during the wet months in any particular location. The positive correlation of shell $\delta^{13}C$ and $\delta^{18}O$ (Fig. 5.3) confirms a dominant hydrological control on both systems across a broad spatial scale. This correlation is unusual in pulmonate snails (Yanes and Fernández-Lopez-de-Pablo, 2017) and possibly in part reflects the influence of precipitation amount on precipitation $\delta^{18}O$ in Australia (Hollins et al., 2018).

4.4.1 Snail shell $\delta^{18}O$ as a quantitative palaeo-precipitation proxy?

A major difficulty in developing a quantitative precipitation-proxy relationship is extracting the 'precipitation amount' signal from all other factors. Although snail shell $\delta^{18}O$ is influenced by many environmental variables, we have demonstrated that clumped isotopes can be used eliminate one confounding influence, by deconstructing snail shell $\delta^{18}O$ into the 'temperature' and 'body fluid' components. Assuming that the body fluid represents 'wet season' precipitation rather than a mean annual signal removes one more source of uncertainty in the relationship, resulting in a coefficient of determination ($R^2 = 0.67$) is comparable to that of existing quantitative calibrations for Australian rainfall (Fig. 5.7) (Tibby et al., 2016; Turney, 2012). This simple model is supported by a realistic mechanism and appears to be applicable across a wide spatial distribution, although I note that confidence in the model may be improved by the addition of shell samples from climates with seasonal rainfall totals around 700–1200 mm (Fig. 5.7).

Variability in snail body fluid $\delta^{18}O$ that is not explained by seasonal precipitation amount is probably due to a range of factors, including the source of the precipitation, anomalous weather events that occurred during snails' lifetimes, and whether the snails inhabiting the shells died >5 years before they were collected, as well as physiological effects arising from snail age, size, and species. These factors may be reasonably straightforward to quantify through a combination of laboratory studies, and observation and collection of live snails from their natural habitats, in conjunction with long-term monitoring of environmental variables including temperature, relative humidity, precipitation amount, and precipitation $\delta^{18}O$. A calibration study such as this was beyond the scope of this thesis, but nevertheless, we provide here a strong foundation for the development of a quantitative proxy.

4.5 Palaeoclimate and beyond

The stable isotope composition of land snail shells has value beyond palaeoprecipitation reconstructions, and could be used to understand aspects of past Australian environments. The preservation of two different signals—a smoothed climate signal via $\delta^{13}C$ and a more transient seasonal signal via $\delta^{18}O$—suggest that differences in temporal changes in $\delta^{13}C$ and $\delta^{18}O$ could be used to identify changes in seasonality at a site, or changes in precipitation $\delta^{18}O$ independent of precipitation amount. The latter may provide insight into past changes in synoptic climatology, providing a direct link to the outputs of climate model simulations, especially those incorporating water isotope information (e.g. Werner et al., 2016; Zhu et al., 2017), which in turn would allow investigation of physical mechanisms responsible for the influence of various ocean-atmosphere circulation patterns on Australian rainfall.

Land snail shells may also provide valuable archaeological information (Leng and Lewis, 2016; Prendergast et al., 2018). If land snail shells are identified in Australian archaeological deposits, shell $\delta^{13}C$ and $\delta^{18}O$ may provide valuable insights into environmental conditions experienced by humans living in Australia throughout the climatic fluctuations of the Late Pleistocene (Hughes et al., 2017; Munt et al., 2018; Reynen et al., 2018).

Although this work suggests that snail shell $\delta^{18}O$ and Δ_{47} may hold the greatest potential for quantitative precipitation reconstructions, if Australian land snails do in fact have a marked preference for C_3 vegetation, then shell $\delta^{13}C$ may be a useful qualitative proxy for annual average environmental conditions. A straightforward test of this assumed dietary preference would be to perform a food preference test (Mølgaard, 1986) i.e. obtain live snails from areas with varying vegetation composition and ascertain any preference by offering native C_3 and C_4 plant material. A test of the influence of snail body size and metabolic rate on shell $\delta^{13}C$ (i.e. species-specific vital effects; Fig. 5.1) would further clarify the $\delta^{13}C$-environment relationship.

5 Conclusions

This study demonstrates that the stable isotope composition of land snail shells in Australia is strongly correlated with both annual and seasonal environmental variables and provides sound mechanistic explanations. A principal control on snail shell $\delta^{18}O$ is precipitation $\delta^{18}O$, which in turn is negatively correlated with precipitation amount. Land snails in Australia are not active throughout the year but rather preferentially sample environmental conditions during the wettest months. Palaeoclimate reconstructions from the $\delta^{18}O$ of land snails will therefore be relevant to seasonal, rather than annual climate. Snails also regulate their

activity to be active during favourable conditions and hence do not sample seasonal average temperatures. Whilst this behaviour inhibits the use of land snail shell Δ_{47} as a palaeotemperature proxy per se, using shell Δ_{47} to extricate the temperature signal results in a clearer relationship of snail $\delta^{18}O$ with precipitation amount. When shell $\delta^{18}O$ values are combined with Δ_{47} to calculate snail body fluid $\delta^{18}O$, we observe a strong correlation with wet season precipitation amount that approaches suitability for a quantitative precipitation proxy.

I also demonstrated that the $\delta^{13}C$ values of snail shells can be evaluated with a snail flux balance model, to derive the $\delta^{13}C$ of the snail's diet. In this dataset, lower $\delta^{13}C$ values generally correlate with areas of high mean annual precipitation. If it can be confirmed that snails consistently target C_3 vegetation at the expense of C_4, the $\delta^{13}C$ of snail shells could be a valuable proxy for plant moisture stress, which in turn reflects mean climate conditions.

6 References cited

Affek, H.P., Bar-Matthews, M., Ayalon, A., Matthews, A., Eiler, J.M., 2008. Glacial/interglacial temperature variations in Soreq cave speleothems as recorded by 'clumped isotope' thermometry. Geochimica et Cosmochimica Acta 72, 5351-5360.

Affek, H.P., Matthews, A., Ayalon, A., Bar-Matthews, M., Burstyn, Y., Zaarur, S., Zilberman, T., 2014. Accounting for kinetic isotope effects in Soreq Cave (Israel) speleothems. Geochimica et Cosmochimica Acta 143, 303-318.

Ansart, A., Vernon, P., 2003. Cold hardiness in molluscs. Acta Oecologica 24, 95-102.

Baker, G.H., 2008. The population dynamics of the mediterranean snails *Cernuella virgata, Cochlicella acuta* (Hygromiidae) and *Theba pisana* (Helicidae) in pasture/cereal rotations in South Australia: a 20-year study. Australian Journal of Experimental Agriculture 48, 1514-1522.

Balakrishnan, M., Yapp, C.J., 2004. Flux balance models for the oxygen and carbon isotope compositions of land snail shells. Geochimica et Cosmochimica Acta 68, 2007-2024.

Barr, C., Tibby, J., Leng, M.J., Tyler, J.J., Henderson, A.C.G., Overpeck, J.T., Simpson, G.L., Cole, J.E., Phipps, S.J., Marshall, J.C., McGregor, G.B., Hua, Q., McRobie, F.H., 2019. Holocene El Niño–Southern Oscillation variability reflected in subtropical Australian precipitation. Scientific Reports 9, 1627.

Bernasconi, S.M., Müller, I.A., Bergmann, K.D., Breitenbach, S.F.M., Fernandez, A., Hodell, D.A., Jaggi, M., Meckler, A.N., Millan, I., Ziegler, M., 2018. Reducing Uncertainties in Carbonate Clumped

Isotope Analysis Through Consistent Carbonate-Based Standardization. Geochemistry, Geophysics, Geosystems 19, 2895-2914.

Blockley, S.P.E., Lane, C.S., Hardiman, M., Rasmussen, S.O., Seierstad, I.K., Steffensen, J.P., Svensson, A., Lotter, A.F., Turney, C.S.M., Bronk Ramsey, C., 2012. Synchronisation of palaeoenvironmental records over the last 60,000 years, and an extended INTIMATE1 event stratigraphy to 48,000 b2k. Quaternary Science Reviews 36, 2-10.

Bowen, G.J., 2017. The Online Isotopes in Precipitation Calculator, version 3.1.

Bowen, G.J., Wassenaar, L.I., Hobson, K.A., 2005. Global application of stable hydrogen and oxygen isotopes to wildlife forensics. Oecologia 143, 337-348.

Bureau of Meteorology, 2010. Average annual rainfall over the period 1961 to 1990. Bureau of Meteorology, Commonwealth of Australia.

Bureau of Meteorology, 2018. Climate statistics for Australian locations. Bureau of Meteorology, Commonwealth of Australia.

Butcher, A.R., Grove, D.I., 2005. Seasonal variation in rates of sporocyst and metacercarial infection by *Brachylaima cribbi* in helicid and hygromiid land snails on the Yorke Peninsula, South Australia. Australian Journal of Zoology 53, 375-382.

Clark, P.U., Shakun, J.D., Marcott, S.A., Mix, A.C., Eby, M., Kulp, S., Levermann, A., Milne, G.A., Pfister, P.L., Santer, B.D., Schrag, D.P., Solomon, S., Stocker, T.F., Strauss, B.H., Weaver, A.J., Winkelmann, R., Archer, D., Bard, E., Goldner, A., Lambeck, K., Pierrehumbert, R.T., Plattner, G.-K., 2016. Consequences of twenty-first-century policy for multi-millennial climate and sea-level change. Nature Clim. Change 6, 360-369.

Cook, B.I., Palmer, J.G., Cook, E.R., Turney, C.S.M., Allen, K., Fenwick, P., O'Donnell, A., Lough, J.M., Grierson, P.F., Ho, M., Baker, P.J., 2016. The paleoclimate context and future trajectory of extreme summer hydroclimate in eastern Australia. Journal of Geophysical Research: Atmospheres 121, 12,820-812,838.

Cook, E.J., van der Kaars, S., 2006. Development and testing of transfer functions for generating quantitative climatic estimates from Australian pollen data. Journal of Quaternary Science 21, 723-733.

Cowie, R.H., 1985. Microhabitat choice and high temperature tolerance in the land snail *Theba pisana* (Mollusca: Gastropoda). Journal of Zoology 207, 201-211.

Daëron, M., Guo, W., Eiler, J., Genty, D., Blamart, D., Boch, R., Drysdale, R., Maire, R., Wainer, K., Zanchetta, G., 2011. $^{13}C^{18}O$ clumping in speleothems: Observations from natural caves and precipitation experiments. Geochimica et Cosmochimica Acta 75, 3303-3317.

Dennis, K.J., Affek, H.P., Passey, B.H., Schrag, D.P., Eiler, J.M., 2011. Defining an absolute reference frame for 'clumped' isotope studies of CO_2. Geochimica et Cosmochimica Acta 75, 7117-7131.

Eagle, R.A., Risi, C., Mitchell, J.L., Eiler, J.M., Seibt, U., Neelin, J.D., Li, G., Tripati, A.K., 2013. High regional climate sensitivity over continental China constrained by glacial-recent changes in temperature and the hydrological cycle. Proceedings of the National Academy of Sciences 110, 8813-8818.

Eiler, J.M., 2011. Paleoclimate reconstruction using carbonate clumped isotope thermometry. Quaternary Science Reviews 30, 3575-3588.

Falster, G., Delean, S., Tyler, J., 2018. Hydrogen Peroxide Treatment of Natural Lake Sediment Prior to Carbon and Oxygen Stable Isotope Analysis of Calcium Carbonate. Geochemistry, Geophysics, Geosystems 19, 3583-3595.

Falster, G., Tyler, J., Grant, K., Tibby, J., Turney, C., Löhr, S., Jacobsen, G., Kershaw, A.P., 2018. Millennial-scale variability in south-east Australian hydroclimate between 30,000 and 10,000 years ago. Quaternary Science Reviews 192, 106-122.

Farquhar, G.D., Ehleringer, J.R., Hubick, K.T., 1989. Carbon Isotope Discrimination and Photosynthesis. Annual Review of Plant Physiology and Plant Molecular Biology 40, 503-537.

Gallant, A.J.E., Phipps, S.J., Karoly, D.J., Mullan, A.B., Lorrey, A.M., 2013. Nonstationary Australasian Teleconnections and Implications for Paleoclimate Reconstructions. Journal of Climate 26, 8827-8849.

Geoscience Australia, 2015. Digital Elevation Model (DEM) of Australia derived from LiDAR 5 Metre Grid, 2018 edition, Canberra.

Ghosh, P., Adkins, J., Affek, H., Balta, B., Guo, W., Schauble, E.A., Schrag, D., Eiler, J.M., 2006. ^{13}C–^{18}O bonds in carbonate minerals: A new kind of paleothermometer. Geochimica et Cosmochimica Acta 70, 1439-1456.

Goodfriend, G.A., 1987. Radiocarbon Age Anomalies in Shell Carbonate of Land Snails from Semi-Arid Areas. Radiocarbon 29, 159-167.

Goodfriend, G.A., Ellis, G.L., 2000. Stable carbon isotope record of middle to late Holocene climate changes from land snail shells at Hinds Cave, Texas. Quaternary International 67, 47-60.

Goodfriend, G.A., Hood, D.G., 1983. Carbon isotope analysis of land snail shells: implications for carbon sources and radiocarbon dating. Radiocarbon 25, 810-830.

Goodfriend, G.A., Magaritz, M., 1987. Carbon and oxygen isotope composition of shell carbonate of desert land snails. Earth and Planetary Science Letters 86, 377-388.

Goodfriend, G.A., Magaritz, M., Gat, J.R., 1989. Stable isotope composition of land snail body-water and its relation to environmental waters and shell carbonate. Geochimica et Cosmochimica Acta 53, 3215-3221.

Goodfriend, G.A., Stipp, J.J., 1983. Limestone and the problem of radiocarbon dating of land-snail shell carbonate. Geology 11, 575-577.

Hattersley, P.W., 1983. The distribution of C3 and C4 grasses in Australia in relation to climate. Oecologia 57, 113-128.

Herbert, A.V., Harrison, S.P., 2016. Evaluation of a modern-analogue methodology for reconstructing Australian palaeoclimate from pollen. Review of Palaeobotany and Palynology 226, 65-77.

Ho, M., Kiem, A.S., Verdon-Kidd, D.C., 2015. A paleoclimate rainfall reconstruction in the Murray-Darling Basin (MDB), Australia: 2. Assessing hydroclimatic risk using paleoclimate records of wet and dry epochs. Water Resources Research 51, 8380-8396.

Hollins, S.E., Hughes, C.E., Crawford, J., Cendon, D.I., Meredith, K.T., 2018. Rainfall isotope variations over the Australian continent - Implications for hydrology and isoscape applications. Science of the Total Environment 645, 630-645.

Hughes, P.J., Sullivan, M.E., Hiscock, P., 2017. Palaeoclimate and human occupation in southeastern arid Australia. Quaternary Science Reviews 163, 72-83.

IAEA/WMO, 2015. Global Network of Isotopes in Precipitation. The GNIP Database.

Jackson, S.T., Williams, J.W., 2004. Modern analogs in Quaternary paleoecology: Here Today, Gone Yesterday, Gone Tomorrow? Annual Review of Earth and Planetary Sciences 32, 495-537.

Kele, S., Breitenbach, S.F.M., Capezzuoli, E., Meckler, A.N., Ziegler, M., Millan, I.M., Kluge, T., Deák, J., Hanselmann, K., John, C.M., Yan, H., Liu, Z., Bernasconi, S.M., 2015. Temperature dependence of oxygen- and clumped isotope fractionation in carbonates: A study of travertines and tufas in the 6–95 °C temperature range. Geochimica et Cosmochimica Acta 168, 172-192.

Kempster, V., Charwat, S., 2003. Soil surface temperature and mortality in land snails: implications for successful management. Australian Journal of Experimental Agriculture 43, 1351-1356.

Kershaw, A.P., Tibby, J., Penny, D., Yezdani, H., Walkley, R., Cook, E.J., Johnston, R., 2004. Latest Pleistocene and Holocene vegetation and environmental history of the Western Plains of Victoria. Proceedings of the Royal Society of Victoria 116, 143-163.

Kim, S.T., O'Neil, J.R., Hillaire-Marcel, C., Mucci, A., 2007. Oxygen isotope fractionation between synthetic aragonite and water: Influence of temperature and Mg^{2+} concentration. Geochimica Et Cosmochimica Acta 71, 4704-4715.

Kohn, M.J., 2010. Carbon isotope compositions of terrestrial C3 plants as indicators of (paleo)ecology and (paleo)climate. Proceedings of the National Academy of Sciences 107, 19691-19695.

Leng, M.J., Lewis, J.P., 2016. Oxygen isotopes in Molluscan shell: Applications in environmental archaeology. Environmental Archaeology 21, 295-306.

Liu, Z., Gu, Z., Wu, N., Xu, B., 2007. Diet control on carbon isotopic composition of land snail shell carbonate. Chin. Sci. Bull. 52, 388-394.

McIntosh, P., Pook, M.J., Risbey, J.S., Hope, P.K., Wang, G., Alves, O., 2008. Australia's Regional Climate Drivers, Canberra, Australia.

Meckler, A.N., Adkins, J.F., Eiler, J.M., Cobb, K.M., 2009. Constraints from clumped isotope analyses of a stalagmite on maximum tropical temperature change through the late Pleistocene. Geochimica Et Cosmochimica Acta 73, A863-A863.

Mølgaard, P., 1986. Food plant preferences by slugs and snails: A simple method to evaluate the relative palatability of the food plants. Biochemical Systematics and Ecology 14, 113-121.

Munt, S., Roberts, A., Gorman, A., 2018. An investigation of human responses to climatic fluctuations at Allen's Cave, South Australia, from ca 40,000 to 5,000BP, by a technological analysis of stone artefacts. Australian Archaeology 84, 67-83.

Nelson, D.M., Urban, M.A., Kershaw, A.P., Hu, F.S., 2016. Late-Quaternary variation in C3 and C4 grass abundance in southeastern Australia as inferred from $\delta^{13}C$ analysis: Assessing the roles of climate, pCO_2, and fire. Quaternary Science Reviews 139, 67-76.

Nicholls, N., Drosdowsky, W., Lavery, B., 1997. Australian rainfall variability and change. Weather 52, 66-72.

O'Connell, L.G., James, N.P., Bone, Y., 2012. The Miocene Nullarbor Limestone, southern Australia; deposition on a vast subtropical epeiric platform. Sedimentary Geology 253-254, 1-16.

O'Leary, M.H., 1981. Carbon isotope fractionation in plants. Phytochemistry 20, 553-567.

Porch, N., 2010. Climate space, bioclimatic envelopes and coexistence methods for the reconstruction of past climates: a method using Australian beetles and significance for Quaternary reconstruction. Quaternary Science Reviews 29, 633-647.

Prendergast, A.L., Pryor, A.J.E., Reade, H., Stevens, R.E., 2018. Seasonal records of palaeoenvironmental change and resource use from archaeological assemblages. Journal of Archaeological Science-Reports 21, 1191-1197.

Prendergast, A.L., Stevens, R.E., Barker, G., O'Connell, T.C., 2015. Oxygen isotope signatures from land snail (Helix melanostoma) shells and body fluid: Proxies for reconstructing Mediterranean and North African rainfall. Chemical Geology 409, 87-98.

Prentice, I.C., Meng, T., Wang, H., Harrison, S.P., Ni, J., Wang, G., 2011. Evidence of a universal scaling relationship for leaf CO_2 drawdown along an aridity gradient. New Phytologist 190, 169-180.

Prior, D.J., 1985. Water-regulatory behaviour in terrestrial gastropods. Biological Reviews 60, 403-424.

Rao, Z., Guo, W., Cao, J., Shi, F., Jiang, H., Li, C., 2017. Relationship between the stable carbon isotopic composition of modern plants and surface soils and climate: A global review. Earth-Science Reviews 165, 110-119.

Reynen, W., Vannieuwenhuyse, D., Morse, K., Monks, C., Balme, J., 2018. What happened after the Last Glacial Maximum? Transitions in site use on an arid inland island in north-western Australia. Archaeology in Oceania 53, 150-162.

Riddle, W.A., 1990. High temperature tolerance in three species of land snails. Journal of Thermal Biology 15, 119-124.

Risbey, J.S., Pook, M.J., McIntosh, P.C., Wheeler, M.C., Hendon, H.H., 2009. On the Remote Drivers of Rainfall Variability in Australia. Monthly Weather Review 137, 3233-3253.

Romaniello, L., Quarta, G., Mastronuzzi, G., D'Elia, M., Calcagnile, L., 2008. ^{14}C age anomalies in modern land snails shell carbonate from Southern Italy. Quaternary Geochronology 3, 68-75.

Sanchez Goñi, M.F., Harrison, S.P., 2010. Millennial-scale climate variability and vegetation changes during the Last Glacial: Concepts and terminology. Quaternary Science Reviews 29, 2823-2827.

Schauble, E.A., Ghosh, P., Eiler, J.M., 2006. Preferential formation of ^{13}C–^{18}O bonds in carbonate minerals, estimated using first-principles lattice dynamics. Geochimica et Cosmochimica Acta 70, 2510-2529.

Segal, E., 1961. Acclimation in molluscs. American Zoologist 1, 235-244.

Smallridge, M.A., Kirby, G.C., 1988. Competitive interactions between the land snails *Theba pisana* (Müller) and *Cernuella Virgata* (Da Costa) from South Australia. Journal of Molluscan Studies 54, 251-258.

Thiagarajan, N., Adkins, J., Eiler, J., 2011. Carbonate clumped isotope thermometry of deep-sea corals and implications for vital effects. Geochimica et Cosmochimica Acta 75, 4416-4425.

Tibby, J., Barr, C., McInerney, F.A., Henderson, A.C.G., Leng, M.J., Greenway, M., Marshall, J.C., McGregor, G.B., Tyler, J.J., McNeil, V., 2016. Carbon isotope discrimination in leaves of the broad-leaved paperbark tree, *Melaleuca quinquenervia*, as a tool for quantifying past tropical and subtropical rainfall. Global Change Biology 22, 3474-3486.

Treble, P.C., Budd, W.F., Hope, P.K., Rustomji, P.K., 2005. Synoptic-scale climate patterns associated with rainfall $\delta^{18}O$ in southern Australia. Journal of Hydrology 302, 270-282.

Tripati, A.K., Eagle, R.A., Thiagarajan, N., Gagnon, A.C., Bauch, H., Halloran, P.R., Eiler, J.M., 2010. ^{13}C–^{18}O isotope signatures and 'clumped isotope' thermometry in foraminifera and coccoliths. Geochimica et Cosmochimica Acta 74, 5697-5717.

Turney, C.S.M., 2012. Surface $\partial^{13}C$ in Australia: A quantified measure of annual precipitation?, in: Haberle, S.G., David, B. (Eds.), Peopled Landscapes. ANU Press, pp. 435-444.

Turney, C.S.M., Jones, R.T., Phipps, S.J., Thomas, Z., Hogg, A., Kershaw, A.P., Fogwill, C.J., Palmer, J., Bronk Ramsey, C., Adolphi, F., Muscheler, R., Hughen, K.A., Staff, R.A., Grosvenor, M., Golledge, N.R., Rasmussen, S.O., Hutchinson, D.K., Haberle, S., Lorrey, A., Boswijk, G., Cooper, A.,

2017. Rapid global ocean-atmosphere response to Southern Ocean freshening during the last glacial. Nature Communications 8, 520.

van der Kaars, S., De Deckker, P., Gingele, F.X., 2006. A 100 000-year record of annual and seasonal rainfall and temperature for northwestern Australia based on a pollen record obtained offshore. Journal of Quaternary Science 21, 879-889.

Viney, N.R., Bates, B.C., 2004. It never rains on Sunday: The prevalence and implications of untagged multi-day rainfall accumulations in the Australian high quality data set. International Journal of Climatology 24, 1171-1192.

Wang, X., Cui, L., Zhai, J., Ding, Z., 2016. Stable and clumped isotopes in shell carbonates of land snails Cathaica sp. and Bradybaena sp. in north China and implications for ecophysiological characteristics and paleoclimate studies. Geochemistry, Geophysics, Geosystems 17, 219-231.

Werner, M., Haese, B., Xu, X., Zhang, X., Butzin, M., Lohmann, G., 2016. Glacial–interglacial changes in $H_2{}^{18}O$, HDO and deuterium excess – results from the fully coupled ECHAM5/MPI-OM Earth system model. Geosci. Model Dev. 9, 647-670.

Yanes, Y., Al-Qattan, N.M., Rech, J.A., Pigati, J.S., Dodd, J.P., Nekola, J.C., 2018. Overview of the oxygen isotope systematics of land snails from North America. Quaternary Research, 1-16.

Yanes, Y., Fernández-Lopez-de-Pablo, J., 2017. Calibration of the stable isotope composition and body size of the arid-dwelling land snail *Sphincterochila candidissima*, a climatic archive abundant in Mediterranean archaeological deposits. The Holocene 27, 890-899.

Yanes, Y., Nekola, J.C., Rech, J.A., Pigati, J.S., 2017. Oxygen stable isotopic disparities among sympatric small land snail species from northwest Minnesota, USA. Palaeogeography, Palaeoclimatology, Palaeoecology 485, 715-722.

Zaarur, S., Olack, G., Affek, H.P., 2011. Paleo-environmental implication of clumped isotopes in land snail shells. Geochimica et Cosmochimica Acta 75, 6859-6869.

Zhang, N., Yamada, K., Kano, A., Matsumoto, R., Yoshida, N., 2018. Equilibrated clumped isotope signatures of land-snail shells observed from laboratory culturing experiments and its environmental implications. Chemical Geology 488, 189-199.

Zhu, J., Liu, Z.Y., Brady, E., Otto-Bliesner, B., Zhang, J.X., Noone, D., Tomas, R., Nusbaumer, J., Wong, T., Jahn, A., Tabor, C., 2017. Reduced ENSO variability at the LGM revealed by an isotope-enabled Earth system model. Geophysical Research Letters 44, 6984-6992.

Supporting information for Chapter Five

Clarifying the climate-isotope relationship in Australian land snail shells using clumped isotopes and flux balance models

Supplementary Table 5.1. Clumped isotope data for all replicate analyses. Temperatures calculated using the Δ_{47}-T calibration equation of Bernasconi et al. (2018). Measurements highlighted in red are not included in the sample average values presented in Table 5.1.

Lab	Sample name	Latitude	Longitude	Species	Specimens in sample	$\delta^{13}C$	$\delta^{18}O$	Δ_{47} (corrected)	Temperature
						‰ VPDB	‰ VPDB	‰	°C
Melbourne	B-116	-31.30	121.51	*Bothriembryon indictus*	5	-4.1	0.2	0.699	17
Melbourne	B-116	-31.30	121.51	*Bothriembryon indictus*	5	-4.0	0.4	0.697	18
Melbourne	B-116	-31.30	121.51	*Bothriembryon indictus*	5	-4.0	0.7	0.694	19
Melbourne	B-116	-31.30	121.51	*Bothriembryon indictus*	5	-4.0	0.4	0.675	24
Melbourne	B-116	-31.30	121.51	*Bothriembryon indictus*	5	-4.0	0.4	0.669	26
Melbourne	B-116	-31.30	121.51	*Bothriembryon indictus*	5	-4.1	0.2	0.666	27
Melbourne	B-116	-31.30	121.51	*Bothriembryon indictus*	5	-4.1	0.2	0.660	29
Melbourne	B-157	-32.32	125.05	*Bothriembryon indictus*	5	-6.1	1.1	0.697	18
Melbourne	B-157	-32.32	125.05	*Bothriembryon indictus*	5	-6.5	1.0	0.690	20
Melbourne	B-157	-32.32	125.05	*Bothriembryon indictus*	5	-6.0	1.0	0.687	21
Melbourne	B-157	-32.32	125.05	*Bothriembryon indictus*	5	-5.9	1.1	0.678	23
Melbourne	B-157	-32.32	125.05	*Bothriembryon indictus*	5	-5.8	0.9	0.676	24
Melbourne	B-157	-32.32	125.05	*Bothriembryon indictus*	5	-6.2	1.1	0.667	27
Melbourne	RP-3-A	-31.96	126.91	*Bothriembryon indictus*	5	-3.7	2.2	0.729	10
Melbourne	RP-3-A	-31.96	126.91	*Bothriembryon indictus*	5	-3.6	2.2	0.715	13
Melbourne	RP-3-A	-31.96	126.91	*Bothriembryon indictus*	5	-3.9	2.3	0.696	18
Melbourne	RP-3-A	-31.96	126.91	*Bothriembryon indictus*	5	-3.6	2.2	0.696	18
Melbourne	RP-3-A	-31.96	126.91	*Bothriembryon indictus*	5	-3.8	2.3	0.689	20
Melbourne	RP-3-A	-31.96	126.91	*Bothriembryon indictus*	5	-3.9	2.3	0.682	22
Melbourne	RP-3-A	-31.96	126.91	*Bothriembryon indictus*	5	-4.1	2.3	0.678	23
Melbourne	RP-3-A	-31.96	126.91	*Bothriembryon indictus*	5	-3.7	2.1	0.645	33
Melbourne	B-166	-32.41	134.52	*Cernuella virgata*	5	-10.6	-3.6	0.704	16
Melbourne	B-166	-32.41	134.52	*Cernuella virgata*	5	-8.7	0.3	0.703	16
Melbourne	B-166	-32.41	134.52	*Cernuella virgata*	5	-8.9	0.0	0.689	20
Melbourne	B-166	-32.41	134.52	*Cernuella virgata*	5	-9.2	-0.2	0.684	21
Melbourne	B-166	-32.41	134.52	*Cernuella virgata*	5	-8.8	0.0	0.672	25
Melbourne	B-166	-32.41	134.52	*Cernuella virgata*	5	-8.6	0.1	0.662	28
Melbourne	B-166	-32.41	134.52	*Cernuella virgata*	5	-8.7	0.2	0.649	32
Melbourne	B-166	-32.41	134.52	*Cernuella virgata*	5	-8.7	0.0	0.647	33
Melbourne	KI-2	-35.84	137.75	*Cochlicella acuta*	5	-9.3	0.1	0.681	22
Melbourne	KI-2	-35.84	137.75	*Cochlicella acuta*	5	-9.2	0.1	0.667	27
Melbourne	KI-2	-35.84	137.75	*Cochlicella acuta*	5	-9.2	0.1	0.666	27
Melbourne	CW-1	-36.26	139.71	*Cernuella virgata*	5	-9.2	0.6	0.696	18
Melbourne	CW-1	-36.26	139.71	*Cernuella virgata*	5	-9.2	0.7	0.686	21
Melbourne	BL-1	-37.12	140.73	*Cernuella virgata*	5	-11.1	-0.1	0.688	20
Melbourne	BL-1	-37.12	140.73	*Cernuella virgata*	5	-11.1	-0.1	0.677	24
Melbourne	BL-1	-37.12	140.73	*Cernuella virgata*	5	-11.1	-0.1	0.671	25
Melbourne	5U6	-37.03	140.80	*Cernuella virgata*	5	-9.9	0.5	0.678	23
Melbourne	5U6	-37.03	140.80	*Cernuella virgata*	5	-9.8	0.5	0.665	27
Melbourne	5U6	-37.03	140.80	*Cernuella virgata*	5	-9.8	0.5	0.639	35
Wollongong	PG-131	-33.38	121.34	*Bothriembryon melo*	5	-6.9	-0.8	0.725	11
Wollongong	PG-131	-33.38	121.34	*Bothriembryon melo*	5	-6.8	-0.3	0.716	13
Wollongong	B-162	-31.55	130.59	*Bothriembryon indictus*	5	-4.1	1.5	0.742	6
Wollongong	B-162	-31.55	130.59	*Bothriembryon indictus*	5	-4.1	1.5	0.728	10
Wollongong	Alice Springs	-23.73	132.87	*Sinumelon expositum*	5	-8.6	1.6	0.752	4
Wollongong	Alice Springs	-23.73	132.87	*Sinumelon expositum*	5	-8.6	2.2	0.745	6
Wollongong	GOC-22B	-16.08	136.53	*Xanthomelon durvillii*	2	-13.9	-5.6	0.741	6
Wollongong	GOC-22B	-16.08	136.53	*Xanthomelon durvillii*	2	-14.3	-5.6	0.728	10
Wollongong	PG-110	-34.07	137.96	*Austrosuccinea australis*	1	-3.8	4.2	0.789	-4
Wollongong	PG-110	-34.07	137.96	*Austrosuccinea australis*	1	-3.7	4.2	0.779	-2
Wollongong	PG-110	-34.07	137.96	*Austrosuccinea australis*	1	-3.8	4.2	0.774	-1
Wollongong	PG-110	-34.07	137.96	*Cernuella virgata*	5	-9.4	0.8	0.830	-13
Wollongong	PG-110	-34.07	137.96	*Cernuella virgata*	5	-9.5	0.9	0.774	-1
Wollongong	GOC-45D	-15.42	141.88	*Crikey steveirwini*	1	-12.3	-1.7	0.719	12
Wollongong	GOC-58A	-17.64	145.46	*Spurlingia gemma*	2	-12.4	0.1	0.773	-1
Wollongong	GOC-58A	-17.64	145.46	*Spurlingia gemma*	2	-12.5	0.3	0.760	2

Supplementary Table 5.2. All inputs to the land snail oxygen isotope steady state flux balance model (Balakrishnan and Yapp, 2004). NDJMA = November through to April, MAMJJASON = March through to November i.e. the austral autumn, winter, and spring. Precipitation $\delta^{18}O$ data obtained from the OIPC (Bowen, 2017). Temperature and relative humidity data downloaded from the SILO database, and are average values for the five years preceding the collection date of the sample. Measured shell $\delta^{18}O$ values are the average of all measurements for each site.

Site name	Latitude	Longitude	Assumed snail active season	Average $\delta^{18}O_{precipitation}$ - active season	Average temperature - active season	Average maximum relative humidity - active season	Average temperature - active season	$^{18}\alpha_k$	1000lnα	$^{18}\alpha_{w\text{-}v}$	$^{18}R_{IN}$	$^{18}R_A$	θ	F_{ev}/n_L	A	B	$\delta^{18}O_{SS}$	$\delta^{18}O_{modelled}$	$\delta^{18}O_{measured}$	$\Delta^{18}O$
				‰ SMOW	°C		°K										‰ SMOW	‰ VPDB	‰ VPDB	
Alice Springs	-23.74	132.87	NDJFMA	-5.7	11.7	82	284.8	1.03	10.49	1.01	994.30	983.92	0.4	0.0004	2.36	0.00	0.67	2.52	-0.40	2.92
GOC-22B	-16.08	136.53	NDJFMA	-4.6	24.4	94	297.6	1.03	9.38	1.01	995.40	986.11	0.4	0.0004	6.67	0.01	-2.42	-3.50	-5.61	2.11
GOC-45D	-15.42	141.88	NDJFMA	-4.8	23.9	93	297.1	1.03	9.42	1.01	995.20	985.87	0.4	0.0004	6.04	0.01	-2.38	-3.35	-1.72	-1.64
GOC-58A	-17.64	145.46	NDJFMA	-4.7	17.9	95	291.0	1.03	9.93	1.01	995.30	985.47	0.4	0.0004	8.76	0.01	-3.01	-2.59	0.20	-2.79
5u6	-37.03	140.80	MAMJJASON	-4.6	7.7	96	280.8	1.03	10.87	1.01	995.40	984.64	0.4	0.0004	9.24	0.01	-2.96	-0.19	-1.02	0.83
B-94	-34.31	138.26	MAMJJASON	-4.1	10.1	91	283.3	1.03	10.64	1.01	995.92	985.38	0.4	0.0004	4.34	0.00	-0.61	1.61	0.95	0.66
BL-1	-37.12	140.73	MAMJJASON	-4.5	11.0	94	284.1	1.03	10.55	1.01	995.47	985.02	0.4	0.0004	7.03	0.01	-2.39	-0.39	-1.62	1.24
CW-1	-36.26	139.71	MAMJJASON	-4.3	12.8	97	285.9	1.03	10.39	1.01	995.70	985.41	0.4	0.0004	12.17	0.01	-3.07	-1.47	-0.91	-0.57
KI-2	-35.84	137.75	MAMJJASON	-4.4	10.6	95	283.7	1.03	10.59	1.01	995.62	985.13	0.4	0.0004	7.48	0.01	-2.37	-0.26	0.25	-0.52
MA0038	-35.70	139.86	MAMJJASON	-4.5	9.2	96	282.4	1.03	10.72	1.01	995.50	984.88	0.4	0.0004	8.81	0.01	-2.79	-0.37	1.42	-1.79
MA0068	-38.23	143.10	MAMJJASON	-5.0	8.5	93	281.6	1.03	10.79	1.01	995.02	984.34	0.4	0.0004	5.75	0.01	-2.35	0.23	0.54	-0.31
MA0083	-37.88	141.08	MAMJJASON	-4.7	8.7	96	281.8	1.03	10.77	1.01	995.27	984.61	0.4	0.0004	9.85	0.01	-3.20	-0.66	0.33	-0.99
MA0219	-35.07	142.33	MAMJJASON	-4.3	10.0	87	283.2	1.03	10.64	1.01	995.75	985.21	0.4	0.0004	3.24	0.00	0.41	2.64	0.72	1.92
MA0220	-34.67	143.56	MAMJJASON	-4.1	10.2	85	283.4	1.03	10.62	1.01	995.92	985.39	0.4	0.0004	2.91	0.00	1.12	3.30	1.73	1.57
PG-103	-34.32	137.72	MAMJJASON	-4.4	9.8	89	283.0	1.03	10.66	1.01	995.57	985.01	0.4	0.0004	3.76	0.00	-0.42	1.85	0.89	0.96
PG-104	-34.58	137.60	MAMJJASON	-4.3	10.2	91	283.3	1.03	10.63	1.01	995.72	985.19	0.4	0.0004	4.58	0.00	-0.99	1.21	0.63	0.58
PG-106	-34.85	137.76	MAMJJASON	-4.3	10.4	90	283.6	1.03	10.61	1.01	995.72	985.21	0.4	0.0004	4.25	0.00	-0.73	1.41	0.60	0.81
PG-107	-34.98	137.51	MAMJJASON	-4.3	10.8	91	283.9	1.03	10.57	1.01	995.75	985.28	0.4	0.0004	4.67	0.00	-1.03	1.03	0.81	0.21
PG-108	-34.54	137.88	MAMJJASON	-4.2	10.2	89	283.4	1.03	10.63	1.01	995.82	985.30	0.4	0.0004	3.76	0.00	-0.17	2.01	0.46	1.55
PG-110	-34.07	137.96	MAMJJASON	-4.2	9.1	93	282.2	1.03	10.74	1.01	995.77	985.14	0.4	0.0004	5.89	0.01	-1.66	0.78	1.49	-0.71
PG-26	-34.29	140.86	MAMJJASON	-4.2	8.7	93	281.9	1.03	10.77	1.01	995.80	985.13	0.4	0.0004	5.75	0.01	-1.57	0.96	-0.73	1.69
PG-27	-34.25	140.62	MAMJJASON	-4.2	7.8	91	281.0	1.03	10.86	1.01	995.77	985.02	0.4	0.0004	4.54	0.00	-0.89	1.85	-0.43	2.28
PG-30	-34.15	140.19	MAMJJASON	-4.2	7.8	92	281.0	1.03	10.85	1.01	995.80	985.05	0.4	0.0004	4.88	0.00	-1.10	1.64	0.44	1.19
PG-50	-33.69	138.93	MAMJJASON	-4.9	6.9	88	280.0	1.03	10.95	1.01	995.12	984.28	0.4	0.0004	3.47	0.00	-0.50	2.46	0.67	1.79
PG-51	-34.40	139.60	MAMJJASON	-4.3	8.2	93	281.3	1.03	10.82	1.01	995.75	985.03	0.4	0.0004	5.49	0.01	-1.49	1.17	0.48	0.69
PG-55	-34.67	139.46	MAMJJASON	-4.5	8.1	93	281.3	1.03	10.83	1.01	995.52	984.80	0.4	0.0004	5.57	0.01	-1.76	0.91	0.20	0.71
PG-56	-32.67	140.17	MAMJJASON	-3.8	8.4	96	281.6	1.03	10.80	1.01	996.20	985.50	0.4	0.0004	9.86	0.01	-2.27	0.33	0.14	0.19
PG-57	-35.27	139.46	MAMJJASON	-4.3	8.6	94	281.8	1.03	10.78	1.01	995.70	985.02	0.4	0.0004	7.14	0.01	-2.18	0.37	0.37	0.00
PG-59	-35.31	140.79	MAMJJASON	-4.6	7.9	93	281.0	1.03	10.85	1.01	995.42	984.68	0.4	0.0004	5.96	0.01	-2.04	0.69	-0.54	1.23
PG-96	-34.21	138.32	MAMJJASON	-4.1	9.0	93	282.2	1.03	10.74	1.01	995.87	985.23	0.4	0.0004	5.69	0.01	-1.47	0.99	1.98	-0.99
PG-97	-33.85	138.41	MAMJJASON	-4.2	8.3	94	281.4	1.03	10.81	1.01	995.82	985.11	0.4	0.0004	6.37	0.01	-1.80	0.83	0.99	-0.16
PG-98	-33.83	138.02	MAMJJASON	-4.2	8.9	94	282.0	1.03	10.76	1.01	995.85	985.20	0.4	0.0004	6.23	0.01	-1.72	0.77	0.77	0.00
PG-99	-33.52	138.06	MAMJJASON	-3.9	9.9	92	283.0	1.03	10.66	1.01	996.10	985.54	0.4	0.0004	4.95	0.00	-0.85	1.42	1.27	0.15
B-116	-31.31	121.51	MAMJJASON	-5.0	9.4	90	282.6	1.03	10.70	1.01	995.02	984.43	0.4	0.0004	4.11	0.00	-1.31	1.06	-0.75	1.81
B-157	-32.32	125.05	MAMJJASON	-4.4	9.3	94	282.5	1.03	10.71	1.01	995.60	984.99	0.4	0.0004	6.96	0.01	-2.23	0.17	0.53	-0.37
B-162	-31.55	130.60	MAMJJASON	-3.4	10.0	89	283.1	1.03	10.65	1.01	996.65	986.09	0.4	0.0004	3.72	0.00	0.71	2.96	1.46	1.50
PG-131	-33.38	121.34	MAMJJASON	-4.9	10.7	93	283.9	1.03	10.58	1.01	995.12	984.65	0.4	0.0004	5.87	0.01	-2.32	-0.25	-0.51	0.26
PG-132	-33.43	121.27	MAMJJASON	-4.9	10.6	93	283.8	1.03	10.59	1.01	995.12	984.64	0.4	0.0004	6.13	0.01	-2.43	-0.33	0.18	-0.51
PG-133	-33.30	121.30	MAMJJASON	-4.9	10.5	93	283.6	1.03	10.60	1.01	995.07	984.57	0.4	0.0004	6.15	0.01	-2.48	-0.35	0.45	-0.80
PG-134	-33.15	121.71	MAMJJASON	-4.9	10.0	92	283.2	1.03	10.64	1.01	995.07	984.54	0.4	0.0004	5.33	0.01	-2.11	0.12	0.41	-0.29
PG-156	-32.35	123.62	MAMJJASON	-4.8	10.3	92	283.4	1.03	10.62	1.01	995.20	984.69	0.4	0.0004	5.33	0.01	-1.98	0.19	1.10	-0.91
PG-157	-32.32	125.05	MAMJJASON	-4.7	10.2	94	283.3	1.03	10.63	1.01	995.35	984.82	0.4	0.0004	6.18	0.01	-2.21	-0.02	0.40	-0.42
PG-159	-31.90	127.02	MAMJJASON	-3.9	11.1	92	284.3	1.03	10.54	1.01	996.10	985.65	0.4	0.0004	4.81	0.00	-0.77	1.21	0.51	0.70
PG-162/163	-31.55	130.62	MAMJJASON	-3.4	10.6	90	283.7	1.03	10.59	1.01	996.65	986.15	0.4	0.0004	4.00	0.00	0.43	2.53	1.14	1.39
PG-162/163A	-31.81	132.24	MAMJJASON	-3.3	10.5	89	283.7	1.03	10.60	1.01	996.75	986.24	0.4	0.0004	3.65	0.00	0.89	3.00	0.92	2.09
PG-166	-32.41	134.52	MAMJJASON	-3.6	11.2	84	284.3	1.03	10.54	1.01	996.42	985.98	0.4	0.0004	2.66	0.00	2.11	4.07	1.16	2.91
PG-167	-32.82	135.16	MAMJJASON	-3.9	10.7	87	283.9	1.03	10.58	1.01	996.10	985.62	0.4	0.0004	3.20	0.00	0.81	2.88	0.72	2.16
PG-168	-32.89	135.12	MAMJJASON	-3.8	10.7	88	283.9	1.03	10.58	1.01	996.22	985.74	0.4	0.0004	3.45	0.00	0.59	2.66	0.65	2.01
PG-171	-33.33	134.88	MAMJJASON	-3.8	10.9	91	284.0	1.03	10.56	1.01	996.20	985.73	0.4	0.0004	4.68	0.00	-0.58	1.45	0.28	1.17
PG-173	-33.49	135.15	MAMJJASON	-3.8	10.3	93	283.4	1.03	10.62	1.01	996.20	985.67	0.4	0.0004	5.40	0.01	-1.01	1.17	0.42	0.75
RP-3-A	-31.96	126.91	MAMJJASON	-3.9	10.6	92	283.8	1.03	10.59	1.01	996.10	985.61	0.4	0.0004	5.08	0.01	-0.93	1.16	0.57	0.59

Supplementary Table 5.3. All inputs to the land snail carbon isotope steady state flux balance model (inverse of the model presented in Balakrishnan and Yapp, 2004). Shell $\delta^{13}C$ values are the average of all measurements for each site. We had no direct measurements to constrain φ, so we performed the calculation with φ = 0, 0.2, and 0.4 for all sites.

Site name	Latitude	Longitude	Temperature	$^{13}\alpha_k$	$^{13}\alpha_{b\text{-}g}$	$^{13}\alpha_{a\text{-}b}$	η	$\delta^{13}C_A$	$^{13}R_A$	φ	F_{rs}/n_b	$\delta^{13}C_{shell}$	G	H	$\delta^{13}C_{SS}$	$^{13}R_{IN}$	$\delta^{13}C_{ingested}$ φ = 0	$\delta^{13}C_{ingested}$ φ = 0.2	$\delta^{13}C_{ingested}$ φ = 0.4
			°C									‰ VPDB			‰ VPDB		**‰ VPDB**	‰ VPDB	‰ VPDB
Alice Springs	-23.73	132.87	20.00	1.00	1.01	1.00	0.02	-8.00	992.00	0.00	0.01	-8.31	6.09	0.01	-10.98	976.12	**-23.88**	-21.30	-18.72
GOC-22B	-16.08	136.53	20.00	1.00	1.01	1.00	0.02	-8.00	992.00	0.00	0.01	-14.09	6.06	0.01	-16.74	970.30	**-29.70**	-27.10	-24.51
GOC-45D	-15.42	141.88	20.00	1.00	1.01	1.00	0.02	-8.00	992.00	0.00	0.01	-12.26	6.07	0.01	-14.92	972.14	**-27.86**	-25.27	-22.68
GOC-58A	-17.64	145.46	20.00	1.00	1.01	1.00	0.02	-8.00	992.00	0.00	0.01	-12.46	6.07	0.01	-15.12	971.94	**-28.06**	-25.47	-22.89
5U6	-37.03	140.80	20.00	1.00	1.01	1.00	0.02	-8.00	992.00	0.00	0.01	-10.20	6.08	0.01	-12.87	974.22	**-25.78**	-23.20	-20.61
B-94	-34.31	138.26	20.00	1.00	1.01	1.00	0.02	-8.00	992.00	0.00	0.01	-9.56	6.09	0.01	-12.23	974.87	**-25.13**	-22.55	-19.97
BL-1	-37.12	140.73	20.00	1.00	1.01	1.00	0.02	-8.00	992.00	0.00	0.01	-11.50	6.08	0.01	-14.16	972.91	**-27.09**	-24.50	-21.92
CW-1	-36.26	139.71	20.00	1.00	1.01	1.00	0.02	-8.00	992.00	0.00	0.01	-9.50	6.09	0.01	-12.17	974.93	**-25.07**	-22.49	-19.91
KI-2	-35.84	137.75	20.00	1.00	1.01	1.00	0.02	-8.00	992.00	0.00	0.01	-9.24	6.09	0.01	-11.91	975.19	**-24.81**	-22.23	-19.65
MA0038	-35.70	139.86	20.00	1.00	1.01	1.00	0.02	-8.00	992.00	0.00	0.01	-9.67	6.09	0.01	-12.34	974.75	**-25.25**	-22.66	-20.08
MA0068	-38.23	143.10	20.00	1.00	1.01	1.00	0.02	-8.00	992.00	0.00	0.01	-9.36	6.09	0.01	-12.03	975.07	**-24.93**	-22.35	-19.77
MA0083	-37.88	141.08	20.00	1.00	1.01	1.00	0.02	-8.00	992.00	0.00	0.01	-8.14	6.10	0.01	-10.81	976.30	**-23.70**	-21.13	-18.55
MA0219	-35.07	142.33	20.00	1.00	1.01	1.00	0.02	-8.00	992.00	0.00	0.01	-9.22	6.09	0.01	-11.89	975.21	**-24.79**	-22.21	-19.63
MA0220	-34.67	143.56	20.00	1.00	1.01	1.00	0.02	-8.00	992.00	0.00	0.01	-11.58	6.07	0.01	-14.24	972.83	**-27.17**	-24.58	-22.00
PG-1	-35.19	143.35	20.00	1.00	1.01	1.00	0.02	-8.00	992.00	0.00	0.01	-8.56	6.09	0.01	-11.23	975.87	**-24.13**	-21.55	-18.97
PG-103	-34.31	137.72	20.00	1.00	1.01	1.00	0.02	-8.00	992.00	0.00	0.01	-10.36	6.08	0.01	-13.02	974.06	**-25.94**	-23.36	-20.77
PG-104	-34.58	137.60	20.00	1.00	1.01	1.00	0.02	-8.00	992.00	0.00	0.01	-9.55	6.09	0.01	-12.22	974.88	**-25.12**	-22.54	-19.96
PG-106	-34.85	137.76	20.00	1.00	1.01	1.00	0.02	-8.00	992.00	0.00	0.01	-10.29	6.08	0.01	-12.96	974.13	**-25.87**	-23.29	-20.70
PG-107	-34.98	137.51	20.00	1.00	1.01	1.00	0.02	-8.00	992.00	0.00	0.01	-9.41	6.09	0.01	-12.08	975.02	**-24.98**	-22.40	-19.82
PG-108	-34.54	137.88	20.00	1.00	1.01	1.00	0.02	-8.00	992.00	0.00	0.01	-9.25	6.09	0.01	-11.92	975.18	**-24.82**	-22.24	-19.66
PG-110	-34.07	137.96	20.00	1.00	1.01	1.00	0.02	-8.00	992.00	0.00	0.01	-9.50	6.09	0.01	-12.17	974.93	**-25.07**	-22.49	-19.91
PG-26	-34.29	140.86	20.00	1.00	1.01	1.00	0.02	-8.00	992.00	0.00	0.01	-8.29	6.10	0.01	-10.96	976.15	**-23.85**	-21.28	-18.70
PG-27	-34.25	140.62	20.00	1.00	1.01	1.00	0.02	-8.00	992.00	0.00	0.01	-7.73	6.10	0.01	-10.40	976.71	**-23.29**	-20.71	-18.14
PG-30	-34.15	140.19	20.00	1.00	1.01	1.00	0.02	-8.00	992.00	0.00	0.01	-8.75	6.09	0.01	-11.42	975.68	**-24.32**	-21.74	-19.16
PG-50	-33.69	138.93	20.00	1.00	1.01	1.00	0.02	-8.00	992.00	0.00	0.01	-9.62	6.09	0.01	-12.29	974.80	**-25.20**	-22.61	-20.03
PG-51	-34.40	139.60	20.00	1.00	1.01	1.00	0.02	-8.00	992.00	0.00	0.01	-9.38	6.09	0.01	-12.05	975.05	**-24.95**	-22.37	-19.79
PG-55	-34.67	139.46	20.00	1.00	1.01	1.00	0.02	-8.00	992.00	0.00	0.01	-9.03	6.09	0.01	-11.70	975.40	**-24.60**	-22.02	-19.44
PG-56	-32.67	140.17	20.00	1.00	1.01	1.00	0.02	-8.00	992.00	0.00	0.01	-8.21	6.10	0.01	-10.88	976.23	**-23.77**	-21.20	-18.62
PG-57	-35.27	139.46	20.00	1.00	1.01	1.00	0.02	-8.00	992.00	0.00	0.01	-9.61	6.09	0.01	-12.28	974.82	**-25.18**	-22.60	-20.02
PG-59	-35.31	140.79	20.00	1.00	1.01	1.00	0.02	-8.00	992.00	0.00	0.01	-8.85	6.09	0.01	-11.52	975.58	**-24.42**	-21.84	-19.26
PG-96	-34.21	138.32	20.00	1.00	1.01	1.00	0.02	-8.00	992.00	0.00	0.01	-10.41	6.08	0.01	-13.07	974.01	**-25.99**	-23.41	-20.82
PG-97	-33.85	138.41	20.00	1.00	1.01	1.00	0.02	-8.00	992.00	0.00	0.01	-9.39	6.09	0.01	-12.06	975.04	**-24.96**	-22.38	-19.80
PG-98	-33.83	138.02	20.00	1.00	1.01	1.00	0.02	-8.00	992.00	0.00	0.01	-9.01	6.09	0.01	-11.68	975.42	**-24.58**	-22.00	-19.42
PG-99	-33.52	138.06	20.00	1.00	1.01	1.00	0.02	-8.00	992.00	0.00	0.01	-8.44	6.09	0.01	-11.11	975.99	**-24.01**	-21.43	-18.85
B-116	-31.30	121.51	20.00	1.00	1.01	1.00	0.02	-8.00	992.00	0.00	0.01	-5.54	6.11	0.01	-8.22	978.92	**-21.08**	-18.51	-15.94
B-157	-32.32	125.05	20.00	1.00	1.01	1.00	0.02	-8.00	992.00	0.00	0.01	-8.04	6.10	0.01	-10.71	976.40	**-23.60**	-21.02	-18.45
B-162	-31.55	130.59	20.00	1.00	1.01	1.00	0.02	-8.00	992.00	0.00	0.01	-3.28	6.13	0.01	-5.96	981.19	**-18.81**	-16.24	-13.67
PG-131	-33.38	121.34	20.00	1.00	1.01	1.00	0.02	-8.00	992.00	0.00	0.01	-6.86	6.10	0.01	-9.53	977.59	**-22.41**	-19.84	-17.26
PG-132	-33.43	121.27	20.00	1.00	1.01	1.00	0.02	-8.00	992.00	0.00	0.01	-6.80	6.10	0.01	-9.47	977.65	**-22.35**	-19.78	-17.20
PG-133	-33.30	121.30	20.00	1.00	1.01	1.00	0.02	-8.00	992.00	0.00	0.01	-7.02	6.10	0.01	-9.69	977.42	**-22.58**	-20.00	-17.42
PG-134	-33.15	121.71	20.00	1.00	1.01	1.00	0.02	-8.00	992.00	0.00	0.01	-6.21	6.11	0.01	-8.89	978.24	**-21.76**	-19.18	-16.61
PG-156	-32.35	123.62	20.00	1.00	1.01	1.00	0.02	-8.00	992.00	0.00	0.01	-4.78	6.12	0.01	-7.46	979.68	**-20.32**	-17.75	-15.18
PG-157	-32.32	125.05	20.00	1.00	1.01	1.00	0.02	-8.00	992.00	0.00	0.01	-7.28	6.10	0.01	-9.95	977.16	**-22.84**	-20.26	-17.68
PG-159	-31.90	127.02	20.00	1.00	1.01	1.00	0.02	-8.00	992.00	0.00	0.01	-6.80	6.10	0.01	-9.47	977.65	**-22.35**	-19.78	-17.20
PG-162/163	-31.55	130.62	20.00	1.00	1.01	1.00	0.02	-8.00	992.00	0.00	0.01	-5.02	6.12	0.01	-7.70	979.44	**-20.56**	-17.99	-15.42
PG-162/163A	-31.81	132.24	20.00	1.00	1.01	1.00	0.02	-8.00	992.00	0.00	0.01	-7.36	6.10	0.01	-10.03	977.08	**-22.92**	-20.34	-17.76
PG-166	-32.41	134.52	20.00	1.00	1.01	1.00	0.02	-8.00	992.00	0.00	0.01	-8.62	6.09	0.01	-11.29	975.81	**-24.19**	-21.61	-19.03
PG-167	-32.82	135.16	20.00	1.00	1.01	1.00	0.02	-8.00	992.00	0.00	0.01	-9.15	6.09	0.01	-11.82	975.28	**-24.72**	-22.14	-19.56
PG-168	-32.89	135.12	20.00	1.00	1.01	1.00	0.02	-8.00	992.00	0.00	0.01	-9.83	6.09	0.01	-12.50	974.59	**-25.41**	-22.82	-20.24
PG-171	-33.33	134.88	20.00	1.00	1.01	1.00	0.02	-8.00	992.00	0.00	0.01	-9.87	6.09	0.01	-12.54	974.55	**-25.45**	-22.86	-20.28
PG-173	-33.49	135.14	20.00	1.00	1.01	1.00	0.02	-8.00	992.00	0.00	0.01	-9.21	6.09	0.01	-11.88	975.22	**-24.78**	-22.20	-19.62
RP-3-A	-31.96	126.91	20.00	1.00	1.01	1.00	0.02	-8.00	992.00	0.00	0.01	-3.99	6.12	0.01	-6.67	980.48	**-19.52**	-16.95	-14.38

Supplementary Table 5.4. As per Supplementary Table 5.2, but replacing temperature data downloaded from the SILO database with Δ_{47} snail growth temperatures.

Site name	Latitude	Longitude	Assumed snail active season	Average $\delta^{18}O_{precipitation}$ - active season	Δ_{47} temperature	Average maximum relative humidity - active season	Shell growth temperature	$^{18}\alpha_k$	1000lnα	$^{18}\alpha_{w\text{-}v}$	$^{18}R_{IN}$	$^{18}R_A$	θ	F_{ev}/n_L	A	B	$\delta^{18}O_{ss}$ - modelled	$\delta^{18}O_{modelled}$	$\delta^{18}O_{measured}$	$\Delta^{18}O$
				‰ SMOW	°C		°K										‰ SMOW	‰ VPDB	‰ VPDB	
GOC-45D	-15.42	141.88	NDJFMA	-5.9	12	93	285	1.03	10.46	1.01	994.15	983.81	0.4	0.0004	5.95	0.01	-3.3	**-1.6**	-1.7	**0.2**
GOC-22B	-16.08	136.53	NDJFMA	-4.6	8	94	281	1.03	10.83	1.01	995.40	984.68	0.4	0.0004	6.66	0.01	-2.3	**0.3**	1.4	**-1.0**
Alice Springs	-23.73	132.87	NDJFMA	-5.4	8	79	281	1.03	10.84	1.01	994.65	983.93	0.4	0.0004	2.07	0.00	2.0	**4.7**	2.2	**2.5**
5U6	-37.03	140.80	MAMJJASON	-5.2	24	90	297	1.03	9.41	1.01	994.82	985.50	0.4	0.0004	4.21	0.00	-1.7	**-2.7**	0.5	**-3.2**
BL-1	-37.12	140.73	MAMJJASON	-5.3	23	91	296	1.03	9.48	1.01	994.67	985.28	0.4	0.0004	4.54	0.00	-2.1	**-2.9**	-0.1	**-2.8**
CW-1	-36.26	139.71	MAMJJASON	-5.1	20	93	293	1.03	9.77	1.01	994.91	985.24	0.4	0.0004	5.75	0.01	-2.5	**-2.5**	0.6	**-3.2**
B-166	-34.31	138.26	MAMJJASON	-4.3	24	82	297	1.03	9.42	1.01	995.69	986.35	0.4	0.0004	2.39	0.00	1.8	**0.8**	-0.4	**1.2**
KI-2	-35.84	137.75	MAMJJASON	-5.1	25	91	298	1.03	9.31	1.01	994.92	985.71	0.4	0.0004	4.39	0.00	-1.8	**-3.1**	0.1	**-3.2**
B-162	-31.55	130.59	MAMJJASON	-4.2	10	87	283	1.03	10.69	1.01	995.77	985.18	0.4	0.0004	3.20	0.00	0.5	**2.8**	1.5	**1.4**
RP-3-A	-31.96	126.91	MAMJJASON	-4.5	20	86	293	1.03	9.77	1.01	995.48	985.80	0.4	0.0004	3.07	0.00	0.3	**0.3**	2.2	**-2.0**
B-157	-32.32	125.05	MAMJJASON	-4.8	22	89	295	1.03	9.57	1.01	995.17	985.69	0.4	0.0004	3.70	0.00	-0.9	**-1.4**	1.0	**-2.4**
B-116	-31.30	121.51	MAMJJASON	-5.3	23	82	296	1.03	9.51	1.01	994.73	985.32	0.4	0.0004	2.36	0.00	0.9	**0.2**	0.4	**-0.1**
PG-131	-33.38	121.34	MAMJJASON	-4.5	12	90	285	1.03	10.49	1.01	995.47	985.08	0.4	0.0004	4.17	0.00	-0.9	**0.9**	-0.6	**1.5**

Chapter 6

Statement of Authorship

Title of Paper	Clumped isotopes in freshwater snail shells: a new quantitative temperature proxy for Australia, and its application to fossil *Glyptophysa* shells from Blanche Cave
Publication Status	☐ Published ☐ Accepted for Publication ☐ Submitted for Publication ☑ Unpublished and Unsubmitted w ork w ritten in manuscript style
Publication Details	Falster, G., Tyler, J., Dux, F., Kluge, T., Drysdale, R., Tibby, J., Reed, L. (2019). Clumped isotopes in freshwater snail shells: a new quantitative temperature proxy for Australia, and its application to fossil *Glyptophysa* shells from Blanche Cave

Principal Author

Name of Principal Author (Candidate)	Georgina Falster		
Contribution to the Paper	Devised study, prepared and analysed samples, interpreted data, wrote manuscript, acted as corresponding author.		
Overall percentage (%)	90 %		
Certification:	This paper reports on original research I conducted during the period of my Higher Degree by Research candidature and is not subject to any obligations or contractual agreements with a third party that would constrain its inclusion in this thesis. I am the primary author of this paper.		
Signature		Date	11/3/2019

Co-Author Contributions

By signing the Statement of Authorship, each author certifies that:

i. the candidate's stated contribution to the publication is accurate (as detailed above);

ii. permission is granted for the candidate in include the publication in the thesis; and

iii. the sum of all co-author contributions is equal to 100% less the candidate's stated contribution.

Name of Co-Author	Jonathan Tyler		
Contribution to the Paper	Provided conceptual guidance, evaluated and edited manuscript.		
Signature		Date	31/1/2019

Name of Co-Author	Florian Dux		
Contribution to the Paper	Assisted with acquisition and processing of clumped isotope data.		
Signature		Date	5.2.2019

Name of Co-Author	Tobias Kluge		
Contribution to the Paper	Assisted with acquisition and processing of clumped isotope data.		
Signature		Date	8.2.2019

Name of Co-Author	Russell Drysdale		
Contribution to the Paper	Provided access to facilities for clumped isotope analysis.		
Signature		Date	31 January 2019

Name of Co-Author	John Tibby		
Contribution to the Paper	Evaluated and edited manuscript.		
Signature		Date	31/1/2019

Name of Co-Author	Liz Reed		
Contribution to the Paper	Provided samples for analysis.		
Signature		Date	11/2/2019

Clumped isotopes in freshwater snail shells: a new quantitative temperature proxy for Australia and its application to fossil *Glyptophysa* shells from Blanche Cave

Abstract

Quantitative reconstructions of past air temperature in Australia are scarce, due in part to a lack of reliable proxies. The rarity and uneven spatial distribution of existing reconstructions limits insights into Australian climates during global climate conditions different to modern, such as the Last Glacial Maximum (LGM; 23–19 thousand years before present; ka BP). Clumped isotope (Δ_{47}) analysis allows calculation of the formation temperature of carbonate minerals, independent of the source water geochemistry or bulk stable isotope composition of the carbonate. Δ_{47} measurements of a terrestrial carbonate phase that grows consistently throughout the year may therefore be a valuable proxy for mean annual temperature. Unlike land snails—which have distinct growth seasons and avoid activity in desiccating conditions—freshwater snails secrete shell carbonate year-round, in equilibrium with their ambient water, potentially providing a temperature proxy that may be applicable across much of the continent. This study reports the first Δ_{47} measurements on Australian freshwater snail shells, excavated from Blanche Cave in south-eastern Australia. The sedimentary sequence at Blanche Cave spans the past 50,000 years and local palaeoenvironmental change is well characterised, offering an ideal setting for a preliminary test of the freshwater snail shell Δ_{47} palaeothermometer. We measured the Δ_{47} of three individual freshwater snail shells (*Glyptophysa* spp)—two from prior to the LGM (approx. 41.3 and 32.4 ka BP) and one from the early deglacial (approx. 15.9 ka BP). Inferred air temperatures between ~0 and 5 °C cooler present (41.3 ka BP) and up to ~10 °C cooler than present (32.4) correspond with local periods of speleothem accumulation and rapid sediment accumulation in the cave, suggesting cool and wet conditions prior to the LGM. An early deglacial air temperature of between 13 and 18 °C degrees coincides with a hiatus in speleothem deposition and a turnover in the small mammal palaeocommunity around the cave. This may represent the onset of conditions more analogous to the modern environment. Combined with existing temperature reconstructions, our new shell Δ_{47} temperatures suggest a consistent trend in late Quaternary temperature variability along the eastern Australian margin i.e. temperatures around 40 ka BP similar to present that steadily decreased into the LGM, then returned to values similar to present by around 15 ka BP. The agreement of the freshwater snail shell Δ_{47} temperatures with existing palaeoclimate records suggests that this may be a valuable new quantitative air temperature proxy, although we emphasise that measurements from individual shells are extremely unlikely to represent long-term climate conditions. Priority should now be placed on measuring the Δ_{47} of modern shells growing in similar environmental waters, and identifying sedimentary accumulations containing multiple fossil shells.

1 Introduction

Quantitative palaeoclimate data are required to interpret palaeoclimate records in the context of modern climates. This is especially important when reconstructing terrestrial climates that probably had very different baselines to the present. The global Last Glacial Maximum (LGM; 23–19 thousand years before present; ka BP) (Clark et al., 2009; Mix et al., 2001) featured a global average temperature approximately six degrees lower than present, extended ice sheets, and lowered sea level, resulting in ocean-atmosphere interactions and terrestrial climate regimes very different to the modern day. The manifestation of LGM conditions in Australia is unclear, in part because our understanding of Australian climates during the LGM is based mostly on qualitative records of change (Chapter 3, this thesis). Although qualitative records are useful for understanding the general nature of the LGM, they preclude direct comparison of fundamental climate variables such as air temperature with historical records or climate model simulations.

There are currently only four quantitative time-series air temperature records that span the LGM for the Australian continent: a pollen-based record of average annual air temperature each from Tullabardine Dam and Lake Selina in Tasmania (Fletcher and Thomas, 2010), a record of average annual air temperature from analysis of fossil bacterial membrane lipids preserved in Lake McKenzie in south-east Queensland (Woltering et al., 2014), and a chironomid-based reconstruction of average February temperature from Welsby Lagoon, also in south-east Queensland (Chang et al., 2015b) (Fig. 6.1). The scarcity and eastern Australian spatial bias of these quantitative temperature records limit our understanding of how Australian climates responded to the major environmental changes that characterised the LGM and by extension, how Australian climates are affected by changes in global climate conditions.

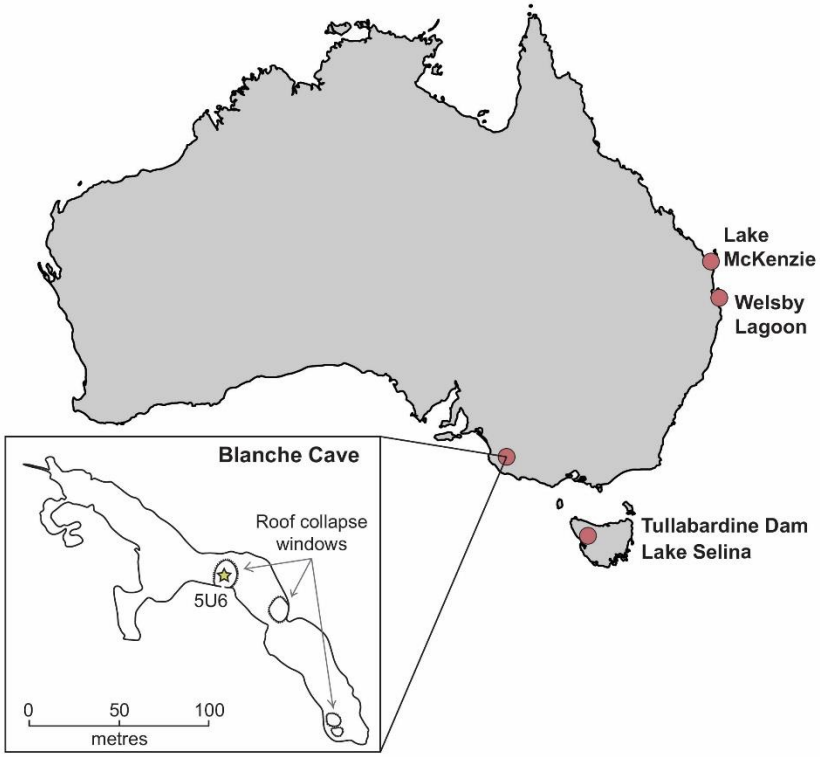

Figure 6.1. Location of sites mentioned in the text i.e. all quantitative palaeotemperature records for Australia during the LGM. Inset map shows a plan view of Blanche Cave, with the location of the three window openings. Approximate location of the excavation is indicated by the yellow star. Cave schematic adapted from Darrénougué et al. (2009).

The dearth of quantitative temperature records reflects the difficulty of accurately reconstructing one variable from the multiple environmental factors that generally influence a palaeoclimate proxy. Table 6.1 provides a summary of methods most frequently used to reconstruct past terrestrial temperatures, along with key advantages and sources of error. Most of these methods rely on quantification of the response of a modern proxy to temperature using a 'training set' (biological proxies), or empirical data (geochemical proxies). These relationships are then applied to fossil material. Where proxies are reliant on biological responses to prevailing environmental conditions, these responses are rarely straightforward. Although advanced numerical techniques may partially overcome non-linear proxy responses to environmental change (eg. Juggins and Birks, 2012; Juggins et al., 2015), there is always uncertainty in biological systems beyond that of one variable, and this can be extremely difficult—if not impossible—to account for (Juggins, 2013). An additional source of uncertainty when reconstructing temperatures from biological assemblages in Australia is that most quantitative methods were developed and tested in the Northern Hemisphere, where there is a greater range of modern analogue climates (Jackson and Williams, 2004; Nielsen and Odgaard, 2004; Porch, 2010). Application of the methods summarised in Table 6.1 would therefore require site-specific calibration, and there are few examples of this for Australian locations or native organisms.

In general, a closer mechanistic relationship between temperature and the proxy provides greater confidence that the relationship is stable through time, resulting in smaller potential for unquantifiable error in the relationship. Geochemical palaeotemperature proxies that are not reliant on modern biology-climate relationships may therefore be particularly promising. Carbonate clumped isotope palaeothermometry is one such geochemical technique, where the results can be reasonably straightforward to interpret in terms of terrestrial temperatures. Clumped isotope analysis is a relatively new tool for calculating the growth temperature of carbonate minerals, and involves measuring the extent to which the rare heavy isotopes ^{13}C and ^{18}O bond—or 'clump'—in the same carbonate ion (Eiler, 2007; Ghosh et al., 2006; Schauble et al., 2006). The actual measured parameter is the excess of the mass 47 CO_2 isotopologue (^{13}C-^{18}O-^{16}O) above the theoretical random distribution of ^{13}C-^{18}O-^{16}O in CO_2 evolved from carbonate by phosphoric acid digestion. This excess is conventionally denoted 'Δ_{47}'. Carbonate Δ_{47} is dependent on the temperature at the time of mineral growth, but largely independent of organism, carbonate phase, or formation water geochemistry (Bernasconi et al., 2018). Carbonate $\delta^{18}O$ and Δ_{47} are measured simultaneously, allowing calculation of the $\delta^{18}O$ of the mineral formation fluid. Clumped isotope analysis therefore offers a uniquely direct perspective on both past temperatures and palaeo-water $\delta^{18}O$.

Table 6.1. List of methods commonly used to infer terrestrial palaeotemperatures, summarising the key advantages and challenges associated with each method. References are provided as examples, and are not exhaustive.

Proxy type	Mechanism	Additional proxy details	How variable is derived	Advantages	Challenges	Selected key references
Biological	Response of species assemblages to environmental change.	Biological indicators include beetles, chironomid midges, cladocerans, non-marine ostracods, diatoms, plant macrofossils, pollen.	Calibration function derived from modern assemblages observed in a range of climates.	May provide high-resolution records	Requires detailed knowledge of organism ecology and phenology	Birks et al. (2010); Brooks and Langdon (2014; Chang et al. (2015); Heiri and Lotter (2005); Herbert and Harrison (2016); Huntley (2012); Juggins (2013); Luoto et al. (2011); Mezquita et al. (2005); Porch (2010)
				Present in many environments	Calibration function requires suitable modern analogue climates, which may not exist	
				May provide detailed climatic information if taxa restricted to a narrow climatic range (eg. beetles)	Different biological proxies from the same reservoir often give different results	
				May provide regional information if indicators have a wide dispersal range (eg. pollen)	Natural variability leads to large errors of reconstruction	
					Fossil assemblages dependent on taphonomy	
Membrane lipids	Certain archaea and algae alter physical properties of their membrane lipids depending on growth temperature.	Fossil membrane lipids preserved in lake and soil sediment.	Empirical calibration of temperature with lipid structure relationships.	Fossil lipids identified in many settings, including soils, peats, lake sediments, hot springs, loess, speleothems	Biased according to seasonality of organism synthesising the lipids	Blaga et al. (2010); Powers et al. (2004); Schouten et al. (2013); Zink et al. (2001)
					Positive identification of non-marine lipid-producing organisms generally unsuccessful	
				Generally high degree of accuracy	Lipid structure also dependent on pH	
					Generally restricted to lakes	
					Absolute temperatures require source-specific calibration	
Calcite Mg/Ca	Substitution of Mg^{2+} into the position of Ca^{2+} in calcite is temperature dependent.	Generally applied to non-marine ostracods	Empirical calibration based on modern organisms.	Ostracods may be common in some lakes	Strong salinity influence on Mg/Ca	Börner et al. (2013); Chivas et al. (1986); Keatings et al. (2006); Saunders et al (2014)
					Species-specific Mg partition coefficient	
					Requires detailed knowledge of organism ecology and phenology	
					Carbonate pre-treatments bias results	
C/N/O stable isotope ratios	Stable isotope ratios ($^{13}C/^{12}C$, $^{15}N/^{14}N$, $^{18}O/^{16}O$), of various carbonate, silica, and organic phases dependent on factors including temperature.	Phases include authigenic and biogenic carbonate, diatom silica, plant matter, bone, teeth, cellulose, and chitin.	Stable isotope ratios measured directly. Annual or seasonal temperatures may be calculated using empirical calibrations based on modern relationships.	Materials with stable isotope compositions fractionated by temperature or temperature-related processes are present in a wide variety of environments	Stable isotope ratios dependent on multiple environmental factors that can be very difficult to isolate	Bailey et al. (2014); Chang et al. (2018); Leng and Barker (2006); Leng and Marshall (2004); Rozanski et al. (2010); Tibby et al. (2016)
					Biogenic carbonates have demonstrated species-specific disequilibrium effects	
				Some phases (eg. bone, teeth) resistant to diagenetic alteration	If biogenic, requires detailed knowledge of organism ecology and phenology	
					Several phases susceptible to diagenetic alteration	
Clumped isotopes	Bonding of ^{13}C and ^{18}O in a carbonate ion is temperature dependent.	Applicable to any carbonate phase.	Calibration equations based on empirical data.	Mineral growth temperature mostly independent of organism, carbonate phase, or source water geochemistry	If biogenic carbonate, requires detailed knowledge of organism ecology and phenology	Bernasconi et al. (2018); Eiler et al. (2011); Eiler et al. (2014); Kelson et al. (2017); Schauble et al. (2006)
					High degree of analytical precision required	
					Disequilibrium effects in some speleothems	

Interpretation of biogenic carbonate Δ_{47} is complicated only by the ecology and phenology of the organisms providing carbonate material. Continental molluscs have provided valuable constraints on terrestrial palaeotemperature (Eagle et al., 2013; Wang et al., 2016; Zaarur et al., 2016) and palaeohydrology (Eagle et al., 2013; Zaarur et al., 2011). Land snails are excellent tracers of hydroclimate as they sample contemporaneous or recent precipitation, however they have narrow environmental tolerances and are only active when temperature and moisture conditions are suitable. Land snail Δ_{47} values are therefore concentrated in a specific range of temperatures (Chapter 5, this thesis). Freshwater snails, on the other hand, grow their shells year-round and display a relatively straightforward relationship with mean air annual temperature (Hren and Sheldon, 2012; Zaarur et al., 2016). Accumulations of freshwater snail shells have also been reported in Australian sediment cores (Ponder et al., 2016).

Freshwater snails therefore offer an ideal source of quantitative palaeotemperature information for Australia, however clumped isotope analysis has never been undertaken on late Quaternary-aged Australian snails. Here the clumped isotope palaeothermometer is applied to freshwater snail shells excavated from the Blanche Cave, south-eastern Australia (Fig. 6.1). Rather than present a new palaeotemperature record per se, the aim of this study is chiefly to gauge the potential for application of the clumped isotope palaeothermometer to fossil freshwater snails in Australia, prior to commencing a detailed 'calibration' study using modern snails.

2 Methods

2.1 Study site

Blanche Cave is one of 26 caves that comprise the Naracoorte Caves system in south-eastern South Australia. The modern climate in the Naracoorte region is Mediterranean, with warm dry summers and cool wet winters (Peel et al., 2007). The mean annual air temperature is 14.9 °C and mean annual precipitation is 491 mm (BOM, 2013) Modern rainfall is delivered mostly between late autumn and early spring (Fig. 6.2).

The Naracoorte Caves formed within the Oligocene-Miocene Gambier Limestone (Wells et al., 1984), and are notable chiefly for their Quaternary vertebrate fossil deposits. These deposits span the past 500,000 years and preserve remarkably diverse vertebrate species assemblages (Prideaux et al., 2007; Reed and Bourne, 2000, 2009). The composition of the cave sediment also provides insight into local and regional palaeoenvironments (Ayliffe et al., 1998; Darrénougué et al., 2009; Desmarchelier et al., 2000; Forbes et al., 2007). The Naracoorte Caves therefore host a concurrent record of faunal and environmental change throughout the late Pleistocene that is unique for Australia.

Three roof collapse windows connect Blanche Cave with the open air (Fig. 6.1). These windows opened prior to 50 ka BP (Macken et al., 2013b), allowing transport and accumulation of terrestrial sediment into Blanche Cave from this time. Sedimentary deposits in the cave are mostly well-stratified and contain both colluvial and aeolian material. Most of the sediment is probably derived from areas proximal to the cave entrances, with a minor distal contribution from the Murray-Darling basin to the north-east (Forbes and Bestland, 2007). Transport of detritus into the cave has been discontinuous, with several sediment layers probably deposited instantaneously during flood events (Macken et al., 2013b).

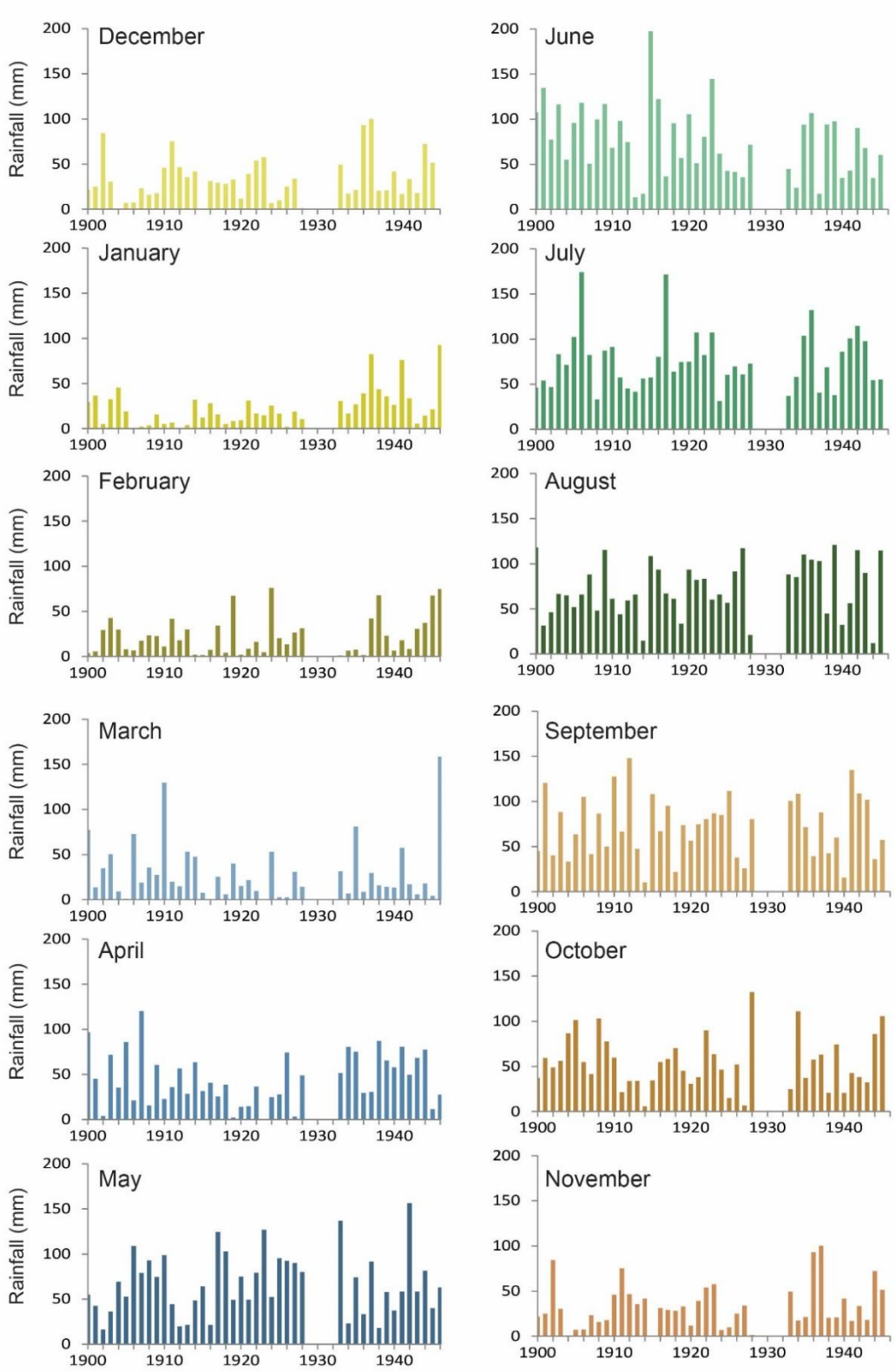

Figure 6.2. Monthly rainfall totals from 1900 to 1947 for Naracoorte. No data was collected between 1929 and 1932. Note that the vertical axis scales are consistent.

Fossilised bones and teeth from over 68 faunal taxa are present in Blanche Cave, including the remains of amphibians, reptiles, birds, and mammals (Reed and Bourne, 2000, 2009). These remains mostly accumulated via owl pellet deposition, pitfall entrapment, and in-situ deaths of cave-dwelling fauna (Laslett, 2006). Gastropod shells of 1–10 mm in diameter are present in several sediment layers, however they have not previously been reported or taxonomically identified (Liz Reed, pers. comm.).

2.2 Chronology

The excavation of pits into the floor of Blanche Cave revealed visually distinct centimetre-scale layers of sediment. In accordance with palaeontological convention, each of these layers has been assigned a name, and these names are maintained in this study (Fig. 6.3).

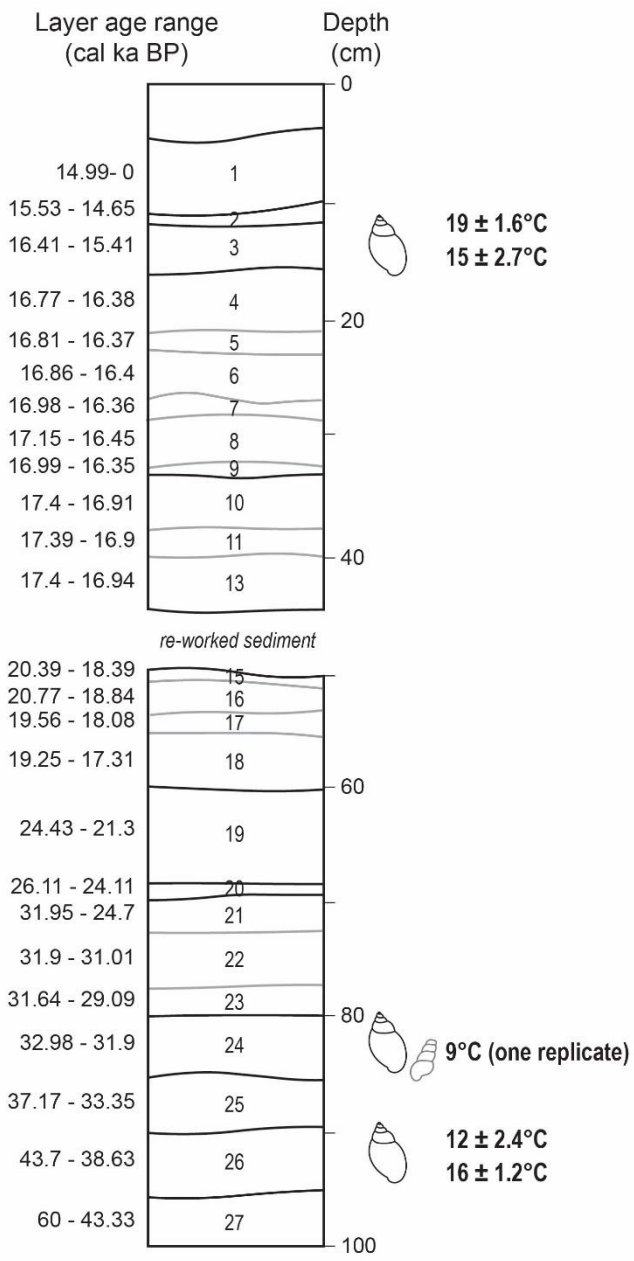

Timing of deposition of the sediment layers has been constrained by a Bayesian age-depth model based on 29 ^{14}C dates on charcoal (Darrénougué et al., 2009; Macken et al., 2013b; St Pierre et al., 2012). The age-depth model provides constraints on the interval of deposition represented by each layer in the form of 'bottom' and 'top' age estimates (Macken et al., 2013b).

The Blanche Cave stratigraphic sequence is therefore constrained chronologically (Macken et al., 2013b; St Pierre et al., 2012), sedimentologically (Darrénougué et al., 2009; Forbes and Bestland, 2007), and palaeontologically (Macken and Reed, 2014), providing an ideal setting for a preliminary assessment of the clumped isotope palaeothermometer.

Figure 6.3. Representative log of the 5U6 excavation site in Blanche Cave, showing stratigraphic position of snail growth temperature estimates calculated from *Glyptophysa* shell Δ_{47} measurements. Depths are to the top of the pit i.e. the modern cave ground level. Adapted from Macken et al. (2013b).

2.3 Sample acquisition

The shells used in this study were excavated in 2006/2007, from a 1 x 1 m grid square near cave window 5U6 (Fig. 6.1). The shells were picked from bags of dry sediment that had previously been sieved to concentrate vertebrate bones. Snail shells were only identified in layers 3 (one specimen), 24 (two specimens), and 26 (one specimen), corresponding with depositional ages of between 16.4 and 15.4 ka BP, 33 and 31.9 ka BP, and 43.7 and 38.6 ka BP, respectively (Fig. 6.3).

2.4 Freshwater snails

Identification of the fossil snails was based on shell morphology and location. The shells from layers 3 and 26, and one of the shells from layer 24 are from freshwater pulmonate gastropods of the *Glyptophysa* (Crosse, 1872) genus (Winster Ponder pers. comm.). The taxonomy of *Glyptophysa* is poorly understood (Ponder et al., 2016) so identification at species level was not possible from the shells alone. *Glyptophysa* shells are globose and sinistral, with a low to elongate spire (Fig. 6.4) (Ponder et al., 2016). In common with most Australian terrestrial gastropods, little is known about the biology, habitat preferences, or environmental tolerances of *Glyptophysa*. *Glyptophysa* snails prefer lentic freshwater habitats including ponds, billabongs, swamps, and slow-moving rivers, and probably attach themselves to water weeds or wood (Ponder et al., 2016). The snails eat algae and detritus, and lay gelatinous eggs that develop directly into juveniles. The snails probably live for one to two years (Winston Ponder, pers. comm.). *Glyptophysa* are found in northern, central, eastern, and south-eastern Australia (Ponder et al., 2016), although the genus is often displaced by morphologically similar alien snails (Ponder et al., 2016; Zukowski and Walker, 2009), so the distribution of the distribution of *Glyptophysa* may have been wider in the past.

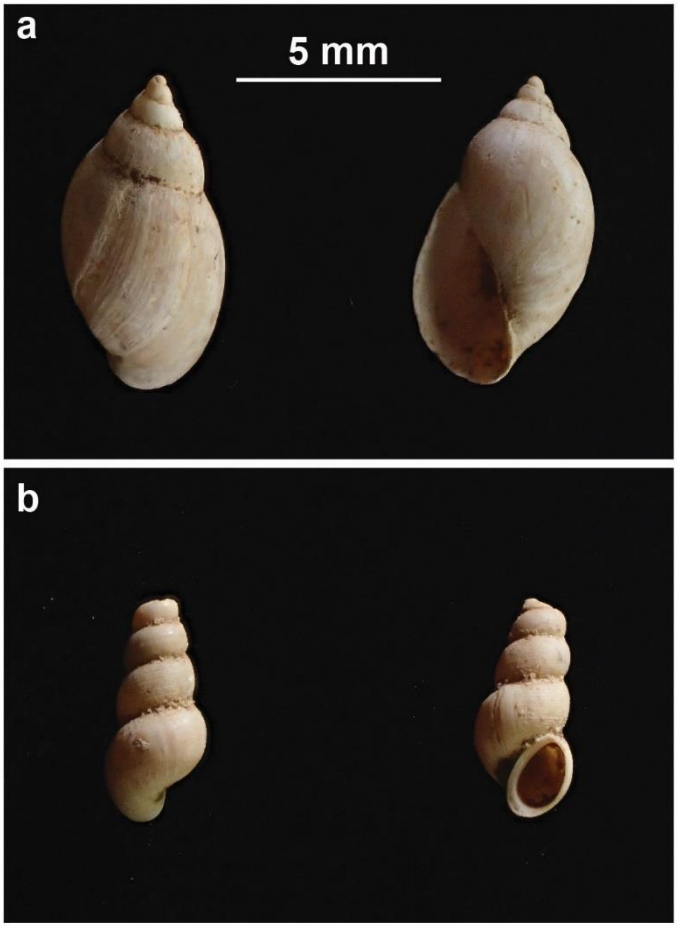

The other shell from layer 24 is from *Coxiella striata* (Reeve, 1842), a freshwater pulmonate gastropod that prefers saline habitats (Williams and Mellor, 1991). *C. striata* have small, elongate dextral shells that are generally spindle-shaped; the top of the spire is often missing in adult shells (Fig. 6.4) (Ponder et al., 2016). *C. striata* are amphibious and are found in ephemeral and permanent salt lakes and coastal marshes (Ponder et al., 2016). The snails probably eat organic detritus, and females deposit eggs singly in capsules coated in sand or mud. *Coxiella* snails likely live for approximately two years (Williams and Mellor, 1991). *C. striata* is found in south-eastern Australia.

Figure 6.4. Photographs of the **a)** *Glyptophysa*, and **b)** *Coxiella striata* shells from layer 24. Scale is the same for all images.

Snails of the *Coxiella* genus have considerable tolerance for desiccating conditions, largely due to behavioural rather than physiological adaptations; they avoid dry conditions by seeking refuge in micro-habitats with more favourable conditions (Williams and Mellor, 1991). The presence of *Coxiella* in ephemeral lakes is dependent in part on the length of time that the lakes contain water, as well as the secular periodicity of inundation (Williams and Mellor, 1991). If the lake is wet for too little time, reproduction and the growth of juveniles to maturity is limited. If the period between lake-filling events is too long, the survival likelihood of adults is decreased.

There are no published data detailing the phenology of Australian freshwater snail taxa. Freshwater snails generally grow throughout the year, possibly with some increase in growth in the warmer months if the snails live in a particularly cold climate (Winston Ponder, pers. comm.). Some snails stop growing at a certain size, but most do not; this information is not available for *Glyptophysa* or *Coxiella*. It was therefore assumed that the shells measured in this study represent the average (mean annual) environmental conditions during the snail's lifetime.

2.5 Sample preparation

The untreated *Coxiella striata* shell from layer 24 weighed only ~5 mg and was therefore too small for clumped isotope analysis which requires minimum total cleaned sample weights of around 10 mg. Prior to isotope analysis, shells were manually cleaned with a toothbrush, then treated with buffered H_2O_2 to dissolve any remaining organic matter (Chapter 2, this thesis). The cleaned shells were finely ground using an agate mortar and pestle, creating a homogeneous powder representing average environmental conditions over the snail's lifespan. This whole-shell sampling approach was necessitated by the small size of the shells. Further details of sample preparation are provided in Appendix 1.

2.6 Clumped isotope analysis

Clumped isotope analysis was performed at The University of Melbourne (UOM) and Heidelberg University (HU) (Table 6.2). Detailed analytical methods for each laboratory are provided in Appendix 1, but the broad approach (extraction, purification, and measurement of CO_2 gas) is common to both laboratories. Briefly, ortho-phosphoric acid was used to transform aliquots of powdered snail shell to gaseous CO_2. The gas was purified by transport of the CO_2 through a trap packed with Porapak™ Q, then a dual inlet mass spectrometer was used to measure the $\delta^{18}O$, $\delta^{13}C$, and Δ_{47} values of the purified gas relative to an ultra-high purity working gas of known isotopic composition.

The raw sample Δ_{47} is calculated as:

$$\Delta_{47} = \left[\left(\frac{R^{47}}{R^{47*}} - 1\right) - \left(\frac{R^{46}}{R^{46*}} - 1\right) - \left(\frac{R^{45}}{R^{45*}} - 1\right)\right] \times 1000$$

where

$$R^i = \frac{mass\ i}{mass\ 44}$$

i.e. the R^i values are abundance ratios of the mass 45, 46, and 47 CO_2 isotopologues, relative to mass 44 CO_2. These values are derived in turn from the measured δ values for each isotopologue in the sample gas, relative to the working gas:

$$\delta^i = \left[\frac{R_{i(sample\ gas)}}{R_{i\ (working\ gas)}} - 1\right] \times 1000$$

The parameter R^{i*} is analogous to R^i, but corresponds to the expected ratios given a stochastic distribution of all possible isotopologues.

The two laboratories use different methods to account for methodological and analytical artifacts, allowing conversion of raw Δ_{47} values into the absolute reference frame (Dennis et al., 2011), and these are described in Appendix 1. In brief: at UOM, a carbon dioxide equilibration scale is used to normalise sample measurements to internationally distributed clumped isotope carbonate standards. At HU, the isotopic composition of a) heated, and b) equilibrated CO_2 gases are used to calibrate the raw sample data into the absolute reference frame (Dennis et al., 2011). The former are heated to 1000 °C to reach a stochastic distribution of isotopologues i.e. Δ_{47} = 0, and the latter are equilibrated with water at 5 or 90 °C. These standardisation steps are necessary to account for mass spectrometric artifacts, allowing inter-laboratory comparison of results (Bernasconi et al., 2018; Dennis et al., 2011). Although the data from both laboratories are presented on the same absolute scale and are theoretically comparable, gas extraction and instrument-specific effects are both non-negligible and poorly understood (Bernasconi et al., 2018) and may result in differences in the calculated temperature of the same sample of up to 10 °C (Dennis et al., 2011). I have therefore differentiated the data from each laboratory on Figure 6.5 (analyses from UOM denoted by a white 'x'). Two shells were analysed in both laboratories. $\delta^{18}O$ and $\delta^{13}C$ values are reported in per mille units relative to the Vienna Pee Dee belemnite standard (VPDB).

Table 6.2. Clumped and stable isotope data for *Glyptophysa* shells from Blanche Cave. Snail growth temperatures calculated using the Δ_{47}-T calibration equation of Bernasconi et al. (2018). $\delta^{18}O_{snail\ body\ fluid}$ calculated using the Δ_{47} temperatures and shell $\delta^{18}O$ (Kim et al., 2007). Air temperatures inferred from snail growth temperatures and the water temperature–air temperature transfer function of Hren and Sheldon (2012). The age range for each layer is the 95.4% probability density range published by Macken et al. (2013). 'n' denotes the number of replicate measurements for each sample. Note that sample 5U6_A3_24 (Heidelberg) has only one replicate, so the reported error (denoted by *) is the long-term standard deviation of laboratory standards. All other errors are standard errors.

Lab	Sample name	Sedimentary layer	Age range of layer (95.4 %)	Genus	Specimens in sample	n	$\delta^{13}C$	$\delta^{18}O$	Δ_{47} (corrected)	Error	Snail growth temperature	Error	$\delta^{18}O_{snail\ body\ fluid}$	Error	Estimated air temperature	Error
			cal yr BP				‰ VPDB	‰ VPDB	‰		°C		‰ VSMOW		°C	
Heidelberg	5U6_A3_3	3	16540 - 15118	*Glyptophysa*	1	3	-8.6	5.5	0.693	0.006	19	1.6	5.9	0.3	18	1.6
Melbourne	5U6_A3_3	3	16540 - 15118	*Glyptophysa*	1	8	-8.9	4.9	0.710	0.010	15	2.7	4.4	0.6	13	3.4
Heidelberg	5U6_A3_24	24	33656 - 31660	*Glyptophysa*	1	1	-7.6	4.1	0.732	*0.013**	9	*2.7**	2.3	*0.6**	5	*4.4**
Heidelberg	5U6_A3_26	26	46473 - 35836	*Glyptophysa*	1	3	-8.9	8.2	0.719	0.009	12	2.4	7.1	0.5	10	3.4
Melbourne	5U6_A3_26	26	46473 - 35836	*Glyptophysa*	1	9	-9.0	7.9	0.705	0.005	16	1.2	7.6	0.3	14	1.5

Results of the analyses and calibrations are listed in Table 6.2 (average values for each sample) and Supplementary Table 6.1 (all measurements). All data are presented in the absolute reference frame (Dennis et al., 2011). Unless otherwise noted, uncertainty is reported as standard error

$$\sigma_{\overline{x}} = \frac{\sigma}{\sqrt{n}}$$

where σ denotes the standard deviation of the Δ_{47} replicates, and n is the number of replicates. For a full description of analytical methods, data reduction processes, and calibration of Δ_{47} to temperature, see Chapter Five Section 2.4 and Appendix 1.

3 Results

3.1 Clumped isotope composition of fossil freshwater snail shells

A summary of the isotope composition (Δ_{47}, $\delta^{18}O$, $\delta^{13}C$) of the three *Glyptophysa* snail shells is provided in Table 6.2, with calculated growth temperatures and snail body water $\delta^{18}O$. Δ_{47} values range from 0.693 ± 0.006 ‰ to 0.732 ‰ (one replicate only), corresponding to growth temperatures between 9 °C and 19 ± 1.6 °C. The coolest temperature is constrained by only one replicate and therefore has high (unquantifiable) uncertainty (at least equivalent to the long-term standard deviation of measurements at HU, which is approximately ± 2.7 °C). This range is comparable to that of the sole published clumped isotope dataset for freshwater snail shells, which inferred growth temperatures of between 18.6 ± 1.9 °C and 29.9 ± 2.1 °C for late glacial to Holocene-aged freshwater snails from the Sea of Galilee, northern Israel (Zaarur et al., 2016). The ~10 °C offset in *absolute* temperatures reflects a similar offset between the modern mean annual air temperatures of Naracoorte and the Sea of Galilee.

3.2 Stable isotope composition of fossil freshwater snail shells

The $\delta^{18}O$ values of these *Glyptophysa* shells range from +4.1 to +8.2 ‰. There are no published $\delta^{18}O$ data from freshwater snail shells in the region (or indeed Australia) for comparison. The $\delta^{18}O$ values are around 5-10 ‰ higher than studies from reasonably similar climates (eg. Apolinarska et al., 2015b; Baroni et al., 2006; Bonadonna et al., 1999; Jones et al., 2002; Stevens et al., 2012), however none of these snails were collected from caves.

The shell $\delta^{18}O$ values correspond to snail body fluid $\delta^{18}O$ values between +2.3 and +7.6 ± 0.3 ‰ (VSMOW) (Table 6.2); snail body fluid $\delta^{18}O$ should be a close approximation of the $\delta^{18}O$ of the ambient water (eg. Fritz and Poplawski, 1974; Leng et al., 1999).

Freshwater pulmonate shell $\delta^{13}C$ values reflect a combination of the $\delta^{13}C$ of dissolved inorganic carbon (DIC) in their ambient water and the $\delta^{13}C$ of their food (Chen et al., 2016; McConnaughey et al., 1997). The DIC in water generally has $\delta^{13}C$ between -3 and +3 ‰ (Leng and Marshall, 2004) and $\delta^{13}C$ of algae and aquatic plant debris eaten by snails falls largely between -35 and -16 ‰ (Keeley and Sandquist, 1992). The $\delta^{13}C$ values of the *Glyptophysa* shells from Blanche Cave range from -9 to -7.6 ‰, well within the range of published studies from elsewhere in the world and consistent with snails deriving carbon mostly from the DIC pool, but with some contribution from dietary plant matter. Controls on the $\delta^{13}C$ of DIC in a water body are complex, including mineralogy and $\delta^{13}C$ of the substrate, isotopic composition of the original inflow water, photosynthesis by aquatic plants, and decomposition of organic matter (McKenzie, 1985). It was not possible to deconvolve these influences from this limited dataset, so whilst the $\delta^{13}C$ values are included in Table 6.2, $\delta^{13}C$ values are not discussed further.

3.3 Interlaboratory comparison

Two *Glyptophysa* shells were measured in both laboratories. The inferred growth temperatures from the two laboratories are within error for both samples, and the offset is not systematic. For one sample the mean Δ_{47} measured at UOM is higher and for the other the Δ_{47} measured at HU is higher. This provides confidence that the data from the two laboratories are comparable. The minor differences between analyses from the two laboratories are probably due to differences in the gas preparation and purification procedures and mass spectrometric artifacts, but may also be the result of imperfect sample grinding and homogenisation.

4 Discussion

The clumped isotope-derived snail growth temperatures—although sparse—are consistent with existing reconstructions of late Quaternary palaeotemperatures in Australia (Fig. 6.5). This suggests that clumped isotope analysis of freshwater snails may be a valuable palaeothermometer for Australia. Although production of a new palaeoclimate record was not a primary goal of this research, not only does this study provide the first quantitative constraint on temperature change in the Naracoorte Cave system, but also reports for the first time the presence of fossil freshwater snails in an Australian cave deposit.

4.1 Freshwater snails in a subterranean cave?

The presence of freshwater snails in otherwise mainly terrestrial cave deposits is enigmatic. Neither *Glyptophysa* nor *Coxiella* are obligate cave dwellers, and nor have they previously been identified in subterranean caves. However, this does not preclude the possibility that these snails lived in Blanche Cave during the late Quaternary. Only five species of cave-dwelling snails have been identified in mainland southern Australia, however surface-dwelling snails have also been observed living in caves (Ponder, 1992; Ponder and Walker, 2003; Ponder et al., 2016). The Australian continental mollusc literature is sparse enough that a great deal remains unknown about the habitat of most native freshwater snails (Ponder and Walker, 2003). Therefore, these freshwater snail shells could either have grown and died in situ, or accumulated in the Blanche Cave deposits in the same manner as other similarly-sized detritus i.e. via owl pellet or aqueous transport.

Most late Quaternary vertebrate remains were deposited in Blanche Cave by owls (Macken et al., 2013b), which roosted in the cave and regurgitated pellets containing the indigestible components of their prey. Two owl species are responsible for the majority of the pellet-derived faunal assemblages—the barn owl (*Tyto alba*) and the masked owl (*Tyto novaehollandiae*) (Macken and Reed, 2014). Neither of these owls—nor any Australian owl—are known to prey on snails (Dickman et al., 1991; Kavanagh, 1996; Kavanagh and Murray, 1996; Law et al., 2013; Morton, 1975; Pavey et al., 2008), suggesting that the snails must have been washed into the cave, or grown in situ.

Blanche Cave has a large window opening, so it is possible that these snails grew outside the cave environment and then were washed into the cave. Both *Glyptophysa* and *Coxiella* prefer lentic environments, so this would require the breaching of a nearby standing waterbody or slow stream and entrainment and transport of these shells into Blanche Cave i.e. a high energy event. The heterogeneity of the sediment layers in Blanche Cave attests to a dynamic cave environment, including discrete cave flooding events (Darrénougué et al., 2009; Macken et al., 2013b). An analogous flood event was observed in Blanche Cave in 2010, when Naracoorte received 145 mm of rain in December, compared with median December rainfall of 26 mm (BOM, 2013). This heavy rainfall resulted in pools of standing water within Blanche Cave (Macken et al., 2013b). Flood events such as this could transport shells into the cave, or transport snail eggs into these cave pools, allowing hatching and in-situ growth of the snails.

The composition of sediments in Blanche Cave provides support for both possibilities. Prior to the LGM, the grain size distribution and sediment geochemistry indicate both aqueous

transport of sediment into the cave and inundation of the cave sediment (i.e. presence of standing water in the cave), probably due to a higher water table and generally wet conditions (Darrénougué et al., 2009). Conversely, most LGM-aged sediment was transported into the cave by the wind, indicating drier conditions corresponding with a lower water table and cessation of aqueous transport into the cave. We did not find any snails in LGM-aged sediment. After around 17 ka BP, sediment composition and morphology suggest a return to wetter conditions. Pollen from aquatic plants is present through sedimentary layers that pre- and post-date the LGM, but not within the LGM sediments (Darrénougué et al., 2009). The aquatic pollen suffers from similar taphonomic ambiguity to the snails; it could have been released by aquatic plants within the cave, or washed in from the surface.

Given the available evidence, I therefore propose that freshwater snails hatched and grew to maturity in or near Blanche Cave, during a wet year that resulted in the pooling of standing water in the cave. These conditions may have been similar to the severe summer storms of December 2010. Whether the snails grew in water within or near the cave makes little difference to the interpretation of the snail growth temperatures, given the reasonably open nature of the cave.

4.2 Late Quaternary temperatures

Although I briefly discuss the isotope-derived temperature estimates in the context of local and regional late Quaternary climates, I emphasise that these analyses are from individual snails and therefore preserve a snapshot into environmental conditions of only one to two years. Given the high inter-annual variability in the local climate (Fig. 6.2), these analyses are very unlikely to be representative of long-term climate, especially given the snails probably hatched during or shortly after an anomalous weather event. Additionally, sedimentological evidence suggests that variable climatic conditions have been a feature of the local Naracoorte climate throughout the late Quaternary (Macken et al., 2013a). Although the aim of this chapter was merely to obtain broadly realistic growth temperatures, in future work, samples should consist of numerous individual shells, to obtain values representative of the mean climate signal for each sediment layer (Apolinarska et al., 2015a). ‘Climate’ is usually defined as the average weather conditions over a certain time period (conventionally 30 years) (Mach et al., 2014) so if snails live for one year, then at least 30 would be required to obtain a climatologically relevant range of values. It will also be important to understand the shell taphonomy, as the shell isotope values may be biased to years featuring extreme weather events analogous to the flood of December 2010.

4.2.1 Palaeoenvironmental implications of snail growth temperatures

Assuming the snails grew to maturity submersed in water, the Δ_{47}-inferred shell growth temperatures represent mean annual water temperature in or around Blanche Cave. Mean annual surface water temperatures are consistently higher than mean annual air temperatures (MAAT) (Hren and Sheldon, 2012). Examination of the Δ_{47}-inferred snail growth temperatures in the context of existing climate reconstructions therefore requires conversion of the growth (i.e. water) temperatures to MAAT. The relationship between air and continental surface water temperatures is independent of water body size, annual climatic conditions, latitude, or elevation, and is described by the transfer function:

$$MAAT\ °C = -0.0318 \times T_{water}^2 + 2.195 \times T_{water} - 12.607;\ R^2 = 0.96$$

where T_{water} is the mean annual water temperature in °C (Hren and Sheldon, 2012). Applying this relationship to the Blanche Cave snail growth temperatures yields mean annual air temperatures between 5 ± 4.4 °C and 18 ± 1.6 °C (Table 6.2, Fig. 6.5). Although there are still uncertainties regarding the seasonality of snail shell growth, water depth, and the nature of the water body where the snails lived, given surface water temperatures rarely equate directly to air temperatures, I suggest that these inferred air temperatures should provide a closer approximation of terrestrial palaeotemperature than snail growth temperatures. I therefore refer to these inferred air temperatures in the remainder of Section 4.2.

4.2.2 Local context

Discrete intervals of speleothem deposition within the Naracoorte Cave system between 50–40 ka BP and 35–20 ka BP probably represent cool temperatures, associated with high effective precipitation (Ayliffe et al., 1998). Speleothems are not currently growing in the caves, suggesting that temperatures during these two accumulation phases were cooler than present, possibly associated with higher average or seasonal rainfall. During the intervening years, the local hydrological balance probably shifted such that potential evaporation exceeded rainfall amount, due to increased temperatures and/or decreased rainfall (Ayliffe et al., 1998). Two of our analyses fall within the speleothem accumulation phases. The Δ_{47} growth temperature of the shell that grew between 46.5 and 35.8 ka BP suggests an average air temperature slightly cooler (estimates between ~0 and ~5 °C cooler) than the modern mean annual air temperature (Fig. 6.5). By 31.7 ka BP, our data suggest that the mean annual air temperature dropped at least several degrees, to almost 10 °C cooler than the modern mean annual temperature, although I reiterate that this temperature estimate is based on the life of one snail. Although we did not find any shells in LGM-aged sediment, an inferred average annual air temperature of between around 13–18 °C during the early deglacial suggests that post-LGM temperatures were almost certainly

warmer than the modern mean annual temperature. Given this coincides with a hiatus in speleothem deposition at Naracoorte, it may be that conditions were more similar to the present day i.e. an excess of potential evaporation over total rainfall, driven in part by higher temperatures. The onset of modern-like warmer and drier conditions overlaps with a turnover in the small mammal palaeocommunity around the cave, which had remained stable prior to and throughout the LGM (Macken and Reed, 2014).

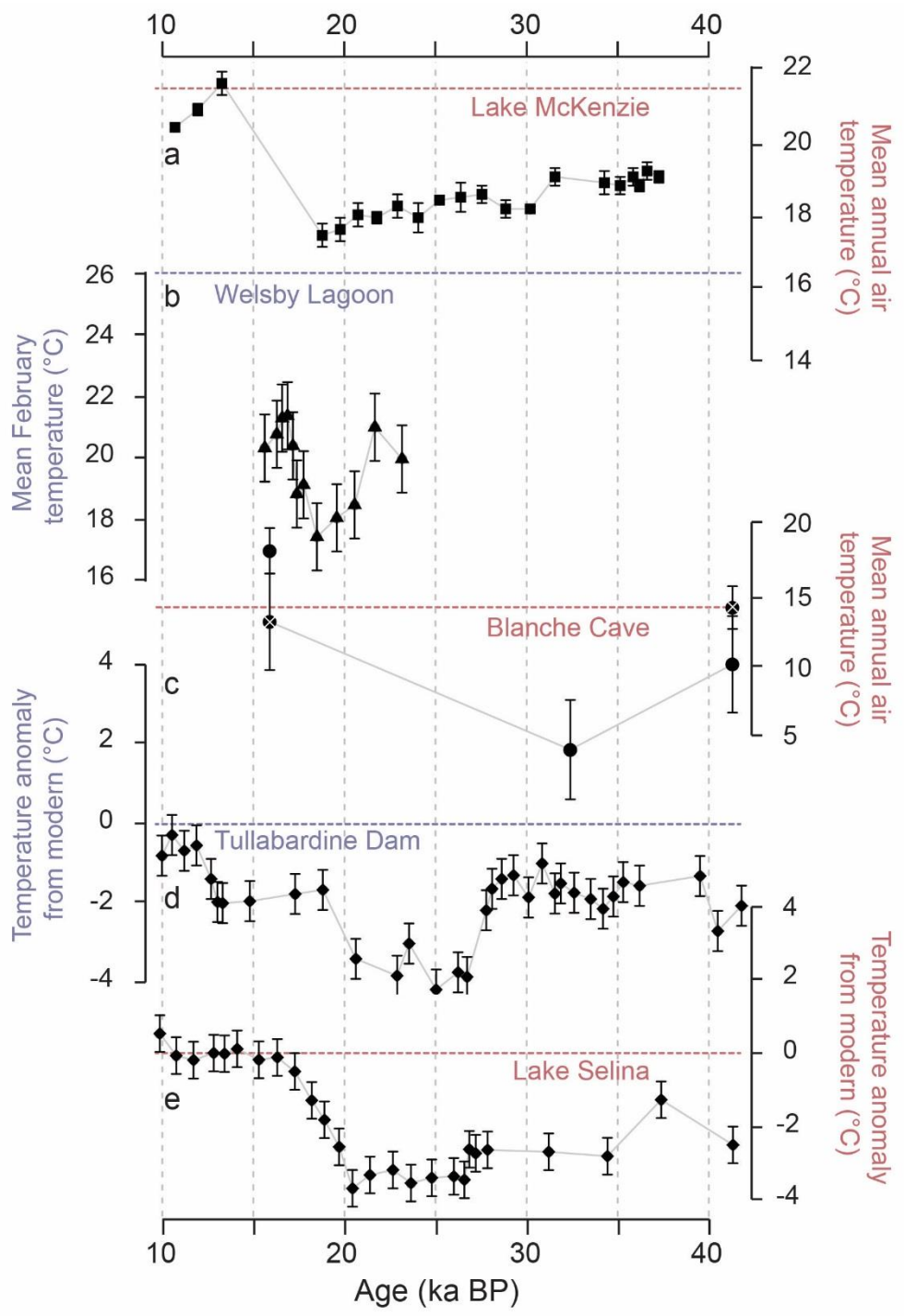

Figure 6.5. Quantitative air temperature estimates from the five sites shown in Fig. 6.1, plotted in latitudinal order from north to south: **a)** mean annual air temperature at Lake McKenzie, estimated from branched glycerol dialkyl glycerol tetraether distributions (Woltering et al., 2014); **b)** mean February temperature at Welsby Lagoon, estimated from fossil chironomid midge assemblages (Chang et al., 2015b); **c)** mean annual air temperatures at Blanche Cave, based on clumped isotope measurements of single freshwater snail shells (this study), converted to air temperature using the transfer function of Hren and Sheldon (2012). White 'x' denotes measurement from UOM; **d-e)** offset from modern mean annual air temperature at **d)** Tullabardine Dam, and **e)** Lake Selina, based on fossil pollen assemblages (Fletcher and Thomas, 2010). The dashed line on each record indicates the equivalent modern value.

4.2.3 Regional context

This new temperature data from Naracoorte is consistent with existing quantitative temperature records from sites to the north and south (Figs. 6.1 & 6.5), implying a consistent trend in late Quaternary temperature variability along the east coast of Australia.

At all sites (except Welsby Lagoon, which is discussed below), mean annual temperatures just prior to the LGM were slightly cooler than present. A further decrease in temperature into the LGM saw absolute temperatures dropping to approximately 4–10 °C below those of the present (Fig. 6.5). This is consistent with two regional-scale estimates of LGM temperatures. Periglacial geomorphology in the Snowy Mountains and Tasmania suggests peak cooling during the LGM saw summer temperatures up to 9 °C and 5 °C cooler than modern, respectively (Galloway, 1965). A record based on amino acid racemisation in emu eggshells from the Australian interior similarly suggests that the average temperature between 45 and 16 ka BP was around 6 °C cooler than modern (Miller et al., 1997). Thus our new clumped isotope data are within existing temperature estimates, providing confidence that freshwater snail shell Δ_{47} may indeed be a valuable palaeotemperature proxy. During the deglacial period, temperatures at all sites except Welsby Lagoon rose to values similar to modern temperatures (Fig. 6.5). There is some disparity in the absolute temperatures, as expected for sites covering a large latitudinal gradient.

The reconstruction from Welsby Lagoon suggests deglacial temperatures that are cooler relative to the modern climate. This may either be due to changes in seasonality during the Late Quaternary, or a bias in the chironomid-based temperature calibration function used to create this record. Chang et al. (2015b) found ‘mean February temperature’ to be the variable most strongly correlated with the composition of chironomid assemblages in south-eastern Australia, although a mechanistic explanation for this choice is not provided. All other temperature reconstructions reflect mean annual conditions. The disparity may therefore reflect a delay in the increase of summer temperatures during the deglacial, relative to a rapid rise in mean annual temperatures. However, modern temperatures at Welsby Lagoon are at the warmest extreme of sites used in the modern calibration dataset (Chang et al., 2015a), and it is therefore likely that the calibration model systematically underestimated the temperature at Welsby Lagoon (Chang et al., 2015b).

I am therefore cautiously optimistic that clumped isotope analysis of freshwater snail shells provides accurate records of mean annual temperature change. Further work should focus on understanding the ecology and phenology of individual species, clarifying the process of freshwater snail shell accumulation in cave deposits, gaining a site-specific understanding of

the relationship between surface water temperature and annual air temperature, and analysing samples composed of multiple individuals.

4.3 Absence of measurable shells from the LGM

The interval lacking freshwater snail shells (32.4–15.9 ka BP) overlaps the estimated duration of LGM conditions in south-eastern Australia (Fogwill et al., 2015; Kershaw et al., 2007; Petherick et al., 2017; Chapter 3, this thesis). The temperature data from the shells provides a clue to this lack of LGM-aged shells in the cave. *Glyptophysa* eggs will not hatch in water temperatures below around 10 °C (Zukowski and Walker, 2009), possibly indicating that not only was this a period of relative aridity (Chapter 3, this thesis), but that temperatures may have remained below around 10 °C. The coolest temperature derived from our shells is slightly below this threshold, although the eggs could have hatched in warmer (summer) temperatures, leaving the hatchlings to grow to adulthood in colder average conditions. Alternatively, relatively dry conditions during this interval (Chapter 3, this thesis) may have corresponded with a lack of flooding events necessary for transport of snails to the cave, or a decrease in effective precipitation (Ayliffe et al., 1998) may have contributed to generally unfavourable conditions for *Glyptophysa*. The latter is supported by the presence of a single *Coxiella striata* shell in the sediment layer deposited between 33.7 and 31.7 ka BP. *C. striata* is tolerant to desiccating conditions and is able to survive periods of exposure (Williams and Mellor, 1991). A lower temperature limit for *C. striata* is unknown and the single shell was too small for clumped isotope analysis.

4.4 A brief discussion of $\delta^{18}O$ values

Given the high uncertainty in the ecology and phenology of *Glyptophysa* in a potentially complex environment, I make only some brief broad comments on possible implications of the *Glyptophysa* shell $\delta^{18}O$ values.

The body fluid of freshwater snails should be in equilibrium with the $\delta^{18}O$ of their environmental waters (Fritz and Poplawski, 1974; Leng et al., 1999). Freshwater snails precipitate their shells using their body fluid, so the $\delta^{18}O$ value of a snail's ambient water source may be approximated from the shell $\delta^{18}O$ value, using clumped isotope analysis to account for the temperature influence (Zaarur et al., 2016). Rather high reconstructed snail body fluid $\delta^{18}O$ values between +2.3 and +7.6 ‰ suggest either precipitation derived from a recycled source (Liu et al., 2010; Winnick et al., 2014), or evaporated water with a long residence time (Markowska et al., 2016; Treble et al., 2013). Such high $\delta^{18}O$ values have not been reported from freshwater snails. However, this is the first work reporting shell $\delta^{18}O$ values from freshwater snails found in caves, where water $\delta^{18}O$ is dependent on percolation pathways, the host rock lithology, evaporation, and residence time, as well as precipitation

$\delta^{18}O$ and temperature. For example, if a large volume of water entered the cave instantaneously along with snail eggs (i.e., a flood event analogous to December 2010), this water may have slowly evaporated, resulting in snail growth within a water source increasingly rich in ^{18}O. A trend of higher snail body fluid $\delta^{18}O$ with higher growth temperatures supports this (Fig. 6.6), perhaps indicating a more rapidly enriched water pool in warmer conditions. If this were the case, it would provide support for in-cave development of the *Glyptophysa*, where snails hatched and grew to maturity inside a gradually diminishing water body. Although highly speculative, this could be easily tested by stable isotope analysis along the growth axis, where I would expect an increase in $\delta^{18}O$ value from the earliest to the latest whorls. I also cannot discount a physiological influence on the shell $\delta^{18}O$ values (Shanahan et al., 2005), and this should be addressed through empirical research before making interpretations of palaeo-water $\delta^{18}O$.

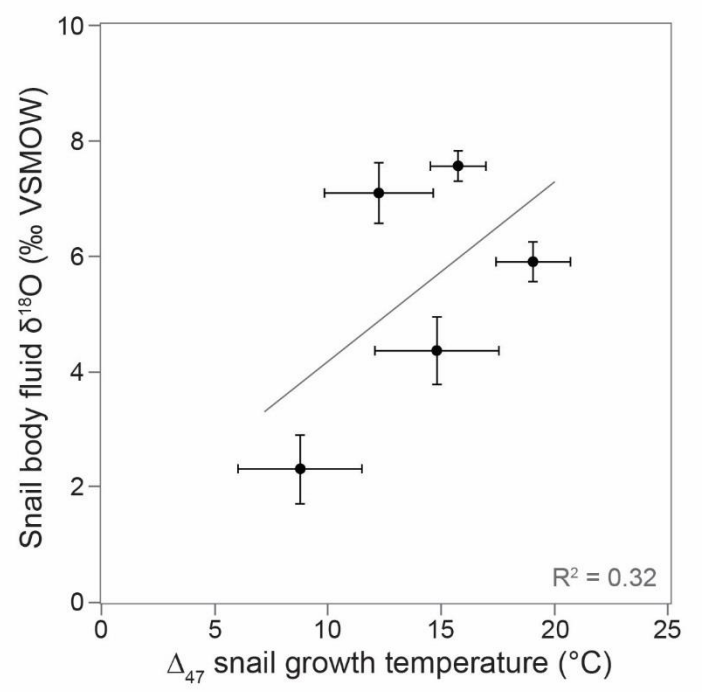

Figure 6.6. Plot showing the relationship between Δ_{47} *Glyptophysa* growth temperatures and the $\delta^{18}O$ of the snail body water i.e. an approximation of the ambient environmental water. Error bars on both axes denote standard error resulting from the Δ_{47} measurements.

5 Conclusions

The results of Δ_{47} analysis of fossil freshwater snail shells from Blanche Cave are consistent with regional palaeotemperature estimates, suggesting that the clumped isotope composition of freshwater snail shells is a plausible quantitative proxy for mean annual air temperature in Australia. As freshwater snails are present across the continent, this new proxy may be widely applicable, allowing reconstruction of both spatial and temporal variability in continental temperatures. A logical next step would be to clarify the relationship of the Δ_{47} and $\delta^{18}O$ values of modern freshwater snail shells with ambient temperature and water $\delta^{18}O$. This will be especially useful if modern and fossil shells co-occur at a site.

Although the aim of this work was a preliminary assessment of the value of applying the clumped isotope palaeothermometer to freshwater snails, our data also provide new insights

into the environmental conditions around Blanche Cave during the late Quaternary. Our results complement existing hydroclimate records, together documenting a shift from cool, wet conditions prior to the LGM, to cooler, dry conditions near the commencement of the LGM, and finally a return to warmer, wetter conditions at the start of the deglacial. This coarse climatic framework would benefit from further analyses, particularly on samples consisting of >1 shell.

6 References cited

Apolinarska, K., Pełechaty, M., Kossler, A., 2015a. Within-sample variability of $\delta^{13}C$ and $\delta^{18}O$ values of freshwater gastropod shells and the optimum number of shells to measure per sediment layer in the Paddenluch palaeolacustrine sequence, Germany. Journal of Paleolimnology 54, 305-323.

Apolinarska, K., Pełechaty, M., Noskowiak, D., 2015b. Differences in stable isotope compositions of freshwater snails from surface sediments of two Polish shallow lakes. Limnologica 53, 95-105.

Ayliffe, L.K., Marianelli, P.C., Moriarty, K.C., Wells, R.T., McCulloch, M.T., Mortimer, G.E., Hellstrom, J.C., 1998. 500 ka precipitation record from southeastern Australia: Evidence for interglacial relative aridity. Geology 26, 147-150.

Bailey, H.L., Henderson, A.C.G., Sloane, H.J., Snelling, A., Leng, M.J., Kaufman, D.S., 2014. The effect of species on lacustrine $\delta^{18}O$ diatom and its implications for palaeoenvironmental reconstructions. Journal of Quaternary Science 29, 393-400.

Baroni, C., Zanchetta, G., Fallick, A.E., Longinelli, A., 2006. Mollusca stable isotope record of a core from Lake Frassina, northern Italy: hydrological and climatic changes during the last 14 ka. The Holocene 16, 827-837.

Bernasconi, S.M., Müller, I.A., Bergmann, K.D., Breitenbach, S.F.M., Fernandez, A., Hodell, D.A., Jaggi, M., Meckler, A.N., Millan, I., Ziegler, M., 2018. Reducing Uncertainties in Carbonate Clumped Isotope Analysis Through Consistent Carbonate-Based Standardization. Geochemistry, Geophysics, Geosystems 19, 2895-2914.

Birks, H.J.B., Heiri, O., Seppä, H., Bjune, A.E., 2010. Strengths and Weaknesses of Quantitative Climate Reconstructions Based on Late-Quaternary Biological Proxies. The Open Ecology Journal 3, 68-110.

Blaga, C.I., Reichart, G.-J., Schouten, S., Lotter, A.F., Werne, J.P., Kosten, S., Mazzeo, N., Lacerot, G., Sinninghe Damsté, J.S., 2010. Branched glycerol dialkyl glycerol tetraethers in lake sediments: Can they be used as temperature and pH proxies? Organic Geochemistry 41, 1225-1234.

Börner, N., De Baere, B., Yang, Q., Jochum, K.P., Frenzel, P., Andreae, M.O., Schwalb, A., 2013. Ostracod shell chemistry as proxy for paleoenvironmental change. Quaternary International 313–314, 17-37.

Bonadonna, F.P., Leone, G., Zanchetta, G., 1999. Stable isotope analyses on the last 30 ka molluscan fauna from Pampa grassland, Bonaerense region, Argentina. Palaeogeography, Palaeoclimatology, Palaeoecology 153, 289-308.

Brooks, S.J., Langdon, P.G., 2014. Summer temperature gradients in northwest Europe during the Lateglacial to early Holocene transition (15–8 ka BP) inferred from chironomid assemblages. Quaternary International 341, 80-90.

Bureau of Meteorology, 2013. Climate statistics for Australian locations - Naracoorte Aerodrome. Bureau of Meteorology, Commonwealth of Australia.

Chang, J.C., Shulmeister, J., Woodward, C., 2015a. A chironomid based transfer function for reconstructing summer temperatures in southeastern Australia. Palaeogeography, Palaeoclimatology, Palaeoecology 423, 109-121.

Chang, J.C., Shulmeister, J., Woodward, C., Steinberger, L., Tibby, J., Barr, C., 2015b. A chironomid-inferred summer temperature reconstruction from subtropical Australia during the last glacial maximum (LGM) and the last deglaciation. Quaternary Science Reviews 122, 282-292.

Chen, F., Feng, J.L., Hu, H.P., 2016. Relationship between the shell geochemistry of the modern aquatic gastropod Radix and water chemistry of lakes of the Tibetan Plateau. Hydrobiologia 771, 239-254.

Chivas, A.R., de Deckker, P., Shelley, J.M.G., 1986. Magnesium content of non-marine ostracod shells: A new palaeosalinometer and palaeothermometer. Palaeogeography, Palaeoclimatology, Palaeoecology 54, 43-61.

Clark, P.U., Dyke, A.S., Shakun, J.D., Carlson, A.E., Clark, J., Wohlfarth, B., Mitrovica, J.X., Hostetler, S.W., McCabe, A.M., 2009. The Last Glacial Maximum. Science 325, 710-714.

Crosse, H., 1872. Description d'un genre nouveau et d'espèces inédites, provinant de la Nouvelle-Calédonie. Journal de Conchyliologie 20, 148-154.

Darrénougué, N., De Deckker, P., Fitzsimmons, K.E., Norman, M.D., Reed, L., van der Kaars, S., Fallon, S., 2009. A late Pleistocene record of aeolian sedimentation in Blanche Cave, Naracoorte, South Australia. Quaternary Science Reviews 28, 2600-2615.

Dennis, K.J., Affek, H.P., Passey, B.H., Schrag, D.P., Eiler, J.M., 2011. Defining an absolute reference frame for 'clumped' isotope studies of CO_2. Geochimica et Cosmochimica Acta 75, 7117-7131.

Desmarchelier, J.M., Goede, A., Ayliffe, L.K., McCulloch, M.T., Moriarty, K., 2000. Stable isotope record and its palaeoenvironmental interpretation for a late Middle Pleistocene speleothem from Victoria Fossil Cave, Naracoorte, South Australia. Quaternary Science Reviews 19, 763-774.

Dickman, C.R., Daly, S.E.J., Connell, G.W., 1991. Dietary Relationships of the Barn Owl and Australian Kestrel on Islands off the Coast of Western Australia. Emu - Austral Ornithology 91, 69-72.

Eagle, R.A., Risi, C., Mitchell, J.L., Eiler, J.M., Seibt, U., Neelin, J.D., Li, G., Tripati, A.K., 2013. High regional climate sensitivity over continental China constrained by glacial-recent changes in temperature and the hydrological cycle. Proceedings of the National Academy of Sciences 110, 8813-8818.

Eiler, J.M., 2007. "Clumped-isotope" geochemistry—The study of naturally-occurring, multiply-substituted isotopologues. Earth and Planetary Science Letters 262, 309-327.

Eiler, J.M., 2011. Paleoclimate reconstruction using carbonate clumped isotope thermometry. Quaternary Science Reviews 30, 3575-3588.

Eiler, J.M., Bergquist, B., Bourg, I., Cartigny, P., Farquhar, J., Gagnon, A., Guo, W., Halevy, I., Hofmann, A., Larson, T.E., Levin, N., Schauble, E.A., Stolper, D., 2014. Frontiers of stable isotope geoscience. Chemical Geology 372, 119-143.

Falster, G., Delean, S., Tyler, J., 2018. Hydrogen Peroxide Treatment of Natural Lake Sediment Prior to Carbon and Oxygen Stable Isotope Analysis of Calcium Carbonate. Geochemistry, Geophysics, Geosystems 19, 3583-3595.

Falster, G., Tyler, J., Grant, K., Tibby, J., Turney, C., Löhr, S., Jacobsen, G., Kershaw, A.P., 2018. Millennial-scale variability in south-east Australian hydroclimate between 30,000 and 10,000 years ago. Quaternary Science Reviews 192, 106-122.

Fletcher, M.-S., Thomas, I., 2010. A quantitative Late Quaternary temperature reconstruction from western Tasmania, Australia. Quaternary Science Reviews 29, 2351-2361.

Fogwill, C.J., Turney, C.S.M., Hutchinson, D.K., Taschetto, A.S., England, M.H., 2015. Obliquity Control On Southern Hemisphere Climate During The Last Glacial. Sci. Rep. 5.

Forbes, M.S., Bestland, E.A., 2007. Origin of the sedimentary deposits of the Naracoorte Caves, South Australia. Geomorphology 86, 369-392.

Forbes, M.S., Bestland, E.A., Wells, R.T., Krull, E.S., 2007. Palaeoenvironmental reconstruction of the Late Pleistocene to Early Holocene Robertson Cave sedimentary deposit, Naracoorte, South Australia. Australian Journal of Earth Sciences 54, 541-559.

Fritz, P., Poplawski, S., 1974. 18O and 13C in the shells of freshwater molluscs and their environments. Earth and Planetary Science Letters 24, 91-98.

Galloway, R.W., 1965. Late Quaternary Climates in Australia. The Journal of Geology 73, 603-618.

Ghosh, P., Adkins, J., Affek, H., Balta, B., Guo, W., Schauble, E.A., Schrag, D., Eiler, J.M., 2006. ^{13}C–^{18}O bonds in carbonate minerals: A new kind of paleothermometer. Geochimica et Cosmochimica Acta 70, 1439-1456.

Heiri, O., Lotter, A.F., 2005. Holocene and Lateglacial summer temperature reconstruction in the Swiss Alps based on fossil assemblages of aquatic organisms: a review. Boreas 34, 506-516.

Herbert, A.V., Harrison, S.P., 2016. Evaluation of a modern-analogue methodology for reconstructing Australian palaeoclimate from pollen. Review of Palaeobotany and Palynology 226, 65-77.

Hren, M.T., Sheldon, N.D., 2012. Temporal variations in lake water temperature: Paleoenvironmental implications of lake carbonate $\delta^{18}O$ and temperature records. Earth and Planetary Science Letters 337-338, 77-84.

Huntley, B., 2012. Reconstructing palaeoclimates from biological proxies: Some often overlooked sources of uncertainty. Quaternary Science Reviews 31, 1-16.

Jackson, S.T., Williams, J.W., 2004. Modern Analogs In Quaternary Paleoecology: Here Today, Gone Yesterday, Gone Tomorrow? Annual Review of Earth and Planetary Sciences 32, 495-537.

Jones, M.D., Leng, M.J., Eastwood, W.J., Keen, D.H., Turney, C.S.M., 2002. Interpreting stable-isotope records from freshwater snail-shell carbonate: a Holocene case study from Lake Gölhisar, Turkey. The Holocene 12, 629-634.

Juggins, S., 2013. Quantitative reconstructions in palaeolimnology: new paradigm or sick science? Quaternary Science Reviews 64, 20-32.

Juggins, S., Birks, H.J.B., 2012. Quantitative environmental reconstructions from biostratigraphical data, In: Birks, H.J.B., Lotter, A.F., Juggins, S., Smol, J.P. (Eds.), Tracking Environmental Change Using Lake Sediments Volume 5: Data Handling and Numerical Techniques. Springer, Dordrechts.

Juggins, S., Simpson, G.L., Telford, R.J., 2015. Taxon selection using statistical learning techniques to improve transfer function prediction. Holocene 25, 130-136.

Kavanagh, R.P., 1996. The breeding biology and diet of the Masked Owl *Tyto novaehollandiae* near Eden, New South Wales. Emu 96, 158-165.

Kavanagh, R.P., Murray, M., 1996. Home range, habitat and behaviour of the Masked Owl *Tyto novaehollandiae* near Newcastle, New South Wales. Emu 96, 250-257.

Keatings, K.W., Holmes, J.A., Heaton, T.H.E., 2006. Effects of pre-treatment on ostracod valve chemistry. Chemical Geology 235, 250-261.

Keeley, J.E., Sandquist, D.R., 1992. Carbon: freshwater plants. Plant, Cell & Environment 15, 1021-1035.

Kelson, J.R., Huntington, K.W., Schauer, A.J., Saenger, C., Lechler, A.R., 2017. Toward a universal carbonate clumped isotope calibration: Diverse synthesis and preparatory methods suggest a single temperature relationship. Geochimica et Cosmochimica Acta 197, 104-131.

Kershaw, A.P., McKenzie, G.M., Porch, N., Roberts, R.G., Brown, J., Heijnis, H., Orr, M.L., Jacobsen, G., Newall, P.R., 2007. A high-resolution record of vegetation and climate through the last glacial cycle from Caledonia Fen, southeastern highlands of Australia. Journal of Quaternary Science 22, 481-500.

Laslett, T., 2006. A palaeoecological study of a Quaternary vertebrate fossil deposit in Blanche Cave, Naracoorte, South Australia. Filnders University, South Australia.

Law, B., Chidel, M., Britton, A., 2013. High predation risk for a small mammal: the eastern pygmy-possum (Cercartetus nanus). Australian Mammalogy 35, 149-152.

Leng, M.J., Lamb, A.L., Lamb, H.F., Telford, R.J., 1999. Palaeoclimatic implications of isotopic data from modern and early Holocene shells of the freshwater snail *Melanoides tuberculata,* from lakes in the Ethiopian Rift Valley. Journal of Paleolimnology 21, 97-106.

Leng, M.J., Marshall, J.D., 2004. Palaeoclimate interpretation of stable isotope data from lake sediment archives. Quaternary Science Reviews 23, 811-831.

Leng, M.J., Barker, P.A., 2006. A review of the oxygen isotope composition of lacustrine diatom silica for palaeoclimate reconstruction. Earth-Science Reviews 75, 5-27.

Liu, Z., Bowen, G.J., Welker, J.M., 2010. Atmospheric circulation is reflected in precipitation isotope gradients over the conterminous United States. Journal of Geophysical Research: Atmospheres 115.

Luoto, T.P., Nevalainen, L., Kultti, S., Sarmaja-Korjonen, K., 2011. An evaluation of the influence of water depth and river inflow on quantitative Cladocera-based temperature and lake level inferences in a shallow boreal lake. Hydrobiologia 676, 143-154.

Mach, K.J., Planton, S., Stechow, C.V. (Eds.), 2014. IPCC 2014 Annex II: Glossary, In: Pachauri, R.K., Meyer, L.A. (Eds.), Climate Change 2014: Synthesis Report. Contribution of Working Groups I, II and III to the Fifth Assessment Report of the Intergovernmental Panel on Climate Change. IPCC, Geneva, Switzerland, pp. 117-130.

Macken, A.C., McDowell, M.C., Bartholomeusz, D.N., Reed, E.H., 2013a. Chronology and stratigraphy of the Wet Cave vertebrate fossil deposit, Naracoorte, and relationship to paleoclimatic conditions of the Last Glacial Cycle in south-eastern Australia. Australian Journal of Earth Sciences 60, 271-281.

Macken, A.C., Staff, R.A., Reed, E.H., 2013b. Bayesian age-depth modelling of Late Quaternary deposits from Wet and Blanche Caves, Naracoorte, South Australia: A framework for comparative faunal analyses. Quaternary Geochronology 17, 26-43.

Macken, A.C., Reed, E.H., 2014. Postglacial reorganization of a small-mammal paleocommunity in southern Australia reveals thresholds of change. Ecological Monographs 84, 563-577.

Markowska, M., Baker, A., Andersen, M.S., Jex, C.N., Cuthbert, M.O., Rau, G.C., Graham, P.W., Rutlidge, H., Mariethoz, G., Marjo, C.E., Treble, P.C., Edwards, N., 2016. Semi-arid zone caves: Evaporation and hydrological controls on $\delta^{18}O$ drip water composition and implications for speleothem paleoclimate reconstructions. Quaternary Science Reviews 131, 285-301.

McConnaughey, T.A., Burdett, J., Whelan, J.F., Paull, C.K., 1997. Carbon isotopes in biological carbonates: Respiration and photosynthesis. Geochimica et Cosmochimica Acta 61, 611-622.

McKenzie, J.A., 1985. Carbon isotopes and productivity in the lacustrine and marine environment, In: Stumm, W. (Ed.), Chemical processes in lakes. Wiley Interscience.

Mezquita, F., Roca, J.R., Reed, J.M., Wansard, G., 2005. Quantifying species–environment relationships in non-marine Ostracoda for ecological and palaeoecological studies: Examples using Iberian data. Palaeogeography, Palaeoclimatology, Palaeoecology 225, 93-117.

Miller, G.H., Magee, J.W., Jull, A.J.T., 1997. Low-latitude glacial cooling in the Southern Hemisphere from amino-acid racemization in emu eggshells. Nature 385, 241.

Mix, A.C., Bard, E., Schneider, R., 2001. Environmental processes of the ice age: land, oceans, glaciers (EPILOG). Quaternary Science Reviews 20, 627-657.

Morton, S.R., 1975. The diet of the Barn Owl *Tyto alba* in Southern Victoria. Emu 75, 31-34.

Nielsen, A.B., Odgaard, B.V., 2004. The use of historical analogues for interpreting fossil pollen records. Vegetation History and Archaeobotany 13, 33-43.

Pavey, C.R., Gorman, J., Heywood, M., 2008. Dietary overlap between the nocturnal letter-winged kite *Elanus scriptus* and barn owl *Tyto alba* during a rodent outbreak in arid Australia. Journal of Arid Environments 72, 2282-2286.

Peel, M.C., Finlayson, B.L., McMahon, T.A., 2007. Updated world map of the Köppen-Geiger climate classification. Hydrology and Earth Systems Science 11, 1633-1644.

Petherick, L.M., Moss, P.T., McGowan, H.A., 2017. An extended Last Glacial Maximum in subtropical Australia. Quaternary International 432, 1-12.

Ponder, W.F., 1992. A new genus and species of aquatic cave-living snail from Tasmanic (Mollusca: Gastropoda: Hydrobiidae). Papers annd Proceedings of the Royal Society of Tasmania 126, 23-28.

Ponder, W. F., Walker, K. F., 2003. From mound springs to mighty rivers: The conservation status of freshwater molluscs in Australia. Aquatic Ecosystem Health and Management 6(1), 19-28.

Ponder, W.F., Halla, A., Shea, M., Clark, S.A., 2016. Australian Freshwater Molluscs.

Porch, N., 2010. Climate space, bioclimatic envelopes and coexistence methods for the reconstruction of past climates: a method using Australian beetles and significance for Quaternary reconstruction. Quaternary Science Reviews 29, 633-647.

Powers, L., Werne, J.P., Vanderwoude, A.J., Sinninghe Damsté, J.S., Hopmans, E.C., Schouten, S., 2010. Applicability and calibration of the TEX_{86} paleothermometer in lakes. Organic Geochemistry 41, 404-413.

Powers, L.A., Werne, J.P., Johnson, T.C., Hopmans, E.C., Damsté, J.S.S., Schouten, S., 2004. Crenarchaeotal membrane lipids in lake sediments: A new paleotemperature proxy for continental paleoclimate reconstruction? Geology 32, 613-616.

Prideaux, G.J., Roberts, R.G., Megirian, D., Westaway, K.E., Hellstrom, J.C., Olley, J.M., 2007. Mammalian responses to Pleistocene climate change in southeastern Australia. Geology 35, 33-36.

Reed, E.H., Bourne, S.J., 2000. Pleistocene fossil vertebrate sites of the South East region of South Australia. Transactions of the Royal Society of South Australia 124, 61-90.

Reed, E.H., Bourne, S.J., 2009. Pleistocene Fossil Vertebrate Sites of the South East Region of South Australia II. Transactions of the Royal Society of South Australia 133, 30-40.

Reeve, L.A., 1842. Conchologia Systematica or Complete System of Conchology: in which the Lepades and Conchiferous Mollusca are described and classified according to their natural organisation and habits. Longman, Brown, Green and Longmans, London.

Rozanski, K., Klisch, M.A., Wachniew, P., Gorczyca, Z., Goslar, T., Edwards, T.W.D., Shemesh, A., 2010. Oxygen-isotope geothermometers in lacustrine sediments: New insights through combined $\delta^{18}O$ analyses of aquatic cellulose, authigenic calcite and biogenic silica in Lake Gościąż, central Poland. Geochimica et Cosmochimica Acta 74, 2957-2969.

Saunders, P., Rogerson, M., Wadhawan, J.D., Greenway, G., Pedley, H.M., 2014. Mg/Ca ratios in freshwater microbial carbonates: Thermodynamic, kinetic and vital effects. Geochimica et Cosmochimica Acta 147, 107-118.

Schauble, E.A., Ghosh, P., Eiler, J.M., 2006. Preferential formation of $^{13}C–^{18}O$ bonds in carbonate minerals, estimated using first-principles lattice dynamics. Geochimica et Cosmochimica Acta 70, 2510-2529.

Schouten, S., Hopmans, E.C., Sinninghe Damsté, J.S., 2013. The organic geochemistry of glycerol dialkyl glycerol tetraether lipids: A review. Organic Geochemistry 54, 19-61.

Shanahan, T.M., Pigati, J.S., Dettman, D.L., Quade, J., 2005. Isotopic variability in the aragonite shells of freshwater gastropods living in springs with nearly constant temperature and isotopic composition. Geochimica et Cosmochimica Acta 69, 3949-3966.

St Pierre, E., Zhao, J.-x., Feng, Y.-x., Reed, E., 2012. U-series dating of soda straw stalactites from excavated deposits: method development and application to Blanche Cave, Naracoorte, South Australia. Journal of Archaeological Science 39, 922-930.

Stevens, R.E., Metcalfe, S.E., Leng, M.J., Lamb, A.L., Sloane, H.J., Naranjo, E., Gonzalez, S., 2012. Reconstruction of late Pleistocene climate in the Valsequillo Basin (Central Mexico) through isotopic analysis of terrestrial and freshwater snails. Palaeogeography Palaeoclimatology Palaeoecology 319, 16-27.

Treble, P.C., Bradley, C., Wood, A., Baker, A., Jex, C.N., Fairchild, I.J., Gagan, M.K., Cowley, J., Azcurra, C., 2013. An isotopic and modelling study of flow paths and storage in Quaternary calcarenite, SW Australia: implications for speleothem paleoclimate records. Quaternary Science Reviews 64, 90-103.

Wang, X., Cui, L., Zhai, J., Ding, Z., 2016. Stable and clumped isotopes in shell carbonates of land snails *Cathaica* sp. and *Bradybaena* sp. in north China and implications for ecophysiological characteristics and paleoclimate studies. Geochemistry, Geophysics, Geosystems 17, 219-231.

Wells, R.T., Moriarty, K., Williams, D.L.G., 1984. The fossil vertebrate deposits of Victoria Fossil Cave, Naracoorte: an introduction to the geology and fauna. The Australian Zoologist 21, 305-333.

Williams, W.D., Mellor, M.W., 1991. Ecology of *Coxiella* (Mollusca, Gastropoda, Prosobranchia), a snail endemic to Australian salt lakes. Palaeogeography Palaeoclimatology Palaeoecology 84, 339-355.

Winnick, M.J., Chamberlain, C.P., Caves, J.K., Welker, J.M., 2014. Quantifying the isotopic 'continental effect'. Earth and Planetary Science Letters 406, 123-133.

Woltering, M., Atahan, P., Grice, K., Heijnis, H., Taffs, K., Dodson, J., 2014. Glacial and Holocene terrestrial temperature variability in subtropical east Australia as inferred from branched GDGT distributions in a sediment core from Lake McKenzie. Quaternary Research 82, 132-145.

Zaarur, S., Affek, H.P., Stein, M., 2016. Last glacial-Holocene temperatures and hydrology of the Sea of Galilee and Hula Valley from clumped isotopes in *Melanopsis* shells. Geochimica et Cosmochimica Acta 179, 142-155.

Zaarur, S., Olack, G., Affek, H.P., 2011. Paleo-environmental implication of clumped isotopes in land snail shells. Geochimica et Cosmochimica Acta 75, 6859-6869.

Zink, K.-G., Leythaeuser, D., Melkonian, M., Schwark, L., 2001. Temperature dependency of long-chain alkenone distributions in recent to fossil limnic sediments and in lake waters. Geochimica et Cosmochimica Acta 65, 253-265.

Zukowski, S., Walker, K.F., 2009. Freshwater snails in competition: alien *Physa acuta* (Physidae) and native *Glyptophysa gibbosa* (Planorbidae) in the River Murray, South Australia. Marine and Freshwater Research 60, 999-1005.

Supporting information for Chapter Six

Clumped isotopes in freshwater snail shells: a new quantitative temperature proxy for Australia, and its application to fossil *Glyptophysa* shells from Blanche Cave

Supplementary Table 6.1. Clumped isotope data for all replicate analyses. Temperatures calculated using the Δ_{47}-T calibration equation of Bernasconi et al. (2018). Measurements highlighted in red are not included in the sample average values presented in Table 6.2. The age range for each layer is the 95.4 % probability density range published by Macken et al. (2013).

Lab	Sample name	Latitude	Longitude	Genus	Sedimentary layer	Age range of layer (95.4 %)	Specimens in sample	$\delta^{13}C$	$\delta^{18}O$	Δ_{47} (corrected)	Temperature
						cal yr BP		‰ VPDB	‰ VPDB	‰	°C
Heidelberg	5U6_A3_3	-37.03	140.80	*Glyptophysa*	3	16540 - 15118	1	-8.7	5.3	0.708	15
Heidelberg	5U6_A3_3	-37.03	140.80	*Glyptophysa*	3	16540 - 15118	1	-8.7	5.5	0.686	21
Heidelberg	5U6_A3_3	-37.03	140.80	*Glyptophysa*	3	16540 - 15118	1	-8.5	5.7	0.685	21
Heidelberg	5U6_A3_24	-37.03	140.80	*Glyptophysa*	24	33656 - 31660	1	-7.5	4.1	0.806	-8
Heidelberg	5U6_A3_24	-37.03	140.80	*Glyptophysa*	24	33656 - 31660	1	-7.4	4.2	0.759	2
Heidelberg	5U6_A3_24	-37.03	140.80	*Glyptophysa*	24	33656 - 31660	1	-7.6	4.1	0.732	9
Heidelberg	5U6_A3_26	-37.03	140.80	*Glyptophysa*	26	46473 - 35836	1	-9.0	8.0	0.742	6
Heidelberg	5U6_A3_26	-37.03	140.80	*Glyptophysa*	26	46473 - 35836	1	-8.9	8.2	0.708	15
Heidelberg	5U6_A3_26	-37.03	140.80	*Glyptophysa*	26	46473 - 35836	1	-8.8	8.4	0.706	16
Melbourne	5U6_A3_3	-37.03	140.80	*Glyptophysa*	3	16540 - 15118	1	-8.9	4.8	0.740	7
Melbourne	5U6_A3_3	-37.03	140.80	*Glyptophysa*	3	16540 - 15118	1	-8.9	4.9	0.738	7
Melbourne	5U6_A3_3	-37.03	140.80	*Glyptophysa*	3	16540 - 15118	1	-8.9	5.0	0.736	8
Melbourne	5U6_A3_3	-37.03	140.80	*Glyptophysa*	3	16540 - 15118	1	-8.8	4.9	0.719	12
Melbourne	5U6_A3_3	-37.03	140.80	*Glyptophysa*	3	16540 - 15118	1	-8.9	4.8	0.719	12
Melbourne	5U6_A3_3	-37.03	140.80	*Glyptophysa*	3	16540 - 15118	1	-8.9	4.8	0.691	20
Melbourne	5U6_A3_3	-37.03	140.80	*Glyptophysa*	3	16540 - 15118	1	-8.8	5.0	0.669	26
Melbourne	5U6_A3_3	-37.03	140.80	*Glyptophysa*	3	16540 - 15118	1	-9.0	4.8	0.666	27
Melbourne	5U6_A3_26	-37.03	140.80	*Glyptophysa*	26	46473 - 35836	1	-9.0	7.9	0.735	8
Melbourne	5U6_A3_26	-37.03	140.80	*Glyptophysa*	26	46473 - 35836	1	-9.0	7.9	0.714	13
Melbourne	5U6_A3_26	-37.03	140.80	*Glyptophysa*	26	46473 - 35836	1	-9.0	8.0	0.713	14
Melbourne	5U6_A3_26	-37.03	140.80	*Glyptophysa*	26	46473 - 35836	1	-9.0	7.8	0.712	14
Melbourne	5U6_A3_26	-37.03	140.80	*Glyptophysa*	26	46473 - 35836	1	-9.0	7.9	0.699	17
Melbourne	5U6_A3_26	-37.03	140.80	*Glyptophysa*	26	46473 - 35836	1	-9.0	7.9	0.698	18
Melbourne	5U6_A3_26	-37.03	140.80	*Glyptophysa*	26	46473 - 35836	1	-9.0	7.8	0.693	19
Melbourne	5U6_A3_26	-37.03	140.80	*Glyptophysa*	26	46473 - 35836	1	-9.0	8.0	0.692	19
Melbourne	5U6_A3_26	-37.03	140.80	*Glyptophysa*	26	46473 - 35836	1	-9.1	7.6	0.690	20

Chapter 7

Discussion and implications for future work

With this thesis, I endeavoured to provide a better understanding of long-term Australian climate variability, through new reconstructions of late Quaternary climate in south-eastern Australia, and new methods that can be applied in future work. Clumped and stable isotope analysis of terrestrial (molluscan) carbonate formed a core component of the study, as a tool to understand past temperature and precipitation. In the following brief discussion, I outline the key outcomes of this thesis in terms of my original aims and then provide a summary of climate variability in south-eastern Australia during the late Quaternary. I also suggest future projects that should result in a more thorough understanding of the nature and drivers of Australian climates on centennial to millennial time scales.

1 Aims

1.1 Provide a new high-resolution, well-dated palaeoclimate record for the late Quaternary, which is of sufficient resolution and quality to compare with regional and distal records

Chapter Three presented a highly resolved record of moisture balance at Lake Surprise, spanning 30–10 thousand years before the year 1950 (ka BP). The x-ray fluorescence and $\delta^{13}C_{OM}$ data comprising the record have an average temporal resolution of approximately one measurement per 5 and 130 years respectively, and together provide a locally coherent record of hydroclimate change. The record is supported by a radiocarbon (^{14}C) chronology constrained by approximately one date per 900 years within the 30–10 ka BP interval, with all ^{14}C analyses performed on concentrated pollen samples, modelled using robust Bayesian methods. The record presented in Chapter Three is therefore one of the most highly resolved, well-constrained palaeoclimate records for the late Quaternary in Australia (Sniderman et al., 2019), capturing sufficient climate variability both for assessment of the regional significance of the record, and detailed comparison with potential remote drivers.

Importantly, the high resolution and temporal security of the record allows tight constraint of:

1. an extended period of relative aridity between 28 and 18.5 ka BP in south-eastern Australia, interspersed with millennial-scale episodes of increased moisture availability
2. peak aridity between 21 and 18.5 ka BP, probably representing the expression of the global LGM

3. a rapid increase in moisture balance between 18 and 16 ka BP
4. maintenance of centennial- to millennial-scale climatic variability throughout the duration of the record.

Both the trends and millennial-scale variability at Lake Surprise are remarkably similar to an existing record of southern Australian aridity (DeDeckker et al., 2012), indicating that both records capture at least a regional signal. Unfortunately, this work also highlighted the scarcity of both regional and distal high-resolution late Quaternary records available for performing detailed comparisons. Modern south-eastern Australian temperature and rainfall are strongly influenced by both zonal circulation features (such as the sub-tropical ridge and the southern westerly winds) and major ocean-atmosphere circulation patterns (such as the El Niño-Southern Oscillation and the Indian Ocean Dipole). Although the strength and latitudinal position of some zonal circulation features may be inferred from single records (e.g. Anderson et al., 2009; Denniston et al., 2013), late Quaternary SST gradients—and hence the nature of their associated ocean-atmosphere circulation patterns—remain a contentious topic in the palaeoceanographic literature, due in part to disparities between reconstructions based on different proxies (Dubois et al., 2009; Gebbie et al., 2016).

I therefore could not draw particularly strong conclusions about the long-term drivers of Australian climate, but rather have provided a foundation for assessing Australian climate—both its key drivers, and the magnitude of its variability on centennial to millennial time scales—as further records become available.

1.2 Develop and test new proxy and numerical methods to improve spatial coverage of palaeoclimate inferences across Australia

The influence of remote drivers of Australian climate often manifests in distinct spatial patterns of temperature or rainfall (Fierro and Leslie, 2014; Jones, 1999; Power et al., 1999; Risbey et al., 2009). I therefore provided new numerical (Chapter 3) and proxy (Chapters 4–6) methods for assessing spatio-temporal palaeoclimate variability. The Monte Carlo Empirical Orthogonal Function (MCEOF) approach used in Chapter Three successfully identified a regional pattern of late Quaternary hydroclimate common to three records in south-eastern Australia and New Zealand. However, this approach also highlighted a clear need for a greater density of high-resolution records, before similar numerical analyses can provide deeper insight into the evolution of Australian climates. I envisage that if a MCEOF analysis could be applied to a larger number of high-resolution records, this may result in the capture of

multiple modes of climate variability, which may in turn be attributed to particular remote drivers. Similarly, the strength of manifestation of various trends in each component record should provide a clearer picture of spatial variability, providing further insight into the contemporaneous climate drivers.

However, robust numerical approaches to understanding spatio-temporal variability—such as MCEOF analysis—rely on well dated, high-resolution datasets, which may not be available for many semi-arid to arid climates. Hence I also developed new proxies for Australian rainfall and temperature that should be applicable across much of the continent, albeit at low temporal resolution. In Chapters Four and Five I found that land snail shells from a wide spatial and climatic gradient across Australia record precipitation amount via two mechanisms: (1) the influence of precipitation amount on the $\delta^{18}O$ of precipitation (a seasonal signal), and (2) the effect of precipitation amount on vegetation $\delta^{13}C$ (an annual to multi-annual signal). These relationships hold regardless of species or regional climatology, confirming that land snail shell isotopes will be a valuable tool to assess spatial palaeoprecipitation variability at a continental scale. In Chapter Six I found that clumped isotope analysis of freshwater snail shells should provide accurate palaeotemperature reconstructions. Although this proxy requires further testing, freshwater snail shells are also found across Australia (Ponder et al., 2016), and therefore should also be useful for continent-scale palaeoclimate reconstruction.

Snail shell isotopes may therefore provide a crucial link between palaeoclimate proxy data and climate model outputs, in the form of 'time slice' evaluation of distinct patterns of spatial variability. For example, synoptic climatology is increasingly used to evaluate the ability of climate models to replicate states of atmospheric circulation (Sheridan and Lee, 2010). Synoptic typing—where regional or local climate conditions are related to discrete circulation patterns—is particularly useful for assessing the performance of models in simulating variables such as temperature and rainfall, as errors in prediction can be more thoroughly interrogated (Gibson et al., 2016; Sheridan and Lee, 2010). Climate model skill in simulating synoptic-scale circulation across Australia varies wildly between different climate models, likely reflecting unrealistic model parameterisation (Gibson et al., 2016). Binning time-series data from a spatial network of proxy records into discrete time intervals—such as the LGM—and then inferring synoptic climatologies would facilitate direct comparison with climate model outputs for the same interval. This approach would be suitable even for records with low (millennial-scale) temporal resolution, as is generally the case for snail shell deposits (e.g. Colonese et al., 2013; Jones et al.,

2002; Prendergast et al., 2015; Yanes et al., 2014). Discrepancies in the proxy and model reconstructions should provide information about model performance, ideally leading to improved model skill, and ultimately more accurate predictions of future climates (Gibson et al., 2016). Conversely, where a good match occurs between proxy and model inferences, this will provide valuable information about the nature and drivers of long-term Australian climate variability, beyond what can be achieved using proxy data alone. A synoptic typing approach to understanding past climates has been applied in New Zealand (Ackerley et al., 2013; Lorrey et al., 2014), but has not been possible in Australia due to a lack of consistent spatial coverage of any one palaeoclimate variable. Application of the new snail shell-based palaeoclimate proxies described in this thesis within a synoptic typing context therefore has the potential to significantly advance understanding of the Australian climate.

The close connection of land snail shell $\delta^{18}O$ with precipitation $\delta^{18}O$ may also provide a direct link with the outputs of state-of-the-art isotope-enabled climate models (Hu et al., 2018; Jones and Dee, 2018). The veracity of climate model outputs incorporating $\delta^{18}O$ information has typically been tested using data from the instrumental period and palaeoclimate data from the past two millennia (Jones and Dee, 2018; PAGES Hydro2k Consortium, 2017). Where suitable fossils shells can be identified, precipitation $\delta^{18}O$ reconstructions from land snail shell $\delta^{18}O$ should facilitate comparison of proxy data and model outputs in a wider range of climate states, allowing both improvements to models and a more holistic understanding of Australian hydroclimate dynamics.

1.3 Develop quantitative methods, and apply to late Quaternary sediment

A crucial step in obtaining quantitative palaeoclimate reconstructions is to have proxy data that reliably reflect environmental conditions. In Chapter Two, I found that both ‘organic’ and ‘treatment’ biases may affect published lake carbonate records, and designed a new method that effectively removes organic matter from bulk sediment samples, whilst avoiding any treatment bias. This work has implications for all published $\delta^{13}C$ and $\delta^{18}O$ values from carbonate from an organic-rich matrix, which may retain either organic or treatment biases, unless specifically assessed by the authors.

Although I do not present a quantitative palaeoprecipitation proxy in this thesis, the strength of the ultimate $\delta^{18}O$-precipitation relationship presented in Chapter Five (R^2 = 0.67) is comparable with that of published Australian quantitative proxy-data calibrations (Chang et al., 2015; Tibby et al., 2016; Turney, 2012). I suggest that with

a direct modern-fossil calibration study and/or analysis of modern shell samples from a more even distribution of seasonal rainfall totals (Fig. 5.7), clumped and stable isotope analysis of fossil land snail shells will provide accurate estimates of past precipitation.

The unexpected presence of freshwater snail shells in Blanche Cave was serendipitous; the clumped isotope composition of freshwater snail shells had previously been shown to provide a relatively straightforward reflection of temperature. Although the temperatures provided in Chapter Six are from single shells and hence technically record weather (rather than climate), they fit well with temperature estimates from existing reconstructions. Clumped isotope analysis of freshwater snail shells therefore has excellent potential to provide quantitative palaeotemperature estimates, subject to modern-fossil calibration studies.

Chapters Five and Six clearly demonstrate the necessity of thoroughly understanding proxy data prior to drawing climatic conclusions. For example, although land snail shell $\delta^{13}C$ probably represents an *annual to multi-annual* signal, land snail shell $\delta^{18}O$ is strongly influenced by the *seasonal* cycle, and these relationships may vary between species. Similarly, the taphonomy of the freshwater snail shells in Blanche Cave suggests that they may record temperatures characteristic of a year with one or more large storm events, rather than representing average climatic conditions. The ecology, phenology, and taphonomy of terrestrial molluscs should therefore be characterised prior to using their shell isotopes as environmental proxies.

2 Synthesis of climate variability in south-eastern Australia during the late Quaternary

The new palaeoclimate information presented in Chapters Three and Six suggest that drivers of south-eastern Australian climate have varied on multi-millennial time scales, in response to major shifts in global ocean-atmosphere circulation patterns during the last glacial-interglacial transition. Dry (Chapter 3) and increasingly cool (Chapter 6) conditions prior to the global LGM gave way to even drier ‘peak’ LGM conditions between 21 and 18.5 ka BP. Millennial-scale hydroclimate variability was maintained throughout this time, although I could not ascribe the sources of this variability in the absence of suitably high-resolution records of potential remote drivers. A distinct peak in moisture balance around 25 ka BP is also evident in other high-resolution records (e.g. Calvo et al., 2007; Petherick et al., 2008; Augustinus et al., 2011), and warrants further investigation. I suggested that the drivers of variability during this time were very different to the modern day, and probably dominated by

cold Southern Ocean processes. Relatively cool sea surface temperatures (SSTs) in the Southern Ocean are likely to have reduced moisture uptake and delivery to south-eastern Australia, and remote influence from the Indian and Pacific oceans may have been dampened by the altered trans-ocean SST gradients (Koutavas and Lynch-Stieglitz, 2003; Otto-Bliesner et al., 2003; Waelbroeck et al., 2009) or generally cooler SSTs in the low latitudes (Lea et al., 2000; Liu et al., 2000; Trend-Staid and Prell, 2002).

Data presented in this thesis suggest that following the LGM, a rapid deglacial climatic shift commenced at around 18 ka BP, culminating in warmer (Chapter 6) and wetter (Chapter 3) conditions, probably more like those of the present. I suggested that this time also saw the beginning of more complex controls on Australian climates, although this hypothesis will only be testable with the generation of more high-resolution records.

3 Next steps to understand long-term Australian climate variability and drivers

With this thesis, I have provided new data and tools for understanding the nature of Australian climate variability on long time scales, and highlighted the effectiveness of clumped and stable isotope analysis of terrestrial gastropod shells as a tool for climate reconstructions. The latter is most effective when combined with a sound knowledge of the ecology, phenology, and taphonomy of the shell-producing animal. In the case of land snails, this is obtainable through use of snail flux balance models, even where empirical calibrations are not easily acquired.

In addition, this thesis has identified priority areas for future related work, for understanding the nature and drivers of long-term climate variability in Australia:

- A holistic understanding of Australian late Quaternary palaeoclimate remains hampered by a lack of temporally continuous records, particularly beyond the south-east of the continent. Modern remote sensing methods, in conjunction with sediment transport models, should aid in the identification of permanent water bodies elsewhere on the continent that could potentially contain late Quaternary sediment accumulations. These may provide relatively ‘low-risk’ targets for acquisition of new sediment cores.
- Although an excellent means of identifying regional spatio-temporal climate variability, the MCEOF approach results in some loss of site-level variability that may have local significance. The recently published Hierarchical Generalised Additive Model (HGAM) approach similarly allows extrication of a

climate signal common to multiple records, but also assesses the deviation of individual sites from this regional trend (Pedersen et al., 2018). A combination of the MCEOF and HGAM approaches may yield detailed information for both regional climate, and local environmental changes.

- Chapters Four, Five, and Six demonstrated snail shell isotopes to be reliable archives of past rainfall (land snails) and temperature (freshwater snails). The isotope-climate relationships will now be improved with species-specific empirical calibrations, which will be especially important for single site studies. This may be readily achieved via growth of snails under controlled conditions in a laboratory, or by collecting live snails of known age from their native environments, along with detailed meteorological information, and local water and plant isotope data. Observational or remotely sensed (e.g. Iyer et al., 2019) data for the activity periods and dietary preferences of individual species would also be highly advantageous. Additionally, defining species-specific kinetic carbon and oxygen isotope fractionation factors was beyond the scope of this thesis, but will be important for the absolute reconstruction of variables such as the $\delta^{18}O$ of precipitation or $\delta^{13}C$ of vegetation.

4 References cited

Ackerley, D., Lorrey, A., Renwick, J., Phipps, S.J., Wagner, S., Fowler, A., 2013. High-resolution modelling of mid-Holocene New Zealand climate at 6000 yr BP. The Holocene 23, 1272-1285.

Anderson, R.F., Ali, S., Bradtmiller, L.I., Nielsen, S.H.H., Fleisher, M.Q., Anderson, B.E., Burckle, L.H., 2009. Wind-Driven Upwelling in the Southern Ocean and the Deglacial Rise in Atmospheric CO_2. Science 323, 1443-1448.

Chang, J.C., Shulmeister, J., Woodward, C., 2015. A chironomid based transfer function for reconstructing summer temperatures in southeastern Australia. Palaeogeography, Palaeoclimatology, Palaeoecology 423, 109-121.

Colonese, A.C., Zanchetta, G., Perlès, C., Drysdale, R.N., Manganelli, G., Baneschi, I., Dotsika, E., Valladas, H., 2013. Deciphering late Quaternary land snail shell $\delta^{18}O$ and $\delta^{13}C$ from Franchthi Cave (Argolid, Greece). Quaternary Research 80, 66-75.
DeDeckker, P., Moros, M., Perner, K., Jansen, E., 2012. Influence of the tropics and southern westerlies on glacial interhemispheric asymmetry. Nature Geoscience 5, 266-269.

Denniston, R.F., Wyrwoll, K.-H., Asmerom, Y., Polyak, V.J., Humphreys, W.F., Cugley, J., Woods, D., LaPointe, Z., Peota, J., Greaves, E., 2013. North Atlantic forcing of millennial-

scale Indo-Australian monsoon dynamics during the Last Glacial period. Quaternary Science Reviews 72, 159-168.

Dubois, N., Kienast, M., Normandeau, C., Herbert, T.D., 2009. Eastern equatorial Pacific cold tongue during the Last Glacial Maximum as seen from alkenone paleothermometry. Paleoceanography 24.

Fierro, A.O., Leslie, L.M., 2014. Relationships between Southeast Australian Temperature Anomalies and Large-Scale Climate Drivers. Journal of Climate 27, 1395-1412.

Gebbie, G., Streletz, G.J., Spero, H.J., 2016. How well would modern-day oceanic property distributions be known with paleoceanographic-like observations? Paleoceanography 31, 472-490.

Gibson, P.B., Uotila, P., Perkins-Kirkpatrick, S.E., Alexander, L.V., Pitman, A.J., 2016. Evaluating synoptic systems in the CMIP5 climate models over the Australian region. Climate Dynamics 47, 2235-2251.

Hu, J., Emile-Geay, J., Nusbaumer, J., Noone, D., 2018. Impact of Convective Activity on Precipitation $\delta^{18}O$ in Isotope-Enabled General Circulation Models. Journal of Geophysical Research: Atmospheres 123.

Iyer, V., Nandakumar, R., Wang, A., Fuller, S.B., Gollakota, S., 2019. Living IoT: A flying Wireless Platform on Live Insects, The 25th Annual International Conference on Mobile Computing and Networking (MobiCom '19). ACM, New York, Los Cabos, Mexico.

Jones, D.A., 1999. Characteristics of Australian land surface temperature variability. Theoretical and Applied Climatology 63, 11-31.

Jones, M.D., Dee, S.G., 2018. Global-scale proxy system modelling of oxygen isotopes in lacustrine carbonates: New insights from isotope-enabled-model proxy-data comparison. Quaternary Science Reviews 202, 19-29.

Jones, M.D., Leng, M.J., Eastwood, W.J., Keen, D.H., Turney, C.S.M., 2002. Interpreting stable-isotope records from freshwater snail-shell carbonate: a Holocene case study from Lake Gölhisar, Turkey. The Holocene 12, 629-634.

Koutavas, A., Lynch-Stieglitz, J., 2003. Glacial-interglacial dynamics of the eastern equatorial Pacific cold tongue-Intertropical Convergence Zone system reconstructed from oxygen isotope records. Paleoceanography 18.

Lea, D.W., Pak, D.K., Spero, H.J., 2000. Climate impact of late quaternary equatorial Pacific sea surface temperature variations. Science 289, 1719-1724.

Liu, Z., Shin, S., Behling, P., Prell, W., Trend-Staid, M., Harrison, S.P., Kutzbach, J.E., 2000. Dynamical and observational constraints on tropical Pacific sea surface temperatures at the last glacial maximum. Geophysical Research Letters 27, 105-108.

Lorrey, A., Fauchereau, N., Stanton, C., Chappell, P., Phipps, S., Mackintosh, A., Renwick, J., Goodwin, I., Fowler, A., 2014. The Little Ice Age climate of New Zealand reconstructed from Southern Alps cirque glaciers: a synoptic type approach. Climate Dynamics 42, 3039-3060.

Otto-Bliesner, B.L., Brady, E.C., Shin, S.I., Liu, Z.Y., Shields, C., 2003. Modeling El Nino and its tropical teleconnections during the last glacial-interglacial cycle. Geophysical Research Letters 30.

PAGES Hydro2k Consortium, 2017. Comparing proxy and model estimates of hydroclimate variability and change over the Common Era. Climate of the Past 13, 1851-1900.

Pedersen, E.J., Miller, D.L., Simpson, G.L., Ross, N., 2018. Hierarchical generalized additive models: an introduction with mgcv. PeerJ Preprints 6, e27320v27321.

Ponder, W.F., Halla, A., Shea, M., Clark, S.A., 2016. Australian Freshwater Molluscs. http://keys.lucidcentral.org/keys/v3/freshwater_molluscs/

Power, S., Tseitkin, F., Mehta, V., Lavery, B., Torok, S., Holbrook, N., 1999. Decadal climate variability in Australia during the twentieth century. International Journal of Climatology 19, 169-184.

Prendergast, A.L., Stevens, R.E., Barker, G., O'Connell, T.C., 2015. Oxygen isotope signatures from land snail (*Helix melanostoma*) shells and body fluid: Proxies for reconstructing Mediterranean and North African rainfall. Chemical Geology 409, 87-98.

Risbey, J.S., Pook, M.J., McIntosh, P.C., Wheeler, M.C., Hendon, H.H., 2009. On the Remote Drivers of Rainfall Variability in Australia. Monthly Weather Review 137, 3233-3253.
Sheridan, S.C., Lee, C.C., 2010. Synoptic climatology and the general circulation model. Progress in Physical Geography 34, 101-109.

Sniderman, J.K.M., Hellstrom, J., Woodhead, J.D., Drysdake, R.N., Bajo, P., Archer, M., Hatcher, L., 2019. Vegetation and Climate Change in Southwestern Australia During the Last Glacial Maximum. Geophysical Research Letters.

Tibby, J., Barr, C., McInerney, F.A., Henderson, A.C.G., Leng, M.J., Greenway, M., Marshall, J.C., McGregor, G.B., Tyler, J.J., McNeil, V., 2016. Carbon isotope discrimination in leaves of the broad-leaved paperbark tree, *Melaleuca quinquenervia*, as a tool for quantifying past tropical and subtropical rainfall. Global Change Biology 22, 3474-3486.

Trend-Staid, M., Prell, W.L., 2002. Sea surface temperature at the Last Glacial Maximum: A reconstruction using the modern analog technique. Paleoceanography 17.

Turney, C.S.M., 2012. Surface $\delta^{13}C$ in Australia: A quantified measure of annual precipitation?, in: Haberle, S.G., David, B. (Eds.), Peopled Landscapes. ANU Press, pp. 435-444.

Waelbroeck, C., Paul, A., Kucera, M., Rosell-Mele, A., Weinelt, M., Schneider, R., Mix, A.C., Abelmann, A., Armand, L., Bard, E., Barker, S., Barrows, T.T., Benway, H., Cacho, I., Chen, M.T., Cortijo, E., Crosta, X., de Vernal, A., Dokken, T., Duprat, J., Elderfield, H., Eynaud, F., Gersonde, R., Hayes, A., Henry, M., Hillaire-Marcel, C., Huang, C.C., Jansen, E., Juggins, S., Kallel, N., Kiefer, T., Kienast, M., Labeyrie, L., Leclaire, H., Londeix, L., Mangin, S., Matthiessen, J., Marret, F., Meland, M., Morey, A.E., Mulitza, S., Pflaumann, U., Pisias, N.G., Radi, T., Rochon, A., Rohling, E.J., Sbaffi, L., Schaefer-Neth, C., Solignac, S., Spero, H., Tachikawa, K., Turon, J.L., 2009. Constraints on the magnitude and patterns of ocean cooling at the Last Glacial Maximum. Nature Geoscience 2, 127-132.

Yanes, Y., Izeta, A.D., Cattáneo, R., Costa, T., Gordillo, S., 2014. Holocene (~4.5–1.7 cal. kyr BP) paleoenvironmental conditions in central Argentina inferred from entire-shell and intra-shell stable isotope composition of terrestrial gastropods. Holocene 24, 1193-1205.

Appendix One: detailed analytical methods

1 Stable carbon and oxygen isotope analyses

Whole snail shells were picked from sediment bags, and five shells were selected for each species present. Shells were selected based on size (larger shells, to avoid juveniles) and degree of preservation (targeting intact shells, without obvious bleaching or degradation, and ideally with some organic matter still attached to indicate a recent death). Where <5 shells from a species were present, all quality shells were used. Each shell was individually cleaned, by breaking the shell into large pieces to expose the interior, extracting any loose soil with forceps or similar, dusting off residual soil with a soft brush, and finally gentle scrubbing with a toothbrush and Milli-Q water. At this stage, for some sites/species, the five shells were combined into one vial; others were kept separate for individual analysis (Appendix 2 Table A3). Each shell or composite shell sample was placed in a vial, and treated with buffered H_2O_2, following the method of Falster et al. (2018). This step was to dissolve any residual organic matter, including the organic matrix within the shell carbonate (Goodfriend, 1990). The cleaned and dried shell samples were finely ground using an agate mortar and pestle, creating a homogeneous powder representing average conditions over the snails' active lifespans.

Carbon and oxygen stable isotope measurements ($\delta^{13}C$ and $\delta^{18}O$) were performed on the powdered shell samples at the University of Melbourne and the University of Wollongong. The $\delta^{13}C$ and $\delta^{18}O$ values are reported in per mille units relative to the Vienna Pee Dee Belemnite (VPDB) standard.

1.1 University of Melbourne

Aliqouts of approximately 1 mg of powdered shell were transferred to borosilicate exetainers then dried overnight in a 40 °C oven with the caps off. After replacing the caps, the exetainers were purged, and then manually injected with 105% H_3PO_4, after which the samples were maintained at 70 °C while gaseous CO_2 evolved from the carbonate. Stable oxygen ($\delta^{18}O$) and carbon ($\delta^{13}C$) measurements were performed on the evolved CO_2 using an AP2003 continuous-flow isotope ratio mass spectrometer, following the standard method of Spötl and Vennemann (2003). Mean analytical precision for $\delta^{13}C$ and $\delta^{18}O$ was ± 0.03‰ and ± 0.07‰, respectively. Results were normalised to the VPDB scale using an internal working standard composed of Carrara Marble (NEW1), which was calibrated against the international standards NBS 18 and NBS 19.

1.2 University of Wollongong

Samples were reacted with 105% H_3PO_4 at 90 °C in an acid-on-individual carbonate MultiPrep system attached to a PRISM III mass spectrometer. Standardisation was based on the NBS 18 ($\delta^{13}C$: -5.04‰, $\delta^{18}O$: -23.01‰), NBS 19 ($\delta^{13}C$: 1.95‰, $\delta^{18}O$: -2.20‰), and Chihauhua ($\delta^{13}C$: -7.91‰, $\delta^{18}O$: -11.68‰) standards. Two of each standard was used at the start of each run and one of each at the end i.e. three standards run three times each. The correction coefficients for slope (always very close to 1) and offset were calculated using linear regressions, for which the R^2 values were always >0.999.

2 Clumped isotope analyses

The general procedures for extracting CO_2 gas from a carbonate sample for clumped isotope analysis are broadly similar to that of stable isotope analysis i.e. digestion of the carbonate with ~104% H_3PO_4 in a sealed reaction vessel at a constant temperature (McCrea, 1950). However, the extremely high precision and accuracy required for accurate clumped isotope measurements necessitates extra CO_2 purification steps, as the measurements are highly susceptible to the presence of non-CO_2 compounds. Purification is typically via various cryogenic and adsorptive techniques tailored to remove non-condensable (O_2, N_2), and condensable (H_2O) contaminants, as well as compounds containing hydrocarbons or halocarbons. Of highest concern are molecules of similar weight to the ^{13}C-^{18}O-^{16}O isotopologue e.g. $^{12}C^{35}Cl$, which can interfere with the measured signal, resulting in anomalously high values.

Manipulation of the CO_2 must be performed under vacuum, to allow pumping of contaminant material from the system. Sample CO_2 gas is manipulated through the vacuum line via cryogenic separation. Liquid nitrogen is used to trap condensable gases, allowing non-condensable compounds to be pumped away. Both H_2O and CO_2 are frozen by liquid nitrogen, so a secondary substance (a mixture of dry ice—$CO_{2(s)}$—and ethanol) is used to separate water vapour from sample CO_2, by virtue of their different freezing points.

The sample CO_2 gas is further purified by passage of the gas through porous adsorptive materials, either passively, or by entrainment in an inert carrier gas. The composition of these materials varies, but separation of CO_2 gas and contaminants is generally based on the polarity of the compounds.

Analysis of the purified sample gas requires a very stable and precise dual-inlet mass spectrometer. The stability requirement arises from the long counting times necessary to detect isotopologues in very low abundance. Stability of the mass spectrometer is required

for accurate results, where precision is maintained over the duration of a measurement cycle.

For this thesis, clumped isotope measurements were performed on the powdered modern snail shell samples (Chapter 5) at the University of Wollongong and the University of Melbourne. Clumped isotope measurements were performed on the powdered fossil snail shell samples (Chapter 6) at Heidelberg University and the University of Melbourne. The powdered modern shell samples were leftover powders from the samples presented in Chapter 4 i.e. each sample consisted of five individual shells that were cleaned and prepared as per described in Section 1.

Fossil snail shells were picked from bags of sediment previously extracted from the excavation pit at site 5U6 (Chapter 6, section 2.3). Sediment from each layer had previously been dried and then stored in separate bags since excavation. Individual sediment bags were emptied into plastic trays, and then the sediment was carefully examined by using a fine paintbrush to gradually sweep the sediment from one side of the tray to the other. All identified shells were sampled. The shells were cleaned and prepared as described in Section 1.

2.1 University of Wollongong

Clumped isotope measurements were performed at the University of Wollongong in 2016, following a modified version of the method described by Ghosh et al. (2006) (Dux, 2015).

2.1.1 Sample preparation

Sample aliquots, each consisting approximately 8 mg of powder, were carefully inserted into the sample chamber of a side-arm reaction vessel. For each sample, 2 mL of ~103% H_3PO_4 was inserted into the side-arm of the vessel, using a disposable polyethylene syringe and a length of flexible tubing. The reaction vessel was evacuated on a vacuum extraction line for between 30 minutes and 2 hours, then closed using a glass stopcock, and removed from the vacuum line. The evacuated vessel was placed in a water bath held at 25 °C for a minimum of 4 hours, to equilibrate both the sample and the H_3PO_4 to the required reaction temperature. The reaction vessel was then slowly tilted to allow the H_3PO_4 to flow from the side-arm into the sample chamber. The carbonate was digested for 12–16 hours at a constant temperature of 25 °C. After digestion was complete, the reaction vessel was removed from the water bath and gas extraction commenced immediately, to avoid any temperature change. Gas extraction was performed on a glass vacuum extraction line, fitted with two large glass traps, and one sample frozen finger port. The gas yield from the shell

samples was measured using a mercury-filled manometer/frozen finger arrangement on the vacuum extraction line; displacement of mercury on expansion of the sample CO_2 gas allowed an estimate of the total volume of CO_2 gas yielded by the sample. This volume was used to detect any loss or gain of gas in subsequent steps. Following the yield measurement, the sample CO_2 was trapped in a frozen finger, and then purified using a temperature-controlled Agilent 7890A gas chromatograph (GC), using a helium carrier gas set to a flow rate of 2 mL/min. An Agilent HP-PLOT-Q column in the GC separated the sample gas from both polar and non-polar contaminants entrained in the sample. Passage of the CO_2 gas through the column was monitored with a non-destructive thermal conductivity detector (TCD). The column was held at -20 °C for the duration of the purification, which was deemed complete when the TCD indicated a return to background signal levels. The purified CO_2 gas was collected by using liquid nitrogen to trap the gas in a stainless steel U-trap, which was then transferred back to the vacuum extraction line. The yield of purified CO_2 gas was measured, and then the gas was sealed in a glass break seal, ready for introduction into the mass spectrometer. After each sample purification, the GC column was heated to 150 °C for 40 minutes while the helium gas flow rate was increased to 5 mL/min, to purge any remaining contaminants.

2.1.2 Mass spectrometric procedures and data evaluation

The purified CO_2 samples were analysed using a Thermo Finnigan MAT 253 mass spectrometer, following the procedure described in detail by Dux (2015). The mass spectrometer was housed in a dedicated room, with temperature controlled to ± 0.1 °C. Each measurement cycle consisted of 12 acquisitions, with 10 cycles per acquisition. Each cycle consisted one set of 26 s integrations of working gas and sample gas through the dual-inlet change-over valve. Each acquisition included a peak centring, background measurement, and an automatic bellows pressure adjustment targeting 8 V on mass 44, on both the sample and working gas bellows. To enable conversion of the data into the absolute reference frame (Dennis et al., 2011), gas standards were also regularly analysed, that had been heated to 1000 °C, or equilibrated with water at 10, 25, or 50 °C. To monitor the accuracy of the conversion to the absolute reference frame (the ‘heated gas line’), carbonate standards Carrara Marble (CM-1) and Sigma (AR) were also periodically measured. The data corrections and transfer of measurements into the absolute reference frame of Dennis et al. (2009) were performed using an in-house macro-enabled Excel spreadsheet. As the acid digestion was performed at 25 °C, no acid reaction temperature correction was necessary (Defliese et al., 2015). Shell $\delta^{13}C$ and $\delta^{18}O$ values are reported relative to the Vienna Pee Dee Belemnite (VPDB) standard.

Temperatures were calculated from the Δ_{47} values, using the calibration of Bernasconi et al. (2018):

$$\Delta_{47} = 0.0449\ (\pm 0.001) * \frac{10^6}{T^2} + 0.167\ (\pm 0.01)$$

where T is the temperature in Kelvin. The $\delta^{18}O$ values of the mineral formation fluid (snail body water) were calculated by using the Δ_{47} temperatures and shell $\delta^{18}O$ as inputs to the water-aragonite oxygen isotope fractionation equation of Kim et al. (2007):

$$1000 \ln \alpha_{aragonite-water} = 17.88\ (\pm 0.13) * \left(\frac{10^3}{T}\right) - 31.14\ (\pm 0.46)$$

In this case, T is the Δ_{47} temperature, and $\alpha_{aragonite-water}$ is the aragonite-water fractionation factor:

$$\alpha_{aragonite-water} = \frac{R_{aragonite}}{R_{water}}$$

where R is the measured ratio of ^{18}O to ^{16}O. $R_{aragonite}$ is measured directly during the clumped isotope measurements, allowing calculation of the R—and hence $\delta^{18}O$—of the formation water. Snail body water $\delta^{18}O$ values are reported relative to the Vienna Standard Mean Ocean Water (VSMOW) standard.

2.1.3 Calculation of average stable and clumped isotope values

Prior to calculating the average values presented in Table 5.1, the data were screened for environmentally unrealistic temperatures, probably indicating sample contamination. These values were not included in the average values, and are highlighted in red in Supplementary Table 5.1.

From the remaining measurements, average Δ_{47} values were calculated as the mean of n (1–3) replicates, with error reported as one standard error (Table 5.1). Standard error is defined as

$$\sigma_{\overline{x}} = \frac{\sigma}{\sqrt{n}}$$

where σ denotes the standard deviation of the Δ_{47} replicates, and n is the number of replicates. Uncertainties in the $\delta^{18}O$ of the snail body fluid are based on the Δ_{47} temperature uncertainties, as the analytical uncertainties were relatively negligible.

2.2 Heidelberg University

Clumped isotope measurements were performed at Heidelberg University in 2017, following the method described by Kluge et al. (2015).

2.2.1 Sample preparation

Sample aliquots, each consisting approximately 8 mg of powder, were carefully inserted into the inlet tube on the side of a glass reaction vessel containing 2 mL 105% H_3PO_4 in the main chamber. The reaction vessel was evacuated for 30 minutes before acid digestion was initiated by dropping the sample from the inlet into the main chamber. The carbonate was digested for 10 minutes at a constant temperature of 90 °C, whilst being stirred continuously. The evolving CO_2 gas was collected in a glass trap cooled by liquid nitrogen. CO_2 evolved from the sample was purified using a conventional off-line glass vacuum line, similar to the procedure described by Dennis and Schrag (2010). In brief, a cryogenic mixture of dry ice ($CO_{2(s)}$) and ethanol was used to separate water from the CO_2 sample gas. The remaining CO_2 gas was passively transported through a trap densely packed with Porapak^{TM} Q held at -35 °C. This purified CO_2 gas was captured in a frozen finger, and immediately transferred to the mass spectrometer for analysis.

2.2.2 Mass spectrometric procedures and data evaluation

The purified CO_2 samples were analysed using a Thermo Fischer Scientific MAT 253 Plus mass spectrometer, following the procedure outlined by Huntington et al. (2009) and Dennis et al. (2011). Each measurement cycle consisted of eight acquisitions, with 10 cycles per acquisition. Each acquisition included a peak centre, background measurements, and a bellows pressure adjustment targeting 6 V. The sample CO_2 was measured relative to an internal working gas standard (Oberlahnstein CO_2). To enable conversion of the data into the absolute reference frame (Dennis et al., 2011), gas standards were also regularly analysed, that had been heated to 1000 °C, or equilibrated with water at 5 °C or 90 °C. To monitor the accuracy of the conversion to the absolute reference frame (the 'heated gas line'), ETH carbonate standards, as well as Richter Marble and HW-II standards were also periodically measured (Meckler et al., 2014). The average values for the period of measurement, reported in the absolute reference frame, are ETH-1: 0.292 ± 0.015‰ (n = 3), ETH-2: 0.305 ± 0.006‰ (n = 3), HW-II: 0.712 ± 0.014‰ (n = 6), and Richter Marble: 0.396 ± 0.019‰ (n = 3). The observed long-term standard deviation of laboratory standards was 0.013‰. Sample contamination was monitored using mass 48 and mass 49 signal, based on the methods outlined by Huntington et al. (2009). The data corrections and transfer of measurements into the absolute reference frame of Dennis et al. (2011) were performed using an in-house Excel spreadsheet. As the acid digestion was performed at 90 °C , a correction of 0.082‰ was applied after conversion to the absolute reference frame, to project the data to an acid reaction temperature of 25 °C (Defliese et al., 2015). Shell $\delta^{13}C$ and $\delta^{18}O$ values are reported relative to the Vienna Pee Dee Belemnite (VPDB) standard. Δ_{47} temperatures and snail body water $\delta^{18}O$ were calculated as described in Section 2.1.2.

2.2.3 Calculation of average stable and clumped isotope values

Prior to calculating the average values presented in Table 6.2 and Figure 6.5, the data were screened for environmentally unrealistic temperatures, probably indicating sample contamination. These values were not included in the average values, and are highlighted in red in Supplementary Table 6.1.

From the remaining measurements, average Δ_{47} values were calculated as the mean of n (1-3) replicates, with error reported as one standard error (Table 6.2). Standard error is defined as

$$\sigma_{\overline{x}} = \frac{\sigma}{\sqrt{n}}$$

where σ denotes the standard deviation of the Δ_{47} replicates, and n is the number of replicates. Where only one measurement was available, the error was assigned the long-term standard deviation of the laboratory standards i.e. 0.013‰. Uncertainties in the $\delta^{18}O$ of the snail body fluid are based on the Δ_{47} temperature uncertainties, as the analytical uncertainties are relatively negligible.

Two samples were measured at both Heidelberg University, and the University of Melbourne, to evaluate possible isotopic biases resulting from the different sample preparation and mass spectriometric procedures. Differences in the $\delta^{13}C$, $\delta^{18}O$, and Δ_{47} measurements were not significant (Fig. 6.5).

2.3 University of Melbourne

Clumped isotope measurements of modern land snail (Chapter 5) and fossil freshwater snail (Chapter 6) shells were performed at the University of Melbourne in 2018, using a modified version of the carbon dioxide equilibration scale to normalise measured clumped isotope values into the absolute reference frame (Dennis et al., 2011). This method relies on internationally distributed standards (Bernasconi et al., 2018; Meckler et al., 2014; Murray et al., 2016) to normalise and calibrate the raw Δ_{47} measurements.

2.3.1 In-line sample preparation

Samples were analysed using a Nu Instruments Perspective-IS stable isotope ratio mass spectrometer, interfaced with the Nu Carb carbonate sample preparation system. This contrasts the sample preparation procedures at the University of Wollongong and Heidelberg University, both of which are derived from the off-line gas preparation and purification process described by Dennis and Schrag (2010).

Sample aliquots, each consisting approximately 400–600 µg of powder, were carefully inserted into individual sample vials, which were placed in the Nu Carb sample carousel. Samples were digested for 10 minutes at a constant temperature of 70 °C, following the automated injection of 120 µL of 104% H_3PO_4. The evolved CO_2 gas was then expanded into a -95 °C water trap. The CO_2 sample gas was purified using an automated cryogenically cooled adsorptive trap apparatus i.e. passage of the gas for 25 minutes through a trap densely packed with Porapak™ Q, held at -34 °C. The purified CO_2 gas was captured in a liquid nitrogen frozen finger, and a pressure transducer was used to calculated total CO_2 yield from each sample powder. The sample gas was transferred into the sample cold finger, within the dual inlet system of the mass spectrometer. Once the sample CO_2 expands, the sample inlet provides a constant depletion volume, which is matched by an identical depletion volume on the reference side of the dual-inlet system. This allows for a constant depletion rate of both sample and reference gas during each measurement cycle. The adsorptive trap apparatus was cleaned between each sample extraction, by active vacuum pumping at 150 °C, for 25 minutes. This cleaning step was to ensure any contaminants from the previous sample extraction were removed.

2.3.2 Mass spectrometric procedures and data evaluation

The purified CO_2 sample was analysed immediately following the automated sample extraction. Each measurement cycle consisted of three acquisitions each for the sample and reference gases, with 20 cycles per acquisition. This equates to 20 minutes of integration time for each analytical replicate. Each acquisition included a zero (no gas) background measurement, as well as automatic peak centring on m/z 45. The reference gas beam was pressure balance to the sample gas beam, and depletes evenly through matched-length capillaries; initial beam balanced (m/z = 44) was set to 80 nA, depleting throughout the measurement cycle to approximately 45 nA.

To account for instrument-specific source scattering effects, and enable conversion of the data into the absolute reference frame, the raw Δ_{47} measurements were calibrated against a suit of carbonate standards of known Δ_{47}. A carbon dioxide equilibration scale (CDES) reference frame was used to calibrate the measured Δ_{47} values to internationally distributed clumped isotope carbonate standards. The CDES is constructed by repeat analysis of the standards ETH-1, ETH-2, ETH-3, and ETH-4, distributed by S. Bernasconi from ETH Zürich, as well as an in-house Carrara Marble standard, NCM. The deviation of the measured Δ_{47} from accepted values was used to create an empirical transfer function, which is then used to project the background-corrected raw sample Δ_{47} values into the absolute reference

frame. The ETH standards were also used to correct sample $\delta^{13}C$ and $\delta^{18}O$ values, which are reported in per mille units relative to the Vienna Pee Dee Belemnite (VPDB) standard. Using the CDES reference frame to transpose the raw Δ_{47} values into the absolute reference frame yielded average offsets of the ETH standards of < ± 0.008‰ from their accepted values. At UOM, standardisation of the raw sample Δ_{47} values is performed for each batch of samples and standards in a particular analytical session; sessions typically span two to three months, in which all analysed standards are used to construct the CDES reference frame. All data presented in this study were obtained during one analytical session.

As the acid digestion was performed at 70 °C , a correction of 0.062‰ was applied after conversion to the absolute reference frame, to project the data to an acid reaction temperature of 25 °C (Defliese et al., 2015). Δ_{47} temperatures and snail body water $\delta^{18}O$ were calculated as described in Section 2.1.2.

2.3.3 Calculation of average stable and clumped isotope values

Prior to calculating the average values presented in Tables 5.1 and 6.2, the data were screened for environmentally unrealistic temperatures, probably indicating sample contamination. These values were not included in the average values, and are highlighted in red in Supplementary Tables 5.1 and 6.1.

From the remaining measurements, average Δ_{47} values were calculated as the mean of n (2-9) replicates, with error reported as one standard error (Tables 5.1 & 6.2). Standard error is defined as

$$\sigma_{\overline{x}} = \frac{\sigma}{\sqrt{n}}$$

where σ denotes the standard deviation of the Δ_{47} replicates, and n is the number of replicates. Uncertainties in the $\delta^{18}O$ of the snail body fluid are based on the Δ_{47} temperature uncertainties, as the analytical uncertainties are relatively negligible.

Two samples were measured at both Heidelberg University, and the University of Melbourne, to evaluate possible isotopic biases resulting from the different sample preparation and mass spectrometric procedures. Differences in the $\delta^{13}C$, $\delta^{18}O$, and Δ_{47} measurements were not significant (Fig. 6.5).

3 References cited

Bernasconi, S.M., Müller, I.A., Bergmann, K.D., Breitenbach, S.F.M., Fernandez, A., Hodell, D.A., Jaggi, M., Meckler, A.N., Millan, I., Ziegler, M., 2018. Reducing Uncertainties in Carbonate Clumped Isotope Analysis Through Consistent Carbonate-Based Standardization. Geochemistry, Geophysics, Geosystems 19, 2895-2914.

Defliese, W.F., Hren, M.T., Lohmann, K.C., 2015. Compositional and temperature effects of phosphoric acid fractionation on Δ_{47} analysis and implications for discrepant calibrations. Chemical Geology 396, 51-60.

Dennis, K.J., Affek, H.P., Passey, B.H., Schrag, D.P., Eiler, J.M., 2011. Defining an absolute reference frame for 'clumped' isotope studies of CO_2. Geochimica et Cosmochimica Acta 75, 7117-7131.

Dennis, K.J., Schrag, D.P., 2010. Clumped isotope thermometry of carbonatites as an indicator of diagenetic alteration. Geochimica Et Cosmochimica Acta 74, 4110-4122.

Dux, F.W., 2015. Applications of clumped-isotope palaeothermometry, School of Earth and Environmental Sciences. University of Wollongong.

Falster, G., Delean, S., Tyler, J., 2018. Hydrogen Peroxide Treatment of Natural Lake Sediment Prior to Carbon and Oxygen Stable Isotope Analysis of Calcium Carbonate. Geochemistry, Geophysics, Geosystems 19, 3583-3595.

Ghosh, P., Adkins, J., Affek, H., Balta, B., Guo, W., Schauble, E.A., Schrag, D., Eiler, J.M., 2006. ^{13}C–^{18}O bonds in carbonate minerals: A new kind of paleothermometer. Geochimica et Cosmochimica Acta 70, 1439-1456.

Goodfriend, G.A., 1990. Rainfall in the Negev Desert during the middle Holocene, based on ^{13}C of organic matter in land snail shells. Quaternary Research 34, 186-197.

Huntington, K.W., Eiler, J.M., Affek, H.P., Guo, W., Bonifacie, M., Yeung, L.Y., Thiagarajan, N., Passey, B., Tripati, A., Daëron, M., Came, R., 2009. Methods and limitations of 'clumped' CO2 isotope (Δ_{47}) analysis by gas-source isotope ratio mass spectrometry. Journal of Mass Spectrometry 44, 1318-1329.

Kim, S.T., O'Neil, J.R., Hillaire-Marcel, C., Mucci, A., 2007. Oxygen isotope fractionation between synthetic aragonite and water: Influence of temperature and Mg^{2+} concentration. Geochimica Et Cosmochimica Acta 71, 4704-4715.

Kluge, T., John, C.M., Jourdan, A.-L., Davis, S., Crawshaw, J., 2015. Laboratory calibration of the calcium carbonate clumped isotope thermometer in the 25–250°C temperature range. Geochimica et Cosmochimica Acta 157, 213-227.

McCrea, J.M., 1950. On the Isotopic Chemistry of Carbonates and a Paleotemperature Scale. The Journal of Chemical Physics 18, 849-857.

Meckler, A.N., Ziegler, M., Millán, M.I., Breitenbach, S.F.M., Bernasconi, S.M., 2014. Long-term performance of the Kiel carbonate device with a new correction scheme for clumped isotope measurements. Rapid Communications in Mass Spectrometry 28, 1705-1715.

Murray, S.T., Arienzo, M.M., Swart, P.K., 2016. Determining the Δ_{47} acid fractionation in dolomites. Geochimica et Cosmochimica Acta 174, 42-53.

Spötl, C., Vennemann, T.W., 2003. Continuous-flow isotope ratio mass spectrometric analysis of carbonate minerals. Rapid Communications in Mass Spectrometry 17, 1004-1006.

Appendix Two: data tables

This appendix comprises three tables. The first table contains all experimental data obtained for Chapter Two. The second table contains a summary of stable isotope and organic geochemical data obtained for Chapter Three. The third table contains all stable isotope data acquired for Chapter Four, and also used in Chapter Five.

1 Table A1

Table A1. Summary of experimental data obtained for Chapter Two. The volume of carbonate measured in each sample was calculated from CO_2 peak heights returned by the CF-IRMS. An entry of 'insufficient signal' indicates that the returned peaks were too small to determine isotope ratios and/or carbonate volumes. NT = no treatment.

Temperature	H_2O_2 pH	Standard	% carbonate		Weight before	Weight after	$\delta^{18}O$		$\delta^{13}C$		CO_2	% carbonate
°C			planned	actual	mg	mg	‰ VPDB	error (1σ)	‰ VPDB	error (1σ)	%	after treatment
4	alkaline	P3	1	1.4	98.3	41.3	-3.4	0.2	-1.0	0.1	0.6	1.2
4	alkaline	P3	1	1.7	101.8	21.5	-1.5	0.2	1.5	0.1	2.7	5.5
4	alkaline	P3	1	0.9	100.0	54.8	-4.0	0.1	-3.2	0.1	0.3	0.6
4	alkaline	P3	1	1.0	98.0	17.6	-1.8	0.2	0.0	0.1	0.7	1.4
4	acidic	P3	1	0.9	98.9	75.0	-12.9	0.3	-24.9	0.2	0.1	0.2
4	acidic	P3	1	1.8	102.5	84.9	-7.1	0.1	-9.6	0.1	0.2	0.5
4	acidic	P3	1	1.3	103.0	81.5	-14.1	0.1	-25.3	0.1	0.2	0.4
4	acidic	P3	1	1.3	100.5	77.0	-14.1	0.1	-25.1	0.1	0.2	0.3
4	alkaline	M2	1	0.9	99.9	27.3	-8.1	0.2	0.7	0.1	0.9	1.7
4	alkaline	M2	1	1.1	99.3	31.8	-7.9	0.2	1.4	0.2	1.2	2.4
4	alkaline	M2	1	1.2	98.8	53.9	-9.2	0.2	-2.5	0.1	0.5	0.9
4	alkaline	M2	1	1.4	101.7	19.5	-7.9	0.1	2.1	0.1	2.6	5.2
4	acidic	M2	1	1.6	101.8	80.0	-14.0	0.2	-25.0	0.3	0.2	0.4
4	acidic	M2	1	1.2	99.3	78.9	-14.0	0.1	-24.9	0.1	0.2	0.4
4	acidic	M2	1	1.8	99.6	77.5	-13.3	0.0	-25.5	0.1	0.2	0.5
4	acidic	M2	1	1.1	99.4	79.0	-13.5	0.1	-25.4	0.1	0.3	0.5
4	alkaline	P3	3	2.8	33.3	2.9	-0.5	0.3	2.2	0.1	13.7	27.5
4	alkaline	P3	3	3.6	36.0	6.6	-0.9	0.2	2.0	0.1	9.2	18.3
4	alkaline	P3	3	3.1	32.9	3.6	-0.5	0.3	2.1	0.1	12.6	25.3
4	alkaline	P3	3	3.4	34.6	2.3	-0.3	0.3	1.8	0.1	5.0	9.9
4	acidic	P3	3	2.6	32.7	23.2	-6.3	0.2	-7.1	0.1	0.6	1.1
4	acidic	P3	3	3.0	31.9	23.1	-5.3	0.2	-5.9	0.1	0.7	1.3
4	acidic	P3	3	3.7	32.2	25.1	-3.6	0.3	-2.8	0.1	0.9	1.7
4	acidic	P3	3	4.1	32.5	24.2	-2.7	0.2	-1.0	0.1	1.4	2.8
4	alkaline	M2	3	4.2	34.6	4.0	-7.4	0.2	2.7	0.1	13.9	27.9
4	alkaline	M2	3	3.6	31.4	2.8	-7.5	0.1	2.8	0.1	15.5	31.0
4	alkaline	M2	3	3.4	33.9	3.0	-7.4	0.2	2.8	0.2	18.6	37.2
4	alkaline	M2	3	4.3	35.2	3.7	-7.5	0.2	2.7	0.2	15.8	31.5
4	acidic	M2	3	3.9	33.0	24.6	-10.4	0.2	-8.4	0.2	0.5	0.9
4	acidic	M2	3	4.8	34.3	26.1	-8.5	0.1	-0.4	0.1	1.6	3.1
4	acidic	M2	3	2.8	34.6	24.5	-9.8	0.2	-5.8	0.1	0.7	1.4
4	acidic	M2	3	4.3	32.6	23.5	-9.5	0.2	-5.3	0.1	0.7	1.5
4	alkaline	P3	5	5.1	18.8	9.5	-2.2	0.3	1.7	0.1	5.2	10.4
4	alkaline	P3	5	5.9	19.4	3.7	-0.8	0.3	2.1	0.1	12.5	25.1
4	alkaline	P3	5	7.5	22.0	4.2	-0.8	0.3	2.1	0.1	15.9	31.8
4	alkaline	P3	5	6.1	20.1	1.9	-0.6	0.3	2.1	0.1	16.6	33.3
4	acidic	P3	5	6.5	21.3	15.5	-2.2	0.2	0.4	0.1	3.1	6.2
4	acidic	P3	5	6.2	19.6	13.2	-2.4	0.2	-0.3	0.1	2.4	4.9
4	acidic	P3	5	4.5	21.6	15.7	-3.0	0.2	-1.5	0.1	1.7	3.3
4	acidic	P3	5	6.3	19.2	13.2	-2.5	0.1	-0.2	0.0	2.2	4.3
4	alkaline	M2	5	9.2	20.5	3.6	-7.7	0.2	2.6	0.1	16.7	33.4
4	alkaline	M2	5	7.2	20.7	2.6	-7.7	0.2	2.7	0.1	22.9	45.9
4	alkaline	M2	5	5.2	21.3	2.5	-7.7	0.1	2.7	0.1	18.0	35.9
4	alkaline	M2	5	3.9	21.3	2.0	-7.5	0.2	2.5	0.1	17.0	34.0
4	acidic	M2	5	6.3	20.4	13.9	-8.5	0.1	0.6	0.1	2.8	5.5
4	acidic	M2	5	5.0	19.2	13.6	-9.0	0.2	-0.5	0.1	1.8	3.7
4	acidic	M2	5	4.8	20.9	14.5	-9.0	0.2	-0.9	0.2	1.9	3.8
4	acidic	M2	5	4.8	21.0	6.5	-12.6	0.2	-7.3	0.2	0.7	1.5
4	alkaline	P3	100	100	1.4	1.3	-0.3	0.3	2.2	0.1	43.4	86.8
4	alkaline	P3	100	100	1.3	1.0	-0.5	0.3	2.2	0.1	47.0	94.0
4	alkaline	P3	100	100	1.0	0.8	-0.4	0.3	2.2	0.1	47.0	93.9
4	alkaline	P3	100	100	1.0	0.9	-0.4	0.2	2.1	0.1	45.5	91.0
4	acidic	P3	100	100	1.2	1.0	-0.5	0.2	2.2	0.1	46.4	92.7
4	acidic	P3	100	100	1.2	1.1	-0.3	0.3	2.3	0.2	44.9	89.9
4	acidic	P3	100	100	1.2	0.8	-0.5	0.3	2.2	0.1	47.2	94.3
4	acidic	P3	100	100	1.2	0.8	-0.5	0.3	2.2	0.2	47.4	94.7
4	alkaline	M2	100	100	1.2	0.9	-7.4	0.2	2.7	0.1	47.4	94.9
4	alkaline	M2	100	100	0.9	0.6	-7.3	0.2	2.7	0.1	46.5	93.1
4	alkaline	M2	100	100	1.3	0.9	-7.5	0.2	2.8	0.1	47.3	94.6
4	alkaline	M2	100	100	1.2	0.9	-7.5	0.1	2.9	0.1	43.0	85.9
4	acidic	M2	100	100	1.6	1.0	-7.4	0.2	2.9	0.1	46.3	92.6
4	acidic	M2	100	100	1.0	0.5	-7.2	0.2	3.1	0.1	49.9	99.8
4	acidic	M2	100	100	1.0	0.6	-7.3	0.2	2.9	0.2	47.2	94.4
4	acidic	M2	100	100	1.1	0.8	-7.4	0.2	2.9	0.1	46.2	92.4
4	alkaline	none	0	0	97.3	20.3	-15.2	0.1	-21.3	1.8	0.1	0.2
4	alkaline	none	0	0	96.8	26.8	-16.2	0.6	-23.8	0.1	0.1	0.2
4	alkaline	none	0	0	108.4	48.2	-14.6	0.3	-24.4	0.1	0.1	0.2
4	alkaline	none	0	0	96.0	11.7	-18.5	0.6	-24.2	0.1	0.1	0.2
4	acidic	none	0	0	101.0	78.9	-13.4	0.1	-24.2	0.2	0.2	0.3
4	acidic	none	0	0	99.6	80.6	-12.6	0.1	-24.6	0.2	0.2	0.4
4	acidic	none	0	0	96.7	78.8	-12.9	0.2	-24.4	0.2	0.2	0.3
4	acidic	none	0	0	93.8	75.4	-13.0	0.1	-24.5	0.3	0.2	0.3
25	alkaline	P3	1	1.0	98.6	32.3	-2.4	0.1	0.6	0.1	1.0	2.0
25	alkaline	P3	1	1.3	100.2	27.6	-1.9	0.1	1.1	0.1	1.7	3.4
25	alkaline	P3	1	1.0	98.7	22.1	-1.6	0.1	1.4	0.2	1.7	3.4
25	alkaline	P3	1	1.0	99.1	13.5	-3.2	0.1	-0.8	0.1	0.7	1.5
25	acidic	P3	1	1.2	99.3	68.8	-7.2	0.1	-11.3	0.1	0.3	0.5

Table A1 contd.

Temperature	H_2O_2 pH	Standard	% carbonate		Weight before	Weight after	$\delta^{18}O$		$\delta^{13}C$		CO_2	% carbonate
°C			planned	actual	mg	mg	‰ VPDB	error (1σ)	‰ VPDB	error (1σ)	%	after treatment
25	acidic	P3	1	0.9	100.5	70.1	-10.8	0.0	-18.3	0.1	0.2	0.4
25	acidic	P3	1	1.2	100.6	74.1	-10.2	0.1	-17.3	0.1	0.2	0.3
25	acidic	P3	1	0.8	101.3	71.6	-10.5	0.2	-17.9	0.1	0.2	0.4
25	alkaline	M2	1	1.0	99.9	16.8	-8.4	0.1	1.6	0.1	1.5	2.9
25	alkaline	M2	1	1.1	99.8	17.3	-8.5	0.1	1.7	0.1	2.1	4.2
25	alkaline	M2	1	1.0	99.6	25.9	-8.8	0.1	1.1	0.1	1.4	2.8
25	alkaline	M2	1	1.0	99.9	30.4	-8.6	0.1	1.0	0.1	1.2	2.3
25	acidic	M2	1	1.3	99.9	73.6	-13.4	0.2	-22.5	0.1	0.2	0.3
25	acidic	M2	1	1.4	100.9	73.8	-12.8	0.1	-19.0	0.1	0.3	0.5
25	acidic	M2	1	1.1	100.3	73.1	-13.5	0.1	-23.5	0.1	0.2	0.3
25	acidic	M2	1	0.8	99.1	71.4	-13.6	0.1	-25.9	0.2	0.1	0.3
25	alkaline	P3	3	3.3	33.6	8.8	-1.8	0.1	1.3	0.1	5.3	10.6
25	alkaline	P3	3	2.7	33.5	7.7	-2.1	0.1	1.2	0.2	4.9	9.7
25	alkaline	P3	3	1.0	33.1	8.5	-2.3	0.1	1.3	0.1	5.9	11.7
25	alkaline	P3	3	3.0	32.0	4.1	-1.3	0.1	1.5	0.2	6.9	13.8
25	acidic	P3	3	2.9	31.8	21.3	-4.5	0.2	-3.1	0.1	1.0	2.0
25	acidic	P3	3	3.6	33.8	22.7	-3.8	0.1	-1.8	0.1	1.3	2.7
25	acidic	P3	3	3.2	32.7	22.4	-4.1	0.1	-2.5	0.1	1.1	2.2
25	acidic	P3	3	4.3	32.8	22.9	-1.9	0.0	1.0	0.0	3.9	7.9
25	alkaline	M2	3	3.4	33.2	8.3	-8.5	0.1	2.2	0.1	5.8	11.5
25	alkaline	M2	3	2.7	32.3	6.8	-8.4	0.1	2.3	0.2	5.4	10.9
25	alkaline	M2	3	2.6	33.1	5.8	-8.4	0.1	2.3	0.1	5.2	10.4
25	alkaline	M2	3	2.8	32.8	4.7	-8.6	0.1	2.2	0.1	4.9	9.9
25	acidic	M2	3	4.1	33.7	23.5	-9.2	0.1	-0.7	0.1	1.4	2.8
25	acidic	M2	3	2.2	33.0	21.1	-10.3	0.2	-4.8	0.1	0.7	1.4
25	acidic	M2	3	3.7	33.5	22.8	-9.4	0.1	-1.4	0.1	1.2	2.5
25	acidic	M2	3	2.8	34.3	22.0	-10.2	0.1	-3.2	0.1	0.9	1.7
25	alkaline	P3	5	4.6	20.8	4.1	-1.2	0.1	1.9	0.1	10.4	20.8
25	alkaline	P3	5	4.4	21.0	4.3	-1.3	0.0	1.8	0.1	8.9	17.9
25	alkaline	P3	5	5.4	20.3	4.7	-1.5	0.1	2.0	0.1	11.3	22.6
25	alkaline	P3	5	6.5	21.4	2.1	-1.0	0.1	2.0	0.2	14.8	29.7
25	acidic	P3	5	3.7	21.1	13.2	-3.4	0.1	-0.9	0.1	1.6	3.1
25	acidic	P3	5	5.1	21.4	12.1	-2.6	0.1	0.4	0.1	2.6	5.2
25	acidic	P3	5	5.6	21.1	11.5	-2.0	0.1	0.9	0.2	2.8	5.7
25	acidic	P3	5	6.2	20.5	12.7	-2.1	0.1	0.8	0.1	3.2	6.3
25	alkaline	M2	5	5.5	20.8	3.3	-8.1	0.1	2.6	0.1	13.7	27.4
25	alkaline	M2	5	4.0	20.4	3.3	-8.2	0.1	2.5	0.1	11.5	22.9
25	alkaline	M2	5	6.0	19.2	2.9	-7.9	0.1	2.6	0.2	15.3	30.6
25	alkaline	M2	5	4.2	20.5	3.4	-8.1	0.1	2.6	0.2	11.1	22.2
25	acidic	M2	5	6.8	24.9	16.1	-8.7	0.1	1.1	0.2	2.8	5.6
25	acidic	M2	5	4.7	19.5	11.3	-9.3	0.1	0.2	0.1	1.6	3.2
25	acidic	M2	5	4.0	21.8	13.1	-9.5	0.2	-0.2	0.2	1.6	3.2
25	acidic	M2	5	4.5	20.5	8.5	-9.3	0.2	0.6	0.2	2.2	4.4
25	alkaline	P3	100	100	1.5	1.3	-0.5	0.1	2.2	0.2	44.2	88.3
25	alkaline	P3	100	100	1.1	1.0	-0.5	0.1	2.2	0.1	45.7	91.4
25	alkaline	P3	100	100	1.1	1.0	-0.3	0.1	2.2	0.1	43.9	87.8
25	alkaline	P3	100	100	1.0	0.8	0.0	0.0	2.4	0.2	37.1	74.1
25	acidic	P3	100	100	1.2	1.1	-0.3	0.1	2.2	0.1	46.4	92.8
25	acidic	P3	100	100	1.1	0.9	-0.3	0.1	2.2	0.1	49.1	98.1
25	acidic	P3	100	100	1.2	1.1	-0.2	0.1	2.3	0.1	42.7	85.4
25	acidic	P3	100	100	1.0	0.7	-0.1	0.1	2.3	0.1	49.5	99.1
25	alkaline	M2	100	100	1.2	1.2	-7.5	0.1	2.9	0.1	44.2	88.3
25	alkaline	M2	100	100	1.3	1.3	-7.7	0.1	2.9	0.1	47.7	95.4
25	alkaline	M2	100	100	1.1	1.0	-7.6	0.1	2.7	0.1	43.7	87.4
25	alkaline	M2	100	100	1.1	1.3	-7.6	0.1	2.8	0.1	39.2	78.4
25	acidic	M2	100	100	0.9	0.6	-7.6	0.1	2.7	0.1	47.7	95.3
25	acidic	M2	100	100	0.9	0.8	-7.6	0.0	2.7	0.1	44.6	89.2
25	acidic	M2	100	100	1.2	0.8	-7.5	0.1	2.7	0.1	44.3	88.6
25	acidic	M2	100	100	1.1	1.0	-7.5	0.0	2.8	0.1	41.5	83.0
25	alkaline	none	0	0	103.5	51.4	-14.8	0.4	-23.9	2.1	0.0	0.1
25	alkaline	none	0	0	100.8	51.2	-14.4	0.2	-26.3	1.5	0.0	0.1
25	alkaline	none	0	0	94.9	39.0	-12.7	4.5	-22.5	7.5	0.0	0.1
25	alkaline	none	0	0	101.0	29.2	-16.4	1.7	-27.1	0.9	0.1	0.1
25	acidic	none	0	0	93.2	69.1	-14.2	0.4	-26.5	0.3	0.1	0.1
25	acidic	none	0	0	95.7	71.3	-16.1	0.3	-27.2	0.1	0.1	0.2
25	acidic	none	0	0	94.2	54.6	-15.3	0.9	-27.0	0.1	0.1	0.1
25	acidic	none	0	0	91.1	66.6	-15.6	0.8	-27.2	0.2	0.1	0.1
50	alkaline	P3	1	1.0	99.7	10.3	-0.6	0.1	2.2	0.1	3.8	7.6
50	alkaline	P3	1	1.0	99.7	9.9	-0.3	0.1	2.3	0.1	3.6	7.1
50	alkaline	P3	1	1.2	99.7	20.3	-0.3	0.1	2.2	0.1	2.4	4.8
50	alkaline	P3	1	0.9	103.2	4.4	0.1	0.0	2.3	0.1	3.5	6.9
50	acidic	P3	1	1.0	99.2	36.1	-11.4	2.4	-24.1	1.6	0.0	0.0
50	acidic	P3	1	0.9	100.7	40.1	-10.8	2.4	-26.2	3.1	0.0	0.0
50	acidic	P3	1	0.7	97.7	34.6	-10.8	2.8	-26.7	4.8	0.0	0.0
50	acidic	P3	1	1.4	100.1	43.6	-11.3	5.0	-30.6	1.6	0.0	0.0
50	alkaline	M2	1	0.9	100.0	9.1	-7.1	0.2	2.9	0.1	1.4	2.7
50	alkaline	M2	1	0.9	100.2	14.9	-7.4	0.1	2.8	0.1	1.7	3.3

Table A1 contd.

Temperature	H_2O_2 pH	Standard	% carbonate		Weight before	Weight after	$\delta^{18}O$		$\delta^{13}C$		CO_2	% carbonate
°C			planned	actual	mg	mg	‰ VPDB	error (1σ)	‰ VPDB	error (1σ)	%	after treatment
50	alkaline	M2	1	0.9	98.9	18.7	-7.4	0.0	2.9	0.1	1.6	3.2
50	alkaline	M2	1	1.5	99.8	17.4	-7.5	0.1	2.9	0.1	3.2	6.3
50	acidic	M2	1	1.2	98.9	44.0	-10.8	2.5	-16.3	1.2	0.0	0.0
50	acidic	M2	1	0.8	99.9	40.4	-14.0	2.6	-24.3	3.0	0.0	0.0
50	acidic	M2	1	0.9	101.2	41.7	-8.0	3.0	-24.2	1.6	0.0	0.0
50	acidic	M2	1	1.1	100.0	30.4	-12.3	1.6	-26.0	4.6	0.0	0.0
50	alkaline	P3	3	3.1	32.4	2.8	-0.2	0.1	2.3	0.1	15.8	31.6
50	alkaline	P3	3	3.8	33.6	3.7	-0.4	0.1	2.3	0.1	15.5	31.0
50	alkaline	P3	3	3.2	32.4	3.8	-0.2	0.2	2.4	0.2	11.2	22.4
50	alkaline	P3	3	2.3	32.5	1.6	-0.2	0.3	2.2	0.0	4.2	8.5
50	acidic	P3	3	3.7	33.9	8.7	-0.5	0.3	1.5	0.1	0.3	0.5
50	acidic	P3	3	3.4	31.3	15.8	-4.2	1.5	-1.7	0.8	0.0	0.1
50	acidic	P3	3	2.6	34.2	9.8	-2.9	1.6	-0.6	1.1	0.1	0.2
50	acidic	P3	3	3.0	32.3	5.2	0.5	1.5	2.4	0.7	0.5	1.0
50	alkaline	M2	3	3.6	32.3	3.6	-7.2	0.1	2.9	0.1	13.7	27.3
50	alkaline	M2	3	3.0	34.0	3.4	-7.3	0.2	2.9	0.1	11.5	22.9
50	alkaline	M2	3	3.5	33.3	4.7	-7.2	0.1	2.9	0.2	10.6	21.2
50	alkaline	M2	3	3.5	33.4	1.1	-7.3	0.2	2.7	0.1	6.6	13.2
50	acidic	M2	3	3.2	33.8	9.3	-7.9	1.4	1.5	1.0	0.2	0.3
50	acidic	M2	3	3.9	32.9	8.5	-6.8	1.4	2.3	0.3	0.3	0.6
50	acidic	M2	3	2.7	33.5	9.2	-9.8	1.3	-0.4	0.6	0.0	0.0
50	acidic	M2	3	3.3	32.3	10.8	-7.1	3.6	-0.3	1.6	0.0	0.0
50	alkaline	P3	5	4.5	19.2	1.9	0.1	0.2	2.4	0.1	16.9	33.8
50	alkaline	P3	5	5.0	21.4	2.1	-0.3	0.2	2.3	0.2	20.5	41.0
50	alkaline	P3	5	5.4	20.0	1.4	-0.2	0.2	2.3	0.1	30.7	61.3
50	alkaline	P3	5	5.5	20.2	1.5	-0.2	0.1	2.3	0.2	41.2	82.4
50	acidic	P3	5	5.4	19.3	3.3	-0.5	0.4	2.0	0.2	1.8	3.7
50	acidic	P3	5	5.0	19.3	5.0	-0.5	0.4	2.1	0.1	0.9	1.8
50	acidic	P3	5	4.4	20.1	6.7	-0.2	0.3	2.5	0.3	0.3	0.6
50	acidic	P3	5	5.3	21.0	6.7	-0.3	0.1	1.9	0.2	0.6	1.2
50	alkaline	M2	5	6.4	20.0	2.6	-7.1	0.1	2.8	0.1	20.5	41.0
50	alkaline	M2	5	5.0	19.2	1.8	-7.3	0.2	2.9	0.1	20.5	41.0
50	alkaline	M2	5	4.1	21.0	2.1	-7.4	0.2	2.8	0.1	15.4	30.7
50	alkaline	M2	5	5.6	20.3	2.8	-7.3	0.2	2.8	0.2	16.7	33.3
50	acidic	M2	5	4.7	20.3	6.4	-8.4	0.1	2.2	0.4	0.3	0.6
50	acidic	M2	5	4.9	21.2	6.5	-7.9	0.1	2.0	0.2	0.2	0.5
50	acidic	M2	5	4.4	20.4	5.6	-6.8	4.1	3.0	1.6	0.1	0.1
50	acidic	M2	5	6.2	19.6	2.8	-7.4	0.8	2.9	0.3	1.5	2.9
50	alkaline	P3	100	100	1.3	1.0	0.2	0.4	2.3	0.3	39.3	78.5
50	alkaline	P3	100	100	1.0	0.8	-0.1	0.4	2.2	0.2	37.1	74.3
50	alkaline	P3	100	100	1.4	0.9	0.4	0.3	2.2	0.2	35.6	71.1
50	alkaline	P3	100	100	1.1	0.7	-0.2	0.2	1.9	0.0	44.4	88.8
50	acidic	P3	100	100	1.1	0.8	-0.8	0.2	2.0	0.0	46.6	93.2
50	acidic	P3	100	100	1.2	0.6	-0.4	0.3	2.2	0.1	46.8	93.6
50	acidic	P3	100	100	1.1	0.8	-0.9	0.2	2.0	0.0	45.3	90.6
50	acidic	P3	100	100	0.7	0.1	-0.5	0.3	2.9	0.2	52.1	104.3
50	alkaline	M2	100	100	0.9	0.6	-7.5	0.2	2.7	0.1	48.7	97.3
50	alkaline	M2	100	100	1.1	1.0	-7.8	0.2	2.8	0.2	43.7	87.5
50	alkaline	M2	100	100	1.2	1.1	-8.0	0.1	2.7	0.2	45.1	90.2
50	alkaline	M2	100	100	0.9	0.6	-7.6	0.2	2.7	0.1	45.8	91.5
50	acidic	M2	100	100	1.2	0.7	-8.1	0.2	2.7	0.0	48.1	96.3
50	acidic	M2	100	100	1.2	0.4	-7.3	0.2	2.9	0.1	49.6	99.1
50	acidic	M2	100	100	0.8	0.4	-7.1	0.2	3.0	0.1	50.4	100.7
50	acidic	M2	100	100	1.2	0.6	-7.6	0.2	2.8	0.1	48.2	96.5
50	alkaline	none	0	0	99.5	4.3	-17.0	0.0	-18.6	2.8	0.2	0.4
50	alkaline	none	0	0	91.3	12.0	insufficient signal					
50	alkaline	none	0	0	86.0	11.2	-16.9	0.1	-24.9	2.3	0.1	0.2
50	alkaline	none	0	0	96.9	2.4	-17.0	0.0	-21.3	0.9	0.3	0.6
50	acidic	none	0	0	95.9	23.5	-14.1	0.6	-30.5	0.1	0.1	0.2
50	acidic	none	0	0	97.8	31.1	insufficient signal					
50	acidic	none	0	0	100.1	17.1	insufficient signal					
50	acidic	none	0	0	93.6	30.8	-21.4	2.3	-30.6	0.2	0.1	0.2
75	alkaline	P3	1	1.1	99.8	26.7	-9.3	0.1	0.9	0.2	1.5	3.1
75	alkaline	P3	1	1.2	99.2	23.4	insufficient signal					
75	alkaline	P3	1	0.9	99.9	22.3	-9.1	0.2	1.0	0.1	1.5	3.0
75	alkaline	P3	1	1.0	101.7	9.6	insufficient signal					
75	acidic	P3	1	0.8	99.5	50.7	-17.3	0.2	-19.9	0.5	0.1	0.1
75	acidic	P3	1	1.0	99.8	54.8	-16.2	0.1	-18.8	0.2	0.1	0.1
75	acidic	P3	1	0.8	99.4	53.7	-18.2	0.7	-19.2	0.8	0.1	0.1
75	acidic	P3	1	1.0	100.8	51.7	-17.6	0.3	-21.4	0.1	0.1	0.1
75	alkaline	M2	1	0.9	102.2	16.3	-10.7	0.1	1.6	0.0	1.6	3.3
75	alkaline	M2	1	1.2	103.2	22.1	-12.3	0.1	1.9	0.1	2.2	4.4
75	alkaline	M2	1	1.0	100.0	20.9	-12.2	0.1	1.9	0.1	1.7	3.3
75	alkaline	M2	1	1.2	100.8	23.4	-12.4	0.1	2.0	0.1	1.9	3.9
75	acidic	M2	1	1.1	101.2	56.7	-15.8	0.2	-12.3	0.3	0.1	0.2
75	acidic	M2	1	0.9	99.5	50.4	-18.1	0.4	-19.3	0.2	0.1	0.1
75	acidic	M2	1	0.9	99.0	53.5	-18.5	0.1	-23.1	0.2	0.1	0.1

Table A1 contd.

Temperature	H_2O_2 pH	Standard	% carbonate		Weight before	Weight after	$\delta^{18}O$		$\delta^{13}C$		CO_2	% carbonate
°C			planned	actual	mg	mg	‰ VPDB	error (1σ)	‰ VPDB	error (1σ)	%	after treatment
75	acidic	M2	1	1.0	99.9	56.1	-17.9	0.4	-20.0	0.1	0.1	0.1
75	alkaline	P3	3	2.6	34.0	5.2	-3.4	0.2	2.1	0.1	7.9	15.8
75	alkaline	P3	3	3.0	33.2	4.3	-3.1	0.2	2.1	0.1	11.0	21.9
75	alkaline	P3	3	3.1	32.4	4.3	-3.3	0.1	2.0	0.2	10.6	21.1
75	alkaline	P3	3	3.0	33.4	1.5	-30.4	1.9	-2.5	1.0	1.5	3.0
75	acidic	P3	3	3.2	32.6	17.2	-4.7	0.1	0.3	0.0	0.9	1.8
75	acidic	P3	3	3.4	34.3	18.5	-4.8	0.1	0.1	0.1	1.0	1.9
75	acidic	P3	3	2.8	32.0	16.5	-5.5	0.2	-0.1	0.0	0.7	1.4
75	acidic	P3	3	3.1	32.8	18.4	-5.5	0.2	-0.1	0.1	0.8	1.6
75	alkaline	M2	3	2.7	32.7	3.5	-10.1	0.2	2.6	0.1	10.0	20.1
75	alkaline	M2	3	2.9	32.9	3.1	-9.8	0.2	2.6	0.1	11.3	22.6
75	alkaline	M2	3	3.8	33.1	4.9	-10.0	0.1	2.8	0.0	11.8	23.6
75	alkaline	M2	3	2.7	34.1	1.6	-9.4	0.1	2.9	0.2	3.7	7.4
75	acidic	M2	3	3.4	33.5	19.0	-11.3	0.1	-0.1	0.0	0.6	1.2
75	acidic	M2	3	3.1	33.7	19.6	-10.4	0.2	0.1	0.0	0.6	1.2
75	acidic	M2	3	2.7	32.6	18.3	-10.7	0.4	-0.2	0.1	0.3	0.7
75	acidic	M2	3	2.7	32.5	17.4	-10.4	0.2	0.5	0.1	0.7	1.4
75	alkaline	P3	5	4.7	20.0	1.2	-1.6	0.2	2.2	0.2	38.3	76.5
75	alkaline	P3	5	5.3	20.2	2.1	-1.6	0.3	2.2	0.1	20.3	40.6
75	alkaline	P3	5	5.2	20.3	2.1	-2.3	0.2	2.2	0.1	21.6	43.1
75	alkaline	P3	5	7.3	19.9	1.1	-2.3	0.1	2.2	0.0	27.9	55.7
75	acidic	P3	5	5.0	20.0	10.6	-2.7	0.2	1.4	0.1	1.7	3.4
75	acidic	P3	5	5.5	20.1	10.6	-2.9	0.1	1.5	0.0	1.7	3.4
75	acidic	P3	5	4.3	19.3	10.0	-2.0	0.2	1.7	0.1	1.5	2.9
75	acidic	P3	5	6.0	19.2	10.3	-3.2	0.2	1.6	0.1	2.1	4.2
75	alkaline	M2	5	5.4	19.9	2.0	-7.6	0.1	2.9	0.1	26.1	52.2
75	alkaline	M2	5	4.7	19.3	1.4	-7.6	0.1	2.9	0.2	31.2	62.4
75	alkaline	M2	5	4.4	19.4	2.0	-7.4	0.1	2.7	0.0	18.0	35.9
75	alkaline	M2	5	5.3	20.5	2.1	-7.3	0.1	2.8	0.1	25.2	50.3
75	acidic	M2	5	5.5	19.8	10.3	-9.1	0.0	2.7	0.1	1.8	3.7
75	acidic	M2	5	5.1	20.0	11.2	-8.4	0.0	2.8	0.0	1.6	3.3
75	acidic	M2	5	5.0	20.0	10.6	-8.8	0.0	2.8	0.0	1.5	3.1
75	acidic	M2	5	5.1	21.3	2.7	-8.7	0.0	2.9	0.1	2.3	4.6
75	alkaline	P3	100	100	1.1	1.0	-0.3	0.1	2.1	0.0	46.8	93.6
75	alkaline	P3	100	100	1.4	1.1	-0.3	0.1	2.1	0.0	46.6	93.2
75	alkaline	P3	100	100	0.9	0.6	-0.3	0.1	2.1	0.1	47.5	95.0
75	alkaline	P3	100	100	0.8	0.4	-0.4	0.1	2.2	0.1	42.8	85.6
75	acidic	P3	100	100	0.9	0.5	-0.2	0.1	2.2	0.1	44.8	89.5
75	acidic	P3	100	100	0.8	0.5	-0.4	0.1	2.2	0.0	50.1	100.2
75	acidic	P3	100	100	1.2	0.8	-0.4	0.1	2.2	0.1	45.5	90.9
75	acidic	P3	100	100	1.1	0.2	-0.3	0.1	2.4	0.0	38.8	77.6
75	alkaline	M2	100	100	1.1	0.9	-7.4	0.1	2.8	0.1	45.9	91.9
75	alkaline	M2	100	100	0.9	0.8	-7.5	0.1	2.7	0.1	48.1	96.2
75	alkaline	M2	100	100	1.0	0.8	-7.4	0.1	2.7	0.0	48.7	97.4
75	alkaline	M2	100	100	1.0	0.7	-7.4	0.1	2.8	0.0	56.6	113.2
75	acidic	M2	100	100	1.1	0.4	-7.3	0.1	2.7	0.0	50.0	99.9
75	acidic	M2	100	100	0.9	0.3	-7.3	0.1	2.9	0.0	47.9	95.8
75	acidic	M2	100	100	0.7	0.4	-7.4	0.0	2.8	0.0	45.2	90.3
75	acidic	M2	100	100	1.0	0.5	-7.4	0.1	2.9	0.0	47.9	95.8
75	alkaline	none	0	0	100.4	22.0	-11.7	0.3	-10.7	0.1	insufficient signal	
75	alkaline	none	0	0	89.3	16.7	insufficient signal					
75	alkaline	none	0	0	95.3	21.5	insufficient signal					
75	alkaline	none	0	0	96.0	14.9	-11.6	0.2	-15.1	insufficient signal		
75	acidic	none	0	0	86.0	34.3	-12.0	0.3	-12.2	insufficient signal		
75	acidic	none	0	0	83.6	32.3	-11.8	0.2	-13.4	insufficient signal		
75	acidic	none	0	0	91.6	38.0	-11.9	0.2	-13.6	insufficient signal		
75	acidic	none	0	0	97.7	34.8	-11.8	0.3	-14.3	insufficient signal		
NT	NT	P3	1	1.2	100.7	102.1	-5.8	0.1	-5.5	0.0	0.4	0.9
NT	NT	P3	1	0.9	99.6	100.5	-7.7	0.1	-8.6	0.1	0.4	0.7
NT	NT	P3	1	0.9	100.4	101.7	-7.6	0.1	-8.1	0.1	0.4	0.8
NT	NT	P3	1	1.1	100.7	67.3	-5.6	0.1	-3.9	0.0	0.5	1.1
NT	NT	P3	3	2.8	32.3	31.9	-3.5	0.1	-0.7	0.0	1.2	2.4
NT	NT	P3	3	3.3	32.9	32.4	-4.1	0.1	-0.2	0.1	1.6	3.1
NT	NT	P3	3	3.3	33.5	32.9	-3.4	0.1	-0.1	0.0	1.5	2.9
NT	NT	P3	3	3.6	34.2	33.2	-3.0	0.1	-0.1	0.1	1.4	2.9
NT	NT	P3	5	6.4	19.8	18.5	-2.0	0.1	1.0	0.1	3.2	6.4
NT	NT	P3	5	5.8	20.0	19.2	-1.9	0.1	1.0	0.0	2.9	5.9
NT	NT	P3	5	4.7	20.0	19.7	-2.3	0.1	0.6	0.1	2.4	4.9
NT	NT	P3	5	4.7	19.6	18.7	-2.3	0.1	0.5	0.0	2.3	4.6
NT	NT	M2	1	1.0	99.4	100.1	-10.0	0.1	-6.9	0.0	0.3	0.7
NT	NT	M2	1	0.8	100.4	100.8	-10.4	0.1	-7.9	0.0	0.4	0.7
NT	NT	M2	1	1.0	100.3	101.2	-10.0	0.1	-6.0	0.0	0.5	0.9
NT	NT	M2	1	1.1	101.3	101.9	-10.1	0.1	-6.0	0.0	0.4	0.8
NT	NT	M2	3	2.8	33.8	32.9	-8.7	0.1	0.5	0.1	1.5	2.9
NT	NT	M2	3	3.1	33.0	32.5	-9.0	0.1	0.1	0.0	1.6	3.2
NT	NT	M2	3	3.8	32.5	32.0	-8.8	0.1	0.3	0.0	1.7	3.4
NT	NT	M2	3	2.9	32.8	15.8	-8.7	0.1	0.3	0.0	1.8	3.7

Table A1 contd.

Temperature	H_2O_2 pH	Standard	% carbonate		Weight before	Weight after	$\delta^{18}O$		$\delta^{13}C$		CO_2	% carbonate
°C			planned	actual	mg	mg	‰ VPDB	error (1σ)	‰ VPDB	error (1σ)	%	after treatment
NT	NT	M2	5	5.5	19.7	18.7	-8.4	0.1	1.3	0.0	2.8	5.5
NT	NT	M2	5	5.9	19.7	18.7	-8.4	0.1	1.3	0.0	2.7	5.3
NT	NT	M2	5	6.2	20.2	18.8	-8.5	0.1	1.3	0.0	2.9	5.7
NT	NT	M2	5	3.9	19.6	18.2	-8.4	0.1	1.1	0.1	2.3	4.6
NT	NT	none	0	0	103.3	103.3	-13.7	0.1	-21.4	0.3	0.2	0.4
NT	NT	none	0	0	95.3	95.3	-13.6	0.1	-21.7	0.2	0.2	0.4
NT	NT	none	0	0	99.1	99.1	-13.6	0.1	-21.6	0.1	0.2	0.4
NT	NT	none	0	0	96.6	96.6	-13.5	0.1	-21.7	0.1	0.2	0.4
NT	NT	P3	100	100	1.1	1.1	-0.3	0.2	2.2	0.0	42.2	84.5
NT	NT	P3	100	100	1.3	1.3	-0.4	0.2	2.2	0.0	42.8	85.7
NT	NT	P3	100	100	1.3	1.3	-0.3	0.1	2.2	0.0	42.6	85.2
NT	NT	P3	100	100	1.0	1.0	-0.3	0.2	2.2	0.0	41.6	83.2
NT	NT	M2	100	100	1.2	1.2	-7.2	0.2	2.8	0.0	42.9	85.8
NT	NT	M2	100	100	0.8	0.8	-7.2	0.1	2.8	0.0	42.9	85.7
NT	NT	M2	100	100	1.2	1.2	-7.3	0.1	2.8	0.0	42.2	84.3
NT	NT	M2	100	100	0.9	0.9	-7.3	0.1	2.8	0.0	44.8	89.5

2 Table A2

Table A2. Stable isotope and organic geochemical data for Lake Surprise core LS04.

Depth	Age	$\delta^{13}C$	C	$\delta^{15}N$	N	C:N
cm	cal. years BP	‰ VPDB	%	‰	%	
926.45	8479	-30.66	33.80	3.06	2.39	16.52
935.05	8546	-30.72	31.40			
937.85	8568	-31.03	25.88			
945.00	8621	-31.43	29.80	2.63	2.22	15.70
950.45	8658	-31.05	23.72			
955.05	8695	-30.64	37.00			
959.60	8732	-31.75	25.73			
965.15	8769	-30.22	31.30	3.46	2.13	17.14
972.75	8829	-32.05	27.94			
974.30	8836	-30.13	34.00			
979.85	8881	-31.40	32.92			
984.90	8918	-31.24	35.30	3.05	2.46	16.75
990.40	8955	-30.95	27.09			
994.80	8992	-29.80	34.70			
997.10	9007	-31.25	30.55			
1005.15	9242	-31.78	47.30	3.07	2.71	20.34
1011.15	9497	-32.03	37.12			
1015.20	9666	-32.39	41.80			
1020.25	9879	-32.07	31.71			
1029.45	10261	-31.29	29.70	3.06	1.97	17.64
1031.90	10388	-33.16	34.31			
1040.00	10728	-30.34	42.00			
1043.85	10898	-32.45	34.01			
1049.25	11110	-31.00	39.40	2.78	2.31	19.93
1053.25	11280	-32.52	39.54			
1059.00	11535	-31.78	47.90			
1062.75	11705	-31.90	22.82			
1070.25	12002	-31.26	39.50	3.02	2.49	18.54
1073.85	12172	-31.76	30.14			
1080.20	12427	-31.43	33.10			
1083.90	12597	-31.98	33.70			
1090.20	12851	-30.76	34.60	4.03	2.18	18.52
1093.50	13021	-31.10	27.81			
1100.35	13276	-32.15	30.20			
1105.85	13384	-30.83	26.77			
1110.10	13457	-31.31	29.90	3.06	2.19	15.96
1113.45	13511	-31.57	26.88			
1120.25	13637	-31.87	28.40			
1129.85	13817	-31.24	30.60	3.66	1.95	18.30
1136.70	13944	-31.58	26.72			
1140.10	13998	-31.87	29.40			
1145.55	14106	-32.22	25.99			
1150.25	14178	-31.89	31.80	4.98	1.91	19.41
1153.00	14232	-31.32	27.73			
1159.95	14359	-31.49	24.60			
1165.10	14449	-33.28	26.16			
1169.00	14521	-30.25	32.70	3.49	1.95	19.52
1173.90	14611	-32.24	26.46			

Table A2 contd.

Depth	Age	$\delta^{13}C$	C	$\delta^{15}N$	N	C:N
cm	cal. years BP	‰ VPDB	%	‰	%	
1177.20	14665	-31.00	27.70			
1180.25	14719	-32.06	27.76			
1185.90	14828	-32.42	37.10	4.12	1.87	23.14
1191.45	14918	-34.03	35.93			
1194.90	14990	-32.67	36.20			
1199.95	15080	-32.62	30.37			
1205.00	15202	-32.21	36.70	4.54	2.14	20.05
1210.15	15324	-32.98	28.83			
1216.35	15471	-32.88	33.80			
1221.60	15617	-33.52	31.39			
1230.15	15813	-30.95	29.10	3.40	2.14	15.81
1235.40	15935	-33.00	33.71			
1240.20	16057	-31.35	33.60			
1242.75	16130	-31.16	33.96			
1250.15	16301	-27.33	33.60	3.91	2.65	14.83
1255.80	16447	-25.93	24.22			
1260.05	16545	-31.78	32.30			
1265.20	16667	-32.29	34.69			
1270.10	16789	-30.95	29.10	4.33	1.88	18.04
1275.65	16936	-26.99	25.63			
1280.20	17033	-25.66	29.70			
1285.30	17156	-25.15	25.14			
1292.30	17326	-24.21	20.30	5.04	1.37	17.28
1296.40	17424	-25.49	21.56			
1300.20	17522	-23.44	23.30			
1306.50	17673	-25.15	25.20			
1310.25	17738	-23.87	22.00	4.95	1.52	16.87
1315.10	17847	-21.94	18.28			
1320.05	17955	-21.78	20.50			
1329.30	18150	-26.11	23.00	5.10	1.64	16.40
1336.50	18323	-22.25	18.61			
1339.65	18388	-23.04	27.80			
1345.75	18518	-22.52	23.36			
1349.50	18604	-21.00	18.40	5.48	1.05	20.54
1357.80	18778	-20.60	18.49			
1360.05	18821	-21.29	25.80			
1366.90	18973	-23.47	29.87			
1371.10	19059	-22.40	27.70	5.31	2.04	15.77
1375.50	19167	-21.85	25.27			
1380.15	19254	-21.61	25.70			
1387.25	19406	-21.88	18.50			
1391.80	19514	-21.18	20.00	5.41	1.28	18.32
1395.85	19600	-21.74	15.40			
1399.45	19665	-22.91	17.10			
1402.00	19724	-23.00	20.93			
1407.60	19834	-22.99	23.50	4.84	1.64	16.73
1413.60	19938	-22.62	22.66			
1420.10	20055	-24.07	27.50			

Table A2 contd.

Depth	Age	$\delta^{13}C$	C	$\delta^{15}N$	N	C:N
cm	cal. years BP	‰ VPDB	%	‰	%	
1429.75	20240	-23.93	24.20	4.55	1.67	16.91
1436.75	20368	-21.89	26.80			
1442.10	20460	-21.60	29.20			
1445.60	20534	-22.62	25.61			
1448.60	20589	-22.65	24.40	4.83	1.56	18.28
1459.85	20792	-23.52	22.20			
1469.70	20976	-23.09	17.04			
1471.70	21013	-22.11	16.30	5.22	1.13	16.80
1479.25	21142	-22.61	16.08			
1483.75	21234	-22.63	18.30			
1489.05	21326	-23.48	15.86			
1492.55	21400	-24.31	14.70	4.71	1.11	15.44
1496.30	21455	-24.51	20.16			
1500.60	21564	-24.54	27.50			
1503.10	21635	-24.59	24.90			
1507.60	21812	-26.59	35.10	4.22	2.21	18.49
1516.05	22096	-26.58	32.01			
1520.05	22238	-24.82	28.60			
1530.20	22593	-24.47	23.60	4.40	1.50	18.35
1539.85	22948	-23.79	25.90			
1546.00	23160	-24.45	25.26			
1549.60	23302	-24.70	25.40	4.40	1.64	18.03
1553.00	23409	-24.22	29.13			
1560.05	23657	-26.66	30.00			
1569.10	23980	-25.49	24.69			
1571.85	24083	-26.80	28.00	4.40	1.83	17.85
1577.80	24289	-26.27	29.44			
1580.15	24367	-26.68	30.00			
1584.60	24530	-27.05	26.67			
1590.95	24757	-30.05	28.70	4.33	1.85	18.04
1598.20	25012	-28.05	30.20			
1602.10	25128	-27.53	28.60			
1607.20	25263	-26.91	25.15			
1611.05	25362	-25.75	22.10	5.30	1.44	17.90
1614.30	25448	-26.02	24.48			
1620.05	25596	-25.17	20.60			
1636.50	26038	-23.27	19.10	5.05	1.26	17.71
1645.30	26245	-22.81	20.90			
1646.30	26271	-22.32	16.13			
1654.85	26505	-23.38	16.90	4.63	1.12	17.67
1659.00	26609	-24.96	17.99			
1662.35	26687	-23.90	19.50			
1667.50	26830	-23.12	22.90			
1673.80	26999	-25.71	31.80	3.96	1.78	20.81
1676.20	27056	-25.57	23.90			
1681.75	27207	-24.07	22.40			
1686.30	27319	-26.04	27.86			
1692.95	27493	-25.01	26.60	3.75	1.70	18.29

Table A2 contd.

Depth	Age	$\delta^{13}C$	C	$\delta^{15}N$	N	C:N
cm	cal. years BP	‰ VPDB	%	‰	%	
1700.85	27695	-27.30	19.60			
1704.90	27774	-28.87	32.12			
1710.30	27878	-28.61	30.90	4.34	2.00	18.03
1715.30	27986	-29.71	34.50			
1720.25	28082	-28.34	34.40			
1738.30	28448	-24.88	22.80			
1742.25	28529	-26.57	28.49			
1744.75	28590	-27.72	28.40			
1754.10	28774	-29.50	33.31			
1756.30	28814	-28.68	28.60	4.71	1.76	18.95
1760.80	28916	-28.26	28.63			
1763.80	28977	-27.93	30.10			
1781.30	29323	-29.80	19.60	5.19	1.09	20.89
1786.55	29445	-27.64	25.90			
1793.20	29568	-27.17	29.00			
1799.65	29710	-28.76	26.30			

3 Table A3

Table A3. Summary of all stable isotope data obtained for Chapter Four and referred to in Chapter Five. Samples with the type 'group' consisted five individuals specimens measured together.

Site name	Latitude	Longitude	Altitude	Species	Sample type	$\delta^{13}C$	$\delta^{18}O$	Lab
			m			‰ VPDB	‰ VPDB	
PG-132	-33.43	121.27	174	*Bothriembryon dux*	group	-6.7	0.2	Melbourne
PG-132	-33.43	121.27	174	*Bothriembryon dux*	group	-6.9	0.1	Wollongong
PG-133	-33.30	121.30	206	*Bothriembryon dux*	individual	-6.6	0.5	Melbourne
PG-133	-33.30	121.30	206	*Bothriembryon dux*	individual	-7.4	0.7	Melbourne
PG-133	-33.30	121.30	206	*Bothriembryon dux*	individual	-7.1	0.3	Melbourne
PG-133	-33.30	121.30	206	*Bothriembryon dux*	individual	-7.4	0.5	Melbourne
PG-133	-33.30	121.30	206	*Bothriembryon dux*	individual	-6.5	0.4	Melbourne
PG-133	-33.30	121.30	206	*Bothriembryon dux*	individual	-7.3	0.3	Wollongong
PG-133	-33.30	121.30	206	*Bothriembryon dux*	individual	-7.0	0.1	Wollongong
PG-133	-33.30	121.30	206	*Bothriembryon dux*	individual	-7.5	0.8	Wollongong
PG-133	-33.30	121.30	206	*Bothriembryon dux*	individual	-7.5	0.6	Wollongong
PG-133	-33.30	121.30	206	*Bothriembryon dux*	individual	-6.5	0.5	Wollongong
PG-133	-33.30	121.30	206	*Bothriembryon dux*	individual	-6.5	0.3	Wollongong
PG-131	-33.38	121.34	178	*Bothriembryon dux*	group	-6.5	-0.4	Melbourne
PG-131	-33.38	121.34	178	*Bothriembryon melo*	group	-7.7	-1.0	Melbourne
PG-131	-33.38	121.34	178	*Bothriembryon dux*	group	-6.4	-0.1	Wollongong
B-116	-31.30	121.51	384	*Bothriembryon indictus*	individual	-5.7	0.9	Melbourne
B-116	-31.30	121.51	384	*Bothriembryon indictus*	individual	-4.5	-1.1	Melbourne
B-116	-31.30	121.51	384	*Bothriembryon indictus*	individual	-5.5	-0.4	Melbourne
B-116	-31.30	121.51	384	*Bothriembryon indictus*	individual	-6.8	-0.7	Melbourne
B-116	-31.30	121.51	384	*Bothriembryon indictus*	individual	-5.0	-1.5	Melbourne
B-116	-31.30	121.51	384	*Bothriembryon indictus*	individual	-4.5	-1.3	Wollongong
B-116	-31.30	121.51	384	*Bothriembryon indictus*	individual	-6.9	-0.8	Wollongong
PG-134	-33.15	121.71	238	*Bothriembryon dux*	individual	-6.3	0.1	Melbourne
PG-134	-33.15	121.71	238	*Bothriembryon dux*	individual	-6.0	0.4	Melbourne
PG-134	-33.15	121.71	238	*Bothriembryon melo*	group	-6.3	0.4	Melbourne
PG-134	-33.15	121.71	238	*Bothriembryon dux*	group	-6.0	0.4	Wollongong
PG-134	-33.15	121.71	238	*Bothriembryon melo*	group	-6.4	0.9	Wollongong
PG-156	-32.35	123.62	180	*Bothriembryon dux*	group	-5.2	1.0	Melbourne
PG-156	-32.35	123.62	180	*Cernuella virgata*	group	-4.7	1.4	Melbourne
PG-156	-32.35	123.62	180	*Bothriembryon dux*	group	-5.0	0.3	Wollongong
PG-156	-32.35	123.62	180	*Cernuella virgata*	group	-4.3	1.7	Wollongong
B-157	-32.32	125.05	131	*Bothriembryon indictus*	individual	-7.9	2.1	Melbourne
B-157	-32.32	125.05	131	*Bothriembryon indictus*	individual	-7.9	1.1	Melbourne
B-157	-32.32	125.05	131	*Bothriembryon indictus*	individual	-8.2	0.3	Melbourne
B-157	-32.32	125.05	131	*Bothriembryon indictus*	individual	-6.4	1.2	Melbourne
B-157	-32.32	125.05	131	*Pleuroxia elfina*	individual	-8.6	0.4	Melbourne
B-157	-32.32	125.05	131	*Pleuroxia elfina*	individual	-7.1	0.0	Melbourne
B-157	-32.32	125.05	131	*Pleuroxia elfina*	individual	-10.3	0.0	Melbourne
B-157	-32.32	125.05	131	*Pleuroxia elfina*	individual	-8.3	1.1	Melbourne
B-157	-32.32	125.05	131	*Pleuroxia elfina*	individual	-8.2	0.1	Melbourne
B-157	-32.32	125.05	131	*Pleuroxia polypleura*	individual	-6.2	0.8	Melbourne
B-157	-32.32	125.05	131	*Pleuroxia polypleura*	individual	-6.1	-1.3	Melbourne
B-157	-32.32	125.05	131	*Pleuroxia polypleura*	individual	-9.5	0.8	Melbourne
B-157	-32.32	125.05	131	*Sinumelon nullarboricum*	group	-8.3	1.2	Melbourne
B-157	-32.32	125.05	131	*Pleuroxia elfina*	individual	-8.6	0.4	Wollongong
B-157	-32.32	125.05	131	*Pleuroxia elfina*	individual	-7.3	-0.1	Wollongong
B-157	-32.32	125.05	131	*Pleuroxia elfina*	individual	-10.3	-0.3	Wollongong
B-157	-32.32	125.05	131	*Pleuroxia polypleura*	individual	-6.1	0.8	Wollongong
B-157	-32.32	125.05	131	*Pleuroxia polypleura*	individual	-9.4	1.1	Wollongong
PG-157	-32.32	125.05	143	*Bothriembryon esperantia*	group	-7.4	1.2	Melbourne
PG-157	-32.32	125.05	143	*Pleuroxia elfina*	group	-7.4	0.2	Melbourne
PG-157	-32.32	125.05	143	*Pleuroxia polypleura*	group	-6.5	-0.5	Melbourne
PG-157	-32.32	125.05	143	*Sinumelon nullarboricum*	group	-7.9	0.5	Melbourne
PG-157	-32.32	125.05	143	*Bothriembryon esperantia*	group	-7.4	1.6	Wollongong
PG-157	-32.32	125.05	143	*Pleuroxia elfina*	group	-7.9	0.3	Wollongong
PG-157	-32.32	125.05	143	*Pleuroxia polypleura*	group	-6.4	-0.5	Wollongong
RP-3-A	-31.96	126.91	29	*Bothriembryon indictus*	individual	-5.3	1.1	Melbourne
RP-3-A	-31.96	126.91	29	*Bothriembryon indictus*	individual	-1.8	1.0	Melbourne
RP-3-A	-31.96	126.91	29	*Bothriembryon indictus*	individual	-5.0	0.7	Melbourne
RP-3-A	-31.96	126.91	29	*Bothriembryon indictus*	individual	-5.8	3.0	Melbourne
RP-3-A	-31.96	126.91	29	*Bothriembryon indictus*	individual	-2.1	2.1	Melbourne
RP-3-A	-31.96	126.91	29	*Bothriembryon indictus*	individual	-6.0	1.3	Melbourne
RP-3-A	-31.96	126.91	29	*Bothriembryon indictus*	individual	-3.9	1.2	Melbourne
RP-3-A	-31.96	126.91	29	*Pleuroxia polypleura*	individual	-2.2	-0.8	Melbourne
RP-3-A	-31.96	126.91	29	*Pleuroxia polypleura*	individual	-3.8	-2.3	Melbourne

Table A3 contd.

Site name	Latitude	Longitude	Altitude	Species	Sample type	$\delta^{13}C$	$\delta^{18}O$	Lab
			m			‰ VPDB	‰ VPDB	
PG-159	-31.90	127.02	63	*Bothriembryon indictus*	group	-5.2	0.3	Melbourne
PG-159	-31.90	127.02	63	*Cernuella virgata*	group	-7.7	0.9	Melbourne
PG-159	-31.90	127.02	63	*Sinumelon nullarboricum*	group	-7.1	0.5	Melbourne
PG-159	-31.90	127.02	63	*Sinumelon nullarboricum*	group	-7.2	0.4	Wollongong
B-162	-31.55	130.59	61	*Bothriembryon indictus*	individual	-2.0	0.6	Melbourne
B-162	-31.55	130.59	61	*Bothriembryon indictus*	individual	-4.3	2.6	Melbourne
B-162	-31.55	130.59	61	*Bothriembryon indictus*	individual	-2.6	0.6	Melbourne
B-162	-31.55	130.59	61	*Bothriembryon indictus*	individual	-4.6	2.0	Melbourne
B-162	-31.55	130.59	61	*Bothriembryon indictus*	individual	-2.9	1.7	Melbourne
PG-162/163	-31.55	130.62	62	*Bothriembryon barretti*	individual	-1.8	1.2	Melbourne
PG-162/163	-31.55	130.62	62	*Bothriembryon barretti*	individual	-7.6	0.7	Melbourne
PG-162/163	-31.55	130.62	62	*Bothriembryon barretti*	individual	-5.8	1.0	Melbourne
PG-162/163	-31.55	130.62	62	*Bothriembryon barretti*	individual	-4.3	1.7	Melbourne
PG-162/163	-31.55	130.62	62	*Bothriembryon barretti*	individual	-2.0	1.6	Wollongong
PG-162/163	-31.55	130.62	62	*Bothriembryon barretti*	individual	-7.8	0.9	Wollongong
PG-162/163	-31.55	130.62	62	*Bothriembryon barretti*	individual	-5.9	1.0	Wollongong
PG-162_163A	-31.81	132.24	37	*Cernuella virgata*	group	-7.6	0.6	Melbourne
PG-162_163A	-31.81	132.24	37	*Cochlicella acuta*	group	-7.4	1.1	Melbourne
PG-162/163A	-31.81	132.24	37	*Cochlicella acuta*	group	-7.1	1.0	Wollongong
Alice Springs	-23.73	132.87	746	*Pleuroxia adcockiana*	individual	-7.3	-1.2	Melbourne
Alice Springs	-23.73	132.87	746	*Pleuroxia adcockiana*	individual	-8.6	-0.8	Melbourne
Alice Springs	-23.73	132.87	746	*Pleuroxia adcockiana*	individual	-8.4	-0.7	Melbourne
Alice Springs	-23.73	132.87	746	*Pleuroxia adcockiana*	individual	-10.2	-2.2	Melbourne
Alice Springs	-23.73	132.87	746	*Pleuroxia adcockiana*	individual	-9.4	0.2	Melbourne
Alice Springs	-23.73	132.87	746	*Sinumelon expositum*	individual	-7.9	-0.7	Melbourne
Alice Springs	-23.73	132.87	746	*Sinumelon expositum*	individual	-8.2	-1.2	Melbourne
Alice Springs	-23.73	132.87	746	*Sinumelon expositum*	individual	-8.3	1.9	Melbourne
Alice Springs	-23.73	132.87	746	*Sinumelon expositum*	individual	-7.3	1.6	Melbourne
Alice Springs	-23.73	132.87	746	*Sinumelon expositum*	individual	-7.5	-1.3	Melbourne
PG-166	-32.41	134.52	80	*Cernuella virgata*	individual	-8.7	0.7	Melbourne
PG-166	-32.41	134.52	80	*Cernuella virgata*	individual	-8.2	1.1	Melbourne
PG-166	-32.41	134.52	80	*Cernuella virgata*	individual	-8.5	1.6	Melbourne
PG-166	-32.41	134.52	80	*Cernuella virgata*	individual	-8.5	1.2	Melbourne
PG-166	-32.41	134.52	80	*Cernuella virgata*	individual	-9.0	1.6	Melbourne
PG-166	-32.41	134.52	80	*Cernuella virgata*	individual	-8.6	0.9	Melbourne
PG-166	-32.41	134.52	80	*Cernuella virgata*	group	-8.8	1.0	Wollongong
PG-171	-33.33	134.88	70	*Cernuella virgata*	individual	-8.4	0.4	Melbourne
PG-171	-33.33	134.88	70	*Cernuella virgata*	individual	-10.2	0.4	Melbourne
PG-171	-33.33	134.88	70	*Cernuella virgata*	individual	-10.6	0.4	Melbourne
PG-171	-33.33	134.88	70	*Cernuella virgata*	individual	-10.6	0.1	Melbourne
PG-171	-33.33	134.88	70	*Cernuella virgata*	individual	-8.9	-0.6	Melbourne
PG-171	-33.33	134.88	70	*Cernuella virgata*	individual	-10.1	0.7	Melbourne
PG-171	-33.33	134.88	70	*Theba pisana*	individual	-9.3	0.9	Melbourne
PG-171	-33.33	134.88	70	*Theba pisana*	individual	-9.6	0.5	Melbourne
PG-171	-33.33	134.88	70	*Theba pisana*	individual	-9.1	0.9	Melbourne
PG-171	-33.33	134.88	70	*Theba pisana*	individual	-10.1	0.5	Melbourne
PG-171	-33.33	134.88	70	*Theba pisana*	individual	-10.5	0.5	Melbourne
PG-171	-33.33	134.88	70	*Cernuella virgata*	individual	-9.4	-0.7	Wollongong
PG-171	-33.33	134.88	70	*Cernuella virgata*	individual	-10.4	0.6	Wollongong
PG-171	-33.33	134.88	70	*Cernuella virgata*	individual	-10.7	0.4	Wollongong
PG-171	-33.33	134.88	70	*Cernuella virgata*	individual	-9.1	-0.4	Wollongong
PG-171	-33.33	134.88	70	*Cernuella virgata*	individual	-10.6	-0.1	Wollongong
PG-171	-33.33	134.88	70	*Theba pisana*	individual	-9.9	0.4	Wollongong
PG-171	-33.33	134.88	70	*Theba pisana*	individual	-9.3	0.8	Wollongong
PG-171	-33.33	134.88	70	*Theba pisana*	individual	-10.0	0.0	Wollongong
PG-171	-33.33	134.88	70	*Theba pisana*	individual	-10.7	0.2	Wollongong
PG-172	-33.34	134.88	77	*Cochlicella acuta*	group	-8.3	0.5	Melbourne
PG-172	-33.34	134.88	77	*Theba pisana*	group	-9.9	0.5	Melbourne
PG-172	-33.34	134.88	77	*Cochlicella acuta*	group	-8.7	0.1	Wollongong
PG-168	-32.89	135.12	112	*Cernuella virgata*	group	-9.8	0.7	Melbourne
PG-173	-33.49	135.14	50	*Cernuella virgata*	group	-9.5	0.4	Melbourne
PG-173	-33.49	135.14	50	*Cochlicella acuta*	group	-8.9	0.4	Melbourne
PG-167	-32.82	135.16	186	*Cernuella virgata*	group	-9.1	0.7	Melbourne
PG-167	-32.82	135.16	186	*Cernuella virgata*	group	-9.2	0.8	Wollongong
GOC-22B	-16.08	136.53	47	*Xanthomelon durvillii*	group	-14.1	-5.6	Wollongong
PG-107	-34.98	137.51	16	*Cernuella virgata*	group	-9.4	1.1	Melbourne

Table A3 contd.

Site name	Latitude	Longitude	Altitude	Species	Sample type	$\delta^{13}C$	$\delta^{18}O$	Lab
			m			‰ VPDB	‰ VPDB	
PG-107	-34.98	137.51	16	*Cochlicella acuta*	group	-9.0	0.7	Melbourne
PG-107	-34.98	137.51	16	*Theba pisana*	group	-9.8	0.7	Melbourne
PG-104	-34.58	137.60	75	*Cernuella virgata*	group	-10.6	0.7	Melbourne
PG-104	-34.58	137.60	75	*Cochlicella acuta*	group	-8.5	0.6	Melbourne
PG-101_102	-33.97	137.70	53	*Cernuella virgata*	individual	-9.7	-0.1	Melbourne
PG-101_102	-33.97	137.70	53	*Cernuella virgata*	individual	-7.7	1.4	Melbourne
PG-101_102	-33.97	137.70	53	*Cernuella virgata*	individual	-9.6	1.7	Melbourne
PG-101_102	-33.97	137.70	53	*Cernuella virgata*	individual	-8.2	2.0	Melbourne
PG-101_102	-33.97	137.70	53	*Cernuella virgata*	individual	-9.1	1.4	Melbourne
PG-103	-34.31	137.72	188	*Cernuella virgata*	group	-9.9	0.6	Melbourne
PG-103	-34.31	137.72	188	*Theba pisana*	group	-10.9	1.2	Melbourne
PG-102	-34.08	137.73	91	*Cernuella virgata*	group	-10.3	1.6	Melbourne
PG-102R	-34.08	137.73	91	*Cernuella virgata*	group	-9.8	1.7	Melbourne
PG-102	-34.08	137.73	91	*Cochlicella acuta*	group	-9.2	1.2	Melbourne
PG-102R	-34.08	137.73	91	*Cochlicella acuta*	group	-9.5	1.0	Melbourne
KI-2	-35.84	137.75	22	*Cernuella virgata*	individual	-6.3	-0.2	Melbourne
KI-2	-35.84	137.75	22	*Cernuella virgata*	individual	-9.2	0.4	Melbourne
KI-2	-35.84	137.75	22	*Cernuella virgata*	individual	-9.2	0.2	Melbourne
KI-2	-35.84	137.75	22	*Cernuella virgata*	individual	-9.6	0.4	Melbourne
KI-2	-35.84	137.75	22	*Cernuella virgata*	individual	-8.4	0.0	Melbourne
KI-2	-35.84	137.75	22	*Cernuella virgata*	individual	-11.2	0.8	Melbourne
KI-2	-35.84	137.75	22	*Cernuella virgata*	individual	-10.8	0.1	Melbourne
PG-106	-34.85	137.76	52	*Cernuella virgata*	group	-10.4	0.7	Melbourne
PG-106	-34.85	137.76	52	*Cochlicella acuta*	group	-9.9	0.2	Melbourne
PG-106	-34.85	137.76	52	*Theba pisana*	group	-10.7	0.9	Melbourne
PG-100	-33.77	137.85	58	*Cernuella virgata*	individual	-9.7	1.9	Melbourne
PG-100	-33.77	137.85	58	*Cernuella virgata*	individual	-8.5	1.1	Melbourne
PG-108	-34.54	137.88	38	*Cochlicella acuta*	group	-8.7	0.5	Melbourne
PG-108	-34.54	137.88	38	*Theba pisana*	group	-9.9	0.4	Melbourne
PG-110	-34.07	137.96	108	*Austrosuccinea australis*	individual	-4.7	3.2	Melbourne
PG-110	-34.07	137.96	108	*Austrosuccinea australis*	individual	-3.5	4.1	Melbourne
PG-110	-34.07	137.96	108	*Austrosuccinea australis*	individual	-5.1	4.2	Melbourne
PG-110	-34.07	137.96	108	*Austrosuccinea australis*	individual	-4.6	3.4	Melbourne
PG-110	-34.07	137.96	108	*Austrosuccinea australis*	individual	-3.3	3.7	Melbourne
PG-110	-34.07	137.96	108	*Cernuella virgata*	individual	-10.1	-0.6	Melbourne
PG-110	-34.07	137.96	108	*Cernuella virgata*	individual	-9.6	2.2	Melbourne
PG-110	-34.07	137.96	108	*Cernuella virgata*	individual	-10.1	0.0	Melbourne
PG-110	-34.07	137.96	108	*Cernuella virgata*	individual	-10.1	-2.6	Melbourne
PG-110	-34.07	137.96	108	*Cernuella virgata*	individual	-9.6	1.3	Melbourne
PG-110	-34.07	137.96	108	*Cochlicella acuta*	individual	-9.6	0.5	Melbourne
PG-110	-34.07	137.96	108	*Cochlicella acuta*	individual	-9.6	1.2	Melbourne
PG-110	-34.07	137.96	108	*Cochlicella acuta*	individual	-8.0	1.3	Melbourne
PG-110	-34.07	137.96	108	*Cochlicella acuta*	individual	-9.2	1.1	Melbourne
PG-110	-34.07	137.96	108	*Cochlicella acuta*	individual	-9.4	1.2	Melbourne
PG-110	-34.07	137.96	108	*Cochlicella acuta*	individual	-9.3	1.4	Wollongong
PG-109	-34.28	137.98	33	*Cernuella virgata*	group	-9.1	0.3	Melbourne
PG-109	-34.28	137.98	33	*Cochlicella acuta*	group	-8.1	1.0	Melbourne
PG-98	-33.83	138.02	124	*Cernuella virgata*	group	-8.8	0.9	Melbourne
PG-98	-33.83	138.02	124	*Cernuella virgata*	group	-9.2	0.6	Wollongong
PG-99	-33.52	138.06	33	*Cernuella virgata*	group	-8.4	1.4	Melbourne
PG-99	-33.52	138.06	33	*Cernuella virgata*	group	-8.5	1.1	Wollongong
PG-94	-34.31	138.26	23	*Cochlicella acuta*	group	-9.1	1.4	Melbourne
PG-94	-34.31	138.26	23	*Theba pisana*	group	-9.8	1.4	Melbourne
B-94	-34.31	138.26	13	*Cochlicella acuta*	individual	-9.5	0.3	Melbourne
B-94	-34.31	138.26	13	*Cochlicella acuta*	individual	-8.4	1.4	Melbourne
B-94	-34.31	138.26	13	*Cochlicella acuta*	individual	-9.4	1.4	Melbourne
B-94	-34.31	138.26	13	*Cochlicella acuta*	individual	-9.3	1.4	Melbourne
B-94	-34.31	138.26	13	*Cochlicella acuta*	individual	-8.1	0.8	Melbourne
B-94	-34.31	138.26	13	*Theba pisana*	individual	-9.8	0.9	Melbourne
B-94	-34.31	138.26	13	*Theba pisana*	individual	-11.1	1.1	Melbourne
B-94	-34.31	138.26	13	*Theba pisana*	individual	-9.8	0.4	Melbourne
B-94	-34.31	138.26	13	*Theba pisana*	individual	-9.8	1.0	Melbourne
B-94	-34.31	138.26	13	*Theba pisana*	individual	-10.3	0.8	Melbourne
PG-95	-34.24	138.29	39	*Cernuella virgata*	group	-10.3	1.1	Melbourne
PG-96	-34.21	138.32	40	*Cernuella virgata*	group	-10.4	2.0	Melbourne
PG-97	-33.85	138.41	123	*Cernuella virgata*	group	-9.4	1.0	Melbourne

Table A3 contd.

Site name	Latitude	Longitude	Altitude	Species	Sample type	$\delta^{13}C$	$\delta^{18}O$	Lab
			m			‰ VPDB	‰ VPDB	
PG-97	-33.85	138.41	123	*Cernuella virgata*	group	-9.4	1.0	Wollongong
PG-50	-33.69	138.93	474	*Cernuella virgata*	group	-9.6	0.7	Melbourne
PG-54	-34.49	139.36	213	*Cernuella virgata*	group	-8.3	1.1	Melbourne
PG-55	-34.67	139.46	124	*Cernuella virgata*	group	-9.0	0.2	Melbourne
PG-57	-35.27	139.46	4	*Cernuella virgata*	group	-9.4	0.5	Melbourne
PG-57	-35.27	139.46	4	*Cochlicella acuta*	group	-9.0	0.7	Melbourne
PG-57	-35.27	139.46	4	*Theba pisana*	group	-10.4	-0.1	Melbourne
PG-51	-34.40	139.60	44	*Cernuella virgata*	group	-9.4	0.5	Melbourne
CW-1	-36.26	139.71	4	*Cernuella virgata*	group	-9.5	-0.9	Melbourne
MA0038	-35.70	139.86	31	*Cernuella virgata*	group	-10.4	1.5	Melbourne
MA0038	-35.70	139.86	31	*Cochlicella acuta*	group	-9.0	1.3	Melbourne
PG-56	-32.67	140.17	85	*Cernuella virgata*	individual	-6.7	0.0	Melbourne
PG-56	-32.67	140.17	85	*Cernuella virgata*	individual	-9.3	0.6	Melbourne
PG-56	-32.67	140.17	85	*Cernuella virgata*	individual	-8.9	0.3	Melbourne
PG-56	-32.67	140.17	85	*Cernuella virgata*	individual	-7.9	-0.5	Melbourne
PG-56	-32.67	140.17	85	*Cernuella virgata*	individual	-8.2	0.3	Melbourne
PG-30	-34.15	140.19	54	*Cernuella virgata*	individual	-9.1	1.3	Melbourne
PG-30	-34.15	140.19	54	*Cernuella virgata*	individual	-9.4	-0.1	Melbourne
PG-30	-34.15	140.19	54	*Cernuella virgata*	individual	-8.3	0.4	Melbourne
PG-30	-34.15	140.19	54	*Cernuella virgata*	individual	-8.2	0.2	Melbourne
PG-27	-34.25	140.62	56	*Cernuella virgata*	group	-7.7	-0.4	Melbourne
BL-1	-37.12	140.73	52	*Cernuella virgata*	group	-11.5	-1.6	Melbourne
PG-59	-35.31	140.79	108	*Cernuella virgata*	group	-8.9	-0.5	Melbourne
5U6	-37.03	140.80	67	*Cernuella virgata*	group	-10.2	-1.0	Melbourne
PG-25D	-34.29	140.86	23	*Cernuella virgata*	group	-7.4	0.6	Melbourne
PG-25D	-34.29	140.86	23	*Pleuroxia elfina*	group	-7.1	1.2	Melbourne
PG-26	-34.29	140.86	24	*Cernuella virgata*	group	-8.3	-0.7	Melbourne
MA0083	-37.88	141.08	70	*Cernuella virgata*	group	-9.3	0.4	Melbourne
MA0083	-37.88	141.08	70	*Cochlicella acuta*	group	-7.0	0.3	Melbourne
GOC-45D	-15.42	141.88	11	*Crikey steveirwini*	group	-12.3	-1.7	Wollongong
MA0219	-35.07	142.33	39	*Cernuella virgata*	group	-9.2	0.7	Melbourne
MA0068	-38.23	143.10	111	*Cornu aspersum*	group	-9.4	0.5	Melbourne
PG-1	-35.19	143.35	63	*Cernuella virgata*	individual	-8.8	1.7	Melbourne
PG-1	-35.19	143.35	63	*Cernuella virgata*	individual	-8.7	1.4	Melbourne
PG-1	-35.19	143.35	63	*Cernuella virgata*	individual	-9.0	1.1	Melbourne
PG-1	-35.19	143.35	63	*Cernuella virgata*	individual	-7.4	1.0	Melbourne
PG-1	-35.19	143.35	63	*Cernuella virgata*	individual	-8.9	0.9	Melbourne
PG-1	-35.19	143.35	63	*Cernuella virgata*	individual	-8.3	0.1	Melbourne
PG-1	-35.19	143.35	63	*Cernuella virgata*	individual	-9.3	-1.2	Melbourne
PG-1	-35.19	143.35	63	*Cernuella virgata*	individual	-7.3	0.7	Melbourne
PG-1	-35.19	143.35	63	*Cernuella virgata*	individual	-9.4	-0.5	Melbourne
PG-1	-35.19	143.35	63	*Cernuella virgata*	individual	-8.6	0.8	Melbourne
MA0220	-34.67	143.56	65	*Cernuella virgata*	individual	-11.6	2.0	Melbourne
MA0220	-34.67	143.56	65	*Cernuella virgata*	individual	-11.6	1.5	Melbourne
GOC-58A	-17.64	145.46	796	*Spurlingia gemma*	group	-12.5	0.2	Wollongong

Appendix Three: publications arising from this thesis

This appendix comprises two published journal articles arising from work undertaken for this thesis. The articles are identical to chapters two and three, aside from some minor formatting changes.

Geochemistry, Geophysics, Geosystems

TECHNICAL REPORTS: METHODS

10.1029/2018GC007575

Key Points:

- Stable isotope values from carbonate preserved within natural lake sediment may be biased by release of CO_2 from organic compounds
- Pretreatment of sediment with acidic hydrogen peroxide causes a treatment bias due partly to carbonate dissolution and reprecipitation
- Pretreatment of sediment with alkaline hydrogen peroxide at 50 °C results in accurate stable isotope values

Supporting Information:

- Supporting Information S1

Correspondence to:
G. Falster,
georgina.falster@adelaide.edu.au

Citation:
Falster, G., Delean, S., & Tyler, J. (2018). Hydrogen peroxide treatment of natural lake sediment prior to carbon and oxygen stable isotope analysis of calcium carbonate. *Geochemistry, Geophysics, Geosystems*, *19*, 3583–3595. https://doi.org/10.1029/2018GC007575

Received 26 MAR 2018
Accepted 30 JUL 2018
Accepted article online 18 AUG 2018
Published online 19 SEP 2018

Hydrogen Peroxide Treatment of Natural Lake Sediment Prior to Carbon and Oxygen Stable Isotope Analysis of Calcium Carbonate

Georgina Falster[1,2], Steven Delean[3], and Jonathan Tyler[1,2]

[1]Department of Earth Sciences, The University of Adelaide, Adelaide, South Australia, Australia, [2]Sprigg Geobiology Centre, The University of Adelaide, Adelaide, South Australia, Australia, [3]Department of Ecology and Evolutionary Biology, The University of Adelaide, Adelaide, South Australia, Australia

Abstract The carbon and oxygen stable isotope ratios ($\delta^{13}C$ and $\delta^{18}O$) of authigenic and biogenic lacustrine carbonates are commonly used as past climate proxies, and these carbonates are often preserved within organic-rich bulk sediment. We measured the $\delta^{13}C$ and $\delta^{18}O$ of carbon dioxide evolved from fine-grained crystalline calcite and biogenic aragonite, mixed with natural organic-rich lake sediment. We found that if the ratio of total inorganic carbon (TIC) to total organic carbon (TOC) in lacustrine bulk sediment is low, then organic compounds evolve detectable CO_2 during phosphoric acid digestion, leading to an "organic bias" in the measured $\delta^{13}C$ and $\delta^{18}O$. We tested the effect of oxidative pretreatment of the bulk sediment with acidic or alkaline hydrogen peroxide (H_2O_2), at a range of temperatures. Pretreatment with acidic H_2O_2 not only had a negligible effect on the TIC/TOC but also resulted in dissolution and reprecipitation of carbonate, and a consequent "treatment bias" that was particularly strong for $\delta^{18}O$. Oxidation with alkaline H_2O_2 removed a greater proportion of organic material, with no evidence for carbonate dissolution at temperatures of ≤50 °C. The $\delta^{13}C$ and $\delta^{18}O$ values obtained from sediment treated with alkaline H_2O_2 at 50 °C were both accurate and precise, even for sediment with very low initial TIC/TOC. Our results show that it is possible to obtain accurate $\delta^{13}C$ and $\delta^{18}O$ values from carbonates preserved within organic-rich lacustrine sediment, suitable for use in paleoclimate reconstructions.

1. Introduction

The stable isotope composition of lacustrine carbonate minerals is dependent on the chemistry, hydrology, and biological productivity of the host lake, which in turn are dependent on ambient environmental conditions. Carbonates therefore record climatic conditions at the time of precipitation, and serve as paleoclimate indicators when preserved in lacustrine sediment. In particular, the $\delta^{13}C$ and $\delta^{18}O$ of authigenic and biogenic lake carbonates have long been used to derive records of a range of climate-related variables, including temperature, hydrology, and lake productivity (e.g., Holmes, 1996; Leng & Marshall, 2004; Stuiver, 1970). For $\delta^{18}O$, fluctuations as small as a few per mille are interpreted to represent major changes in temperature and hydroclimate (e.g., Holmes et al., 2016; Hyvåinen et al., 1990; McCrea, 1950; Schwander et al., 2000; von Grafenstein et al., 1992). It is therefore critical that reported stable isotope values are accurate and precise.

The accumulative natures of lakes is such that lacustrine sediment is often a rich source of materials that may be used as paleoclimate proxies, including allochthonous and autochthonous organic material as well as various carbonate phases. While this compositional variety is excellent for the creation of multiproxy paleoclimate reconstructions, lacustrine carbonates consequently are often preserved in a matrix that has a low ratio of total inorganic carbon (TIC) to total organic carbon (TOC). Oehlerich et al. (2013) and Lebeau et al. (2014) demonstrated that when using the phosphoric acid (H_3PO_4) digestion method to measure carbonate stable isotope ratios of bulk sediment with low TIC/TOC (<0.3), organic compounds release CO_2, leading to bias in the measured $\delta^{13}C$ and $\delta^{18}O$ that is dependent on the specific sample matrix. For coarse-grained carbonates, such as large snail, bivalve, or foraminiferal shells, manual cleaning is typically sufficient to remove much of the organic material (Keatings et al., 2006). For fine-grained carbonates, such as very small ostracod shells and authigenic carbonate, this may not be possible, in which case the TIC/TOC may be raised by oxidizing as much of the organic material as possible prior to analysis of the sediment.

Methods commonly used to oxidize organic matter prior to stable isotope analysis are bleaching with sodium hypochlorite (NaOCl) or hydrogen peroxide (H_2O_2), or thermal treatments (vacuum roasting, plasma ashing).

However, both chemical and thermal pretreatment methods are demonstrated sources of error in isotope determinations, with different methods resulting in different biases (Grottoli et al., 2005; Lebeau et al., 2014; Nagtegaal et al., 2012; Serrano et al., 2008; Wierzbowski, 2007). After several decades of debate, there is yet no consensus in either the literature or stable isotope geochemistry community as to which method results in the most accurate carbonate $\delta^{13}C$ and $\delta^{18}O$, or indeed whether pretreatment is necessary. This is in part due to the wide compositional variety in lacustrine sediment, including carbonate phase, TIC/TOC, and specific organic compounds, all of which may respond differently to the same treatment. In paleoclimate studies where lake sediment has been subjected to oxidative treatment prior to analysis, many different methods are used, and with low methodological consistency, for example, temperature and duration of reaction, concentration, and purity of reagent. Comparison of isotope proxy data from different laboratories may therefore potentially be misleading, in the absence of quantitative assessment of potential treatment effects on carbonate $\delta^{13}C$ and $\delta^{18}O$.

Several studies have tested the effect of chemical pretreatment on the stable isotope composition of specific carbonate phases, including foraminiferal calcite (Fallet et al., 2009; Feldmeijer et al., 2013; Ganssen, 1981; Serrano et al., 2008), coral aragonite (Boiseau & Juillet-Leclerc, 1997; Grottoli et al., 2005; Nagtegaal et al., 2012), ostracod calcite (Keatings et al., 2006), and siderite (Lebeau et al., 2014). The findings from these studies are not consistent (see Table 1). Wierzbowski (2007) performed perhaps the most universally applicable study, and investigated the effect of NaOCl, H_2O_2, and vacuum roasting treatments on skeletal and inorganic calcites and aragonites, mixed with a variety of pure organic compounds. Results from this study indicated that pretreatment may introduce severe isotopic biases, and is generally unnecessary. However, this study was conducted on mixtures with TIC/TOC $\geq$ 0.85.

Pretreatment with NaOCl typically leads to negative bias in both $\delta^{13}C$ and $\delta^{18}O$ (Table 1), which is likely due to both isotope exchange between the carbonate and the NaOCl, and precipitation of calcium hydroxide; authors therefore generally suggest avoiding oxidation with NaOCl (Keatings et al., 2006; Wierzbowski, 2007). Thermal treatments are similarly prone to inducing bias, through disruption of the carbonate structure, and isotope exchange with internal water (Boiseau & Juillet-Leclerc, 1997; Keatings et al., 2006; Wierzbowski, 2007). Commercially available laboratory-grade H_2O_2 is acidic, leading to partial dissolution of carbonate, and has been reported to be less effective in the removal of organic material than NaOCl (Gaffey & Bronnimann, 1993). However, no isotope exchange occurs between H_2O_2 and carbonate (Boiseau & Juillet-Leclerc, 1997). Pretreatment with H_2O_2 therefore has the potential to result in accurate stable isotope values, if carbonate dissolution can be prevented by raising the pH of the solution (cf. Fallet et al., 2009). Alkaline H_2O_2 is not routinely used as an oxidative reagent, as a high pH promotes rapid decomposition of H_2O_2, particularly at the higher temperatures that may be used to speed up oxidation (Hosking, 1932; Mikutta et al., 2005). Fine-grained lacustrine carbonates are likely to be particularly susceptible to partial dissolution by acidic H_2O_2; however, the efficacy of alkaline H_2O_2 in oxidative pretreatment of natural lake sediment has not been directly tested.

The aim of this study is therefore to test the effect of treatment with both acidic and alkaline H_2O_2 on the measured $\delta^{13}C$ and $\delta^{18}O$ of fine-grained calcium carbonate within a natural lake sediment matrix. We also test the effect of carrying out the reaction at different temperatures. We measured the $\delta^{13}C$ and $\delta^{18}O$ of treated and untreated simulated very low TIC/TOC lake sediment, created by mixing fine-grained carbonate standards—one crystalline calcite and one relatively poorly structured aragonite—with carbonate-free lake sediment from Lake Purrumbete, a maar lake in the Newer Volcanics Province of south-eastern Australia. This province hosts several crater lakes that preserve long sediment records, potentially representing valuable paleoclimate archives (e.g., Chivas et al., 1986; Cook, 2009; Falster et al., 2018; Timms, 1976; Wilkins et al., 2013). We evaluated the influence of both the organic matter and the oxidative treatments, by comparison with the stable isotope composition of the pure, untreated carbonate. We designed the experiment to test the following hypotheses:

1. Organic matter will be more efficiently oxidized by acidic than alkaline H_2O_2, but the former will lead to partial dissolution of carbonate.
2. Higher TIC/TOC will result in less contribution of organic material to the measured CO_2, with negligible influence above TIC/TOC = 0.3 (cf. Oehlerich et al., 2013).
3. Increasing reaction temperature will result in more efficient oxidation of organic material.

Table 1
Summary of Published Results of Three Most Commonly Used Treatments for the Removal of Organic Matter From Carbonates—Bleaching With Sodium Hypohlorite (NaOCl) or Hydrogen Peroxide (H_2O_2), and Thermal Treatments (Vacuum Roasting or Plasma Ashing)

Treatment	Methodological detail	Carbonate phase	Change in stable isotope composition relative to untreated samples	Authors' possible explanations for observations	Reference
NaOCl	5%, 18 hr, room temperature	Biogenic aragonite	Negative shift in $\delta^{13}C$, no change in $\delta^{18}O$	Isotope exchange with reagent, precipitation of $Ca(OH)_2$	Wierzbowski (2007)
	5%, 18 hr, room temperature	Biogenic calcite	Negative shift in $\delta^{13}C$ and $\delta^{18}O$	Isotope exchange with reagent, precipitation of $Ca(OH)_2$	Wierzbowski (2007)
	Household bleach, 5.25%, 24 hr	Coral aragonite	Negative shift in $\delta^{13}C$ and $\delta^{18}O$	Partial dissolution of carbonate, isotope exchange with reagent	Grottoli et al. (2005)
	Reagent grade, 5%, 24 hr, room temperature	Coral aragonite	No change		Nagtegaal et al. (2012)
	10%, 10 min, 20 °C	Foraminiferal calcite	No change		Serrano et al. (2008)
	5%, 18 hr, room temperature	Inorganic aragonite	No change		Wierzbowski (2007)
	5%, 18 hr, room temperature	Inorganic calcite	No change		Wierzbowski (2007)
	5%, 18 hr, room temperature	Inorganic calcite (ground)	Negative shift in $\delta^{13}C$ and $\delta^{18}O$	Isotope exchange with reagent, precipitation of $Ca(OH)_2$	Wierzbowski (2007)
	5%, 4 hr, room temperature	Ostracod calcite	Negative shift in $\delta^{13}C$ and $\delta^{18}O$, increase in variability	Isotope exchange with reagent	Keatings et al. (2006)
	3.5%, three days, room temperature	Siderite	Negative shift in $\delta^{13}C$ (not significant), no change in $\delta^{18}O$	Partial dissolution of carbonate	Lebeau et al. (2014)
H_2O_2	30%, 12 hr, room temperature	Biogenic aragonite	No change		Wierzbowski (2007)
	30%, 12 hr, room temperature	Biogenic calcite	No change		Wierzbowski (2007)
	30%, 24 hr	Coral aragonite	Negative shift in $\delta^{13}C$, no change in $\delta^{18}O$, increase in variability	Partial dissolution of carbonate, precipitation of $Ca(OH)_2$, possible isotope exchange with reagent	Grottoli et al. (2005)
	30%, 12 hr, room temperature	Coral aragonite	Variable, but mainly negative shifts in $\delta^{13}C$ and $\delta^{18}O$	Elimination of organic matter, partial dissolution of carbonate	Boiseau and Juillet-Leclerc (1997)
	30%, 10 min, 20 °C	Foraminiferal calcite	No change in $\delta^{13}C$, negative shift in $\delta^{18}O$	Partial dissolution of carbonate	Serrano et al. (2008)
	10%, 1 hr, room temperature	Foraminiferal calcite	No change		Feldmeijer et al. (2013)
	10%, 20 min, buffered to pH = 7.5 with ammonia	Foraminiferal calcite	No change		Ganssen (1981)
	30%, 12 hr, room temperature	Inorganic calcite	No change in $\delta^{13}C$, negative shift or no change in $\delta^{18}O$	Partial dissolution of carbonate	Wierzbowski (2007)
	5%, 80 °C, 15 min	Ostracod calcite	Negative shift in $\delta^{13}C$, no change in $\delta^{18}O$, increase in variability	Potential isotope exchange with reagent	Keatings et al. (2006)
	30%, three days, room temperature	Siderite	Negative shift in $\delta^{13}C$ and $\delta^{18}O$ (not significant)	Partial dissolution of carbonate	Lebeau et al. (2014)
Thermal	Plasma ashing, 125 °C, 16 hr	Ostracod calcite	No change		Keatings et al. (2006)
	Plasma ashing, 5–33 hr	Siderite	Negative shift in $\delta^{13}C$ (not significant), no change in $\delta^{18}O$		Lebeau et al. (2014)
	Vacuum roasting, 200 °C, 30 min	Foraminiferal calcite	No change		Ganssen (1981)
	Vacuum roasting, 200 °C, 45 min	Biogenic aragonite	No change in $\delta^{13}C$, negative shift in $\delta^{18}O$	Isotope exchange with internal water	Wierzbowski (2007)
	Vacuum roasting, 200 °C, 45 min	Biogenic calcite	No change		Wierzbowski (2007)
	Vacuum roasting, 340–350 °C, 45 min	Biogenic aragonite	No change in $\delta^{13}C$, negative shift in $\delta^{18}O$	Isotope exchange with internal water	Wierzbowski (2007)
	Vacuum roasting, 340–350 °C, 45 min	Biogenic calcite	No change		Wierzbowski (2007)

Table 1 *(continued)*

Treatment	Methodological detail	Carbonate phase	Change in stable isotope composition relative to untreated samples	Authors' possible explanations for observations	Reference
	Vacuum roasting, 340–350 °C, 45 min	Inorganic aragonite	No change		Wierzbowski (2007)
	Vacuum roasting, 340–350 °C, 45 min	Inorganic calcite	No change		Wierzbowski (2007)
	Vacuum roasting, 350 °C, 2 hr	Coral aragonite	Negative shift in $\delta^{13}C$ and $\delta^{18}O$	Conversion of aragonite to calcite, presence of organic carbon	Boiseau and Juillet-Leclerc (1997)
	Vacuum roasting, 380 °C, 1 hr	Ostracod calcite	Negative shift in $\delta^{13}C$ and $\delta^{18}O$, increase in variability	Disruption of calcite lattice facilitating isotope exchange with atmospheric CO_2	Keatings et al. (2006)
	Vacuum roasting, 400 °C, 60 min	Foraminiferal calcite	No change		Ganssen (1981)
	Vacuum roasting, 450 °C, 45 min	Biogenic aragonite	Negative shift in $\delta^{13}C$ and $\delta^{18}O$	Isotope exchange with internal water	Wierzbowski (2007)
	Vacuum roasting, 450 °C, 45 min	Biogenic calcite	No change		Wierzbowski (2007)
	Vacuum roasting, 450 °C, 45 min	Inorganic aragonite	No change		Wierzbowski (2007)
	Vacuum roasting, 450 °C, 45 min	Inorganic calcite	Negative shift or no change in $\delta^{13}C$, no change in $\delta^{18}O$		Wierzbowski (2007)

Note. For the sake of clarity, we only report findings from studies that specifically tested for the effects of these treatments.

2. Materials and Methods

2.1. Preparation of Experimental Material

We simulated realistic, very low TIC/TOC lake sediment by mixing natural lake sediment with two different calcium carbonate standards of known $\delta^{13}C$ and $\delta^{18}O$. The sediment was obtained from core PB86–5 A, a core raised from near the southern margin of Lake Purrumbete in 1986. Lake Purrumbete is a large, deep (>40 m), cheimomictic freshwater maar located in south-eastern Australia (38°16′48″S, 143°13′48″E; Timms, 1976). The lake is contained by a ring of basaltic phreatomagmatic deposits, and the water is alkaline and eutrophic (Ollier, 1967; Tibby et al., 2011). The lake sediment has a high organic matter content (24%), including substantial plant matter, and a low C/N ratio of ~12.5 (Timms, 1976). Two fine-grained calcium carbonate standards were used: M2 ($\delta^{13}C$: 2.8‰ Vienna Pee Dee belemnite (VPDB), $\delta^{18}O$: −7.26‰ VPDB), and P3 ($\delta^{13}C$: 2.23‰ VPDB, $\delta^{18}O$: −0.31‰ VPDB). M2 is a calcite marble, formed during Devonian-aged contact metamorphism of a Silurian limestone, and collected from Marulan, New South Wales. P3 is aragonitic shell carbonate from a giant clam (*Tridacna gigas*), collected live in the 1980s from Palm Island, Queensland.

To ensure that no carbonate was present aside from the two standards, the Lake Purrumbete sediment was acidified prior to creating the mixtures. Approximately 250 cm^3 wet sediment was taken from the top 30 cm of the core, and placed in a large beaker with 200 mL of 1% hydrochloric acid. The sediment was agitated every 30 min for 2 hr, and then the solution was made up to 1 L with ultrapure water, and left to react overnight. After a total of 24 hr of reaction time, the supernatant was decanted off, and the beaker was refilled with ultrapure water, stirred, and left to settle. The rinsing process was repeated 3 times, before the sediment was placed in a freeze drier. The dry sediment was homogenized by gentle grinding with an agate mortar and pestle.

The acid-treated Lake Purrumbete sediment was analyzed with an elemental analyzer to determine the $\delta^{13}C$ of the organic matter, and check for carbonate content. Four subsamples of approximately 2 mg were weighed into silver capsules, and four into tin capsules. Testing for residual carbonate was via the acid-fumigation method—approximately 50 μL deionized water was added to each silver capsule, and then subsamples were acidified for 4 hr in concentrated hydrochloric acid vapor and then left to dry overnight in a 40 °C oven (e.g., Harris et al., 2001). Once dry, the silver capsules were placed inside tin capsules and crimped. The acidified sediment was analyzed alongside the four nonacidified samples. The $\delta^{13}C$ values were

Table 2
Summary of Treatments Applied to Mixtures of Fine-Grained Carbonate in Varying Concentrations, Within Natural Lake Sediment Obtained From Lake Purrumbete

Parameter	Variables
$CaCO_3$ material	M2 (calcite marble), P3 (biogenic aragonite)
$CaCO_3$ concentration	1, 3, 5% (0, 100%)
Oxidizing agent	Acidic 18% H_2O_2, alkaline 18% H_2O_2 (no treatment)
Reaction temperature	4 °C, 25 °C, 50 °C, 75 °C (no treatment)

Note. All reactions were carried out for 24 hr, with each possible combination of variables tested in quadruplicate. To assess the effect of the different oxidative pretreatments, we also measured the $\delta^{13}C$ and $\delta^{18}O$ and of pure lake sediment and pure carbonate (0 and 100% carbonate), as well as mixtures that were not subject to any pretreatment.

indistinguishable (−23.09 ± 0.1‰ VPDB) and uncorrelated with carbon content, and sediment was therefore regarded as carbonate-free.

Pretreatment parameters tested were the pH of the oxidizing agent (H_2O_2), and the temperature at which oxidation occurred. For each combination of reagent and temperature, sufficient Lake Purrumbete sediment was added to 1 mg of each of the pure reference carbonates to make mixtures of approximately 1, 3, and 5% carbonate. Samples containing 0 and 100% carbonate were also subject to each pretreatment. Prior to oxidation at each temperature, two solutions of fresh 18% H_2O_2 were prepared from reagent-grade 30% H_2O_2: one pure (pH ≈ 4), and one buffered to a pH of 8 using sodium hydroxide (NaOH), following the NIOZ protocol outlined in Fallet et al. (2009; hereafter referred to as acidic H_2O_2 and alkaline H_2O_2). In brief, the acidic 18% H_2O_2 solution was prepared by mixing 300 mL 30% H_2O_2 with 200 mL ultrapure water, and the alkaline 18% H_2O_2 solution was prepared by mixing 20 mL 0.5 M NaOH, 240 mL 30% H_2O_2, and 200 mL ultrapure water. All samples were tested in quadruplicate, resulting in a total of 324 samples; a summary of all tested variables is provided in Table 2.

2.2. Organic Matter Oxidation

To test oxidation at 4 °C, the NaOH, 30% H_2O_2, and ultrapure water were refrigerated overnight prior to preparation of the oxidizing solutions as above. A 2-mL aliquot of reagent was added to each vial, and gently shaken to thoroughly mix the reagent with the sediment. The samples were placed in a refrigerator at 4 °C, and gently agitated every 15 min. After 1 hr of reaction time, a further 2 mL of reagent was added. This procedure was repeated until a total of 10 mL of reagent had been added to each vial. Each time the samples were agitated, the pH of several vials was measured using pH indicator paper, to check that the pH did not fluctuate by more than one unit. The samples were subsequently agitated each hour for 5 hr, and then left to react in the refrigerator overnight. After a total reaction time of 24 hr, each vial was filled with ultrapure water and centrifuged, and then the supernatant liquid was decanted. The samples were rinsed 4 times with ultrapure water and then freeze-dried.

To test oxidation at 25 °C, the above procedure was repeated, but the reaction was performed out in a room with the temperature controlled at 25 °C, using solutions that were previously equilibrated to room temperature. For oxidation at 50 °C and 75 °C, the reaction was carried out in an oven.

2.3. Sample Analysis

2.3.1. Stable Isotope Analysis

All pretreated samples were transferred to borosilicate exetainers for stable isotope analysis at the University of Adelaide. We also analyzed samples at each concentration that had not undergone any pretreatment. Samples were digested in 105% H_3PO_4 at 70 °C for a minimum of 1 hr, and measurements were made on the evolved CO_2 gas following the method of Spötl and Vennemann (2003). Measurements were made on a Nu Instruments GasPrep in-line with a Nu-Horizon continuous flow isotope ratio mass spectrometer. Standardization was based on in-house ANU-P3 ($\delta^{13}C$: 2.24‰, $\delta^{18}O$: −0.32‰), UAC-1 ($\delta^{13}C$: −15‰, $\delta^{18}O$: −18.4‰), and IAEA CO-8 ($\delta^{13}C$: −5.76‰, $\delta^{18}O$: −22.7‰) standards, which have been calibrated against international standards. Analytical precision (1σ) for replicate measurements of the standards was ±0.1‰. The CO_2 peak heights returned by the continuous flow isotope ratio mass spectrometer were used to calculate the volume of carbonate measured in each sample, which in turn was used to approximate the posttreatment carbonate concentration. Seven of the 324 samples returned CO_2 peak sizes that were too small for reliable calculation of isotopic composition. The $\delta^{13}C$ and $\delta^{18}O$ values are reported in per mille units relative to the Vienna Pee Dee belemnite (VPDB) standard.

2.3.2. Scanning Electron Microscope Imaging

To investigate any structural or mineralogical alteration to the carbonate during pretreatment, the simulated lake sediment was imaged using a Phillips XL30 field emission scanning electron microscope equipped with a thin film energy-dispersive X-ray spectroscopy detector, at 30-mm working distance and 10-kV accelerating

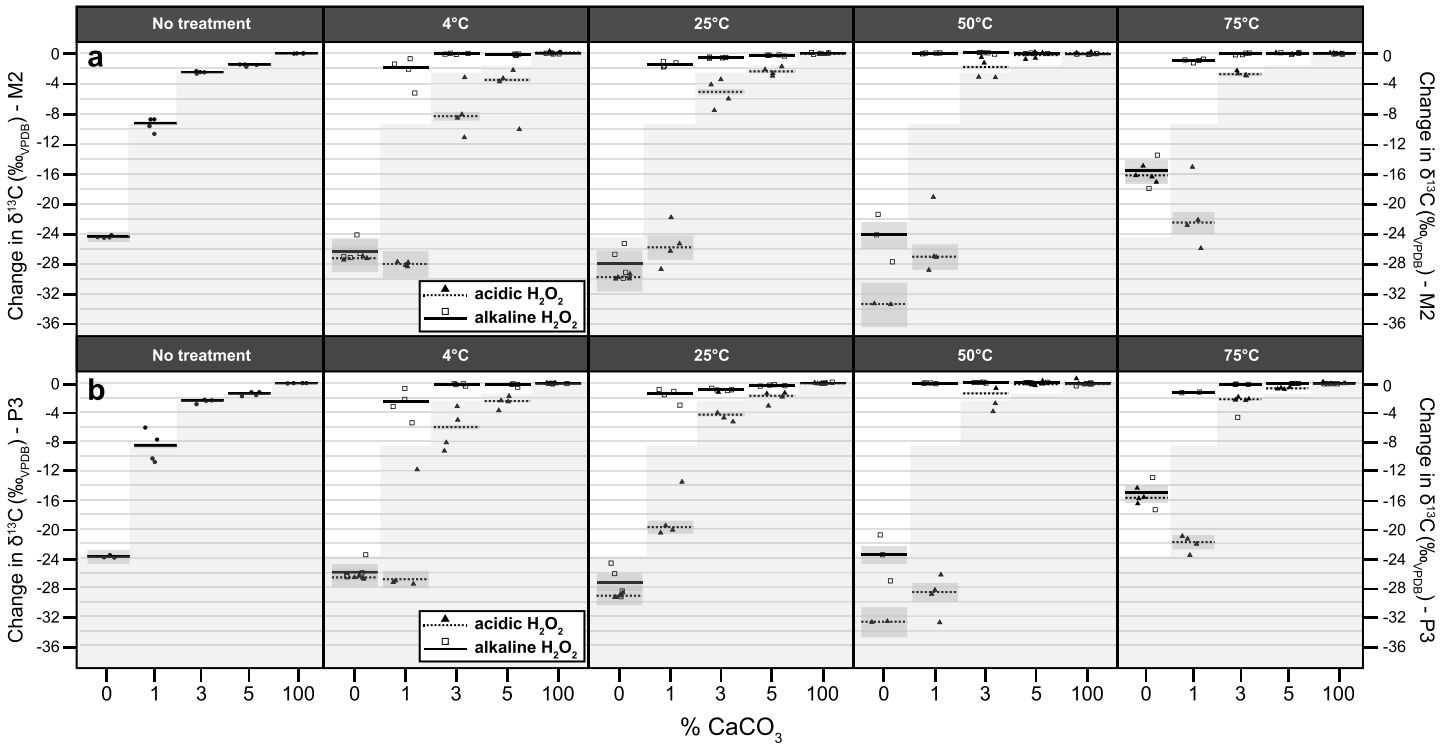

Figure 1. (a) Comparison of the effect of oxidative pretreatments on the measured $\delta^{13}C$ of mixtures of M2 carbonate standard (calcite; $\delta^{13}C$: 2.8‰ VPDB) in varying concentrations, within natural lake sediment. Sediment mixtures were treated with 18% H_2O_2 (dotted line/filled triangles) or 18% H_2O_2 that was buffered to a pH of 8 with NaOH (solid line/outlined squares), at four different temperatures. Values are presented as deviations from the $\delta^{13}C$ of pure, untreated M2 carbonate. Horizontal bars denote the fitted model value for each combination of experimental parameters, and gray windows show the 95% confidence interval. Points denote the partial residuals from individual analyses. The leftmost panel shows results from mixtures of M2 carbonate and lake sediment that were not subject to any pretreatment; these are shown as gray steps on each plot window for comparison. (b) All as per (a) but for the P3 carbonate standard (aragonite; $\delta^{13}C$: 2.23‰ VPDB).

voltage. We imaged untreated carbonate grains, as well as mixtures of sediment and carbonate that were treated with either acidic or alkaline H_2O_2, in both cases at 25 °C.

2.4. Statistical Analysis

We used a balanced three-way analysis of variance to determine whether the treatment parameters (acidic or alkaline H_2O_2, reaction temperature) and initial carbonate concentration resulted in significantly different $\delta^{13}C$ and $\delta^{18}O$ values. The response variables ($\delta^{13}C$ and $\delta^{18}O$) were rescaled so that all values were positive prior to analysis. We used robust linear models for model fitting because the variance more closely approximated a *t*-distribution than a Gaussian distribution. We used type II sums of squares and set α to 0.05 a priori. All analysis of variance computations were performed using the "MASS" package (Venables & Ripley, 2002) in R (R Core Team, 2017) and estimated marginal mean effects were calculated using the "visreg" package (Breheny & Burchett, 2017). Estimates were back-transformed to their original scale for plotting.

3. Results

For each carbonate standard, the highest-order interaction among all three factors (temperature, reagent, and carbonate concentration) was significant for both $\delta^{13}C$ and $\delta^{18}O$ (Table S1 in the supporting information). The $\delta^{13}C$ and $\delta^{18}O$ data are presented in Figures 1 and 2 as deviation from the stable isotope composition of the pure, untreated carbonate.

For samples that were not subject to any pretreatment, the measured $\delta^{13}C$ and $\delta^{18}O$ of all mixtures differed significantly from the true values for both the M2 and P3 standards (Figures 1 and 2 and Table S1). Detectable CO_2 was evolved from the pure lake sediment, which returned the most negative $\delta^{13}C$ and $\delta^{18}O$ values. The values of all mixtures were negatively biased, and the bias increased with decreasing carbonate concentration.

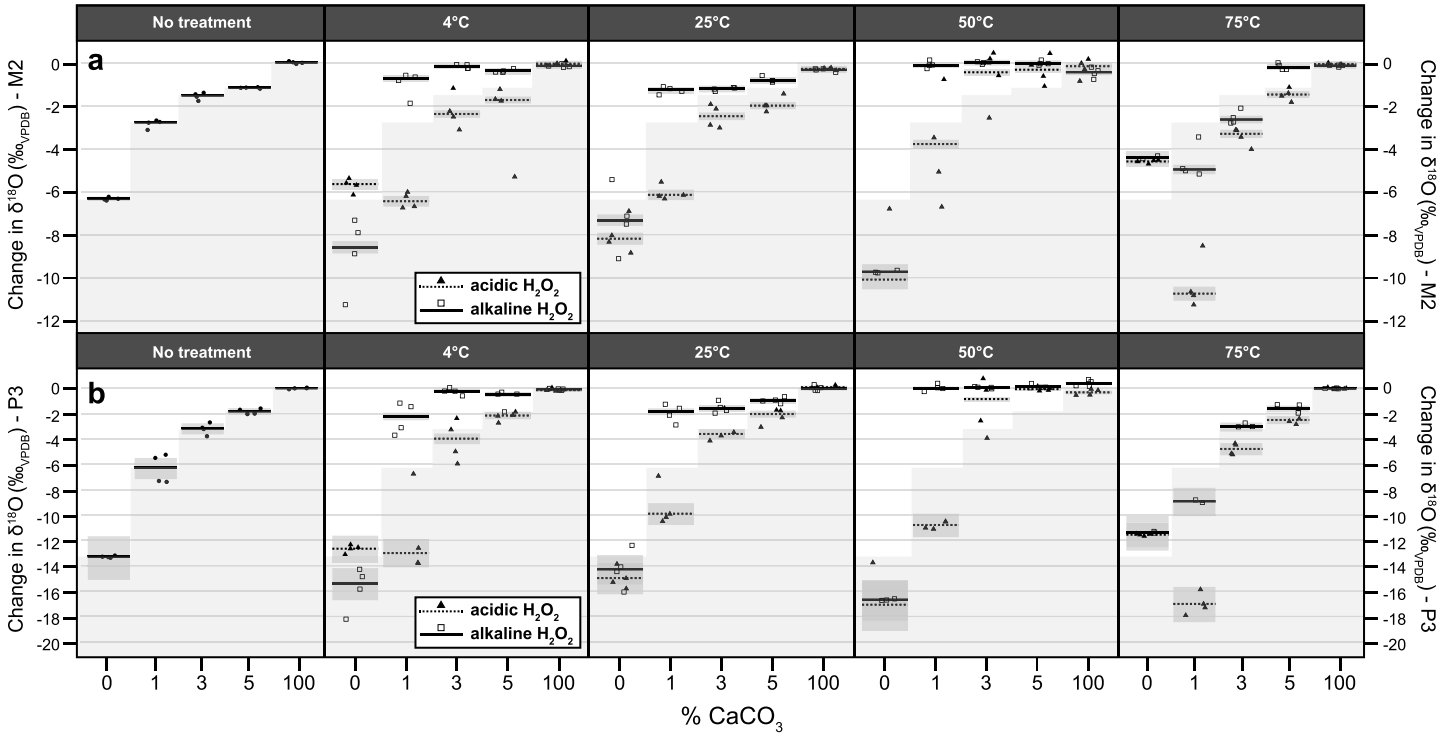

Figure 2. Same as Figure 1 but for $\delta^{18}O$ (M2 $\delta^{18}O$: −7.26‰ VPDB; P3 $\delta^{18}O$: −0.31‰ VPDB).

The posttreatment carbonate concentrations for the eight different treatments fell into two distinct populations—samples subject to oxidation by acidic H_2O_2 at the four temperatures and samples subject to oxidation by alkaline H_2O_2 at the four temperatures (Figure 3). In all cases, the posttreatment carbonate concentration was significantly higher in the samples treated with alkaline H_2O_2. A linear relationship with slopes ranging from 5 to 10.9 indicates a high degree of organic matter removal (Figure 3a). Conversely, samples oxidized with acidic H_2O_2 lie along slopes between 0.4 and 1.1, indicating either very little removal of organic matter, or in fact some loss of carbonate (Figure 3b). For alkaline H_2O_2 and acidic H_2O_2, the most organic matter removal occurred at 75 °C and 25 °C, respectively.

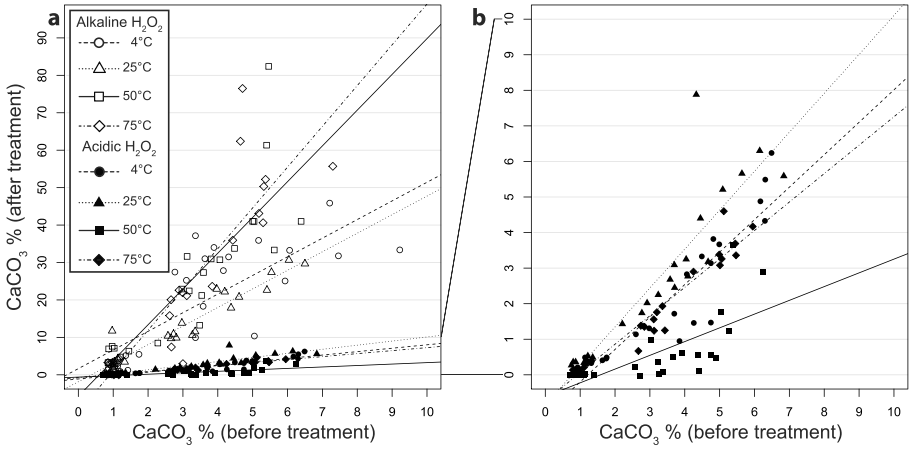

Figure 3. Cross plots showing the percentage of calcium carbonate after treatment with either acidic (pH ≈ 4) or alkaline (pH ≈ 8) H_2O_2 at four different temperatures, compared with the initial percentage within natural lake sediment. (a) All samples plotted on the same axes, showing two distinct populations: samples that were treated with acidic H_2O_2 (lower slopes) and samples that were treated with alkaline H_2O_2 (higher slopes). (b) Only samples that were treated with acidic H_2O_2, with the same scale on the *x* and *y* axes.

Both the pH of the H_2O_2 and the temperature of reaction had a significant effect on the measured $\delta^{13}C$ and $\delta^{18}O$ of the simulated lake sediment (Table S1), with a larger effect at lower starting carbonate concentrations (Figures 1 and 2). Pretreatment of the simulated lake sediment with alkaline H_2O_2 resulted in model $\delta^{13}C$ values that were invariably more accurate than both the sediment that was not pretreated, and the sediment that was treated with acidic H_2O_2 (Figure 1). The $\delta^{18}O$ values of sediment treated with alkaline H_2O_2 were generally more accurate than those resulting from pretreatment with acidic H_2O_2, or from sediment that was not pretreated (Figure 2). The major exception to this was treatment at 75 °C, where the accuracy of the $\delta^{18}O$ values was not improved by any pretreatment. For both standards, the most accurate values were returned by mixtures subject to oxidation with alkaline H_2O_2 at 50 °C.

The negative bias in $\delta^{18}O$ was much greater for the P3 (biogenic aragonite; $\delta^{18}O$: −0.31‰ VPDB) standard than the M2 (crystalline calcite; $\delta^{18}O$: −7.26‰ VPDB) standard (note the difference in the scale of the *y* axis in Figures 2a and 2b). Where samples of 100% carbonate were subject to pretreatment, in all cases, the $\delta^{13}C$ values were both accurate and precise. The $\delta^{18}O$ values are slightly less accurate, and display some scatter, especially for samples treated with acidic H_2O_2.

4. Discussion

Our results clearly demonstrate that $\delta^{13}C$ and $\delta^{18}O$ values of fine-grained carbonate in very low concentrations within natural lake sediment, measured with no pretreatment, differ significantly from those of the pure carbonate. This confirms the findings of similar studies (e.g., Lebeau et al., 2014), indicating that sediment with low TIC/TOC is affected by an "organic bias," and requires pretreatment in order to obtain accurate C and O stable isotope determinations. For lake sediment that was treated with H_2O_2 to oxidize organic matter prior to analysis, different reaction parameters resulted in significant differences in both the efficacy of organic matter removal, and the measured $\delta^{13}C$ and $\delta^{18}O$.

Bias in the measured stable isotope composition of pretreated sediment/carbonate mixtures was almost uniformly negative, that is, toward the values returned from analysis of carbonate-free lake sediment. This effect was particularly strong in samples with extremely low TIC/TOC, and in sediment that was subject to oxidation with acidic H_2O_2. The effect was also larger for $\delta^{18}O$ at high temperatures, indicating that chemical treatment of carbonate at high temperature could be particularly detrimental to accurate oxygen stable isotope analyses.

For paleoclimate studies where oxidation of organic matter is required, H_2O_2 is generally used in its pure form despite being acidic, as it has been considered a less effective oxidizing agent if buffered to an alkaline pH (Gaffey & Bronnimann, 1993; Hosking, 1932). H_2O_2 is thermodynamically unstable, and decomposes into water and oxygen; this decomposition is accelerated by both high pH, and the higher temperatures that are often applied to reduce reaction time (Nicoll & Smith, 1955; Schultz et al., 1999). However, our results indicate that oxidation with alkaline H_2O_2 removes around 5 times as much organic matter as oxidation with acidic H_2O_2 (Figure 3). This apparent contradiction may be due in part to the composition of the Lake Purrumbete sediment. The molecular composition of the organic matter in Lake Purrumbete has not been determined; however, the sediment contains abundant plant material (Timms, 1976). Vascular plants produce lignin, a complex organic polymer that is resistant to diagenesis, so that it is preferentially preserved in lake sediment (Meyers & Ishiwatari, 1993). Solubilization of lignin by H_2O_2 has been shown to be more effective at high pH, owing to increased presence of molecular oxygen and other radical species produced by the rapid decomposition of H_2O_2 (Xiang & Lee, 2000). The ability for these species to degrade lignin is increased at higher temperatures; this fits well with our results, where the greatest removal of organic matter by alkaline H_2O_2 occurred at 75 °C (Figure 3). This also suggests that lignins contribute to residual organic carbon in mixtures treated with acidic H_2O_2, and confirms that specific lake sediment composition is an important factor in choice of reagent; for example, for lake sediment that is rich in terrestrial plant matter, the organic bias may be more effectively reduced by oxidation with alkaline H_2O_2.

Not only did oxidation with alkaline H_2O_2 remove a much larger proportion of organic matter from the simulated lake sediment samples than oxidation with acidic H_2O_2, but it also resulted in uniformly more accurate $\delta^{13}C$ and $\delta^{18}O$. This must be due in part to the greater increase in TIC/TOC (cf. Oehlerich et al., 2013), resulting in relatively less organic bias.

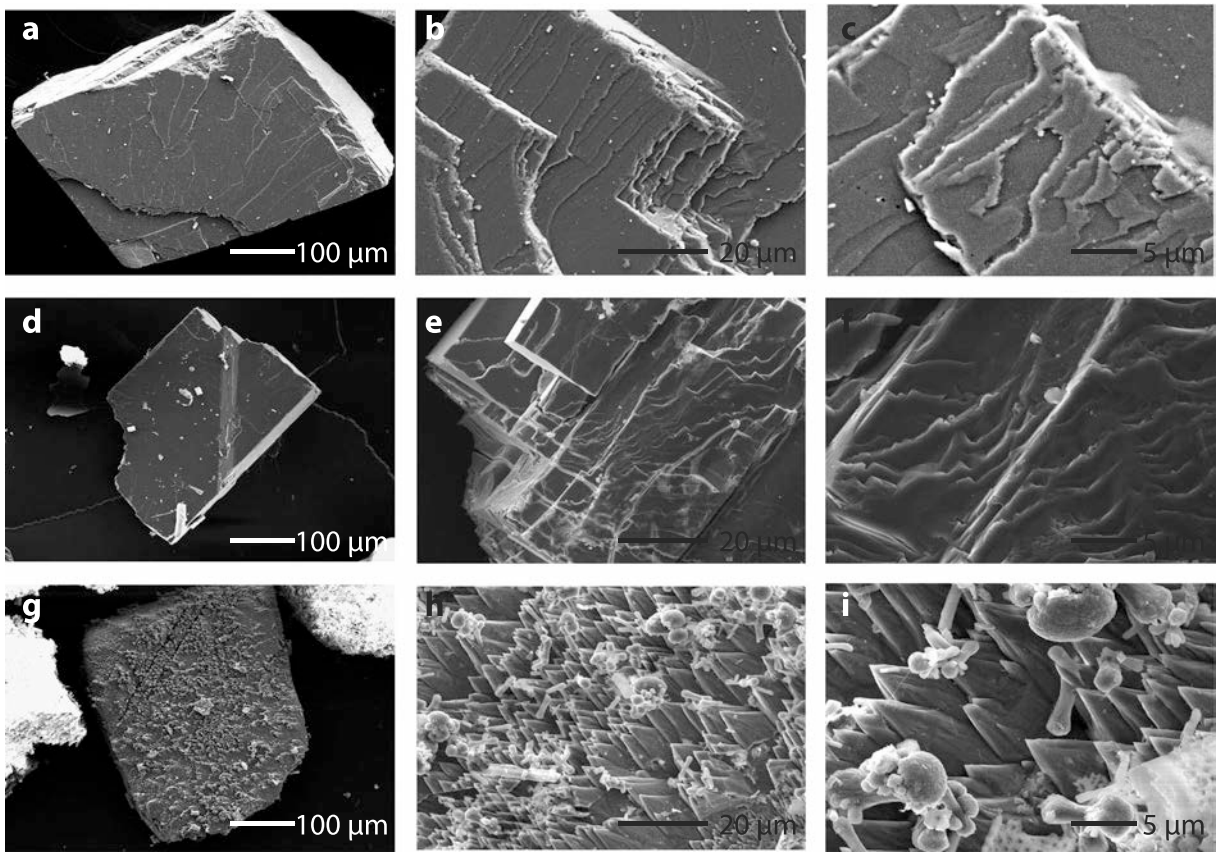

Figure 4. Scanning electron micrographs of M2 calcite grains, showing the effect of acidic or alkaline oxidative pretreatment on crystal morphology. Both reactions were carried out for 24 hr, at 25 °C. (a–c) M2 standard prior to any pretreatment: regular, plate-like calcite crystalline morphology. (d–f) M2 carbonate after reaction with alkaline 18% H_2O_2. Note that the crystal structure remains unchanged at all scales. (g–i) M2 carbonate after reaction with acidic 18% H_2O_2, in the presence of natural lake sediment. Note the appearance of new carbonate morphologies, including elongated laminated microparticles on the grain surface, with rhombohedral calcite crystals, alongside with dumbbell-like crystals, and cauliflower-like polycrystalline aggregates typical of vaterite (h and i).

The deviation of values following exposure to acidic H_2O_2 is also a strong argument for partial dissolution of fine-grained carbonate, that is, a "treatment bias." This is supported by the scanning electron microscope imaging. Images of the standards prior to treatment reveal distinct carbonate morphologies: M2 grains are characterized by well-defined platy calcite layers (Figures 4a–4c), and P3 grains are composed of relatively poorly structured aragonite (Figures 5a–5c). Grains that were subject to the alkaline H_2O_2 pretreatment are structurally indistinguishable from untreated grains, both at the scale of an entire grain and on a submicron scale (Figures 4a–4f and 5a–5f). However, grains within sediment treated with the acidic H_2O_2 show major structural changes on the surface of the grains, as well as the appearance of new carbonate morphologies (Figures 4g–4i and 5g–5i). M2 calcite grains developed a surficial morphology characterized by elongate rhombohedral crystals, and adhered to the grain surfaces were discrete rhombohedral calcite crystals, dumbbell-shaped crystals, and cauliflower-like polycrystalline aggregates (Figures 4h and 4i). The latter are characteristic of vaterite (Boyjoo et al., 2014), a metastable polymorph of calcium carbonate ($CaCO_3$) that may form subject to certain conditions including pH, water chemistry, presence of organic compounds, and the substrate (Pochitalkina et al., 2016; Ren et al., 2011; Zhao et al., 2011). The surficial structure of the P3 aragonite grains was altered from an irregular thalloid texture (Figure 5b) to elongate platy crystals (Figure 5h). Individual needle-shaped crystals and clusters of rod-like crystals—both typical aragonite morphologies—also appeared, alongside rare cauliflower-shaped aggregates similar to those seen on the M2 carbonate (Figures 5h and 5i). The composition—including presence of organic compounds—of a solution from which $CaCO_3$ precipitates is an important factor in determining the morphology of $CaCO_3$ crystals (Konopacka-Łyskawa et al., 2017). The variety of morphologies present in samples treated with acidic H_2O_2 indicates unequivocally that new carbonate was precipitated during the reaction. By contrast, the absence

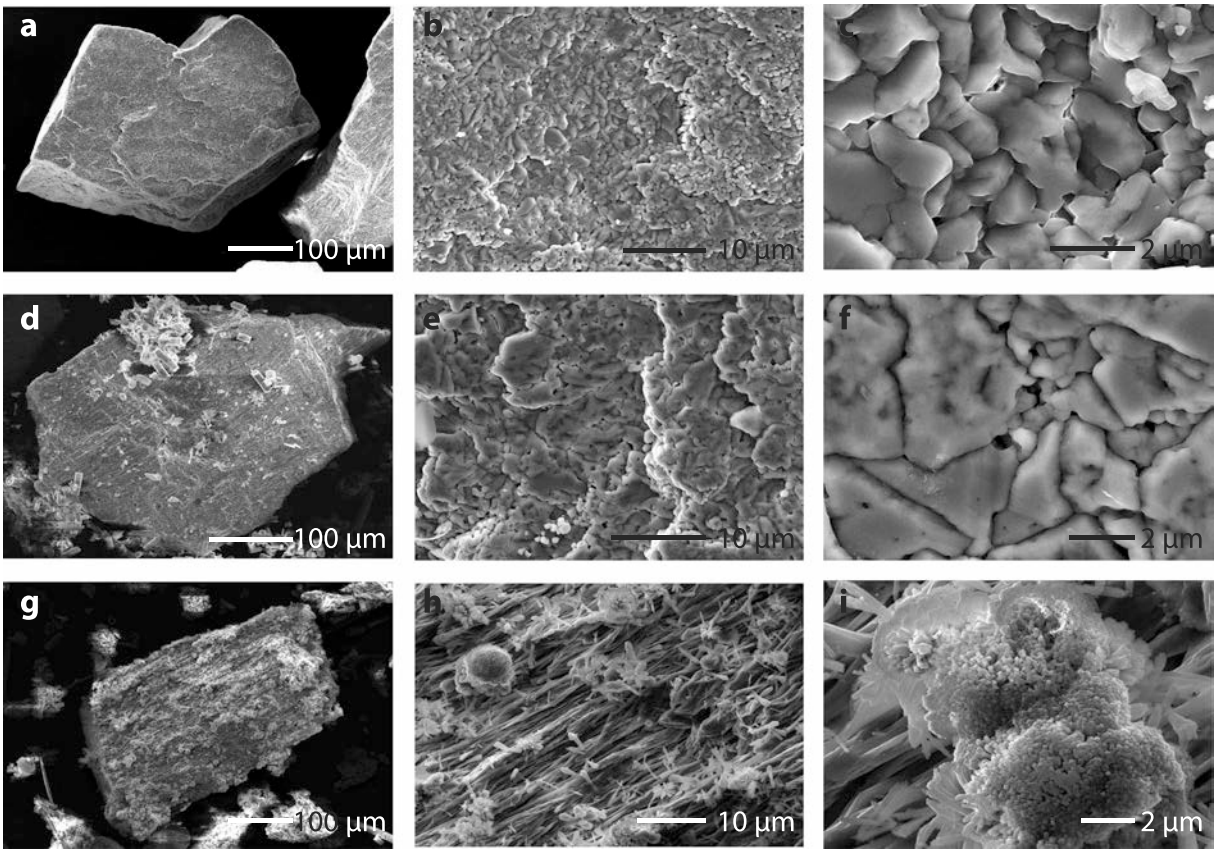

Figure 5. Scanning electron micrographs of P3 aragonite grains, as per Figure 4. (a–c) P3 standard prior to any pretreatment: an aragonite crystal with irregular thalloid surface morphology. (d–f) P3 carbonate after reaction with alkaline 18% H_2O_2. Note that the crystal structure remains unchanged at all scales. (g–i) P3 carbonate after reaction with acidic 18% H_2O_2, in the presence of natural lake sediment. Note the appearance of new carbonate morphologies, including discrete needle-like and cauliflower-shaped crystals (h) alongside aggregates of rod-like crystals (i).

of new carbonate morphologies in the samples treated with alkaline H_2O_2 suggests that dissolution and reprecipitation was prevented by buffering the H_2O_2 to pH 8.

While the alkaline H_2O_2 treatment resulted in more accurate $\delta^{13}C$ and $\delta^{18}O$ values than the acidic H_2O_2 at all tested temperatures, the temperature of reaction also had a significant influence on the measured values. During treatment with alkaline H_2O_2 at 4 °C and 25 °C, the $\delta^{13}C$ and $\delta^{18}O$ of both carbonates at 1% concentration maintained a negative bias of several per mille, and this bias was also present at 3 and 5% in the $\delta^{18}O$ of samples treated at 25 °C. These are the two temperatures at which the least organic matter was removed (Figure 3), resulting in lower TIC/TOC at the time of measurement. Given there was no evidence for the precipitation of new carbonate during treatment with alkaline H_2O_2, it is likely that the residual organic matter evolved detectable CO_2, resulting in an organic bias.

The $\delta^{13}C$ of the mixtures treated at 75 °C was accurate for starting concentrations of 3 and 5%, and only slightly offset at 1%. However, the $\delta^{18}O$ values are heavily biased, with negative offsets of up to -5 and -9‰ in mixtures of 1% M2 and P3 carbonates, respectively (Figure 2). There was also generally no improvement on samples that were subject to no pretreatment. The organic bias in these samples was most likely minimal, given that this was the treatment at which the most organic matter was removed (Figure 3), and so this must represent a treatment bias. The similarity in $\delta^{18}O$ between the samples treated with acidic versus alkaline H_2O_2 at 75 °C suggests that at high temperatures, some new carbonate precipitation did occur. At temperatures over $>$70 °C, H_2O_2 decomposes rapidly, particularly at an alkaline pH (Schultz et al., 1999). We did not image samples treated at high temperature; however, at a temperature $>$70 °C, the supply of alkaline reagent may have been exhausted (Mikutta et al., 2005), allowing acidic oxidation products to lower the solution pH sufficiently to dissolve carbonate. Hence, 50 °C was the only temperature at which treatment with alkaline H_2O_2 did not result in any discernible organic or treatment bias.

Regarding the use of $\delta^{13}C$ and $\delta^{18}O$ from fine-grained lacustrine carbonate for paleoclimate reconstructions, our results demonstrate that with appropriate pretreatment, lake sediment with very low TIC/TOC may indeed yield accurate values that may be used to interpret past environmental change. However, given the large between-treatment range—especially for $\delta^{18}O$, which is commonly used in quantitative climate reconstructions—a degree of circumspection is essential when comparing published results where different H_2O_2 treatment parameters were used. This will be particularly important where pretreatment was carried out at a high temperature, with an acidic reagent, or on sediment that has very low starting TIC/TOC. We also note that these results are specific to the Lake Purrumbete sediment and that sediments containing different organic compounds will almost certainly result in different degrees of bias (Mikutta et al., 2005; Oehlerich et al., 2013). Nevertheless, alkaline H_2O_2 is clearly efficient in removal of organic compounds commonly found in lakes, and provides a starting point for determination of optimal treatment parameters for a wider variety of lake sediments. For individual lakes, a straightforward test may be to acidify a sediment subsample, subject this subsample to oxidation by alkaline H_2O_2 at varying temperatures and durations, and in this way determine optimal parameters for removal of organic compounds specific to the sediment. Our results may also be applicable to diatom $\delta^{18}O$ studies, where it is essential that all organic material in the surrounding sediment is removed prior to analysis (Leng & Barker, 2006; Tyler et al., 2007).

One parameter not tested here is the temperature at which H_3PO_4 digestion occurs prior to analysis. In our case, this was performed at 70 °C. However, digestion at lower temperatures for a longer time period may result in a lower organic bias. This should be tested in future work.

5. Conclusions

The $\delta^{13}C$ and $\delta^{18}O$ of fine-grained carbonate preserved within organic-rich lacustrine sediments may provide valuable information about how the climate has varied in the past. If the TIC/TOC of the measured bulk sediment is low (<0.3; Oehlerich et al., 2013), then an organic bias arises due to contribution of CO_2 evolved from organic compounds. The TIC/TOC may be raised by oxidation of organic matter with H_2O_2; however, this may induce a treatment bias resulting from dissolution and reprecipitation of carbonate under acidic conditions. We tested the effects of pretreatment with acidic or alkaline H_2O_2 at different temperatures, on the measured $\delta^{13}C$ and $\delta^{18}O$ of very small amounts (≤5%) of fine-grained carbonate standards within a natural lake sediment matrix, and present the following key findings and recommendations:

1. Pretreatment of lacustrine sediment with alkaline H_2O_2 at 50 °C results in accurate carbonate $\delta^{13}C$ and $\delta^{18}O$ values, even for initial carbonate concentrations as low as 1%. This combination of treatment parameters not only avoids the bias associated with partial dissolution of carbonate but also is more efficient in the oxidation of some organic compounds. This may be particularly relevant to lacustrine sediment that contains a high proportion of material derived from vascular land plants.
2. Oxidation of organic material with acidic H_2O_2 results in partial dissolution and reprecipitation of carbonate, leading to a treatment bias. Oxidation with hot (75 °C) alkaline H_2O_2 also results in a treatment bias, possibly due to the production of organic acids in conjunction with rapid decomposition of the alkaline reagent. We recommend avoiding treatment with hot or acidic H_2O_2 in all cases.
3. Scanning electron microscope imaging of sediment before and after treatment is a useful tool to determine if new carbonate has precipitated during treatment; the appearance of new crystal morphologies is a reliable positive indicator of carbonate dissolution and reprecipitation.
4. The lack of methodological consistency in oxidative pretreatments that is evident in the paleoclimatological literature, even between H_2O_2-based treatments, may preclude rigorous comparison of climate interpretations derived from the absolute $\delta^{13}C$ and $\delta^{18}O$ values of lacustrine carbonates.

Acknowledgments
This research was supported in part by an ARC Discovery Project (grant DP140014093). The authors are grateful to Mark Rollog for the assistance in lab analyses. Professor Allan Chivas kindly provided carbonate standard material. G. Falster was supported during this research by an Australian Government Research Training Program Scholarship and an AINSE Limited Postgraduate Research Award (grant ALNSTU11873). Anne Juillet-Leclerc and one anonymous reviewer provided suggestions which improved the clarity of the manuscript. Experimental data are provided in Table S2 in the supporting information.

References

Boiseau, M., & Juillet-Leclerc, A. (1997). H_2O_2 treatment of recent coral aragonite: Oxygen and carbon isotopic implications. *Chemical Geology*, *143*(3-4), 171–180. https://doi.org/10.1016/S0009-2541(97)00112-5

Boyjoo, Y., Pareek, V. K., & Liu, J. (2014). Synthesis of micro and nano-sized calcium carbonate particles and their applications. *Journal of Materials Chemistry A*, *2*(35), 14,270–14,288. https://doi.org/10.1039/C4TA02070G

Breheny, P., & Burchett, W., 2017. visreg: Visualization of regression models, R package version 2.4–1 ed.

Chivas, A. R., Deckker, P. D., & Shelley, J. M. G. (1986). Magnesium and strontium in non-marine ostracod shells as indicators of palaeosalinity and palaeotemperature. *Hydrobiologia*, *143*(1), 135–142. https://doi.org/10.1007/BF00026656

Cook, E. J. (2009). A record of late Quaternary environments at lunette-lakes Bolac and Turangmoroke, western Victoria, Australia, based on pollen and a range of non-pollen palynomorphs. *Review of Palaeobotany and Palynology*, *153*(3-4), 185–224. https://doi.org/10.1016/j.revpalbo.2008.07.001

Core Team, R. (2017). *R: A Language and Environment for Statistical Computing*. Vienna, Austria: R Foundation for Statistical Computing.

Fallet, U., Boer, W., van Assen, C., Greaves, M., & Brummer, G.-J. A. (2009). A novel application of wet oxidation to retrieve carbonates from large organic-rich samples for ocean-climate research. *Geochemistry, Geophysics, Geosystems*, *10*, Q08004. https://doi.org/10.1029/2009GC002573

Falster, G., Tyler, J., Grant, K., Tibby, J., Turney, C., Löhr, S., et al. (2018). Millennial-scale variability in south-east Australian hydroclimate between 30,000 and 10,000 years ago. *Quaternary Science Reviews*, *192*, 106–122. https://doi.org/10.1016/j.quascirev.2018.05.031

Feldmeijer, W., Metcalfe, B., Scussolini, P., & Arthur, K. (2013). The effect of chemical pretreatment of sediment upon foraminiferal-based proxies. *Geochemistry, Geophysics, Geosystems*, *14*, 3996–4014. https://doi.org/10.1002/ggge.20233

Gaffey, S. J., & Bronnimann, C. E. (1993). Effects of bleaching on organic and mineral phases in biogenic carbonates. *Journal of Sedimentary Petrology*, *63*(4), 752–754. https://doi.org/10.1306/D4267BE0-2B26-11D7-8648000102C1865D

Ganssen, G. (1981). Isotopic analysis of foraminifera shells: Interference from chemical treatment. *Palaeogeography, Palaeoclimatology, Palaeoecology*, *33*(1-3), 271–276. https://doi.org/10.1016/0031-0182(81)90043-2

Grottoli, A. G., Rodrigues, L. J., Matthews, K. A., Palardy, J. E., & Gibb, O. T. (2005). Pre-treatment effects on coral skeletal $\delta^{13}C$ and $\delta^{18}O$. *Chemical Geology*, *221*(3-4), 225–242. https://doi.org/10.1016/j.chemgeo.2005.05.004

Harris, D., Horwath, W. R., & van Kessel, C. (2001). Acid fumigation of soils to remove carbonates prior to total organic carbon or carbon-13 analysis. *Soil Science Society of America Journal*, *65*(6), 1853–1856. https://doi.org/10.2136/sssaj2001.1853

Holmes, J. A. (1996). Trace-element and stable-isotope geochemistry of non-marine ostracod shells in quaternary palaeoenvironmental reconstruction. *Journal of Paleolimnology*, *15*(3), 223–235. https://doi.org/10.1007/BF00213042

Holmes, J. A., Tindall, J., Roberts, N., Marshall, W., Marshall, J. D., Bingham, A., et al. (2016). Lake isotope records of the 8200-year cooling event in western Ireland: Comparison with model simulations. *Quaternary Science Reviews*, *131*, 341–349. https://doi.org/10.1016/j.quascirev.2015.06.027

Hosking, J. S. (1932). The influence of hydrogen-ion concentration on the decomposition of soil organic matter by hydrogen peroxide. *The Journal of Agricultural Science*, *22*(01), 92–100. https://doi.org/10.1017/S0021859600053119

Hyvåinen, H., Martma, T., & Punning, J.-M. (1990). Stable isotope and pollen stratigraphy of a Holocene lake marl section from NE Finland. *Boreas*, *19*, 17–24.

Keatings, K. W., Holmes, J. A., & Heaton, T. H. E. (2006). Effects of pre-treatment on ostracod valve chemistry. *Chemical Geology*, *235*(3-4), 250–261. https://doi.org/10.1016/j.chemgeo.2006.07.003

Konopacka-Łyskawa, D., Kościelska, B., & Karczewski, J. (2017). Controlling the size and morphology of precipitated calcite particles by the selection of solvent composition. *Journal of Crystal Growth*, *478*, 102–110. https://doi.org/10.1016/j.jcrysgro.2017.08.033

Lebeau, O., Busigny, V., Chaduteau, C., & Ader, M. (2014). Organic matter removal for the analysis of carbon and oxygen isotope compositions of siderite. *Chemical Geology*, *372*, 54–61. https://doi.org/10.1016/j.chemgeo.2014.02.020

Leng, M. J., & Barker, P. A. (2006). A review of the oxygen isotope composition of lacustrine diatom silica for palaeoclimate reconstruction. *Earth-Science Reviews*, *75*(1-4), 5–27. https://doi.org/10.1016/j.earscirev.2005.10.001

Leng, M. J., & Marshall, J. D. (2004). Palaeoclimate interpretation of stable isotope data from lake sediment archives. *Quaternary Science Reviews*, *23*(7-8), 811–831. https://doi.org/10.1016/j.quascirev.2003.06.012

McCrea, J. M. (1950). On the isotopic chemistry of carbonates and a paleotemperature scale. *The Journal of Chemical Physics*, *18*(6), 849–857. https://doi.org/10.1063/1.1747785

Meyers, P. A., & Ishiwatari, R. (1993). Lacustrine organic geochemistry—An overview of indicators of organic matter sources and diagenesis in lake sediments. *Organic Geochemistry*, *20*(7), 867–900. https://doi.org/10.1016/0146-6380(93)90100-P

Mikutta, R., Kleber, M., Kaiser, K., & Jahn, R. (2005). Organic matter removal from soils using hydrogen peroxide, sodium hypochlorite, and disodium peroxodisulfate. *Soil Science Society of America Journal*, *69*(1), 120–135. https://doi.org/10.2136/sssaj2005.0120

Nagtegaal, R., Grove, C. A., Kasper, S., Zinke, J., Boer, W., & Brummer, G.-J. A. (2012). Spectral luminescence and geochemistry of coral aragonite: Effects of whole-core treatment. *Chemical Geology*, *318–319*, 6–15.

Nicoll, W. D., & Smith, A. F. (1955). Stability of dilute alkaline solutions of hydrogen peroxide. *Industrial and Engineering Chemistry*, *47*(12), 2548–2554. https://doi.org/10.1021/ie50552a051

Oehlerich, M., Baumer, M., Lücke, A., & Mayr, C. (2013). Effects of organic matter on carbonate stable isotope ratios ($\delta^{13}C$, $\delta^{18}O$ values)—Implications for analyses of bulk sediments. *Rapid Communications in Mass Spectrometry*, *27*(6), 707–712. https://doi.org/10.1002/rcm.6492

Ollier, C. D. (1967). Maars their characteristics, varieties and definition. *Bulletin Volcanologique*, *31*(1), 45–73. https://doi.org/10.1007/BF02597005

Pochitalkina, I. A., Kekin, P. A., Morozov, A. N., Kondakov, D. F., & Petropavlovskii, I. A. (2016). Morphology of calcium carbonate prepared via homogeneous synthesis. *Russian Journal of Inorganic Chemistry*, *61*(11), 1392–1396. https://doi.org/10.1134/S0036023616110152

Ren, D., Feng, Q., & Bourrat, X. (2011). Effects of additives and templates on calcium carbonate mineralization in vitro. *Micron*, *42*(3), 228–245. https://doi.org/10.1016/j.micron.2010.09.005

Schultz, M. K., Biegalski, S. R., Inn, K. G. W., Yu, L., Burnett, W. C., Thomas, J. L. W., & Smith, G. E. (1999). Optimizing the removal of carbon phases in soils and sediments for sequential chemical extractions by coulometry. *Journal of Environmental Monitoring*, *1*(2), 183–190. https://doi.org/10.1039/a900534j

Schwander, J., Eicher, U., & Ammann, B. (2000). Oxygen isotopes of lake marl at Gerzensee and Leysin (Switzerland), covering the younger Dryas and two minor oscillations, and their correlation to the GRIP ice core. *Palaeogeography, Palaeoclimatology, Palaeoecology*, *159*(3-4), 203–214. https://doi.org/10.1016/S0031-0182(00)00085-7

Serrano, O., Serrano, L., & Mateo, M. A. (2008). Effects of sample pre-treatment on the $\delta^{13}C$ and $\delta^{18}O$ values of living benthic foraminifera. *Chemical Geology*, *257*(3-4), 218–220. https://doi.org/10.1016/j.chemgeo.2008.09.013

Spötl, C., & Vennemann, T. W. (2003). Continuous-flow isotope ratio mass spectrometric analysis of carbonate minerals. *Rapid Communications in Mass Spectrometry*, *17*(9), 1004–1006. https://doi.org/10.1002/rcm.1010

Stuiver, M. (1970). Oxygen and carbon isotope ratios of fresh-water carbonates as climatic indicators. *Journal of Geophysical Research*, *75*(27), 5247–5257. https://doi.org/10.1029/JC075i027p05247

Tibby, J., Penny, D., Leahy, P., & Kershaw, A. P. (2011). Vegetation and water quality responses to Holocene climate variability in Lake Purrumbete, western Victoria. *Terra Australis*, *43*, 359–373.

Timms, B. V. (1976). A comparative study of the limnology of three Maar Lakes in western Victoria. I. Physiography and Physicochemical Features. *Australian Journal of Marine and Freshwater Research*, *27*(1), 35–60. https://doi.org/10.1071/MF9760035

Tyler, J. J., Leng, M. J., & Sloane, H. J. (2007). The effects of organic removal treatment on the integrity of $\delta^{18}O$ measurements from biogenic silica. *Journal of Paleolimnology*, *37*(4), 491–497. https://doi.org/10.1007/s10933-006-9030-9

Venables, W. N., & Ripley, B. D. (2002). *Modern Applied Statistics with S* (4th ed.). New York: Springer.

von Grafenstein, U., Erlenkeuser, H., Müller, J., & Kleinmann-Eisenmann, A. (1992). Oxygen isotope records of benthic ostracods in Bavarian lake sediments. *Naturwissenschaften*, *79*(4), 145–152. https://doi.org/10.1007/BF01134431

Wierzbowski, H. (2007). Effects of pre-treatments and organic matter on oxygen and carbon isotope analyses of skeletal and inorganic calcium carbonate. *International Journal of Mass Spectrometry*, *268*(1), 16–29. https://doi.org/10.1016/j.ijms.2007.08.002

Wilkins, D., Gouramanis, C., Deckker, P. D., Fifield, L. K., & Olley, J. (2013). Holocene lake-level fluctuations in lakes Keilambete and Gnotuk, southwestern Victoria, Australia. *The Holocene*, *23*(6), 784–795. https://doi.org/10.1177/0959683612471983

Xiang, Q., & Lee, Y. Y. (2000). Oxidative cracking of precipitated hardwood lignin by hydrogen peroxide. *Applied Biochemistry and Biotechnology*, *84*, 153–162.

Zhao, Y., Li, S., Yu, L., Liu, Y., Wang, X., & Jiao, J. (2011). The preparation of calcium carbonate crystals regulated by mixed cationic/cationic surfactants. *Journal of Crystal Growth*, *324*(1), 278–283. https://doi.org/10.1016/j.jcrysgro.2011.03.052

Quaternary Science Reviews 192 (2018) 106–122

Contents lists available at ScienceDirect

Quaternary Science Reviews

journal homepage: www.elsevier.com/locate/quascirev

Millennial-scale variability in south-east Australian hydroclimate between 30,000 and 10,000 years ago

Georgina Falster [a, b, *], Jonathan Tyler [a, b], Katharine Grant [c], John Tibby [d, b], Chris Turney [e], Stefan Löhr [f], Geraldine Jacobsen [g], A. Peter Kershaw [h]

[a] Department of Earth Sciences, University of Adelaide, North Terrace, South Australia, 5005, Australia
[b] Sprigg Geobiology Centre, University of Adelaide, North Terrace, South Australia, 5005, Australia
[c] Research School of Earth Sciences, Australian National University, Canberra, ACT, 2601, Australia
[d] Department of Geography, Environment and Population, University of Adelaide, North Terrace, South Australia, 5005, Australia
[e] Palaeontology, Geobiology and Earth Archives Research Centre, and ARC Centre of Excellence in Australian Biodiversity and Heritage School of Biological, Earth and Environmental Sciences, University of New South Wales, Sydney, NSW, 2052, Australia
[f] Department of Earth & Planetary Sciences and Macquarie University Marine Research Centre, Macquarie University, North Ryde, 2109, Australia
[g] Centre for Accelerator Science, Australian Nuclear Science and Technology Organisation, Lucas Heights, NSW, 2232, Australia
[h] School of Earth, Atmosphere and Environment, Monash University, Melbourne, Victoria, 3800, Australia

ARTICLE INFO

Article history:
Received 13 November 2017
Received in revised form
11 April 2018
Accepted 21 May 2018
Available online 1 June 2018

Keywords:
Palaeoclimatology
Quaternary
Last glacial maximum (LGM)
Australasia
Lake sediment
Scanning XRF
Carbon isotopes
Monte Carlo empirical orthogonal function

ABSTRACT

Global climate variability during the late Quaternary is commonly investigated within the framework of the 'bipolar seesaw' pattern of asynchronous temperature variations in the northern and southern polar latitudes. The terrestrial hydrological response to this pattern in south-eastern Australia is not fully understood, as continuous, high-resolution, well-dated proxy records for the hydrological cycle in the region are sparse. Here we present a well-dated, highly resolved record of moisture balance spanning 30000–10000 calendar years before present (30–10 ka BP), based on x-ray fluorescence and organic carbon isotope ($\delta^{13}C_{OM}$) measurements of a sedimentary sequence from Lake Surprise in south-eastern Australia. The data provide a locally coherent record of the hydrological cycle. Elevated Si (reflecting windblown quartz and clays), and relatively high $\delta^{13}C_{OM}$, indicate an extended period of relative aridity between 28 and 18.5 ka BP, interrupted by millennial-scale episodes of decreased Si and $\delta^{13}C_{OM}$, suggesting increased moisture balance. This was followed by a rapid deglacial shift to low Si and $\delta^{13}C_{OM}$ at 18.5 ka BP, indicative of wetter conditions. We find that these changes are coeval with other records from south-eastern Australia and New Zealand, and use a Monte Carlo Empirical Orthogonal Function approach to extract a common trend from three high-resolution records. Our analyses suggest that drivers of the regional hydrological cycle have varied on multi-millennial time scales, in response to major shifts in global atmosphere-ocean dynamics during the last glacial-interglacial transition. Southern Ocean processes were the dominant control on hydroclimate during glacial times, via a strong influence of cold sea surface temperatures on moisture uptake and delivery onshore. Following the last deglaciation (around 18 ka BP), the southward migration of cold Southern Ocean fronts likely resulted in the establishment of conditions more like those of the present day. Millennial-scale variability in records from the region is dominated by a persistent ca. 2300-year periodicity, consistent with other records across the Southern Hemisphere mid-latitudes; however, this pervasive periodicity is not obviously linked to the 'bipolar seesaw' and the mechanism remains equivocal.

1. Introduction

The late Quaternary (defined here as 30000–10000 calendar years before present; 30–10 ka BP) is the most recent period in the geological record that is characterised by abrupt shifts in global atmosphere and ocean circulation (Thomas, 2016). Unravelling

* Corresponding author. Department of Earth Sciences, University of Adelaide, North Terrace, South Australia, 5005, Australia.
E-mail address: georgina.falster@adelaide.edu.au (G. Falster).

https://doi.org/10.1016/j.quascirev.2018.05.031
0277-3791/

patterns of climate variability during this period is key to understanding long-term atmosphere-ocean dynamics, and their environmental impact on centennial to millennial time scales. High-resolution methane-synchronised ice core records from the northern and southern polar regions are characterised by marked, asynchronous climate changes during the late Quaternary (c.f. the 'bipolar seesaw'), and much research has been devoted to understanding the mechanisms driving these high-latitude climate phase relationships (Blunier et al., 1998; Broecker, 1998; Blunier and Brook, 2001; EPICA Community Members, 2006). However, the manifestation of these events in the terrestrial hydrological cycle beyond the high latitudes is less well constrained. This is particularly the case in the Southern Hemisphere (SH) mid-latitudes (defined here as spanning 25–45°S) where a relative dearth of continuous, high-resolution records has limited our ability to investigate the timing and drivers of change (Vandergoes et al., 2005; Bayon et al., 2017).

Within the ocean-dominated SH mid-latitudes, coastal sites in southern Australia and New Zealand (NZ) are highly sensitive to atmosphere-ocean interactions (Gentilli, 1971; Barrows et al., 2007; Gouramanis et al., 2013), and hence are ideally located to investigate long-term drivers of terrestrial hydroclimate. Large-scale climate systems that directly influence modern southern Australian and NZ climates include the mid-latitude Southern Westerly Winds (SWW) (Hall and Visbeck, 2002; Cai et al., 2005; Meneghini et al., 2007; Pepler et al., 2016), Southern Ocean and Antarctic ice sheet dynamics (Pezza et al., 2008; Williams and Stone, 2009), and zonal sea surface temperature (SST) gradients including the El Niño Southern Oscillation (ENSO) and the Indian Ocean Dipole (IOD) (Ashok et al., 2007; Risbey et al., 2009; Pepler et al., 2014; Forootan et al., 2016). However, the extent to which these systems influence southern Australian and NZ hydroclimate on multi-millennial time scales is not clear, especially considering the confounding effect of the sea level changes associated with glacial cycles (Clark and Mix, 2002).

A range of sedimentological, palaeoecological and geochemical tracers respond strongly to changes in the terrestrial hydrological cycle, and accordingly, there are over 60 hydroclimate-related proxy records from southern Australia and New Zealand, that span the late Quaternary (Table 1, Fig. 1). Early work, relying largely on fragmentary aeolian deposits, suggested that the last glacial period was cold, windy, and mostly dry relative to deglacial and interglacial periods (Bowler, 1976). This hypothesis has been generally supported by subsequent hydroclimate records (e.g. Gingele et al., 2001; Petherick et al., 2009; Barrell et al., 2013; Petherick et al., 2013), though some exceptions have been reported (Shulmeister et al., 2016; Treble et al., 2016; Barr et al., 2017).

Unfortunately, most records shown in Table 1 are fragmentary, or at too coarse a resolution to reliably identify millennial-scale variability. This is primarily because the largely arid to semi-arid climates of south-eastern Australia in particular are generally not conducive to continuous accumulation of sediments. The region therefore suffers from a limited network of high-resolution, temporally well-constrained, late Quaternary hydroclimate proxy records, limiting precise inter-site comparison of climatic events on both regional and global scales. This is problematic, as single-site reconstructions may be confounded by local or proxy-specific effects, rather than providing a robust representation of regional palaeoclimate that may be directly compared with high-resolution and precisely dated palaeoclimate records from more distal locations (Turney et al., 2006; Moss et al., 2013; Petherick et al., 2013; Harrison et al., 2016; Prentice et al., 2017).

This uncertainty has resulted in ambiguity in the expression of the Last Glacial Maximum (LGM) in southern Australia and NZ. The global LGM is generally considered to have occurred between 23 and 19 ka BP, when sea level was at a minimum and the global climate was relatively stable (Mix et al., 2001; Clark et al., 2009). However, the LGM has no formal stratigraphic definition *per se* (Hughes and Gibbard, 2014), and numerous Southern Hemisphere (including Australian and NZ) palaeoclimate records preserve evidence for an 'extended LGM' that manifests as a period of extreme aridity, and most likely commenced between 32 and 28 ka BP (e.g. Heusser et al., 1999; Williams et al., 2006; Kershaw et al., 2007; Newnham et al., 2007; Fogwill et al., 2015; Petherick et al., 2017), but possibly as early as ~38 ka BP (e.g. Barrows et al., 2001; Petherick et al., 2008). Furthermore, some high-resolution records from southern Australia and NZ preserve evidence for (a) two relatively arid phases centred around ~31 and 22 ka BP, separated by an interval of increased moisture balance around ~24 ka BP (Alloway et al., 2007; Petherick et al., 2008; 2017; Augustinus et al., 2011), or (b) variable hydroclimate superimposed on generally dry conditions (Moss et al., 2013). The timing, nature, and spatial distribution of LGM conditions in southern Australia and NZ is therefore equivocal, highlighting the need for more highly resolved palaeoclimate records.

Here we present a new high-resolution, multi-proxy hydroclimate record spanning 30–10 ka BP from Lake Surprise, a small, steep-walled crater lake located in south-eastern Australia (38°03′42″S, 141°55′22″E; Fig. 1). Lake Surprise is a sensitive archive of climate variability, lying at the modern northern margin of influence of the SWW (Hendon et al., 2007; Barr et al., 2014), with climate variability also modulated by the IOD and ENSO (Ashok et al., 2007; Risbey et al., 2009; Ummenhofer et al., 2009). Using comprehensive radiocarbon (^{14}C) dating in combination with high-resolution quantitative elemental composition data, and the carbon isotope composition of bulk organic matter, we infer past changes in aeolian input and variation in plant water stress within a robust geochronological framework. We subsequently apply a Monte Carlo Empirical Orthogonal Function (MCEOF) approach to key published records to objectively define a regionally coherent record of hydroclimate change. These records are all from south-eastern Australia and NZ, so we then use our findings to explore the timing and potential drivers of change in this region.

2. Methods

2.1. Study site and core acquisition

Lake Surprise occupies the crater complex of Mt Eccles, a dormant scoria cone volcano composed of nepheline hawaiite, located in the Newer Volcanics Province of south-eastern Australia (Fig. 1; Timms, 1975; Irving and Green, 1976; Boyce, 2013). Cosmogenic exposure dating of the surrounding Tyrendarra lava flow, which originated in Mt Eccles, indicates that the eruption of the volcano probably occurred 36 ± 3 ka BP (Gillen et al., 2010). Radiocarbon dates from lakes and swamps that formed following drainage diversion due to the extrusion of the Tyrendarra basalt provide minimum eruption ages of between 32 and 29 ka BP (Head et al., 1991; Builth et al., 2008); this chronological discrepancy is most likely due to the time taken for the porous basalt substrate to mature sufficiently to allow the accumulation of water and sediment. Following the eruption of Mt Eccles - and several other volcanos that erupted around the same time - there appears to have been no further volcanic activity in the Newer Volcanics Province until approximately the mid-Holocene (Sherwood et al., 2004). Based on analysis of archaeological evidence of human patterns of occupation of Australia, it is likely that Indigenous people lived in the general area from before the eruption of Mt Eccles (O'Connor and Allen, 2015), however there is no strong evidence for their exploitation of the landscape prior to the mid-Holocene (Builth

Table 1
Records of late Quaternary hydroclimate variability (spanning the majority of the period 30–10 ka BP), from southern Australia and New Zealand. Listed by country, in order of decreasing latitude. Map reference numbers correspond to Fig. 1.

Country	Site name	Hydroclimate proxy(s)	Reference(s)	Latitude	Longitude	Map reference
Australia	Welsby Lagoon	Pollen, charcoal, total organic carbon content	Moss et al. (2013); Barr et al. (2017)	27°27′00″S	153°28′00″E	1
	Tortoise Lagoon	Pollen, charcoal, clastic sediment flux, particle size analysis	Moss et al. (2013); Petherick et al. (2017)	27°30′59″S	153°28′26″E	2
	Native Companion Lagoon	ICP-MS trace element analysis, pollen, charcoal, particle size analysis	Petherick et al. (2008); Petherick et al. (2009), Moss et al. (2013)	27°40′36″S	153°24′39″E	3
	Lake Eyre	Dates (OSL, TL, AMS ^{14}C, TIMS U-Th, amino acid racemisation determinations on bird eggshells and molluscs) from lake and lake-margin sediments	Magee et al. (2004)	28°31′2″S	137°13′51″E	4
	Lake Mega-Frome	OSL, TL, and ^{14}C dates from lake palaeoshorelines	Cohen et al. (2011)	29°49′34″S	140°10′6″E	5
	Little Llangothlin Lagoon	OSL dating of geomorphology (lake margin shoreline features) via GPR, and sediments in a couple of cores	Shulmeister et al. (2016)	30° 5′9″S	151°46′53″E	6
	Lake Eyre, Lake Frome	OSL dating of palaeoshorelines	Cohen et al. (2015)	30°43′19″S	139°49′43″E	4, 7
	Lake Frome	Pollen	Singh and Luly (1991)	30°43′19″S	139°49′43″E	7
	Ulungra Springs	Pollen	Dodson and Wright (1989)	31°44′25″S	149° 5′38″E	8
	Burraga Swamp	Pollen	Sweller and Martin (2001)	32° 5′50″S	151°35′29″E	9
	Mairs Cave	MC-ICP-MS growth-phase, δ^{18}O, δ^{13}C, and trace element analyses on speleothems	Cohen et al. (2011); Treble et al. (2016)	32°13′25″S	138°53′5″E	10
	Redhead Lagoon	Pollen, charcoal	Williams (2005); Williams et al. (2006)	32°59′43″S	151°43′22″E	11
	Lachlan River	OSL dates from river terraces	Kemp and Rhodes (2010)	33°21′34″S	147°40′41″E	12
	Mountain Lagoon	Pollen	Robbie and Martin (2007)	33°26′40″S	150°38′15″E	13
	Willandra Lakes	^{14}C and TL dates within stratigraphic sections	Bowler (1998); Bowler et al. (2003); Bowler et al. (2012)	33°42′31″S	143° 4′18″E	14
	Darling Lakes	δ^{18}O (emu eggshells)	Miller and Fogel (2016)	33°42′31″S	143° 4′18″E	15
	Lake Baraba	Pollen, charcoal, LOI	Black et al. (2006)	34°13′S	150°13′E	16
	Murrumbidgee Valley	TL dates from riverine source-bordering dunes	Page et al. (2001)	35° 4′13″S	147°12′38″E	17
	Lake George	^{14}C dates on abandoned lake shorelines, pollen, ostracod ecology, charcoal	Coventry (1976); Singh et al. (1981); De Deckker (1982); Singh and Geissler (1985)	35° 6′37″S	149°26′5″E	18
	Lake Tyrrell	OSL dating of dune sediments	Stone (2006)	35°14′17″S	142°50′28″E	19
	Kelly Hill Caves	U/Th dates from speleothems	Cohen et al. (2011)	35°58′31″S	136°54′15″E	20
	Snowy Mountains	^{10}Be dates from glacial moraines	Barrows et al. (2001)	36°25′25″S	148°16′37″E	21
	Marine Core MD03-2611	Scanning XRF (Fe and Ti), XRD	DeDeckker et al. (2012)	36°43′48″S	136°32′54″E	22
	Naracoorte Caves (including Blanche Cave, Robertson Cave, Wet Cave)	^{230}Th/^{234}U ages from speleothems and flowstones, XRF-derived major element geochemistry, LA-ICP-MS-derived REE and trace element composition, Nd isotopes, pollen, morphological analysis of quartz grains, grain size analysis, petrography, NMR, δ^{13}C and δ^{15}N (bulk sediment), δ^{13}C (charcoal), XRD	Ayliffe et al. (1998); Moriarty et al. (2000); Forbes et al. (2007); Darrénougué et al. (2009); Macken et al. (2013); Macken and Reed (2014)	37° 4′50″S	140°48′38″E	23
	Caledonia Fen	Pollen, charcoal, magnetic susceptibility, δ^{13}C (pollen grains)	Kershaw et al. (2007); Nelson et al. (2016)	37°20′0″S	146°43′60″E	24
	Lake Leake	Pollen	Dodson (1975)	37°37′27″S	140°36′14″E	25
	Wyrie Swamp	Pollen	Dodson (1977)	37°38′0″S	140°16′56″E	26
	Lake Turangmoroke	Pollen, palynomorphs, charcoal	Cook (2009)	37°43′33″S	142°53′34″E	27
	Lake Bolac	Pollen, palynomorphs, charcoal	Cook (2009)	37°43′49″S	142°51′39″E	28
	Lake Keilambete	^{14}C dates within stratigraphic sections	Bowler and Hamada (1971)	38°12′28″S	142°52′35″E	29
	Tower Hill	Pollen, microfauna, diatoms, charcoal, δ^{13}C (pollen grains)	D'Costa et al. (1989); Nelson et al. (2016)	38°19′1″S	142°21′46″E	30
	Marine core E55-6	Pollen, charcoal	Harle (1997)	38°51′12″S	141° 3′48″E	31
	Egg Lagoon	Mollusc assemblages, pollen, charcoal	D'Costa et al. (1993)	39°38′39″S	143°59′30″E	32
	Pulbeena Swamp	Pollen	Colhoun et al. (1982)	40°52′35″S	145° 8′36″E	33
	Tullabardine Dam	Pollen, charcoal	Colhoun and Geer (1986)	41°40′30″S	145°39′8″E	34
	Lake Selina	Pollen, charcoal, NMR intensity	Colhoun et al. (1999)	41°52′43″S	145°36′32″E	35
	Central Ice Plateau	^{36}Cl and ^{10}Be dates on glacial moraines	Barrows et al. (2002)	41°58′44″S	145°36′36″E	36
	Hazards Lagoon	Pollen, charcoal	Mackenzie and Moss (2017)	42°10′20″S	148°17′21″E	37
	Tasman Sea (deep sea cores)	Sedimentology (aeolian content, dry bulk density), particle size analysis of mineral fraction	Hesse (1994); Hesse and McTainsh (1999)	Multiple locations within the Tasman Sea		n/a
	Australian Highlands (Snowy Mountains, Tasmania)	Presence of periglacial landforms and LGM-aged lake shorelines	Galloway (1965)	Multiple locations		n/a
New Zealand	Marine Core S803	Pollen	Wright et al. (1995)	36°41′49″S	176°36′22″E	38
	Onepoto Maar	Sediment grain size, XRF (Al, Ti, Ni, Cr, Fe/Mn), TOC, TN, TS, δ^{13}C and δ^{15}N (bulk sediment), biogenic silica, diatoms, cladocerans, pollen, charcoal	Kattel and Augustinus (2010); Augustinus et al. (2011); Augustinus et al. (2012)	36°48′31″S	175°45′05″E	39
	Mt. Richmond	Pollen	Sandiford et al. (2002)	36°55′58″S	174°50′26″E	40
	Kohuora Crater	Pollen, charcoal	Newnham et al. (2007)	36°58′42″S	174°50′34″E	41
	Pukaki Crater	Pollen, charcoal	Sandiford et al. (2003)	36°58′57″S	174°48′38″E	42
	Central Taranaki	XRD determination of aerosolic quartz	Alloway et al. (1992)	39° 6′11″S	174°15′17″E	43
	North Island	^{3}He surface dates on glacial moraines, tephrochronology, tephrostratigraphy	Eaves et al. (2016)	39° 7′48″S	175°39′0″E	44
	Marine Core P69	Pollen	McGlone (2001)	40°23′48″S	177°59′48″E	45

Table 1 (*continued*)

Country	Site name	Hydroclimate proxy(s)	Reference(s)	Latitude	Longitude	Map reference
	North-West Nelson	Pollen, charcoal	Shulmeister et al. (2003)	41° 5′57″S	172°38′5″E	46
	Mt. Arthur	$\delta^{18}O$ and $\delta^{13}C$ (speleothem)	Hellstrom et al. (1998)	41°12′35″S	172°43′46″E	47
	Hollywood Cave	$\delta^{18}O$ and $\delta^{13}C$ (speleothem)	Whittaker et al. (2011)	41°57′0″S	171°28′0″E	48
	Okarito Bog	Pollen	Vandergoes et al. (2013)	43°14′30″S	170°13′6″E	49
	Galway Tarn	Pollen	Vandergoes et al. (2013)	43°24′30″S	169°52′24″E	50
	Skiffington Swamp	Pollen	Vandergoes et al. (2013)	43°25′15″S	169°59′30″E	51
	Rakaia Valley	IRSL dates within sedimentary sections	Shulmeister et al. (2010)	43°27′49″S	171°36′9″E	52
	Southern Alps Icefield	Topographically-constrained ice sheet modelling	Golledge et al. (2012)	43°42′1″S	170°4′6″E	53
	Lake Ohau	^{10}Be surface exposure dates on terminal moraines	Putnam et al. (2013)	44°13′20″S	169°51′17″E	54
	South Island	^{36}Cl and ^{10}Be dates and tephrochronology of glacial landforms	Barrows et al. (2013)	Multiple locations on the South Island of New Zealand		n/a
	Offshore NZ (marine cores)	Mass accumulation rates of terrigenous and biogenic sediments	Carter et al. (2000)	Multiple locations around New Zealand		n/a

et al., 2008).

The Mt Eccles crater complex is an amalgam of three contiguous craters (Boutakoff, 1963), resulting in an elongate lake with large littoral areas at each end (Fig. 1b; Timms, 1975). The crater walls are high and steep, protecting Lake Surprise from wind disturbance (Fig. 1c). This limits deep mixing, resulting in a sharp boundary between the oxygenated epilimnion and the anoxic hypolimnion (Timms, 1975). The lake has no fluvial input or output, such that the hydrological balance is mainly a function of precipitation and evaporation (Barr et al., 2014), and detrital input is restricted to run-off from the crater walls and wind-blown particles. The lake water level is also maintained by some groundwater input. The lake water is hard, and slightly alkaline (Timms, 1975). The modern climate at Lake Surprise is temperate, with a mean daily temperature of 13.6 °C and mean annual precipitation of 798 mm recorded at Heywood Forestry, approximately 45 km to the west (Peel et al., 2007; BOM, 2013). Precipitation is winter-dominated, with the majority delivered by prevailing westerly and south-westerly winds that bring moist air onshore from the Southern Ocean. The area is also affected by north-easterly and north-westerly winds, especially in the warmer months (Gentilli, 1971).

The modern crater slopes are dominated by a *Eucalyptus viminalis* woodland with abundant *Acacia melanoxylon*, and ground cover is predominantly composed of bracken, with some grasses on the drier slopes (Tibby et al., 2006). The shallow water margins of the lake support a variable, but generally narrow, band of aquatic vegetation composed mainly of emergent macrophytes, but incorporating floating plants in sheltered open water (Tibby et al., 2006).

Here we present data from core LS04, which was retrieved from the deepest point of Lake Surprise in March 2004 in a contemporary water depth of approximately 10.4 m (Barr et al., 2014). The core was recovered from 1 to 13 m using a hand-operated Livingstone sampler, and core recovery was extended to the base of the sequence at 18.4 m using a piston sampler operated with a winch and pulley system (Builth et al., 2008). All core segments were split longitudinally, and have been stored at 4 °C since acquisition.

The sediment in the analysed section of core LS04 (9.25–18.4m) is uniformly very dark brown and very fine-grained, with few

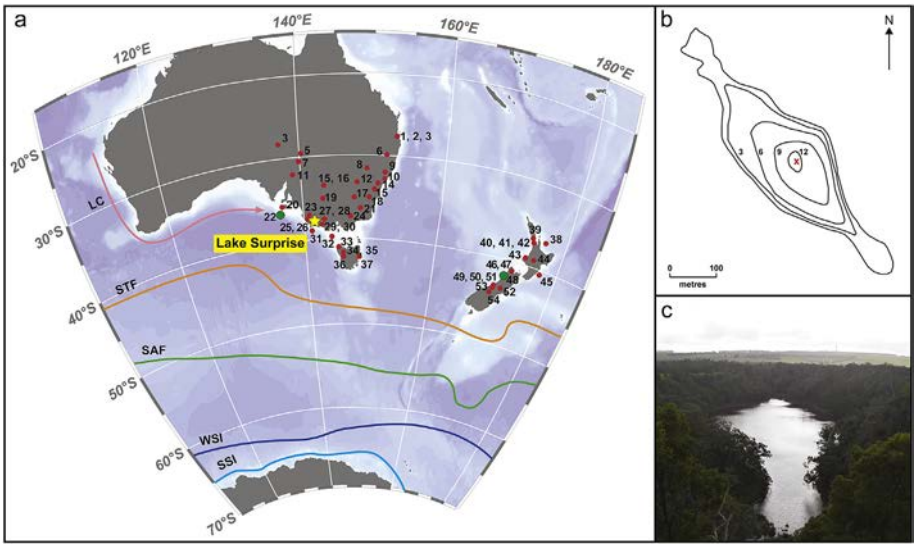

Fig. 1. Location of sites mentioned in the text: **a**) Records of hydroclimate variability for southern Australia and New Zealand during the period 30-10 ka BP (Table 1), with the approximate modern position of the Southern Ocean subtropical front (STF), subantarctic front (SAF), maximum winter sea ice extent (WSI), and maximum summer sea ice extent (SSI), as well as the Leeuwin Current (LC). Location of published records included in the MCEOF analysis shown in green. Southern Ocean fronts and sea ice distribution adapted from Gersonde et al. (2005); Leeuwin Current path adapted from De Deckker et al. (2012). Map generated using the Ocean Data View software; **b**) Bathymetry of Lake Surprise, with depth contours in metres, and core location shown by the red cross; **c)** Lake Surprise, looking north-west from the rim of the Mt Eccles crater. (For interpretation of the references to colour in this figure legend, the reader is referred to the Web version of this article.)

visible grains or sedimentary features. The absence of any desiccation or erosion features indicates perennial water in the lake since the onset of sedimentation. Due to the limited nature of the catchment, core LS04 therefore provides a continuous record of the surrounding vegetation, as well as pluvial, colluvial, and aeolian input to Lake Surprise.

2.2. Chronological control

A chronology for core LS04 has been defined by a total of 32 accelerator mass spectrometry (AMS) ^{14}C dates, all obtained from concentrated pollen samples. Sixteen AMS ^{14}C dates existed for Lake Surprise prior to this study (Supp. Table 1).

Here we report sixteen new AMS ^{14}C dates, all within the 30–10 ka BP period. The location of each sample was selected in order to have AMS ^{14}C dates at sufficient spacing to identify change points in sediment accumulation rate. Wet sediment samples of approximately 5–10 g were sieved to retain the 5–150 μm fraction. The samples were reacted with 10 % HCl at 60 °C for 20 minutes to remove carbonates, and then with 40 % HF at room temperature overnight to remove silicate minerals. The organic matter was separated from mineral residue using LST heavy liquid with a specific gravity of 1.8. To remove humic acids, the <1.8 g/mL sample fraction was reacted with 10 % NaOH at 60 °C for 30 minutes repeatedly until the supernatant was completely clear. The samples were reacted with 5 % NaOCl for 5 minutes at room temperature to reduce the level of organic contamination (e.g. chitin, cellulose), and then once more with 10 % HCl for 10 minutes at room temperature. Each sample was rinsed three times with 18 MΩ Milli-Q water between each step.

The concentrated pollen samples were screened for contamination under an optical microscope, then transferred to a clean vial and dried in a 60 °C oven overnight. The pollen samples were then combusted and graphitised for AMS ^{14}C analysis on the STAR accelerator mass spectrometer at the Australian Nuclear Science and Technology Organisation (Hua et al., 2001; Fink et al., 2004).

All radiocarbon ages were calibrated to calendar ages using the SH radiocarbon calibration curve (SHCal13; Hogg et al., 2013). We developed a composite age-depth model in R using the 'Bacon' software for Bayesian age modelling (Blaauw and Christen, 2011). Calibrated ages are reported as 'ka BP' – thousands of calendar years before the year 1950 (Supp. Fig. 1).

2.3. XRF core scanning

High-resolution elemental analyses of core LS04 were obtained using an Avaatech XRF core scanner at the Australian National University. Half-core segments were covered with 4 μm SPEX SamplePrep Ultralene film to prevent desiccation of the sediment and avoid contamination of the instrument. Measurements were acquired every 2 mm at 10 kv, with a 500 μA current and count time of 20 s, and with a 2 mm down-core slit size and a 12 mm across-core slit size. Only elements that were reliably detected above background levels were included in subsequent analysis (i.e. Si, S, Ca, Ti, Mn, and Fe) (Supp Fig. 2).

The semi-quantitative scanning XRF count data were converted to quantitative element concentrations (Fig. 2) using wavelength-dispersive (WD) XRF analyses of 10 discrete sub-samples from core LS04, following the multivariate log ratio calibration method outlined by Weltje et al. (2015) and applied by Grant et al. (2017). The location for each sample was selected using Ward's method in conjunction with a Euclidean distance matrix to divide the count data into ten clusters. The data point closest to the cluster centroid was selected for sampling. The predictive power of the calibration was assessed by plotting the measured values against the values predicted by the calibration model (Supp Fig. 3). High r^2 values and p-values « 0.05 for all elements indicates a robust calibration.

WD-XRF analyses were performed at the Commonwealth Scientific and Industrial Research Organisation's (CSIRO) Waite Campus. Approximately one gram of oven-dried (105°C) sample was weighed into a Pt/Au crucible with 4 g of 12–22 lithium borate flux. To remove organic matter, the mixtures were slowly heated to 700 °C in a furnace, held at 700 °C for seven hours, and then slowly cooled overnight. Each oxidised mixture was heated to 1050 °C until completely liquefied, and then poured into a Pt/Au mould and rapidly cooled. The resulting glass discs were analysed on a PANalytical Axios Advanced WD-XRF system using the CSIRO in-house silicates calibration programme (Supp. Table 2).

Principal Components Analysis (PCA) was used to identify major patterns of change in the calibrated data (Fig. 2). The data were scaled according to variance to give each element equal importance, and the mean was subtracted from each analysis. The PCA was performed on the centred and scaled data, using the 'vegan' package (Okansen et al., 2008) in R (R Core Team, 2017). The number of principal components (PCs) that are likely to contain meaningful information was determined using a 'broken-stick' model (Bennett, 1996), which compares the variance explained by each PC with that expected from a random distribution (Fig. 2b). Results from the PCA are provided in Supp. Table 3. A principal curve was also fitted to the PCA axis scores, to isolate a single vector that describes the majority of variance in the XRF data. The principal curve was fitted using the 'analogue' package in R (Simpson, 2007; Simpson and Oksanen, 2016).

2.4. Mineral identification

Bulk mineralogy of ten samples was determined using x-ray diffractometry (XRD) performed on randomly oriented powders. The samples were dried in a freeze-drier, and lightly ground using an agate mortar and pestle. Powder diffraction patterns were collected using a Bruker D8 Advance x-ray diffractometer with a Cu-radiation source. Minerals were identified using Bruker Diffrac. Eva software and Crystallography Open Database reference patterns. Phase identification was complicated by the abundant presence of biogenic opal in all samples, particularly for low abundance phases. Interpretation of the x-ray diffractograms was therefore assisted by SEM imaging and mineral mapping of several samples. Samples for imaging were embedded in resin, manually polished, ion polished (Hitachi IM4000 Argon Ion Mill) and carbon coated. SEM analyses were performed on an FEI Teneo LoVac field emission SEM equipped with dual EDS (energy dispersive x-ray spectroscopy) detectors (Bruker XFlash Series 6), at a 13 mm working distance and 15 kV accelerating voltage. Back-scatter electron images and EDS spectra (2 μm step size, 16 ms acquisition time) for mineral mapping were collected sequentially using the FEI Maps Mineralogy software, followed by classification of the individual EDS spectra using the FEI Nanomin software. Mineral classification is achieved by comparing EDS spectra collected in the mapped area against reference spectra collected on known mineral standards. A summary of minerals identified in each sample is provided in Supp. Table 4, with qualitative estimates of relative mineral abundance.

2.5. Organic matter elemental and stable isotope ratios

Concentrations of organic carbon (total organic carbon; TOC) and nitrogen (total nitrogen; TN), and the $^{13}C/^{12}C$ isotope ratio of the bulk organic matter ($\delta^{13}C_{OM}$) were determined on samples that were freeze-dried and lightly ground in a ball mill. $\delta^{13}C_{OM}$ and TOC were determined at 5 cm resolution from 9.25 to 18.4 m, and TN at 10 cm resolution. Sub-samples of approximately 2 mg were

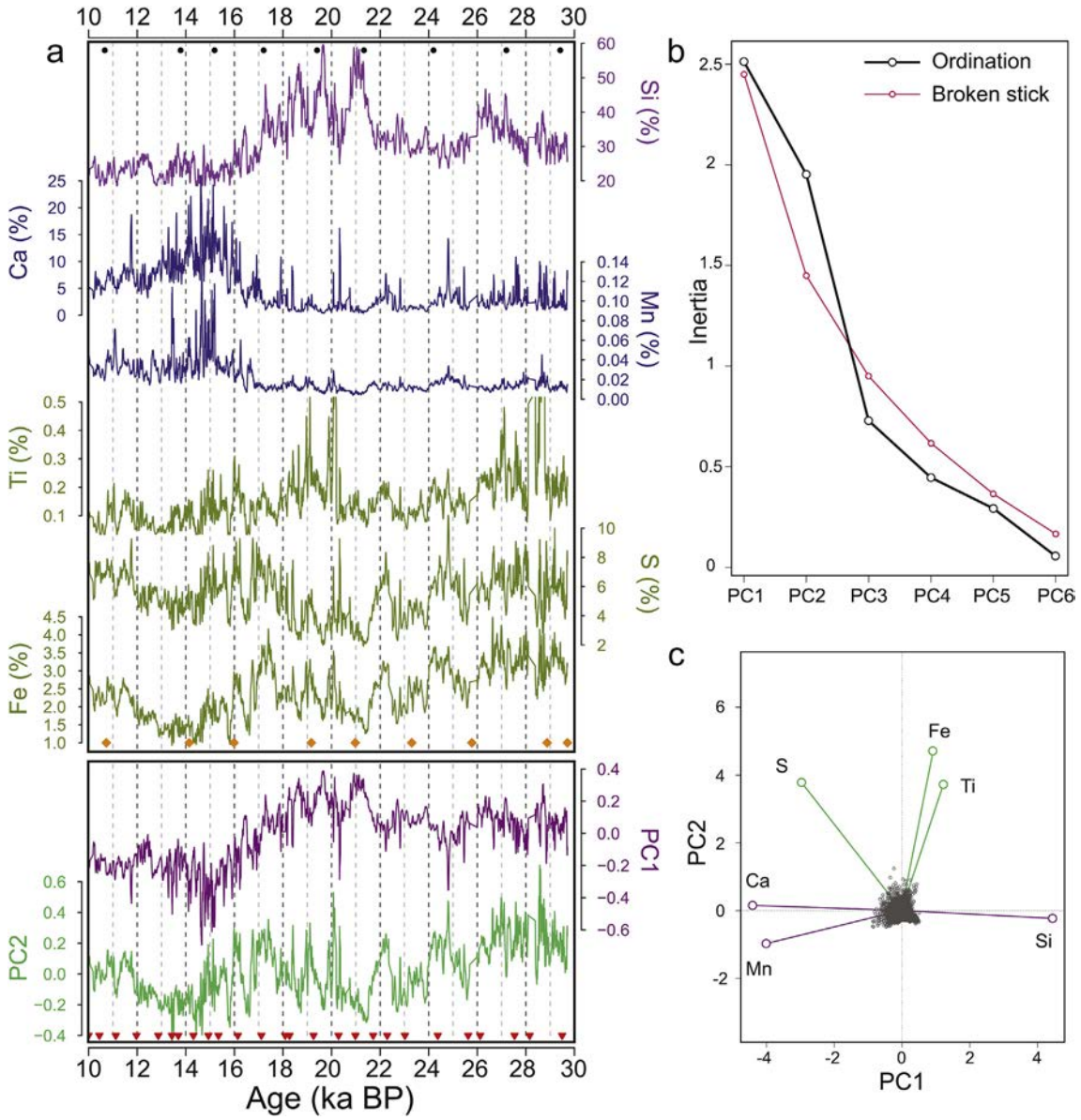

Fig. 2. Calibrated Lake Surprise scanning XRF data, and results of the Principal Components Analysis (PCA): **a)** Upper panel: Five-point running mean of calibrated concentrations for all elements detected above background levels. Black points denote the location of WD-XRF calibration samples (Supp. Table 2). Orange diamonds denote the location of XRD samples (Supp. Table 4). Lower panel: First and second principal components of the scanning XRF data. Note strong similarity between PC1 and Si, and PC2 and Ti/Fe/S. Red triangles denote the location of age control points; **b)** Broken stick test performed on the PCA of the scanning XRF data, indicating that the first two principal components preserve interpretable information; **c)** Biplot representation of the PCA, showing the loadings of each sample (grey circles) and element (vectors) on the first two principal components. (For interpretation of the references to colour in this figure legend, the reader is referred to the Web version of this article.)

weighed into silver capsules. Carbonate was removed from the sub-samples via acid fumigation, whereby approximately 50 μL deionised water was added to each capsule, then sub-samples were acidified for four hours in concentrated hydrochloric acid vapour and dried overnight in a 40 °C oven (e.g. Harris et al., 2001). Once dry, the silver capsules were placed inside larger tin capsules and crimped. The acid fumigation step was omitted for TN analyses.

All capsules were combusted in a Eurovector elemental analyser, and the evolved gas was transferred to a Nu Horizon isotope-ratio mass spectrometer. Standardisation was based on in-house glycine ($\delta^{13}C$: −31.2‰), glutamic acid ($\delta^{13}C$: −16.72‰) and triphenylamine ($\delta^{13}C$: −29.3‰) standards which have been calibrated against international standards. Analytical precision (1σ) for replicate measurements of the standards was ± 0.06 ‰. Each run of samples also included at least 10 % replicate analyses. $\delta^{13}C_{OM}$ is reported in per mille units relative to the Vienna Pee Dee belemnite standard (VPDB) (Supp Fig. 4).

2.6. Multi-proxy synthesis

Published hydroclimate reconstructions for southern Australia and New Zealand were systematically reviewed, and are summarised in Table 1. We used the following four criteria to screen these records for inclusion in a regional data synthesis alongside the record from Lake Surprise: (1) the record is continuous through the majority of the period 30–10 ka BP, (2) the data have been interpreted to primarily reflect the terrestrial hydrological cycle, (3) the record is independently dated with a minimum of one date per

2000 years, and (4) the data have an average time resolution per sample of 200 years or less. In addition to our new record from Lake Surprise, two records met all criteria - a speleothem $\delta^{13}C$ record from Hollywood Cave, on the south island of New Zealand (Whittaker et al., 2011), and an XRF-derived record of Ti variation from ocean core MD03-2611, located south of South Australia (De Deckker et al., 2012) (green circles in Fig. 1a). No suitable records exist for western Australia.

We used the Monte Carlo Empirical Orthogonal Function (MCEOF) approach to identify significant trends common to all records. Our method follows Anchukaitis and Tierney (2012) using code modified from Tyler et al. (2015). To maintain consistency in the chronological control, we updated each age-depth model using the 'Bacon' software in R (Blaauw and Christen, 2011). We extracted an ensemble of 1000 individual iterations from the Bayesian age-depth model for each site, and, for each iteration, each dataset was modelled using a Generalised Additive Model (GAM). This replaces the interpolation step of previous studies, which potentially alters the variance structure of the data (Tyler et al., 2015). GAMs were fitted using the Mixed GAM Computational Vehicle ('mgcv') package (Wood, 2006) in R, with model parameters estimated using the 'restricted maximum likelihood' method (Fig. 3a). In each case, the data were resampled from the GAM at consistent intervals and truncated to the period 29–11 ka BP. The time period was defined by the limit of overlapping coverage of the three datasets. The data were standardised to unit variance, and PCA was performed for each age realisation. For each EOF, 68% and 90% confidence intervals were calculated, to provide estimates of the error in the EOFs associated with age model determination (Fig. 3).

Significance testing was performed using two 'Rule N' tests

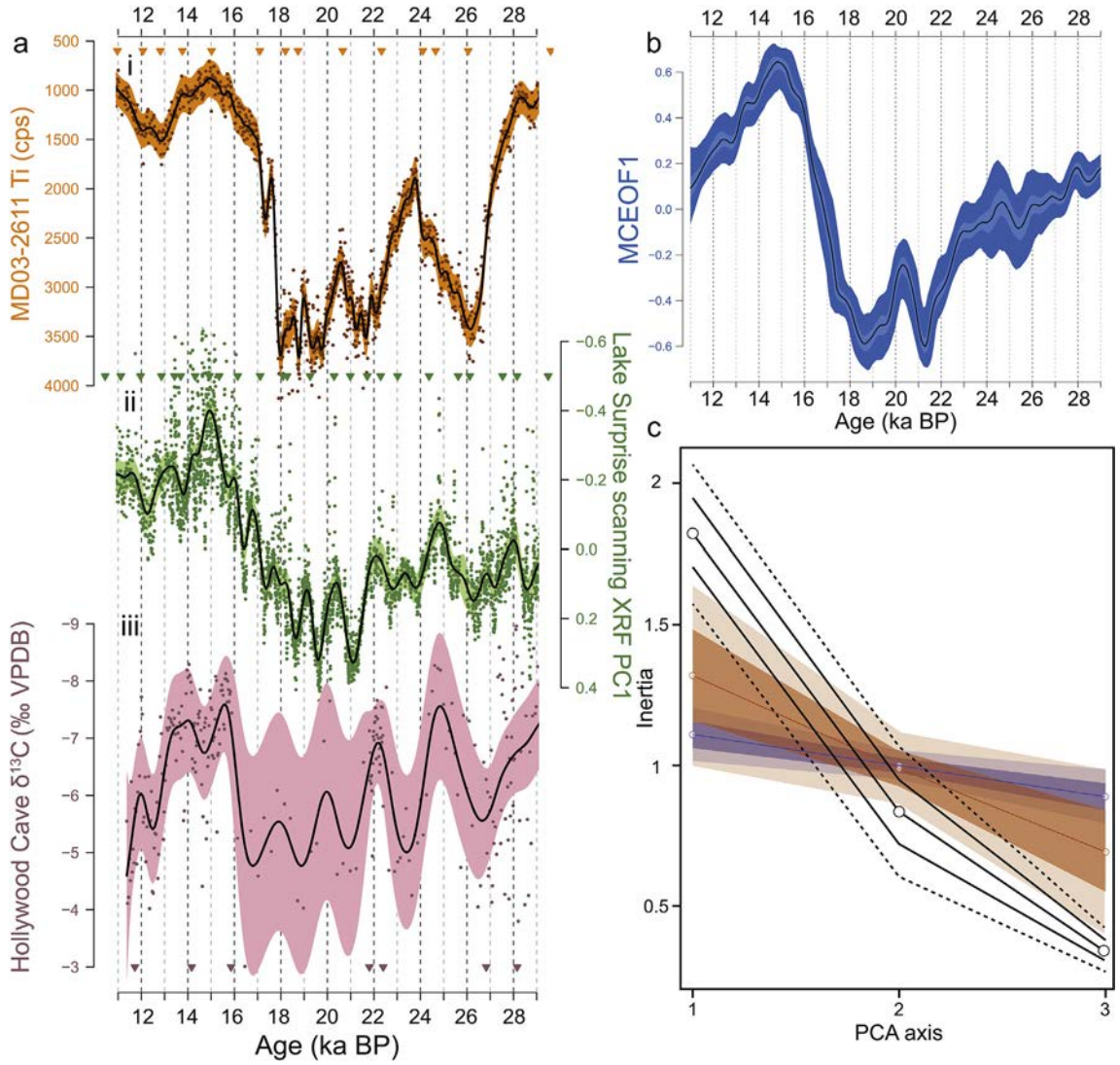

Fig. 3. Results of the MCEOF analysis on three key hydroclimate records from the south-east Australia and NZ region: **a)** Example Generalised Additive Models (GAMs) derived for each site, using published age models. **i)** Total counts per second (cps) of Ti from core MD03-2611, located south of South Australia (Fig. 1). Interpreted to reflect regional aridity in southern Australia (De Deckker et al., 2012); **ii)** Lake Surprise scanning XRF PC1 (this study); **iii)** Speleothem $\delta^{13}C$ from Hollywood Cave in New Zealand, interpreted to reflect changes in precipitation (Whittaker et al., 2011). Black line = GAM, shading = 95% confidence interval, points = individual data points, triangles = age control points on published chronologies. For input to the MCEOF analysis, a GAM was derived for each of 1000 age ensemble members extracted from a Bayesian age-depth model created using the 'Bacon' software in R (Blaauw and Christen, 2011); **b)** Results of the MCEOF analysis. Black line = median timeseries, dark and light shading = 90% and 68% confidence intervals; **c)** Variance explained by each MCEOF, compared with simulated random and red noise. White circles with a black outline represent the ensemble mean, with one and two standard deviations shown by solid and dashed black lines, respectively. The blue line shows the mean of the white noise test, with one and two standard deviations shown by the dark and light blue envelopes. The same applies for the orange envelope, but showing results of the red noise test, following Anchukaitis and Tierney (2012). (For interpretation of the references to colour in this figure legend, the reader is referred to the Web version of this article.)

following Anchukaitis and Tierney (2012). For the null hypotheses, we generated 1000 sets of synthetic timeseries, using (1) Gaussian white noise, and (2) 'red noise', with parameters derived from the autoregressive structure of the component timeseries. The synthetic timeseries were then input to the PCA as described above, and the eigenvalues compared with those from the actual data (Fig. 3c).

2.7. Spectral analysis

To investigate characteristic timescales of variability in the data, we performed spectral analysis on the Lake Surprise XRF PC1, PC2, and $\delta^{13}C_{OM}$ timeseries, as well as each component record of the MCEOF analysis, and several other timeseries for comparison. We used Lomb-Scargle periodograms to identify frequencies present in each timeseries, as the Lomb-Scargle method may be applied to unevenly spaced timeseries, avoiding the need for an interpolation step that may introduce artificial periodicities to the data. Lomb-Scargle periodograms were computed using the 'lomb' package in R (Ruf, 1999), along with estimates of the significance ($\alpha = 0.05$) of spectral peaks (Supp Fig. 5).

3. Results

3.1. Chronology

The core chronology indicates continuous sediment accumulation in Lake Surprise from ~30 ka BP until the time of coring in 2004 (Supp Table 1, Supp Fig. 1). All ages are shown as median calibrated radiocarbon ages with 2σ errors. The modelled sediment accumulation for the bottom section of core LS04 shows a reasonably consistent accumulation rate between 30 and 13 ka BP, with a decrease in accumulation rate between 25 and 23 ka BP, and peaks in the accumulation rate at 22–21 ka BP, 20–19.5 ka BP, and 17.5 ka BP. A sharp drop in accumulation rate between 13 and 10 ka BP is followed by a rapid return to higher accumulation rates.

3.2. Geochemical analyses

3.2.1. Inorganic geochemistry and mineralogy

The Avaatech XRF scans yielded interpretable data for six elements, and each has been calibrated to quantitative WD-XRF measurements (Si, S, Ca, Ti, Mn, Fe – Supp Fig. 3). The elemental trends fall visually into three distinct groups, within which elements display similar stratigraphic variation: (1) Si; (2) Ca and Mn; (3) Fe, Ti and S (Fig. 2). Ca and Mn are mostly present only in trace concentrations, except for a broad peak between 17 and 12 ka BP which corresponds to the only core section where the calcite tests of ostracods are preserved. This is reflected in the XRD data, where calcite is abundant between 14 and 15.9 ka BP, but absent from the remainder of the samples (Supp. Table 4).

Si is by far the most abundant inorganic element, and is present as both quartz and biogenic opal (diatoms and sponge spicules were both identified by visual inspection of the sediment), as well as a range of silicate minerals. The x-ray diffractograms indicate that amorphous (biogenic) silica is a major component of the sediment throughout the core. The abundance of quartz, feldspars, and clays is relatively variable, and these minerals are likely the main contributors to downcore variability in Si, although this is difficult to quantify given that amorphous silica does not manifest as a distinct pattern in the diffractograms, but rather a diffuse 'hump'. Moderate to abundant quartz is present in all samples from 28.8 to 15.9 ka BP, but subsequently decreases and is present only in trace to minor amounts between 14 and 8.5 ka BP. Similarly, feldspars and silt-sized illite/kaolinite aggregates are present in minor to moderate amounts from 29.7 to 19.1 ka BP, but were either not identified, or present only in trace amounts in younger samples.

PCA performed on the calibrated XRF data captures the two dominant trends in the first two principal components (PC1 and PC2). Both axes are significant according to the broken stick test, and summarise the majority of the variance in the dataset (Fig. 2, Supp. Table 3). PC1 explains 42 % of the total variability, and is strongly dominated by Si. PC1 is relatively stable between 30 and 21 ka BP, with minor negative peaks at 24.8 and 22 ka BP (Fig. 2). The pattern of change during the global LGM features an increase in both variability and absolute values, with distinct negative peaks at 20 and 19 ka BP. PC1 then exhibits a gradual decline until ca. 15 ka BP, followed by a slight increase to the start of the Holocene, and then relatively stable values during the early Holocene (Fig. 2).

PC2 explains a further 33 % of the total variance, and is strongly correlated to Ti, Fe, and S; the former two are elements that are present both in the Lake Surprise catchment, and in Australian dust sources (De Deckker et al., 2012; Petherick et al., 2009). The overall variability of PC2 is dominated by a cyclicity with a period of ca. 2300 years (significant at 95 % confidence level; Supp Fig. 5), superimposed on a slight decreasing trend from 30 to 21 ka BP, and an overall increase from 15 ka BP into the Holocene, along with a reduction in variability (Fig. 2).

A plot of the first and second principal components yields a 'horseshoe' shape (Fig. 2c). This is characteristic of a long environmental gradient in the data that is not sufficiently captured by

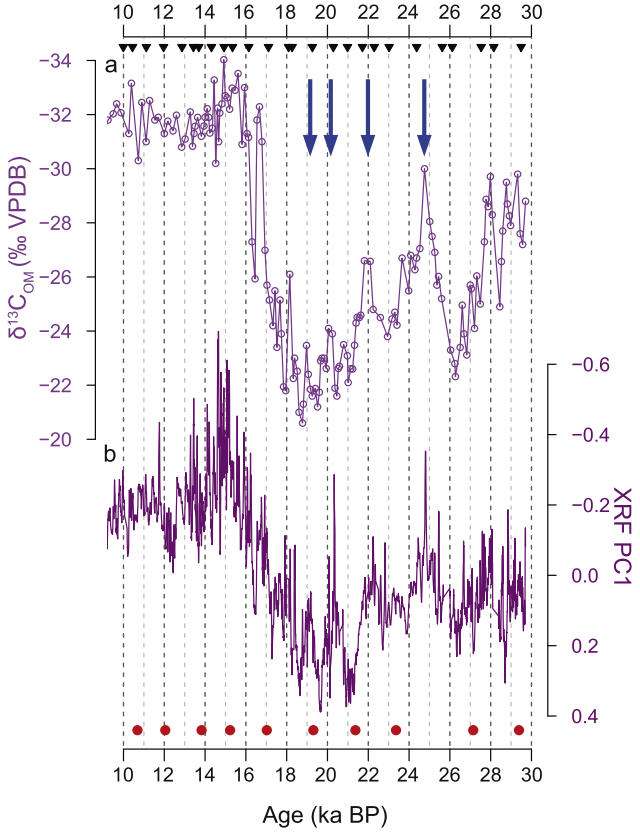

Fig. 4. Selected data from the 30-10 ka BP geochemical record from Lake Surprise: **a**) Bulk sediment carbon isotope ratios ($\delta^{13}C_{OM}$), interpreted to reflect plant moisture stress; **b**) First principal component (PC1) of the calibrated scanning XRF dataset, interpreted to reflect aeolian deposition of Si in the lake. Blue arrows indicate periods of increased effective moisture within the relatively arid LGM. Filled triangles denote ^{14}C age control points. Red circles denote the location of XRD samples (Supp. Table 4). (For interpretation of the references to colour in this figure legend, the reader is referred to the Web version of this article.)

an unconstrained ordination, but may be more accurately modelled by fitting a principal curve. The principal curve for the Lake Surprise XRF data describes 80 % of the total variance, however, the trend is near identical to PC1.

3.2.2. Organic geochemistry

TOC concentrations in core LS04 are highly variable, with a range of 33 % around a mean of 27 % and median of 28 %. The broad trend is characterised by fluctuations around a mean that is relatively stable between 30 and 20 ka BP, then follows a slight upward trend from 20 to 10 ka BP. Organic C:N ratios are relatively invariant, with a range of 8 around a mean and median of 18. There is no long-term trend in the mean C:N throughout the analysed section of the core (Supp. Fig. 4).

The $\delta^{13}C_{OM}$ is also highly variable, with a range of 13‰ around a mean and median of −28 ‰. $\delta^{13}C_{OM}$ increases by ~4 ‰ between 28 and 26 ka BP, then rapidly decreases to ~ -30 ‰ by 25 ka BP. This is followed by an overall increase to the highest values of ~ -21‰ at 21–18.5 ka BP, punctuated by distinct millennial-scale periods of lower $\delta^{13}C_{OM}$. A sharp negative shift of over 10 ‰ between 18 and 16 ka BP is interrupted by a brief return to more positive values at 16.5 ka BP. The remainder of the record from 16 to 10 ka BP features relatively stable values around −32 ‰, the most negative in the record (Fig. 4). $\delta^{13}C_{OM}$ is linearly correlated with XRF PC1 ($r^2 = 0.56$, $p \ll 0.05$) (Supp. Fig. 6).

4. Discussion

Our new high-resolution data from the sediments of Lake Surprise complement existing palaeoecological data (Builth et al., 2008), and record distinct climate variability in south-eastern Australia throughout the period from 30 to 10 ka BP. The highly resolved age-depth model for Lake Surprise makes it one of the most well constrained late Quaternary palaeoclimate records for southern Australia. The constraint of climate fluctuations at Lake Surprise allows for robust inter-site comparison; both (1) regionally, to determine the geographic significance of these events, and (2) globally, to establish likely mechanisms underpinning the variability.

4.1. Interpretation of Lake Surprise geochemical data

4.1.1. XRF and mineralogical data

High-resolution core scanning is increasingly used to characterise the elemental composition of lake sediments (e.g. Hahn et al., 2014; Turner et al., 2015; Weltje et al., 2015; Burrows et al., 2016), which varies as a function of the accumulation of autochthonous and allochthonous minerals. This in turn is driven by the flux of alluvial and aeolian sediment, as well as changes in lake water chemistry. The elemental composition therefore archives various environmental and climate processes, including lake hydrological balance, exposure and inundation of littoral areas, biogeochemical cycling, catchment erosion and dust deposition (Davies et al., 2015). These factors are difficult to deconvolve, however here we propose likely scenarios, given the specific environmental setting.

At Lake Surprise, scanning XRF PC1 is dominated by Si (Fig. 2c), and may therefore represent the deposition of aeolian sediment (quartz, feldspars, and clays), colluvial feldspars and clays, or biogenic opal from diatoms and sponge spicules. Diatom concentration data are currently not available for these sediments, however variation in opal peak heights on the x-ray diffractograms is not consistent with trends in XRF Si (Supp. Table 4, Fig. 2). This suggests a primary lithogenic driver of Si variability. Abundant quartz silt is associated with high Si between ~28 and 17 ka BP, and this must represent aeolian deposition, given the catchment bedrock is basaltic (Irving and Green, 1976). An aeolian source is supported by the low concentration of plagioclase and apparent absence of lithic grains, which together indicate a predominance of distally-versus locally-sourced detritus. Secondary clay minerals (kaolinite, smectite, and illite) were present in sufficient abundances to be detected via bulk powder XRD only prior to 19 ka BP, also corresponding to high Si, and the occurrence of kaolinite as discrete, silt-size aggregates indicates that it was windblown.

Comparison with regional palaeoclimate records provides support for this interpretation. Despite sampling and age uncertainties, the majority of palaeoclimate records for south-eastern Australia indicate that 30–18.5 ka BP (high Si at Lake Surprise) was generally dry relative to the deglacial (lower Si at Lake Surprise). The consequent reduction in vegetation cover probably increased sediment deflation in sediment source areas to the north-east and north-west, and this would have been supplemented by the lower sea level providing a greater potential source area on the exposed continental shelf along the path of the prevailing westerly winds (Hesse and McTainsh, 1999, 2003; Petherick et al., 2013). Furthermore, PC1 follows a similar trend to two direct records of aeolian dust accumulation from eastern Australia (Supp. Fig. 7) (De Deckker et al., 2012; Petherick et al., 2009). We are therefore confident in the inference that at Lake Surprise, an increase in PC1 reflects increased aeolian sediment supply, potentially due to (1) reduced regional vegetation cover in source areas to the west, north-east, and north-west (depending on seasonal wind direction), and (2) lower sea level resulting in an overall greater potential sediment source area.

PC2 is dominated by the concentrations of Ti, Fe, and S (Fig. 2c). Ti is redox-insensitive, and accumulates in lacustrine sediments following detrital input via catchment erosion or aeolian deposition. Fe preservation in lacustrine sediments is affected both by detrital input (bound to clay minerals, and deposited in the lake without reaction), and, to a lesser extent, by redox conditions in the lake (Davison, 1993; Davies et al., 2015). The strong correspondence of the Fe and Ti profiles (Fig. 2a) suggests that first-order variability in Fe at Lake Surprise relates to the former i.e. changes in lithogenic detrital input. Fe and Ti in Lake Surprise may have originated from both local and distal sources. The basalt that forms the crater walls contains Fe- and Ti-bearing minerals, including olivine, labradorite, and augite, however, windblown dust in Australia tends to be rich in goethite (Petherick et al., 2009), and may supply clay-bound Fe. According to the XRD and SEM EDS-based mineral mapping analysis, potentially Ti- and Fe-bearing minerals in the Lake Surprise sediments include clays (Fe only), and rutile and ilmenite, present as 2–3 μm grains. Each of these minerals may be colluvially transported from the basaltic crater walls, or wind-blown, and may therefore reflect either changes in catchment weathering and erosion, or a different mode of aeolian deposition to that preserved in PC1.

Sulphur is largely delivered to lake water via deposition of marine aerosols, and leaching from catchment soils (Davies et al., 2015), with subsequent accumulation in the lake sediments dependent on lake water chemistry. Sulphur in the Lake Surprise sediment therefore reflects (1) the amount of S being delivered to the lake, and (2) the occurrence of conditions conductive to the preservation of sulphate minerals. Regarding (1), Chivas et al. (1991) found that the majority of sulphate in modern southern and central Australian lakes is of marine origin, with comparatively little from weathering of local bedrock. This may therefore provide support to an aeolian control on PC2.

Potential mechanisms for preservation of S in the Lake Surprise sediments are rather more complex than those for its delivery. Sulphur is present in Lake Surprise as iron sulphide minerals, including pyrite (during the early last deglacial), and jarosite (abundant in one sample only, around 28.8 ka BP). Pyrite is present

only in trace to minor quantities during the early last interglacial-glacial transition (LGIT), and may reflect increased supply of S to the lake due to a strengthening of the onshore south-westerly winds, which are prevalent over the modern Lake Surprise particularly during winter (Gentilli, 1971).

Jarosite is a mineral that precipitates in acidic, saline lake waters, and has been identified as an early diagenetic phase in several such settings in southern Australia (e.g. Alpers et al., 1992; Benison and Bowen, 2013). Factors that may cause the acidic conditions necessary for jarosite precipitation in lakes include the oxidation of sulphides, seepage of acidic groundwater, or large inputs of acid rain (Long et al., 1992). In each of these cases, jarosite precipitation is also dependent on evaporative concentration of constituent ions, generally resulting in crusts or cements, but there is no evidence for these in the Lake Surprise sediments. However, jarosite (Bani et al., 2009) and schwertmannite (a metastable mineral that tends to alter to jarosite) (Ohsawa et al., 2014) have also been identified in modern volcanic lakes, where precipitation is a result of degassing of sulphur-rich gas into the lake water following eruptive activity. We therefore speculate that the unique appearance of jarosite in the Lake Surprise sediments, early in the lake's history, was the result of some similar residual degassing activity following the eruption of Mt Eccles several thousand years prior.

Sulphur is also present in Lake Surprise as gypsum, which precipitates in lake environments under evaporative conditions. There is no evidence for periods of a dry lake bed in core LS04, which was taken from the deepest part of Lake Surprise. However, minor gypsum is present in the early Holocene section of the core, when we might expect higher lake levels (Supp. Table 4) (Petherick et al., 2013). This is counter-intuitive, as evaporative minerals would be expected to accumulate during the driest periods in a lake's history. We suggest that this may be a result of the unusual morphology of Lake Surprise. It is possible that gypsum precipitated in the large littoral areas at either end of the lake during periods of relatively low lake level (Fig. 1b). When lake level rose during periods of increased moisture balance, sediment was washed down to the core site in the profundal zone. Gypsum in core LS04 may therefore signify an increase in water depth following a period of relative aridity.

Given the complex controls on the elements that load most strongly on PC2, it is difficult to confidently ascribe PC2 to a specific environmental variable. One driver that is common to all three elements, however, is westerly and south-westerly wind strength, which influences the delivery of both marine sulphate and Fe- and Ti-bearing sediment to the lake, and colluvial weathering of the crater walls. This may indicate that whilst PC1 is representative of regional sediment availability, PC2 records the local influence of changes in wind strength.

Although negatively correlated with PC1, Ca and Mn are present only in trace amounts other than a broad peak between 17 and 12 ka BP (Fig. 2), corresponding with the only analysed section of LS04 with an accumulation of calcite ostracod tests. Ostracods are cosmopolitan organisms that occur across a wide spectrum of environmental conditions in south-eastern Australia (e.g. De Deckker, 1982; Chivas et al., 1986). The ostracod proliferation in these sediments may reflect changes in water oxygen profile, habitat availability, water chemistry, or taphonomic conditions, and will be the subject of future investigation.

4.1.2. Organic geochemical data

The $\delta^{13}C$ of bulk organic matter (OM) in a lake may have several controls, dependent in part on the OM source. The C:N ratio of OM is commonly used to separate autochthonous and allochthonous sources of OM in lakes; C:N values of OM from terrestrial and aquatic plants are typically >20 and < 10, respectively (Meyers and Ishiwatari, 1993). C:N in the LS04 OM is stratigraphically stable around a mean of 18, and the aquatic/terrestrial pollen ratio is consistently low (Builth et al., 2008). These lines of evidence suggest a dominant contribution of terrestrial plants to the OM (Supp. Fig. 8).

Three main factors affect the $\delta^{13}C_{OM}$ of terrestrial plants: (1) the photosynthetic pathway used by the source plants, where more arid conditions favour a dominance of C_4 (less negative $\delta^{13}C$) over C_3 (more negative $\delta^{13}C$) plant types, (2) changes in stomatal conductivity in C_3 plants, where increased moisture stress results in closure of stomatal pores and reduced discrimination against ^{13}C (i.e. less negative $\delta^{13}C$), and (3) partial pressure of atmospheric CO_2 (ρCO_2), where lower ρCO_2 results in reduced discrimination against ^{13}C during photosynthesis in C_3 plants (O'Leary, 1981; Farquhar et al., 1989; Prentice et al., 2011; Schubert and Jahren, 2012; Rao et al., 2017). With respect to (3), a shift of approximately −2 ‰ in $\delta^{13}C_{OM}$ may be ascribed to the ~100 ppm rise in ρCO_2 between the LGM and the Holocene (Schubert and Jahren, 2012, 2015). This is much smaller than the deglacial shift of approximately −10 ‰ recorded at Lake Surprise (Fig. 4), indicating a relatively minor influence of ρCO_2 on $\delta^{13}C_{OM}$ variability. Regarding factors (1) and (2), a reduction in effective moisture results in less negative $\delta^{13}C_{OM}$ values in both cases (Stewart et al., 1995; Kohn, 2010; Prentice et al., 2011; Rao et al., 2017).

We also acknowledge potential minor environmental impacts from (1) the local Indigenous people, and (2) fire. However, regarding (1), there is no definitive evidence for Indigenous people modifying the surrounding environmental until the mid-Holocene (Builth et al., 2008). Regarding (2), the pollen to charcoal ratio does not vary much through the record, indicating at most a minor influence of fire on the environmental variability (Builth et al., 2008). Hence, given the limited effect of glacial-interglacial atmospheric ρCO_2 and the relatively low and invariant contribution of autochthonous OM to Lake Surprise, we interpret changes in $\delta^{13}C_{OM}$ as an indirect tracer of terrestrial plant moisture stress, which is a direct response to local hydroclimate variability.

4.2. Hydroclimate change at Lake Surprise

Lake Surprise scanning XRF PC1 (interpreted to reflect increased aeolian sediment supply to Lake Surprise during periods of aridity) and $\delta^{13}C_{OM}$ (interpreted to reflect terrestrial vegetation moisture stress) are positively correlated (Supp Fig. 6), and provide a locally coherent record of changes in the hydrological cycle. This interpretation is supported by pollen data from Lake Surprise (Builth et al., 2008). Evidence for a slight increase in aeolian input to the lake from 28 to 18 ka BP coincides with relatively high $\delta^{13}C_{OM}$, and a dominance of open herbaceous grassland and semi-arid shrublands over forest or woodland. Together, these data suggest that 28–18 ka BP was a period of aridity both at Lake Surprise and in the surrounding region. During this time, local vegetation was subject to greater moisture stress; regional pollen records clearly indicate reduced tree and shrub cover during the glacial period (e.g. Builth et al., 2008; Cook, 2009), most likely resulting in increased supply of aeolian sediment to the lake. The timing is in agreement with palaeoclimate records from northern and eastern Australia (De Deckker, 2001; Petherick et al., 2008) and New Zealand (Hellstrom et al., 1998; Suggate and Almond, 2005; Alloway et al., 2007; Newnham et al., 2007), which all record arid conditions and increased dust transport coincident with local glacial maxima in New Zealand from around 28 ka BP, significantly earlier than the global LGM (Mix et al., 2001).

Within this interval, peak aridity occurs between 21 and 18.5 ka BP, possibly representing the expression of the global LGM at Lake Surprise. However, the Lake Surprise data also record distinct

millennial-scale episodes of increased effective moisture, centred on 24.8, 22, 20, and 19 ka BP (indicated by arrows on Fig. 4). These are reflected in reduced detrital input in conjunction with lower $\delta^{13}C_{OM}$, and are also coeval with peaks in *Eucalyptus* pollen at the expense of Asteraceae (Builth et al., 2008). In south-eastern Australia, expansion of eucalypts most likely reflects a regional increase in effective precipitation (Builth et al., 2008), and this adds weight to our interpretation of a succession of humid intervals within an arid period. The alternation of wetter and drier conditions at Lake Surprise provides further evidence that the global LGM in south-eastern Australia was not a prolonged, stable period of cold and dry conditions, but rather that the climate remained variable (Moss et al., 2013; Petherick et al., 2013; Reeves et al., 2013).

The period of increased moisture balance at 24.8 ka BP is particularly distinct, and coincides with the climate amelioration proposed for both Australia and New Zealand (Alloway et al., 2007; Newnham et al., 2007; Petherick et al., 2008; Augustinus et al., 2011), concurrent with oscillating lake levels in the Willandra region (Bowler et al., 2012) and warming in the Southern Ocean to the south of Australia (Calvo et al., 2007). The interpretation of a wetter period at 24.8 ka BP in our well-dated record provides strong support for the regional nature of this event, indicating that it may have been a period of major environmental change at least in southern Australia.

A major deglacial shift in hydroclimate commences at 18.5 ka BP at Lake Surprise, approximately concomitant with the rapid rise in global sea level (Clark and Mix, 2002). The transition is marked in the geochemical data by reduced detrital input and a sharp reduction in plant moisture stress. This implies a rapid transition from the period of peak aridity, to relatively moist conditions at the start of the LGIT, possibly with a decreased source area for aeolian sediment. The geochemical shift precedes a more gradual transition in the palaeoecological data, from open herbaceous vegetation to Casuarinaceae woodland (Builth et al., 2008). This lag implies a delayed response of the vegetation to deglacial climate change, perhaps due to the time taken for long-lived trees to become established following a major climatic shift (Builth et al., 2008).

The transition to deglacial conditions is interrupted by a temporary return to drier conditions at 16.5 ka BP, after which the $\delta^{13}C_{OM}$ remains remarkably stable. The inorganic geochemical data continues to exhibit variability, suggesting some disparity between local conditions within the crater rim, and regional climate. Detrital input to the lake decreases to a minimum around 14.5 ka BP, signifying a period of peak moisture balance for the period 30–10 ka BP. The subsequent increase in detrital input between 14.5 and 12 ka BP implies a minor drying into a relatively stable couple of millennia at the beginning of the Holocene (Fig. 4).

4.3. Multi-site analysis

There is a growing demand for objective numerical approaches to inferring regional-scale climate variability, through integration of multiple palaeoclimate records that have secure chronological control and high temporal resolution (Shakun and Carlson, 2010; Shanahan et al., 2015). The MCEOF method is one such approach, and incorporates the chronological uncertainty inherent in individual records. The MCEOF method has been applied to late Holocene records from Africa and southern Australia (Anchukaitis and Tierney, 2012; Tierney et al., 2013; Tyler et al., 2015), but until now has not been used for longer time periods.

The Lake Surprise record exhibits clear visual similarity with numerous high and low resolution records of climate variability from the region, but most notably with the two records that met the criteria for inclusion in the MCEOF analysis: a speleothem $\delta^{13}C$ record from the south island of New Zealand (Whittaker et al., 2011), and an XRF-derived record of Ti variation from offshore South Australia (De Deckker et al., 2012 (Fig. 1 & Supp. Fig. 9). The coherence between the records is remarkable given that the records are derived from disparate proxies spanning a longitudinal distance of over 2000 km, and points to a regional hydroclimate signal that transcends the influence of local or proxy-specific factors. The visual similarity is confirmed by the MCEOF analysis, which isolated one mode of hydroclimate variability (EOF1) that contains interpretable information, and explains 61% of the common variance (Fig. 3b–c). The trend described by EOF1 is broadly consistent with Australian aeolian sedimentation records (Petherick et al., 2008; Darrénougué et al., 2009, Petherick et al., 2009; Fitzsimmons et al., 2013), as well as many additional records of terrestrial Australasian hydroclimate that did not meet the criteria for inclusion in the MCEOF analysis; examples are provided in Fig. 5. To test the robustness of the MCEOF analysis, we tried including several records that failed to meet criteria 3) or 4) i.e. chronological or sampling resolution. In each case, the first mode of variability was almost indistinguishable from EOF1, apart from some loss of finer-scale variability.

This consistency indicates that the trends and millennial-scale variability observed in the three records reflect the regional hydrological cycle in south-eastern Australasia between 30 and 10 ka BP, and that the trend is accurately captured by the MCEOF analysis.

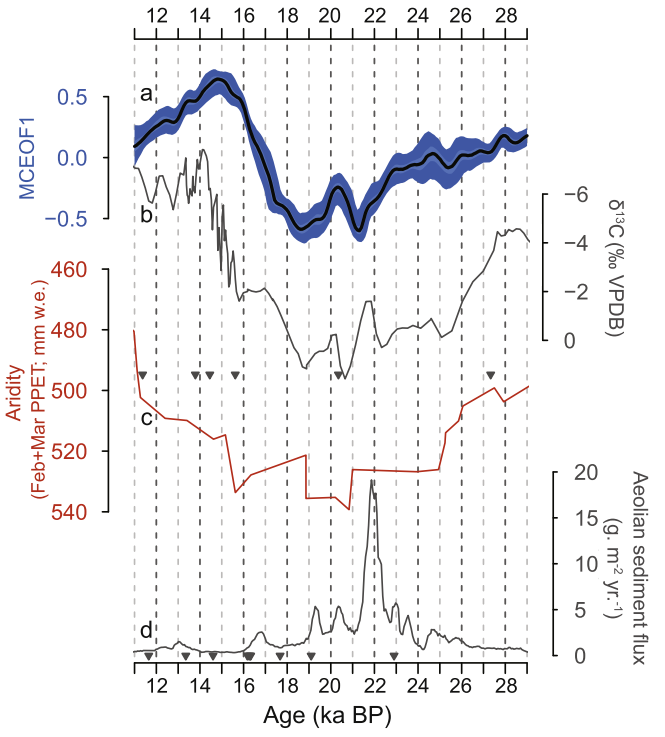

Fig. 5. Comparison of the first Empirical Orthogonal Function (MCEOF1) of three high-resolution hydroclimate records, with Australian and New Zealand hydroclimate records not included in the MCEOF analysis: **a**) MCEOF1, representing regional hydroclimate change in the south-east Australian and NZ region, during the period from 29 to 11 ka BP. Black line = median timeseries, dark and light shading = 90% and 68% confidence intervals, respectively; **b**) Speleothem $\delta^{13}C$ from Mt. Arthur in New Zealand, interpreted to reflect changes in regional forest productivity (Hellstrom et al., 1998); **c**) aridity index (February and March point-potential evapotranspiration, in mm of water equivalent) for arid southern Australia, derived from the $\delta^{18}O$ of emu eggshells (Miller and Fogel, 2016); **d**) total aeolian sediment flux to Native Companion Lagoon (Petherick et al., 2009). Timeseries **a**)-**c**) oriented so that 'up' indicates a wetter climate. Location of age control points for **b**) and **d**) denoted by grey triangles.

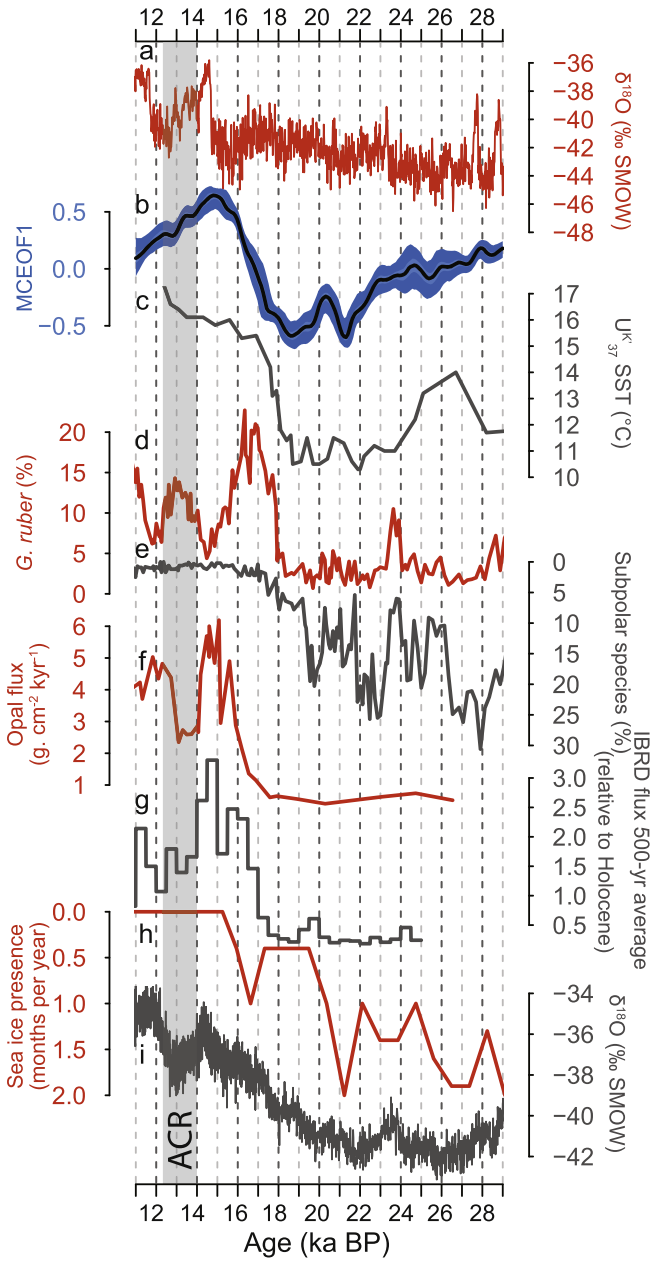

Fig. 6. Trends in south-east Australian and NZ hydroclimate, compared with a range of global palaeoclimate records: **a**) $\delta^{18}O$ record from NGRIP ice core, indicative of mean annual surface air temperature in the NH high latitudes (WAIS Divide Project Members, 2013); **b**) Regional south-east Australian and NZ hydroclimate (this study). Black line = median timeseries, dark and light shading = 90% and 68% confidence intervals, respectively; **c**) Mean annual SST for offshore south-eastern Australia, derived using the $U^{K'}_{37}$ alkenone index (Lopes dos Santos et al., 2013); **d-e** Percentages of planktic foraminifera from core MD03-2611, located south of Australia near the modern location of the subtropical front: **d**) *Globigerinoides ruber*, a subtropical near-surface dweller that tracks the position of the Leeuwin Current, and **e**) subpolar species, indicative of subantarctic/Antarctic water masses, and hence the proximity of the subantarctic front (SAF) (De Deckker et al., 2012); **f**) Biogenic silica flux south of the Antarctic Polar Front, indicative of the rate of upwelling in the Southern Ocean (Anderson et al., 2009); **g**) 500-yr average of iceberg-rafted debris flux to the Scotia Sea, relative to the Holocene average. Reflects iceberg flux from the Antarctic ice sheet (Weber et al., 2014); **h**) Duration of sea-ice presence (months per year) over a core location near the LGM maximum winter sea ice extent, in the Indian sector of the Southern Ocean (Crosta et al., 2004); **i**) $\delta^{18}O$ record from WDC ice core, indicative of mean annual surface air temperature in the SH high latitudes (WAIS Divide Project Members, 2013). Records are plotted from north to south, and are oriented so that 'up' indicates a warmer/wetter climate. Approximate duration of the Antarctic Cold Reversal (ACR) highlighted by grey window.

The pattern of change in EOF1 indicates a gradual decrease in regional moisture balance from 30 ka BP to 23.5 ka BP, with a small reversal at ca. 24.5 ka BP. The lowest values of EOF1 occur between 21.5 and 18.5 ka BP, indicating peak aridity at this time, but punctuated by a moisture peak at 21–20 ka BP. The minor 24.5 ka BP event coincides with the period of increased moisture balance identified in the Lake Surprise multi-proxy record (Fig. 4), but is considerably less distinct. This may reflect smoothing due to incorporation of the chronological uncertainty, especially considering that this is a period of relatively sparse age control for Hollywood Cave (Fig. 3aii). Nevertheless, this provides some evidence that this wetter period within a generally arid interval may have been a regional event that lasted for up to 1500 years. This is relatively brief considering the low sediment accumulation rates characteristic of many Australian wetlands in particular, where data can only be collected at millennial-scale resolution, and is a possible reason for the event remaining largely undetected in hydroclimate records for south-eastern Australia and NZ.

The rapid deglacial switch from relatively dry to relatively wet conditions observed at Lake Surprise is maintained in EOF1, where the transition occurs between 18.5 and 16 ka BP, and is then followed by an overall decrease in moisture balance into the Holocene.

4.4. Potential drivers of regional hydroclimate

Between 29 ka BP and 16 ka BP, the EOF1 pattern of change is comparable to records of SH ocean and atmospheric circulation, within dating uncertainty (Anderson et al., 2009; De Deckker et al., 2012; Lopes dos Santos et al., 2013; Weber et al., 2014; WAIS Divide Project Members, 2015) (Fig. 6b–i). Relatively arid conditions in south-eastern Australia and New Zealand were associated with increased sea ice extent around Antarctica, along with reduced wind strength and cooler SSTs in the Southern Ocean south of Australia i.e. the dominant moisture source for the region. This relationship is unsurprising for coastal margin climates that are strongly subject to variations in both SST and atmospheric circulation (Mullan, 1998; Watterson, 2001). The decrease in latent heat flux from the ocean implies a weakened continental hydrological cycle (e.g. Hesse and McTainsh, 1999; Hesse and McTainsh, 2003), and consequent widespread reduction in precipitation. This is likely to have been compounded by the lower eustatic sea level (Clark and Mix, 2002), as each site lay further from the moisture source offshore.

Hesse and McTainsh (1999) and Shulmeister et al. (2016) suggested that the strength and position of the SWW (i.e. the key mechanism for the delivery of the moisture onshore) did not vary greatly over the past 25 ka BP. If this were the case, then SH SST must have had a greater influence than wind strength on regional hydroclimate during the last glacial period. This is supported by slight increases in Southern Ocean SST, coincident with southward migration of the cold subantarctic front (Fig. 1a) (Lopes dos Santos et al., 2013), which match the timing of the peaks in regional moisture balance inferred from EOF1, particularly at 21–20 ka BP (Fig. 6).

The onset of more rapid Antarctic warming post 18 ka BP was associated with i) melting of the ice sheet (Weber et al., 2014), ii) reduced sea ice extent (Crosta et al., 2004; Ferry et al., 2015), iii) poleward displacement of the cold subantarctic front (De Deckker et al., 2012), iv) increased upwelling strength in the Southern Ocean (Anderson et al., 2009), and v) a rapid increase in SST off the southern coast of Australia between 18 and 16 ka BP (Lopes dos Santos et al., 2013) (Fig. 6). This was matched by a switch from arid to more humid conditions in south-eastern Australia and New Zealand, implying a re-invigoration of the hydrological cycle. The Australian sites may also been affected by the opening of the

Indonesian Throughflow, and renewed delivery of warm Indian Ocean water to southern Australia by the Leeuwin Current (Figs. 1a and 6d) (Gingele et al., 2001; De Deckker et al., 2012).

The Last Glacial-Interglacial Transition (LGIT) in each of the SH high latitude records (Fig. 6c–i) is characterised by a reasonably uniform warming/wetting trend between 18 and 12 ka BP, interrupted by a two-millennia duration event. This event coincides with the Antarctic Cold Reversal (ACR), a millennial-scale high latitude cooling event which occurred between ca. 14 and 12.2 ka BP (grey window in Fig. 6) (Pedro et al., 2016). The stabilisation of the Antarctic ice sheet and northward migration of cold SO fronts (Fig. 1) during the ACR is reflected in EOF1 as a slight increase in the rate of decline of the moisture balance, also consistent with a weakening of the SWW at this time (Anderson et al., 2009).

Following these major shifts in SH ocean-atmosphere circulation between 18 and 15 ka BP, the strength of the relationship between EOF1 and SH high latitude drivers weakens. Likewise, the rapid climate shift that characterises the start of the Holocene in many palaeoclimate records from both the SH and NH high latitudes is not present in EOF1, which instead reflects a continued gradual drying trend until at least 11 ka BP (Fig. 6). A parsimonious explanation may simply be that with the removal of a strong SO influence on south-east Australian and NZ climates, a more complex array of climate drivers – including the modern drivers that originate in the equatorial regions, such as ENSO and the IOD (e.g. Ashok et al., 2007) - began to exert a stronger influence on the SH mid-latitudes.

Our data and analyses therefore suggest that the mechanisms controlling the regional hydrological cycle in south-eastern Australasia varied over multi-millennial time scales, with a strong dominant Southern Ocean influence during the last glacial giving way to more complex drivers during the deglacial and early Holocene. These conclusions are corroborated by Bayon et al. (2017), who use sediment provenance proxy data from a marine core from southern Australia to advocate a combined northern- and southern high latitude control on SH subtropical climates during the last glacial period (90–20 ka BP). It is important to note, however, that any potential mechanism remains equivocal without additional high-resolution reconstructions of SST and terrestrial hydroclimate across the region.

4.5. Spectral analysis

Spectral analysis performed on the Lake Surprise data returned no persistent frequencies in the $\delta^{13}C_{OM}$ or XRF PC1 records, but yielded two significant peaks in XRF PC2, centred around 1600 and 2300 years (Supp. Fig. 5). A significant peak at 2300 ± 200 years is also present in the hydroclimate records from Hollywood Cave and core MD03-2611 (Supp. Fig. 5), both of which are well-dated, and sampled at appropriate resolution to discern cyclicity on millennial time scales. This hints at a climate oscillation that is consistent on at least a regional scale. Intriguingly, a similar periodicity is present in several late Pleistocene climate reconstructions from a diverse geographical range, including northern Australian hydroclimate (De Deckker, 2001; Denniston et al., 2013), East African hydroclimate (van Bree et al., 2014), Antarctic air temperature (WAIS Divide Project Members, 2015), and iceberg rafted debris in the Southern Ocean (Weber et al., 2014) (Supp Fig. 5), as well as two low-resolution records of sea-ice presence around Antarctica, where the cycle is present but not significant (Crosta et al., 2004; Ferry et al., 2015). We acknowledge that this is only a tiny fraction of all late Pleistocene records, however due to aliasing, a signal can only be identified in records that are both well dated, and of sufficiently high resolution. However, the occurrence of this periodicity in a broad range of high-resolution records suggests that a ca. 2300 year cycle may be a real climatic feature of late Quaternary climate, but also poses the significant challenge of identifying the driver of a potentially globally coherent climate response.

One such link has previously been proposed for the persistence of a ca. 2300 year cycle throughout climate records of the Holocene. The presence of this periodicity in both solar activity and palaeoclimate proxy records has led to the suggestion that cyclical changes in solar insolation may be a contributing influence on millennial-scale climate variation in south-east Australia (McGowan et al., 2010) as well as a broad range of climatic regimes globally (e.g. Damon and Jirikowic, 1992; Engels and van Geel, 2012; Scafetta et al., 2016; Soon et al., 2014; Steinhilber et al., 2009; van Bree et al., 2014). A potential causal relationship between small changes in solar irradiance and global climate remains elusive for the Holocene (Haigh, 2007; Versteegh, 2005), and this uncertainty is amplified considering the only record of cosmogenic ^{14}C production that extends beyond the Holocene does not preserve any significant periodicity (Hughen et al., 2006). Additionally, the direct influence of solar irradiance on climate variability is likely to be small in comparison to that of ocean and atmospheric circulation on glacial-interglacial timescales, and requires amplification by internal climate processes (de Garidel-Thoron et al., 2001; Khider et al., 2014; Ogurtsov et al., 2010). Nonetheless, a persistent spectral signature across a broad range of climatic zones for at least 30,000 years does suggest a consistent external forcing apparently independent of a 'bipolar seesaw' mechanism, and a solar origin of the 2300-year periodicity should probably not be discounted, although we also acknowledge the possibility that the periodicity is a heterodyne of higher-frequency cycles (Clemens, 2005). This potential modulation of global millennial-scale climate variability warrants further investigation, and will require further well dated, high-resolution records of both climate, and solar activity.

5. Conclusions

1. A multi-proxy record of late Quaternary (30–10 ka BP) hydroclimate change from Lake Surprise, south-eastern Australia, is accompanied by a well-constrained age-depth model, allowing detailed comparison with existing records.
2. Quantitative high-resolution XRF data provide a record of aeolian sediment supply to the lake, whilst the carbon isotope composition of bulk organic matter reflects local terrestrial vegetation moisture stress. Together these data provide a coherent record of hydroclimate change in south-eastern Australia.
3. The onset of arid 'LGM-like' conditions at Lake Surprise occurred around 28 ka BP, providing further evidence that the LGM in the SH mid-latitudes may have commenced considerably earlier than the global LGM around 23 ka BP. Similarly, a period of increased moisture balance around 24.8 ka BP is coincident with similar events in Australian and New Zealand records, suggesting that this climate amelioration may have been a regional event. The combined proxy data indicate that peak aridity was reached at Lake Surprise between ~21–18.5 ka BP, but also that climatic variability persisted throughout the LGM.
4. An MCEOF approach was used to extract a pattern of change (EOF1) that is common to three high-resolution, well-dated hydroclimate records from south-eastern Australia and NZ. EOF1 incorporates the chronological uncertainty inherent in each record, and is free from site-specific idiosyncrasies. We argue that EOF1 is representative of changes in the regional hydrological cycle, and consequently explore the relationship of this pattern with potential drivers, with a higher degree of confidence than may be obtained from a traditional single-site approach.

5. Evidence for a regionally coherent early LGM is ambiguous in EOF1, as is an interval of increased moisture balance at 25-24 ka BP. However, this may be a result of smoothing due to the geochronological uncertainty in the component records. EOF1 indicates that peak aridity in south-eastern Australia and NZ occurred between ~21.5–18.5 ka BP.
6. Our analysis indicates that drivers of the regional hydrological cycle varied over multi-millennial time scales. At the end of the last glacial period (30–18.5 ka BP), a strong Southern Ocean influence led to cold SSTs south of Australia and NZ, resulting in a weakened terrestrial hydrological cycle, and widespread aridity. During the last glacial-interglacial transition, retreating Antarctic sea ice and a southward migration of the subantarctic front resulted in a marked decrease in Southern Ocean influence on south-eastern Australian and NZ hydroclimate, making way for more complex controls on regional hydroclimate, potentially similar to those of the modern day.
7. A ca. 2300 year periodicity that is present in climate records from a broad range of climate regimes globally is also present in the component records of the MCEOF, and may represent a solar modulation of millennial-scale climate variability. However, a mechanism for this influence remains equivocal.

Declarations of interest

None.

Acknowledgements

This research was partially funded by an ARC Discovery Project (grant number DP140014093). The authors would like to thank AINSE Limited for providing a Postgraduate Research Award to G. Falster to enable acquisition of new radiocarbon dates (grant number ALNSTU11873). G. Falster received support for this research through the provision of an Australian Government Research Training Program Scholarship. The authors also acknowledge the financial support from the Australian Government for the Centre for Accelerator Science at ANSTO through the National Collaborative Research Infrastructure Strategy. The authors are grateful to Mark Rollog, Peter Self, and Tony Hall for assistance in lab analyses, and to Dave Heslop for providing the Matlab script for calibration of the XRF scanner data. Cameron Barr is also thanked for his contribution to initial discussions of the data. The comments of two anonymous reviewers greatly increased the quality of the manuscript.

Appendix A. Supplementary data

Supplementary data related to this article can be found at https://doi.org/10.1016/j.quascirev.2018.05.031.

References

Alloway, B.V., Stewart, R.B., Neall, V.E., Vucetich, C.G., 1992. Climate of the last glaciation in New Zealand, based on aerosolic quartz influx in an andesitic terrain. Quat. Res. 38, 170–179.
Alloway, B.V., Lowe, D.J., Barrell, D.J.A., Newnham, R.M., Almond, P.C., Augustinus, P.C., Bertler, N.A.N., Carter, L., Litchfield, N.J., McGlone, M.S., Shulmeister, J., Vandergoes, M.J., Williams, P.W., 2007. Towards a climate event stratigraphy for New Zealand over the past 30 000 years (NZ-INTIMATE project). J. Quat. Sci. 22, 9–35.
Alpers, C.N., Rye, R.O., Nordstrom, D.K., White, L.D., King, B.-S., 1992. Chemical, crystallographic and stable isotopic properties of alunite and jarosite from acid—hypersaline Australian lakes. Chem. Geol. 96, 203–226.
Anchukaitis, K.J., Tierney, J.E., 2012. Identifying coherent spatiotemporal modes in time-uncertain proxy paleoclimate records. Clim. Dynam. 41, 1291–1306.
Anderson, R.F., Ali, S., Bradtmiller, L.I., Nielsen, S.H.H., Fleisher, M.Q., Anderson, B.E., Burckle, L.H., 2009. Wind-driven upwelling in the Southern Ocean and the deglacial rise in atmospheric CO_2. Science 323, 1443–1448.
Ashok, K., Nakamura, H., Yamagata, T., 2007. Impacts of ENSO and Indian Ocean Dipole events on the Southern Hemisphere storm-track activity during austral winter. J. Clim. 20, 3147–3163.
Augustinus, P., D'Costa, D., Deng, Y., Hagg, J., Shane, P., 2011. A multi-proxy record of changing environments from ca. 30 000 to 9000 cal. a BP: Onepoto maar palaeolake, Auckland, New Zealand. J. Quat. Sci. 26, 389–401.
Augustinus, P., Cochran, U., Kattel, G., D'Costa, D., Shane, P., 2012. Late Quaternary paleolimnology of Onepoto maar, Auckland, New Zealand: Implications for the drivers of regional paleoclimate. Quat. Int. 253, 18–31.
Ayliffe, L.K., Marianelli, P.C., Moriarty, K.C., Wells, R.T., McCulloch, M.T., Mortimer, G.E., Hellstrom, J.C., 1998. 500 ka precipitation record from south-eastern Australia: evidence for interglacial relative aridity. Geology 26, 147–150.
Bani, P., Oppenheimer, C., Varekamp, J.C., Quinou, T., Lardy, M., Carn, S., 2009. Remarkable geochemical changes and degassing at Voui crater lake, Ambae volcano, Vanuatu. J. Volcanol. Geoth. Res. 188, 347–357.
Barr, C., Tibby, J., Gell, P., Tyler, J., Zawadzki, A., Jacobsen, G.E., 2014. Climate variability in south-eastern Australia over the last 1500 years inferred from the high-resolution diatom records of two crater lakes. Quat. Sci. Rev. 95, 115–131.
Barr, C., Tibby, J., Moss, P.T., Halverson, G.P., Marshall, J.C., McGregor, G.B., Stirling, E., 2017. A 25,000-year record of environmental change from Welsby Lagoon, North Stradbroke Island, in the Australian subtropics. Quat. Int. 449, 106–118.
Barrell, D.J.A., Almond, P.C., Vandergoes, M.J., Lowe, D.J., Newnham, R.M., 2013. A composite pollen-based stratotype for inter-regional evaluation of climatic events in New Zealand over the past 30,000 years (NZ-INTIMATE project). Quat. Sci. Rev. 74, 4–20.
Barrows, T.T., Stone, J.O., Fifield, L.K., Cresswell, R.G., 2001. Late Pleistocene glaciation of the Kosciuszko Massif, Snowy Mountains, Australia. Quat. Res. 55, 179–189.
Barrows, T.T., Stone, J.O., Fifield, L.K., Cresswell, R.G., 2002. The timing of the Last Glacial Maximum in Australia. Quat. Sci. Rev. 21, 159–173.
Barrows, T.T., Juggins, S., De Deckker, P., Calvo, E., Pelejero, C., 2007. Long-term sea surface temperature and climate change in the Australian–New Zealand region. Paleoceanography 22.
Barrows, T.T., Almond, P., Rose, R., Keith Fifield, L., Mills, S.C., Tims, S.G., 2013. Late Pleistocene glacial stratigraphy of the Kumara-Moana region, West Coast of south island, New Zealand. Quat. Sci. Rev. 74, 139–159.
Bayon, G., De Deckker, P., Magee, J.W., Germain, Y., Bermell, S., Tachikawa, K., Norman, M.D., 2017. Extensive wet episodes in Late Glacial Australia resulting from high-latitude forcings. Sci. Rep. 7, 44–54.
Benison, K.C., Bowen, B.B., 2013. Extreme sulfur-cycling in acid brine lake environments of Western Australia. Chem. Geol. 351, 154–167.
Bennett, K.D., 1996. Determination of the number of zones in a biostratigraphical sequence. New Phytol. 132, 155–170.
Blaauw, M., Christen, J.A., 2011. Flexible paleoclimate age-depth models using an autoregressive gamma process. Bayesian Analysis 6, 457–474.
Black, M.P., Mooney, S.D., Martin, H.A., 2006. A >43,000-year vegetation and fire history from lake Baraba, New South Wales, Australia. Quat. Sci. Rev. 25, 3003–3016.
Blunier, T., Brook, E.J., 2001. Timing of millennial-scale climate change in Antarctica and Greenland during the last glacial period. Science 291, 109–112.
Blunier, T., Chappellaz, J., Schwander, J., Dallenbach, A., Stauffer, B., Stocker, T.F., Raynaud, D., Jouzel, J., Clausen, H.B., Hammer, C.U., Johnsen, S.J., 1998. Asynchrony of Antarctic and Greenland climate change during the last glacial period. Nature 394, 739–743.
Boutakoff, N., 1963. The Geology and Geomorphology of the Portland Area. Department of Mines Melbourne, Victoria.
Bowler, J.M., 1976. Aridity in Australia: age, origins and expression in aeolian landforms and sediments. Earth Sci. Rev. 12, 279–310.
Bowler, J.M., 1998. Willandra Lakes revisited: environmental framework for human occupation. Archaeol. Ocean. 33, 120–155.
Bowler, J.M., Hamada, T., 1971. Late Quaternary Stratigraphy and Radiocarbon Chronology of Water Level Fluctuations in Lake Keilambete, Victoria. Nature 232, 330–332.
Bowler, J.M., Johnston, H., Olley, J.M., Prescott, J.R., Roberts, R.G., Shawcross, W., Spooner, N.A., 2003. New ages for human occupation and climatic change at Lake Mungo, Australia. Nature 421, 837.
Bowler, J.M., Gillespie, R., Johnston, H., Boljkovac, K., 2012. Wind v water: glacial maximum records from the Willandra Lakes. In: Haberle, S.G., David, B. (Eds.), Peopled Landscapes: Archaeological and Biogeographic Approaches to Landscapes. ANU E-Press, Canberra, pp. 271–296.
Boyce, J., 2013. The Newer Volcanics Province of southeastern Australia: a new classification scheme and distribution map for eruption centres. Aust. J. Earth Sci. 60, 449–462.
Broecker, W.S., 1998. Paleocean circulation during the Last Deglaciation: a bipolar seesaw? Paleoceanography 13, 119–121.
Builth, H., Kershaw, A.P., White, C., Roach, A., Hartney, L., McKenzie, M., Lewis, T., Jacobsen, G., 2008. Environmental and cultural change on the Mt Eccles lava-flow landscapes of southwest Victoria, Australia. Holocene 18, 413–424.
Bureau of Meteorology, 2013. Climate Statistics for Australian Locations - Heywood Forestry. Bureau of Meteorology, Commonwealth of Australia.
Burrows, M.A., Heijnis, H., Gadd, P., Haberle, S.G., 2016. A new late Quaternary palaeohydrological record from the humid tropics of northeastern Australia.

Palaeogeogr. Palaeoclimatol. Palaeoecol. 451, 164–182.
Cai, W., Shi, G., Cowan, T., Bi, D., Ribbe, J., 2005. The response of the Southern Annular Mode, the East Australian Current, and the southern mid-latitude ocean circulation to global warming. Geophys. Res. Lett. 32.
Calvo, E., Pelejero, C., De Deckker, P., Logan, G.A., 2007. Antarctic deglacial pattern in a 30 kyr record of sea surface temperature offshore South Australia. Geophys. Res. Lett. 34, 1–6.
Carter, L., Neil, H.L., McCave, I.N., 2000. Glacial to interglacial changes in non-carbonate and carbonate accumulation in the SW Pacific Ocean, New Zealand. Palaeogeogr. Palaeoclimatol. Palaeoecol. 162, 333–356.
Chivas, A.R., Deckker, P.D., Shelley, J.M.G., 1986. Magnesium and strontium in non-marine ostracod shells as indicators of palaeosalinity and palaeotemperature. Hydrobiologia 143, 135–142.
Chivas, A.R., Andrews, A.S., Lyons, W.B., Bird, M.I., Donnelly, T.H., 1991. Isotopic constraints on the origin of salts in Australian playas. 1. Sulphur. Palaeogeogr. Palaeoclimatol. Palaeoecol. 84, 309–332.
Clark, P.U., Mix, A.C., 2002. Ice sheets and sea level of the Last Glacial Maximum. Quat. Sci. Rev. 21, 1–7.
Clark, P.U., Dyke, A.S., Shakun, J.D., Carlson, A.E., Clark, J., Wohlfarth, B., Mitrovica, J.X., Hostetler, S.W., McCabe, A.M., 2009. The Last Glacial Maximum. Science 325, 710–714.
Clemens, S.C., 2005. Millennial-band climate spectrum resolved and linked to centennial-scale solar cycles. Quat. Sci. Rev. 24, 521–531.
Cohen, T.J., Nanson, G.C., Jansen, J.D., Jones, B.G., Jacobs, Z., Treble, P., Price, D.M., May, J.-H., Smith, A.M., Ayliffe, L.K., Hellstrom, J.C., 2011. Continental aridification and the vanishing of Australia's megalakes. Geology 39, 167–170.
Cohen, T.J., Jansen, J.D., Gliganic, L.A., Larsen, J.R., Nanson, G.C., May, J.-H., Jones, B.G., Price, D.M., 2015. Hydrological transformation coincided with megafaunal extinction in central Australia. Geology 43, 195–198.
Colhoun, E.A., Geer, G.V.D., 1986. Holocene to Middle Last Glaciation Vegetation History at Tullabardine Dam, Western Tasmania. Proc. R. Soc. Lond. Ser. B Biol. Sci.s 229, 177–207.
Colhoun, E.A., van de Geer, G., Mook, W.G., 1982. Stratigraphy, pollen analysis, and paleoclimatic interpretation of Pulbeena Swamp, northwestern Tasmania. Quat. Res. 18, 108–126.
Colhoun, E.A., Pola, J.S., Barton, C.E., Heijnis, H., 1999. Late Pleistocene vegetation and climate history of lake Selina, western Tasmania. Quat. Int. 57–58, 5–23.
Cook, E.J., 2009. A record of late Quaternary environments at lunette-lakes Bolac and Turangmoroke, Western Victoria, Australia, based on pollen and a range of non-pollen palynomorphs. Rev. Palaeobot. Palynol. 153, 185–224.
Coventry, R.J., 1976. Abandoned shorelines and the late Quaternary history of Lake George, New South Wales. J. Geol. Soc. Aust. 23, 249–273.
Crosta, X., Sturm, A., Armand, L., Pichon, J.-J., 2004. Late Quaternary sea ice history in the Indian sector of the Southern Ocean as recorded by diatom assemblages. Mar. Micropaleontol. 50, 209–223.
D'Costa, D.M., Edney, P., Kershaw, A.P., Deckker, P.D., 1989. Late Quaternary palaeoecology of Tower Hill, Victoria, Australia. J. Biogeogr. 16, 461–482.
D'Costa, D.M., Grindrod, J., Ogden, R., 1993. Preliminary environmental reconstructions from late Quaternary pollen and mollusc assemblages at Egg Lagoon, King Island, Bass Strait. Aust. J. Ecol. 18, 351–366.
Damon, P.E., Jirikowic, J.L., 1992. The sun as a low-frequency harmonic oscillator. Radiocarbon 34, 199–205.
Darrénougué, N., De Deckker, P., Fitzsimmons, K.E., Norman, M.D., Reed, L., van der Kaars, S., Fallon, S., 2009. A late Pleistocene record of aeolian sedimentation in Blanche Cave, Naracoorte, south Australia. Quat. Sci. Rev. 28, 2600–2615.
Davies, S.J., Lamb, H.F., Roberts, S.J., 2015. Micro-xrf core scanning in palaeolimnology: recent developments. In: Croudace, I.W., Rothwell, R.G. (Eds.), Micro-XRF Studies of Sediment Cores: Applications of a Non-destructive Tool for the Environmental Sciences. Springer Netherlands, Dordrecht, pp. 189–226.
Davison, W., 1993. Iron and manganese in lakes. Earth Sci. Rev. 34, 119–163.
De Deckker, P., 1982. Late Quaternary ostracods from Lake George, New South Wales. Alcheringa 6, 305–318.
De Deckker, P., 2001. Late Quaternary cyclic aridity in tropical Australia. Palaeogeogr. Palaeoclimatol. Palaeoecol. 170, 1–9.
De Deckker, P., Moros, M., Perner, K., Jansen, E., 2012. Influence of the tropics and southern westerlies on glacial interhemispheric asymmetry. Nat. Geosci. 5, 266–269.
De Garidel-Thoron, T., Beaufort, L., Linsley, B.K., Dannenmann, S., 2001. Millennial-scale dynamics of the east Asian winter monsoon during the last 200,000 years. Paleoceanography 16, 491–502.
Denniston, R.F., Wyrwoll, K.-H., Asmerom, Y., Polyak, V.J., Humphreys, W.F., Cugley, J., Woods, D., LaPointe, Z., Peota, J., Greaves, E., 2013. North Atlantic forcing of millennial-scale Indo-Australian monsoon dynamics during the Last Glacial period. Quat. Sci. Rev. 72, 159–168.
Dodson, J.R., 1975. Vegetation history and water fluctuations at Lake Leake, Southeastern South Australia. II*. 50,000 B.P. To 10,000 B.P. Aust. J. Bot. 23, 815–831.
Dodson, J., 1977. Late Quaternary palaeoecology of Wyrie Swamp, southeastern South Australia. Quat. Res. 8, 97–114.
Dodson, J., Wright, R., 1989. Humid to Arid to Subhumid Vegetation Shift on Pilliga Sandstone, Ulungra Springs, New South Wales. Quat. Res. 32, 182–192.
Eaves, S.R., Mackintosh A, N., Winckler, G., Schaefer, J.M., Alloway, B.V., Townsend, D.B., 2016. A cosmogenic ^{3}He chronology of late Quaternary glacier fluctuations in North Island, New Zealand (39°S). Quat. Sci. Rev. 132, 40–56.
Engels, S., van Geel, B., 2012. The effects of changing solar activity on climate: contributions from palaeoclimatological studies. J. Space Weather Space Climate 2. A09.
EPICA Community Members, 2006. One-to-one coupling of glacial climate variability in Greenland and Antarctica. Nature 444, 195–198.
Farquhar, G.D., Ehleringer, J.R., Hubick, K.T., 1989. Carbon isotope discrimination and photosynthesis. Annu. Rev. Plant Physiol. Plant Mol. Biol. 40, 503–537.
Ferry, A.J., Crosta, X., Quilty, P.G., Fink, D., Howard, W., Armand, L.K., 2015. First records of winter sea ice concentration in the southwest Pacific sector of the Southern Ocean. Paleoceanography 30, 1525–1539.
Fink, D., Hotchkis, M., Hua, Q., Jacobsen, G., Smith, A.M., Zoppi, U., Child, D., Mifsud, C., van der Gaast, H., Williams, A., Williams, M., 2004. The ANTARES AMS facility at ANSTO. Nucl. Instrum. Methods Phys. Res. Sect. B Beam Interact. Mater. Atoms 223, 109–115.
Fitzsimmons, K.E., Cohen, T.J., Hesse, P.P., Jansen, J., Nanson, G.C., May, J.-H., Barrows, T.T., Haberlah, D., Hilgers, A., Kelly, T., Larsen, J., Lomax, J., Treble, P., 2013. Late Quaternary palaeoenvironmental change in the Australian drylands. Quat. Sci. Rev. 74, 78–96.
Fogwill, C.J., Turney, C.S.M., Hutchinson, D.K., Taschetto, A.S., England, M.H., 2015. Obliquity control on Southern Hemisphere climate during the last glacial. Sci. Rep. 5 https://doi.org/10.1038/srep11673.
Forbes, M.S., Bestland, E.A., Wells, R.T., Krull, E.S., 2007. Palaeoenvironmental reconstruction of the Late Pleistocene to Early Holocene Robertson Cave sedimentary deposit, Naracoorte, south Australia. Aust. J. Earth Sci. 54, 541–559.
Forootan, E., Khandu, Awange, J.L., Schumacher, M., Anyah, R.O., van Dijk, A.I.J.M., Kusche, J., 2016. Quantifying the impacts of ENSO and IOD on rain gauge and remotely sensed precipitation products over Australia. Rem. Sens. Environ. 172, 50–66.
Galloway, R.W., 1965. Late Quaternary climates in Australia. J. Geol. 73, 603–618.
Gentilli, J., 1971. Climates of Australia and New Zealand. In: Landsberg, H.E. (Ed.), World Survey of Climatology. Elsevier Publishing Company, The Netherlands.
Gersonde, R., Crosta, X., Abelmann, A., Armand, L., 2005. Sea-surface temperature and sea ice distribution of the Southern Ocean at the EPILOG Last Glacial Maximum—a circum-Antarctic view based on siliceous microfossil records. Quat. Sci. Rev. 24, 869–896.
Gillen, D., Honda, M., Chivas, A.R., Yatsevich, I., Patterson, D.B., Carr, P.F., 2010. Cosmogenic ^{21}Ne exposure dating of young basaltic lava flows from the Newer Volcanic Province, western Victoria, Australia. Quat. Geochronol. 5, 1–9.
Gingele, F.X., De Deckker, P., Hillenbrand, C.D., 2001. Late Quaternary fluctuations of the Leeuwin Current and palaeoclimates on the adjacent land masses: clay mineral evidence. Aust. J. Earth Sci. 48, 867–874.
Golledge, N.R., Mackintosh, A.N., Anderson, B.M., Buckley, K.M., Doughty, A.M., Barrell, D.J.A., Denton, G.H., Vandergoes, M.J., Andersen, B.G., Schaefer, J.M., 2012. Last Glacial Maximum climate in New Zealand inferred from a modelled Southern Alps icefield. Quat. Sci. Rev. 46, 30–45.
Gouramanis, C., De Deckker, P., Switzer, A.D., Wilkins, D., 2013. Cross-continent comparison of high-resolution Holocene climate records from southern Australia — deciphering the impacts of far-field teleconnections. Earth Sci. Rev. 121, 55–72.
Grant, K.M., Rohling, E.J., Westerhold, T., Zabel, M., Heslop, D., Konijnendijk, T., Lourens, L., 2017. A 3 million year index for North African humidity/aridity and the implication of potential pan-African Humid periods. Quat. Sci. Rev. 171, 100–118.
Hahn, A., Kliem, P., Oehlerich, M., Ohlendorf, C., Zolitschka, B., 2014. Elemental composition of the Laguna Potrok Aike sediment sequence reveals paleoclimatic changes over the past 51 ka in southern Patagonia, Argentina. J. Paleolimnol. 52, 349–366.
Haigh, J.D., 2007. The sun and the Earth's climate. Living Rev. Sol. Phys. 4, 2.
Hall, A., Visbeck, M., 2002. Synchronous variability in the Southern Hemisphere atmosphere, sea ice, and ocean resulting from the annular mode. J. Clim. 15, 3043.
Harle, K.J., 1997. Late Quaternary vegetation and climate change in southeastern Australia: palynological evidence from marine core E55-6. Palaeogeogr. Palaeoclimatol. Palaeoecol. 131, 465–483.
Harris, D., Horwath, W.R., van Kessel, C., 2001. Acid fumigation of soils to remove carbonates prior to total organic carbon or carbon-13 analysis. Soil Sci. Soc. Am. J. 65, 1853–1856.
Harrison, S.P., Bartlein, P.J., Prentice, I.C., 2016. What have we learnt from palaeoclimate simulations? J. Quat. Sci. 31, 363–385.
Head, L., D'Costa, D., Edney, P., 1991. Pleistocene dates for volcanic activity in western Victoria and implications for Aboriginal occupation. In: Williams, M.A.J., De Deckker, P., Kershaw, A.P. (Eds.), The Cainozoic in Australia: a Re-appraisal of the Evidence. Geological Society of Australia, pp. 302–308.
Hellstrom, J., McCulloch, M., Stone, J., 1998. A detailed 31,000-year record of climate and vegetation change, from the isotope geochemistry of two New Zealand speleothems. Quat. Res. 50, 167–178.
Hendon, H.H., Thompson, D.W.J., Wheeler, M.C., 2007. Australian rainfall and surface temperature variations associated with the Southern Hemisphere annular mode. J. Clim. 20, 2452–2467.
Hesse, P.P., 1994. The record of continental dust from Australia in Tasman Sea Sediments. Quat. Sci. Rev. 13, 257–272.
Hesse, P.P., McTainsh, G.H., 1999. Last Glacial Maximum to early Holocene wind strength in the mid-latitudes of the Southern Hemisphere from aeolian dust in the Tasman Sea. Quat. Res. 52, 343–349.
Hesse, P.P., McTainsh, G.H., 2003. Australian dust deposits: modern processes and the Quaternary record. Quat. Sci. Rev. 22, 2007–2035.
Heusser, L., Heusser, C., Kleczkowski, A., Crowhurst, S., 1999. A 50,000-yr pollen

record from Chile of South American millennial-scale climate instability during the last glaciation. Quat. Res. 52, 154–158.
Hogg, A.G., Quan, H., Blackwell, P.G., Mu, N., Buck, C.E., Guilderson, T.P., Heaton, T.J., Palmer, J.G., Reimer, P.J., Reimer, R.W., Turney, C.S.M., Zimmerman, S.R.H., 2013. SHCAL13 Southern Hemisphere calibration, 0-50,000 years cal BP. Radiocarbon 55, 1889–1903.
Hua, Q., Jacobsen, G.E., Zoppi, U., Lawson, E.M., Williams, A.A., Smith, A.M., McGann, M.J., 2001. Progress in radiocarbon target preparation at the ANTARES AMS Centre. Radiocarbon 43, 275–282.
Hughen, K., Southon, J., Lehman, S., Bertrand, C., Turnbull, J., 2006. Marine-derived ^{14}C calibration and activity record for the past 50,000 years updated from the Cariaco Basin. Quat. Sci. Rev. 25, 3216–3227.
Hughes, P.D., Gibbard, P.L., 2014. Evaluating the concept of a global "last glacial maximum" (LGM): a terrestrial perspective. In: Rocha, R., Pais, J., Kullberg, J.C., Finney, S. (Eds.), STRATI 2013: First International Congress on Stratigraphy at the Cutting Edge of Stratigraphy. Springer International Publishing, Cham, pp. 943–945.
Irving, A.J., Green, D.H., 1976. Geochemistry and petrogenesis of the newer basalts of Victoria and South Australia. J. Geol. Soc. Aust. 23, 45–66.
Kattel, G.R., Augustinus, P.C., 2010. Cladoceran-inferred environmental change during the LGM to Holocene transition from Onepoto maar paleolake, Auckland, New Zealand. N. Z. J. Geol. Geophys. 53, 31–42.
Kemp, J., Rhodes, E.J., 2010. Episodic fluvial activity of inland rivers in southeastern Australia: Palaeochannel systems and terraces of the Lachlan River. Quat. Sci. Rev. 29, 732–752.
Kershaw, A.P., McKenzie, G.M., Porch, N., Roberts, R.G., Brown, J., Heijnis, H., Orr, M.L., Jacobsen, G., Newall, P.R., 2007. A high-resolution record of vegetation and climate through the last glacial cycle from Caledonia Fen, southeastern highlands of Australia. J. Quat. Sci. 22, 481–500.
Khider, D., Jackson, C.S., Stott, L.D., 2014. Assessing millennial-scale variability during the Holocene: a perspective from the western tropical Pacific. Paleoceanography 29, 143–159.
Kohn, M.J., 2010. Carbon isotope compositions of terrestrial C3 plants as indicators of (paleo)ecology and (paleo)climate. Proc. Natl. Acad. Sci. 107, 19691–19695.
Long, D.T., Fegan, N.E., McKee, J.D., Lyons, W.B., Hines, M.E., Macumber, P.G., 1992. Formation of alunite, jarosite and hydrous iron oxides in a hypersaline system: lake Tyrrell, Victoria, Australia. Chem. Geol. 96, 183–202.
Lopes dos Santos, R.A., Spooner, M.I., Barrows, T.T., De Deckker, P., Sinninghe Damsté, J.S., Schouten, S., 2013. Comparison of organic ($U^{K'}_{37}$, TEX^{H}_{86}, LDI) and faunal proxies (foraminiferal assemblages) for reconstruction of late Quaternary sea surface temperature variability from offshore southeastern Australia. Paleoceanography 28, 377–387.
Macken, A.C., McDowell, M.C., Bartholomeusz, D.N., Reed, E.H., 2013. Chronology and stratigraphy of the Wet Cave vertebratefossil deposit, Naracoorte, and relationship to paleoclimatic conditions of the Last Glacial Cycle in southeastern Australia. Aust. J. Earth Sci. 60, 271–281.
Macken, A.C., Reed, E.H., 2014. Postglacial reorganization of a small-mammal paleocommunity in southern Australia reveals thresholds of change. Ecol. Monogr. 84, 563–577.
Mackenzie, L., Moss, P., 2017. A late Quaternary record of vegetation and climate change from Hazards Lagoon, eastern Tasmania. Quat. Int. 432, 58–65.
Magee, J.W., Miller, G.H., Spooner, N.A., Questiaux, D., 2004. Continuous 150 k.y. monsoon record from Lake Eyre, Australia: insolation-forcing implications and unexpected Holocene failure. Geology 32, 885–888.
McGlone, M.S., 2001. A late Quaternary pollen record from marine core P69, southeastern North Island, New Zealand. N. Z. J. Geol. Geophys. 44, 69–77.
McGowan, H.A., Marx, S.K., Soderholm, J., Denholm, J., 2010. Evidence of solar and tropical-ocean forcing of hydroclimate cycles in southeastern Australia for the past 6500 years. Geophys. Res. Lett. 37. L10705.
Meneghini, B., Simmonds, I., Smith, I.N., 2007. Association between Australian rainfall and the Southern Annular Mode. Int. J. Climatol. 27, 109–121.
Meyers, P.A., Ishiwatari, R., 1993. Lacustrine organic geochemistry—an overview of indicators of organic matter sources and diagenesis in lake sediments. Org. Geochem. 20, 867–900.
Miller, G.H., Fogel, M.L., 2016. Calibrating $\delta^{18}O$ in *Dromaius novaehollandiae* (emu) eggshell calcite as a paleo-aridity proxy for the Quaternary of Australia. Geochem. Cosmochim. Acta 193, 1–13.
Mix, A.C., Bard, E., Schneider, R., 2001. Environmental processes of the ice age: land, oceans, glaciers (EPILOG). Quat. Sci. Rev. 20, 627–657.
Moriarty, K.C., McCulloch, M.T., Wells, R.T., McDowell, M.C., 2000. Mid-Pleistocene cave fills, megafaunal remains and climate change at Naracoorte, South Australia: towards a predictive model using U-Th dating of speleothems. Palaeogeogr. Palaeoclimatol. Palaeoecol. 159, 113–143.
Moss, P.T., Tibby, J., Petherick, L., McGowan, H., Barr, C., 2013. Late Quaternary vegetation history of North Stradbroke Island, Queensland, eastern Australia. Quat. Sci. Rev. 74, 257–272.
Mullan, A.B., 1998. Southern Hemisphere sea-surface temperatures and their contemporary and lag association with New Zealand temperature and precipitation. Int. J. Climatol. 18, 817–840.
Nelson, D.M., Urban, M.A., Kershaw, A.P., Hu, F.S., 2016. Late-Quaternary variation in C3 and C4 grass abundance in southeastern Australia as inferred from $\delta^{13}C$ analysis: Assessing the roles of climate, pCO2, and fire. Quat. Sci. Rev. 139, 67–76.
Newnham, R.M., Lowe, D.J., Giles, T., Alloway, B.V., 2007. Vegetation and climate of Auckland, New Zealand, since ca. 32 000 cal. yr ago: support for an extended LGM. J. Quat. Sci. 22, 517–534.
O'Leary, M.H., 1981. Carbon isotope fractionation in plants. Phytochemistry 20, 553–567.
Ogurtsov, M.G., Raspopov, O.M., Oinonen, M., Jungner, H., Lindholm, M., 2010. Possible manifestation of nonlinear effects when solar activity affects climate changes. Geomagn. Aeron. 50, 15–20.
Ohsawa, S., Sugimori, K., Yamauchi, H., Koeda, T., Inaba, H., Kataoka, Y., Kagiyama, T., 2014. Brownish discoloration of the summit crater lake of Mt. Shinmoe-dake, Kirishima Volcano, Japan: volcanic–microbial coupled origin. Bull. Volcanol. 76, 809.
Okansen, J., Kindt, R., Legendre, P., O'Hara, B., Simpson, G.L., Solymos, P., Stevens, M.H.H., Wagner, H., 2008. Vegan: Community Ecology Package.
O'Connor, J.F., Allen, J., 2015. The process, biotic impact, and global implications of the human colonization of Sahul about 47,000 years ago. J. Archaeol. Sci. 56, 73–84.
Page, K.J., Dare-Edwards, A.J., Owens, J.W., Frazier, P.S., Kellett, J., Price, D.M., 2001. TL chronology and stratigraphy of riverine source bordering sand dunes near Wagga Wagga, New South Wales, Australia. Quat. Int. 83, 187–193.
Pedro, J.B., Bostock, H. C, Bitz, C.M., He, F., Vandergoes, M.J., Steig, E.J., Chase, B.M., Krause, C.E., Rasmussen, S.O., Markle, B.R., Cortese, G., 2016. The spatial extent and dynamics of the Antarctic Cold Reversal. Nat. Geosci. 9, 51–55.
Peel, M.C., Finlayson, B.L., McMahon, T.A., 2007. Updated world map of the Köppen-Geiger climate classification. Hydrology and Earth Sysem. Sciences 11, 1633–1644.
Pepler, A., Timbal, B., Rakich, C., Coutts-Smith, A., 2014. Indian Ocean Dipole overrides ENSO's influence on cool season rainfall across the eastern seaboard of Australia. J. Clim. 27, 3816–3826.
Pepler, A.S., Alexander, L.V., Evans, J.P., Sherwood, S.C., 2016. Zonal winds and southeast Australian rainfall in global and regional climate models. Clim. Dynam. 46, 123–133.
Petherick, L., McGowan, H., Moss, P., 2008. Climate variability during the Last Glacial Maximum in eastern Australia: evidence of two stadials? J. Quat. Sci. 23, 787–802.
Petherick, L.M., McGowan, H.A., Kamber, B.S., 2009. Reconstructing transport pathways for late Quaternary dust from eastern Australia using the composition of trace elements of long traveled dusts. Geomorphology 105, 67–79.
Petherick, L., Bostock, H., Cohen, T.J., Fitzsimmons, K., Tibby, J., Fletcher, M.-S., Moss, P., Reeves, J., Mooney, S., Barrows, T., Kemp, J., Jansen, J., Nanson, G., Dosseto, A., 2013. Climatic records over the past 30 ka from temperate Australia - a synthesis from the Oz-INTIMATE workgroup. Quat. Sci. Rev. 74, 58–77.
Petherick, L.M., Moss, P.T., McGowan, H.A., 2017. An extended Last Glacial Maximum in subtropical Australia. Quat. Int. 432, 1–12.
Pezza, A.B., Durrant, T., Simmonds, I., Smith, I., 2008. Southern Hemisphere synoptic behavior in extreme phases of SAM, ENSO, sea ice extent, and southern Australia rainfall. J. Clim. 21, 5566–5584.
Prentice, I.C., Meng, T., Wang, H., Harrison, S.P., Ni, J., Wang, G., 2011. Evidence of a universal scaling relationship for leaf CO_2 drawdown along an aridity gradient. New Phytol. 190, 169–180.
Prentice, I.C., Cleator, S.F., Huang, Y.H., Harrison, S.P., Roulstone, I., 2017. Reconstructing ice-age palaeoclimates: quantifying low-CO_2 effects on plants. Global Planet. Change 149, 166–176.
Putnam, A.E., Schaefer, J.M., Denton, G.H., Barrell, D.J.A., Birkel, S.D., Andersen, B.G., Kaplan, M.R., Finkel, R.C., Schwartz, R., Doughty, A.M., 2013. The last glacial maximum at 44°S documented by a ^{10}Be moraine chronology at Lake Ohau, southern Alps of New Zealand. Quat. Sci. Rev. 62, 114–141.
R Core Team, 2017. R: a Language and Environment for Statistical Computing. R Foundation for Statistical Computing, Vienna, Austria.
Rao, Z., Guo, W., Cao, J., Shi, F., Jiang, H., Li, C., 2017. Relationship between the stable carbon isotopic composition of modern plants and surface soils and climate: a global review. Earth Sci. Rev. 165, 110–119.
Reeves, J.M., Barrows, T.T., Cohen, T.J., Kiem, A.S., Bostock, H.C., Fitzsimmons, K.E., Jansen, J.D., Kemp, J., Krause, C., Petherick, L., Phipps, S.J., OZ-INTIMATE Members, 2013. Climate variability over the last 35,000 years recorded in marine and terrestrial archives in the Australian region: an OZ-INTIMATE compilation. Quat. Sci. Rev. 74, 21–34.
Risbey, J.S., Pook, M.J., McIntosh, P.C., Wheeler, M.C., Hendon, H.H., 2009. On the remote drivers of rainfall variability in Australia. Mon. Weather Rev. 137, 3233–3253.
Robbie, A., Martin, H.A., 2007. The history of the vegetation from the Last Glacial Maximum at Mountain Lagoon, Blue Mountains, New South Wales. Proc. Linn. Soc. N. S. W. 128, 57–80.
Ruf, T., 1999. The Lomb-Scargle periodogram in biological rhythm research: Analysis of incomplete and unequally spaced time-series. Biol. Rhythm. Res. 30, 178–201.
Sandiford, A., Horrocks, M., Newnham, R., Ogden, J., Alloway, B., 2002. Environmental change during the Last Glacial Maximum (c. 25 000-c. 16 500 years BP) at Mt Richmond, Auckland Isthmus, New Zealand. J. Roy. Soc. N. Z. 32, 155–167.
Sandiford, A., Newnham, R., Alloway, B., Ogden, J., 2003. A 28 000–7600 cal yr BP pollen record of vegetation and climate change from Pukaki Crater, northern New Zealand. Palaeogeogr. Palaeoclimatol. Palaeoecol. 201, 235–247.
Scafetta, N., Milani, F., Bianchini, A., Ortolani, S., 2016. On the astronomical origin of the Hallstatt oscillation found in radiocarbon and climate records throughout the Holocene. Earth Sci. Rev. 162, 24–43.
Schubert, B.A., Jahren, A.H., 2012. The effect of atmospheric CO_2 concentration on carbon isotope fractionation in C_3 land plants. Geochem. Cosmochim. Acta 96,

29–43.
Schubert, B.A., Jahren, A.H., 2015. Global increase in plant carbon isotope fractionation following the Last Glacial Maximum caused by increase in atmospheric pCO_2. Geology 43, 435–438.
Shakun, J.D., Carlson, A.E., 2010. A global perspective on Last Glacial Maximum to Holocene climate change. Quat. Sci. Rev. 29, 1801–1816.
Shanahan, T.M., McKay, N.P., Hughen, K.A., Overpeck, J.T., Otto-Bliesner, B., Heil, C.W., King, J., Scholz, C.A., Peck, J., 2015. The time-transgressive termination of the African Humid Period. Nat. Geosci. 8, 140–144.
Sherwood, J., Oyston, B., Kershaw, A.P., 2004. The age and contemporary environments of Tower Hill volcano, southwest Victoria, Australia. Proc. Roy. Soc. Vic. 116, 71–78.
Shulmeister, J., McLea, W.L., Singer, C., McKay, R.M., Hosie, C., 2003. Late Quaternary pollen records from the lower Cobb Valley and adjacent areas, north-west Nelson, New Zealand. N. Z. J. Botany 41, 503–533.
Shulmeister, J., Thackray, G.D., Rieser, U., Hyatt, O.M., Rother, H., Smart, C.C., Evans, D.J.A., 2010. The stratigraphy, timing and climatic implications of glaciolacustrine deposits in the middle Rakaia Valley, South Island, New Zealand. Quat. Sci. Rev. 29, 2362–2381.
Shulmeister, J., Kemp, J., Fitzsimmons, K.E., Gontz, A., 2016. Constant wind regimes during the Last Glacial Maximum and early Holocene: evidence from Little Llangothlin Lagoon, New England Tablelands, eastern Australia. Clim. Past 12, 1435–1444.
Simpson, G.L., 2007. Analogue Methods in Palaeoecology: Using the Analogue Package, p. 29, 2007 22.
Simpson, G.L., Oksanen, J., 2016. Analogue: Analogue Matching and Modern Analogue Technique Transfer Function Models, R Package Version 0.17-0 Ed.
Singh, G., Geissler, E.A., 1985. Late Cainozoic history of vegetation, fire, lake levels and climate, at Lake George, New South Wales, Australia. Philos. Trans. R. Soc. Lond. Ser. B Biol. Sci. 311, 379–447.
Singh, G., Luly, J., 1991. Changes in vegetation and seasonal climate since the last full glacial at Lake Frome, South Australia. Palaeogeogr. Palaeoclimatol. Palaeoecol. 84, 75–86.
Singh, G., Opdyke, N.D., Bowler, J.M., 1981. Late Cainozoic stratigraphy, palaeomagnetic chronology and vegetational history from Lake George, N.S.W. J. Geol. Soc. Aust. 28, 435–452.
Soon, W., Velasco Herrera, V.M., Selvaraj, K., Traversi, R., Usoskin, I., Chen, C.-T.A., Lou, J.-Y., Kao, S.-J., Carter, R.M., Pipin, V., Severi, M., Becagli, S., 2014. A review of Holocene solar-linked climatic variation on centennial to millennial timescales: Physical processes, interpretative frameworks and a new multiple cross-wavelet transform algorithm. Earth Sci. Rev. 134, 1–15.
Steinhilber, F., Beer, J., Fröhlich, C., 2009. Total solar irradiance during the Holocene. Geophys. Res. Lett. 36. L19704.
Stewart, G.R., Turnbull, M.H., Schmidt, S., Erskine, P.D., 1995. ^{13}C natural abundance in plant communities along a rainfall gradient: a biological integrator of water availability. Funct. Plant Biol. 22, 51–55.
Stone, T., 2006. Last glacial cycle hydrological change at Lake Tyrrell, southeast Australia. Quat. Res. 66, 176–181.
Suggate, R.P., Almond, P.C., 2005. The Last Glacial Maximum (LGM) in western South Island, New Zealand: implications for the global LGM and MIS 2. Quat. Sci. Rev. 24, 1923–1940.
Sweller, S., Martin, H.A., 2001. A 40,000 year vegetation history and climatic interpretations of Burraga Swamp, Barrington Tops, New South Wales. Quat. Int. 83, 233–244.
Thomas, Z.A., 2016. Using natural archives to detect climate and environmental tipping points in the Earth System. Quat. Sci. Rev. 152, 60–71.
Tibby, J., Kershaw, A.P., Builth, H., Philibert, A., White, C., 2006. Environmental change and variability in south-western Victoria: changing constraints and opportunities for occupation and land use. In: David, B., Barker, B., McNiven, I.J. (Eds.), The Social Archaeology of Australian Indigenous Societies. Aboriginal Studies Press, Canberra, pp. 254–269.
Tierney, J.E., Smerdon, J.E., Anchukaitis, K.J., Seager, R., 2013. Multidecadal variability in East African hydroclimate controlled by the Indian Ocean. Nature 493, 389–392.
Timms, B.V., 1975. Basic limnology of two crater lakes in western Victoria. Proc. Roy. Soc. Vic. 87, 159–166.
Treble, P.C., Baker, A., Ayliffe, L.K., Cohen, T.C., Hellstrom, J.C., Gagan, M.K., Frisia, S., Drysdale, R.N., Griffiths, A.D., Borsato, A., 2016. Hydroclimate of the Last Glacial Maximum and deglaciation in southern Australia's arid margin interpreted from speleothem records (23-15 ka). Clim. Past Discuss 2016, 1–43.
Turner, J.N., Holmes, N., Davis, S.R., Leng, M.J., Langdon, C., Scaife, R.G., 2015. A multiproxy (micro-XRF, pollen, chironomid and stable isotope) lake sediment record for the Lateglacial to Holocene transition from Thomastown Bog, Ireland. J. Quat. Sci. 30, 514–528.
Turney, C.S.M., Haberle, S., Fink, D., Kershaw, A.P., Barbetti, M., Barrows, T.T., Black, M., Cohen, T.J., Corrège, T., Hesse, P.P., Hua, Q., Johnston, R., Morgan, V., Moss, P., Nanson, G., van Ommen, T., Rule, S., Williams, N.J., Zhao, J.X., D'Costa, D., Feng, Y.X., Gagan, M., Mooney, S., Xia, Q., 2006. Integration of ice-core, marine and terrestrial records for the Australian Last Glacial Maximum and Termination: a contribution from the OZ INTIMATE group. J. Quat. Sci. 21, 751–761.
Tyler, J.J., Mills, K., Barr, C., Sniderman, J.M.K., Gell, P.A., Karoly, D.J., 2015. Identifying coherent patterns of environmental change between multiple, multivariate records: an application to four 1000-year diatom records from Victoria, Australia. Quat. Sci. Rev. 119, 94–105.
Ummenhofer, C.C., England, M.H., McIntosh, P.C., Meyers, G.A., Pook, M.J., Risbey, J.S., Gupta, A.S., Taschetto, A.S., 2009. What causes southeast Australia's worst droughts? Geophys. Res. Lett. 36.
van Bree, L.G.J., Rijpstra, W.I.C., Cocquyt, C., Al-Dhabi, N.A., Verschuren, D., Sinninghe Damsté, J.S., de Leeuw, J.W., 2014. Origin and palaeoenvironmental significance of C25 and C27 n-alk-1-enes in a 25,000-year lake-sedimentary record from equatorial East Africa. Geochem. Cosmochim. Acta 145, 89–102.
Vandergoes, M.J., Newnham, R.M., Preusser, F., Hendy, C.H., Lowell, T.V., Fitzsimons, S.J., Hogg, A.G., Kasper, H.U., Schluchter, C., 2005. Regional insolation forcing of late Quaternary climate change in the Southern Hemisphere. Nature 436, 242–245.
Vandergoes, M.J., Newnham, R.M., Denton, G.H., Blaauw, M., Barrell, D.J.A., 2013. The anatomy of Last Glacial Maximum climate variations in south Westland, New Zealand, derived from pollen records. Quat. Sci. Rev. 74, 215–229.
Versteegh, G.J.M., 2005. Solar forcing of climate. 2: evidence from the past. Space Sci. Rev. 120, 243–286.
WAIS Divide Project Members, 2013. Onset of deglacial warming in West Antarctica driven by local orbital forcing. Nature 500, 440–444.
WAIS Divide Project Members, 2015. Precise interpolar phasing of abrupt climate change during the last ice age. Nature 520, 661–665.
Watterson, I.G., 2001. Wind-induced rainfall and surface temperature anomalies in the Australian region. J. Clim. 14, 1901.
Weber, M.E., Clark, P.U., Kuhn, G., Timmermann, A., Sprenk, D., Gladstone, R., Zhang, X., Lohmann, G., Menviel, L., Chikamoto, M.O., Friedrich, T., Ohlwein, C., 2014. Millennial-scale variability in Antarctic ice-sheet discharge during the last deglaciation. Nature 510, 134–138.
Weltje, G.J., Bloemsma, M.R., Tjallingii, R., Heslop, D., Röhl, U., Croudace, I.W., 2015. Prediction of geochemical composition from XRF core scanner data: a new multivariate approach including automatic selection of calibration samples and quantification of uncertainties. In: Croudace, I.W., Rothwell, R.G. (Eds.), Micro-XRF Studies of Sediment Cores. Springer, Netherlands, pp. 507–534.
Whittaker, T.E., Hendy, C.H., Hellstrom, J.C., 2011. Abrupt millennial-scale changes in intensity of Southern Hemisphere westerly winds during marine isotope stages 2–4. Geology 39, 455–458.
Williams, A.A.J., Stone, R.C., 2009. An assessment of relationships between the Australian subtropical ridge, rainfall variability, and high-latitude circulation patterns. Int. J. Climatol. 29, 691–709.
Williams, N.J., 2005. The Environmental Reconstruction of the Last Glacial Cycle at Redhead Lagoon in Coastal, Eastern Australia. PhD Thesis. The University of Sydney, Sydney.
Williams, N.J., Harle, K.J., Gale, S.J., Heijnis, H., 2006. The vegetation history of the last glacial–interglacial cycle in eastern New South Wales, Australia. J. Quat. Sci. 21, 735–750.
Wood, S.N., 2006. Generalized Additive Models: an Introduction with R. Chapman and Hall/CRC Boca Raton, Florida.
Wright, I.C., McGlone, M.S., Nelson, C.S., Pillans, B.J., 1995. An integrated Late Quaternary (Stage 3 to Present-day) paleoclimate and paleoceanographic record from offshore northern New Zealand. Quat. Res. 44, 283–293.